

Abstract

HARRIS III, JOHN LEROY. Seismic Analysis and Design of Type FR Steel Frames Using Displacement-Based Design and Advanced Analysis. (Under the direction of Mervyn J. Kowalsky.)

Current design office methodologies for seismic design of steel moment frames include forced-based methods for calculating equivalent lateral forces and a static elastic analysis. Research has revealed erroneous assumptions in forced-based methods and proposes that displacement-based methods, due to modeling inelastic systems, result in more reasonable lateral force distributions. Additionally, LRFD¹ member design interaction equations implicitly account for geometric and material non-linear effects. This philosophy does not satisfy compatibility between actual inelastic member response and the elastic system as assumed by a conventional elastic analysis.

Displacement-based lateral force distributions in combination with a second-order inelastic static analysis that sufficiently determines the limit state strength and stability of a structural system, or “Advanced Analysis,” is advantageous to the design of steel moment frames. Second-order geometric and material non-linear effects are directly accounted for in the analysis. This allows engineers to predict actual frame behavior with greater accuracy and results in a more efficient and economical frame. Another advantage is that force reduction factors outlined in current seismic codes are not required since the frame is designed for inelastic behavior. This approach eliminates discrepancies between initially assumed force reduction factors and final frame ductility capacity. Also, individual member capacity checks outlined in design specifications are similarly not required.

The goal of this research is to advance the validity and accuracy of displacement-based design methods and Advanced Analysis for the engineering of seismic resistant steel moment frames. This research will allow the development of alternate seismic analysis and design procedures, as well as refined practical methods that can be incorporated in a design office.

1) Manual of Steel Construction – Load and Resistance Factor Design, American Institute of Steel Construction

**SEISMIC ANALYSIS AND DESIGN OF TYPE FR STEEL
FRAMES USING DISPLACEMENT-BASED DESIGN AND
ADVANCED ANALYSIS**

by

JOHN LEROY HARRIS III

A thesis submitted to the Graduate Faculty of
North Carolina State University
in partial fulfillment of the
requirements for the Degree of
Master of Science

CIVIL AND ENVIRONMENTAL ENGINEERING

Raleigh

2002

APPROVED BY:

Tasnim Hassan

James Nau

Chair of Advisory Committee

Mervyn Kowalsky

Unquestioned answers are more dangerous than unanswered questions

Unknown

Dedicated to

My future students – I hope I will be able to inspire them half as well as my teachers inspired me.

Biography

John Harris was born August 8, 1970 in Rome, NY and spent his childhood years in Chicago, IL, and Raleigh, NC. After completing his Bachelor of Science degree in Civil Engineering at North Carolina State University in 1994, he worked as a Structural Engineer in Raleigh, NC, Atlanta, GA, and New York, NY, with special interest in steel structures. Additionally, John is a registered Professional Engineer and an active member of AISC, SSRC, and ASCE. For the past several years, he has participated with various industry committees, most notably, Committee on Manuals and Textbooks for AISC and Task Group #29 – 2nd Order Inelastic Analysis for SSRC. It was the experience with these groups that led John to return to North Carolina State University with an interest in researching Advanced Analysis techniques for steel structures. While at NCSU, John met Mervyn Kowalsky, who strengthened John's concentration in earthquake engineering, and began researching displacement-based seismic design and Advanced Analysis of steel frames. John completed his Master of Science degree in August 2002.

John can be reached by email at: jlh3@bellsouth.net

Acknowledgements

I am sincerely grateful to the following while preparing this document.

- God, for giving me the ability to think, though at times incorrectly.
- My family and friends, whom without their support I would be a starving musician.
- Brian Lanier, Kirk Stanford, Randall Wilson, Joel Howard, Todd Garrison, Scott Wirgau, and Tyler Durden, for putting up with my raving discussions, most notably, the ones concerning my ironic views that people should not live in severe earthquake prone regions. For the scientific exploration, I do submit.
- My mentor and friend, JC Smith, for the ability to see the truths in his vision.
- My committee members, Jim Nau and Tasnim Hassan, for their support, wisdom, guidance, and their ability to let go at 4:30 on Friday.
- My committee chair, Mervyn Kowalsky, for showing me the light and then reinforcing the brick wall I banged my head against with #18 bars at 4”.

Table of Contents

List of Tables	x	
List of Figures	xv	
List of Symbols	xxvi	
List of Abbreviations	xxxix	
PART 1	INTRODUCTION, SIMPLIFICATIONS AND ASSUMPTIONS	1
1.0	Introduction	2
1.1	Current Research	4
1.2	Simplifications, Assumptions, and Constant Variables	7
1.2.1	Simplifications	7
1.2.2	Assumptions	8
1.2.3	Constant Variables	9
PART 2	DISPLACEMENT-BASED DESIGN	11
2.0	Introduction	12
2.1	SEAOC Specification on Performance-based Design	12
2.1.1	Ductility	16
2.2	Section Curvature	16
2.2.1	Yield Curvature	16
2.2.2	Equivalent Plastic Curvature	18
2.2.3	First-yield Curvature	21
2.2.4	Curvature Reduction for Combined Load Effects	22
2.2.4.1	Reduction for Axial Compression	22
2.2.4.2	Reduction for Shear	26
2.2.4.3	Reduction for Torsion	27
2.2.5	Material Overstrength Factor	27
2.2.6	Summary of Curvatures	29

2.3	Member Rotation	29
2.3.1	Stability Functions (No Transverse Loads – No Support Displacement)	29
2.3.2	Stability Functions (No Transverse Loads – Support Displacement)	32
2.3.3	Stability Functions (Transverse Loads)	34
2.3.4	Column-to-Beam Stiffness Factor	39
2.3.5	Summary of Plastic Rotation Capacities	42
2.4	Global System Response	43
2.4.1	Design System Displacement	46
2.4.2	System Ductility	47
2.4.3	Effective System Damping	48
2.4.4	Effective System Period and Stiffness, and Base Shear	50
2.4.5	System Analysis and Elastic Displacement Profiles	52
	2.4.5.1 Equivalent Yield Analysis	54
2.4.6	System Overstrength and Capacity Design	58
	2.4.6.1 Material Overstrength Factors	59
	2.4.6.2 Performance Overstrength Factors	59
	2.4.6.3 Capacity Design	65
	2.4.6.4 Member Design	69
	2.4.6.4.1 Beams	70
	2.4.6.4.2 Columns	70
2.5	Displacement-based Design	73
2.5.1	FR-4	79
2.5.2	FR-4-W21	94
2.5.3	FR-4-W24	97
2.5.4	FR-4a	100

	2.5.5	FR-4b	109
	2.5.6	FR-8	116
	2.5.7	FR-8-W27	126
	2.5.8	FR-16	136
PART 3		ADVANCED ANALYSIS	152
3.0		Introduction	153
	3.1	Advanced Analysis	155
	3.2	Advanced Analysis Methods	156
		3.2.1 Material Non-linearities	157
		3.2.2 Geometric Non-linearities	161
	3.3	Advanced Analysis and Displacement-Based Design	162
		3.3.1 FR-4	165
		3.3.2 FR-4-W21	166
		3.3.3 FR-4-W24	167
		3.3.4 FR-4a	168
		3.3.5 FR-4b	169
		3.3.6 FR-8	170
		3.3.7 FR-8-W27	171
	3.4	References	173
PART 4		VERIFICATION	174
4.0		Introduction	175
	4.1	FR-4	176
		4.1.1 Displacement Profiles	176
		4.1.2 Base Shear	189
	4.2	FR-4-W21	194
		4.2.1 Displacement Profiles	194
		4.2.2 Base Shear	199

4.3	FR-4-W24	200
	4.3.1 Displacement Profiles	200
	4.3.2 Base Shear	205
4.4	FR-4a	206
	4.4.1 Displacement Profiles	206
	4.4.2 Base Shear	211
4.5	FR-4b	213
	4.5.1 Displacement Profiles	213
	4.5.2 Base Shear	218
4.6	FR-8	220
	4.6.1 Displacement Profiles	220
	4.6.2 Base Shear	231
4.7	FR-8-W27	234
	4.7.1 Displacement Profiles	234
	4.7.2 Base Shear	239
4.8	FR-16	241
	4.8.1 Displacement Profiles	241
	4.8.2 Base Shear	252
4.9	Sources of Variation	255
PART 5	CONCLUSION AND FUTURE RESEARCH	263
5.0	Conclusion	264
5.1	Future Research	267
PART 6	APPENDIX AND REFERENCES	269
A	Design Response Spectrums	270
A.1	Acceleration Response Spectrums	271
A.2	Displacement Response Spectrums	272
A.3	Velocity Response Spectrums	275

B	Time-Histories	277
B.1	TH-1 Design Response Spectrums (Artificial)	277
B.2	TH-2 Design Response Spectrums (Artificial)	279
B.3	TH-3 Design Response Spectrums (El Centro)	281
B.4	TH-4 Design Response Spectrums (Kobe)	283
B.5	TH-5 Design Response Spectrums (Loma Prieta)	285
B.6	TH-6 Design Response Spectrums (Cape Mendocino)	287
B.7	TH-7 Design Response Spectrums (Tabas)	289
B.8	TH-8 Design Response Spectrums (Petrolia)	291
B.9	TH-9 Design Response Spectrums (Vina Del Mar)	293
B.10	TH-10 Design Response Spectrums (Northridge)	295
B.11	TH-11 Design Response Spectrums (Tokachi-Oki)	297
B.12	TH-12 Design Response Spectrums (Taft)	299
C	References	301

List of Tables

Table 1.1-1	Frame description	4
Table 2.1-1	Structural performance levels	13
Table 2.1-2	Design level earthquakes	14
Table 2.1-3	Basic safety performance objective	15
Table 2.2.3-1	Recommended design magnitude of compressive residual stresses	21
Table 2.2.5-1	Recommended material overstrength factors	28
Table 2.2.6-1	Recommended equivalent plastic curvatures	29
Table 2.3.3-1	Elastic fixed-end moments	38
Table 2.3.5-1	Recommended equivalent plastic rotation capacities	42
Table 2.3.5-2	Recommended equivalent plastic rotation capacities with axial force	42
Table 2.4-1	Recommended target interstory drifts corresponding to rotation demands	44
Table 2.4-2	Inelastic Displacement Profiles	44
Table 2.5-1	Frame descriptions	73
Table 2.5-2	Target interstory drifts per performance level	74
Table 2.5-3	Target peak ground accelerations per performance level	75
Table 2.5.1-1	Floor equivalent plastic rotations (FR-4)	81
Table 2.5.1-2	SP-1 target displacements (FR-4)	83
Table 2.5.1-3	SP-2 target displacements (FR-4)	83
Table 2.5.1-4	SP-3 target displacements (FR-4)	83
Table 2.5.1-5	SP-4 target displacements (FR-4)	84
Table 2.5.1-6	SP-1 SDOF system properties (FR-4)	85
Table 2.5.1-7	SP-2 SDOF system properties (FR-4)	85
Table 2.5.1-8	SP-3 SDOF system properties (FR-4)	86

Table 2.5.1-9	SP-4 SDOF system properties (FR-4)	86
Table 2.5.1-10	SP-4 effective system properties (FR-4)	88
Table 2.5.1-11	SP-3 effective system properties (FR-4)	88
Table 2.5.1-12	SP-2 effective system properties (FR-4)	89
Table 2.5.1-13	SP-1 effective system properties (FR-4)	89
Table 2.5.1-14	Equivalent static lateral forces (FR-4)	90
Table 2.5.4-1	Floor equivalent plastic rotations (FR-4a)	101
Table 2.5.4-2	SP-1 target displacements (FR-4a)	103
Table 2.5.4-3	SP-2 target displacements (FR-4a)	103
Table 2.5.4-4	SP-3 target displacements (FR-4a)	103
Table 2.5.4-5	SP-1 target displacements (FR-4a)	103
Table 2.5.4-6	SP-1 SDOF system properties (FR-4a)	104
Table 2.5.4-7	SP-2 SDOF system properties (FR-4a)	105
Table 2.5.4-8	SP-3 SDOF system properties (FR-4a)	105
Table 2.5.4-9	SP-4 SDOF system properties (FR-4a)	105
Table 2.5.4-10	SP-4 effective system properties (FR-4a)	106
Table 2.5.4-11	SP-3 effective system properties (FR-4a)	106
Table 2.5.4-12	SP-2 effective system properties (FR-4a)	106
Table 2.5.4-13	SP-1 effective system properties (FR-4a)	106
Table 2.5.4-14	Equivalent static lateral forces (FR-4a)	107
Table 2.5.5-1	Floor equivalent plastic rotations (FR-4b)	110
Table 2.5.5-2	SP-1 target displacements (FR-4b)	110
Table 2.5.5-3	SP-2 target displacements (FR-4b)	110
Table 2.5.5-4	SP-3 target displacements (FR-4b)	111
Table 2.5.5-5	SP-4 target displacements (FR-4b)	111
Table 2.5.5-6	SP-1 SDOF system properties (FR-4b)	112
Table 2.5.5-7	SP-2 SDOF system properties (FR-4b)	112

Table 2.5.5-8	SP-3 SDOF system properties (FR-4b)	112
Table 2.5.5-9	SP-4 SDOF system properties (FR-4b)	113
Table 2.5.5-10	SP-4 effective system properties (FR-4b)	113
Table 2.5.5-11	SP-3 effective system properties (FR-4b)	113
Table 2.5.5-12	SP-2 effective system properties (FR-4b)	113
Table 2.5.5-13	SP-1 effective system properties (FR-4b)	113
Table 2.5.5-14	Equivalent static lateral forces (FR-4b)	114
Table 2.5.6-1	Floor equivalent plastic rotations (FR-8)	117
Table 2.5.6-2	Elastic SP-1 target displacements (FR-8)	118
Table 2.5.6-3	SP-2 target displacements (FR-8)	118
Table 2.5.6-4	SP-3 target displacements (FR-8)	118
Table 2.5.6-5	SP-4 target displacements (FR-8)	119
Table 2.5.6-6	Elastic SP-1 SDOF system properties (FR-8)	120
Table 2.5.6-7	SP-2 SDOF system properties (FR-8)	120
Table 2.5.6-8	SP-3 SDOF system properties (FR-8)	121
Table 2.5.6-9	SP-4 SDOF system properties (FR-8)	121
Table 2.5.6-10	SP-4 effective system properties (FR-8)	122
Table 2.5.6-11	SP-3 effective system properties (FR-8)	123
Table 2.5.6-12	SP-2 effective system properties (FR-8)	123
Table 2.5.6-13	Elastic SP-1 effective system properties (FR-8)	123
Table 2.5.6-14	Equivalent static lateral forces (FR-8)	123
Table 2.5.7-1	Floor equivalent plastic rotations (FR-8-W27)	127
Table 2.5.7-2	Elastic SP-1 target displacements (FR-8-W27)	127
Table 2.5.7-3	SP-2 target displacements (FR-8-W27)	128
Table 2.5.7-4	SP-3 target displacements (FR-8-W27)	128
Table 2.5.7-5	SP-4 target displacements (FR-8-W27)	128
Table 2.5.7-6	Elastic SP-1 SDOF system properties (FR-8-W27)	129

Table 2.5.7-7	SP-2 SDOF system properties (FR-8-W27)	130
Table 2.5.7-8	SP-3 SDOF system properties (FR-8-W27)	130
Table 2.5.7-9	SP-4 SDOF system properties (FR-8-W27)	131
Table 2.5.7-10	SP-4 effective system properties (FR-8-W27)	131
Table 2.5.7-11	SP-3 effective system properties (FR-8-W27)	131
Table 2.5.7-12	SP-2 effective system properties (FR-8-W27)	131
Table 2.5.7-13	Elastic SP-1 effective system properties (FR-8-W27)	132
Table 2.5.7-14	Equivalent static lateral forces (FR-8-W27)	132
Table 2.5.8-1	Floor equivalent plastic rotations (FR-16)	137
Table 2.5.8-2	Elastic SP-1 target displacements (FR-16)	138
Table 2.5.8-3	SP-2 target displacements (FR-16)	139
Table 2.5.8-4	SP-3 target displacements (FR-16)	140
Table 2.5.8-5	SP-4 target displacements (FR-16)	141
Table 2.5.8-6	Elastic SP-1 SDOF system properties (FR-16)	143
Table 2.5.8-7	SP-2 SDOF system properties (FR-16)	144
Table 2.5.8-8	SP-3 SDOF system properties (FR-16)	145
Table 2.5.8-9	SP-4 SDOF system properties (FR-16)	146
Table 2.5.8-10	SP-4 effective system properties (FR-16)	146
Table 2.5.8-11	SP-3 effective system properties (FR-16)	147
Table 2.5.8-12	SP-2 effective system properties (FR-16)	147
Table 2.5.8-13	Elastic SP-1 effective system properties (FR-16)	147
Table 2.5.8-14	Equivalent static lateral forces (FR-16)	148
Table 4-1	Selected time-histories	175
Table 4.1.1-1	FR-4 Displacements at effective height	178
Table 4.1.2-1	FR-4 Maximum base shears	189
Table 4.2.1-1	FR-4-W21 Displacement at effective height	196
Table 4.2.2-1	FR-4-W21 Base shears	199

Table 4.3.1-1	FR-4-W24 Displacement at effective height	202
Table 4.3.2-1	Base shears (FR-4-W24)	205
Table 4.4.1-1	FR-4a Displacement at effective height	208
Table 4.4.2-1	FR-4a Base shears	211
Table 4.5.1-1	FR-4b Displacement at effective height	215
Table 4.5.2-1	FR-4b Base shears	218
Table 4.6.1-1	FR-8 Displacement at effective height	222
Table 4.6.2-1	FR-8 Base shears	231
Table 4.7.1-1	FR-8-W27 Displacement at effective height	236
Table 4.7.2-1	FR-8-W27 Base shears	239
Table 4.8.1-1	FR-16 Displacement at effective height	243
Table 4.8.2-1	FR-16 Base shears	252
Table A-1	Design Peak Ground Accelerations	270

List of Figures

Figure 1.1-1	Building plan	5
Figure 1.2.1-1	Member Force-Displacement graph of structural steel beam	7
Figure 1.2.1-2	Cyclic behavior of structural steel with Baushinger Effect	8
Figure 2.1-1	System Force-displacement graph	12
Figure 2.1-2	Graphical representation of structural performance levels	13
Figure 2.1-3	Structural Performance Objectives	14
Figure 2.2.2-1	Normalized moment-curvature graph	19
Figure 2.2.2-2	Elasto-perfectly plastic moment-curvature graph	19
Figure 2.2.3-1	Plastic flexural behavior of wide-flange with residual stresses	21
Figure 2.2.4.1-1	Idealized interaction diagram for steel beam-column	25
Figure 2.3.1-1	Beam-column subjected to end moments and axial force	30
Figure 2.3.2-1	Beam-Column subjected to end moments, axial force, and support displacement	33
Figure 2.3.3-1	Beam-Column subjected to end moments, axial force, and transverse load	34
Figure 2.3.3-2	Moment comparison	38
Figure 2.4-1	SDOF representation of actual system	43
Figure 2.4-1	Recommended Inelastic Displacement Profiles	45
Figure 2.4.3-1	Effective damping vs. ductility graph	50
Figure 2.4.4-1	Displacement Response Spectra	50
Figure 2.4.4-2	System force-displacement graph	52
Figure 2.4.5-1	Displacement profile ranges of frames	54
Figure 2.4.5.1-1	Non-linear yield displacement profile at SP-1 performance level	56
Figure 2.4.5.1-2	Normalized target drift to EQ level comparison	57
Figure 2.4.6.2-1	System Force-Deformation Graph including System Overstrength	64
Figure 2.4.6.2-2	System Force-Deformation Graph including System Overstrength	64

Figure 2.4.6.3-1	Reduced cross-section at plastic hinge length	68
Figure 2.5-1	EQ I Displacement Response Spectrum (PGA Reduction Factor = 0.125)	76
Figure 2.5-2	EQ II Displacement Response Spectrum (PGA Reduction Factor = 0.45)	76
Figure 2.5-3	EQ III Displacement Response Spectrum (PGA Reduction Factor = 0.8)	77
Figure 2.5-4	EQ IV Displacement Response Spectrum (PGA Reduction Factor = 1.0)	77
Figure 2.5-5	Equivalent damping vs. displacement ductility	78
Figure 2.5.1-1	Frame schematic (FR-4)	79
Figure 2.5.1-2	Target displacement profiles (FR-4)	84
Figure 2.5.1-3	Equal displacement approximation	87
Figure 2.5.1-3	System force-displacement graph (FR-4)	89
Figure 2.5.1-4	System force-displacement graph (FR-4)	92
Figure 2.5.1-5	Final frame schematic (FR-4)	93
Figure 2.5.1-6	SP-1 displacement profile (FR-4)	93
Figure 2.5.2-1	System force-displacement graph (FR-4-W21)	95
Figure 2.5.2-2	Final Schematic (FR-4-W21)	96
Figure 2.5.2-3	SP-1 displacement profile (FR-4-W21)	96
Figure 2.5.3-1	System force-displacement graph (FR-4-W24)	98
Figure 2.5.3-2	Final schematic (FR-4-W24)	98
Figure 2.5.3-3	SP-1 displacement profile (FR-4-W24)	99
Figure 2.5.4-1	Frame schematic (FR-4a)	100
Figure 2.5.4-2	Beam Rotation Chart	101
Figure 2.5.4-3	Beam rotation ductility chart	102
Figure 2.5.4-4	Target displacement profiles (FR-4a)	104
Figure 2.5.4-5	System force-displacement graph with Overstrength (FR-4a)	107

Figure 2.5.4-6	Final frame schematic (FR-4a)	108
Figure 2.5.4-7	SP-1 displacement profile (FR-4a)	108
Figure 2.5.5-1	Frame schematic (FR-4b)	109
Figure 2.5.5-2	Target displacement profiles (FR-4b)	111
Figure 2.5.5-3	System force-displacement graph (FR-4b)	114
Figure 2.5.5-4	Final frame schematic (FR-4b)	115
Figure 2.5.5-5	SP-1 displacement profile (FR-4b)	115
Figure 2.5.6-1	Final frame schematic (FR-8)	116
Figure 2.5.6-2	Target displacement profiles (FR-8)	119
Figure 2.5.6-3	Elastic and pseudo-elastic non-linear displacement profiles	122
Figure 2.5.6-4	System force-displacement graph (FR-8)	124
Figure 2.5.6-5	Final frame schematic (FR-8)	125
Figure 2.5.6-6	Elastic SP-1 Displacement Profile (FR-8)	126
Figure 2.5.7-1	Target displacement profiles (FR-8-W27)	129
Figure 2.5.7-2	System force-displacement graph (FR-8-W27)	133
Figure 2.5.7-3	Final Frame schematic (FR-8-W27)	134
Figure 2.5.7-4	Elastic SP-1 Displacement Profile (FR-8-W27)	135
Figure 2.5.8-1	Final frame schematic (FR-16)	136
Figure 2.5.8-2	Target displacement profiles (FR-16)	142
Figure 2.5.8-3	System force-displacement graph (FR-16)	149
Figure 2.5.8-4	Final frame schematic (FR-16)	150
Figure 2.5.8-5	Elastic SP-1 Displacement Profile (FR-16)	151
Figure 3.2.1-1	Two-surface stiffness degrading plastic hinge interaction diagram	158
Figure 3.2.1-2	Parabolic plastic hinge stiffness degradation function	159
Figure 3.2.1-3	CRC tangent stiffness degradation function	160
Figure 3.2.1-4	Normalized axial force-strain relationship	160
Figure 3.2.2-1	Further reduced CRC tangent stiffness degradation function	162

Figure 3.2.2-2	Comparison of strength curves	162
Figure 3.3.1-1	FR-4 System Force-Displacement Graph	165
Figure 3.3.1-2	FR-4 SP-1 Displacement Profile	165
Figure 3.3.2-1	FR-4-W21 System Force-Displacement Graph	166
Figure 3.3.2-2	FR-4-W21 SP-1 Displacement Profile	166
Figure 3.3.3-1	FR-4-W21 System Force-Displacement Graph	167
Figure 3.3.3-2	FR-4-W24 SP-1 Displacement Profile	167
Figure 3.3.4-1	FR-4a System Force-Displacement Graph	168
Figure 3.3.5-1	FR-4b System Force-Displacement Graph	169
Figure 3.3.5-2	FR-4b SP-1 Displacement profile	169
Figure 3.3.6-1	FR-8 System Force-Displacement Graph	170
Figure 3.3.6-2	FR-8 SP-1 Displacement Profile	170
Figure 3.3.7-1	FR-8-W27 System Force-Displacement Graph	171
Figure 3.3.7-2	FR-8-W27 SP-1 Displacement profile	171
Figure 4.1.1-1	FR-4 Maximum displacement envelopes (SP-1:EQ I)	176
Figure 4.1.1-2	FR-4 Maximum displacement envelopes (SP-2:EQ II)	177
Figure 4.1.1-3	FR-4 Maximum displacement envelopes (SP-3:EQ III)	177
Figure 4.1.1-4	Maximum displacement envelopes (SP-4:EQ IV)	178
Figure 4.1.1-5	FR-4 Nodal displacements as function of time (TH-1:EQ I)	180
Figure 4.1.1-6	FR-4 Interstory drifts as function of time (TH-1:EQ I)	181
Figure 4.1.1-7	FR-4 Nodal displacements as function of time (TH-1:EQ II)	182
Figure 4.1.1-8	FR-4 Interstory drifts as function of time (TH-1:EQ II)	182
Figure 4.1.1-9	FR-4 Nodal displacements as function of time (TH-1:EQ III)	183
Figure 4.1.1-10	FR-4 Interstory drifts as function of time (TH-1:EQ III)	184
Figure 4.1.1-11	FR-4 Nodal displacements as function of time (TH-1:EQ IV)	184
Figure 4.1.1-12	FR-4 Interstory drifts as function of time (TH-1:EQ IV)	185
Figure 4.1.1-13	FR-4 Nodal displacements as function of time (TH-9:EQ IV)	186

Figure 4.1.1-14	FR-4 Maximum interstory drift envelopes (SP-1:EQ I)	187
Figure 4.1.1-15	FR-4 Maximum interstory drift envelopes (SP-2:EQ II)	187
Figure 4.1.1-16	FR-4 Maximum interstory drift envelopes (SP-3:EQ III)	188
Figure 4.1.1-17	FR-4 Maximum interstory drift envelopes (SP-4:EQ IV)	188
Figure 4.1.2-1	FR-4 System force-displacement graph	190
Figure 4.1.2-2	FR-4 Maximum story shear envelopes (SP-1:EQ I)	191
Figure 4.1.2-3	FR-4 Maximum story shear envelopes (SP-2:EQ II)	191
Figure 4.1.2-4	FR-4 Maximum story shear envelopes (SP-3:EQ III)	192
Figure 4.1.2-5	FR-4 Maximum story shear envelopes (SP-1:EQ I)	192
Figure 4.1.2-6	FR-4 story shears as function of time (TH-1:EQ III)	193
Figure 4.2.1-1	FR-4-W21 Maximum displacement envelopes (SP-1:EQ I)	194
Figure 4.2.1-2	FR-4-W21 Maximum displacement envelopes (SP-2:EQ II)	195
Figure 4.2.1-3	FR-4-W21 Maximum displacement envelopes (SP-3:EQ III)	195
Figure 4.2.1-4	FR-4-W21 Maximum displacement envelopes (SP-4:EQ IV)	196
Figure 4.2.1-5	FR-4-W21 Maximum interstory drift envelope (SP-1:EQ I)	197
Figure 4.2.1-6	FR-4-W21 Maximum interstory drift envelope (SP-2:EQ II)	197
Figure 4.2.1-7	FR-4-W21 Maximum interstory drift envelope (SP-3:EQ III)	198
Figure 4.2.1-8	FR-4-W21 Maximum interstory drift envelope (SP-4:EQ IV)	198
Figure 4.2.2-1	FR-4-W21 System force-displacement graph	199
Figure 4.3.1-1	FR-4-W24 Maximum displacement envelopes (SP-1:EQ I)	200
Figure 4.3.1-2	FR-4-W24 Maximum displacement envelopes (SP-2:EQ II)	201
Figure 4.3.1-3	FR-4-W24 Maximum displacement envelopes (SP-3:EQ III)	201
Figure 4.3.1-4	FR-4-W24 Maximum displacement envelopes (SP-4:EQ IV)	202
Figure 4.3.1-5	FR-4-W24 Maximum interstory drift envelope (SP-1:EQ I)	203
Figure 4.3.1-6	FR-4-W24 Maximum interstory drift envelope (SP-2:EQ II)	203
Figure 4.3.1-7	FR-4-W24 Maximum interstory drift envelope (SP-3:EQ III)	204
Figure 4.3.1-8	FR-4-W24 Maximum interstory drift envelope (SP-4:EQ IV)	204

Figure 4.3.2-1	FR-4-W24 System force-displacement graph	205
Figure 4.4.1-1	FR-4a Maximum displacement envelopes (SP-1:EQ I)	206
Figure 4.4.1-2	FR-4a Maximum displacement envelopes (SP-2:EQ II)	207
Figure 4.4.1-3	Fr-4a Maximum displacement envelopes (SP-3:EQ III)	207
Figure 4.4.1-4	FR-4a Maximum displacement envelopes (SP-4:EQ IV)	208
Figure 4.4.1-5	FR-4a Maximum interstory drift envelope (SP-1:EQ I)	209
Figure 4.4.1-6	FR-4a Maximum interstory drift envelope (SP-2:EQ II)	209
Figure 4.4.1-7	FR-4a Maximum interstory drift envelope (SP-3:EQ III)	210
Figure 4.4.1-8	FR-4a Maximum interstory drift envelope (SP-4:EQ IV)	210
Figure 4.4.2-1	FR-4a System force-displacement graph	211
Figure 4.5.2-2	FR-4a Maximum story shears (TH-1)	212
Figure 4.5.2-3	FR-4a Maximum story shears (TH-2)	212
Figure 4.5.1-1	FR-4b Maximum displacement envelopes (SP-1:EQ I)	213
Figure 4.5.1-2	FR-4b Maximum displacement envelopes (SP-2:EQ II)	214
Figure 4.5.1-3	Fr-4b Maximum displacement envelopes (SP-3:EQ III)	214
Figure 4.5.1-4	FR-4b Maximum displacement envelopes (SP-4:EQ IV)	215
Figure 4.5.1-5	FR-4b Maximum interstory drift envelope (SP-1:EQ I)	216
Figure 4.5.1-6	FR-4b Maximum interstory drift envelope (SP-2:EQ II)	216
Figure 4.5.1-7	FR-4b Maximum interstory drift envelope (SP-3:EQ III)	217
Figure 4.5.1-8	FR-4b Maximum interstory drift envelope (SP-4:EQ IV)	217
Figure 4.5.2-1	FR-4b System force-displacement graph	218
Figure 4.5.2-2	FR-4b Maximum story shears (TH-1)	219
Figure 4.5.2-3	FR-4b Maximum story shears (TH-2)	219
Figure 4.6.1-1	FR-8 Maximum displacement envelopes (SP-1:EQ I)	220
Figure 4.6.1-2	FR-8 Maximum displacement envelopes (SP-2:EQ II)	221
Figure 4.6.1-3	FR-8 Maximum displacement envelopes (SP-3:EQ III)	221
Figure 4.6.1-4	FR-8 Maximum displacement envelopes (SP-4:EQ IV)	222

Figure 4.6.1-5	FR-8 Nodal displacements as function of time (TH-1:EQ I)	223
Figure 4.6.1-6	FR-8 Interstory drifts as function of time (TH-1:EQ I)	224
Figure 4.6.1-7	FR-8 Nodal displacements as function of time (TH-1:EQ II)	225
Figure 4.6.1-8	FR-8 Interstory drifts as function of time (TH-1:EQ II)	225
Figure 4.6.1-9	FR-8 Nodal displacements as function of time (TH-1:EQ III)	226
Figure 4.6.1-10	FR-8 Interstory drifts as function of time (TH-1:EQ III)	227
Figure 4.6.1-11	FR-8 Nodal displacements as function of time (TH-1:EQ IV)	227
Figure 4.6.1-12	FR-8 Interstory drifts as function of time (TH-1:EQ IV)	228
Figure 4.6.1-14	FR-8 Maximum interstory drift envelope (SP-1:EQ I)	229
Figure 4.6.1-15	FR-8 Maximum interstory drift envelope (SP-2:EQ II)	229
Figure 4.6.1-16	FR-8 Maximum interstory drift envelope (SP-3:EQ III)	230
Figure 4.6.1-17	FR-8 Maximum interstory drift envelope (SP-4:EQ IV)	230
Figure 4.6.2-1	FR-8 System force-displacement graph	231
Figure 4.6.2-2	FR-8 Maximum story shear envelopes (SP-1:EQ I)	232
Figure 4.6.2-3	FR-8 Maximum story shear envelopes (SP-2:EQ II)	232
Figure 4.6.2-4	FR-8 Maximum story shear envelopes (SP-3:EQ III)	233
Figure 4.6.2-5	FR-8 Maximum story shear envelopes (SP-4:EQ IV)	233
Figure 4.7.1-1	FR-8-W27 Maximum displacement envelopes (SP-1:EQ I)	234
Figure 4.7.1-2	FR-8-W27 Maximum displacement envelopes (SP-2:EQ II)	235
Figure 4.7.1-3	FR-8-W27 Maximum displacement envelopes (SP-3:EQ III)	235
Figure 4.7.1-4	FR-8-W27 Maximum displacement envelopes (SP-4:EQ IV)	236
Figure 4.7.1-5	FR-8-W27 Maximum interstory drift envelope (SP-1:EQ I)	237
Figure 4.7.1-6	FR-8-W27 Maximum interstory drift envelope (SP-2:EQ II)	237
Figure 4.7.1-7	FR-8-W27 Maximum interstory drift envelope (SP-3:EQ III)	238
Figure 4.7.1-8	FR-8-W27 Maximum interstory drift envelope (SP-4:EQ IV)	238
Figure 4.7.2-1	FR-8-W27 System force-displacement graph	239
Figure 4.7.2-2	FR-8-W27 Maximum story shears (TH-1)	240

Figure 4.7.2-2	FR-8-W27 Maximum story shears (TH-2)	240
Figure 4.8.1-1	FR-16 Maximum displacement envelopes (SP-1:EQ I)	241
Figure 4.8.1-2	FR-16 Maximum displacement envelopes (SP-2:EQ II)	242
Figure 4.8.1-3	FR-16 Maximum displacement envelopes (SP-3:EQ III)	242
Figure 4.8.1-4	FR-16 Maximum displacement envelopes (SP-4:EQ IV)	243
Figure 4.8.1-5	FR-16 Nodal displacements as function of time (TH-1:EQ I)	244
Figure 4.8.1-6	FR-16 Interstory drifts as function of time (TH-1:EQ I)	245
Figure 4.8.1-7	FR-16 Nodal displacements as function of time (TH-1:EQ II)	246
Figure 4.8.1-8	FR-16 Interstory drifts as function of time (TH-1:EQ II)	246
Figure 4.8.1-9	FR-16 Nodal displacements as function of time (TH-1:EQ III)	247
Figure 4.8.1-10	FR-16 Interstory drifts as function of time (TH-1:EQ III)	248
Figure 4.8.1-11	FR-16 Nodal displacements as function of time (TH-1:EQ IV)	248
Figure 4.8.1-12	FR-16 Interstory drifts as function of time (TH-1:EQ IV)	249
Figure 4.8.1-14	FR-16 Maximum interstory drift envelope (SP-1:EQ I)	250
Figure 4.8.1-15	FR-16 Maximum interstory drift envelope (SP-2:EQ II)	250
Figure 4.8.1-16	FR-16 Maximum interstory drift envelope (SP-3:EQ III)	251
Figure 4.8.1-17	FR-16 Maximum interstory drift envelope (SP-4:EQ IV)	251
Figure 4.8.2-1	FR-16 System force-displacement graph	252
Figure 4.8.2-2	FR-16 Maximum story shear envelopes (SP-1:EQ I)	253
Figure 4.8.2-3	FR-16 Maximum story shear envelopes (SP-2:EQ II)	253
Figure 4.8.2-4	FR-16 Maximum story shear envelopes (SP-3:EQ III)	254
Figure 4.8.2-5	FR-16 Maximum story shear envelopes (SP-4:EQ IV)	254
Figure 4.9-1	MCE (EQ IV) Design displacement response spectrums (5% damping)	255
Figure 4.9-2	MCE (EQ IV) Design displacement response spectrums (10% damping)	256
Figure 4.9-3	MCE (EQ IV) Design displacement response spectrums (15% damping)	256

Figure 4.9-4	MCE (EQ IV) Design displacement response spectrums (20% damping)	257
Figure 4.9-5	MCE (EQ IV) Design displacement response spectrums (25% damping)	257
Figure 4.9-6	Displacement variations at effective system height (FR-4)	258
Figure 4.9-7	Displacement variations at effective system height (FR-8)	259
Figure 4.9-8	Displacement variations at effective system height (FR-16)	259
Figure 4.9-9	Range of effective system periods (FR-4)	260
Figure 4.9-10	Range of effective system periods (FR-8)	261
Figure 4.9-11	Range of effective system periods (FR-16)	261
Figure A.1-1	EQ I Acceleration Response Spectrum	271
Figure A.1-2	EQ II Acceleration Response Spectrum	271
Figure A.1-3	EQ III Acceleration Response Spectrum	272
Figure A.1-4	EQ IV Acceleration Response Spectrum	272
Figure A.2-1	EQ I Displacement Response Spectra	273
Figure A.2-2	EQ II Displacement Response Spectra	273
Figure A.2-3	EQ III Displacement Response Spectra	274
Figure A.2-4	EQ IV Displacement Response Spectra	274
Figure A.3-1	EQ I Velocity Response Spectra	275
Figure A.3-2	EQ II Velocity Response Spectra	275
Figure A.3-3	EQ III Velocity Response Spectra	276
Figure A.3-4	EQ IV Velocity Response Spectra	276
Figure B.1-1	Time-History (TH-1)	277
Figure B.1-2	Acceleration Response Spectra (TH-1)	277
Figure B.1-3	Displacement Response Spectra (TH-1)	278
Figure B.1-4	Velocity Response Spectra (TH-1)	278
Figure B.2-1	Time-History (TH-2)	279

Figure B.2-2	Acceleration Response Spectra (TH-2)	279
Figure B.2-3	Displacement Response Spectra (TH-2)	280
Figure B.2-4	Velocity Response Spectra (TH-2)	280
Figure B.3-1	Time-History (TH-3)	281
Figure B.3-2	Acceleration Response Spectra (TH-3)	281
Figure B.3-3	Displacement Response Spectra (TH-3)	282
Figure B.3-4	Velocity Response Spectra (TH-3)	282
Figure B.4-1	Time-History (TH-4)	283
Figure B.4-2	Acceleration Response Spectra (TH-4)	283
Figure B.4-3	Displacement Response Spectra (TH-4)	284
Figure B.4-4	Velocity Response Spectra (TH-4)	284
Figure B.5-1	Time-History (TH-5)	285
Figure B.5-2	Acceleration Response Spectra (TH-5)	285
Figure B.5-3	Displacement Response Spectra (TH-5)	286
Figure B.5-4	Velocity Response Spectra (TH-5)	286
Figure B.6-1	Time-History (TH-6)	287
Figure B.6-2	Acceleration Response Spectra (TH-6)	287
Figure B.6-3	Displacement Response Spectra (TH-6)	288
Figure B.6-4	Velocity Response Spectra (TH-6)	288
Figure B.7-1	Time-History (TH-7)	289
Figure B.7-2	Acceleration Response Spectra (TH-7)	289
Figure B.7-3	Displacement Response Spectra (TH-7)	290
Figure B.7-4	Velocity Response Spectra (TH-7)	290
Figure B.8-1	Time-History (TH-8)	291
Figure B.8-2	Acceleration Response Spectra (TH-8)	291
Figure B.8-3	Displacement Response Spectra (TH-8)	292
Figure B.8-4	Velocity Response Spectra (TH-8)	292

Figure B.9-1	Time-History (TH-9)	293
Figure B.9-2	Acceleration Response Spectra (TH-9)	293
Figure B.9-3	Displacement Response Spectra (TH-9)	294
Figure B.9-4	Velocity Response Spectra (TH-9)	294
Figure B.10-1	Time-History (TH-10)	295
Figure B.10-2	Acceleration Response Spectra (TH-10)	295
Figure B.10-3	Displacement Response Spectra (TH-10)	296
Figure B.10-4	Velocity Response Spectra (TH-10)	296
Figure B.11-1	Time-History (TH-11)	297
Figure B.11-2	Acceleration Response Spectra (TH-11)	297
Figure B.11-3	Displacement Response Spectra (TH-11)	298
Figure B.11-4	Velocity Response Spectra (TH-11)	298
Figure B.12-1	Time-History (TH-12)	299
Figure B.12-2	Acceleration Response Spectra (TH-12)	299
Figure B.12-3	Displacement Response Spectra (TH-12)	300
Figure B.12-4	Velocity Response Spectra (TH-12)	300

List of Symbols

b_f	Flange width
c	Distance from extreme compression fiber to neutral axis
d	Section depth
g	Acceleration of gravity
$h_{eff\ sys}$	System effective height
h_i	Floor height
h_n	Total frame height
h_w	Height of web (inside of flange to inside of flange) (also d_w)
n	Number of stories
r	Radius of gyration
t_f	Flange thickness
t_w	Web thickness
w	Uniform load
y_o	Distance from extreme compression to centroidal axis
A_g	Gross cross-sectional area
E	Nominal Modulus of Elasticity
F_L	Nominal yield stress including residual stresses
F_r	Nominal compressive residual stress
F_x	Lateral force
F_y	Nominal material yield stress
F_{ye}	Material yield stress including material overstrength (AISC)
G	Nominal Shear Modulus

G	Stiffness ratio of interconnecting columns to beams
I_x	Moment of inertia about major axis
K	Slenderness factor
$K_{eff\ sys}$	System effective stiffness
$K_{el\ sys}$	System elastic stiffness
L	Member length
L_b	Beam length
L_c	Column length
M	Applied moment
$M_{A,B}$	Moment at end A or B
$M_{eff\ sys}$	System effective mass
M_{EQ}	Moment due to earthquake
M_G	Moment due to transverse load(s)
M_i	Floor mass
M_n	Nominal section flexural resistance
M_o	Total section plastic moment capacity
M_p	Section plastic moment capacity
M_{pc}	Reduced section plastic moment capacity for presence of axial force
M_{ps}	Reduced section plastic moment capacity for presence of shear force
M_{pt}	Reduced section plastic moment capacity for presence of torsion
M_{pr}	Reduced section plastic moment capacity
M_r	Section plastic moment capacity
M_T	Moment due to translation

M_y	Section yield moment capacity
P	Applied axial force (compression or tension)
P_n	Nominal section axial resistance
P_u	Ultimate axial force (compression or tension)
P_y	Axial plastic nominal material yield stress
R	Force reduction factor
R_y	Material overstrength factor (AISC)
S_1	One (1) second period spectral acceleration
S_F	Shape factor
s_{ii}	Beam-column stiffness coefficient
S_S	Short period spectral acceleration
S_x	Elastic section modulus about major axis
T	Period
$T_{eff\ sys}$	System effective period
T_p	Section plastic torsion capacity
T_{pt}	Reduced section plastic torsion capacity for presence of torsion
V	Shear force
V_b	Base shear
V_n	Nominal section shear resistance
V_p	Plastic shear capacity
V_u	Ultimate shear force
W_i	Floor weight
Z_x	Plastic section modulus about major axis

α_s	Plastic moment capacity reduction factor for shear
β	Ratio of SP-4 lateral force to performance level lateral force
Δ	Displacement
Δ_{di}	Design, or target, nodal displacement
$\Delta_{d,sys}$	System design, or target, displacement
$\Delta_{p,sys}$	Post-yield system displacement
Δ_y	Yield displacement
$\Delta_{y,sys}$	System yield displacement
ε_y	Nominal material yield strain
$\varepsilon_{y'}$	Nominal material first-yield strain
λ	Column-to-beam stiffness factor
λ_o	Total member overstrength
$\theta_{A,B}$	Member rotation at end A or B
θ_d	Design joint rotation
θ_G	Member rotation due to transverse load(s)
θ_p	<i>Equivalent</i> member plastic rotation capacity
θ_T	Target joint rotation
θ_y	Member yield rotation capacity
ϕ	Curvature
ϕ_y	Section yield curvature
ϕ_p	<i>Equivalent</i> section plastic curvature
$\phi_{y'}$	Section first-yield curvature

ϕ_x	Resistance factor
ϕ_m^o	Material overstrength
ϕ_{ph}^o	Member overstrength from plastic hinge sequencing
ϕ_{phi}^o	Floor member overstrength from plastic hinge sequencing
ϕ_{phsys}^o	System member overstrength from plastic hinge sequencing
ϕ_s^o	Member overstrength
ϕ_{sys}^o	System member overstrength
ϕ_{sf}^o	Overstrength from shape factor
ϕ_{sh}^o	Overstrength from strain hardening
ϕ_{si}^o	Floor member overstrength
ϕ_{sr}^o	Overstrength from strain rate
σ	Stress
σ_c	Compressive Stress
σ_t	Tensile Stress
Ω_i	Floor performance overstrength
Ω_{sys}	System performance overstrength
μ	Ductility
μ_{Δ}	Displacement ductility
$\mu_{\Delta sys}$	System displacement ductility
μ_{θ}	Rotation ductility
ζ	Damping
$\zeta_{eff sys}$	System effective damping

List of Abbreviations

AISC	American Institute of Steel Construction
ARS	Acceleration Response Spectra
CRC	Column Research Council
DBD	Displacement-based Design
DFRD	Demand and Resistance Factor Design
DRS	Displacement Response Spectra
EPP	Elasto-perfectly Plastic
EQ	Earthquake
EYA	Equivalent Yield Analysis
FBD	Force-based Design
FEMA	Federal Emergency Management Agency
IBC	International Building Code
LRFD	Load and Resistance Factor Design
MCE	Maximum Considered Earthquake
MDOF	Multi-degree-of-freedom
NEHRP	National Earthquake Hazards Reduction Program
PBSE	Performance-based Seismic Engineering
PGA	Peak Ground Acceleration
SDOF	Single-degree-of-freedom
SEAOC	Structural Engineers Association of California
SP	Structural Performance Level
VRS	Velocity Response Spectra

PART 1

INTRODUCTION,
SIMPLIFICATIONS AND ASSUMPTIONS

1.0 Introduction

The objective of this research is to outline an alternate seismic engineering philosophy to the current codified force-based design (FBD) approach for seismic resistant steel moment frames known as Performance-based Seismic Engineering (PBSE). Performance-based engineering is any design methodology in which the final analytical outcome is measured against a performance limit state. These limit states can be quantitatively measured by forces, strains, rotations, or displacements, and are representative of member or system damage levels. It is the limit state form that delineates the design methodology into respective performance-based groups. Since displacements are the most convenient practice of system and member evaluation, the analytical method employed in this research to achieve PBSE is Displacement-based Design (DBD).

Current design office methodologies for seismic design of steel moment frames include forced-based methods for calculating equivalent lateral forces and a static elastic analysis. Research has revealed erroneous assumptions in forced-based methods and proposes that displacement-based methods, due to modeling inelastic systems, result in more reasonable lateral force distributions. In some respects the current FBD philosophy incorporates certain aspects of PBSE. That is current seismic codes require the design engineer to check service level and ultimate displacement demands against code requirements. Similarly, elastic force demands are checked against ultimate plastic capacities. However, these are grossly approximated since an elastic analysis cannot account for inelastic redistribution and higher mode effects are incorporated only by a top level concentrated force with no evaluation of the stiffness and strength of individual floors. Additionally, the final ductility demand is determined by the amplification of service level displacements, albeit with no requirements to insure that the final ductility capacity does in fact match the initially assumed force reduction factor. This implies that a ductility capacity can be assigned to a structural system regardless of its geometry and member strengths (*Priestley and Kowalsky, 2000*). Additionally, that the stiffness of a structure solely determines its displacement response (*Priestley and Kowalsky, 2000*).

Furthermore, current seismic codes limit inelastic story drifts to 0.02 or 0.025 depending on the initially “assumed” 1st mode period. These values are based on early research reporting that steel beams can accommodate post-yield rotations in the range of 0.01 to 0.015 radians – assuming an elastic rotation capacity of 0.01 radians (*AISC Seismic Provisions*, 2000). These rotation values have been subsequently revised based on later research; however, the codified inelastic drift requirements have not been similarly revised. As a consequence, code drift limits tend to reduce design ductility levels to values significantly less than what can actually be accommodated (*Priestley and Kowalsky*, 2000). Ultimately, the system will not be able to accommodate the full ductility demand (assumed equal to the force reduction factor by current seismic codes). Thus producing higher than expected seismic forces and possibly leading to either unexpected damage or damage levels in excess of desired. Furthermore, FBD procedures were developed based on the results from early scale model research and current research is noting that those results are not appropriate for determining or predicting the behavior of larger complex systems.

It is the expectation that the proposed DBD procedures will eliminate the fundamental problems inherent in FBD methods by means of reverse engineering. That is the final ductility demand, or damage level, is the starting point of the design process, not the approximate final result. Therefore, the initial system stiffness and respective member strengths are the final design results. It is out of the scope of this document to discuss current FBD procedures except for, where needed, providing information confirming respective erroneous assumptions.

1.1 Current Research

In this document, eight (8) fixed base steel moment frames, listed in Table 1.1-1, will be analyzed and designed in accordance with the proposed DBD method (Part 2).

Frame ID	Stories	Bay 1	Bay 2	Bay 3	Height
FR-4	4	25'-0" (7620)	25'-0" (7620)	25'-0" (7620)	52'-0" (15850)
FR-4-W21	4	25'-0" (7620)	25'-0" (7620)	25'-0" (7620)	52'-0" (15850)
FR-4-W24	4	25'-0" (7620)	25'-0" (7620)	25'-0" (7620)	52'-0" (15850)
FR-4a	4	22'-6" (6858)	30'-0" (9144)	22'-6" (6858)	52'-0" (15850)
FR-4b	4	27'-6" (8382)	20'-0" (6096)	27'-6" (8382)	52'-0" (15850)
FR-8	8	25'-0" (7620)	25'-0" (7620)	25'-0" (7620)	52'-0" (31700)
FR-8-W27	8	25'-0" (7620)	25'-0" (7620)	25'-0" (7620)	104'-0" (31700)
FR-16	16	25'-0" (7620)	25'-0" (7620)	25'-0" (7620)	208'-0" (63400)

Table 1.1-1. Frame description

The selected test frame is the center frame (left to right) in the building plan shown in Fig. 1.1-1 (neglecting the floor openings).

The majority of procedures used throughout this document are in accordance with preliminary DBD specifications developed by the Structural Engineers Association of California (SEAOC) as part of *Vision 2000*. Several additional procedures will be introduced and incorporated within the boundaries set by the previous specification. Two of these procedures are Capacity Design, for the design of beams and columns, and Equivalent Yield

Analysis, for the design of multi-story frames where the “yield” displacement profile is non-linear.

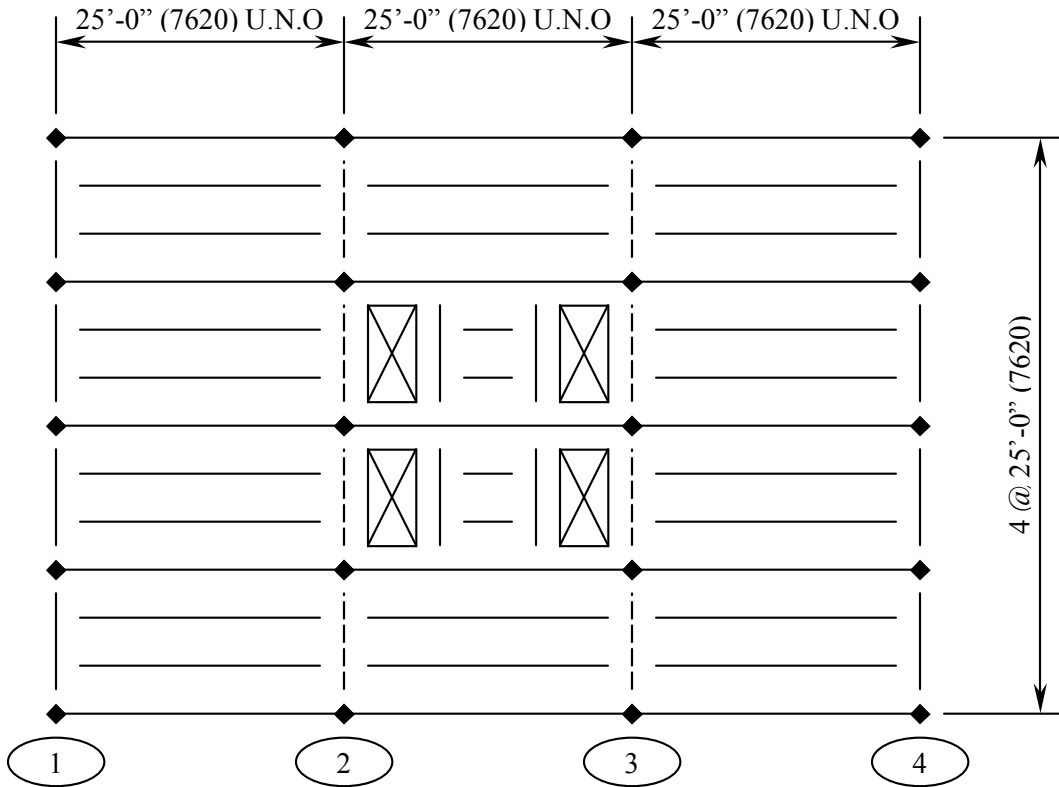


Figure 1.1-1. Building plan

Additionally, a limit state second-order inelastic static analysis, or “Advanced Analysis” will be used to analyze the frames designed by the proposed method (Part 3). The distinct difference between Advanced Analysis and a standard elastic analysis, including a push-over analysis, besides the obvious inclusion of inelastic response, is that all design uncertainties and imperfections inherent in current steel design interaction equations are included in the analysis. Thus eliminating the incompatibility between elastic analysis demands and inelastic capacities. The analysis results will be compared to the predicted values not necessarily as an acceptance analysis of the proposed method but to outline the initial use of Advanced Analysis techniques for the design of seismic resistant steel frames.

Finally, the frames will be analyzed in a second-order inelastic dynamic analysis subject to twelve (12) time-histories representing a wide analytical range of ground motions (Part 4). Two of the time-histories are artificially generated to approximate the MCE design

acceleration response spectra developed in accordance with current IBC/NEHRP seismic provisions. Whereas the other *actual* time-histories are intensity normalized to the MCE design acceleration response spectra. The predicted, or “as designed”, response from the proposed method will be compared to the analysis results for applicability and to highlight future research needs.

This research represents the *fundamental* procedures outlining the preliminary development of Displacement-Based Design of steel moment frames. The analysis and design, including behavior, of steel structures increases in complexity as the number of joints increase. Behavior of steel frames is separated from analysis and design, though correlation exists, to emphasize the fact that in DBD the final behavior of the system justifies the analysis and design, not vice versa as in current force-based design procedures. Hence, several simplifications and assumptions have been used, outlined in Section 1.2, more for assistance in the basic understanding of steel response than for accuracy in the early development of the proposed procedures. It is the hope of the author to continue this research forward, continually revising the process for accuracy and simplicity, in order to develop a systematic design procedure.

Lastly, a large number of graphs are presented in both the numerical implementation (2.5) and verification (Part 4) sections in anticipation that the reader will, beyond the limited discussions contained within, conduct their own examination into the behavioral characteristics of steel moment frames subjected to strong ground motions.

1.2 Simplifications, Assumptions, and Constant Variables

The following items are used throughout this document, unless specifically noted otherwise.

1.2.1 Simplifications

1. Member Behavior

The bi-linear elasto-perfectly plastic approximation of the actual force-displacement response, shown in Fig. 1.1.1-1, is used as the hysteretic function. It is understood that structural steel exhibits the Baushinger Effect during loading/unloading, shown in Fig. 1.1.1-2; hence, the Ramberg-Osgood hysteresis is a more accurate approximation. However, for simplicity in the early development of the proposed method, the EPP approximation is used.

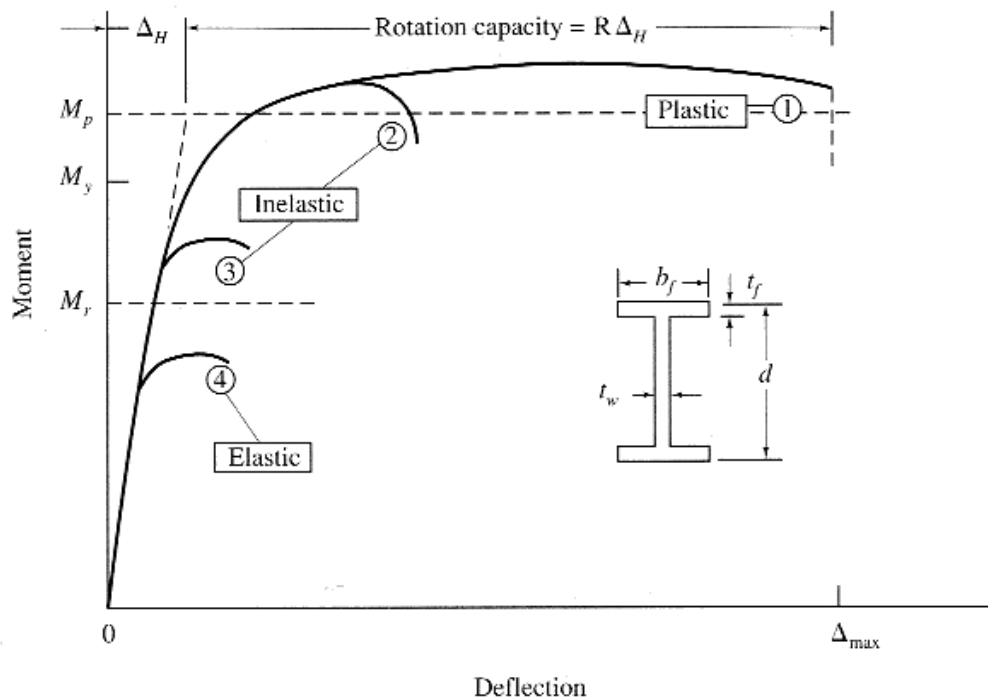


Figure 1.2.1-1. Member force-displacement graph of structural steel beam (Salmon and Johnson, 1996)

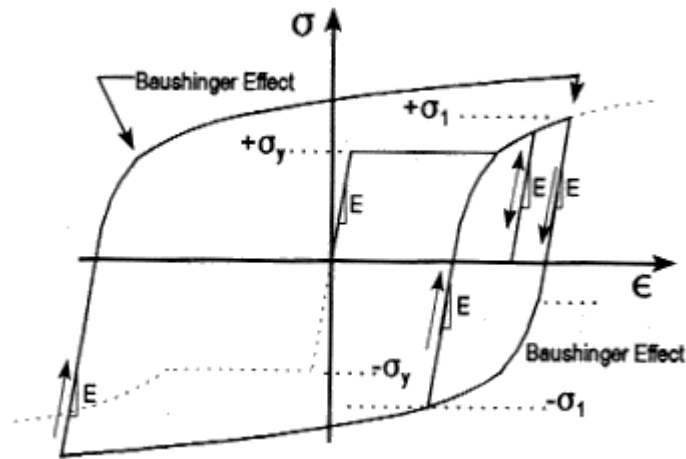


Figure 1.2.1-2. Cyclic behavior of structural steel with Baushinger Effect (Uang et al, 1998)

1.2.2 Assumptions

1. All elements are initially straight and prismatic, and plane cross-sections remain plane after deformation. (*Chen and Kim, 1997*)
2. Local buckling and lateral-torsional buckling are not considered. All members are assumed to be fully compact and adequately braced to prevent out-of-plane deformations. (*Chen and Kim, 1997*) Hence, full plastic moment capacity is achieved (with reductions for the presence of axial and shear forces).
3. Large rigid-body displacements are allowed, but member deformations and strains are small. (*Chen and Kim, 1997*)
4. The element stiffness formulation is based on conventional beam-column stability functions, including axial and bending deformations, but not those associated with shear. Element bowing effects are neglected. (*Chen and Kim, 1997*)
5. The formulation is limited by its ability to model plastic hinges only at the element ends. (*Chen and Kim, 1997*)

6. Plastic hinges can sustain inelastic rotations only. Strain hardening and stiffness degradation is not considered. (*Chen and Kim, 1997*)
7. All members are fabricated from isotropic homogeneous material
8. No composite action is considered.
9. All joints are assumed perfectly rigid and complete force transfer is assumed.
10. Vertical accelerations are small and are neglected.
11. Demand Factor and Resistance Design (DRFD) is not utilized. That is allowable service level displacements are not factored for uncertainties in analysis, construction, and design in suit with the LRFD philosophy.
12. Panel zone effects are neglected.
13. Soil-Structure interaction is not considered.

1.2.3 Constant Variables

1. Nominal Material Properties

$$F_y = 50 \text{ ksi (345 MPa)}$$

$$E = 29000 \text{ ksi (200 GPa)}$$

$$\varepsilon_y = \frac{F_y}{E} = 0.001724$$

$$G = 11200 \text{ ksi (77.2 GPa)}$$

2. Design Response Spectrum

The Maximum Considered Earthquake (MCE) response spectrums were formulated in accordance with IBC/NEHRP (2000) seismic provisions with the following constant parameters (equivalent to Zone 4):

Soil Type D

$$S_s = 1.684 \text{ in/sec}^2 \text{ (43 mm/sec}^2\text{)}$$

$$S_1 = 0.60 \text{ in/sec}^2 \text{ (15 mm/sec}^2\text{)}$$

$$\zeta = 5\% \text{ (Viscous Damping)}$$

$T = 4$ seconds – DRS is considered constant

3. Gravity Loads

$$\text{Dead Load} = 100 \text{ psf (4.8 KPa)}$$

$$\text{Live Load} = 100 \text{ psf (4.8 KPa)}$$

(30% is considered in the total weight of the structure)

$$\text{Node Type 1} = 30.5 \text{ kips (135.7 kN)} \text{ – Exterior Joint}$$

$$\text{Node Type 2} = 60.8 \text{ kips (270.4 kN)} \text{ – Interior Joint}$$

Modification to nodal concentrated gravity forces for frames with varying bay lengths are modified as required.

PART 2

DISPLACEMENT-BASED DESIGN

2.0 Introduction

The majority of material presented herein is based on preliminary DBD procedures outlined by the SEAOC committee on PBSE and introduced in the SEAOC *Recommended Lateral Force Requirements and Commentary*, 1999 Edition, in Appendix I, *Tentative Guidelines for Performance-Based Seismic Engineering*. Several procedures not outlined by SEAOC will be additionally incorporated in subsequent sections. Due to complexities and variations in frame analysis procedures, the reader is referred to the numerical implementation of DBD procedures in Section 2.5 for additional information not discussed in detail in prior sections (2.1 to 2.4).

2.1 SEAOC Specification for Performance-Based Design

Fig. 2.1-1 shows a complete system force-displacement graph from which all codified seismic design principles, including limit states, are based.

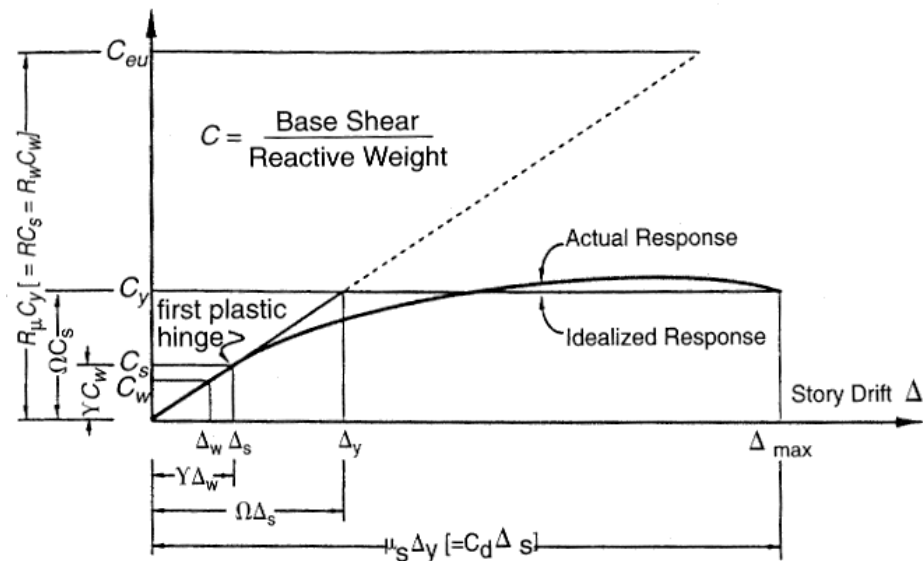


Figure 2.1-1. System force-displacement graph (Uang, 1991)

The SEAOC PBSE committee proposes five design limit states, or structural performance levels, that when coupled with varying earthquake levels provide a design performance objective. The importance of using different earthquake levels is for the ability to determine

the structural integrity of a system at various stages along the force-displacement curve. The proposed limit states are defined in Table 2.1-1 and graphically represented in Fig. 2.1-2.

Performance Level	Qualitative Description	Definition
SP-1	Operational (Service)	Yield mechanism; damage is negligible
SP-2	Occupiable	Damage is minor to moderate; some repair is required
SP-3	Life Safe	Damage is moderate to major; extensive repairs are required
SP-4	Near Collapse	Damage is major; repairs may be uneconomically feasible
SP-5	Collapse	Collapse is imminent

Table 2.1-1. Structural Performance Levels (SEAOC Blue Book, 1999)

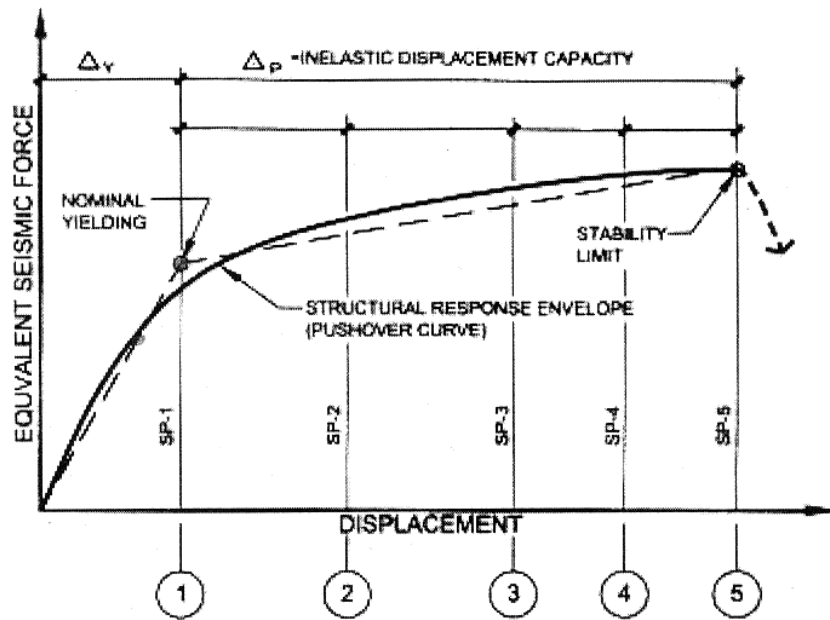
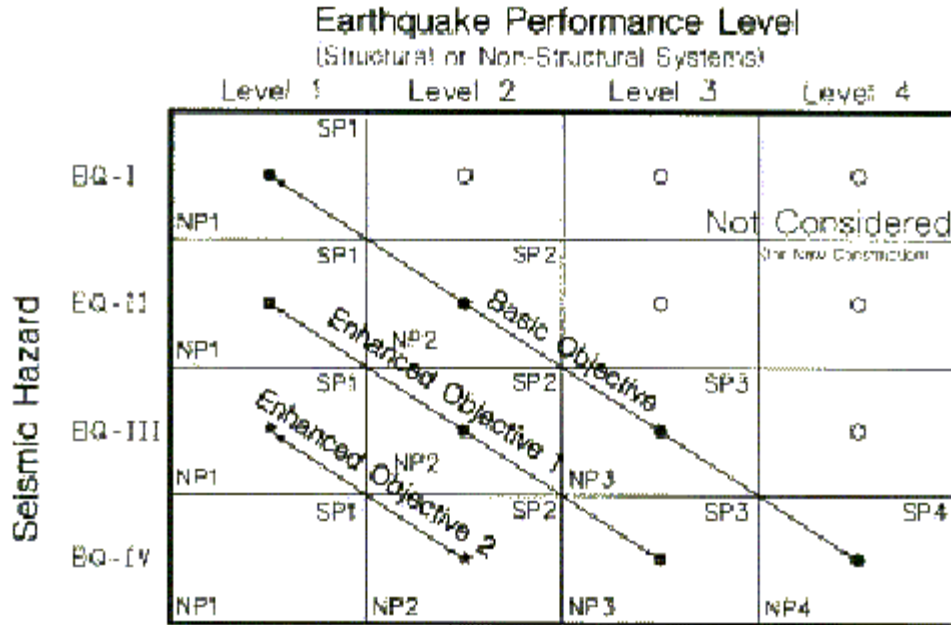


Figure 2.1-2. Graphical representation of structural performance levels

(SEAOC Blue Book, 1999; modified: Harris)

In addition to structural performance levels, SEAOC also stipulates associated non-structural performance levels. For this research importance is set on the determination of the general procedures for structural performance and design; therefore, non-structural performance levels will be neglected.

The design engineer selects the design performance objective of the system in accordance with damage level requirements and assigns earthquake levels, based on mean return period and annual probability of exceedance, to each respective performance level.



Commentary:

1. The performance objective matrix illustrates the typical performance levels to be achieved at each hazard level to meet the three defined performance objectives.
2. Meeting one performance level at one hazard level does not indicate that the specified performance objective is met. Performance should be checked at each hazard level to verify that the selected objective is met.
3. The performance objectives illustrated above indicate the same performance objectives for both structural and nonstructural systems. Alternatively, separate and different objectives can be selected for the structural and nonstructural systems.

Figure 2.1-3. Structural performance objectives (SEAOB Blue Book, 1999)

EQ	Description	Probability of Exceedance	Other Definition	Mean Return Period (yrs)	Annual Probability of Exceedance
EQ-I	Frequent	87%/50 yrs	—	25	4%
EQ-II	Occasional	50%/50 yrs	—	72	1.4%
EQ-III	Rare	—	2/3 MCE	250-800	0.12%-0.4%
EQ-IV	Maximum considered	—	MCE	800-2,500	0.04%-0.12%

Table 2.1-2. Design level earthquakes (SEAOB Blue Book, 1999)

For this research the Basic Safety Objective (BSO) is selected, hence, the performance levels with associated earthquake levels are indicated in Table 2.1-3.

Performance Level	Earthquake Level
SP-1	EQ I
SP-2	EQ II
SP-3	EQ III
SP-4	EQ IV (MCE)

Table 2.1-3. Basic safety performance objective

In truth, the design engineer can associate any earthquake level with any performance level. For example, if the system were required to remain “operational” (SP-1) at the maximum considered earthquake (MCE), then EQ IV would be associated with the SP-1 performance level. Hence, all other performance and earthquake levels (I, II, and III) can be neglected. Though this example might be uneconomical, it emphasizes that a selected performance level and respective earthquake level are initially independent. As will be shown subsequently, once the controlling design performance level is determined, performance levels and earthquake levels are in fact dependent. This dependence will allow the design engineer to design a system to respond in accordance with the complete performance objective and not just match one performance level (controlling).

In accordance with the current PBSE code, the design engineer constructs the design response spectrums associated with each earthquake level based on specified effective peak ground accelerations. It should be mentioned that this procedure is slightly revised in this document as discussed in Section 2.5.

This section outlines the fundamental design approach of DBD and presents the concept of limit state seismic design. Hence, all subsequent sections will recall performance levels and objectives stated here.

2.1.1 Ductility

Ductility, μ , represents a damage level indicator and can be quantified by the ratio of response to yield response. This response action can be measured by section curvature, member rotation, element strain, or displacements. However, these ductility actions typically do not generate the same results. That is curvature ductility will not equal displacement ductility. Though it is assumed by current seismic codes that displacement ductility is equal to rotation ductility, which is similarly equivalent to the force reduction factor, R , employed in force-based design. Since displacements are the easiest form of measurement for the design engineer to visualize and evaluate, it is the preferred choice of ductility measurement and the main quantifier in displacement-based seismic design.

$$\mu_{\Delta} = \frac{\Delta}{\Delta_y} \quad (2.1-1)$$

where

$$\Delta_y = \text{Yield displacement (in, mm)}$$

Prior to discussing the global design procedures encompassing DBD once the performance objective has been selected, the relationship between member and system response needs to be addressed. That is section curvature and member rotation play an important role in predicting the global response of a system subjected to strong ground motion and, ultimately, the quantitative measure of the frame ductility capacity.

2.2 Section Curvature

2.2.1 Yield Curvature

From mechanics, the section curvature, ϕ , for a beam subjected to a bending moment about the major centroidal axis is defined as

$$\phi = \frac{M}{EI_x} \quad (2.2.1-1)$$

where

M = Applied moment (*k in, N mm*)

E = Nominal Modulus of Elasticity (*ksi, MPa*)

I_x = Moment of Inertia about the major centroidal axis (*in⁴, mm⁴*)

Evaluating Eq. (2.2.1-1) at full yield (i.e. all extreme compression and tension fibers are yielding), we have

$$\phi_y = \frac{M_y}{EI_x} \quad (2.2.1-2)$$

where

M_y = Section yield moment capacity (*k in, N mm*)

Eq. (2.2.1-2) can be further expanded using the following known classical relationships.

$$M_y = S_x \phi_m^o F_y \quad (2.2.1-3)$$

$$y_o = \frac{d}{2} \quad (2.2.1-4)$$

$$S_x = \frac{I_x}{y_o} \quad (2.2.1-5)$$

$$\varepsilon_y = \frac{F_y}{E} \quad (2.2.1-6)$$

where

S_x = Elastic section modulus (*in³, mm³*)

F_y = Nominal yield stress (*ksi, MPa*)

y_o = Distance from extreme compression fiber to major centroidal axis (*in, mm*)

d = Depth of section (*in, mm*)

ε_y = Nominal yield strain from Hooke's Law

ϕ_m^o = Material overstrength factor (discussed in Section 2.2.5)

Substituting Eqs. (2.2.1-3) through (2.2.1-6) into Eq. (2.2.1-2), the section curvature of an element subjected to pure bending at yield is

$$\phi_y = \frac{M_y}{EI_x} = \frac{S_x \phi_m^o F_y}{EI_x} = \frac{2 \phi_m^o \varepsilon_y}{d} \quad (2.2.1-7)$$

Evaluation of Eq. (2.2.1-7) shows that the yield curvature is dependent only on section geometry, independent of strength (*Priestley and Kowalsky, 2000*). Furthermore, evaluation of Eq. (2.2.1-1) in the whole range of member behavior concludes that stiffness is proportional to strength. The proportionality between strength and stiffness contradicts the FBD assumption that an initial stiffness, and, ultimately, the elastic system period, can be determined independent of strength. That is the action of allocating strength between members also changes the stiffness from the initial assumption, and, hence, implies an iterative analysis procedure (*Priestley and Kowalsky, 2000*). Furthermore, the determination of a non-dimensional section yield curvature indicates that the yield drift of frames might possess the same independence (*Priestley, 2000*).

2.2.2 Equivalent Plastic Curvature

Eqs. (2.2.1-1) and (2.2.1-2) outline the moment-curvature relationship of an elastic section represented by the straight line in Fig. 2.2.2-1. Post-yield section curvatures can be determined by Eq. (2.2.2-1) and similarly graphed in Fig. 2.2.2-1.

$$M = S_F \left(1 - \frac{1}{3} \left(\frac{\phi_y}{\phi} \right)^2 \right) M_y \quad (2.2.2-1)$$

where

S_F = Shape factor (see Eq. 2.2.2-3)

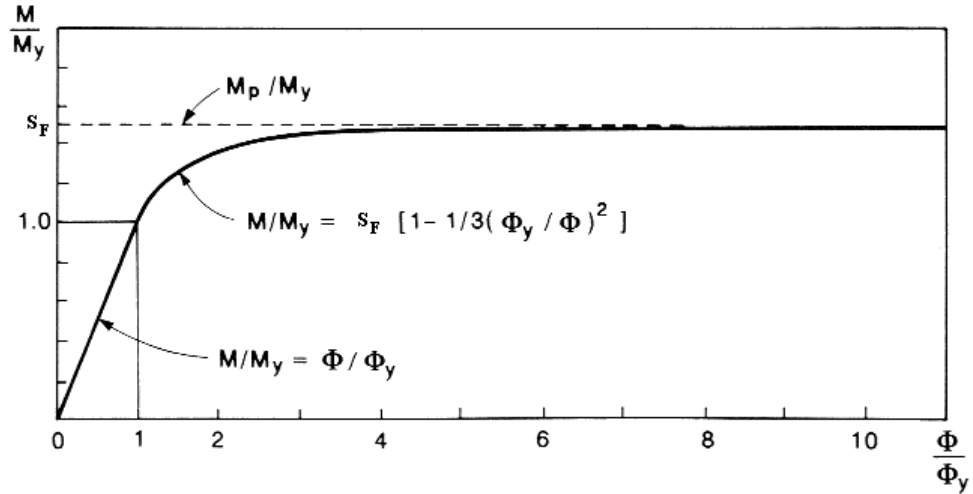


Figure 2.2.2-1. Normalized moment-curvature graph (Chen et al, 1995: modified: Harris)

Due to the iterative nature of an exact non-linear analysis, the bi-linear idealization, shown in Figure 2.2.2-2, is recommended for its simplicity. In this elasto-perfectly plastic idealization, the element is assumed to behave elastically up to the plastic moment, where all plastic rotations occur at a zero length plastic hinge and the plastic curvature increases indefinitely with constant plastic moment capacity (Chen et al, 1995)

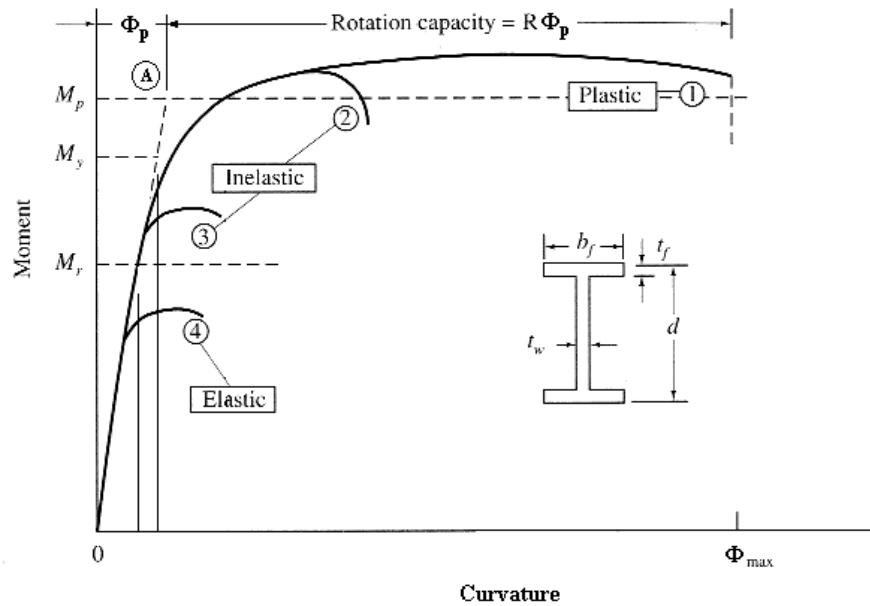


Figure 2.2.2-2. Elasto-perfectly plastic moment-curvature graph

(Salmon and Johnson, 1996: modified: Harris)

This idealization results in a considerable simplification of the analysis procedure without significant compromise in the accuracy of the computed plastic limit load (*Chen et al*, 1995).

Similar to the previous derivation of the section yield curvature, we substitute Eqs. (2.2.2-2) and (2.2.2-3) into Eq. (2.2.1-1).

$$M_p = Z_x \phi_m^o F_y \quad (2.2.2-2)$$

$$S_F = \frac{Z_x}{S_x} \quad (2.2.2-3)$$

where

M_p = Section plastic moment capacity (*k in, kN mm*)

Z_x = Geometric plastic section modulus (*in³, mm³*)

Hence, the *equivalent* plastic section curvature in accordance with the bi-linear approximation, represented by point A in Figure 2.2.2-2, can be expressed as

$$\phi_p = \frac{M_p}{EI_x} = \frac{2S_F \phi_m^o \varepsilon_y}{d} \approx \frac{2.28 \phi_m^o \varepsilon_y}{d} \quad (2.2.2-4)$$

The shape factor, S_F , for North American wide flange sections can be approximated as 1.14 in lieu of the actual value. However, in some cases it will be necessary for the design engineer to include a modification factor during the member design stage representing the ratio of actual to assumed shape factor, discussed subsequently in Section 2.4.6. Again, it shall be emphasized that Eq. (2.2.2-4) is the *equivalent* plastic section curvature of an element subjected to pure full plastic bending (i.e. no axial load effects). Furthermore, the *equivalent* plastic section curvature replaces the yield curvature, ϕ_y , in the determination of curvature ductility.

$$\mu_\phi = \frac{\phi}{\phi_p} \quad (2.2.2-5)$$

2.2.3 First-Yield Curvature

An additional curvature that needs to be discussed is the curvature at first-yield. As a result of the cooling process steel inherently contains residual stresses. The magnitude of these stresses varies depending on section geometry. Fig. 2.2.3-1 shows an example of residual stress distribution and its effect on the behavior of a wide-flange section.

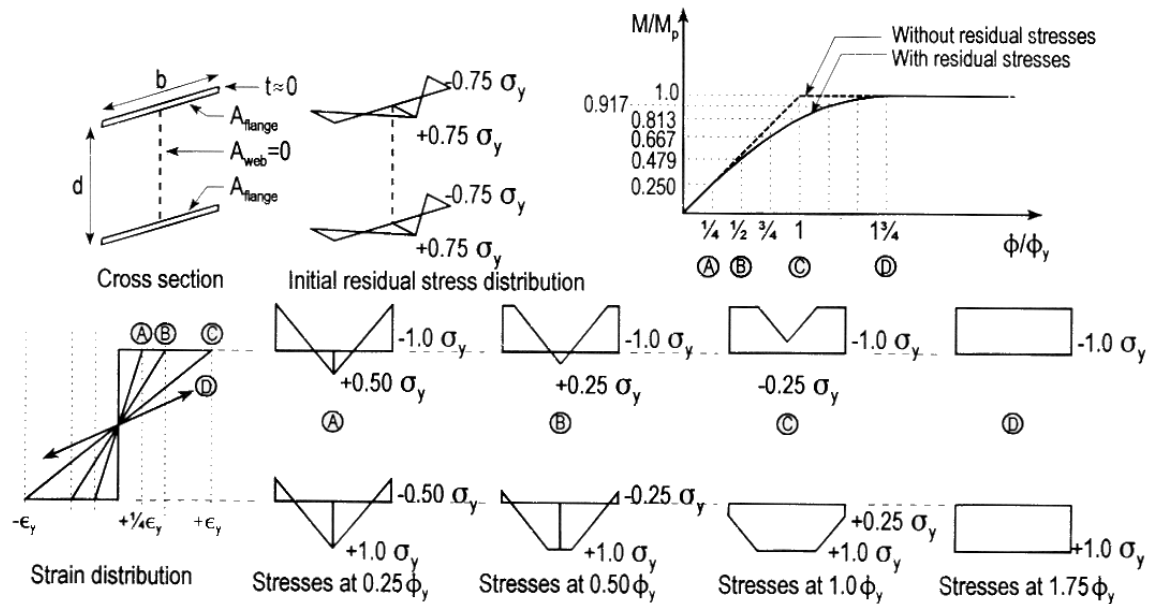


Figure 2.2.3-1. Flexural behavior of wide-flange with residual stresses (Uang et al, 1998)

In accordance with AISC specifications, the design magnitude of compressive residual stresses, F_r , is shown in Table 2.2.3-1.

F_y	F_r	Ratio
36 ksi (250 MPa)	10 ksi (69 MPa)	0.72
50 ksi (345 MPa)	16.5 ksi (114 MPa)	0.67

Table 2.2.3-1. Recommended design magnitude of compressive residual stresses (AISC)

Similar to the previous derivations,

$$M_r = S_x \phi_m^o F_L \quad (2.2.3-1)$$

$$\epsilon_{y'} = \frac{F_L}{E} \quad (2.2.3-2)$$

$$\varepsilon_{y'} \approx 0.7\varepsilon_y \quad (2.2.3-3)$$

where

M_r = Section elastic moment capacity at first-yield (*k in, kN mm*)

$F_L = F_y - F_r$ (*ksi, MPa*)

F_r = Nominal compressive residual stress (*ksi, MPa*)

$\varepsilon_{y'}$ = Nominal first-yield strain from Hooke's Law

Hence, the section curvature at first-yield can be expressed by

$$\phi_{y'} = \frac{M_r}{EI_x} = \frac{2\phi_m^o \varepsilon_{y'}}{d} \approx \frac{1.4\phi_m^o \varepsilon_y}{d} \quad (2.2.3-4)$$

Although, residual stresses can be large, they have no impact on the plastic moment capacity of a section (*Uang et al, 1998*)

2.2.4 Curvature Reduction for Combined Load Effects

2.2.4.1 Reduction for Axial Compression

The previous sections derived the section curvature of an element subjected to pure bending. However, the application of an axial force affects the yield curvature by reducing the allowable magnitude of the applied moment. From mechanics, the stress distribution for a member subjected to combined loading is

$$\sigma = \frac{M}{S_x} \pm \frac{P}{A_g} \quad (2.2.4.1-1)$$

For axial compression, the stress at the extreme compression fiber at yield is

$$\sigma_c = \frac{M}{S_x} + \frac{P}{A_g} = F_y \quad (2.2.4.1-2)$$

Similarly, at the extreme tension fiber, the flexural stress from Eq. (2.2.4.1-2) is

$$\sigma_t = \frac{M}{S_x} = F_y - \frac{P}{A_g} \quad (2.2.4.1-3)$$

Substituting Eq. (2.2.4.1-3) into Eq. (2.2.4.1-1), we have

$$\sigma_t = \frac{M}{S_x} - \frac{P}{A_g} = \left(F_y - \frac{P}{A_g} \right) - \frac{P}{A_g} = F_y - \frac{2P}{A_g} \quad (2.2.4.1-4)$$

Applying

$$P_y = A_g F_y \quad (2.2.4.1-5)$$

the resulting tensile stress can be expressed as

$$\sigma_t = F_y - \frac{2P}{A_g} = F_y - \frac{2PF_y}{P_y} = F_y \left(1 - \frac{2P}{P_y} \right) \quad (2.2.4.1-6)$$

Since the overstength factor, ϕ_m^o , is included in the final curvature calculation, it should not be additionally included in the previous equations.

Applying Hooke's Law and evaluating the strain distribution, we have from similar triangles

$$\frac{\varepsilon_y}{c} = \frac{\varepsilon_y \left(1 - \frac{2P}{P_y} \right)}{d - c} \quad (2.2.4.1-7)$$

Solving Eq. (2.2.4.1-7) for c , the distance from the extreme compression fiber to the neutral axis, we have

$$c = \frac{d}{2 \left(1 - \frac{P}{P_y} \right)} \quad (2.2.4.1-8)$$

By trigonometry and including ϕ_m^o to denote the variation in material strength, the section yield curvature for a member subjected to bending and an axial force can be expressed as

$$\phi_y = \frac{2\phi_m^o \varepsilon_y}{d} \left(1 - \frac{P}{P_y}\right) \quad (2.2.4.1-9)$$

It can be seen from Eq. (2.2.4.1-9) that the reduced yield moment capacity is dependent on the magnitude of axial load and can be expressed as

$$M_{yc} = \left(1 - \frac{P}{P_y}\right) M_y \quad (2.2.4.1-10)$$

It should be mentioned, as similar notations will be used subsequently, that the 2nd subscript denotes the load effect causing the reduction.

Similarly, the *equivalent* plastic and first-yield curvatures become respectively

$$\phi_p = \frac{2S_F \phi_m^o \varepsilon_y}{d} \left(1 - \frac{P}{P_y}\right) \approx \frac{2.28 \phi_m^o \varepsilon_y}{d} \left(1 - \frac{P}{P_y}\right) \quad (2.2.4.1-11)$$

$$\phi_{y'} = \frac{2\phi_m^o \varepsilon_{y'}}{d} \left(1 - \frac{P}{P_y}\right) \approx \frac{1.4 \phi_m^o \varepsilon_y}{d} \left(1 - \frac{P}{P_y}\right) \quad (2.2.4.1-12)$$

The reduced plastic moment capacity can similarly be expressed by Eqs. (2.2.4.1-13) and (2.2.4.1-14) and graphically shown in Fig. 2.2.4.1-1.

For $0 \leq P \leq 0.15P_y$

$$M_{pc} = M_p \quad (2.2.4.1-13)$$

For $0.15P_y \leq P \leq P_y$

$$M_{pc} = 1.18 \left(1 - \frac{P}{P_y}\right) M_p \quad (2.2.4.1-14)$$

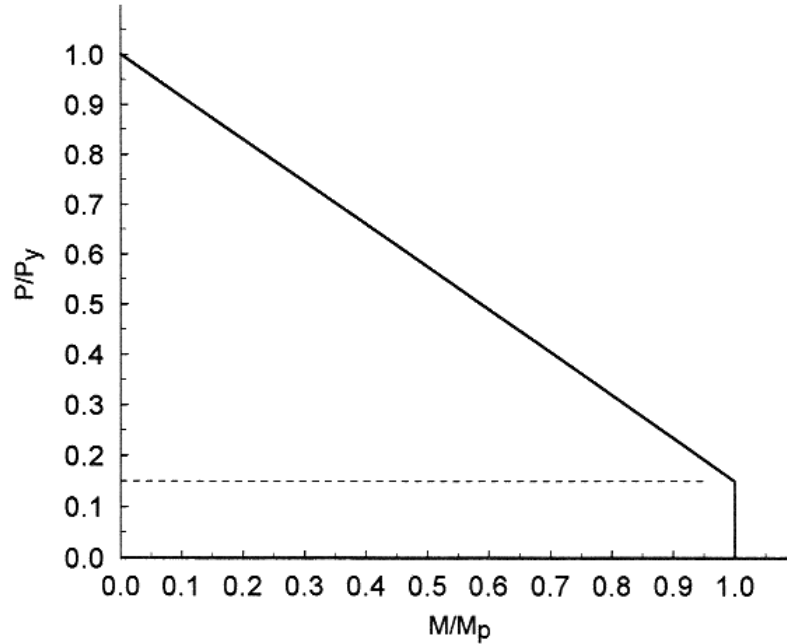


Figure 2.2.4.1-1. Idealized interaction diagram for steel beam-column (Uang et al, 1998)

Eq. (2.2.4.1-14) is slightly conservative; therefore, the difference between it and Eq. (2.2.4.1-15), extracted directly from Eq. (2.2.4.1-11), is negligible.

$$M_{pc} = S_F \left(1 - \frac{P}{P_y} \right) M_p \approx 1.14 \left(1 - \frac{P}{P_y} \right) M_p \quad (2.2.4.1-15)$$

Evaluation of Eq. (2.2.4.1-15) indicates that P should be limited to $0.15P_y$ as an upper bound criteria for beam-columns with an expected ductility greater than 3 (typical of beams in moment frames). This leads to an applied moment capacity of $0.85M_p$, which is approximately equal to M_y . It shall be noted that taking M_{pc} as M_p for values of P less than $0.15P_y$ leads to a maximum error less than 5% (Uang et al, 1998). Additionally, until the axial force exceeds 30% of the axial plastic value, the reduction in moment capacity is typically less than 10% for wide flange sections (Uang et al, 1998)

Normally this criterion is not a concern for beams in moment frames since the axial load ratio is small due to the large cross-sectional area typical of these members. Furthermore, Capacity Design principals, discussed subsequently, will eliminate this requirement for columns above the base columns. However, base columns with fixed bases are subjected to

high axial loads from gravity and additive beam shears, high lateral shears, and high moment demands (including $P-\Delta$ and $P-\delta$ moments) normally accompanied with high rotation demands. Thus requiring the base columns to maintain structural integrity while stressed into the inelastic region. Hence, care is required in the design of base columns.

2.2.4.2 Reduction for Shear

Likewise, the plastic moment capacity is reduced for the presence of high shear forces. In accordance with the Von Mises yield criterion and assuming that the web carries the shear force, the plastic shear capacity can be expressed as

$$V_p = t_w d_w \frac{F_y}{\sqrt{3}} \quad (2.2.4.2-1: \text{Chen et al, 1995})$$

Therefore, the reduced plastic moment capacity can be obtained by

$$\text{For } 0 \leq V \leq \frac{2}{3}V_p$$

$$M_{ps} = M_p \quad (2.2.4.2-2: \text{Chen et al, 1995})$$

$$\text{For } \frac{2}{3}V_p \leq V \leq V_p$$

$$M_{ps} = (1 - \alpha_s)M_p = \left(1 - \frac{\frac{3}{4} \left(\frac{V}{V_p} \right)^2}{1 + \frac{4b_f t_f d_f}{t_w d_w^2}} \right) M_p \quad (2.2.4.2-3: \text{Chen et al, 1995})$$

Hence, Eq. (2.2.4.1-11) is modified to account for the presence of shear.

$$\phi_p = \frac{M_{pr}}{EI_x} = \frac{2S_F \phi_m^o \varepsilon_y}{d} \left(1 - \frac{P}{P_y} - \alpha_s \right) \quad (2.2.4.2-4)$$

Similarly, the total reduced plastic moment capacity can be expressed as

$$M_{pr} = S_F \left(1 - \frac{P}{P_y} - \alpha_s \right) M_p \approx 1.14 \left(1 - \frac{P}{P_y} - \alpha_s \right) M_p \quad (2.2.4.2-8)$$

The effect of shear force on the plastic moment capacity of member in frames is negligible due to high shear and moment occurring in localized zones where strain hardening of material will set in quickly, thus permitting the moment capacity to exceed the plastic value (*Chen et al*, 1995). Therefore, the full plastic moment, not including the effect from axial force, can be used in the design of framed members as long as the shear force does not exceed the plastic shear capacity, V_p .

2.2.4.3 Reduction for Torsion

The plastic moment capacity of a wide flange section may still be reduced further with the presence of torsion. Good design details accounting for torsional load paths normally will eliminate this occurrence. Hence, this topic will be neglected for this document. For convenience following the procedures as previous reduction factors, the interaction equation for flexure and torsion is

$$\left(\frac{M_{pt}}{M_p} \right)^2 + \left(\frac{T_{pt}}{T_p} \right)^2 = 1 \quad (2.2.4.3-1: \text{Uang et al, 1998})$$

2.2.5 Material Overstrength Factor

Recent studies have reported an increase in the margin between the actual yield strength and nominal specified yield strength (*Uang et al*, 1998). For non-ductile steel design this fact has no great importance; however, for seismic design, where localized portions of members are required to yield for energy dissipation, this has an adverse effect possibly leading to unexpected damage. Not only does this prevent the formation of plastic hinges when expected it also effects force demands on other members, thus possibly overloading adjacent members. To account for this effect the nominal local yield strength must be modified by the material overstrength.

$$\phi_m^o = \frac{F_{y actual}}{F_{y nominal}} \quad (2.2.5-1)$$

Due to the conservative nature of accounting for material overstrength, care shall be used in assuming and using a global material overstrength factor. In truth, the material overstrength factor should only be applied to critical regions required to dissipate energy.

Due to increases in quality control during the mill process and advancement in manufacturing technology, the material overstrength factor, ϕ_m^o , for new structural steel can be taken as unity. However, for older steel, and with the absence of certified test coupons, values for ϕ_m^o are listed in Table 2.2.5-1.

F_y	$\phi_m^o (R_y)$
36 ksi (250 MPa)	1.5
50 ksi (345 MPa)	1.3

Table 2.2.5-1. Recommended material overstrength factors (AISC)

It should be mentioned that AISC *Seismic Provisions* use R_y to represent material overstrength factor ($F_{ye} = R_y F_y$). In accordance with other published seismic engineering material, overstrengths will be notated as in the previous equations where the subscript denotes type and the superscript, o , signifies the variable as an overstrength. Additionally, the strengthening effect from strain hardening, ϕ_{sh}^o , should not be included in the member *equivalent* plastic curvature calculation. However, it should be included in the determination of the ultimate plastic moment capacity and ductility calculation.

2.2.6 SUMMARY OF CURVATURES

ϕ_p	Theoretical	Simplified: Beam ($\phi_m^o = 1$)	Simplified: Beam- Column ($\phi_m^o = 1$)
First-Yield	$\frac{2\phi_m^o \varepsilon_y}{d} \left(1 - \frac{P}{P_y}\right)$	$\frac{1.4\varepsilon_y}{d}$	$\frac{1.4\varepsilon_y}{d} \left(1 - \frac{P}{P_y}\right)$
Yield	$\frac{2\phi_m^o \varepsilon_y}{d} \left(1 - \frac{P}{P_y}\right)$	$\frac{2\varepsilon_y}{d}$	$\frac{2\varepsilon_y}{d} \left(1 - \frac{P}{P_y}\right)$
Plastic ^{1,2}	$\frac{2S_F \phi_m^o \varepsilon_y}{d} \left(1 - \frac{P}{P_y} - \alpha_s\right)$	$\frac{2.28\varepsilon_y}{d}$	$\frac{2.28\varepsilon_y}{d} \left(1 - \frac{P}{P_y}\right)$

Notes:

1: For $V \leq \frac{2}{3}V_p$, no reduction in plastic moment capacity

2: For $P \leq 0.15P_y$, no reduction in plastic moment capacity

Table 2.2.6-1. Recommended equivalent plastic curvatures

2.3 Member Rotation

Stability functions will be employed in the determination of member rotation capacities. The benefit of using stability functions in the analysis of a beam-column is that second-order effects and the effect of an axial force on the bending stiffness of the element are accounted (*Chen et al, 1997*). Additionally, only one element is needed for the analysis of a member.

2.3.1 Stability Functions (No Transverse Loads – No Support Displacement)

Fig. 2.3.1-1 shows a typical beam-column subjected to end moments and an axial force.

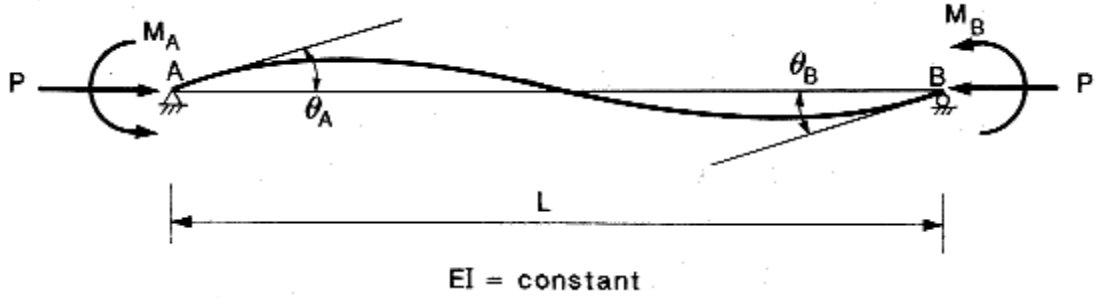


Figure 2.3.1-1. Beam-column subjected to end moments and axial force

(Chen et al, 1997; modified: Harris)

From structural theory, the deflection formula of the beam-column shown in Fig. 2.3.1-1 is

$$y_{(x)} = \frac{M_A}{EI k^2} \left(\frac{\cos kL}{\sin kL} \sin kx - \cos kx - \frac{x}{L} + 1 \right) + \frac{M_B}{EI k^2} \left(\frac{1}{\sin kL} \sin kx - \frac{x}{L} \right) \quad (2.3.1-1)$$

where

$$k = \sqrt{\frac{P}{EI}} \quad (2.3.1-2)$$

The slopes at the ends of the beam are determined from the 1st derivative of Eq. (2.3.1-1) using the respective boundary conditions at $x = 0$ and $x = L$.

$$\theta_A = \frac{M_A L}{EI} \left(\frac{kL \cos kL - \sin kL}{(kL)^2 \sin kL} \right) + \frac{M_B L}{EI} \left(\frac{kL - \sin kL}{(kL)^2 \sin kL} \right) \quad (2.3.1-3)$$

$$\theta_B = \frac{M_A L}{EI} \left(\frac{kL - \sin kL}{(kL)^2 \sin kL} \right) + \frac{M_B L}{EI} \left(\frac{kL \cos kL - \sin kL}{(kL)^2 \sin kL} \right) \quad (2.3.1-4)$$

Solving Eqs. (2.3.1-3) and (2.3.1-4) for M_A and M_B in terms of θ_A and θ_B , we determine

$$M_A = \frac{EI}{L} (s_{ii} \theta_A + s_{ij} \theta_B) \quad (2.3.1-5)$$

$$M_B = \frac{EI}{L} (s_{ji} \theta_A + s_{jj} \theta_B) \quad (2.3.1-6)$$

where

$$s_{ii} = s_{jj} = \frac{kL \sin kL - (kL)^2 \cos kL}{2 - 2 \cos kL - kL \sin kL} \quad (2.3.1-7)$$

$$s_{ij} = s_{ji} = \frac{(kL)^2 - kL \sin kL}{2 - 2 \cos kL - kL \sin kL} \quad (2.3.1-8)$$

In the specific case when $P = 0$, using L'Hospital rule, Eq. (2.3.1-5) and (2.3.1-6) are simplified to the standard first-order slope-deflection equations.

$$M_A = \frac{EI}{L}(4\theta_A + 2\theta_B) \quad (2.3.1-9)$$

$$M_B = \frac{EI}{L}(2\theta_A + 4\theta_B) \quad (2.3.1-10)$$

Solving Eqs. (2.3.1-3), (2.3.1-4), (2.3.1-9), and (2.3.1-10) for equal end plastic moments, in accordance with the elasto-perfectly plastic approximation, we have

Case 1: $0.15P_y \leq P \leq P_y$ (Compression)

$$\theta_{pA} = \theta_{pB} = \frac{M_{pr}L}{EI} \left(\frac{kL + kL \cos kL - 2 \sin kL}{(kL)^2 \sin kL} \right) \quad (2.3.1-11)$$

Case 2: $0 \leq P \leq 0.15P_y$ (Compression)

$$\theta_{pA} = \theta_{pB} = \frac{M_{pr}L}{6EI} \quad (2.3.1-12)$$

Substituting the appropriate plastic curvatures, ϕ_p , from Table 2.2.6-1 into Eq.(2.3.1-11) and (2.3.1-12), we have

Case 1: $0.15P_y \leq P \leq P_y$ (Compression)

$$\theta_{pA} = \theta_{pB} = \phi_p L \left(\frac{kL + kL \cos kL - 2 \sin kL}{(kL)^2 \sin kL} \right) \quad (2.3.1-13)$$

Case 2: $0 \leq P \leq 0.15P_y$ (Compression)

$$\theta_{pA} = \theta_{pB} = \phi_p \frac{L}{6} \quad (2.3.1-14)$$

In the special case when P is tensile the slope-deflection equations ((2.3.1-5) and (2.3.1-6)) are valid with following modifications

$$s_{ii} = s_{jj} = \frac{(kL)^2 \cosh kL - kL \sinh kL}{2 - 2 \cosh kL + kL \sinh kL} \quad (2.3.1-15)$$

$$s_{ij} = s_{ji} = \frac{kL \sinh kL - (kL)^2}{2 - 2 \cosh kL + kL \sinh kL} \quad (2.3.1-16)$$

and the case for $P < 0$ (Tension) can be readily derived.

2.3.2 Stability Functions (No Transverse Loads – Support Displacement)

If the beam-column behavior is additionally accompanied by sideways as shown in Figure 2.3.2-1, the slope-deflection equations are modified to

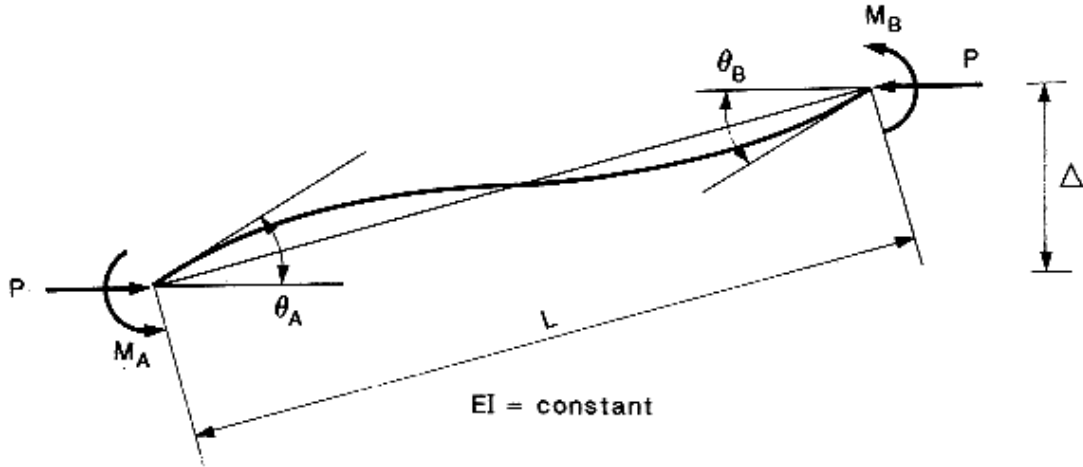


Figure 2.3.2-1. Beam-Column subjected to end moments, axial force, and support displacement

(Chen et al, 1997: modified: Harris)

Case 1: $0.15P_y \leq P \leq P_y$ (Compression)

$$M_A = \frac{EI}{L} (s_{ii}\theta_A + s_{ij}\theta_B - (s_{ii} + s_{ij})\frac{\Delta}{L}) \quad (2.3.2-1)$$

$$M_B = \frac{EI}{L} (s_{ji}\theta_A + s_{jj}\theta_B - (s_{ji} + s_{jj})\frac{\Delta}{L}) \quad (2.3.2-2)$$

Case 2: $0 \leq P \leq 0.15P_y$ (Compression)

$$M_A = \frac{EI}{L} \left(4\theta_A + 2\theta_B - 6\frac{\Delta}{L} \right) \quad (2.3.2-3)$$

$$M_B = \frac{EI}{L} \left(2\theta_A + 4\theta_B - 6\frac{\Delta}{L} \right) \quad (2.3.2-4)$$

where

Δ = Relative joint translation (in, mm).

Solving Eqs. (2.3.2-1) and (2.3.2-2) for θ_p , similar to the previous derivations, we have

Case 1: $0.15P_y \leq P \leq P_y$ (Compression)

$$\theta_{pA} = \theta_{pB} = \phi_p L \left(\frac{2 - kL \cot kL}{(kL)^2} \right) + \frac{\Delta}{L} \quad (2.3.2-5)$$

Case 2: $0 \leq P \leq 0.15P_y$ (Compression)

$$\theta_{pA} = \theta_{pB} = \phi_p \frac{L}{6} + \frac{\Delta}{L} \quad (2.3.2-6)$$

Although not discussed in detail, these equations may also be modified to determine the approximate plastic moment demand at the base column and similarly used to determine the required depth of the base column. However, this process would be iterative in nature since an initial Moment of Inertia and cross-sectional area must be assumed at the start. This process could in fact assist in eliminating some of the design penalties associated with steel base columns in seismic resisting frames, discussed subsequently in Section 2.4.

2.3.3 Stability Functions (Transverse Loads)

The presence of a transverse load(s) increases the complexity of the derivation of the stability functions of a beam-column mainly due to the uncertain effect of the column-to-beam stiffness. For simplicity, the derivation of a true simple-span beam is shown with no axial force.

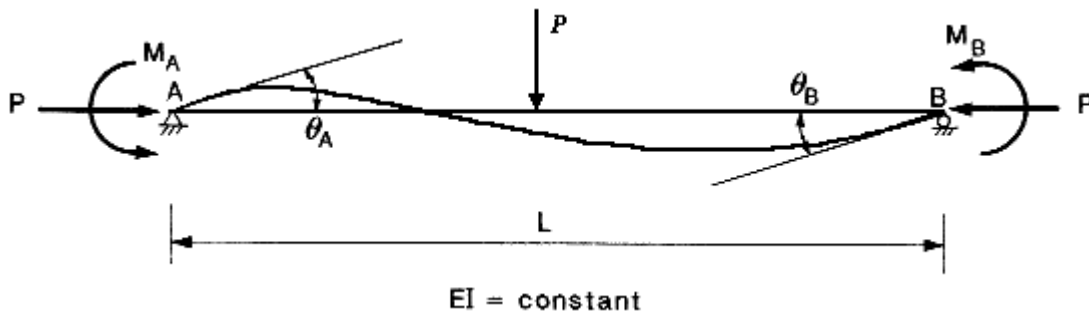


Figure 2.3.3-1. Beam-Column subjected to end moments, axial force, and transverse load

(Chen et al, 1997; modified: Harris)

Re-arranging and modifying Eqs. (2.3.2-3) and (2.3.2-4) including the presence of transverse loads, we determine

$$\theta_A = \frac{L}{3EI} \left(M_A - \frac{M_B}{2} \right) + \frac{\Delta}{L} + \theta_{AG} \quad (2.3.3-1: \text{Chen et al, 1995})$$

$$\theta_B = \frac{L}{3EI} \left(-M_B + \frac{M_A}{2} \right) + \frac{\Delta}{L} + \theta_{BG} \quad (2.3.3-2: \text{Chen et al, 1995})$$

where

θ_{iG} = Respective slope from transverse loads for the i^{th} end

Setting the end moments equal to the moment due to translation only, $M_A = M_B = M_T$, with no support displacement, we have

$$\theta_A = \frac{M_T L}{6EI} + \theta_{AG} \quad (2.3.3-3)$$

$$\theta_B = \frac{M_T L}{6EI} + \theta_{BG} \quad (2.3.3-4)$$

In the elastic range of the member, the respective end moment is the sum of the moment due to translation and transverse loads.

$$M = M_G + M_T \quad (2.3.3-5)$$

As plastic hinges develop and the member continues to deform into the inelastic range, the member undergoes moment redistribution. A simplified approximation to the final result of moment redistribution is to assume that the moment due to translation “takes up” the entire plastic moment capacity of the member. The member now behaves similar to a simple-span member subjected to transverse loads with equal constant plastic moments on both ends. However, plastic hinges in such a member do not form simultaneously, and successive formation of plastic hinges requires one plastic hinge to deform further into the inelastic region. This fact should not concern the design engineer momentarily for the objective is to

ensure that the system remains stable in the inelastic region when hinges have formed at both ends of the beam.

Recall from mechanics that the elastic rotation of a simple-span member subjected to a uniform transverse load, w , is

$$\theta_{AG} = -\theta_{BG} = \frac{wL^3}{24EI} = \frac{wL^2}{12} \frac{L}{2EI} \text{ or } \frac{wL^2}{8} \frac{L}{3EI} \quad (2.3.3-6)$$

Since it is assumed the member will behave as a simple-span beam once plastic hinges form at both ends, Eqs. (2.3.3-3), (2.3.3-4), and (2.3.3-6) are valid for determining the rotation ductility demand. However, the effect of column-to-beam stiffness should be incorporated into for the determination of beam rotations in the elastic region. For example if the column-to-beam stiffness is greater than 8 (typical of interior joints with beams on both sides of the column) the elastic beam rotation, for all intents and purposes, is equal to zero. As the stiffness ratio decreases the elastic beam rotation can range from

$$\theta_G = 0 \rightarrow \frac{wL^3}{24EI}$$

corresponding to a range of elastic fixed-end moments

$$M_G = \frac{wL^2}{8} \rightarrow \frac{wL^2}{24}$$

Here in lies the difficulty of determining the actual member rotations due to transverse loads and seismic forces, since columns are not normally finalized until after Capacity Design procedures have been implemented. For structures in high seismic regions, the ratio of gravity moment to plastic moment demand for earthquake levels representative at the SP-1 performance level is small, typically on the order of 25% for girders and decreases further for beams depending on framing configurations. Therefore, including the effect of Capacity Design procedures on column selection, the effect of transverse loads on the *equivalent* plastic rotation capacity of a beam can be neglected (i.e. $M_T = M_p$). However, for frames in low seismic regions where the ratio of moments approaches unity, this effect should be

included in the determination of the plastic rotation capacity. Hence, expanding Eqs. (2.3.3-3) and (2.3.3-4), we have

$$\theta_{pA} = \frac{M_T L}{6EI} + \frac{wL^3}{24EI} = \frac{M_{pr} L}{6EI} + \frac{M_G L}{2EI} \quad (2.3.3-7)$$

$$\theta_{pB} = \frac{M_T L}{6EI} - \frac{wL^3}{24EI} = \frac{M_{pr} L}{6EI} - \frac{M_G L}{2EI} \quad (2.3.3-8)$$

where the assumed maximum elastic first-order fixed-end gravity moment is

$$M_G = \frac{wL^2}{12} \quad (2.3.3-9)$$

It should be mentioned that care should be used when assuming the maximum fixed-end moment. The design engineer should not over-estimate the actual fixed-end moment.

Therefore, Eqs. (2.3.3-7) and (2.3.3-8) are simplified to

$$\theta_{pA} = \phi_p L \left(\frac{1}{6} + \frac{M_G}{2M_{pr}} \right) \quad (2.3.3-10)$$

$$\theta_{pB} = \phi_p L \left(\frac{1}{6} - \frac{M_G}{2M_{pr}} \right) \quad (2.3.3-11)$$

Evaluation of Eqs. (2.3.3-10) and (2.3.3-11), and illustrated in Fig. 2.3.3-2, shows that the plastic moment capacity needs to be at least twice the simple-span gravity moment in order for no plastic hinges to form along the span of the member prior to the use of Capacity Design. Additionally, the second plastic hinge will form when the respective moment is increased by twice the gravity moment.

$$M_A = M_T + M_G = M_p \quad (2.3.3-12)$$

$$M_B = M_T - M_G = (M_p - M_G) - M_G = M_p - 2M_G \quad (2.3.3-13)$$

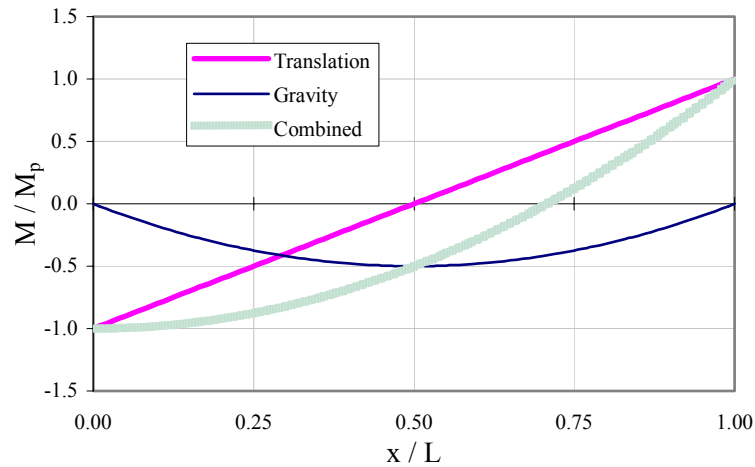


Figure 2.3.3-2. Normalized moment comparison

It shall be noted that Eq. (2.3.3-9) is an approximation of the actual elastic fixed-end gravity moment in determining the additional rotation due to transverse loads. In an actual moment frame, the ratio of column-to-beam stiffness delineates the magnitude of the elastic fixed-end moment and member rotations. Typical ranges for elastic fixed-end moments in a moment frame are summarized in Table 2.3.3-1.

Location	Fixed-end Moment
Exterior Joint – End Span	$\frac{wL^2}{12} \rightarrow \frac{wL^2}{24}$
Interior Joint – End Span	$\frac{wL^2}{9} \rightarrow \frac{wL^2}{12}$
Interior Span	$\frac{wL^2}{8} \rightarrow \frac{wL^2}{12}$

Table 2.3.3-1. Elastic fixed-end moments

Alternatively, the following equations can possibly be used in determining the *equivalent* plastic rotation capacity

$$M_A = \frac{EI}{L} \left[s_{ii}(\theta_A - \theta_{AG}) + s_{ij}(\theta_B - \theta_{BG}) - (s_{ii} + s_{ij}) \frac{\Delta}{L} \right] \quad (2.3.3-14: \text{Chen et al, 1991})$$

$$M_B = \frac{EI}{L} \left[s_{ji}(\theta_A - \theta_{AG}) + s_{jj}(\theta_B - \theta_{BG}) - (s_{ji} + s_{jj}) \frac{\Delta}{L} \right] \quad (2.3.3-15: \text{Chen et al, 1991})$$

Similarly, the rotation capacity of a member subjected to axial compression and transverse load(s) (no transverse support displacement) can be determined by

$$\theta_{pA} = \frac{M_{pr}L}{EI} \left(\frac{kL + kL \cos kL - 2 \sin kL}{(kL)^2 \sin kL} \right) + \frac{M_G}{2M_{pr}} \left(\frac{3 \left(\tan \frac{kL}{2} - \frac{kL}{2} \right)}{\left(\frac{kL}{2} \right)^2 \tan \frac{kL}{2}} \right)$$

(2.3.3-16: *Chen et al, 1991: modified: Harris*)

$$\theta_{pB} = \frac{M_{pr}L}{EI} \left(\frac{kL + kL \cos kL - 2 \sin kL}{(kL)^2 \sin kL} \right) - \frac{M_G}{2M_{pr}} \left(\frac{3 \left(\tan \frac{kL}{2} - \frac{kL}{2} \right)}{\left(\frac{kL}{2} \right)^2 \tan \frac{kL}{2}} \right)$$

(2.3.3-16: *Chen et al, 1991: modified: Harris*)

Due to complexities in frame configurations and transverse load effects, further research is required when beams are either subjected to very high transverse loads or a frame is located in a low seismic region.

2.3.4 Column-to-Beam Stiffness Factor

The previous plastic rotation capacity derivations assume basically a simple-span condition with applied end moments and axial force; however, in a framed structure there are no true simple-span conditions. Therefore, the need arises to incorporate a column-to-beam stiffness factor, λ . Currently, there are no procedures outlining the determination of this value. The proposed method is a conceptual procedure and therefore future research is required.

By assuming that each floor behaves independently of the others and then evaluating each floor, the column-to-beam stiffness can be approximated by evaluating the total axial load to

total horizontal force on the respective floor. Hence, this factor is sometimes referred to as a floor stiffness factor.

$$\lambda = \left(\frac{1}{1 - \frac{\sum P\Delta}{\sum FL}} \right) \quad (2.3.4-1)$$

Alternatively, another possible form is

$$\lambda = \left(\frac{1}{1 - \frac{\sum P}{\sum P_{e2}}} \right) \quad (2.3.4-2)$$

where

$$P_{e2} = \frac{AF_y}{\lambda_c^2} \quad (2.3.4-3)$$

$$\lambda_c = \frac{KL}{r\pi} \sqrt{\frac{F_y}{E}} \quad (2.3.4-4)$$

The previous equations are the global second-order amplification factor, B_2 , from AISC LRFD specification. The difficulty in using the alternate form is that the slenderness factor, K , is required to determine the effective length of the column, KL . Therefore, Eq. (2.3.4-1) is the preferred expression to determine the column-to-beam stiffness factor. Additionally, when story columns are extremely stiff, λ can actually be less than unity. This occurs when axial loads are extremely high compared to horizontal seismic forces, possibly due to extremely long bay lengths. Therefore, there may be cases when the upper floors will have a value greater than unity while the lower floor values are less than unity. This effect can be compensated for in the selection of beam depths between floors. Furthermore, the effect of joint deformation (panel zone) and member shear deformation should be included. This factor is then applied to the plastic rotation capacities determined in the previous sections to

represent the effect of floor stiffness. It should also be mentioned that this factor could also be evaluated for each column in a frame. This will most likely be the case when a frame is comprised of different bay lengths. As noted, this is a conceptual procedure and additional research is required for both alternate methods and accuracy. It is assumed for this research that λ is constant for each floor and based on preliminary experimental data is set equal to 1.10.

Additionally, this factor may also be applied to the determination of the elastic rotation when a beam is subjected to high transverse load(s). Therefore Eq. (2.3.3-6) can be modified to incorporate the column-to-beam stiffness factor for the moment side and an additional stiffness factor incorporated for the rotation side.

$$\theta_{AG} = -\theta_{BG} = \lambda \frac{wL^2}{12} \left(\frac{L}{(2+G)EI} \right) \quad (2.3.4-5)$$

where

$$G = \frac{\sum \frac{I_c}{L_c}}{\sum \frac{I_b}{L_b}} \quad (2.3.4-6)$$

Additionally, G should include the inelastic stiffness reduction factor, τ , and adjustment factors for beams with different end conditions as outlined in AISC LRFD specification.

2.3.5 Summary of Plastic Rotation Capacities

θ_p	$0 < P \leq 0.15P_y$
Case 1	$\theta_p = \lambda\phi_p \frac{L}{6}$
Case 2	$\theta_p = \lambda\left(\phi_p \frac{L}{6} + \frac{\Delta}{L}\right)$
Case 3	$\theta_{pA} = \lambda\phi_p L \left(\frac{1}{6} + \frac{M_G}{2M_{pr}} \right)$ $\theta_{pB} = \lambda\phi_p L \left(\frac{1}{6} - \frac{M_G}{2M_{pr}} \right)$

Table 2.3.5-1. Recommended equivalent plastic rotation capacities

θ_p	$0.15P_y < P \leq P_y$
Case 1	$\theta_p = \lambda\phi_p L \left(\frac{kL + kL \cos kL - 2 \sin kL}{(kL)^2 \sin kL} \right)$
Case 2	$\theta_p = \lambda\left(\phi_p L \left(\frac{2 - kL \cot kL}{(kL)^2} \right) + \frac{\Delta}{L}\right)$
Case 3	$\theta_{pA} = \lambda\phi_p L \left(\left(\frac{kL + kL \cos kL - 2 \sin kL}{(kL)^2 \sin kL} \right) + \frac{M_G}{2M_{pr}} \left(\frac{3 \left(\tan \frac{kL}{2} - \frac{kL}{2} \right)}{\left(\frac{kL}{2} \right)^2 \tan \frac{kL}{2}} \right) \right)$ $\theta_{pB} = \lambda\phi_p L \left(\left(\frac{kL + kL \cos kL - 2 \sin kL}{(kL)^2 \sin kL} \right) - \frac{M_G}{2M_{pr}} \left(\frac{3 \left(\tan \frac{kL}{2} - \frac{kL}{2} \right)}{\left(\frac{kL}{2} \right)^2 \tan \frac{kL}{2}} \right) \right)$

Table 2.3.5-2. Recommended equivalent plastic rotation capacities with axial force

2.4 Global System Response

The previous two sections (2.2 and 2.3) outlined the curvature and rotation mechanics of a member in a structural frame including the approximate column-to-beam, or floor, stiffness factor, λ . The subsequent sections will discuss the global seismic response of a system employed in DBD.

The fundamental principal of Displacement-based Design is to represent the actual structure as an equivalent single-degree-of-freedom (SDOF) system as shown in Fig. 2.4-1. This method of representation is known as the “substitute structure” (Shibata and Sozen, 1970).

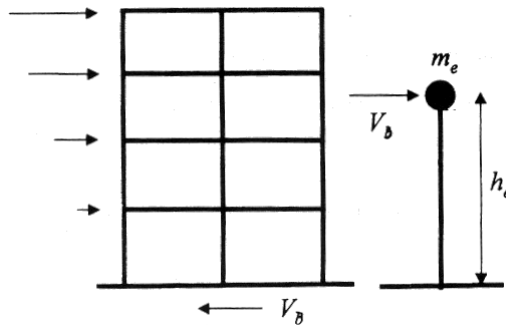


Figure 2.4-1. SDOF representation of actual system (Priestley and Kowalsky, 2000)

The aim of DBD is to represent a damage level in accordance with required ductility demands. As mentioned previously, the easiest form of ductility measurement is with displacements, which can similarly be expressed by interstory drifts, θ_i , or joint rotations. Hence, the design engineer now can begin to see the relationship between member and system response. That is member ductility targets can be determined by

$$\mu_\theta = \frac{\theta_i}{\theta_p} \quad (2.4-1)$$

where

θ_p = Equivalent plastic rotation capacity (Section 2.3)

Target interstory drifts, θ_T , are selected to define the desired performance level, or limit state, corresponding to the respective damage level or desired ductility demand. Here in lies

the fundamental difficulty of performance-based design. That is the quantitative definition of the degree of damage corresponding to each performance level and the prediction of the earthquake magnitudes leading to the attainment of the pre-defined damage level (*Mazzolani et al, 2000*). Currently, SEAOC recommends the following drift values for a steel SMRF:

Performance Level	Target Drift Limit, θ_T (radians)
SP-1	0.005
SP-2	0.018
SP-3	0.032
SP-4	0.040

Table 2.4-1. Recommended target story drifts corresponding to rotation demands (*SEAOC Blue Book, 1999*)

Based on the selected interstory drift limits and considering the inelastic system displacement shape function at the respective performance levels, the target, or design, displacement profiles can be determined.

For this research, the estimated inelastic displacement profiles are shown in Table 2.4-2.

n	Δ_{di}
$n \leq 4$	$\theta_T h_i$
$4 < n < 20$	$\theta_T h_i \left(1 - \frac{(n-4)h_i}{32h_n} \right)$
$n \geq 20$	$\theta_T h_i \left(1 - \frac{h_i}{2h_n} \right)$

Table 2.4-2. Inelastic displacement profiles (*Priestley and Kowalsky, 2000*)

where

n = number of stories

h_i = respective story height (*in, mm*)

h_n = Total frame height (*in, mm*)

SEAOC specifications recommend the inelastic design displacement profiles shown in Fig. 2.4-2.

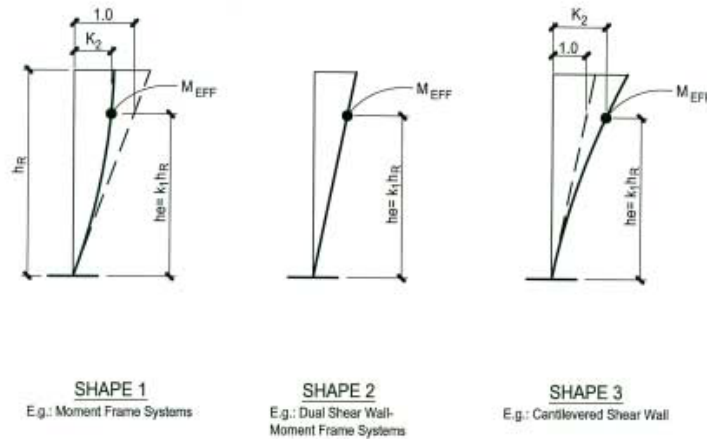


Table AppB-7. K factors for Equations AppB-1 and AppB-8

# Stories	K_1 Effective Height Factor				K_2 Shape Factor					K_3 Effective Mass Factor $= M_{eff}/M$			
	Shape 1	Shape 2	Shape 3		Shape 1	Shape 2	Shape 3			Shape 1	Shape 2	Shape 3	
			HIL=2	HIL=5			$\mu = 1$	$\mu = 2$	$\mu = 5$			HIL=2	HIL=5
1	1.00	1.00	1.00	1.00	1.00	1.00	0.60	0.75	0.88	1.00	1.00	1.00	1.00
2	0.83	0.83	0.90	0.85	1.00	1.00	0.60	0.75	0.88	0.90	0.90	0.90	0.85
3	0.78	0.78	0.85	0.77	1.00	1.00	0.60	0.75	0.88	0.85	0.85	0.85	0.75
4	0.75	0.75	0.85	0.77	1.00	1.00	0.60	0.75	0.88	0.85	0.85	0.85	0.75
5	0.73	0.74	0.85	0.77	0.98	1.00	0.60	0.75	0.88	0.85	0.84	0.85	0.75
10	0.67	0.70	0.85	0.77	0.87	1.00	0.60	0.75	0.88	0.84	0.79	0.85	0.75
15	0.62	0.69	0.85	0.77	0.79	1.00	0.60	0.75	0.88	0.83	0.77	0.85	0.75
20	0.57	0.68	0.85	0.77	0.73	1.00	0.60	0.75	0.88	0.82	0.77	0.85	0.75
50	0.56	0.68	—	0.77	0.72	1.00	0.60	0.75	0.88	0.82	0.77	—	0.75

Where μ =displacement ductility

Figure 2.4-2. Recommended inelastic displacement profiles (SEAOC “Blue Book”, 1999)

It should be mentioned that these formulas approximate the values given in Fig. 2.4-2. Additionally, the relationship between displacement and story drifts (or member rotations) can be evaluated. As indicated in Table 2.4-2, the assumed displacement profile for frames four (4) stories or less is linear. Therefore, it can be assumed that system displacement ductility equals the member rotation ductility. However, for frames with more than four (4) stories the assumed displacement profile is non-linear and, hence, indicates that the displacement ductility will not equal the member rotation ductility. This fact will be discussed further in Section 2.4.5

2.4.1 Design System Displacement

Using the nodal masses and design nodal displacements at each desired performance level, the design system displacement, $\Delta_{d\ sys}$, can be determined from Eq. (2.4.1-1). This represents the lateral displacement of the effective system mass, $M_{eff\ sys}$, at the effective system height, $h_{eff\ sys}$. The subscript “sys” is included in the effective system variables at this point for clarity and subsequently will be dropped. The effective system mass and height are determined from Eqs. (2.4.1-2) and (2.4.1-3).

$$\Delta_{d\ sys} = \frac{\sum_{i=1}^n M_i \Delta_{di}^2}{\sum_{i=1}^n M_i \Delta_{di}} \quad (2.4.1-1)$$

$$M_{eff\ sys} = \frac{\sum_{i=1}^n M_i \Delta_{di}}{\Delta_{d\ sys}} = \frac{\sum_{i=1}^n W_i \Delta_{di}}{g \Delta_{d\ sys}} \quad (2.4.1-2)$$

$$h_{eff\ sys} = \frac{\sum_{i=1}^n M_i \Delta_{di} h_i}{\sum_{i=1}^n M_i \Delta_{di}} \quad (2.4.1-3)$$

where

n = number of floors

M_i = total mass at floor i ($\frac{lbs s^2}{ft}$, mm)

Δ_{di} = design floor displacement at floor i (in , mm)

h_i = floor height above floor $i-1$ (in , mm)

W_i = total weight of floor i (lbs , N)

$g = \text{acceleration of gravity } (32.2 \frac{ft}{s^2}, 9.81 \frac{m}{s^2})$

2.4.2 System Ductility

Ductility is the quantitative measure of member deformation beyond the elastic limit without considerable loss in either strength or stiffness. In suit with the principals of the “substitute structure” analysis, the target system displacement ductility demand, $\mu_{\Delta_{sys}}$, can be represented by either the kinematic or cyclic ductility relationship.

Kinematic Ductility:

$$\mu_{\Delta_{sys}} = \frac{\Delta_{d.sys}}{\Delta_{y.sys}} \quad (2.4.2-1)$$

Cyclic Ductility:

$$\mu_{\Delta_{sys}} = \frac{\Delta_{p.sys}}{\Delta_{y.sys}} + 1 \quad (2.4.2-2: \text{Mazzolani et al, 1996})$$

where

$$\Delta_{p.sys} = \text{Post-yield plastic displacement (in, mm)}$$

The difference between the two is the later takes into account the possible changes of the origin of the inelastic excursion (*Mazzolani et al, 1996*).

The importances of the system yield and design displacement variables can now be recognized. Fundamentally, they determine the target ductility (quantified by displacements) for a given performance level and, similarly, is considered the primary damage level indicator. However, the current problem with this maximum displacement criterion is it treats post SP-1 system displacements and respective damage levels independently. That is there is no inclusion of the number of allowable inelastic excursions, or cycles, that the

system and comprising subassemblies can be subjected. Therefore, further research is required in this area.

Furthermore, the selection of an accurate system yield displacement at the SP-1 level is necessary for a reasonable measure of system ductility. Currently, this cannot be accomplished by choosing the yield drift equal to 0.005 as suggested, since the plastic rotation capacity is a function of beam depth. Additionally, by setting the SP-1 drift limit at the initial design stage prior to analysis or member selection, the engineer is in fact tending more towards the current design philosophy.

Furthermore, current relationships between system ductility and force reduction factors can be evaluated based on the “equal displacement” and “equal energy” principal.

$$R = \mu \text{ for long period structures} \quad (2.4.2-3)$$

$$R = \sqrt{2\mu - 1} \text{ for short period structures} \quad (2.4.2-4)$$

$$R = 1 + \frac{(\mu - 1)T}{0.7} \text{ for } 0 < T \leq 0.7 \quad (2.4.2-5: \text{Paulay and Priestley, 1998})$$

It can be seen that the target system ductility, corresponding to the required energy dissipation and force reduction factor, is a direct function of the mass, strength and stiffness of the system. However, there are currently few design codes that adopt force reduction factors based on the natural period of the system (*Paulay and Priestley, 1998*).

It should be mentioned that it is assumed in current FBD that member ductility is equal to system ductility, even for large complex systems. This is well represented when the displacement profiles are linear. However, for systems that respond in a non-linear function, it is clear that member ductility does not equal system ductility since member ductility demands will vary vertically. Again, this will be discussed further in Section 2.4.5.

2.4.3 Effective System Damping

The ability of a structure to dissipate energy during an earthquake is known as damping. Whereas the damping coefficient is selected so that the vibration energy it dissipates is

equivalent to the energy dissipated by all the damping mechanisms (*Chopra, 2001*). While current design codes assume elastic systems inherently contain 5% elastic viscous damping, there are no guidelines in quantifying the additional damping due to inelastic behavior at large deformations, known as hysteretic damping. Hence, the total equivalent damping can be expressed by the sum of the elastic viscous and hysteretic damping. An enormous amount of research has been conducted in determining member hysteretic functions; however, there are few relationships for quantifying the effects of member damping on the system damping. Additionally, this is extremely difficult to approximate or generalize due to plastic hinge sequencing being a function of both earthquake characteristics and member overstrengths, discussed further in Section 2.4.6. Therefore, further research is required to accurately determine member-system damping relationships for steel frames.

By assuming a proportional relationship between system and member damping, by use of available material hysteretic functions, a closed form equation can be derived representing the effective system damping in terms of the system ductility demand. For example, the Takeda Model (member level) can be used to determine the effective system damping for reinforced concrete frames.

$$\zeta_{eff\ sys} = 0.05 + \frac{1 - \left(\left(\frac{1-r}{\sqrt{\mu_{\Delta,sys}}} \right) - r \sqrt{\mu_{\Delta,sys}} \right)}{\pi} \quad (2.4.3-1: \textit{Takeda et al, 1970})$$

where

r = slope of the inelastic curve

Figure 2.4.3-1 shows a plot of several effective damping curves for different systems.

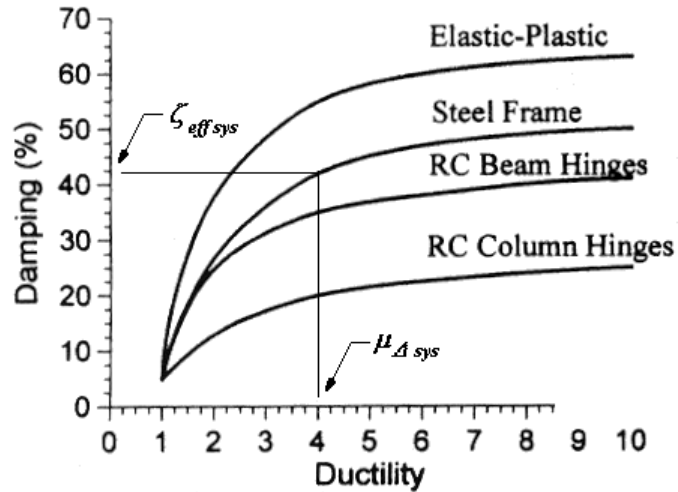


Figure 2.4.3-1. Effective damping vs. ductility graph (Priestley and Kowalsky, 2000: modified: Harris)

Once the system hysteretic function is determined and an effective damping curve constructed, the engineer enters the graph with the target system ductility demand and determines the respective effective system damping.

2.4.4 Effective System Period and Stiffness, and Base Shear

With the effective system damping and design system displacement of the equivalent SDOF system determined, the effective system period can be obtained from the respective DRS, as shown in Figure 2.4.4-1.

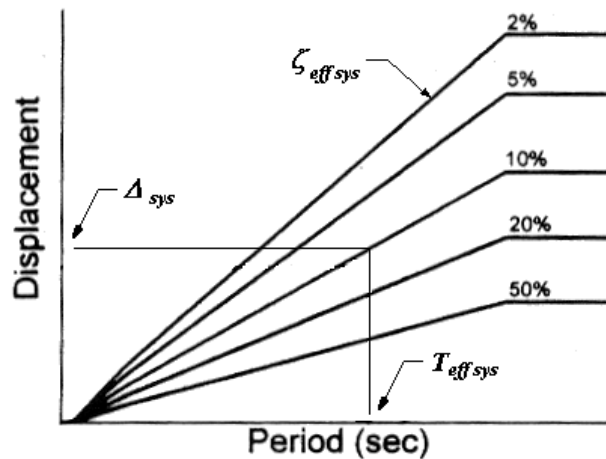


Figure 2.4.4-1. Displacement response spectra (Priestley and Kowalsky, 2000: modified: Harris)

The design engineer can now begin to see the dependence of earthquake level and target demands. Since T_{eff} is determined from the respective DRS, which is a function of earthquake level.

The effective system stiffness and base shear can be determined from Eqs. (2.4.4-1) and (2.4.4-2).

$$K_{eff\ sys} = 4\pi^2 \frac{M_{eff\ sys}}{T_{eff\ sys}^2} \quad (2.4.4-1)$$

$$V_b = K_{eff\ sys} \Delta_{d\ sys} = F \quad (2.4.4-2)$$

This process is repeated for each performance level and the initial elastic stiffness is determined from the performance level with the maximum base shear.

$$K_{el\ sys} = K_{eff\ sys} \left(\frac{\mu_{\Delta\ sys}}{r\mu_{\Delta\ sys} - r + 1} \right) \quad (2.4.4-3)$$

where

r = Post-yield stiffness/elastic stiffness, typically equal to 0.05 to 0.01 depending on structural system

The idealized system force-deformation graph can now be constructed as shown in Figure 2.4.4-2. Furthermore, it is during this process that the controlling performance level is actually determined by the maximum base shear.

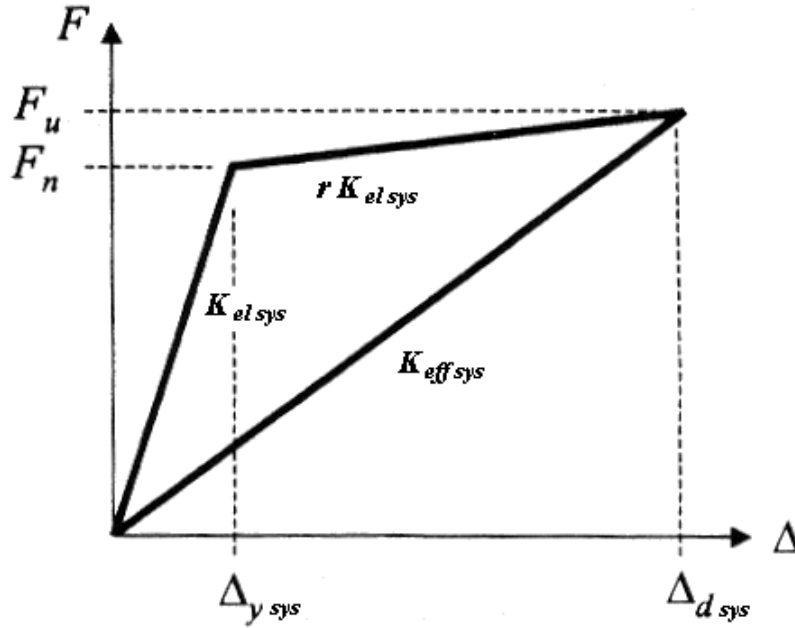


Figure 2.4.4-2. System force-displacement graph (Priestley and Kowalsky, 2000; modified: Harris)

2.4.5 System Analysis and Elastic Displacement Profiles

With the yield base shear at the SP-1 performance level determined, it is then vertically distributed using Eq. (2.4.5-1).

$$F_{xi} = V_b \frac{M_i \Delta_{di}}{\sum_{i=1}^n M_i \Delta_{di}} \quad (2.4.5-1)$$

The design engineer then analyzes the system for the lateral static forces with a standard elastic analysis package. Since steel members are designed for their respective plastic moment capacity, the results from the elastic analysis are used as the plastic moment demands in the member selection process. The engineer selects the required members maintaining the beam depths selected previously when determining the design displacement profiles. The engineer should also make note of any shape factors well in excess of the assumed 1.14 used in determining the plastic rotation capacity. Additionally, the columns can be designed using Capacity Design procedures, including second-order amplification factors if not included in the analysis, while maintaining consistency with the column-to-beam stiffness factor.

Here in lies the fundamental difficulty in analyzing a system with forces generated at the SP-1 performance level. It is assumed that the target inelastic displacement profile, SP-3 for example, is the same at the SP-1 level. That is they have the same shape function and differ only by magnitude. Recall that in order to obtain the selected profiles the strong column/weak beam (SCWB) design philosophy is applied. This, with additional capacity design procedures, will insure that no undesired plastic hinges form in the columns, other than the base, and allow plastic hinges to form only at the ends of beams.

For frames four (4) stories or less, the SCWB philosophy will provide linear inelastic displacement profiles, as indicated in Table 2.4-2. This fact, in combination with current steel design procedures, will allow the design engineer to assume that the displacement profile at the SP-1 level, representative of the global yield mechanism, is equivalent to the inelastic displacement profiles at subsequent performance levels. That is the inelastic displacement profile can be used as the shape function at the SP-1 performance level. Therefore, to delineate the profiles, the SP-1 displacement profile shall be referred to as the pseudo-elastic displacement profile, since it simulates the formation of the global yield mechanism. However, as discussed subsequently, penalties arise in the selection of the base columns and thus possibly preventing the formation of plastic hinges at the column bases at the SP-1 level. This will affect the pseudo-elastic displacement profile and vertical force distribution of the yield base shear at the SP-1 performance level used in the elastic analysis. Ultimately, this will affect the assumption of constant inelastic displacement shape functions for all performance levels.

For frames with more than four (4) stories, the relationship between the inelastic and pseudo-elastic displacement profile becomes more complex. As can be seen in Fig. 2.4.5-1, the pseudo-elastic profile can take a range of profiles, dependent on stiffness distribution.

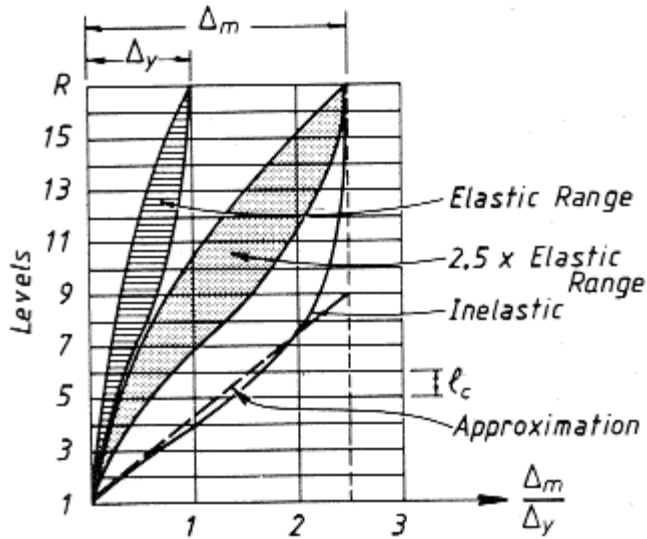


Figure 2.4.5-1. Displacement profile ranges of frames (Pauly and Priestley, 1996)

It is now apparent that the use of a constant force reduction factor, R , or displacement amplification factor, C_d , as specified in current seismic codes for determining the inelastic displacement demand is a truly a misconception. Therefore, it would seem plausible for the engineer to analyze the system for a range of possible pseudo-elastic displacement profiles and design for the worst demands. This procedure should be further researched for suitability. Furthermore, since the target displacement profiles are non-linear, the system displacement ductility in all likelihood will not equal the member rotation ductility.

Upon further research, it will be assumed that the pseudo-elastic displacement profile is equivalent to post-yield displacement profiles (i.e. constant shape function).

2.4.5.1 Equivalent Yield Analysis

Equivalent Yield Analysis (EYA) is a concept adopted by the author for the elastic analysis of multi-story frames where the pseudo-elastic displacement profile is non-linear. This concept separates conceptual hinge formation into various levels (note this is not the same thing as plastic hinge sequencing which affects the design base shear). That is groups of plastic hinges assumed to form simultaneously are assigned to the same level. For example, for linear pseudo-elastic displacement profiles it is assumed that all desired hinges form simultaneously and, likewise, all are assigned to the first level. Additionally, this process

recognizes that an elastic analysis will only determine first level plastic hinge demands. Hence, an elastic analysis is suitable for analyzing systems with linear pseudo-elastic displacement profiles. However, for non-linear pseudo-elastic displacement profiles, the target yield drift implies that a majority of the floors below the effective height will in fact be inelastic by some degree, shown in Fig. 2.4.5.1-1, thus providing multi-level plastic hinge formations. This cannot be accurately analyzed by an elastic analysis without modification to the stiffness of the floors, done by reducing the moment of inertia of the beams, making it difficult and time-consuming for the design engineer.

It can be noticed that at the SP-1 level the system ductility, following the procedures described previously, is less than unity. This is due to not all beam ends forming conceptual plastic hinges. In recognition of this and the limitations of an elastic analysis, the design engineer can reduce the yield base shear at the SP-1 performance level to an *elastic* base shear by multiplying through by the system displacement ductility (less than unity). The *elastic* base shear can then be vertically distributed using the *elastic* displacement profile, or profiles, and the system analyzed in a standard elastic analysis package. By doing so, the elastic analysis will provide the first level plastic hinge demands, normally at the lowest two floors. The term *elastic* is used to represent the behavior or force demands of a completely elastic system and does not refer to a full non-reduced earthquake. The other design demands for members above the first two floors can be determined by dividing the elastic analysis results by the respective floor rotation ductility. This procedure is an attempt to simplify the analysis of multi-story seismic resistant steel frames using the DBD philosophy, and thus shall be further researched.

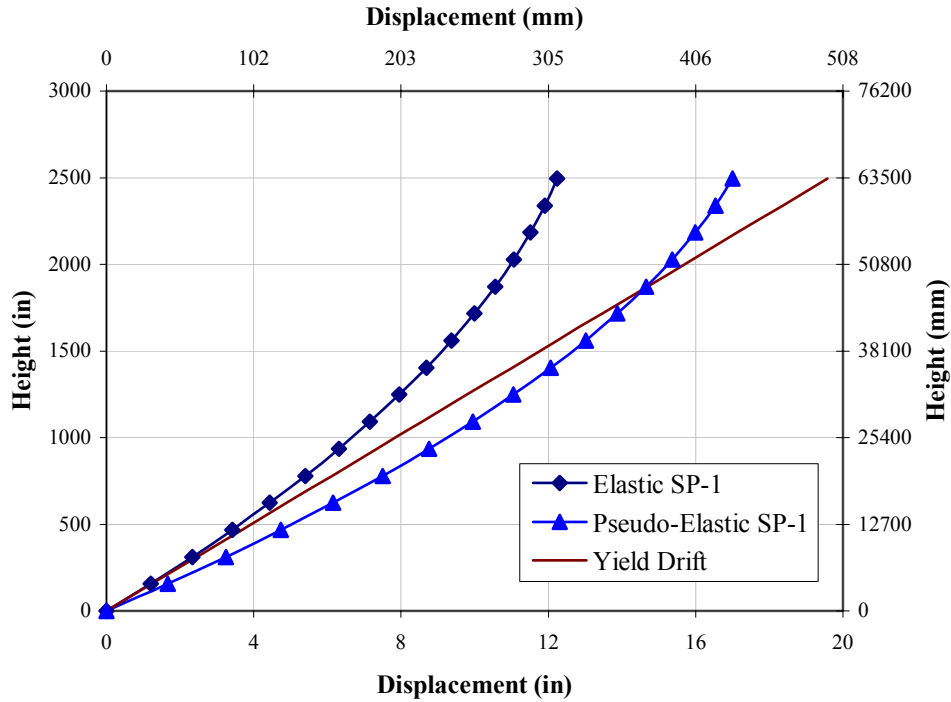


Figure 2.4.5.1-1. Non-linear yield displacement profile at SP-1 performance level

This analysis procedure still does not provide a solution to the ultimate question of what displacement profile should be used at the pseudo-elastic (SP-1) or *elastic* level. Using the distributed *elastic* base shear to size the members for frames with non-linear displacement profiles, plastic hinges in all likelihood will not form at the column bases. Additionally, higher mode effects are more prominent as the frames get taller. Therefore, SP-1 level displacement profiles, or range of, and any respective *elastic* displacement profiles deserve additional research. It shall be emphasized that for linear displacement profiles the terms pseudo-elastic and *elastic* are synonymous for no design displacement profile modifications (and lateral forces) are required in the determination of the first level plastic hinge demands. Numerical implementation of this process is discussed in Section 2.5.

Another difficulty in the current SEAOC specifications is that the use of fixed MCE PGA reduction factors does not allow the design engineer to match all performance levels. For example, assuming that SP-4 controls the design of a frame (i.e. largest base shear), hence, the required *elastic* and pseudo-elastic system variables are thus determined from system

characteristics determined at the controlling performance level. It would seem plausible that the change in target interstory drift between performance levels should match the change in design earthquake levels. That is the ratio of performance target to SP-4 target would equal the ratio of desired EQ level to EQ IV. Simply, the target drift dictates the required demand. Additionally, once the SP-1 interstory drift target is determined based on beam depths, the design engineer can then determine the required EQ I level, not before as suggested by fixing the SP-1 target prior to selecting member depths. Fig. 2.4.5.1-2 shows an example of matching EQ levels with target drifts.

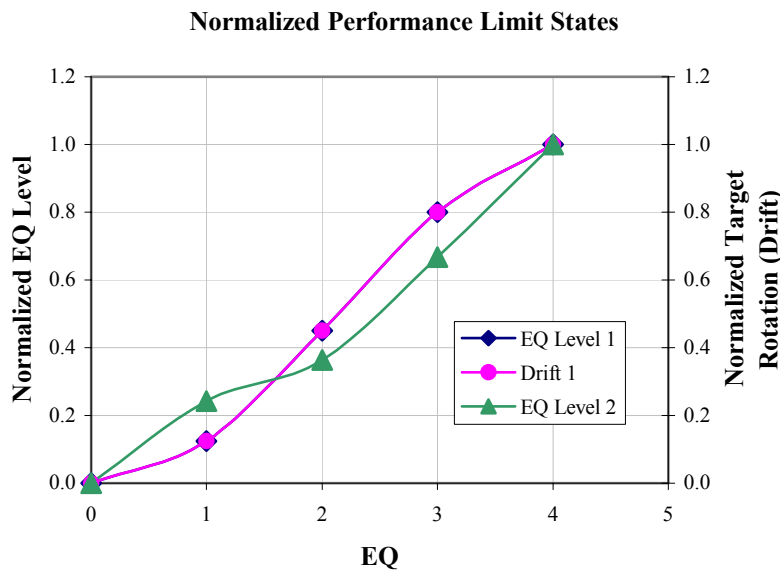


Figure 2.4.5.1-2. Normalized target drift to EQ level comparison

In Figure 2.4.5.1-2, EQ Level 2 and Drift 1 represent the normalized fixed MCE PGA reduction factors and target drifts specified by SEAOC. As can be seen, theoretically only EQ IV, representative of SP-4 in this document, can be matched. If the slopes of the normalized earthquake level factors and targets are not co-linear, the design engineer will most likely find that the damage level and the associated target displacement are not achievable. It shall also be noted that EQ I (SP-1) is determined from the 0.005 drift ratio specified by SEAOC. However, subsequently, this value will be modified to suit the respective selected system configuration. Furthermore, by matching the EQ level with the drift ratio, it seems plausible that the design engineer could theoretically match all displacement profiles, with some modifications for performance overstrengths, system

uncertainties, and earthquake uncertainties. Earthquake uncertainties, though out of the scope of this document, are developed from the need to represent the unlikelihood of an earthquake actually having the full intensity of the design spectra specified in seismic codes. The advantage of doing so is that the engineer would be able to determine a more accurate force-displacement graph for the complete performance objective of the system. In truth, once the controlling performance level is determined, there is no need to examine or modify the other performance levels since the elastic system properties will be developed based on the controlling performance level. However, the idea behind the proposed method is to be able to predict system behavior, and damage level, anywhere along the force-displacement graph. Therefore, the modifications as discussed are used.

The previous sections (2.0-2.4) outlined the fundamental procedures involved in DBD of steel moment frames. As can be seen, this design concept is very simple with the only complexities occurring in the determination of the “substitute structure” characteristics, design displacements (*Priestly and Kowalsky, 2000*). The last step that needs to be discussed is the design of members, including Capacity Design.

2.4.6 System Overstrength and Capacity Design

The penalty for using steel in seismic resistant frames, not including members with reduced cross-sections at plastic hinge locations, is that the design engineer in all likelihood will not be able to proportion member plastic capacities to exactly match what is required by analysis. Hence, it is necessary to incorporate overstrength factors into the seismic design of steel structures. Furthermore, in accordance with the recommended SCWB philosophy, for the design of non-ductile structural elements or portions of critical members where inelastic behavior is not desired, Capacity Design procedures should be employed to protect these members/regions from actions that could cause failure (*Paulay and Priestley, 1996*). The key difference between overstrength factors and Capacity Design is that the later employs the overstrength factors in the design of ductile and non-ductile members.

There are two main types of overstrength factors employed in seismic design of steel frames: 1) material (partly discussed previously in Section 2.2.6) and 2) performance. While both

factors are required for the design of steel frames, the later can only be determined during the analysis/design stage.

2.4.6.1 Material Overstrength Factors

Randomness of the yield strength, or material overstrength, ϕ_m^o , of a member effects the formation of plastic hinges, and as a consequence, the ultimate behavior of the system (Mazzolani, 1996). Additionally, the dependence of yield strength upon plate thickness has to be taken into account for the prevention of premature collapse (local buckling) (Mezzolani, 1996) and to account for the elongated range of inelastic action prior to full plastification of thick flange plates. It shall be noted that the first is considered in current seismic codes by minimum width-thickness ratios and the later is accounted for in the shape factor variable. Therefore, post-yield displacements should be calculated based on these conditions and, therefore, it is necessary to account for the effects of material overstrength and plate thickness in the determination of member *equivalent* plastic rotation capacities. Since strain hardening effects post-yield response it will be placed in the member overstrength factor and should not be included in the determination of rotation capacity. Furthermore, since ductility is measured by the ratio of ultimate to yield response, material overstrength factors should be incorporated at the member level and not as a global overstrength.

2.4.6.2 Performance Overstrength Factors

System performance overstrength is composed of two factors that affect the global performance of a system. The first factor is member, or flexural, overstrength, ϕ_s^o , which represents a member being stronger than required. Displacement profiles are determined based on the locations and conceptual formation of acceptable plastic hinges; therefore, in order to meet the target value, the desired plastic hinges must form when expected. When the results of an elastic analysis are used to determine the required plastic moment capacity, it is not always the case that the geometric plastic moment capacity of the member equals that which is required by analysis. For example, if analysis requires a plastic section modulus of 360 in^3 ($5.90\text{E}+06 \text{ mm}^3$), the closest acceptable plastic section modulus could be

375 in³ (6.15E+06 mm³). This leads to a member overstrength factor of 375/360 = 1.04. While this example value may be considered negligible for a structure located in a high seismic area, higher member overstrength factors are expected for deeper heavier sections due to a wider range of available plastic moduli. Additionally, this factor is calculated for each location of a system where plastic hinges are expected to form.

Depending on the shape factor, S_F , used in the determination of plastic rotation capacity, an additional factor is incorporated to represent the ratio of the actual shape factor to the initially assumed shape factor. For example, if a W30x99 ($S_F = 1.16$) is selected and the rotation capacity was determined assuming an average value of 1.14, the shape factor overstrength, ϕ_{sf}^o , is 1.16/1.14 = 1.02. There are also cases when this is a reduction factor. Other factors included in the member overstrength factor are strain rate, ϕ_{sr}^o , and strain hardening, ϕ_{sh}^o . Therefore, the need arises to incorporate these effects into DBD in order to accurately predict global system response.

The member overstrength at a plastic hinge location can be determined from Eq. (2.4.6.2-1).

$$\phi_{s_j}^o = \phi_{sr}^o \phi_{sh}^o \phi_m^o \frac{M_p}{\phi_{sf}^o M_{EQ}} = \frac{\lambda_o M_p}{M_{EQ}} = \frac{M_o}{M_{EQ}} \quad (2.4.6.2-1)$$

where

j = desired plastic hinge location

M_p = Plastic moment capacity (k in, kN mm)

M_{EQ} = Plastic moment demand (k in, N mm)

M_o = Plastic moment capacity including all overstrength factors (k in, kN mm)

λ_o = Total overstrength factor

ϕ_m^o = Overstrength effect from material overstrength

ϕ_{sf}^o = Overstrength effect from deviation in initial assumed shape factor

ϕ_{sr}^o = Overstrength effect from strain rate

ϕ_{sh}^o = Overstrength effect from strain hardening

Upon further research, the overstrength factors for the effect of strain rate and strain hardening should be taken as unity. It can further be noticed that by designing the maximum rotation capacity (at SP-4) of a member to 0.04 radians, there is a possibility that the member has not entered into the strain hardening region. In certain situations it is equally important to compare the sum of the overstrengths of a number of interrelated members with the total demand made on the same members (*Paulay and Priestley, 1996*). Floor overstrengths are established by evaluating the individual member overstrengths per floor, including the column bases, and can be determined from Eq. (2.4.6.2-2).

$$\phi_{si}^o = \frac{\sum_{j=1}^k M_{oj}}{\sum_{j=1}^k M_{EQj}} \quad (2.4.6.2-2)$$

where

i = Floor number including base

k = Number of desired plastic hinge locations for floor i

This will allow the design engineer to compare total shear forces per floor against lateral seismic forces as will be shown in Part 4. Similarly, the system member overstrength can be determined by evaluating each floor from Eq. (2.4.6.2-3).

$$\phi_{s.sys}^o = \frac{\sum_{i=1}^n M_{oi}}{\sum_{i=1}^n M_{EQi}} \leq 1.5 \quad (2.4.6.2-3)$$

where

n = number of floors

The system member overstrength factor should have an upper limit of 1.5 at which point the design engineer should re-evaluate either the system configuration or beam depths used in determining the design displacement profiles. Additionally, it should be noted that the member overstrength is primarily for beams without reduced cross-sections, RBS or “dog bones,” at desired plastic hinge locations. The use of RBS beams will fundamentally eliminate this factor; however, care is needed in the use of these types of beams in order to prevent local buckling and additional lateral braces should be included.

The second major contributor to the system performance overstrength factor is plastic hinge sequencing, ϕ_{ph}^o . Technically this is not a true overstrength; however, since there is relationship between it and floors overstrengths it is included here. This factor attempts to represent the additional strength required in a system when desired plastic hinges do not form when expected. Hinge sequencing occurs when a floor, since it is designed that all bays in a floor yield simultaneously, due to member overstrengths, dynamically attracts higher demands than expected. Thus altering the equivalent lateral force distribution. Once the “overloaded” floor has formed a yield mechanism, the elastic floors then begin attracting higher demands beyond that which was expected. Ultimately, the system could respond in an apparent higher mode due to reduced stiffness in localized portions of the system. This factor is additionally employed to represent increased demands when earthquake induced higher mode effects govern system behavior. Higher mode effects occur when the earthquake intensity is extremely powerful and inputs a large amount of energy into the system.

While this factor does not play a large part in the design of critical regions, it will contribute to the design of columns. There are a couple of ways to incorporate this factor into the design of a system. The displacement profiles can be modified by a dynamic amplification factor, as suggested by Mesa and Priestley (2002), thus increasing the equivalent static lateral loads to represent the increased demands. However, due to the relationship between hinge sequencing and floor overstrength, this process would place an increased demand on the system thereby inadvertently contributing to the member overstrength factor. The second method is to determine the relationship between both factors presented. The design engineer

would apply this factor to the demands, in addition to member overstrengths, during design. It should be noted that this procedure is conceptual and requires additional research. For this research the floor plastic hinge sequencing factor, ϕ_{phi}^o , is assumed equal to 1.2 for all floors.

$$\phi_{phi}^o = \lambda \sqrt{\phi_{si}^o} \approx 1.2 \leq 1.3 \quad (2.4.6.2-4)$$

$$\phi_{ph\ sys}^o = \frac{\sum_{i=1}^n \phi_{phi}^o}{n} \approx 1.2 \quad (2.4.6.2-5)$$

Eq. (2.4.6.2-5) is averaged to account for the fact that not all floor hinge sequencing factors will occur simultaneously. The system hinge sequencing factor should have an upper limit of 1.3 at which point the design engineer should re-evaluate either the system configuration or beam depths used in determining the design displacement profiles.

The floor and system performance overstrength factor can be determined by the multiplication of the member overstrength and plastic hinge sequencing factors.

$$\Omega_i = \phi_{si}^o \phi_{phi}^o \quad (2.4.6.2-6)$$

$$\Omega_{sys} = \phi_{s\ sys}^o \phi_{ph\ sys}^o \quad (2.4.6.2-7)$$

The performance overstrength factor fundamentally leads to an energy dissipation capacity and available ductility different from predicted (*Mazzolani*, 1996). Therefore the need arises to incorporate these factors into the design of steel frames.

The system performance overstrength factor is then applied to the post-yield predicted performance values to determine the “as designed” system force-displacement graph.

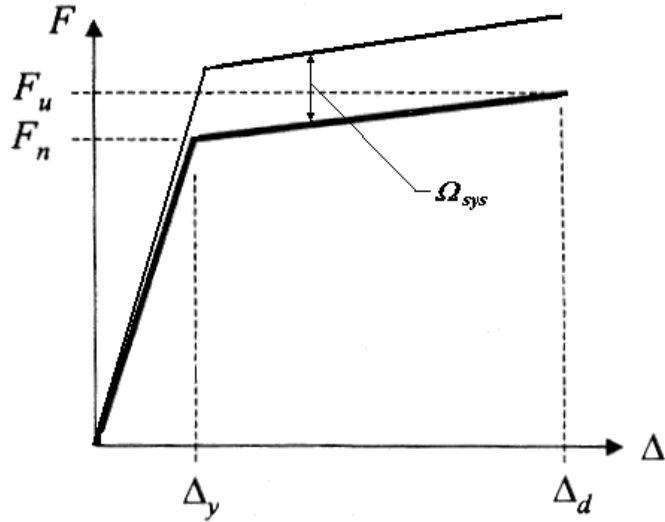


Figure 2.4.6.2-1. System Force-Deformation Graph including System Overstrength

(Prestley and Kowalsky, 2000: modified: Harris)

Additionally, it seems plausible that the performance overstrength factor is additionally a function of inelastic behavior. For example, in the SP-1 (pseudo-elastic) range, member overstrengths take precedence over hinge sequencing for plastic hinges have not yet likely formed. Once plastic hinges begin to form, the member overstrength factor remains constant and hinge sequencing starts to take affect as shown in Fig. 2.4.6-2.

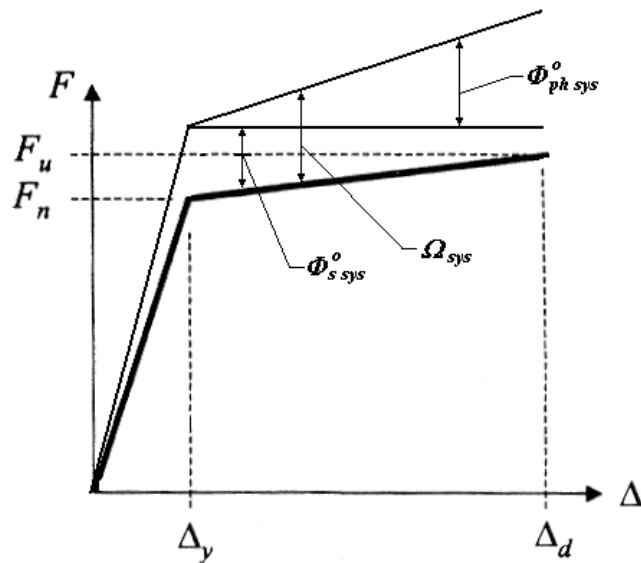


Figure 2.4.6.2-2. System Force-Deformation Graph including System Overstrength

(Prestley and Kowalsky, 2000: modified: Harris)

Current seismic codes specify a generalized system overstrength value to be used in the analysis/design of a steel frame. However, this procedure is erroneous since it applies a system overstrength factor prior to the design of any members (similar to applying a force-reduction factor prior to member selection). The previous procedure defines the correct procedure, albeit conceptual, for determining the system overstrength, which is after the member design process. Additionally, if the code specified overstrength factor is used to increase the applied horizontal earthquake forces, the system overstrength has not been determined and the resulting demands will merely force the system to be proportionally stiffer and stronger. Similarly, there will still be inherent member overstrengths when designing the members for the increased demands. Therefore, it is recommended that no overstrength factors be used prior to designing members. Furthermore, the use of a system overstrength factor in the design of all members is conservative and, ultimately, contributes to the frame being stiffer and stronger than required. Hence it is recommended that floor overstrengths be used in the design of members. Future research is thus required to determine the relationship between floor and system performance overstrengths.

2.4.6.3 Capacity Design

Prior to discussing Capacity Design it is important to define the strength definitions inherent in capacity design procedures. A majority of this information has been directly taken from other references (*Paulay and Priestley, 1996, Priestley et al, 2000*) and the reader is referred to these references for further information.

Required Strength (S_u)

Strength demand determined by factored analysis using prescribed loads and forces.

$$S_u = \gamma_y S \quad (2.4.6.3-1)$$

where

S = Strength demand from analysis

γ_y = Respective load factor for load effect y

Load factors are determined in accordance with AISC *LRFD Manual of Steel Construction* with amendments specified in the *Seismic Provisions*. Though there has been disagreement what load factor should be used for equivalent lateral seismic forces between codes, it is recommended that the load factor be unity.

Nominal Strength (S_n)

Nominal strength of a section of a member determined by established theory predicting a prescribed limit state with respect to failure of that section.

$$\phi_x S_n \geq S_u \quad (2.4.6.3-2)$$

where

ϕ_x = Respective strength reduction factor for resistance x

Resistance factors are determined in accordance with the AISC *LRFD Manual of Steel Construction* with amendments specified in the *Seismic Provisions*. It is recommended that the resistance factor for critical regions of seismic force resisting members be unity. Non-ductile members and elastic portions of critical members should use standard reduction factors.

Probable Strength (S_p)

Probable strength of a section taking into account material strength greater than nominal strength prescribed by the respective design code.

$$S_p = \phi_p^o \phi_x S_n \geq S_u \quad (2.4.6.3-3)$$

where

ϕ_p^o = Probable strength factor (greater than 1.0)

The difference between the probable strength factor and material overstrength factor, ϕ_m^o , is that the later is more of an actual value, whereas the probable strength factor represents the

mean of a series of material overstrength factors. For all intents and purposes they are identical and, hence, are interchangeable.

Overstrength (S_o)

Strength of section taking into account all possible factors that may contribute to the expected strength exceeding the nominal strength.

$$S_o = \lambda_o \phi_x S_n \quad (2.4.6.3-4)$$

where

λ_o = Overstrength factor including strain rate, ϕ_{sr}^o , strain hardening, ϕ_{sh}^o , and material overstrength, ϕ_m^o or ϕ_p^o

During seismic activity, it is the actual strength, S_o , that will develop not the nominal strength, S_n (*Paulay and Priestley, 1996*). It shall be noted for clarity, that the member overstrength, ϕ_s^o , is the total strength of the critical section compared to the demand, while S_o , or M_o in the case for flexure, is the actual total capacity of the critical section including all overstrength factors.

In the capacity design of steel structures for earthquake resistance, distinct regions (plastic hinges) of desired members of the primary lateral force resisting system are chosen and designed and detailed for energy dissipation under severe imposed deformations (*Paulay and Priestley, 1996*). All other structural members and regions adjacent to plastic hinges where the formation of plastic hinges is undesirable must be protected against actions that could cause failure. This includes other failure modes in the critical regions, such as shear failure, local buckling, and lateral-torsional buckling. It can be thought that Capacity Design serves two purposes: 1) protection of non-ductile members from inelastic action and 2) protection of critical regions from other undesirable failure modes. Capacity Design procedures of steel moment frames are outlined as follows:

- 1) Desirable plastic hinge regions are clearly defined in accordance with the SCWB philosophy. The mechanism should be chosen such that the target displacement ductility can be developed, which DBD attempts to determine and such insofar the design engineer designs for. As discussed previously, this is an iterative cycle during the design period since overstrengths affect the formation of plastic hinges, hence, design forces and lateral nodal displacements.
- 2) Non-ductile regions of members containing plastic hinges are protected by providing strengths that can resist increased demands originating from plastic hinge overstrengths. These regions are in theory designed to remain elastic irrespective of the intensity of the ground motion or magnitudes of inelastic deformations (*Paulay and Priestley, 1996*). Here in lies an inherent problem with prismatic steel sections. While RBS or “dog bone” beams can support this procedure by providing two distinct section strengths, standard prismatic sections cannot separate the critical region and non-ductile section strengths. One option is to add strength to the non-ductile region by use of cover plates or other strength enhancement modifications outside of the critical region. Similarly, the beam can also be modified to contain full plastic hinge length strength modifications as shown in Fig. 2.4.6.3-1.

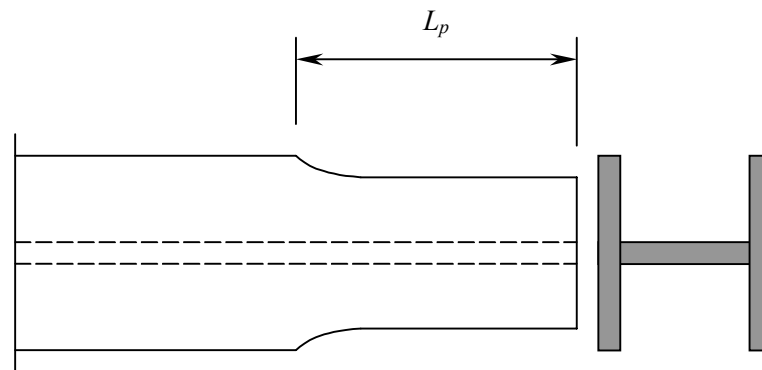


Figure 2.4.6.3-1. Reduced cross-section at plastic hinge

In this scenario, the non-ductile portion of the beam is designed for the maximum moment demand including overstrength factors to provide strengths in excess of the plastic hinge capacity of the critical section. The entire critical region, or plastic hinge length, L_p , is then modified, incorporating all detailing requirements set forth

in the AISC *Seismic Provisions* (i.e. limiting width-thickness ratios to prevent local buckling) to provide the necessary strength distinctions. This process is similar to the design of RBS or “dog bone” beams. However, since the entire beam is designed for the maximum moment demand, therefore leading to thicker plates (including the web), the engineer is normally not penalized by the instability of the RBS. The reader is referred to work by C.M. Uang for further information on the instability of RBS beams (Uang, 2000). Furthermore, providing the reduced section to the column face reduces the maximum allowable moment transferred into the column. Additionally, the design engineer should be aware of any strength excess in this region and, therefore, should be incorporated in the initial design stage (plastic rotation capacity).

- 3) Non-ductile members, such as columns, are then designed to resist the forces, including overstrength, originating from adjacent critical regions. Since standard reduction factors are incorporated in the design of these members there is an additional factor of safety from undesirable modes of inelastic response. However, questions arise about how to ensure the formation of column base hinges as well as insure the protection of adjacent regions. Reduced column sections, or RCS, columns can possibly be used, though only under strict design and detailing procedures, which have not yet been specified.

A capacity design approach adopted for the design of seismic resistant steel frames is able to predict and assure satisfactory inelastic response under conditions for which sophisticated dynamic analysis can yield no more than crude estimates (Paulay and Priestley, 1996). This is due to the fact that capacity-designed structures cannot develop undesirable plastic hinges, thus leading to undesirable modes of inelastic deformations and, ultimately, a failure mechanism. Therefore, the system is insensitive to earthquake characteristics, except the magnitude of inelastic flexural deformations (Paulay and Priestley, 1996).

2.4.6.4 Member Design

The design of members for a capacity-designed steel frame can be performed by procedures outlined in this section.

2.4.6.4.1 Beams

With the demands from an analysis, the beam can be sized using the depths used to determine the target displacement ductility. Material and performance overstrengths are determined and used in the calculation of the plastic hinge capacity of the critical regions, including axial and shear capacities that subsequently are protected from undesirable modes of failure. The non-ductile region of the member is then protected from inelastic response by increasing the axial, moment, and shear demand by the respective overstrength factors. The section is then designed to satisfactorily resist these increased demands. The design forces used in the design of beams can be determined from Eqs. (2.4.6.4.1-1) to (2.4.6.4.1-6).

Critical Sections:

$$M_u = M_G \pm M_{EQ} = M_{pr} \quad (2.4.6.4.1-1)$$

$$0.9 \leq \frac{M_{pr}}{M_u} \leq 1.1 \quad (2.4.6.4.1-1a)$$

$$V_u = V_G \pm \phi_{si}^o \phi_{phi}^o V_{EQ} \leq \phi_x V_n \quad (2.4.6.4.1-2)$$

$$P_u = P_G \pm \phi_{si}^o \phi_{phi}^o P_{EQ} \leq \phi_x P_n \quad (2.4.6.4.1-3)$$

Non-ductile Sections:

$$M_u = M_G \pm \phi_{si}^o \phi_{phi}^o M_{EQ} \leq \phi_x M_n \quad (2.4.6.4.1-4)$$

$$V_u = V_G \pm \phi_{si}^o \phi_{phi}^o V_{EQ} \leq \phi_x V_n \quad (2.4.6.4.1-5)$$

$$P_u = P_G \pm \phi_{si}^o \phi_{phi}^o P_{EQ} \leq \phi_x P_n \quad (2.4.6.4.1-6)$$

2.4.6.4.2 Columns

In the case where the beam plastic moment capacity is in excess of that which is required, including the effects of strain rate and strain hardening, the corresponding additional moment and shear required to form the plastic hinge in the beam(s) is transferred into the column. Thus increasing the column axial load (beam shear), in certain cases, lateral moment, and

shear demand. This increase must be considered in design to prevent the formation of an undesirable plastic hinge in the column. Plastic hinge sequencing additionally affects the lateral shear and moment demands in the columns. To account for this effect, the column moments, shear, and axial force, minus the gravity load, obtained from the elastic analysis shall be multiplied by the floor performance overstrength factor determined when designing the connecting beam(s). Due to moment redistribution, for regular frames configured in accordance with recommendations in Section 2.3, the floor performance overstrength factor may be used in lieu of individual local performance overstrength factors. It should be noted that while the column moments include the additional $P-\Delta$ and $P-\delta$ moment from gravity loads, increasing the total moment does not lead to excessive column sizes. This may additionally be thought of as a precautionary measure to insure that plastic hinges do not form in the column. Hence, the design forces used in the design of columns can be determined from Eqs. (2.4.6.4.2-1) to (2.4.6.4.2-3).

$$M_u = M_G \pm \phi_{si}^o \phi_{phi}^o M_{EQ} \leq \phi_x M_n \quad (2.4.6.4.2-1)$$

$$V_u = V_G \pm \phi_{si}^o \phi_{phi}^o V_{EQ} \leq \phi_x V_n \quad (2.4.6.4.2-2)$$

$$P_u = P_G \pm \phi_{si}^o \phi_{phi}^o P_{EQ} \leq \phi_x P_n \quad (2.4.6.4.2-3)$$

The biggest penalty occurs in the design of column bases. Capacity design at the first and second floor, depending on column height, normally controls the column size at the base due to prismatic member shapes. This, with the addition of high shear and axial forces further increased for the effect of plastic hinge sequencing and member overstrengths, can dictate rather high plastic moment capacities in the columns. Thus either preventing the formation of plastic hinges or formation of simultaneous plastic hinges at the column bases at the SP-1 level. Therefore, the SP-1 level displacement profile should incorporate this fact and further reinforces that idea that a range of possible profiles be used in design. The engineer would then design for the worst-case scenario from the ranges of displacement profiles. The design forces used to verify the capacity of the column base are determined from Eqs. (2.4.6.4.2-4) to (2.4.6.4.2-6).

$$M_u = M_G \pm M_{EQ} = M_{pr} \quad (2.4.6.4.2-4)$$

$$0.9 \leq \frac{M_{pr}}{M_u} \leq 1.1 \quad (2.4.6.4.2-4a)$$

$$V_u = V_G \pm \phi_{sys}^o \phi_{ph sys}^o V_{EQ} \leq \phi_x V_n \quad (2.4.6.4.2-5)$$

$$P_u = P_G \pm \phi_{sys}^o \phi_{ph sys}^o P_{EQ} \leq \phi_x P_n \quad (2.4.6.4.2-6)$$

Note that the system overstrengths are used in lieu of the floor overstrength. While it seems plausible that base columns could in fact be modified, or RCS, similar to reduced cross-section in beams, there is a lack of information on this topic to justify its use. Furthermore, stability issues of the column and the effect of RCS on the structural integrity of the system should be further examined.

There are additional design choices that need to be considered in the design of columns. The most important being joint rotation and vertical stiffness distribution. During the design stage, the design engineer should select column sizes that allow all joints in a floor to have approximately equal rotations. This will also provide beam design moment to be approximately the same, considering gravity loads do not cause large moment deviations in adjacent bays. Additionally, there should not be large stiffness variations from floor to floor, as is observed when different beam depths and/or column depths are used. In the event that different beam depths are used in adjacent floors, column sizes should be selected to counteract the additional moment and shear demand placed on the lower floor while maintaining equivalent joint rotations. The design of steel frames for seismic resistance is no longer justified by the selection of least weight beams and columns to satisfy demand and codified displacement control, but for the engineer to design a system where the behavior is dictated from the start. This is in contrast to current seismic design where the frame behavior is the final product, and even then grossly approximated. This sometimes requires members to have capacities in excess of the demand, and should therefore be incorporated in the design as an overstrength factor. Likewise, the true monetary savings comes from the level of repairs required after being subjected to certain earthquake intensities.

2.5 Displacement-Based Design

This section will implement the procedures outlined in Sections 2.1 to 2.4 for the displacement-based design of seismic resistant steel moment frames. The frames listed in Table 1.1-1 will be analyzed and designed accordingly (see Table 2.5-1 for the respective section).

Stories	Frame ID *	Section
4	FR-4	2.5.1
4	FR-4-W21	2.5.2
4	FR-4-W24	2.5.3
4	FR-4a	2.5.4
4	FR-4b	2.5.5
8	FR-8	2.5.6
8	FR-8a	2.5.7
16	FR-16	2.5.8

* - Schematics of each frame are included in the respective section.

Table 2.5-1. Frame descriptions

The first two steps in DBD of steel moment frames shall be addressed here, for they are constant throughout each frame analysis. Therefore, subsequent sections will begin at Step 3.

Step 1: Select target or design interstory drifts.

As outlined in Section 2.4, the design engineer selects target drifts representative of the desired level of damage and assigns them to respective performance levels. The drift values shown in Table 2.5-2 are the SEAOC BSO drift recommendations and will be used throughout (not including SP-1). In truth, the design engineer has complete freedom in the selection of the target drift. For example, if the design engineer requires that the structure remain serviceable or “operational” at the EQ III level with a target ductility of 0.9 (completely elastic), the service or “yield” drift, including the 10% reduction, would correspond to the SP-1 performance level, and EQ IV would correspond to SP-2.

Performance Level ²	Target Drift Limit, θ_T (radians)
SP-1 – Operational	0.005 ¹
SP-2 – Occupiable	0.018
SP-3 – Life Safe	0.032
SP-4 ³ – Near Collapse	0.040

Notes:

1. 0.005 is chosen and will be subsequently modified to represent system yield behavior.
2. Basic Safety Objective (BSO) is chosen with no limits placed for restricting non-structural damage.
3. With BSO, SP-4 corresponds to the MCE (EQ IV).

Table 2.5-2. Target interstory drifts per performance level

In this research more importance is placed on the development of the fundamental procedures; therefore, no additional limits are placed on the drift targets to control damage levels in non-structural items (i.e. cladding, MEP equipment). In truth, the mechanical and electrical equipment is normally more valuable than the structural framework, and therefore, target drift limits should incorporate non-structural damage control measures (*Paulay and Priestley, 1996*).

Step 2: Determine Displacement Response Spectra (DRS) for each earthquake level.

Based on location characteristics and soil type, the DRS for each required design earthquake level is constructed in accordance with current seismic codes (IBC/NEHRP), illustrated in Figs. 2.5-1 to 2.5-4. Since EQ IV has been selected as the maximum or “near collapse” performance level, it is assigned to the MCE and assumed initially to be the controlling design level earthquake. Therefore all other earthquake levels (I, II, and III) are a reduced level of this. The design peak ground acceleration (PGA) for each earthquake level is thus determined by multiplying the ratio of target drift to ultimate target drift by the MCE PGA, Eq. (2.5-1).

$$PGA_i = PGA_{MCE} \frac{\theta_{Ti}}{\theta_{Tu}} \quad (2.5-1)$$

Performance Level	MCE PGA Reduction Factor	PGA
SP-1 – Operational	0.125 ¹ (0.005/0.04)	0.084 ¹
SP-2 – Occupiable	0.45 (0.018/0.04)	0.30
SP-3 – Life Safe	0.80 (0.032/0.04)	0.54
SP-4 – Near Collapse	1.00 (0.04/0.04)	0.67 ← MCE PGA

Notes:

1. Based on a target drift of 0.005 and will be subsequently modified to represent system yield

Table 2.5-2. Target peak ground accelerations per performance level

This process differs slightly from the current SEAOC procedure using fixed peak ground accelerations representative of discrete earthquake mean return periods. In this procedure, the mean return periods in effect change in order to allow the engineer to attempt to match all performance levels. However, the PGA is only one factor that affects earthquake intensity, duration and frequency content of the strong motion additionally contribute to the destructive power of an earthquake (*Paulay and Priestley, 1996*). Furthermore, the factor for the number of inelastic excursions is considered inherent in the preceding factors.

What cannot be predicted at this moment with accuracy is which performance level will ultimately control the design of the structure (i.e. by means of maximum base shear). Furthermore, at all times the design engineer must be aware of two critical situations. The first being that the current codified design level earthquake (IBC/NEHRP = $\frac{2}{3}$ MCE) is in fact met, and the second that the “operational” or service level earthquake is representative of an acceptable service level earthquake by means of return period comparison. The prior is normally met by including the MCE as one of the design earthquakes.

Additional damping curves can be constructed in the respective DRS from the 5% damping curve using the Eurocode relationship, Eq. (2.5-2).

$$\Delta_{\zeta\%} = \Delta_{5\%} \sqrt{\frac{7}{2 + \zeta\%}} \quad (2.5-2)$$

**Design Displacement Response Spectrum for EQ I
SP-1 (Operational)**

IBC: $S_s = 168.4$, $S_1 = 60$, Site Class = D

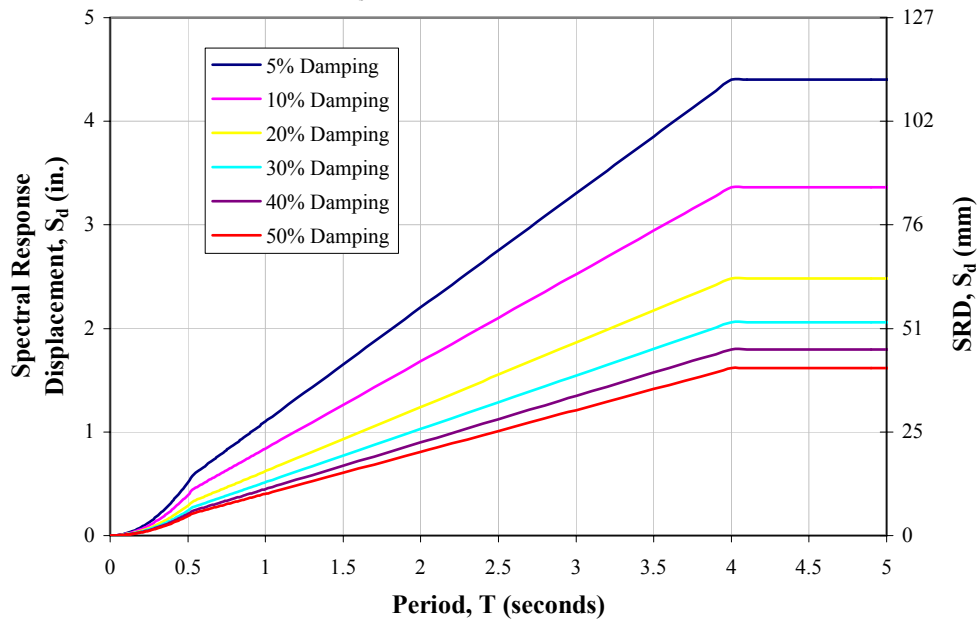


Figure 2.5-1. EQ I Displacement Response Spectrum (PGA Reduction Factor = 0.125)

**Design Displacement Response Spectrum for EQ II
SP-2 (Occupiable)**

IBC: $S_s = 168.4$, $S_1 = 60$, Site Class = D

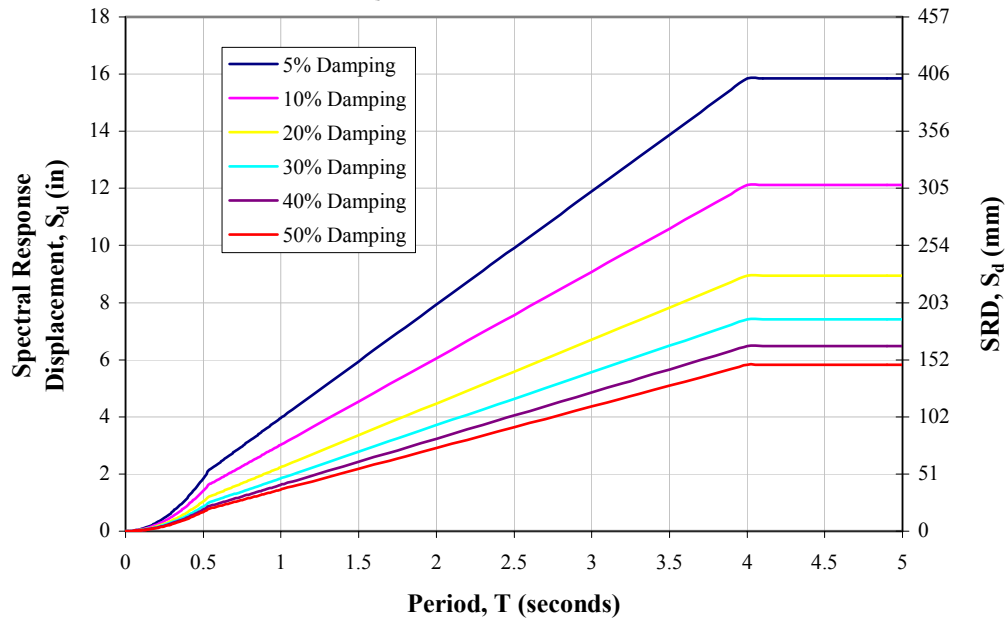


Figure 2.5-2. EQ II Displacement Response Spectrum (PGA Reduction Factor = 0.45)

**Design Displacement Response Spectrum for EQ III
SP-3 (Life Safe)**

IBC: $S_s = 168.4$, $S_1 = 60$, Site Class = D

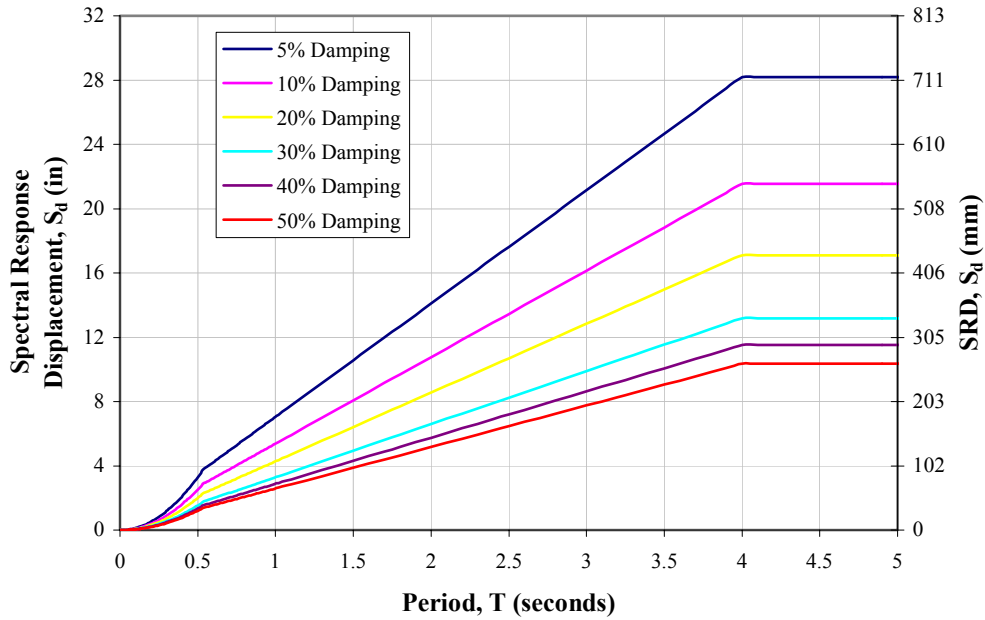


Figure 2.5-3. EQ III Displacement Response Spectrum (PGA Reduction Factor = 0.8)

**Design Displacement Response Spectrum for EQ IV
SP-4 (MCE - Collapse)**

IBC: $S_s = 168.4$, $S_1 = 60$, Site Class = D

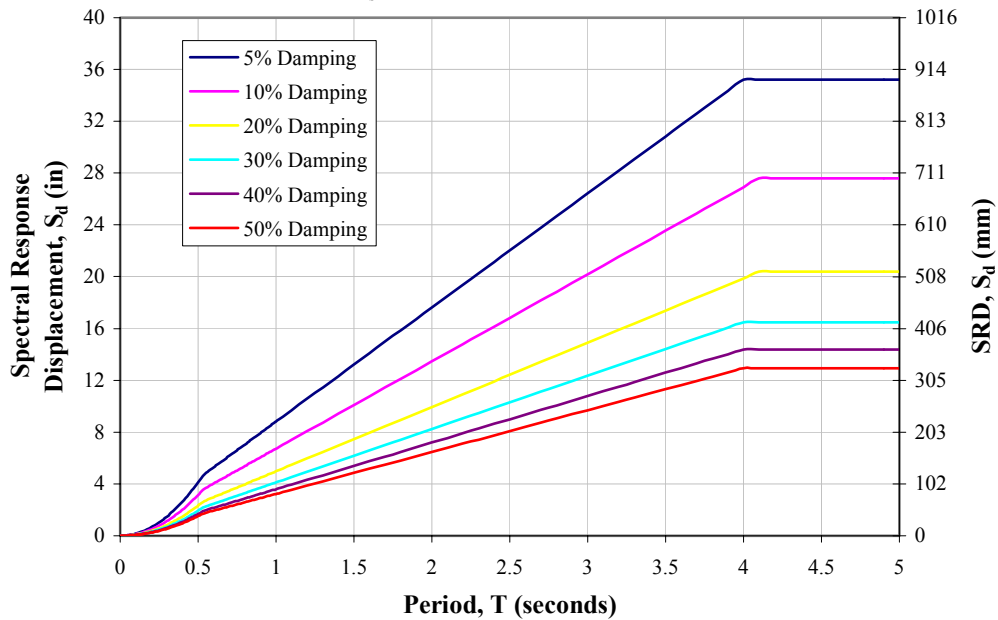


Figure 2.5-4. EQ IV Displacement Response Spectrum (PGA Reduction Factor = 1.0)

In addition to constructing the respective Displacement Response Spectrums, system damping vs. displacement ductility graph is constructed from the desired hysteretic function. For this research, the elasto-perfectly plastic approximation is used for simplicity and basic understanding of DBD procedures. It should be noted that more accurate results are obtained by using a more complex non-linear hysteretic function that includes the Baushinger Effect. The system damping graph represents the amount of expected global damping at various levels of ductility. For this research, the approximate function developed by the author is used and represents a combination of values specified by SEAOC and other references.

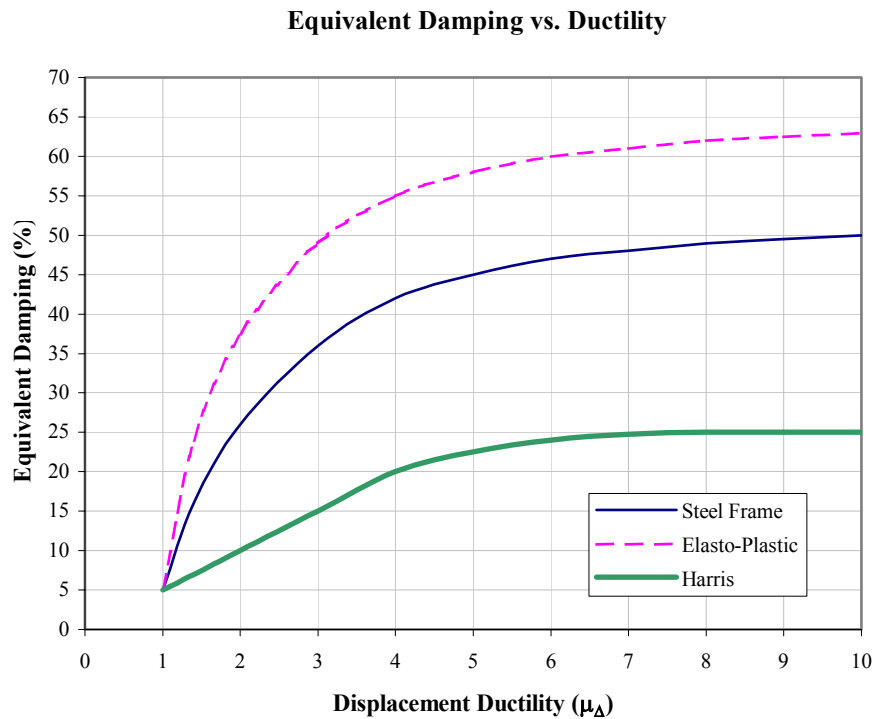


Figure 2.5-5. Equivalent damping vs. displacement ductility (Data from Priestley and Kowalsky, 2000)

Noting the importance of this graph, more accurate damping vs. ductility functions should be further researched.

The remaining DBD steps are frame dependent and are included in the discussion of the various frames listed in Table 2.5-1.

2.5.1 Four (4) Story Frame (FR-4)

Step 3: Determine initial beam depths and plastic rotations.

Once the frame configuration has been finalized as shown in Fig. 2.5.1-1, the design

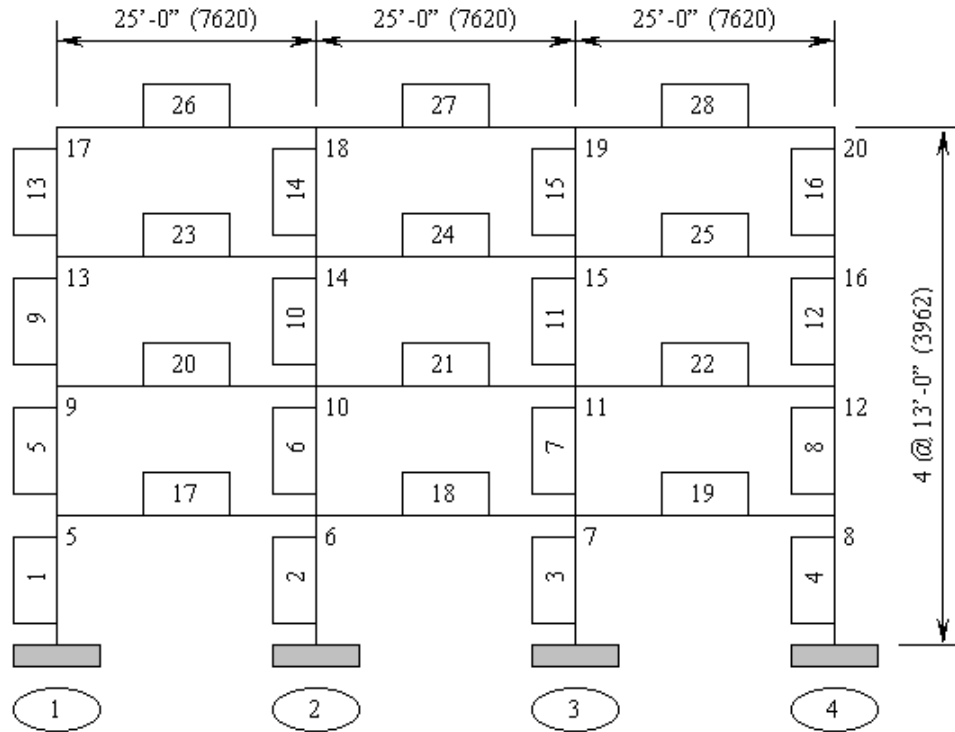


Figure 2.5.1-1. Frame schematic (FR-4)

engineer can start the iterative beam selection process. For simplicity, the design engineer can choose a beam that has a plastic moment capacity that can easily satisfy two times the simple-span gravity load moment demand as discussed in Section 2.3.

$$M_p = 2 \left(\frac{wL^2}{8} \right) \quad (2.5.1-1)$$

For this frame, W24's have been chosen as the beam depths for the wide range of available plastic moment capacities satisfying Eq. (2.5.1-1). Additionally, since the bay lengths are equal, the same beam depth can be used throughout. The question arises what beam depth to use in the upper floors where the moment demands are reduced and would imply the use of lighter shallower beams. For example, the lightest W24 is a W24x55 (W610x82) while the

moment demand would lead the design engineer to select possibly a W18x40 (W460x60). However, the design engineer should be aware of vertical stiffness irregularities. That is by using a W18 at say the top floor in lieu of a W24, the reduced stiffness would in fact cause a higher moment demand on the floor directly below thus possibly affecting the plastic hinge sequencing factor. However, in the same light, since the W24 is stronger than required it will adversely attract higher dynamic demands thus forcing the formation of plastic hinges prior to the lower floors and, likewise, affecting the plastic hinge sequencing factor. For elastic design this is satisfactory; however, in seismic engineering of steel frames, the goal is to, as at least close as possible, design the beams to form plastic hinges simultaneously. While it is true that the beams are sized according to moment demand, the W18 beam in fact has a different plastic rotation capacity thus leading to a local ductility demand different from a W24 beam. Therefore, it can be noted that upper floors will typically possess higher floor overstrengths. If the columns are not designed for this effect, plastic hinges will likely form in the lower columns and a soft story mechanism will develop. Therefore, not only is it necessary to examine the moment demand but additionally the vertical stiffness distribution.

This does emphasize the important point that the effect of the member overstrengths must be considered during the design stage. Additionally, the stronger portions of a frame will increase the plastic hinge sequencing factor by attracting a larger percentage of dynamic inertia forces. That is to say that the equivalent static lateral force distribution will not match the inertia forces, and in effect could force the frame to behave essentially in a higher mode regardless of earthquake characteristics. For capacity-designed frames, these effects are incorporated in the design and, hence, should not concern the design engineer beyond the determination of the numerical representation of these effects.

With the initial beam depths selected, the plastic rotation capacities for each beam can be determined, neglecting axial and shear forces, by employing Eq. (2.5.1-2). The term “yield” is sometimes used to represent the distinction between elastic and inelastic member and system behavior, whereas the synonymous term “plastic” is used in accordance with current steel design notation.

$$\theta_p = \lambda \phi_p \frac{L}{6} = \lambda S_F \phi_m^o \varepsilon_y \frac{L_b}{3d} = 0.42 \varepsilon_y \frac{L_b}{d} \quad (2.5.1-2)$$

where

$$\lambda = 1.10 \text{ (see Section 2.3.5)}$$

$$S_F = 1.14$$

$$\phi_m^o = 1.0$$

$$\varepsilon_y = \frac{F_y}{E} = \frac{50}{29000} = 0.001724$$

Though for this example constant beam depths are selected, system design is based on floor yield mechanisms. Therefore, the floor *equivalent* plastic rotation capacity is set equal to the minimum of all the beams contained in a floor. It might also be justifiable to take the average of the all the local plastic rotations capacities.

Floor (i)	L_{b1}	L_{b2}	L_{b3}	d_1	d_2	d_3	θ_{p1}	θ_{p2}	θ_{p3}	θ_{pi}
Ground	0	0	0	0	0	0	0.00000	0.00000	0.00000	0.00000
2	300	300	300	24	24	24	0.00905	0.00905	0.00905	0.00905
3	300	300	300	24	24	24	0.00905	0.00905	0.00905	0.00905
4	300	300	300	24	24	24	0.00905	0.00905	0.00905	0.00905
Roof	300	300	300	24	24	24	0.00905	0.00905	0.00905	0.00905
$\theta_{p,sys} \Rightarrow$ Average:										0.00905
$\theta_{p,sys} \Rightarrow$ Minimum:										0.00905
EQ I Factor:										1.81

Table 2.5.1-1. Floor equivalent plastic rotations (FR-4)

The system plastic rotation capacity can be determined by either taking the average of the floor rotations or the minimum floor rotation. For this example, it is obvious that the two methods yield the same result.

Similarly, the EQ I modification factor can be determined. Recall that 0.005 was selected as the SP-1 design interstory drift, corresponding to EQ I for this example. As seen, the system

rotation capacity is 0.00905. Note this value would change if different beam depths were selected. The EQ I modification factor would then be $0.00905/0.005 = 1.81$, which leads to a MCE PGA reduction factor of $0.125*1.81 = 0.226$. This in fact leads to an earthquake level closer to the SEAOC recommended mean return period for the service level earthquake. Hence, the DRS for EQ I, Fig. 2.5-1, would then need to be modified using the revised PGA equal to $0.151g$ ($0.226*0.67$). In fact, altering the PGA for EQ I changes the design return period for this performance level.

Additionally as a side note, some engineers believe that interstory drifts within the system elastic region should be limited for the comfort level of the inhabitants, for example, using 0.005 as the target drift at the SP-1 level. However, the author believes this to be slightly misleading. In trying to control the elastic interstory drift the design engineer would be placed into a windmill and possibly find the targets unachievable. Target interstory drift ratios within the elastic region place unneeded stiffness requirements on the frame, which possibly could fail drift targets at high-level earthquakes. In lieu of controlling the interstory drift during low-level earthquakes (EQ I), the structural accelerations should be controlled in order to reduce human perception or awareness of motion. In addition, the engineer shall be careful in assuming an elastic structural system at low-level earthquakes. Low-level earthquakes do not necessarily indicate that local ductility capacities will not exceed yield. To reduce the possibility of local yielding, local curvature ductility shall be examined and section geometry revised if required to obtain the drift target and limit hinge sequencing.

Step 4: Determine target displacement profiles.

The recommended nodal design displacement profiles from the target rotations determined in Step 1 and 3 for a four (4) story frame is determined from Table 2.4-2.

$$\Delta_{di} = \theta_{Ti} h_i \quad (2.5.1-3)$$

The design rotation, θ_{di} , can then be determined from the respective design displacement profile, thus leading to the expected floor rotation ductility, μ_{θ} .

$$\theta_{di} = \frac{\Delta_{di\text{ Drift}}}{h_i} = \frac{\Delta_{di} - \Delta_{di-1}}{h_i} \quad (2.5.1-4)$$

$$\mu_{\theta} = \frac{\theta_{di}}{\theta_{pi}} = \frac{\theta_{Ti}}{\theta_{pi}} \quad (\text{for linear target displacement profiles}) \quad (2.5.1-5)$$

Target Displacements: SP-1 (Operational)

Floor (i)	θ_{Ti}	β	μ_{θ}	Δ_{di}	$\Delta_{di\text{ Drift}}$	θ_{di}	$\Delta_{Ti\text{ Drift}}$	Δ_{Ti}	h_{floor}	h_i
Ground	0.00000	0.000	0.00	0.00	0.00	0.0000	0.00	0.00	0	0
2	0.00905	1.17	1.00	1.41	1.41	0.0091	1.41	1.41	156	156
3	0.00905	1.17	1.00	2.82	1.41	0.0091	1.41	2.82	156	312
4	0.00905	1.17	1.00	4.24	1.41	0.0091	1.41	4.24	156	468
Roof	0.00905	1.17	1.00	5.65	1.41	0.0091	1.41	5.65	156	624

Table 2.5.1-2. SP-1 target displacements (FR-4)

Target Displacements: SP-2 (Occupiable)

Floor (i)	θ_{Ti}	β	μ_{θ}	Δ_{di}	$\Delta_{di\text{ Drift}}$	θ_{di}	$\Delta_{Ti\text{ Drift}}$	Δ_{Ti}	h_{floor}	h_i
Ground	0.000	0.00	0.00	0.00	0.00	0.0000	0.00	0.00	0	0
2	0.018	1.12	1.99	2.81	2.81	0.0180	2.81	2.81	156	156
3	0.018	1.12	1.99	5.62	2.81	0.0180	2.81	5.62	156	312
4	0.018	1.12	1.99	8.42	2.81	0.0180	2.81	8.42	156	468
Roof	0.018	1.12	1.99	11.23	2.81	0.0180	2.81	11.23	156	624

Table 2.5.1-3. SP-2 target displacements (FR-4)

Target Displacements: SP-3 (Life Safe)

Floor (i)	θ_{Ti}	β	μ_{θ}	Δ_{di}	$\Delta_{di\text{ Drift}}$	θ_{di}	$\Delta_{Ti\text{ Drift}}$	Δ_{Ti}	h_{floor}	h_i
Ground	0.000	0.00	0.00	0.00	0.00	0.0000	0.00	0.00	0	0
2	0.032	1.04	3.54	4.99	4.99	0.0320	4.99	4.99	156	156
3	0.032	1.04	3.54	9.98	4.99	0.0320	4.99	9.98	156	312
4	0.032	1.04	3.54	14.98	4.99	0.0320	4.99	14.98	156	468
Roof	0.032	1.04	3.54	19.97	4.99	0.0320	4.99	19.97	156	624

Table 2.5.1-4. SP-3 target displacements (FR-4)

Target Displacements: SP-4 (Near Collapse)

Floor (i)	θ_{Ti}	β	μ_{θ}	Δ_{di}	$\Delta_{di \text{ Drift}}$	θ_{di}	$\Delta_{Ti \text{ Drift}}$	Δ_{Ti}	h_{floor}	h_i
Ground	0.00	0.00	0.00	0.00	0.00	0.0000	0.00	0.00	0	0
2	0.04	1.00	4.42	6.24	6.24	0.0400	6.24	6.24	156	156
3	0.04	1.00	4.42	12.48	6.24	0.0400	6.24	12.48	156	312
4	0.04	1.00	4.42	18.72	6.24	0.0400	6.24	18.72	156	468
Roof	0.04	1.00	4.42	24.96	6.24	0.0400	6.24	24.96	156	624

Table 2.5.1-5. SP-4 target displacements (FR-4)

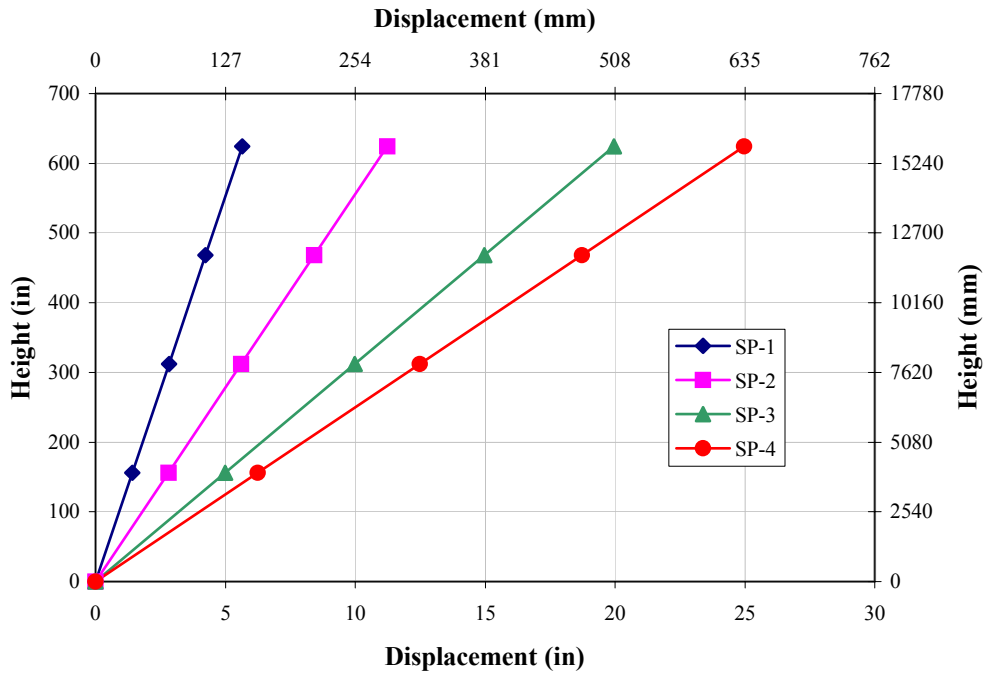


Figure 2.5.1-2. Target displacement profiles (FR-4)

Step 5: Determine effective system displacements.

Using the nodal masses and design displacements determined in Step 4, the effective height, mass, and lateral displacement of the equivalent SDOF system, or “substitute structure” can be determined for each performance level.

$$M_{eff \text{ sys}} = \frac{\sum_{i=1}^n M_i \Delta_{di}}{\Delta_{d \text{ sys}}} = \frac{\sum_{i=1}^n W_i \Delta_{di}}{g \Delta_{d \text{ sys}}} \quad (2.5.1-6)$$

$$h_{eff\ sys} = \frac{\sum_{i=1}^n M_i \Delta_{di} h_i}{\sum_{i=1}^n M_i \Delta_{di}} \quad (2.5.1-7)$$

$$\Delta_{d\ sys} = \frac{\sum_{i=1}^n M_i \Delta_{di}^2}{\sum_{i=1}^n M_i \Delta_{di}} \quad (2.5.1-8)$$

The system displacement ductility can be determined by

$$\mu_{\Delta} = \frac{\Delta_d}{\Delta_y} \quad (2.5.1-9)$$

where

$$\Delta_y = \theta_{T\ sys} h_{eff} = \theta_{p\ sys} h_{eff} \text{ at the SP-1 performance level}$$

SDOF System Properties: SP-1 (Operational)

	Gravity:	32.2						
Floor (i)	W_i	M_i	$M_i \Delta_i$	$M_i \Delta_i^2$	$M_i \Delta_i h_i$	$\Delta_{d\ sys}$	4.24	in.
Ground	0	0	0	0	0	$M_{eff\ sys}$	18925	83% of total
2	182.81	5677	8017	11320	1250635	$h_{eff\ sys}$	468	75% of total
3	182.81	5677	16034	45282	5002539	$\Delta_{y\ sys}$	4.24	in.
4	182.81	5677	24051	101884	11255714	k	1.00	
Roof	182.81	5677	32068	181126	20010157	$\mu_{\Delta\ sys}$	1.00	
Total: Σ	731.25	22710	80169	339612	37519045			

Table 2.5.1-6. SP-1 SDOF system properties (FR-4)

SDOF System Properties: SP-2 (Occupiable)

	Gravity:	32.2						
Floor (i)	W_i	M_i	$M_i \Delta_i$	$M_i \Delta_i^2$	$M_i \Delta_i h_i$	$\Delta_{d\ sys}$	8.42	in.
Ground	0	0	0	0	0	$M_{eff\ sys}$	18925	83% of total
2	182.81	5677	15942	44766	2486977	$h_{eff\ sys}$	468	75% of total
3	182.81	5677	31884	179062	9947907	$\Delta_{y\ sys}$	4.24	in.
4	182.81	5677	47826	402890	22382790	k	1.00	
Roof	182.81	5677	63769	716249	39791627	$\mu_{\Delta\ sys}$	1.99	
Total: Σ	731.25	22710	159422	1342967	74609301			

Table 2.5.1-7. SP-2 SDOF system properties (FR-4)

SDOF System Properties: SP-3 (Life Safe)

		Gravity: 32.2								
Floor (i)	W_i	M_i	$M_i \Delta_i$	$M_i \Delta_i^2$	$M_i \Delta_i h_i$	$\Delta_{d,sys}$	14.98	in.		
Ground	0	0	0	0	0	$M_{eff,sys}$	18925		83%	of total
2	182.81	5677	28342	141481	4421292	$h_{eff,sys}$	468		75%	of total
3	182.81	5677	56683	565925	17685168	$\Delta_{y,sys}$	4.24	in.		
4	182.81	5677	85025	1273332	39791627	k	1.00			
Roof	182.81	5677	113366	2263701	70740671	$\mu_{\Delta,sys}$	3.54			
Total: Σ	731.25	22710	283416	4244440	132638758					

Table 2.5.1-8. SP-3 SDOF system properties (FR-4)

SDOF System Properties: SP-4 (Near Collapse)

		Gravity: 32.2								
Floor (i)	W_i	M_i	$M_i \Delta_i$	$M_i \Delta_i^2$	$M_i \Delta_i h_i$	$\Delta_{d,sys}$	18.72	in.		
Ground	0	0	0	0	0	$M_{eff,sys}$	18925		83%	of total
2	182.81	5677	35427	221065	5526615	$h_{eff,sys}$	468		75%	of total
3	182.81	5677	70854	884258	22106460	$\Delta_{y,sys}$	4.24	in.		
4	182.81	5677	106281	1989581	49739534	k	1.00			
Roof	182.81	5677	141708	3537034	88425839	$\mu_{\Delta,sys}$	4.42			
Total: Σ	731.25	22710	354270	6631938	165798447					

Table 2.5.1-9. SP-4 SDOF system properties (FR-4)

As stated in AISC *Seismic Provisions*, the inelastic rotation of beams is approximately equal to the inelastic drift, hence, evaluating the effective system properties, it can be seen that for linear displacement profiles, $\mu_{\Delta} = \mu_{\theta}$. However, this is not always the case as will be shown in subsequent analysis examples. Therefore, this suggestion should be a final result and not an initial approximation. Furthermore, current codes imply that the structural ductility is equal to the member ductility (Priestley et al, 1996) and following the “equal displacement” approximation, translates to the force reduction factor, R , being equal to the system displacement ductility, μ_{Δ} .

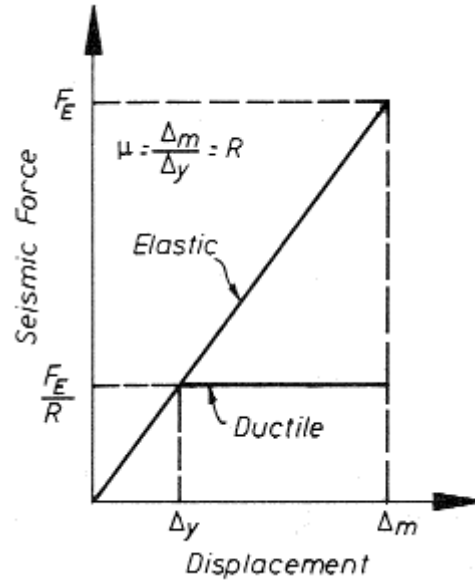


Figure 2.5.1-3. Equal displacement approximation (Paulay and Priestley, 1992)

Current seismic codes (IBC/NEHRP) stipulate that the force reduction factor for a steel special moment frame is eight (8). However, the maximum system displacement ductility at SP-4 for this frame is 4.42. This begins to show that the force reduction factor is in fact dependent on frame configuration, including member geometry, and period. Frames with different bay configurations and/or beam depths will similarly produce different displacement ductilities. Again it shall be noted, that this should be a final result rather than an initial assumption. The difficulty in initially assuming a force reduction factor is the final check to determine if in fact the system contains the ductility capacity required to meet the initial assumed value.

Step 6: Determine effective system properties and base shear.

A system damping vs. displacement ductility graph can be constructed from the desired hysteretic function as shown in Fig. 2.5-5. The design engineer enters the graph with the desired system displacement ductility demand determined in Step 5 and obtains the effective system damping.

Additionally, the effective system period can be determined by entering the respective DRS from Step 2 with the design system displacement determined in Step 5. The effective system stiffness of the equivalent SDOF system can then be determined.

$$K_{eff\ sys} = 4\pi^2 \frac{M_{eff\ sys}}{T_{eff\ sys}^2} \quad (2.5.1-10)$$

Similarly, the effective SDOF system moment of inertia and expected base shear in the considered direction can be established.

$$I_{eff\ sys} = \frac{K_{eff\ sys} h_{eff\ sys}^3}{3E} \quad (2.5.1-11)$$

$$V_b = K_{eff\ sys} \Delta_{d\ sys} \quad (2.5.1-12)$$

The initial stiffness and respective SDOF moment of inertia can be determined considering a positive post-yield stiffness.

$$K_i = K_{eff\ sys} \left(\frac{\mu_\Delta}{r\mu_\Delta - r + 1} \right) \quad (2.5.1-13)$$

where r represents the ratio of post-yield stiffness to initial stiffness. For this document it is assumed that a steel frame will establish a r value of 0.05.

Effective System Properties: SP-4 (Near Collapse)

$\zeta_{eff\ sys}$	22%		$I_{eff\ sys}$	57873	in ⁴
$T_{eff\ sys}$	3.9	sec.	r	0.05	
$K_{eff\ sys}$	49120	lbs/in.	$I_{i\ sys}$	218407	in ⁴
$V_{b\ sys}$	920	Kips			

Table 2.5.1-10. SP-4 effective system properties (FR-4)

Effective System Properties: SP-3 (Life Safe)

$\zeta_{eff\ sys}$	18%		$I_{eff\ sys}$	69612	in ⁴
$T_{eff\ sys}$	3.556	sec.	r	0.05	
$K_{eff\ sys}$	59083	lbs/in.	$I_{i\ sys}$	218409	in ⁴
$V_{b\ sys}$	885	Kips			

Table 2.5.1-11. SP-3 effective system properties (FR-4)

Effective System Properties: SP-2 (Occupiable)

$\zeta_{eff,sys}$	10%		$I_{eff,sys}$	115304	in ⁴
$T_{eff,sys}$	2.763	sec.	r	0.05	
$K_{eff,sys}$	97865	lbs/in.	$I_{i,sys}$	218491	in ⁴
$V_{b,sys}$	824	Kips			

Table 2.5.1-12. SP-2 effective system properties (FR-4)

Effective System Properties: SP-1 (Operational)

$\zeta_{eff,sys}$	5%		$I_{eff,sys}$	218531	in ⁴
$T_{eff,sys}$	2.007	sec.			
$K_{eff,sys}$	185479	lbs/in.			
$V_{by,sys}$	786	Kips			
$V_{b,sys,.005}$	434	Kips			

Table 2.5.1-13. SP-1 effective system properties (FR-4)

With the initial base shear and design displacements determined the target system force-deformation response graph can be plotted as shown in Fig. 2.5.1-3.

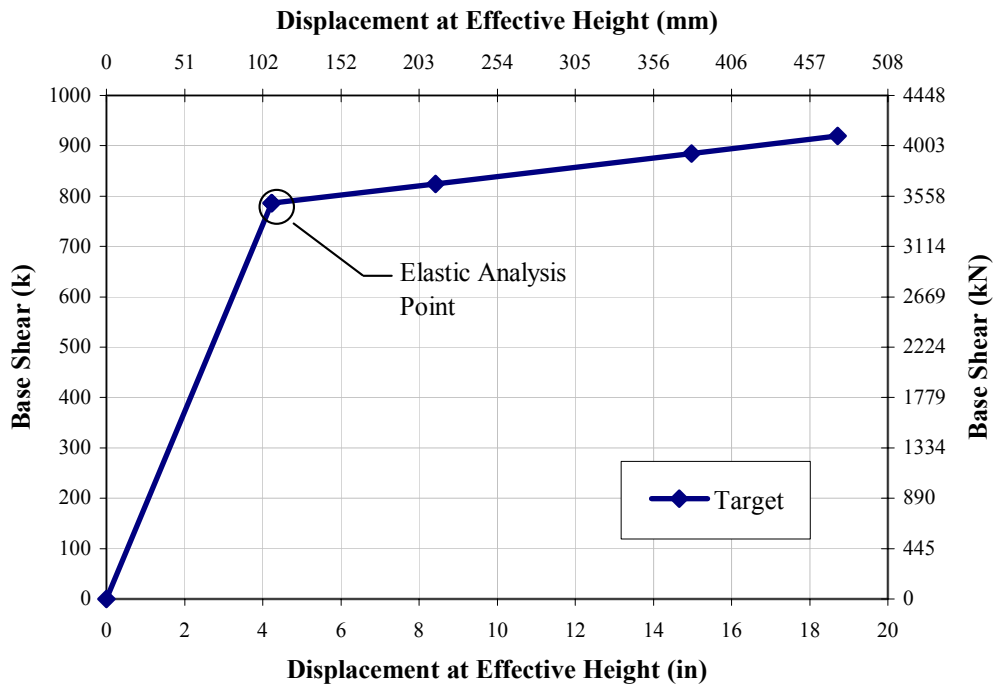


Figure 2.5.1-3. System force-displacement graph (FR-4)

As seen in Fig. 2.5.1-3, the design base shear steadily increases from SP-1 to SP-4, which happens to be the maximum design base shear. This proves that the initially assumed target interstory drifts and corresponding PGA reduction factor from step 1 and 2 were appropriately chosen. That is SP-4 was assumed to be the controlling design performance level, and, hence, the other PGA reduction factors (ratio of target to maximum) were proportioned accordingly. If during this step one of the other performance levels (possibly by using different target drifts in Step 1) dictates a higher expected base shear than the assumed controlling level the design engineer would need to return to step 2 and re-calculate the PGA reduction factors accordingly. Additionally, the term PGA reduction factor would then be misleading, for any performance level beyond the controlling level would in fact be a PGA amplification factor. For example, if SP-3, with an example target drift of 0.26, controlled with the highest design base shear, the SP-4 PGA reduction factor would then be $0.04/0.026 = 1.54$ (amplification) and hence would be applied to EQ III when constructing the EQ IV earthquake spectrums (but not greater than the MCE PGA).

Step 7: Vertical base shear distribution and analysis.

The base shears determined in Step 6 can be vertically distributed by

$$F_{xi} = V_b \frac{M_i \Delta_{di}}{\sum_{i=1}^n M_i \Delta_{di}} \quad (2.5.1-14)$$

Equivalent Static Lateral Forces (kips):

	SP-1		SP-2		SP-3		SP-4	
Floor (i)	F_{yi}	$F_{yi} \Omega_{sys}$	F_i	$F_i \Omega_{sys}$	F_i	$F_i \Omega_{sys}$	F_i	$F_i \Omega_{sys}$
Ground	0	0	0	0	0	0	0	0
2	79	118	82	124	88	133	92	138
3	157	236	165	247	177	265	184	276
4	236	354	247	371	265	398	276	414
Roof	314	471	330	495	354	531	368	552
Total:	786	1179	824	1237	885	1327	920	1379

Table 2.5.1-14. Equivalent static lateral forces (FR-4)

Since steel members are designed for the plastic moment demand using the elasto-perfectly plastic bi-linear approximation, the SP-1 design base shear can be used to analyze and design the system using a standard elastic analysis. Though it is noted that a true elastic analysis, including a push-over analysis, is conservative, possibly over-estimating the frame strength. As will be discussed in Part 3, a 2nd order inelastic limit-state static analysis or “Advanced Analysis” is the recommended analysis procedure. Additionally, since the design displacement profile is linear, there is no lateral force modifications required (following EYA guidelines).

An elastic 2nd order analysis, or $P-\Delta$ analysis, was utilized to analyze the test frame for the equivalent static lateral forces, determined at the SP-1 performance level, and gravity loads. It is assumed that the demands from the uniformly distributed gravity loads are small compared to the seismic moment demands and are considered negligible as discussed previously. Therefore, gravity loads were applied at the joints as concentrated loads (see Section 1.2.3).

As previously discussed in Section 2.4.6, the design engineer should implement Capacity Design procedures during the analysis and design stage. During the design process member overstrengths were calculated and similarly used in the design of the columns. The system member overstrength factor was determined to be approximately 1.25, with the top floor having the largest floor overstrength, and the plastic hinge sequencing factor was assumed to be 1.2. This leads to a system performance overstrength factor, Ω_{sys} , of approximately 1.5. This factor is then applied to the expected system force-deformation graph determined in step 6 as shown in Fig. 2.5.1-4. Since strength is proportional to stiffness, the system overstrength factors affect both the base shear capacity and target displacement. The system yield displacement is a function of beam geometry; therefore, this value does not change if the beam depths do not change. However, the base shear capacity increases due to member overstrength of the beams and base columns. In order to account for this effect, the design base shear capacity is increased by the system member overstrength while maintaining the same system yield displacement. Additionally, the corner point can then be located by applying the plastic hinge sequencing factor to the previously adjusted base shear and

multiply the system yield displacement by the ratio of system overstrength to system member overstrength.

$$\Delta_p = \Delta_y \frac{\Omega_{sys}}{\phi_{s,sys}^o} \quad (2.5.1-15)$$

The remaining performance levels are modified by increasing the predicted base shear by the system overstrength factor while maintaining the same target displacement. In theory, if the static lateral forces were increased by the respective floor overstrength factor and then analyzed, the moment demands at the desired plastic hinges would match the plastic moment capacity if all other mechanisms remain constant.

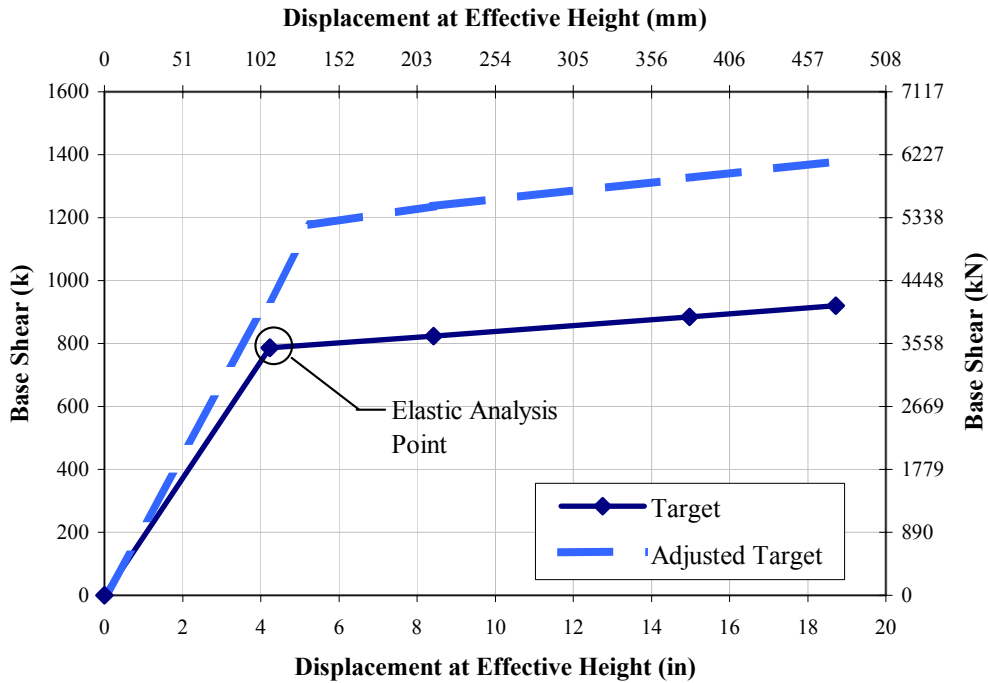


Figure 2.5.1-4. System force-displacement graph (FR-4)

The final frame design is shown in Fig. 2.5.1-5 and SP-1 pseudo-elastic displacement profile is shown in Fig. 2.5.1-6.

Evaluating the results from the elastic analysis, the base hinges have not yet formed, including the capacity reduction for the effects of axial load and shear. Therefore, the lower stiffer portion of the frame behaves similar to a braced frame while producing increased displacement demands on the stronger upper floors as seen in Fig. 2.5.1-6. In effect this is the first indication of hinge sequencing since the upper floors have a higher displacement demand, hence, a higher rotation demand. This will ultimately allow plastic hinges to develop in the upper floors prior to the any plastic hinges forming in the base and/or the lower floors. This will additionally produce variations in final local displacement and rotation ductility. Still there is good agreement between the predicted target displacement profile and the elastic analysis results.

The only technique currently used to check the formation of plastic hinges in this process is to evaluate the force demands (interaction equations) from the elastic analysis. If base hinges had formed, the elastic analysis would need to be re-run with true hinges and applied concentrated plastic moments at the base. Since the displacement profiles are linear allowing the use of a non-modified elastic analysis and using the bi-linear elasto-perfectly plastic approximation, the design is satisfactory. Additionally, the small variations in profiles are of no great concern for capacity design will incorporate any additional design factors.

2.5.2 Four (4) Story Frame (FR-4-W21)

In addition to the previously described and designed four (4) story frame (FR-4), two other similar frames were designed while maintaining the same targets determined previously in Section 2.5.1. The first frame (FR-4-W21) was designed using only W21 (W530) beams while maintaining the same demand and targets determined by the SP-1 performance level using all W24 (W610) beams. The complete system force-displacement graph is shown in Fig. 2.5.2-1.

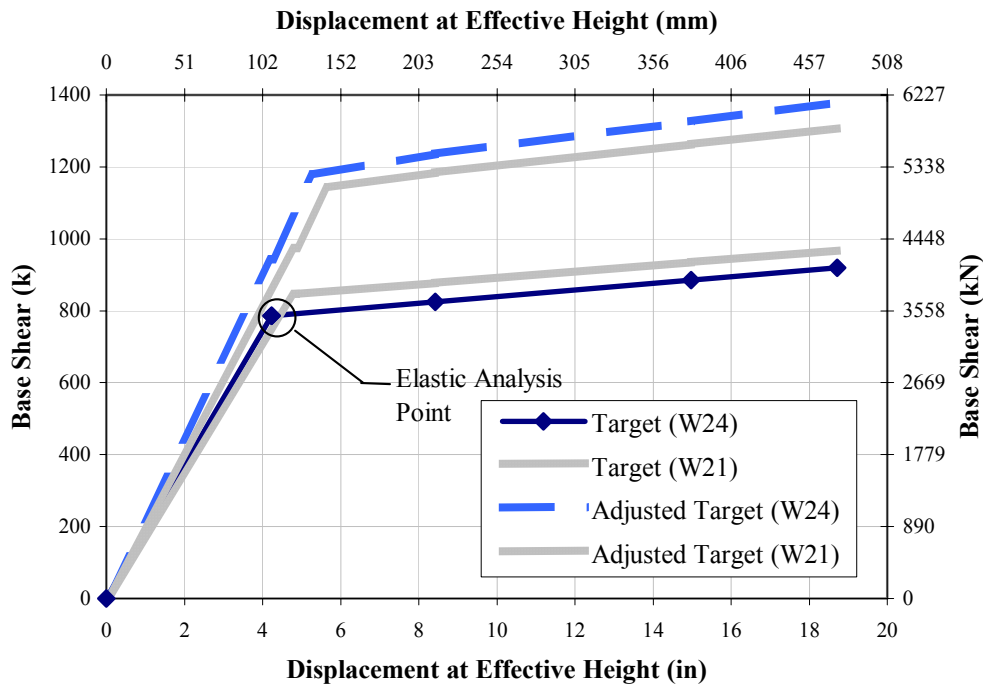


Figure 2.5.2-1. System force-displacement graph (FR-4-W21)

The shaded curves in Fig. 2.5.2-1 represent the predicted values for a frame if W21 (W530) beams were actually used in the procedures detailed previously. Due to the decreased beam depths there is an increase in the W21 system yield displacement capacity of this frame. This results in an increase in the effective period at the SP-1 performance level. Therefore, there is a slight increase in the design base shear and decrease in the system displacement ductility. Additionally, the W21 system member overstrength is reduced due to closer spacing of adjacent plastic moment capacities indicating an overall decrease in the expected “as designed” base shear. The final frame design is shown in Fig. 2.5.2-2 and the SP-1 displacement profile is shown in Fig. 2.5.2-3.

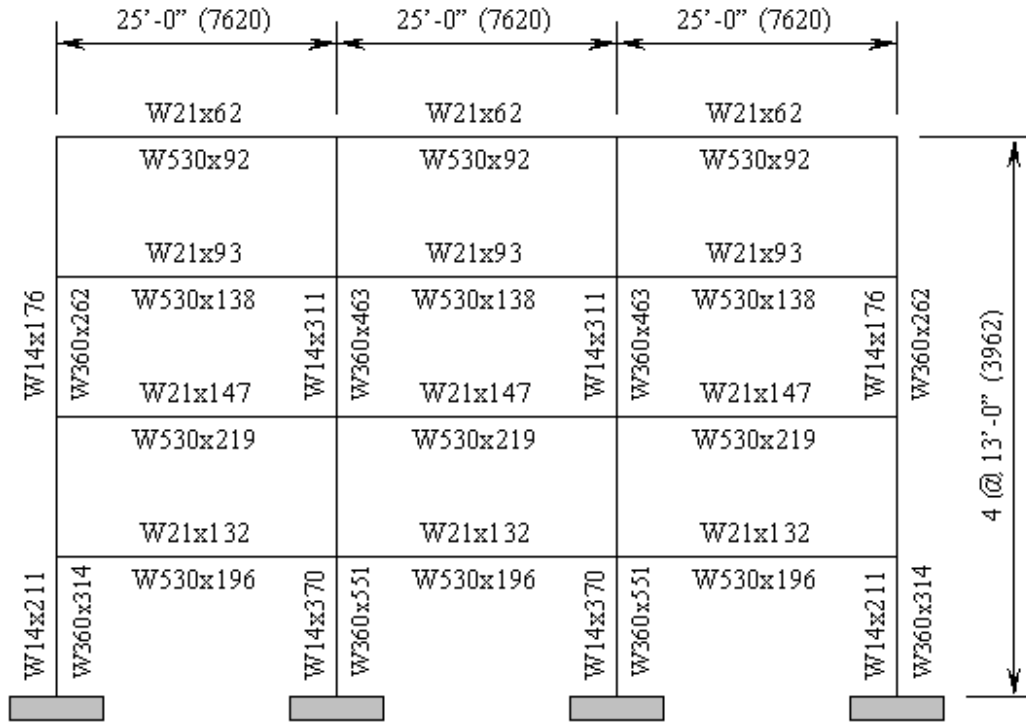


Figure 2.5.2-2. Final Schematic (FR-4-W21)

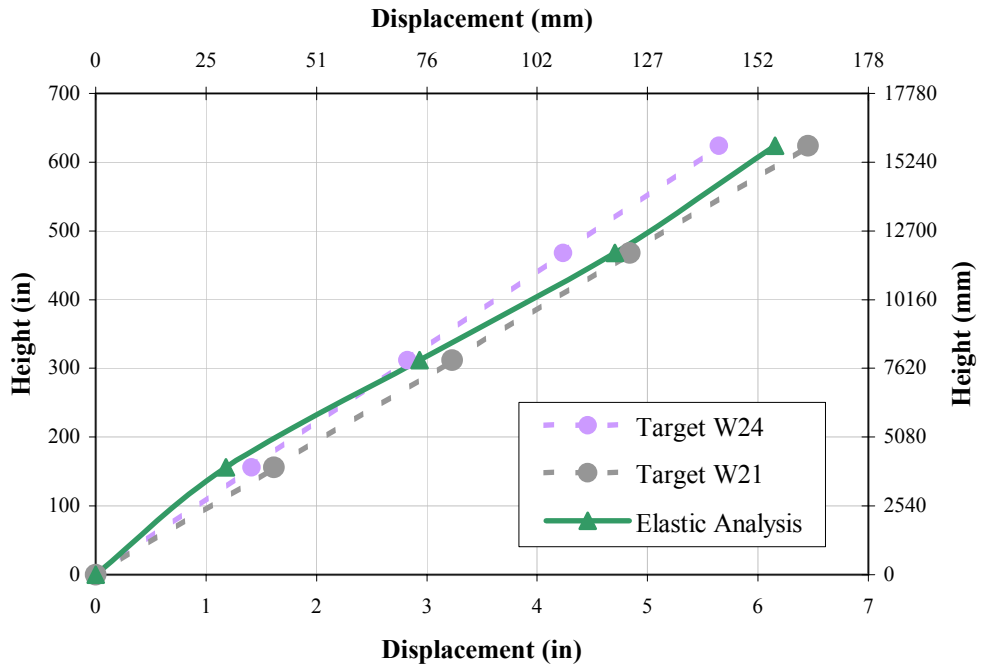


Figure 2.5.2-3. SP-1 displacement profile (FR-4-W21)

As can be seen in Fig. 2.5.2-3, similar to the previous FR-4 discussion, the base hinges have not yet formed. In fact the base is stronger than required since the same FR-4 columns were used in this test frame, thus providing a higher total base column member overstrength than that determined for FR-4. This overstrength is counteracted in the determination of the system member overstrength by the reduced beam member overstrength. Furthermore, the reduced stiffness, by use of W21 (W520) beams, has produced increased displacement demands in the upper floors tending towards the W21 target displacement profile. The purpose of this test frame is to show the importance of accurate target calculations while consistently maintaining the initial assumptions on the final frame behavior.

2.5.3 Four (4) Story Frame (FR-4-W24)

The second frame (FR-4-W24) was designed by reducing the SP-1 static lateral forces by the system member overstrength factor, $\phi_{sys}^o = 1.25$, while maintaining W24 (W610) beams and the same columns as designed previously in Section 2.5.1. It seems plausible that the design engineer can attempt to counteract the strengthening effect of member overstrengths by incorporating them into the design as a reduction factor to the applied lateral forces. Therefore, when the actual member overstrengths take effect, the frame behavior would be as initially predicted with the only unforeseen overstrengths coming from plastic hinge sequencing. That is the same system overstrength value is still developed, $\Omega_{sys} = 1.5$, and is applied to the elastic analysis point. The system force-displacement graph is shown in Fig. 2.5.3-1.

In fact this process would decrease the system stiffness and strength of the frame. The system yield displacement and design displacement ductility remain constant with the only decrease occurring in the base shear. Ultimately, this procedure under-predicts the damage level at the SP-1 performance level and, therefore, an increase in lateral. Furthermore, this process is more time consuming than correctly applying the overstrength to post-yield predicted values and likewise is not recommended.

The final frame design is shown in Fig. 2.5.2-2 and the SP-1 displacement profile is shown in Fig. 2.5.2-3.

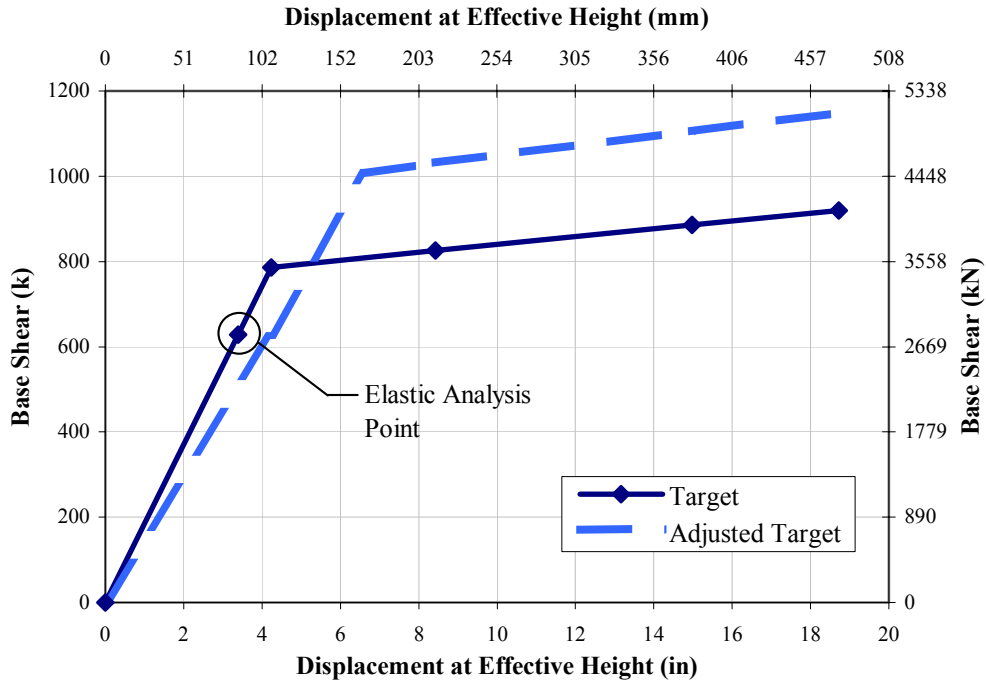


Figure 2.5.3-1. System force-displacement graph (FR-4-W24)

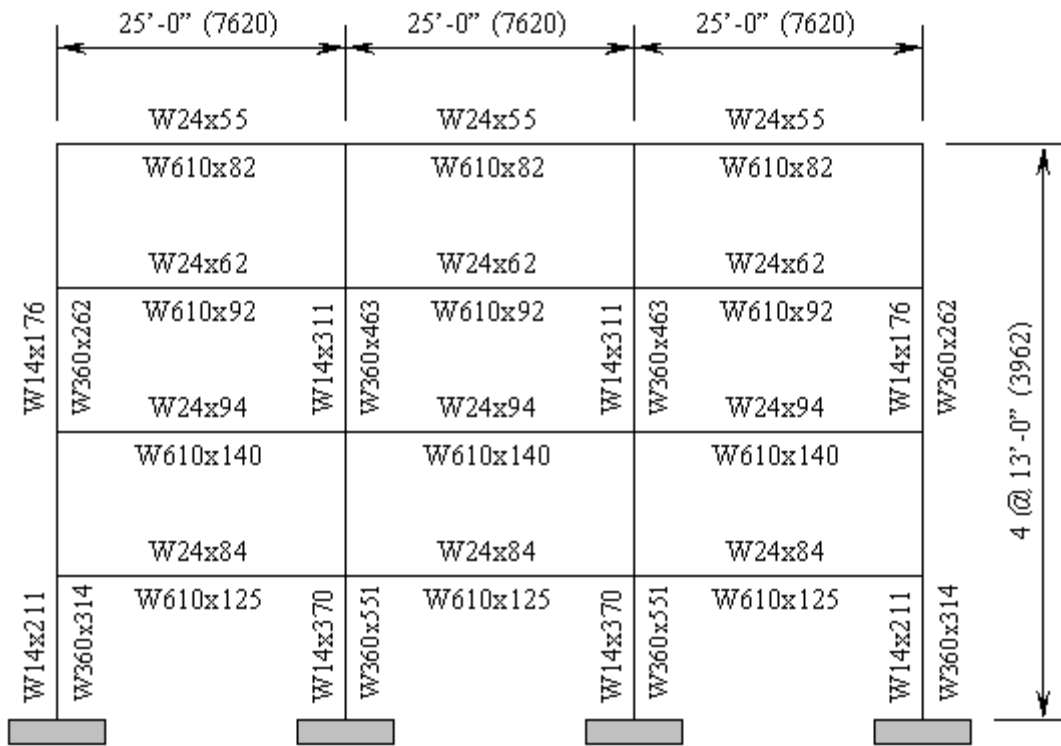


Figure 2.5.3-2. Final schematic (FR-4-W24)

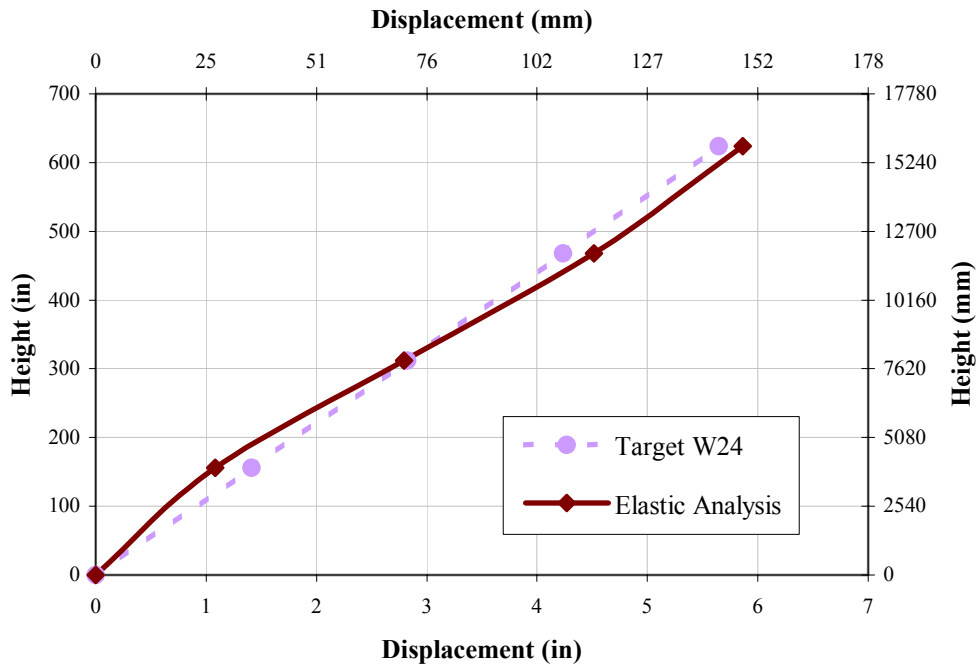


Figure 2.5.3-3. SP-1 displacement profile (FR-4-W24)

Reducing the SP-1 lateral forces in order to inherently account for the system member overstrength reduces the frame stiffness as expected. Hence, when subjected to the actual SP-1 lateral forces, increased lateral displacements are seen in Fig. 2.5.2-6. Due to the same column sizes being used as FR-4, thus preventing hinges from forming at the base, there is a decrease in lateral displacements in the lower floors. Additionally, though there is an increase in the total base column member overstrength, there is an overall decrease in the system member overstrength, seen in Fig. 2.5.3-1. In fact the column sizes can be reduced with the anticipation that this will result in increased lateral displacements. It is also clear that plastic hinges will form prior to obtaining the required strength at the SP-1 level (global yield mechanism) due to the use of reduced demands to determine the plastic capacities. This will ultimately under-predict the damage level at the SP-1 performance level. It is for this reason that this procedure is not recommended. Furthermore, this procedure will lead to inaccurate ultimate displacement ductility and, hence, unrepresentative of the final damage level.

Since the bay lengths are different and the same floor target plastic rotation is desired, the design engineer can select the beam depth for the short bays from Fig. 2.5.4-2 (developed using the same equations and factors as previously used in FR-4).

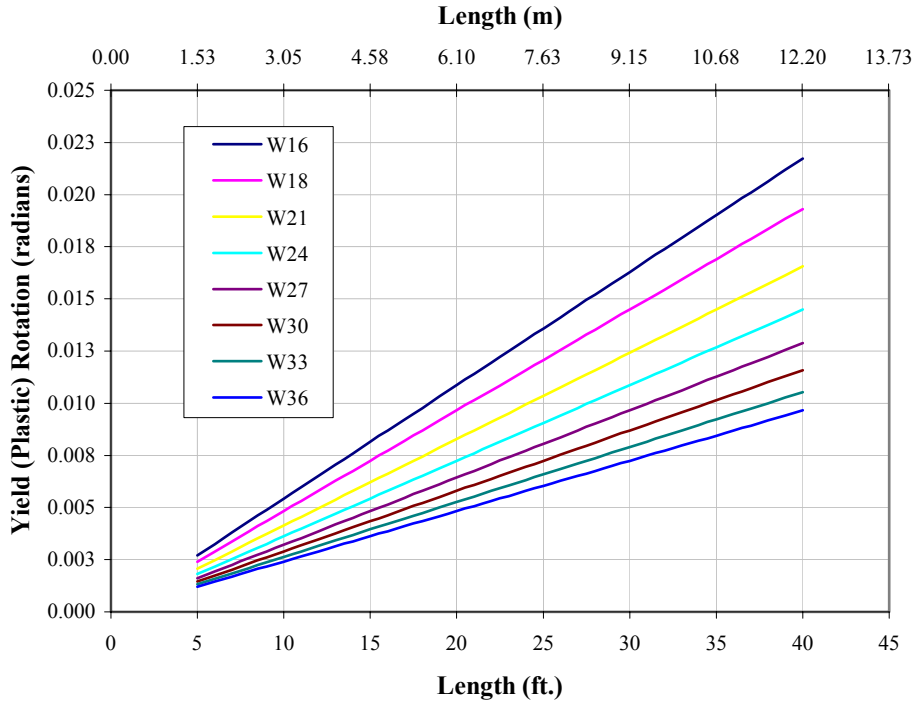


Figure 2.5.4-2. Beam Rotation Chart

The design engineer enters Fig. 2.5.4-2 with the rotation target of the longest bay and the length of the other bays and determines the required beam depth. Since a W24 was selected for the beam depth for the 30'-0" (9.15 m) bay, the corresponding beam depth for the 22'-6" (6.86 m) bay with approximately the same plastic rotation is a W18.

Floor (i)	L_{b1}	L_{b2}	L_{b3}	d_1	d_2	d_3	θ_{p1}	θ_{p2}	θ_{p3}	θ_{pi}
Ground	0	0	0	0	0	0	0.00000	0.00000	0.00000	0.00000
2	270	360	270	18	24	18	0.01086	0.01086	0.01086	0.01086
3	270	360	270	18	24	18	0.01086	0.01086	0.01086	0.01086
4	270	360	270	18	24	18	0.01086	0.01086	0.01086	0.01086
Roof	270	360	270	18	24	18	0.01086	0.01086	0.01086	0.01086
$\theta_{p\ sys} \Rightarrow$ Average:										0.01086
$\theta_{p\ sys} \Rightarrow$ Minimum:										0.01086
EQ I Factor:										2.17

Table 2.5.4-1. Floor equivalent plastic rotations (FR-4a)

It is by coincidence that the plastic rotation capacity for the W24 and W18 are identical for the respective bay lengths. Note that the EQ I factor has also been modified according to the revised system plastic rotation capacity, leading to a PGA reduction factor for EQ I of 0.271. This begins to show that the system yield mechanism is a function of system configuration. Furthermore, the assumed force reduction factor, R , in current seismic design is in fact not constant for respective frames (i.e. SMRF) and, therefore, is a function of beam geometry and system configuration. This means that two identical steel moment frames (overall dimensions and height) consisting of different bay lengths and beam depths will not have identical force reduction factors, nor will they have the same level of damage if subjected to identical earthquakes. Similar to Fig. 2.5.4-3, a graph can be constructed of expected rotation ductility versus beam length.

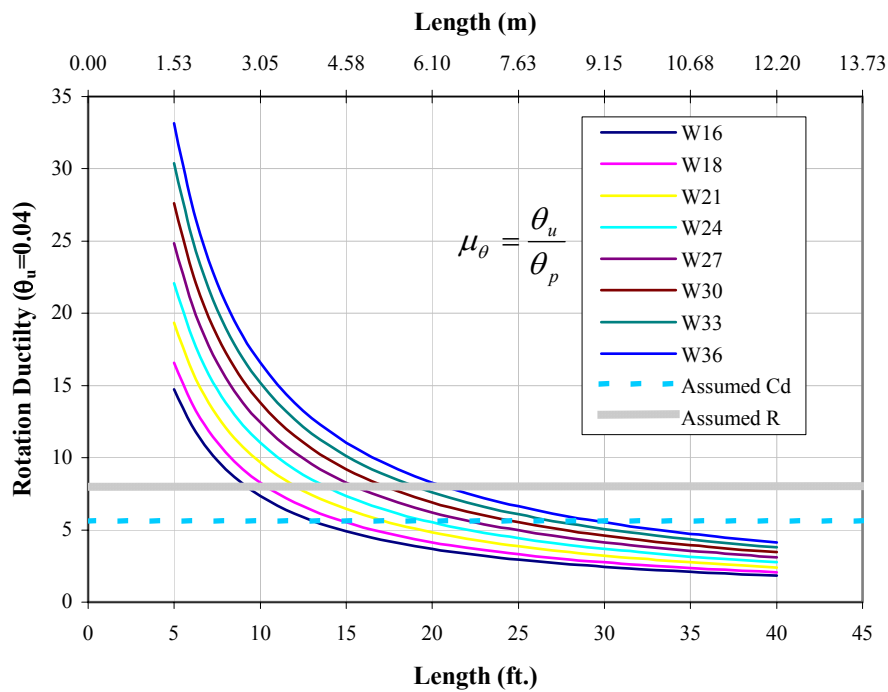


Figure 2.5.4-3. Beam rotation ductility chart

As can be seen in Fig. 2.5.4-3, theoretically the assumed force reduction factor occurs at a distinct point based on beam depth and length for a given ultimate rotation target. Hence, specifying a force reduction factor prior to beam selection and determination of rotation capacity is invalid.

Step 4: Determine target displacement profiles.

Target Displacements: SP-1 (Operational)

Floor (i)	θ_{Ti}	β	μ_{θ}	Δ_{di}	Δ_{di} Drift	θ_{di}	Δ_{Ti} Drift	Δ_{Ti}	h_{floor}	h_i
Ground	0.0000	0.000	0.00	0.00	0.00	0.0000	0.00	0.00	0	0
2	0.0109	1.13	1.00	1.69	1.69	0.0109	1.69	1.69	156	156
3	0.0109	1.13	1.00	3.39	1.69	0.0109	1.69	3.39	156	312
4	0.0109	1.13	1.00	5.08	1.69	0.0109	1.69	5.08	156	468
Roof	0.0109	1.13	1.00	6.78	1.69	0.0109	1.69	6.78	156	624

Table 2.5.4-2. SP-1 target displacements (FR-4a)

Target Displacements: SP-2 (Occupiable)

Floor (i)	θ_{Ti}	β	μ_{θ}	Δ_{di}	Δ_{di} Drift	θ_{di}	Δ_{Ti} Drift	Δ_{Ti}	h_{floor}	h_i
Ground	0.000	0.00	0.00	0.00	0.00	0.000	0.00	0.00	0	0
2	0.018	1.10	1.66	2.81	2.81	0.018	2.81	2.81	156	156
3	0.018	1.10	1.66	5.62	2.81	0.018	2.81	5.62	156	312
4	0.018	1.10	1.66	8.42	2.81	0.018	2.81	8.42	156	468
Roof	0.018	1.10	1.66	11.23	2.81	0.018	2.81	11.23	156	624

Table 2.5.4-3. SP-2 target displacements (FR-4a)

Target Displacements: SP-3 (Life Safe)

Floor (i)	θ_{Ti}	β	μ_{θ}	Δ_{di}	Δ_{di} Drift	θ_{di}	Δ_{Ti} Drift	Δ_{Ti}	h_{floor}	h_i
Ground	0.000	0.00	0.00	0.00	0.00	0.000	0.00	0.00	0	0
2	0.032	1.03	2.95	4.99	4.99	0.032	4.99	4.99	156	156
3	0.032	1.03	2.95	9.98	4.99	0.032	4.99	9.98	156	312
4	0.032	1.03	2.95	14.98	4.99	0.032	4.99	14.98	156	468
Roof	0.032	1.03	2.95	19.97	4.99	0.032	4.99	19.97	156	624

Table 2.5.4-4. SP-3 target displacements (FR-4a)

Target Displacements: SP-4 (Near Collapse)

Floor (i)	θ_{Ti}	β	μ_{θ}	Δ_{di}	Δ_{di} Drift	θ_{di}	Δ_{Ti} Drift	Δ_{Ti}	h_{floor}	h_i
Ground	0.00	0.00	0.00	0.00	0.00	0.00	0.00	0.00	0	0
2	0.04	1.00	3.68	6.24	6.24	0.04	6.24	6.24	156	156
3	0.04	1.00	3.68	12.48	6.24	0.04	6.24	12.48	156	312
4	0.04	1.00	3.68	18.72	6.24	0.04	6.24	18.72	156	468
Roof	0.04	1.00	3.68	24.96	6.24	0.04	6.24	24.96	156	624

Table 2.5.4-5. SP-4 target displacements (FR-4a)

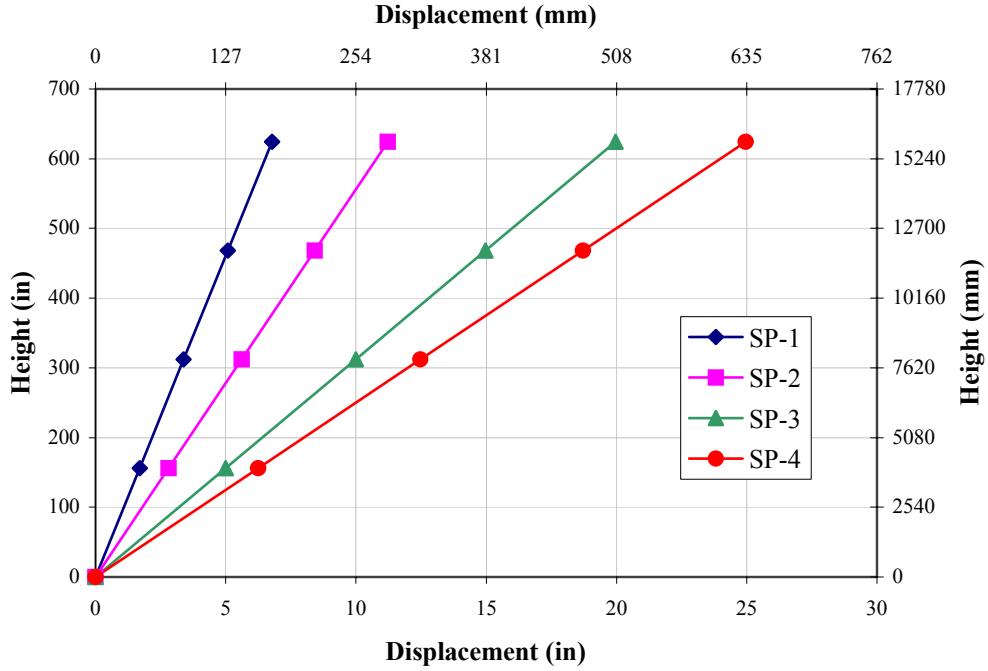


Figure 2.5.4-4. Target displacement profiles (FR-4a)

Step 5: Determine effective system displacements.

SDOF System Properties: SP-1 (Operational)

Gravity:		32.2			
Floor (i)	W_i	M_i	$M_i \Delta_i$	$M_i \Delta_i^2$	$M_i \Delta_i h_i$
Ground	0	0	0	0	0
2	182.81	5677	9620	16301	1500762
3	182.81	5677	19241	65206	6003047
4	182.81	5677	28861	146712	13506856
Roof	182.81	5677	38481	260822	24012189
Total: Σ	731.25	22710	96203	489041	45022854

$\Delta_{d,sys}$	5.08	in.	
$M_{eff,sys}$	18925	83%	of total
$h_{eff,sys}$	468	75%	of total
$\Delta_{y,sys}$	5.08	in.	
k	1.00		
$\mu_{\Delta,sys}$	1.00		

Table 2.5.4-6. SP-1 SDOF system properties (FR-4a)

SDOF System Properties: SP-2 (Occupiable)

Gravity:		32.2					
Floor (i)	W_i	M_i	$M_i \Delta_i$	$M_i \Delta_i^2$	$M_i \Delta_i h_i$	$\Delta_{d,sys}$	8.42 in.
Ground	0	0	0	0	0	$M_{eff,sys}$	18925 83% of total
2	182.81	5677	15942	44766	2486977	$h_{eff,sys}$	468 75% of total
3	182.81	5677	31884	179062	9947907	$\Delta_{y,sys}$	5.08 in.
4	182.81	5677	47826	402890	22382790	k	1.00
Roof	182.81	5677	63769	716249	39791627	$\mu_{\Delta,sys}$	1.66
Total: Σ	731.25	22710	159422	1342967	74609301		

Table 2.5.4-7. SP-2 SDOF system properties (FR-4a)

SDOF System Properties: SP-3 (Life Safe)

Gravity:		32.2					
Floor (i)	W_i	M_i	$M_i \Delta_i$	$M_i \Delta_i^2$	$M_i \Delta_i h_i$	$\Delta_{d,sys}$	14.98 in.
Ground	0	0	0	0	0	$M_{eff,sys}$	18925 83% of total
2	182.81	5677	28342	141481	4421292	$h_{eff,sys}$	468 75% of total
3	182.81	5677	56683	565925	17685168	$\Delta_{y,sys}$	5.08 in.
4	182.81	5677	85025	1273332	39791627	k	1.00
Roof	182.81	5677	113366	2263701	70740671	$\mu_{\Delta,sys}$	2.95
Total: Σ	731.25	22710	283416	4244440	132638758		

Table 2.5.4-8. SP-3 SDOF system properties (FR-4a)

SDOF System Properties: SP-4 (Near Collapse)

Gravity:		32.2					
Floor (i)	W_i	M_i	$M_i \Delta_i$	$M_i \Delta_i^2$	$M_i \Delta_i h_i$	$\Delta_{d,sys}$	18.72 in.
Ground	0	0	0	0	0	$M_{eff,sys}$	18925 83% of total
2	182.81	5677	35427	221065	5526615	$h_{eff,sys}$	468 75% of total
3	182.81	5677	70854	884258	22106460	$\Delta_{y,sys}$	5.08 in.
4	182.81	5677	106281	1989581	49739534	k	1.00
Roof	182.81	5677	141708	3537034	88425839	$\mu_{\Delta,sys}$	3.68
Total: Σ	731.25	22710	354270	6631938	165798447		

Table 2.5.4-9. SP-4 SDOF system properties (FR-4a)

Evaluation of the previous data reveals that the force reduction factor is in fact dependent on frame configuration, including member geometry, and period. Furthermore, frames with different bay configurations and/or beam depths will have different ductility capacities. This contradicts the assumption in current FBD that all frames in a structure can be designed to yield simultaneously. That is parallel frames with different bay lengths and beam depths will

not yield simultaneously unless beam depths are selected in proportion to the bay lengths as discussed previously.

Step 6: Determine effective system properties and base shear.

Effective System Properties: SP-4 (Near Collapse)

$\zeta_{eff\ sys}$	18%		$I_{eff\ sys}$	67921	in ⁴
$T_{eff\ sys}$	3.6	sec.	r	0.05	
$K_{eff\ sys}$	57648	lbs/in.	$I_{i\ sys}$	220540	in ⁴
$V_{b\ sys}$	1079	Kips			

Table 2.5.4-10. SP-4 effective system properties (FR-4a)

Effective System Properties: SP-3 (Life Safe)

$\zeta_{eff\ sys}$	15%		$I_{eff\ sys}$	82120	in ⁴
$T_{eff\ sys}$	3.274	sec.	r	0.05	
$K_{eff\ sys}$	69700	lbs/in.	$I_{i\ sys}$	220476	in ⁴
$V_{b\ sys}$	1044	Kips			

Table 2.5.4-11. SP-3 effective system properties (FR-4a)

Effective System Properties: SP-2 (Occupiable)

$\zeta_{eff\ sys}$	10%		$I_{eff\ sys}$	137520	in ⁴
$T_{eff\ sys}$	2.53	sec.	r	0.05	
$K_{eff\ sys}$	116721	lbs/in.	$I_{i\ sys}$	220641	in ⁴
$V_{b\ sys}$	1278	Kips			

Table 2.5.4-12. SP-2 effective system properties (FR-4a)

Effective System Properties: SP-1 (Operational)

$\zeta_{eff\ sys}$	5%		$I_{eff\ sys}$	220504	in ⁴
$T_{eff\ sys}$	1.998	sec.			
$K_{eff\ sys}$	187153	lbs/in.			
$V_{by\ sys}$	951	Kips			
$V_{b\ sys\ .005}$	438	Kips			

Table 2.5.4-13. SP-1 effective system properties (FR-4a)

Step 7: Vertical base shear distribution and analysis.

Equivalent Static Lateral Forces:

Floor (i)	SP-1		SP-2		SP-3		SP-4	
	F_{yi}	$F_{yi} \Omega_{sys}$	F_i	$F_i \Omega_{sys}$	F_i	$F_i \Omega_{sys}$	F_i	$F_i \Omega_{sys}$
Ground	0	0	0	0	0	0	0	0
2	95	124	98	128	104	136	108	140
3	190	247	197	256	209	271	216	281
4	285	371	295	383	313	407	324	421
Roof	381	495	393	511	418	543	432	561
Total:	951	1237	983	1278	1044	1357	1079	1403

Table 2.5.4-14. Equivalent static lateral forces (FR-4a)

The system member overstrength factor was determined to be approximately 1.10 and the plastic hinge sequencing factor was assumed to be 1.2. This leads to a system performance overstrength factor, Ω_{sys} , of approximately 1.3. This factor is then applied to the expected system force-deformation graph shown in Fig. 2.5.4-5.

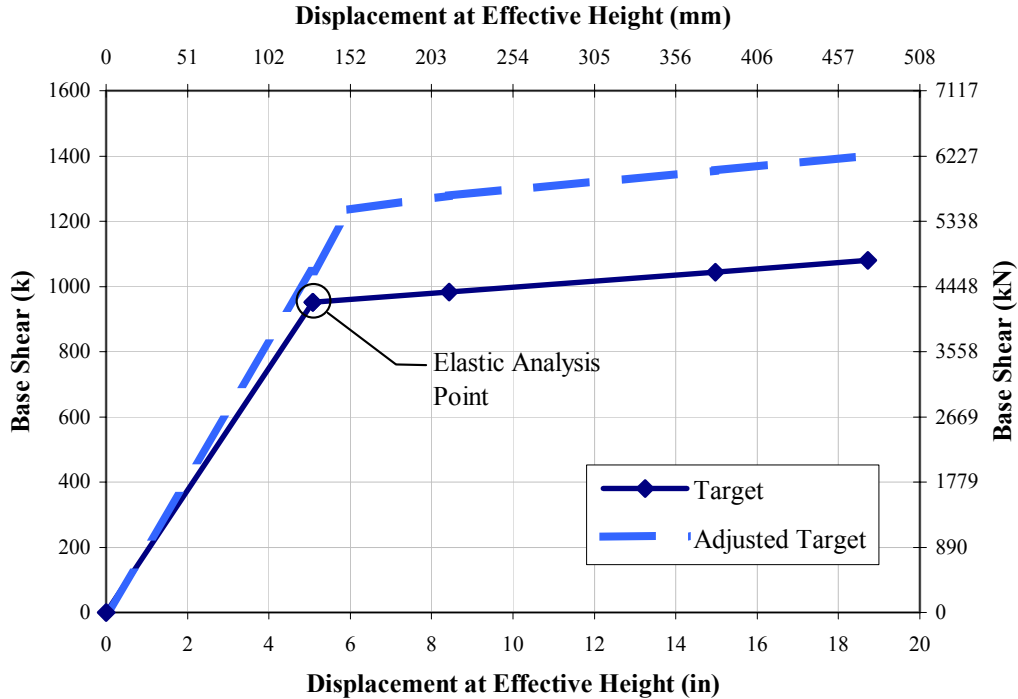


Figure 2.5.4-5. System force-displacement graph with Overstrength (FR-4a)

The final frame design is shown in Fig. 2.5.4-6 and the SP-1 displacement profile is shown in Fig. 2.5.4-7.

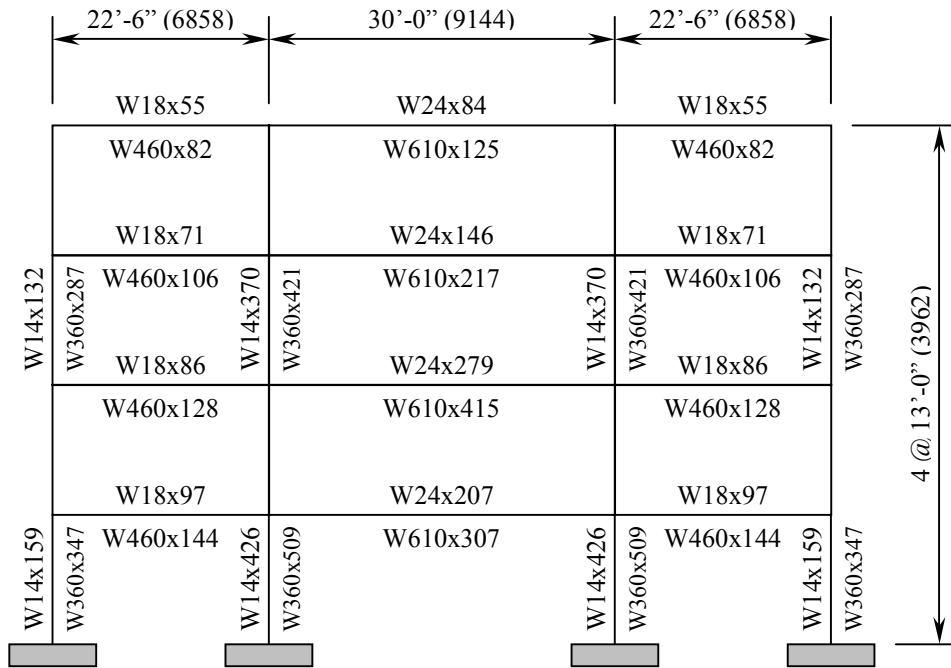


Figure 2.5.4-6. Final frame schematic (FR-4a)

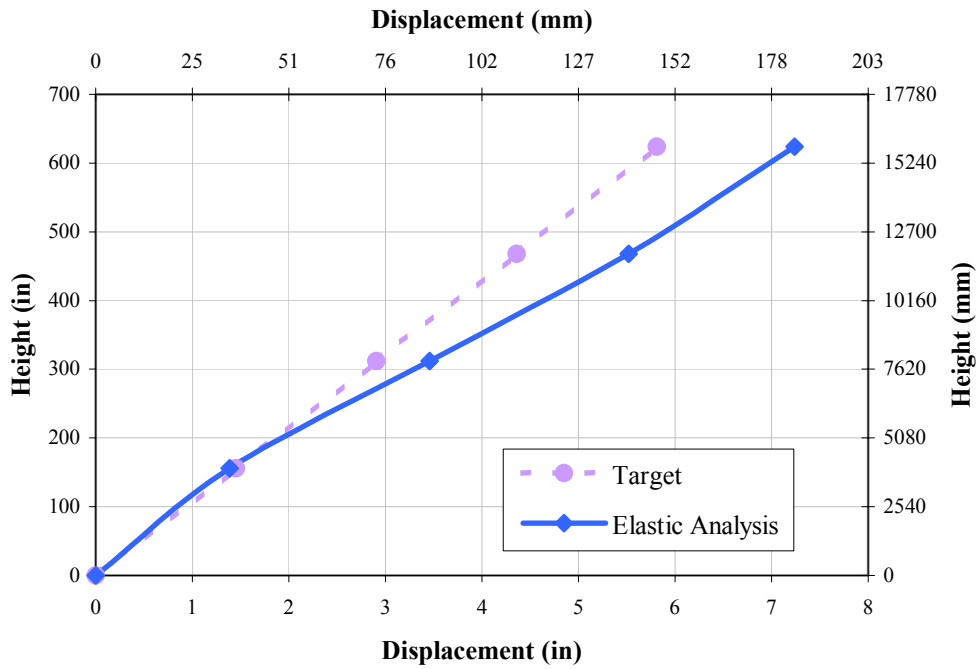


Figure 2.5.4-7. SP-1 displacement profile (FR-4a)

2.5.5 Four (4) Story Frame (FR-4b)

The second alternate frame (FR-4b), shown in Fig. 2.5.5-1, evaluates the behavior of a frame incorporating long bay lengths. . The reader is referred back to Section 2.5.1 (FR-4) for repeated information purposely not restated.

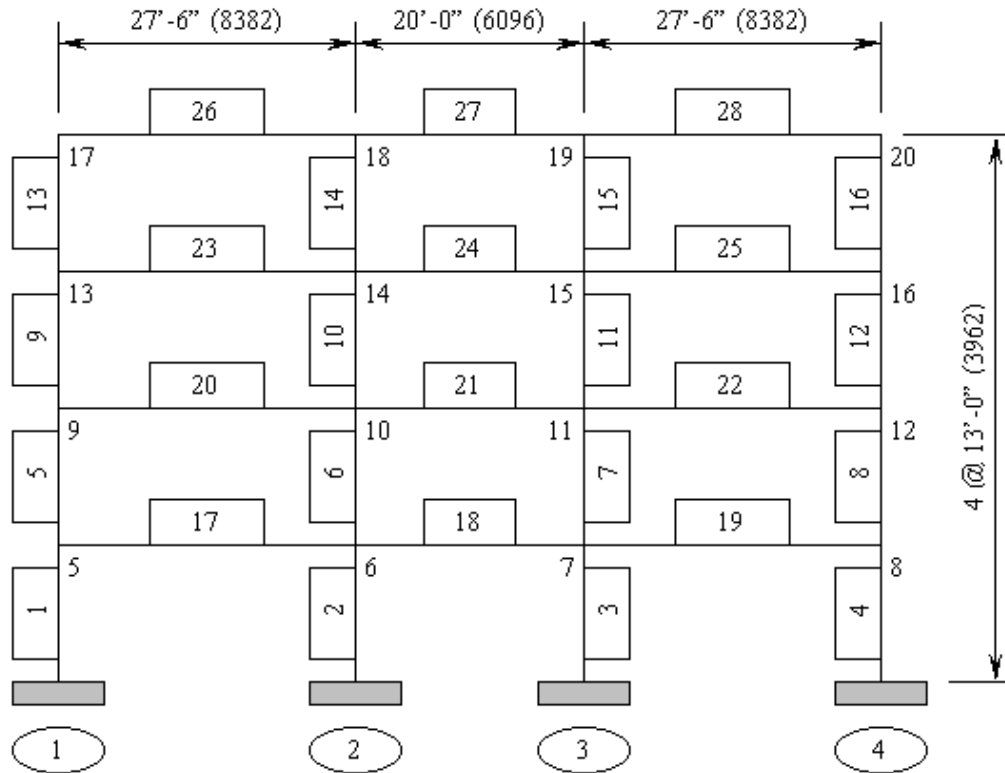


Figure 2.5.5-1. Frame schematic (FR-4b)

Step 3: Determine initial beam depths and plastic rotations.

For this frame, a W24 has been chosen as the beam depths for bay 1 and 3. Since the bay lengths are different and the same floor target rotation is desired, the design engineer selects the beam depth for the short bay from the beam rotation chart (Fig. 2.5.4-2). Since a W24 was selected for the beam depth for the 27'-6" (8.38 m) bay, the corresponding beam depth for the 20'-0" (6.09 m) bay with approximately the same plastic rotation is a W18.

Floor (i)	L_{b1}	L_{b2}	L_{b3}	d_1	d_2	d_3	θ_{p1}	θ_{p2}	θ_{p3}	θ_{pi}
Ground	0	0	0	0	0	0	0.00000	0.00000	0.00000	0.00000
2	330	240	330	24	18	24	0.00996	0.00966	0.00996	0.00966
3	330	240	330	24	18	24	0.00996	0.00966	0.00996	0.00966
4	330	240	330	24	18	24	0.00996	0.00966	0.00996	0.00966
Roof	330	240	330	24	18	24	0.00996	0.00966	0.00996	0.00966
									$\theta_{p\ sys} \Rightarrow$ Average:	0.00966
									$\theta_{p\ sys} \Rightarrow$ Minimum:	0.00966
									EQ I Factor:	1.93

Table 2.5.5-1. Floor equivalent plastic rotations (FR-4b)

It is by coincidence that the plastic rotation for the W24 and W18 are identical for the respective bay lengths. The EQ I factor is also modified according to the revised system plastic rotation capacity, leading to a PGA reduction factor for EQ I of 0.241.

Step 4: Determine target displacement profiles.

Target Displacements: SP-1 (Operational)

Floor (i)	θ_{Ti}	β	μ_{θ}	Δ_{di}	$\Delta_{di\ Drift}$	θ_{di}	$\Delta_{Ti\ Drift}$	Δ_{Ti}	h_{floor}	h_i
Ground	0.0000	0.000	0.00	0.00	0.00	0.0000	0.00	0.00	0	0
2	0.00966	1.16	1.00	1.51	1.51	0.0097	1.51	1.51	156	156
3	0.00966	1.16	1.00	3.01	1.51	0.0097	1.51	3.01	156	312
4	0.00966	1.16	1.00	4.52	1.51	0.0097	1.51	4.52	156	468
Roof	0.00966	1.16	1.00	6.02	1.51	0.0097	1.51	6.02	156	624

Table 2.5.5-2. SP-1 target displacements (FR-4b)

Target Displacements: SP-2 (Occupiable)

Floor (i)	θ_{Ti}	β	μ_{θ}	Δ_{di}	$\Delta_{di\ Drift}$	θ_{di}	$\Delta_{Ti\ Drift}$	Δ_{Ti}	h_{floor}	h_i
Ground	0.000	0.00	0.00	0.00	0.00	0.000	0.00	0.00	0	0
2	0.01800	1.11	1.86	2.81	2.81	0.0180	2.81	2.81	156	156
3	0.01800	1.11	1.86	5.62	2.81	0.0180	2.81	5.62	156	312
4	0.01800	1.11	1.86	8.42	2.81	0.0180	2.81	8.42	156	468
Roof	0.01800	1.11	1.86	11.23	2.81	0.0180	2.81	11.23	156	624

Table 2.5.5-3. SP-2 target displacements (FR-4b)

Target Displacements: SP-3 (Life Safe)

Floor (i)	θ_{Ti}	β	μ_{θ}	Δ_{di}	Δ_{di} Drift	θ_{di}	Δ_{di} Drift	Δ_{di}	h_{floor}	h_i
Ground	0.000	0.00	0.00	0.00	0.00	0.000	0.00	0.00	0	0
2	0.03200	1.04	3.31	4.99	4.99	0.0320	4.99	4.99	156	156
3	0.03200	1.04	3.31	9.98	4.99	0.0320	4.99	9.98	156	312
4	0.03200	1.04	3.31	14.98	4.99	0.0320	4.99	14.98	156	468
Roof	0.03200	1.04	3.31	19.97	4.99	0.0320	4.99	19.97	156	624

Table 2.5.5-4. SP-3 target displacements (FR-4b)

Target Displacements: SP-4 (Near Collapse)

Floor (i)	θ_{Ti}	β	μ_{θ}	Δ_{di}	Δ_{di} Drift	θ_{di}	Δ_{di} Drift	Δ_{di}	h_{floor}	h_i
Ground	0.00	0.00	0.00	0.00	0.00	0.00	0.00	0.00	0	0
2	0.04	1.00	4.14	6.24	6.24	0.04	6.24	6.24	156	156
3	0.04	1.00	4.14	12.48	6.24	0.04	6.24	12.48	156	312
4	0.04	1.00	4.14	18.72	6.24	0.04	6.24	18.72	156	468
Roof	0.04	1.00	4.14	24.96	6.24	0.04	6.24	24.96	156	624

Table 2.5.5-5. SP-4 target displacements (FR-4b)

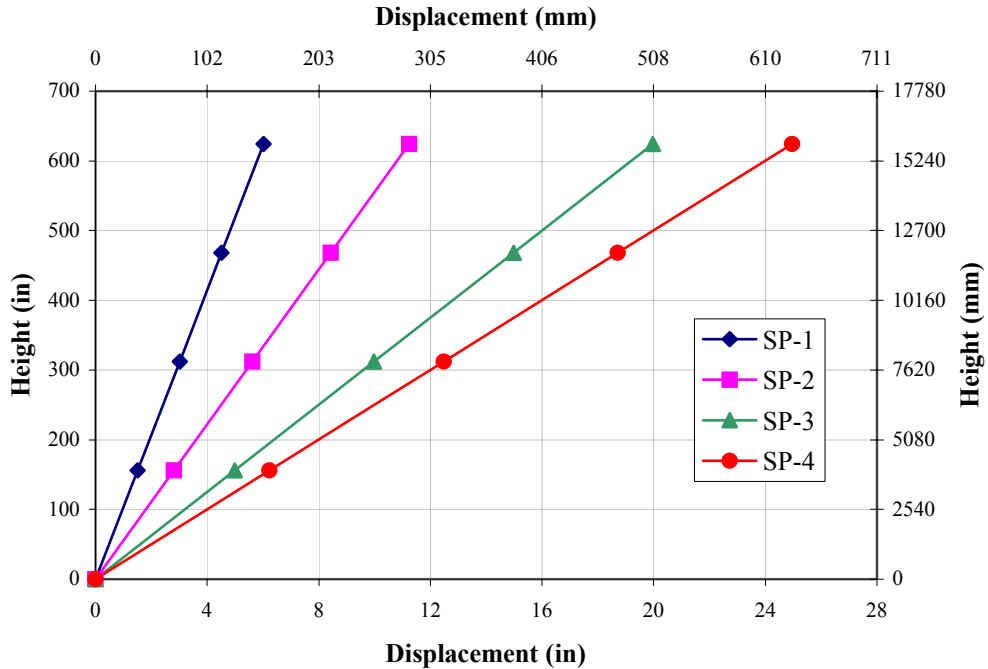


Figure 2.5.5-2. Target displacement profiles (FR-4b)

Step 5: Determine effective system displacements.

SDOF System Properties: SP-1 (Operational)

Gravity:		32.2							
Floor (i)	W_i	M_i	$M_i \Delta_i$	$M_i \Delta_i^2$	$M_i \Delta_i h_i$	$\Delta_{d,sys}$	4.52	in.	
Ground	0	0	0	0	0	$M_{eff,sys}$	18925	83%	of total
2	182.81	5677	8551	12880	1334010	$h_{eff,sys}$	468	75%	of total
3	182.81	5677	17103	51520	5336042	$\Delta_{y,sys}$	4.52	in.	
4	182.81	5677	25654	115921	12006094	k	1.0		
Roof	182.81	5677	34205	206082	21344168	$\mu_{\Delta,sys}$	1.00		
Total: Σ	731.25	22710	85513	386403	40020315				

Table 2.5.5-6. SP-1 SDOF system properties (FR-4b)

SDOF System Properties: SP-2 (Occupiable)

Gravity:		32.2							
Floor (i)	W_i	M_i	$M_i \Delta_i$	$M_i \Delta_i^2$	$M_i \Delta_i h_i$	$\Delta_{d,sys}$	8.42	in.	
Ground	0	0	0	0	0	$M_{eff,sys}$	18925	83%	of total
2	182.81	5677	15942	44766	2486977	$h_{eff,sys}$	468	75%	of total
3	182.81	5677	31884	179062	9947907	$\Delta_{y,sys}$	4.52	in.	
4	182.81	5677	47826	402890	22382790	k	1.0		
Roof	182.81	5677	63769	716249	39791627	$\mu_{\Delta,sys}$	1.86		
Total: Σ	731.25	22710	159422	1342967	74609301				

Table 2.5.5-7. SP-2 SDOF system properties (FR-4b)

SDOF System Properties: SP-3 (Life Safe)

Gravity:		32.2							
Floor (i)	W_i	M_i	$M_i \Delta_i$	$M_i \Delta_i^2$	$M_i \Delta_i h_i$	$\Delta_{d,sys}$	14.98	in.	
Ground	0	0	0	0	0	$M_{eff,sys}$	18925	83%	of total
2	182.81	5677	28342	141481	4421292	$h_{eff,sys}$	468	75%	of total
3	182.81	5677	56683	565925	17685168	$\Delta_{y,sys}$	4.52	in.	
4	182.81	5677	85025	1273332	39791627	k	1.00		
Roof	182.81	5677	113366	2263701	70740671	$\mu_{\Delta,sys}$	3.31		
Total: Σ	731.25	22710	283416	4244440	132638758				

Table 2.5.5-8. SP-3 SDOF system properties (FR-4b)

SDOF System Properties: SP-4 (Near Collapse)

	Gravity:	32.2						
Floor (i)	W_i	M_i	$M_i \Delta_i$	$M_i \Delta_i^2$	$M_i \Delta_i h_i$	$\Delta_{d,sys}$	18.72	in.
Ground	0	0	0	0	0	$M_{eff,sys}$	18925	83% of total
2	182.81	5677	35427	221065	5526615	$h_{eff,sys}$	468	75% of total
3	182.81	5677	70854	884258	22106460	$\Delta_{y,sys}$	4.52	in.
4	182.81	5677	106281	1989581	49739534	k	1.00	
Roof	182.81	5677	141708	3537034	88425839	$\mu_{A,sys}$	4.14	
Total: Σ	731.25	22710	354270	6631938	165798447			

Table 2.5.5-9. SP-4 SDOF system properties (FR-4b)

Step 6: Determine effective system properties and base shear.

Effective System Properties: SP-4 (Near Collapse)

$\zeta_{eff,sys}$	20%		$I_{eff,sys}$	60959	in ⁴
$T_{eff,sys}$	3.8	sec.	r	0.05	
$K_{eff,sys}$	51739	lbs/in.	$I_{i,sys}$	218249	in ⁴
$V_{b,sys}$	969	Kips			

Table 2.5.5-10. SP-4 effective system properties (FR-4b)

Effective System Properties: SP-3 (Life Safe)

$\zeta_{eff,sys}$	17%		$I_{eff,sys}$	73528	in ⁴
$T_{eff,sys}$	3.46	sec.	r	0.05	
$K_{eff,sys}$	62407	lbs/in.	$I_{i,sys}$	218420	in ⁴
$V_{b,sys}$	935	Kips			

Table 2.5.5-11. SP-3 effective system properties (FR-4b)

Effective System Properties: SP-2 (Occupiable)

$\zeta_{eff,sys}$	9%		$I_{eff,sys}$	122101	in ⁴
$T_{eff,sys}$	2.685	sec.	r	0.05	
$K_{eff,sys}$	103633	lbs/in.	$I_{i,sys}$	218201	in ⁴
$V_{b,sys}$	873	Kips			

Table 2.5.5-12. SP-2 effective system properties (FR-4b)

Effective System Properties: SP-1 (Operational)

$\zeta_{eff,sys}$	5%		$I_{eff,sys}$	218313	in ⁴
$T_{eff,sys}$	2.008	sec.			
$K_{eff,sys}$	185294	lbs/in.			
$V_{by,sys}$	837	Kips			
$V_{b,sys}.005$	434	Kips			

Table 2.5.5-13. SP-1 effective system properties (FR-4b)

Step 7: Vertical base shear distribution and analysis.

Equivalent Static Lateral Forces (kips):

Floor (i)	SP-1		SP-2		SP-3		SP-4	
	F_{yi}	$F_{yi} \Omega_{sys}$	F_i	$F_i \Omega_{sys}$	F_i	$F_i \Omega_{sys}$	F_i	$F_i \Omega_{sys}$
Ground	0	0	0	0	0	0	0	0
2	84	117	87	122	93	131	97	136
3	167	234	175	244	187	262	194	271
4	251	352	262	367	280	393	291	407
Roof	335	469	349	489	374	523	387	542
Total:	837	1172	873	1222	935	1308	969	1356

Table 2.5.5-14. Equivalent static lateral forces (FR-4b)

The system member overstrength factor was determined to be approximately 1.20 and the plastic hinge sequencing factor was assumed to be 1.2. This leads to a system performance overstrength factor, Ω_{sys} , of approximately 1.4. This factor is then applied to the expected system force-deformation graph shown in Fig. 2.5.5-3.

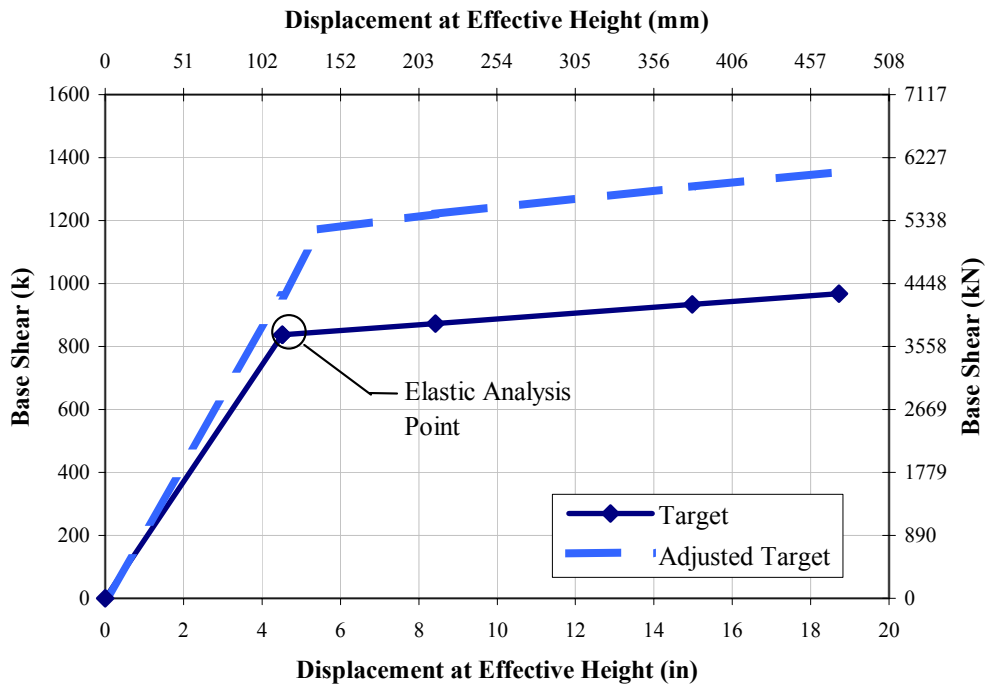


Figure 2.5.5-3. System force-displacement graph (FR-4b)

The final frame design is shown in Fig. 2.5.5-4 and the SP-1 displacement profile is shown in Fig. 2.5.5-5.

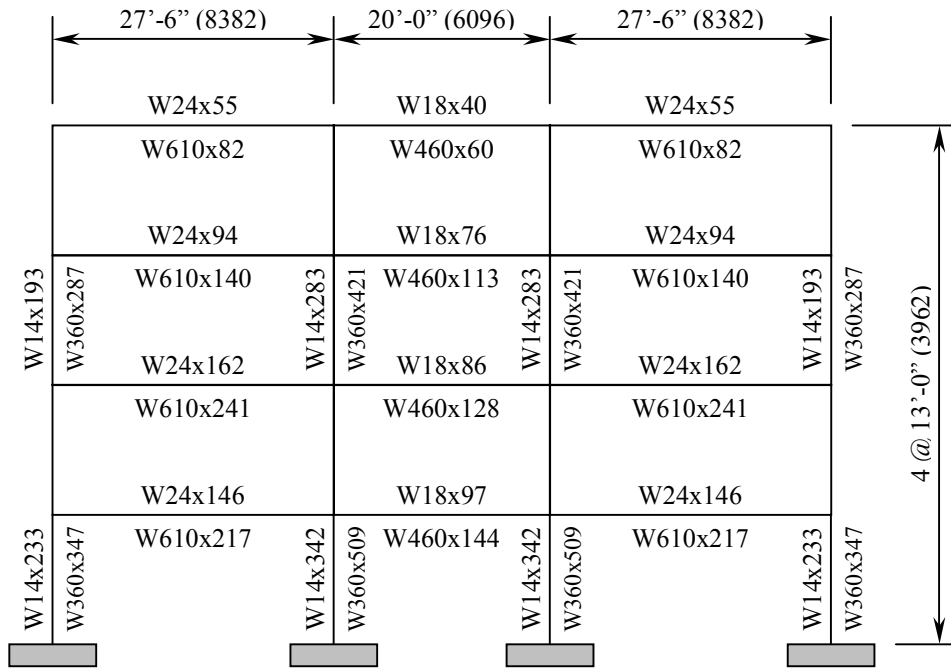


Figure 2.5.5-4. Final frame schematic (FR-4b)

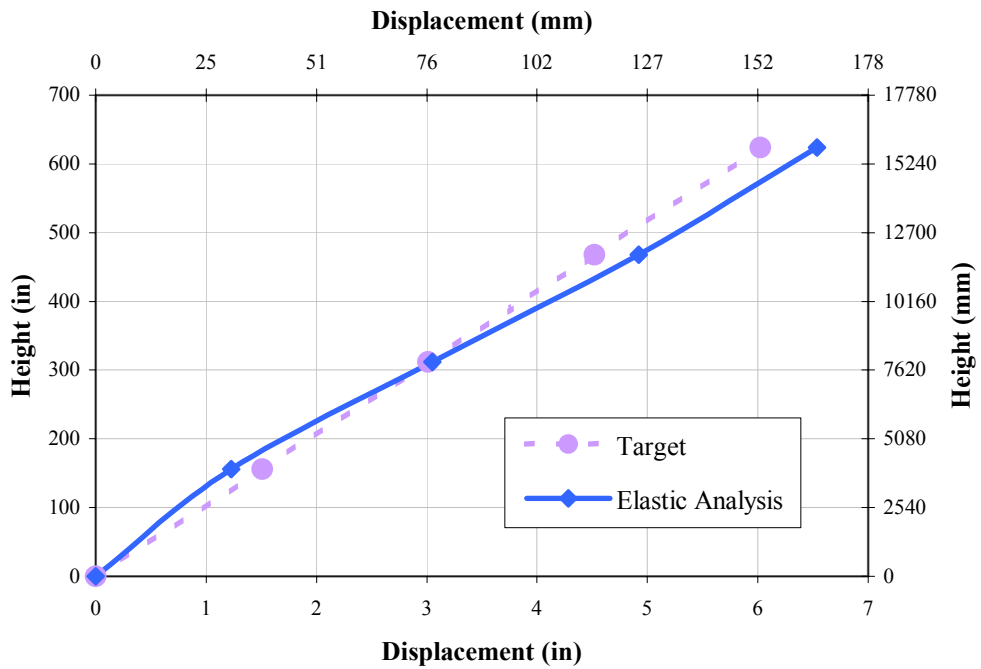


Figure 2.5.5-5. SP-1 displacement profile (FR-4b)

2.5.6 Eight (8) Story Frame (FR-8)

Step 3: Determine initial beam depths and plastic rotations.

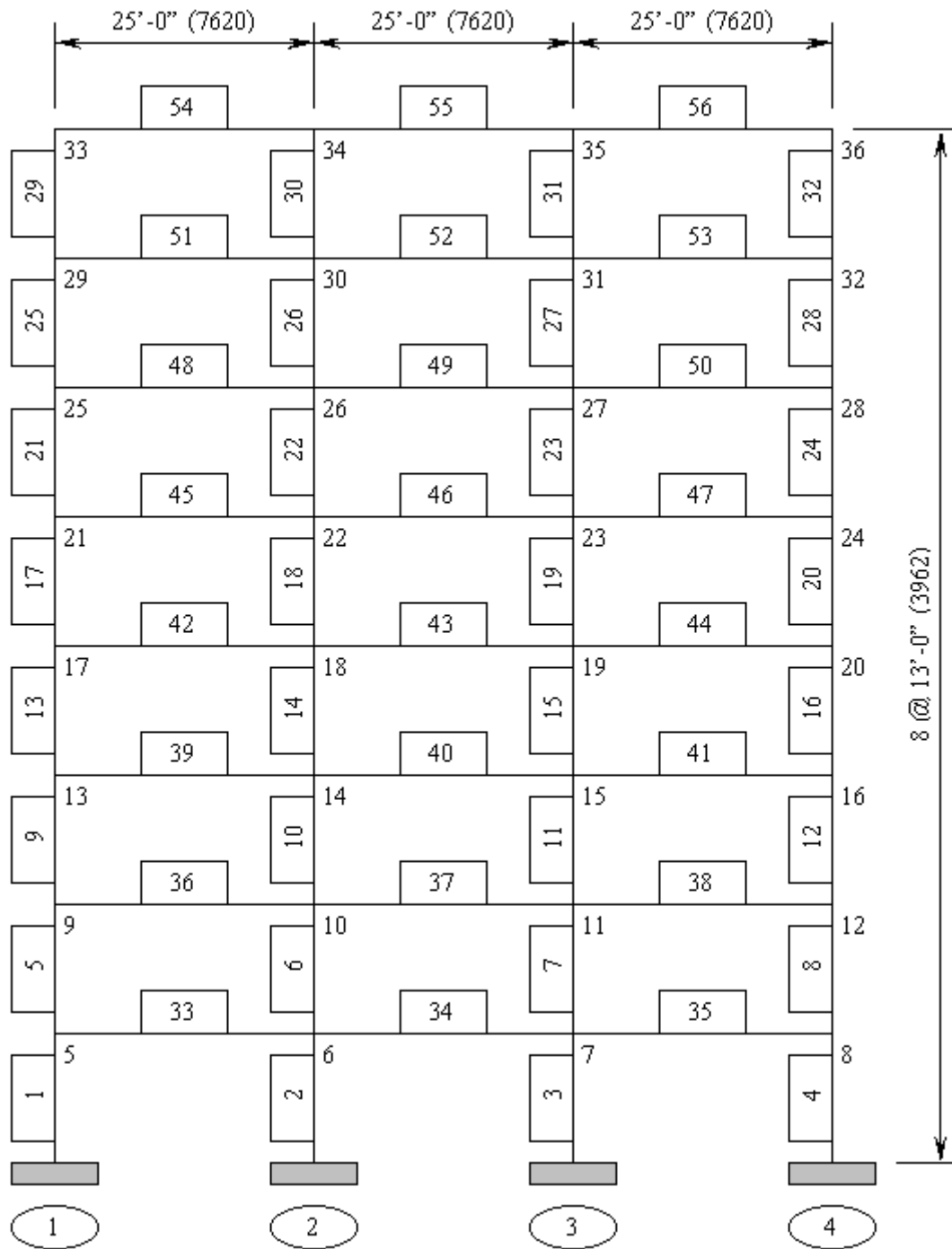


Figure 2.5.6-1. Frame schematic (FR-8)

For this frame, W24's have been chosen as the beam depths. Additionally, since the bay lengths are all the same, the same beam depth is used through out.

Floor (i)	L_{b1}	L_{b2}	L_{b3}	d_1	d_2	d_3	θ_{p1}	θ_{p2}	θ_{p3}	θ_{pi}
Ground	0	0	0	0	0	0	0.00000	0.00000	0.00000	0.00000
2	300	300	300	24	24	24	0.00905	0.00905	0.00905	0.00905
3	300	300	300	24	24	24	0.00905	0.00905	0.00905	0.00905
4	300	300	300	24	24	24	0.00905	0.00905	0.00905	0.00905
5	300	300	300	24	24	24	0.00905	0.00905	0.00905	0.00905
6	300	300	300	24	24	24	0.00905	0.00905	0.00905	0.00905
7	300	300	300	24	24	24	0.00905	0.00905	0.00905	0.00905
8	300	300	300	24	24	24	0.00905	0.00905	0.00905	0.00905
Roof	300	300	300	24	24	24	0.00905	0.00905	0.00905	0.00905
$\theta_{p,sys} \Rightarrow$ Average:										0.00905
$\theta_{p,sys} \Rightarrow$ Minimum:										0.00905
EQ I Factor:										1.81

Table 2.5.6-1. Floor equivalent plastic rotations (FR-8)

The system rotation capacity corresponding to the SP-1 performance level is 0.00905, leading to an EQ I modification factor of $0.00905/0.005 = 1.81$ and MCE PGA Reduction Factor of $0.125*1.81 = 0.226$.

Step 4: Determine target displacement profiles.

The recommended nodal design displacement profiles from the target rotations determined in Step 1 and 3 for an eight (8) story frame is determined from Table 2.4-2.

$$\Delta_{di} = \theta_T h_i \left(1 - \frac{(n-4)h_i}{32h_n} \right) \quad (2.5.6-1)$$

The design rotation, θ_{di} , can then be determined from the design displacement profile, thus leading to the expected floor rotation ductility, μ_θ . Note that θ_{di} will not always equal θ_{Ti} , as is the case for linear displacement profiles.

Target Displacements: *Elastic* SP-1 (Operational)

Floor (i)	θ_{Ti}	β	μ_{θ}	Δ_{di}	Δ_{di} Drift	θ_{di}	Δ_{Ti} Drift	Δ_{Ti}	h_{floor}	h_i
Ground	0.00000	0.000	0.00	0.00	0.00	0.0000	0.00	0.00	0	0
2	0.00905	1.28	0.98	1.39	1.39	0.0089	1.41	1.41	156	156
3	0.00905	1.28	0.95	2.74	1.35	0.0086	1.41	2.82	156	312
4	0.00905	1.28	0.92	4.04	1.30	0.0083	1.41	4.24	156	468
5	0.00905	1.28	0.89	5.30	1.26	0.0081	1.41	5.65	156	624
6	0.00905	1.28	0.86	6.51	1.21	0.0078	1.41	7.06	156	780
7	0.00905	1.28	0.83	7.68	1.17	0.0075	1.41	8.47	156	936
8	0.00905	1.28	0.80	8.80	1.13	0.0072	1.41	9.88	156	1092
Roof	0.00905	1.28	0.77	9.88	1.08	0.0069	1.41	11.30	156	1248

Table 2.5.6-2. *Elastic* SP-1 target displacements (FR-8)

Target Displacements: SP-2 (Occupiable)

Floor (i)	θ_{Ti}	β	μ_{θ}	Δ_{di}	Δ_{di} Drift	θ_{di}	Δ_{Ti} Drift	Δ_{Ti}	h_{floor}	h_i
Ground	0.000	0.00	0.00	0.00	0.00	0.0000	0.00	0.00	0	0
2	0.018	1.11	1.96	2.76	2.76	0.0177	2.81	2.81	156	156
3	0.018	1.11	1.90	5.44	2.68	0.0172	2.81	5.62	156	312
4	0.018	1.11	1.83	8.03	2.59	0.0166	2.81	8.42	156	468
5	0.018	1.11	1.77	10.53	2.50	0.0160	2.81	11.23	156	624
6	0.018	1.11	1.71	12.94	2.41	0.0155	2.81	14.04	156	780
7	0.018	1.11	1.65	15.27	2.33	0.0149	2.81	16.85	156	936
8	0.018	1.11	1.58	17.51	2.24	0.0143	2.81	19.66	156	1092
Roof	0.018	1.11	1.52	19.66	2.15	0.0138	2.81	22.46	156	1248

Table 2.5.6-3. SP-2 target displacements (FR-8)

Target Displacements: SP-3 (Life Safe)

Floor (i)	θ_{Ti}	β	μ_{θ}	Δ_{di}	Δ_{di} Drift	θ_{di}	Δ_{Ti} Drift	Δ_{Ti}	h_{floor}	h_i
Ground	0.000	0.00	0.00	0.00	0.00	0.0000	0.00	0.00	0	0
2	0.032	1.04	3.48	4.91	4.91	0.0315	4.99	4.99	156	156
3	0.032	1.04	3.37	9.67	4.76	0.0305	4.99	9.98	156	312
4	0.032	1.04	3.26	14.27	4.60	0.0295	4.99	14.98	156	468
5	0.032	1.04	3.15	18.72	4.45	0.0285	4.99	19.97	156	624
6	0.032	1.04	3.04	23.01	4.29	0.0275	4.99	24.96	156	780
7	0.032	1.04	2.93	27.14	4.13	0.0265	4.99	29.95	156	936
8	0.032	1.04	2.82	31.12	3.98	0.0255	4.99	34.94	156	1092
Roof	0.032	1.04	2.71	34.94	3.82	0.0245	4.99	39.94	156	1248

Table 2.5.6-4. SP-3 target displacements (FR-8)

Target Displacements: SP-4 (Near Collapse)

Floor (i)	θ_{Ti}	β	μ_{θ}	Δ_{di}	$\Delta_{di\ Drift}$	θ_{di}	$\Delta_{Ti\ Drift}$	Δ_{Ti}	h_{floor}	h_i
Ground	0.00	0.00	0.00	0.00	0.00	0.0000	0.00	0.00	0	0
2	0.04	1.00	4.35	6.14	6.14	0.0394	6.24	6.24	156	156
3	0.04	1.00	4.21	12.09	5.95	0.0381	6.24	12.48	156	312
4	0.04	1.00	4.07	17.84	5.75	0.0369	6.24	18.72	156	468
5	0.04	1.00	3.94	23.40	5.56	0.0356	6.24	24.96	156	624
6	0.04	1.00	3.80	28.76	5.36	0.0344	6.24	31.20	156	780
7	0.04	1.00	3.66	33.93	5.17	0.0331	6.24	37.44	156	936
8	0.04	1.00	3.52	38.90	4.97	0.0319	6.24	43.68	156	1092
Roof	0.04	1.00	3.38	43.68	4.78	0.0306	6.24	49.92	156	1248

Table 2.5.6-5. SP-4 target displacements (FR-8)

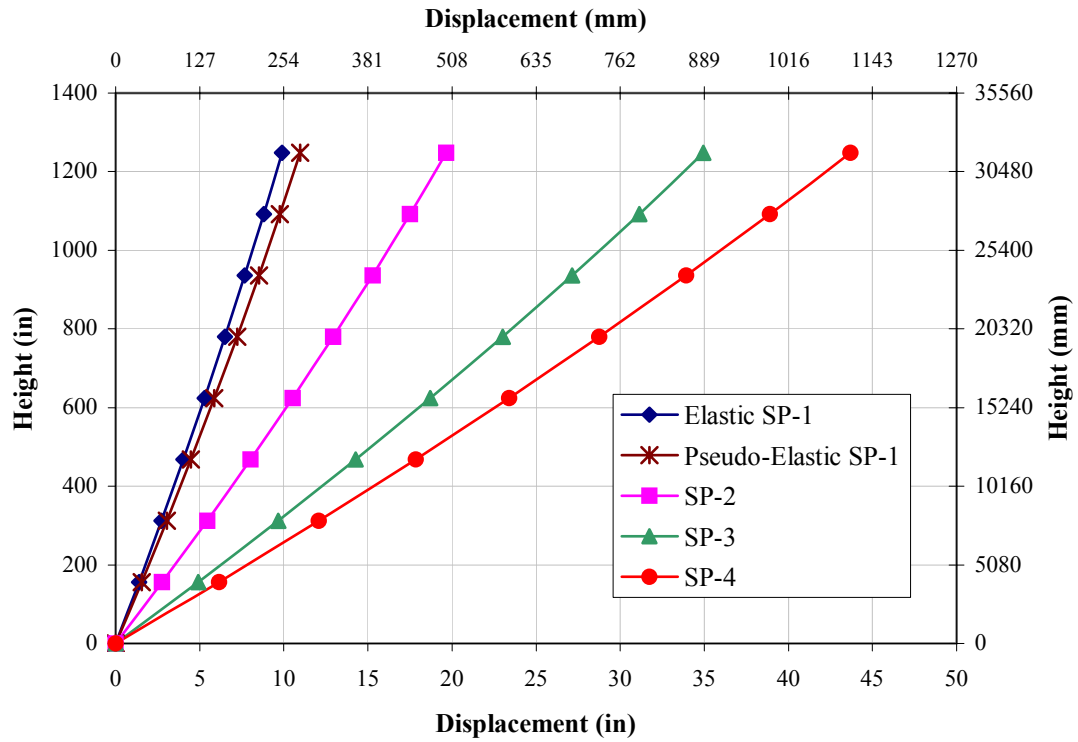


Figure 2.5.6-2. Target displacement profiles (FR-8)

Step 5: Determine effective system displacements.

SDOF System Properties: Elastic SP-1 (Operational)

Gravity:		32.2							
Floor (i)	W_i	M_i	$M_i \Delta_i$	$M_i \Delta_i^2$	$M_i \Delta_i h_i$	$\Delta_{d,sys}$	7.13	in.	
Ground	0.00	0	0	0	0	$M_{eff,sys}$	36903	81%	of total
2	182.81	5677	7892	10969	1231094	$h_{eff,sys}$	874	70%	of total
3	182.81	5677	15533	42496	4846210	$\Delta_{y,sys}$	7.91	in.	
4	182.81	5677	22923	92556	10728102	k	0.90		
5	182.81	5677	30063	159193	18759523	$\mu_{\Delta,sys}$	0.90		
6	182.81	5677	36953	240517	28823225				
7	182.81	5677	43592	334704	40801962				
8	182.81	5677	49980	439995	54578486				
Roof	182.81	5677	56118	554700	70035551				
Total: Σ	1462.50	45419	263054	1875129	229804152				

Table 2.5.6-6. Elastic SP-1 SDOF system properties (FR-8)

SDOF System Properties: SP-2 (Occupiable)

Gravity:		32.2							
Floor (i)	W_i	M_i	$M_i \Delta_i$	$M_i \Delta_i^2$	$M_i \Delta_i h_i$	$\Delta_{d,sys}$	14.18	in.	
Ground	0.00	0	0	0	0	$M_{eff,sys}$	36903	81%	of total
2	182.81	5677	15693	43378	2448118	$h_{eff,sys}$	874	70%	of total
3	182.81	5677	30888	168046	9637035	$\Delta_{y,sys}$	7.91	in.	
4	182.81	5677	45585	366005	21333597	k	0.90		
5	182.81	5677	59783	629516	37304651	$\mu_{\Delta,sys}$	1.79		
6	182.81	5677	73483	951105	57317041				
7	182.81	5677	86685	1323557	81137615				
8	182.81	5677	99389	1739923	108533218				
Roof	182.81	5677	111595	2193513	139270696				
Total: Σ	1462.50	45419	523102	7415042	456981970				

Table 2.5.7-6. SP-2 SDOF system properties (FR-8)

SDOF System Properties: SP-3 (Life Safe)

		Gravity: 32.2					
Floor (i)	W_i	M_i	$M_i \Delta_i$	$M_i \Delta_i^2$	$M_i \Delta_i h_i$		
Ground	0.00	0	0	0	0		
2	182.81	5677	27899	137095	4352209		
3	182.81	5677	54912	531108	17132506		
4	182.81	5677	81039	1156755	37926395		
5	182.81	5677	106281	1989581	66319379		
6	182.81	5677	130637	3005960	101896962		
7	182.81	5677	154108	4183095	144244649		
8	182.81	5677	176692	5499016	192947943		
Roof	182.81	5677	198391	6932586	247592348		
Total: Σ	1462.50	45419	929959	23435196	812412391		

$\Delta_{d,sys}$	25.20	in.	
$M_{eff,sys}$	36903		81% of total
$h_{eff,sys}$	874		70% of total
$\Delta_{y,sys}$	7.91	in.	
k	0.90		
$\mu_{\Delta,sys}$	3.19		

Table 2.5.6-8. SP-3 SDOF system properties (FR-8)

SDOF System Properties: SP-4 (Near Collapse)

		Gravity: 32.2					
Floor (i)	W_i	M_i	$M_i \Delta_i$	$M_i \Delta_i^2$	$M_i \Delta_i h_i$		
Ground	0.00	0	0	0	0		
2	182.81	5677	34873	214210	5440262		
3	182.81	5677	68640	829856	21415633		
4	182.81	5677	101299	1807430	47407993		
5	182.81	5677	132851	3108721	82899224		
6	182.81	5677	163296	4696813	127371203		
7	182.81	5677	192634	6536086	180305811		
8	182.81	5677	220865	8592213	241184929		
Roof	182.81	5677	247989	10832165	309490435		
Total: Σ	1462.50	45419	1162449	36617494	1015515489		

$\Delta_{d,sys}$	31.50	in.	
$M_{eff,sys}$	36903		81% of total
$h_{eff,sys}$	874		70% of total
$\Delta_{y,sys}$	7.91	in.	
k	0.90		
$\mu_{\Delta,sys}$	3.98		

Table 2.5.6-9. SP-4 SDOF system properties (FR-8)

As stated previously, it is not always the case that the displacement ductility is equal to the floor rotation ductility. This can be seen when evaluating the floor rotation ductility against the system displacement ductility for any of the previous performance levels. In fact the system displacement ductility is approximately the average of the floor rotation ductilities.

For non-linear displacement profiles, the SP-1 performance level will always yield a system displacement ductility less than unity. However, the system yield displacement is used to determine the system characteristics and base shear at the SP-1 level. Hence, the

displacement profile simulating the global yield mechanism (pseudo-elastic profile) will require the floors below the effective height to yield by some degree, as seen in Fig. 2.5.6-3. Therefore, modifications must be made since an elastic analysis is not suitable to determine the design demands. For non-linear displacement profiles in accordance with the Equivalent Yield Analysis, the displacement ductility (less than unity) is used to reduce the SP-1 base shear to an *elastic* base shear. The design of the system is then based on the reduced SP-1 lateral forces using the *elastic* displacement profile.

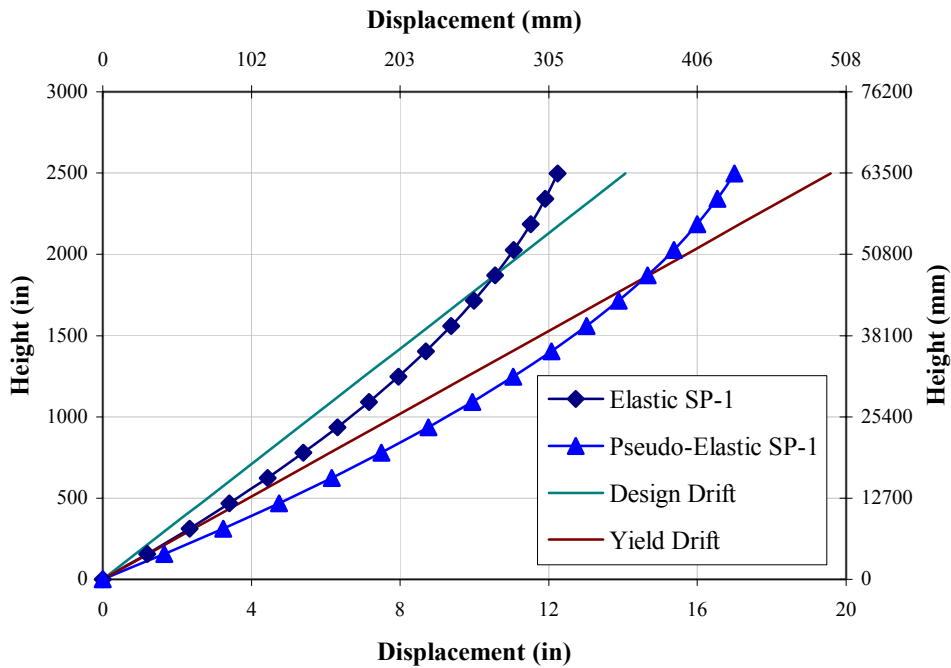


Figure 2.5.6-3. Elastic and pseudo-elastic non-linear displacement profiles

Step 6: Determine effective system properties and base shear.

Effective System Properties: SP-4 (Near Collapse)

$\zeta_{eff,sys}$	20%		$I_{eff,sys}$	276879	in ⁴
$T_{eff,sys}$	6.35	sec.	R	0.05	
$K_{eff,sys}$	36130	lbs/in.	$I_{i,sys}$	959784	in ⁴
$V_{b,sys}$	1138	Kips			

Table 2.5.6-10. SP-4 effective system properties (FR-8)

Effective System Properties: SP-3 (Life Safe)

$\zeta_{eff\ sys}$	18%		$I_{eff\ sys}$	334066	in ⁴
$T_{eff\ sys}$	5.781	sec.	r	0.05	
$K_{eff\ sys}$	43593	lbs/in.	$I_{i\ sys}$	959681	in ⁴
$V_{b\ sys}$	1099	Kips			

Table 2.5.6-11. SP-3 effective system properties (FR-8)

Effective System Properties: SP-2 (Occupiable)

$\zeta_{eff\ sys}$	9%		$I_{eff\ sys}$	556513	in ⁴
$T_{eff\ sys}$	4.479	sec.	r	0.05	
$K_{eff\ sys}$	72620	lbs/in.	$I_{i\ sys}$	959577	in ⁴
$V_{b\ sys}$	1029	Kips			

Table 2.5.6-12. SP-2 effective system properties (FR-8)

Effective System Properties: Elastic SP-1 (Operational)

$\zeta_{eff\ sys}$	5%		$I_{eff\ sys}$	959564	in ⁴
$T_{eff\ sys}$	3.411	sec. (Yield)			
$K_{eff\ sys}$	125215	lbs/in (Yield)			
$V_{b\ sys}$	893	Kips			
$V_{by\ sys}$	990	Kips (Yield)			

Table 2.5.6-13. Elastic SP-1 effective system properties (FR-8)

Step 7: Vertical base shear distribution and analysis.

Equivalent Static Lateral Forces:

	Elastic SP-1		SP-2		SP-3		SP-4	
Floor (i)	F_{yi}	$F_{yi} \Omega_{sys}$	F_i	$F_i \Omega_{sys}$	F_i	$F_i \Omega_{sys}$	F_i	$F_i \Omega_{sys}$
Ground	0	0	0	0	0	0	0	0
2	27	40	31	42	33	44	34	46
3	53	79	61	82	65	88	67	91
4	78	116	90	121	96	129	99	134
5	102	153	118	159	126	169	130	176
6	125	188	145	195	154	208	160	216
7	148	222	171	230	182	246	189	255
8	170	254	196	264	209	282	216	292
Roof	190	285	220	296	234	316	243	328
Total:	893	1337	1029	1390	1099	1483	1138	1536

Table 2.5.6-14. Equivalent static lateral forces (FR-8)

The system member overstrength factor was determined to be approximately 1.25 and the plastic hinge sequencing factor was assumed to be 1.2. This leads to a system performance overstrength factor, Ω_{sys} , of approximately 1.5. This factor is then applied to the expected system force-displacement graph starting at the *elastic* system as shown in Fig. 2.5.6-4. Since a portion of the system overstrength, mainly the member overstrength, is accounted for in the reduced *elastic* SP-1 value, the actual system post-yield system overstrength is similarly reduced by the system displacement ductility. This leads to a post-yield system overstrength of 1.35 (1.5*0.9). Additionally, the design demands per floor were increased to the pseudo-elastic SP-1 level by dividing the demand by the respective floor rotation ductility (less than unity).

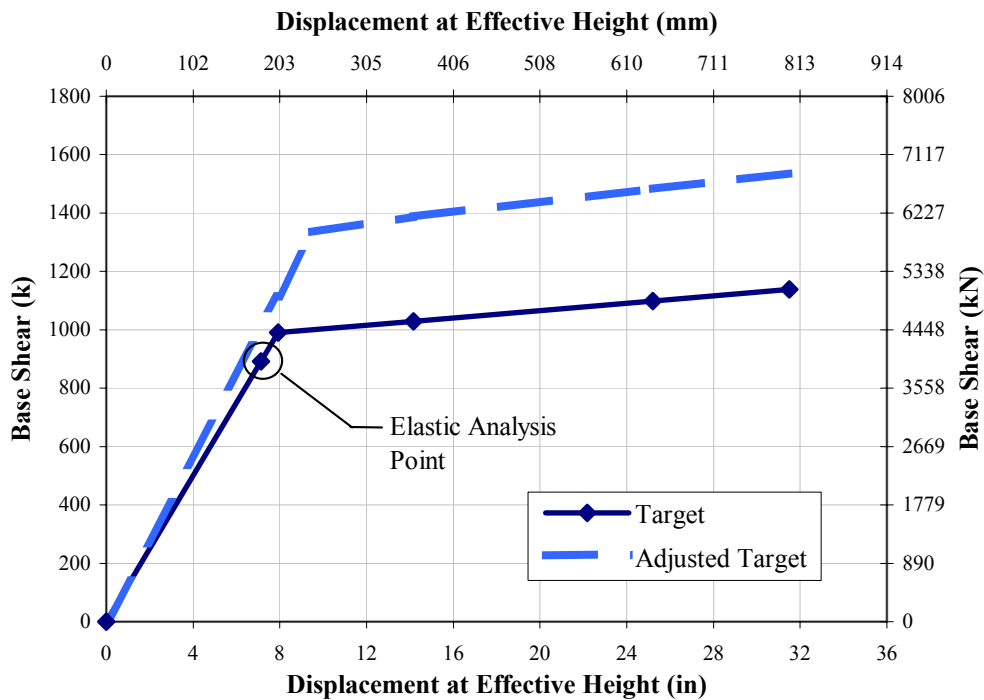


Figure 2.5.6-4. System force-displacement graph (FR-8)

The final frame design is shown in Fig. 2.5.6-5 and the *elastic* SP-1 displacement profile is shown in Fig. 2.5.6-6.

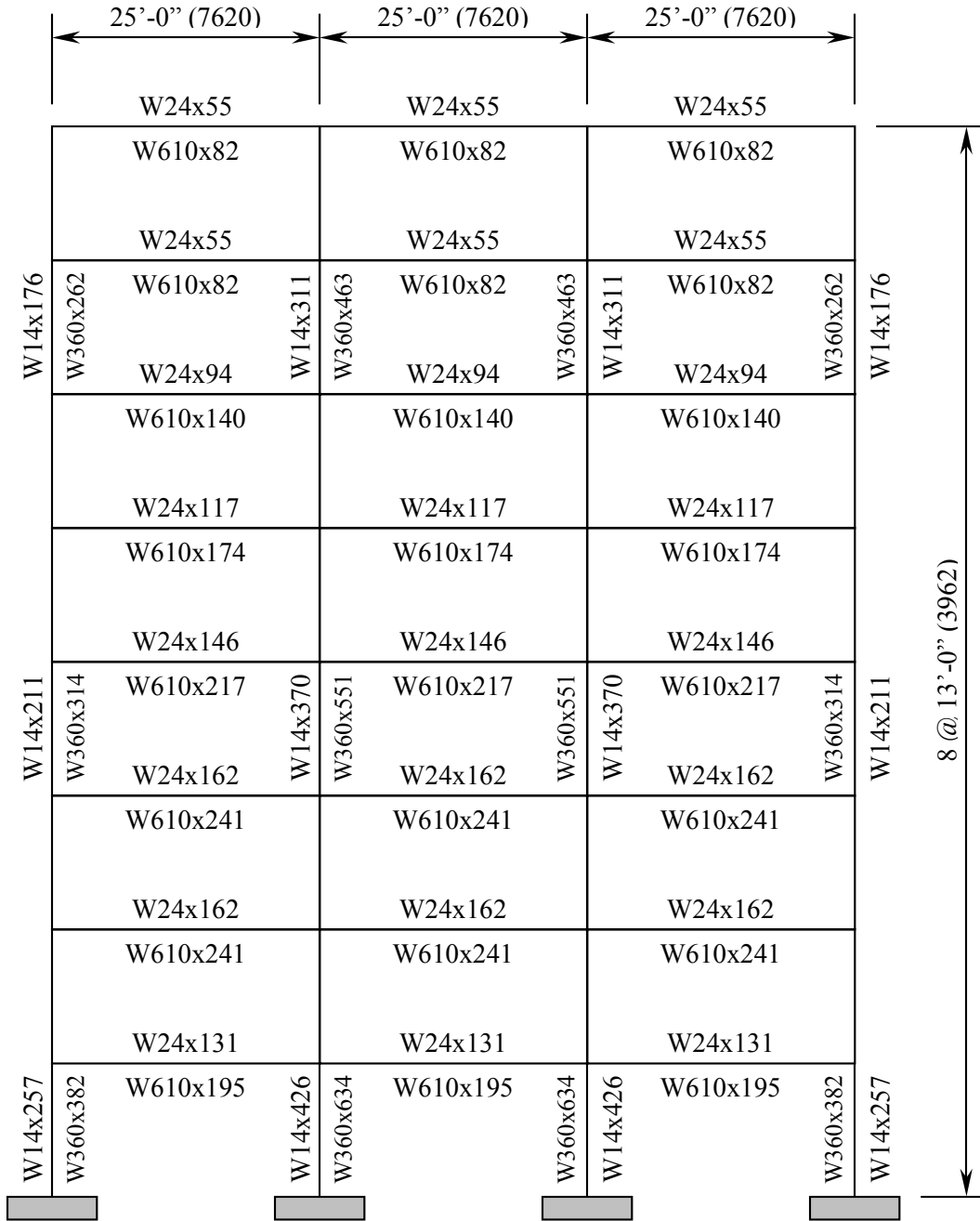


Figure 2.5.6-5. Final frame schematic (FR-8)

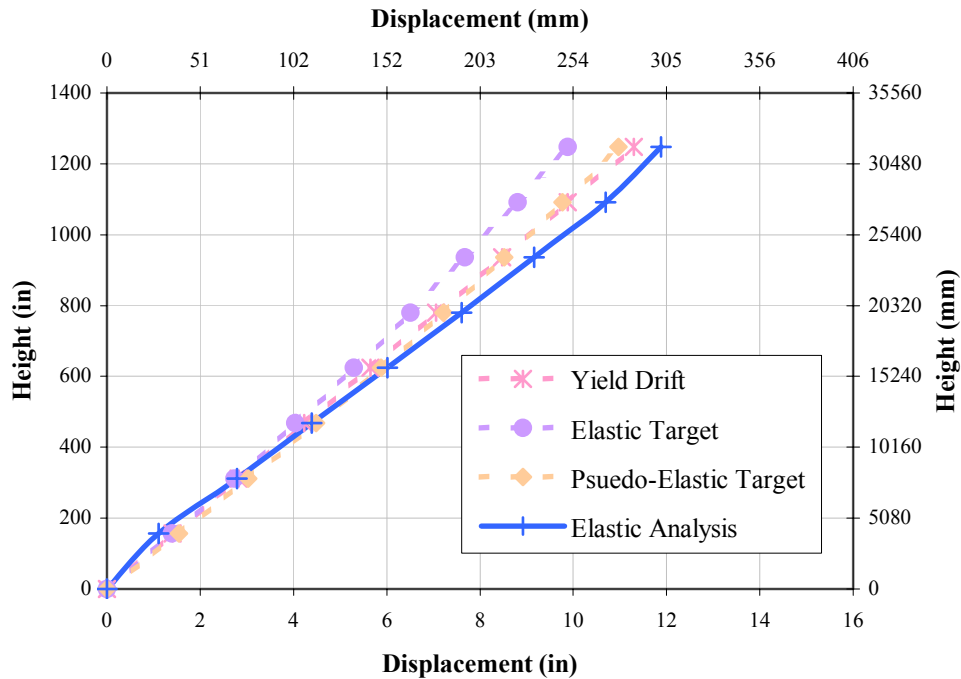


Figure 2.5.6-6. Elastic SP-1 Displacement Profile (FR-8)

As can be seen in Fig. 2.5.6-6, the base hinges have not formed and the lower stiffer portion of the frame behaves similar to a braced frame. Similarly, large lateral displacements are evident in the upper floors. It should be mentioned that non-linear profiles result in fairly high floor overstrength factors in the upper floors. Furthermore, the use of Equivalent Yield Analysis is conceptual and *elastic* displacement profiles require future research.

2.5.7 Eight (8) Story Frame (FR-8-W27)

Step 3: Determine initial beam depths and plastic rotations.

For this frame, W24's have been chosen as the beam depths for the upper four floors and W27 for the lower four floors. Additionally, since the bay lengths are all the same, the same beam depth is used through out.

Floor (i)	L_{b1}	L_{b2}	L_{b3}	d_1	d_2	d_3	θ_{p1}	θ_{p2}	θ_{p3}	θ_{pi}
Ground	0	0	0	0	0	0	0.00000	0.00000	0.00000	0.00000
2	300	300	300	27	27	27	0.00805	0.00805	0.00805	0.00805
3	300	300	300	27	27	27	0.00805	0.00805	0.00805	0.00805
4	300	300	300	27	27	27	0.00805	0.00805	0.00805	0.00805
5	300	300	300	27	27	27	0.00805	0.00805	0.00805	0.00805
6	300	300	300	24	24	24	0.00905	0.00905	0.00905	0.00905
7	300	300	300	24	24	24	0.00905	0.00905	0.00905	0.00905
8	300	300	300	24	24	24	0.00905	0.00905	0.00905	0.00905
Roof	300	300	300	24	24	24	0.00905	0.00905	0.00905	0.00905
$\theta_{p,sys} \Rightarrow$ Average:										0.00855
$\theta_{p,sys} \Rightarrow$ Minimum:										0.00805
EQ I Factor:										1.71

Table 2.5.7-1. Floor equivalent plastic rotations (FR-8-W27)

The system rotation capacity corresponding to the SP-1 performance level is 0.00855. The average value is recommended since some yielding is expected at the SP-1 level. Therefore the EQ I modification factor is $0.00855/0.005 = 1.71$ and the corresponding MCE PGA Reduction Factor is $0.125*1.71 = 0.214$.

Step 4: Determine target displacement profiles.

Target Displacements: Elastic SP-1 (Operational)

Floor (i)	θ_{Ti}	β	μ_{θ}	Δ_{di}	$\Delta_{di, Drift}$	θ_{di}	$\Delta_{di, Drift}$	Δ_{di}	h_{floor}	h_i
Ground	0.00805	0.00	0.00	0.00	0.00	0.0000	0.00	0.00	0	0
2	0.00805	1.29	1.05	1.31	1.31	0.0084	1.33	1.33	156	156
3	0.00805	1.29	1.01	2.58	1.27	0.0081	1.33	2.67	156	312
4	0.00805	1.29	0.98	3.81	1.23	0.0079	1.33	4.00	156	468
5	0.00905	1.29	0.95	5.00	1.19	0.0076	1.33	5.33	156	624
6	0.00905	1.29	0.81	6.15	1.15	0.0073	1.33	6.67	156	780
7	0.00905	1.29	0.78	7.25	1.10	0.0071	1.33	8.00	156	936
8	0.00905	1.29	0.75	8.31	1.06	0.0068	1.33	9.34	156	1092
Roof	0.00805	1.29	0.72	9.34	1.02	0.0065	1.33	10.67	156	1248

Table 2.5.7-2. Elastic SP-1 target displacements (FR-8-W27)

Target Displacements: SP-2 (Occupiable)

Floor (i)	θ_{Ti}	β	μ_{θ}	Δ_{di}	$\Delta_{di\ Drift}$	θ_{di}	$\Delta_{Ti\ Drift}$	Δ_{Ti}	h_{floor}	h_i
Ground	0.000	0.00	0.00	0.00	0.00	0.0000	0.00	0.00	0	0
2	0.018	1.11	2.20	2.76	2.76	0.0177	2.81	2.81	156	156
3	0.018	1.11	2.13	5.44	2.68	0.0172	2.81	5.62	156	312
4	0.018	1.11	2.06	8.03	2.59	0.0166	2.81	8.42	156	468
5	0.018	1.11	1.99	10.53	2.50	0.0160	2.81	11.23	156	624
6	0.018	1.11	1.71	12.94	2.41	0.0155	2.81	14.04	156	780
7	0.018	1.11	1.65	15.27	2.33	0.0149	2.81	16.85	156	936
8	0.018	1.11	1.58	17.51	2.24	0.0143	2.81	19.66	156	1092
Roof	0.018	1.11	1.52	19.66	2.15	0.0138	2.81	22.46	156	1248

Table 2.5.7-3. SP-2 target displacements (FR-8-W27)

Target Displacements: SP-3 (Life Safe)

Floor (i)	θ_{Ti}	β	μ_{θ}	Δ_{di}	$\Delta_{di\ Drift}$	θ_{di}	$\Delta_{Ti\ Drift}$	Δ_{Ti}	h_{floor}	h_i
Ground	0.000	0.00	0.00	0.00	0.00	0.0000	0.00	0.00	0	0
2	0.032	1.04	3.92	4.91	4.91	0.0315	4.99	4.99	156	156
3	0.032	1.04	3.79	9.67	4.76	0.0305	4.99	9.98	156	312
4	0.032	1.04	3.67	14.27	4.60	0.0295	4.99	14.98	156	468
5	0.032	1.04	3.54	18.72	4.45	0.0285	4.99	19.97	156	624
6	0.032	1.04	3.04	23.01	4.29	0.0275	4.99	24.96	156	780
7	0.032	1.04	2.93	27.14	4.13	0.0265	4.99	29.95	156	936
8	0.032	1.04	2.82	31.12	3.98	0.0255	4.99	34.94	156	1092
Roof	0.032	1.04	2.71	34.94	3.82	0.0245	4.99	39.94	156	1248

Table 2.5.7-4. SP-3 target displacements (FR-8-W27)

Target Displacements: SP-4 (Near Collapse)

Floor (i)	θ_{Ti}	β	μ_{θ}	Δ_{di}	$\Delta_{di\ Drift}$	θ_{di}	$\Delta_{Ti\ Drift}$	Δ_{Ti}	h_{floor}	h_i
Ground	0.00	0.00	0.00	0.00	0.00	0.0000	0.00	0.00	0	0
2	0.04	1.00	4.89	6.14	6.14	0.0394	6.24	6.24	156	156
3	0.04	1.00	4.74	12.09	5.95	0.0381	6.24	12.48	156	312
4	0.04	1.00	4.58	17.84	5.75	0.0369	6.24	18.72	156	468
5	0.04	1.00	4.43	23.40	5.56	0.0356	6.24	24.96	156	624
6	0.04	1.00	3.80	28.76	5.36	0.0344	6.24	31.20	156	780
7	0.04	1.00	3.66	33.93	5.17	0.0331	6.24	37.44	156	936
8	0.04	1.00	3.52	38.90	4.97	0.0319	6.24	43.68	156	1092
Roof	0.04	1.00	3.38	43.68	4.78	0.0306	6.24	49.92	156	1248

Table 2.5.7-5. SP-4 target displacements (FR-8-W27)

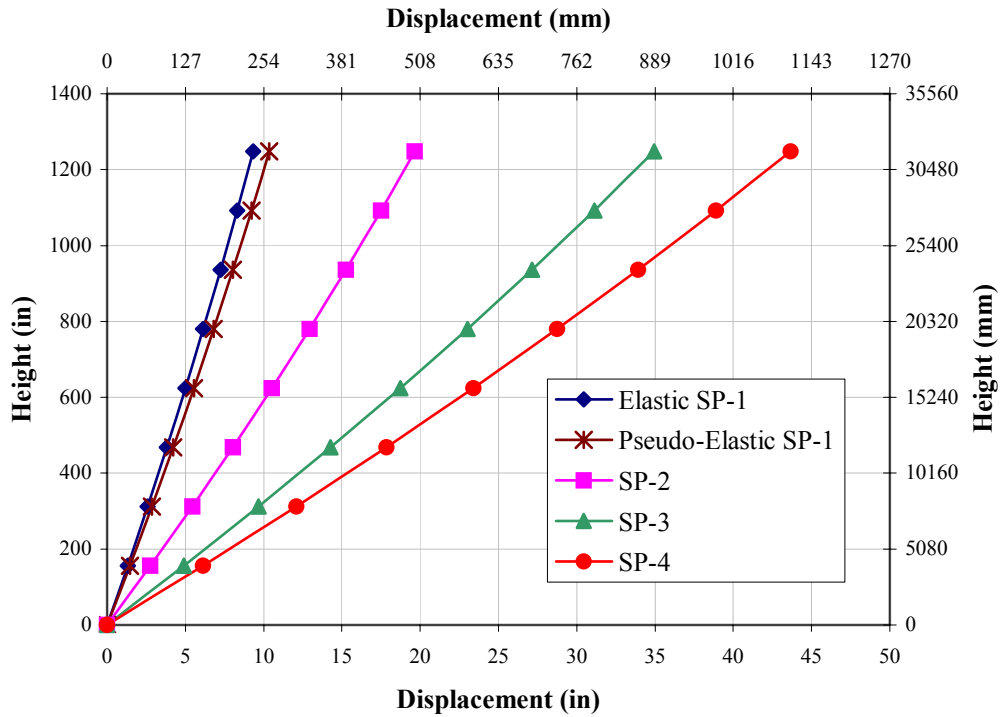


Figure 2.5.7-1. Target displacement profiles (FR-8-W27)

Step 5: Determine effective system displacements.

SDOF System Properties: Elastic SP-1 (Operational)

Gravity:		32.2			
Floor (i)	W_i	M_i	$M_i \Delta_i$	$M_i \Delta_i^2$	$M_i \Delta_i h_i$
Ground	0.00	0	0	0	0
2	182.81	5677	7453	9784	1162700
3	182.81	5677	14670	37905	4576976
4	182.81	5677	21650	82558	10132096
5	182.81	5677	28393	141996	17717327
6	182.81	5677	34900	214535	27221935
7	182.81	5677	41170	298547	38535186
8	182.81	5677	47204	392465	51546348
Roof	182.81	5677	53001	494778	66144687
Total: Σ	1462.50	45419	248440	1672569	217037254

$\Delta_{d,sys}$	6.73	in.	
$M_{eff,sys}$	36903		81% of total
$h_{eff,sys}$	874		70% of total
$\Delta_{y,sys}$	7.47	in.	
k	0.90		
$\mu_{\Delta,sys}$	0.90		

Table 2.5.7-6. Elastic SP-1 SDOF system properties (FR-8-W27)

SDOF System Properties: SP-2 (Occupiable)

Gravity:		32.2							
Floor (i)	W_i	M_i	$M_i \Delta_i$	$M_i \Delta_i^2$	$M_i \Delta_i h_i$	$\Delta_{d,sys}$	14.18	in.	
Ground	0.00	0	0	0	0	$M_{eff,sys}$	36903	81%	of total
2	182.81	5677	15693	43378	2448118	$h_{eff,sys}$	874	70%	of total
3	182.81	5677	30888	168046	9637035	$\Delta_{y,sys}$	7.47	in.	
4	182.81	5677	45585	366005	21333597	k	0.90		
5	182.81	5677	59783	629516	37304651	$\mu_{\Delta,sys}$	1.90		
6	182.81	5677	73483	951105	57317041				
7	182.81	5677	86685	1323557	81137615				
8	182.81	5677	99389	1739923	108533218				
Roof	182.81	5677	111595	2193513	139270696				
Total: Σ	1462.50	45419	523102	7415042	456981970				

Table 2.5.7-7. SP-2 SDOF system properties (FR-8-W27)

SDOF System Properties: SP-3 (Life Safe)

Gravity:		32.2							
Floor (i)	W_i	M_i	$M_i \Delta_i$	$M_i \Delta_i^2$	$M_i \Delta_i h_i$	$\Delta_{d,sys}$	25.20	in.	
Ground	0.00	0	0	0	0	$M_{eff,sys}$	36903	81%	of total
2	182.81	5677	27899	137095	4352209	$h_{eff,sys}$	874	70%	of total
3	182.81	5677	54912	531108	17132506	$\Delta_{y,sys}$	7.47	in.	
4	182.81	5677	81039	1156755	37926395	k	0.90		
5	182.81	5677	106281	1989581	66319379	$\mu_{\Delta,sys}$	3.37		
6	182.81	5677	130637	3005960	101896962				
7	182.81	5677	154108	4183095	144244649				
8	182.81	5677	176692	5499016	192947943				
Roof	182.81	5677	198391	6932586	247592348				
Total: Σ	1462.50	45419	929959	23435196	812412391				

Table 2.5.7-8. SP-3 SDOF system properties (FR-8-W27)

SDOF System Properties: SP-4 (Near Collapse)

		Gravity:	32.2							
Floor (i)	W_i	M_i	$M_i \Delta_i$	$M_i \Delta_i^2$	$M_i \Delta_i h_i$	$\Delta_{d,sys}$	31.50	in.		
Ground	0.00	0	0	0	0	$M_{eff,sys}$	36903	81%	of total	
2	182.81	5677	34873	214210	5440262	$h_{eff,sys}$	874	70%	of total	
3	182.81	5677	68640	829856	21415633	$\Delta_{y,sys}$	7.47	in.		
4	182.81	5677	101299	1807430	47407993	k	0.90			
5	182.81	5677	132851	3108721	82899224	$\mu_{\Delta,sys}$	4.22			
6	182.81	5677	163296	4696813	127371203					
7	182.81	5677	192634	6536086	180305811					
8	182.81	5677	220865	8592213	241184929					
Roof	182.81	5677	247989	10832165	309490435					
Total: Σ	1462.50	45419	1162449	36617494	1015515489					

Table 2.5.7-9. SP-4 SDOF system properties (FR-8-W27)

Step 6: Determine effective system properties and base shear.

Effective System Properties: SP-4 (Near Collapse)

$\zeta_{eff,sys}$	21%		$I_{eff,sys}$	265881	in ⁴
$T_{eff,sys}$	6.48	sec.	R	0.05	
$K_{eff,sys}$	34695	lbs/in.	$I_{i,sys}$	966027	in ⁴
$V_{b,sys}$	1093	Kips			

Table 2.5.7-10. SP-4 effective system properties (FR-8-W27)

Effective System Properties: SP-3 (Life Safe)

$\zeta_{eff,sys}$	17%		$I_{eff,sys}$	320291	in ⁴
$T_{eff,sys}$	5.904	sec.	r	0.05	
$K_{eff,sys}$	41795	lbs/in.	$I_{i,sys}$	966072	in ⁴
$V_{b,sys}$	1053	Kips			

Table 2.5.7-11. SP-3 effective system properties (FR-8-W27)

Effective System Properties: SP-2 (Occupiable)

$\zeta_{eff,sys}$	10%		$I_{eff,sys}$	532007	in ⁴
$T_{eff,sys}$	4.581	sec.	r	0.05	
$K_{eff,sys}$	69422	lbs/in.	$I_{i,sys}$	966381	in ⁴
$V_{b,sys}$	984	Kips			

Table 2.5.7-12. SP-2 effective system properties (FR-8-W27)

Effective System Properties: *Elastic* SP-1 (Operational)

$\zeta_{eff\ sys}$	5%		$I_{eff\ sys}$	966352	in^4
$T_{eff\ sys}$	3.399	sec. (Yield)			
$K_{eff\ sys}$	126100	lbs/in (Yield)			
$V_{b\ sys}$	849	Kips			
$V_{by\ sys}$	5%	Kips (Yield)			

Table 2.5.7-13. Elastic SP-1 effective system properties (FR-8-W27)

Step 7: Vertical base shear distribution and analysis.

Equivalent Static Lateral Forces:

Floor (i)	<i>Elastic</i> SP-1		SP-2		SP-3		SP-4	
	F_{yi}	$F_{yi} \Omega_{sys}$	F_i	$F_i \Omega_{sys}$	F_i	$F_i \Omega_{sys}$	F_i	$F_i \Omega_{sys}$
Ground	0	0	0	0	0	0	0	0
2	25	38	30	40	32	43	33	44
3	50	75	58	78	62	84	65	87
4	74	111	86	116	92	124	95	129
5	97	145	112	152	120	163	125	169
6	119	179	138	187	148	200	154	207
7	141	211	163	220	175	236	181	244
8	161	242	187	252	200	270	208	280
Roof	181	271	210	283	225	303	233	315
Total:	849	1271	984	1328	1053	1422	1093	1475

Table 2.5.7-14. Equivalent static lateral forces (FR-8-W27)

The system member overstrength factor was determined to be approximately 1.25 and the plastic hinge sequencing factor was assumed to be 1.2. This leads to a system performance overstrength factor, Ω_{sys} , of approximately 1.5. This factor is then applied to the expected system force-deformation graph starting at the *elastic* system as shown in Fig. 2.5.7-3. Since a portion of the system overstrength is accounted for in the reduced SP-1 value, the actual post-yield system overstrength is 1.35 (1.5*0.9). Additionally, the demands per floor were increased to the SP-1 level by dividing the demand by the respective floor rotation ductility (less than unity).

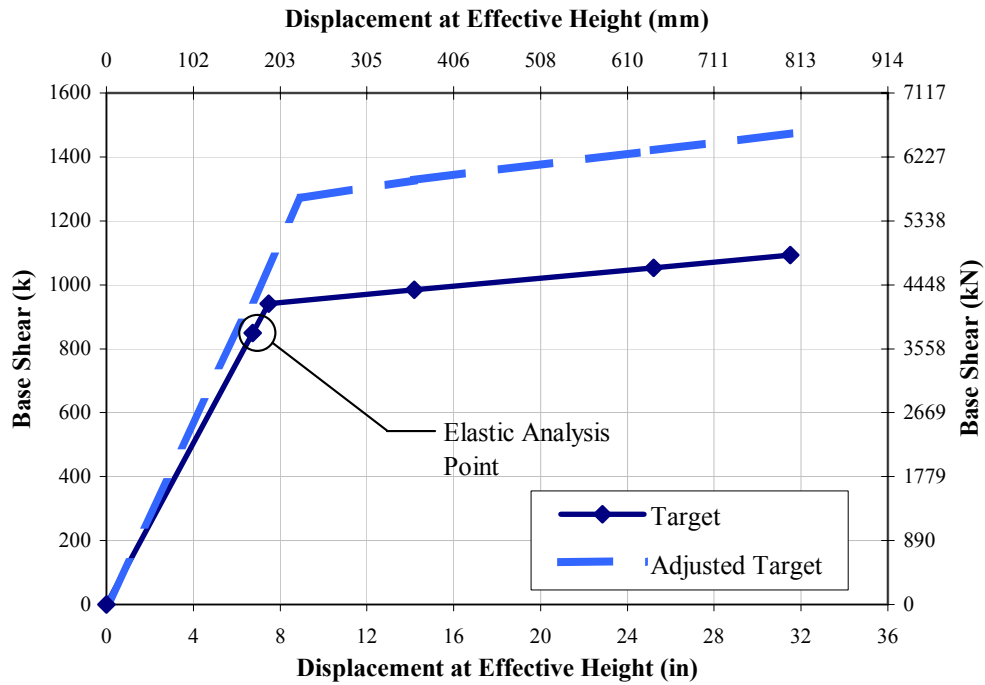


Figure 2.5.7-2. System force-displacement graph (FR-8-W27)

The final frame design is shown in Fig. 2.5.7-4 and the *elastic* SP-1 displacement profile is shown in Fig. 2.5.7-5.

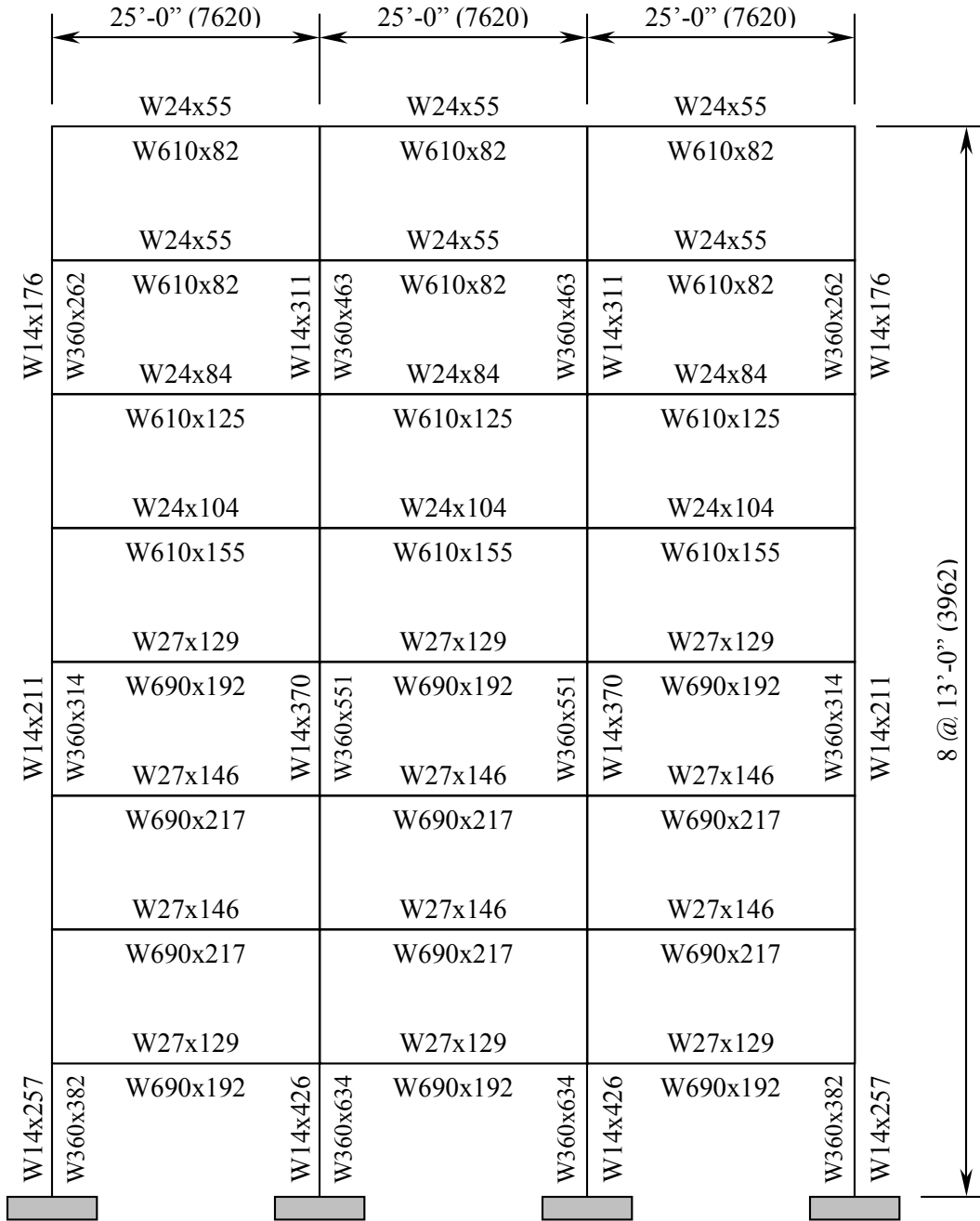


Figure 2.5.7-3. Final Frame schematic (FR-8-W27)

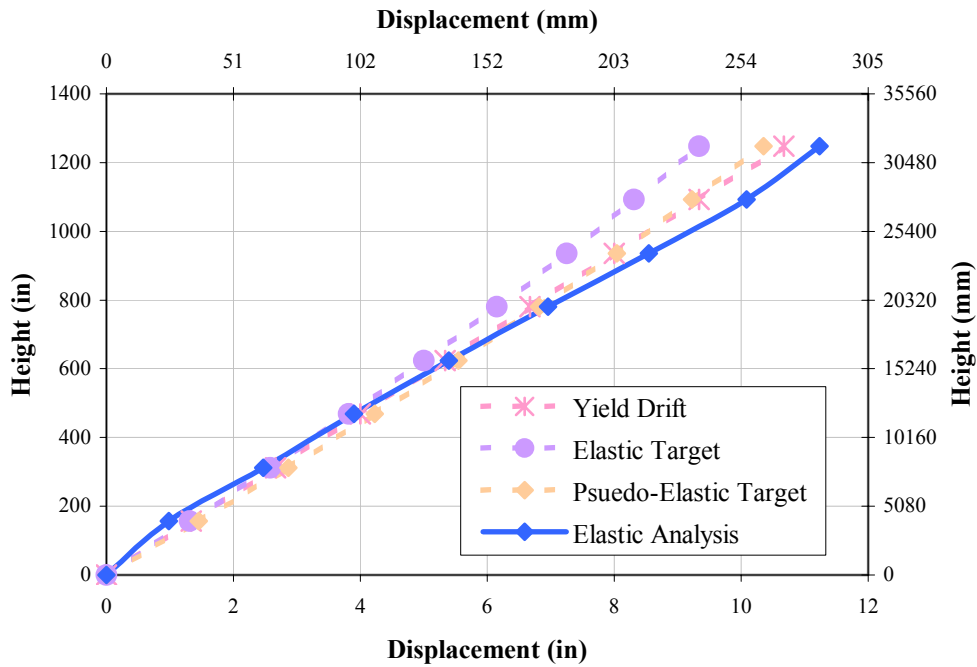


Figure 2.5.7-4. Elastic SP-1 Displacement Profile (FR-8-W27)

The same response is evident with both FR-8-W27 and FR-8. Although it cannot be accurately seen in the previous graph, all stories have slightly decreased lateral displacement demands. This should be expected since the use of W27 beams in the lower four floors changes the system stiffness and strength. Ultimately, there is reasonable agreement with the *elastic* displacement profile and actual displacement demands for both FR-8 and FR-8-W27. However, one might consider that steel frames respond linearly up to eight (8) stories.

2.5.8 Sixteen (16) Story Frame (FR-16)

Step 3: Determine initial beam depths and plastic rotations.

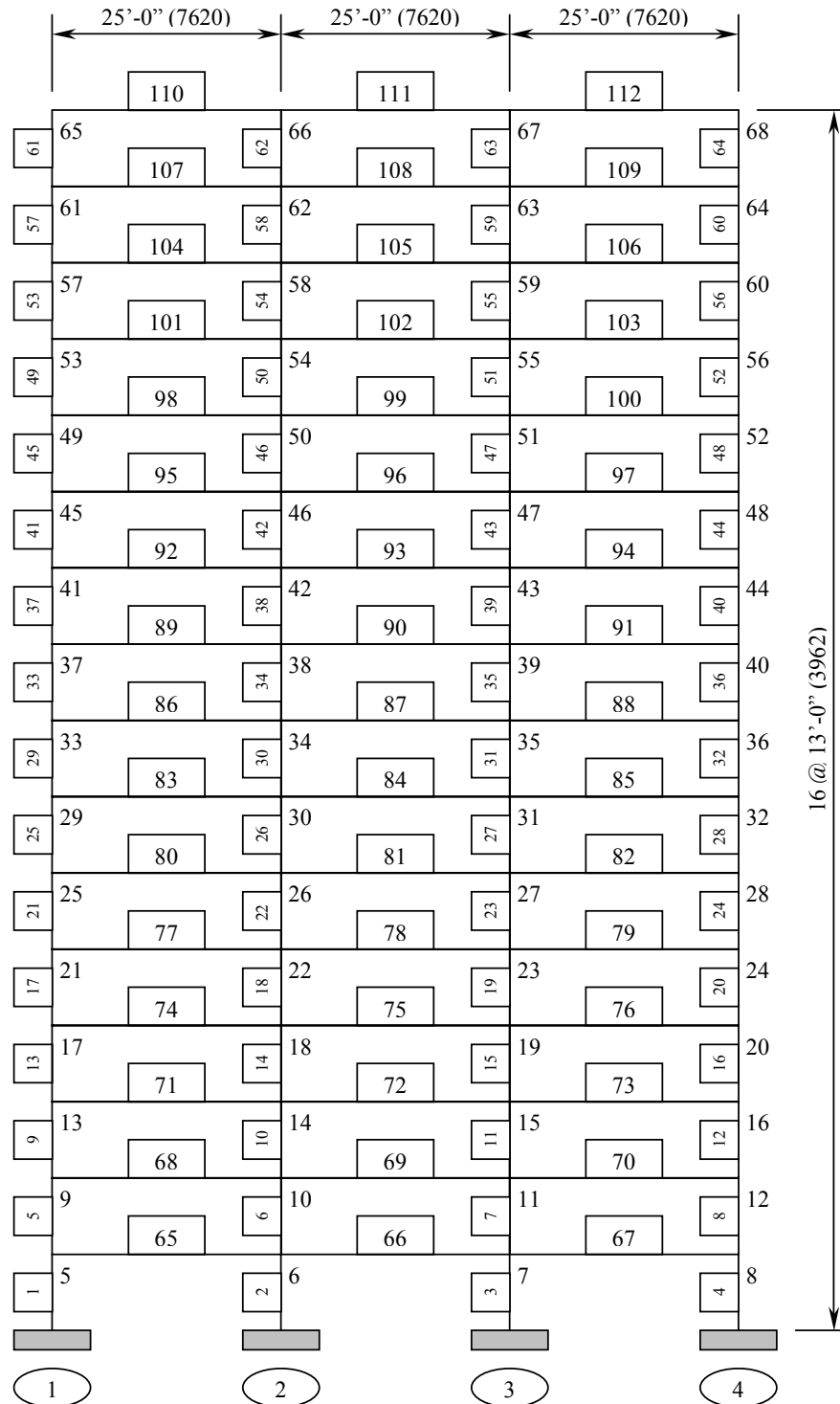


Figure 2.5.8-1. Frame schematic (FR-16)

Floor (i)	L_{b1}	L_{b2}	L_{b3}	d_1	d_2	d_3	θ_{p1}	θ_{p2}	θ_{p3}	θ_{pi}
Ground	0	0	0	0	0	0	0.00000	0.00000	0.00000	0.00000
2	300	300	300	30	30	30	0.00724	0.00724	0.00724	0.00724
3	300	300	300	30	30	30	0.00724	0.00724	0.00724	0.00724
4	300	300	300	30	30	30	0.00724	0.00724	0.00724	0.00724
5	300	300	300	30	30	30	0.00724	0.00724	0.00724	0.00724
6	300	300	300	30	30	30	0.00724	0.00724	0.00724	0.00724
7	300	300	300	30	30	30	0.00724	0.00724	0.00724	0.00724
8	300	300	300	30	30	30	0.00724	0.00724	0.00724	0.00724
9	300	300	300	30	30	30	0.00724	0.00724	0.00724	0.00724
10	300	300	300	30	30	30	0.00724	0.00724	0.00724	0.00724
11	300	300	300	27	27	27	0.00805	0.00805	0.00805	0.00805
12	300	300	300	27	27	27	0.00805	0.00805	0.00805	0.00805
13	300	300	300	27	27	27	0.00805	0.00805	0.00805	0.00805
14	300	300	300	24	24	24	0.00905	0.00905	0.00905	0.00905
15	300	300	300	24	24	24	0.00905	0.00905	0.00905	0.00905
16	300	300	300	24	24	24	0.00905	0.00905	0.00905	0.00905
Roof	300	300	300	24	24	24	0.00905	0.00905	0.00905	0.00905
									$\theta_{p,sys} \Rightarrow$ Average:	0.00784
									$\theta_{p,sys} \Rightarrow$ Minimum:	0.00724
									EQ I Factor:	1.57

Table 2.5.8-1. Floor equivalent plastic rotations (FR-16)

The system rotation capacity corresponding to the SP-1 performance level is 0.00784. Therefore, the EQ I modification factor is $0.00784/0.005 = 1.57$ and the MCE PGA Reduction Factor of $0.125*1.57 = 0.196$.

Step 4: Determine target displacement profiles.

Target Displacements: *Elastic SP-1 (Operational)*

Floor (i)	θ_{Ti}	β	μ_{θ}	Δ_{di}	$\Delta_{di \text{ Drift}}$	θ_{di}	$\Delta_{Ti \text{ Drift}}$	Δ_{Ti}	h_{floor}	h_i
Ground	0.00000	0.00	0.00	0.00	0.00	0.0000	0.00	0.00	0	0
2	0.00724	1.58	1.06	1.20	1.20	0.0077	1.22	1.22	156	156
3	0.00724	1.58	1.01	2.33	1.14	0.0073	1.22	2.45	156	312
4	0.00724	1.58	0.96	3.41	1.08	0.0069	1.22	3.67	156	468
5	0.00724	1.58	0.91	4.44	1.02	0.0066	1.22	4.90	156	624
6	0.00724	1.58	0.85	5.40	0.97	0.0062	1.22	6.12	156	780
7	0.00724	1.58	0.80	6.31	0.91	0.0058	1.22	7.34	156	936
8	0.00724	1.58	0.75	7.16	0.85	0.0055	1.22	8.57	156	1092
9	0.00724	1.58	0.70	7.95	0.79	0.0051	1.22	9.79	156	1248
10	0.00724	1.58	0.65	8.69	0.74	0.0047	1.22	11.01	156	1404
11	0.00805	1.58	0.54	9.37	0.68	0.0044	1.22	12.24	156	1560
12	0.00805	1.58	0.50	9.99	0.62	0.0040	1.22	13.46	156	1716
13	0.00805	1.58	0.45	10.56	0.56	0.0036	1.22	14.69	156	1872
14	0.00905	1.58	0.36	11.06	0.51	0.0032	1.22	15.91	156	2028
15	0.00905	1.58	0.32	11.51	0.45	0.0029	1.22	17.13	156	2184
16	0.00905	1.58	0.28	11.90	0.39	0.0025	1.22	18.36	156	2340
Roof	0.00905	1.58	0.24	12.24	0.33	0.0021	1.22	19.58	156	2496

Table 2.5.8-2. Elastic SP-1 target displacements (FR-16)

Target Displacements: SP-2 (Occupiable)

Floor (i)	θ_{Ti}	β	μ_{θ}	Δ_{di}	$\Delta_{di \text{ Drift}}$	θ_{di}	$\Delta_{ti \text{ Drift}}$	Δ_{ti}	h_{floor}	h_i
Ground	0.00000	0.00	0.00	0.00	0.00	0.0000	0.00	0.00	0	0
2	0.01800	1.10	2.43	2.74	2.74	0.0176	2.81	2.81	156	156
3	0.01800	1.10	2.31	5.35	2.61	0.0167	2.81	5.62	156	312
4	0.01800	1.10	2.19	7.83	2.48	0.0159	2.81	8.42	156	468
5	0.01800	1.10	2.08	10.18	2.35	0.0150	2.81	11.23	156	624
6	0.01800	1.10	1.96	12.39	2.22	0.0142	2.81	14.04	156	780
7	0.01800	1.10	1.84	14.48	2.08	0.0134	2.81	16.85	156	936
8	0.01800	1.10	1.73	16.43	1.95	0.0125	2.81	19.66	156	1092
9	0.01800	1.10	1.61	18.25	1.82	0.0117	2.81	22.46	156	1248
10	0.01800	1.10	1.50	19.94	1.69	0.0108	2.81	25.27	156	1404
11	0.01800	1.10	1.24	21.50	1.56	0.0100	2.81	28.08	156	1560
12	0.01800	1.10	1.14	22.92	1.43	0.0091	2.81	30.89	156	1716
13	0.01800	1.10	1.03	24.22	1.29	0.0083	2.81	33.70	156	1872
14	0.01800	1.10	0.82	25.38	1.16	0.0075	2.81	36.50	156	2028
15	0.01800	1.10	0.73	26.41	1.03	0.0066	2.81	39.31	156	2184
16	0.01800	1.10	0.64	27.31	0.90	0.0058	2.81	42.12	156	2340
Roof	0.01800	1.10	0.54	28.08	0.77	0.0049	2.81	44.93	156	2496

Table 2.5.8-3. SP-2 target displacements (FR-16)

Target Displacements: SP-3 (Life Safe)

Floor (i)	θ_{Ti}	β	μ_{θ}	Δ_{di}	$\Delta_{di \text{ Drift}}$	θ_{di}	$\Delta_{di \text{ Drift}}$	Δ_{ri}	h_{floor}	h_i
Ground	0.00000	0.00	0.00	0.00	0.00	0.0000	0.00	0.00	0	0
2	0.03200	1.03	4.32	4.88	4.88	0.0313	4.99	4.99	156	156
3	0.03200	1.03	4.11	9.52	4.64	0.0298	4.99	9.98	156	312
4	0.03200	1.03	3.90	13.92	4.41	0.0283	4.99	14.98	156	468
5	0.03200	1.03	3.69	18.10	4.17	0.0268	4.99	19.97	156	624
6	0.03200	1.03	3.49	22.04	3.94	0.0253	4.99	24.96	156	780
7	0.03200	1.03	3.28	25.74	3.71	0.0238	4.99	29.95	156	936
8	0.03200	1.03	3.07	29.21	3.47	0.0223	4.99	34.94	156	1092
9	0.03200	1.03	2.87	32.45	3.24	0.0208	4.99	39.94	156	1248
10	0.03200	1.03	2.66	35.45	3.00	0.0193	4.99	44.93	156	1404
11	0.03200	1.03	2.21	38.22	2.77	0.0178	4.99	49.92	156	1560
12	0.03200	1.03	2.02	40.76	2.54	0.0163	4.99	54.91	156	1716
13	0.03200	1.03	1.83	43.06	2.30	0.0148	4.99	59.90	156	1872
14	0.03200	1.03	1.46	45.12	2.07	0.0133	4.99	64.90	156	2028
15	0.03200	1.03	1.30	46.96	1.83	0.0118	4.99	69.89	156	2184
16	0.03200	1.03	1.13	48.56	1.60	0.0103	4.99	74.88	156	2340
Roof	0.03200	1.03	0.97	49.92	1.37	0.0088	4.99	79.87	156	2496

Table 2.5.8-4. SP-3 target displacements (FR-16)

Target Displacements: SP-4 (Near Collapse)

Floor (i)	θ_{Ti}	β	μ_{θ}	Δ_{di}	Δ_{di} Drift	θ_{di}	Δ_{Ti} Drift	Δ_{Ti}	h_{floor}	h_i
Ground	0.00000	0.00	0.00	0.00	0.00	0.0000	0.00	0.00	0	0
2	0.04000	1.00	5.39	6.09	6.09	0.0391	6.24	6.24	156	156
3	0.04000	1.00	5.14	11.90	5.80	0.0372	6.24	12.48	156	312
4	0.04000	1.00	4.88	17.40	5.51	0.0353	6.24	18.72	156	468
5	0.04000	1.00	4.62	22.62	5.22	0.0334	6.24	24.96	156	624
6	0.04000	1.00	4.36	27.54	4.92	0.0316	6.24	31.20	156	780
7	0.04000	1.00	4.10	32.18	4.63	0.0297	6.24	37.44	156	936
8	0.04000	1.00	3.84	36.51	4.34	0.0278	6.24	43.68	156	1092
9	0.04000	1.00	3.58	40.56	4.05	0.0259	6.24	49.92	156	1248
10	0.04000	1.00	3.32	44.31	3.75	0.0241	6.24	56.16	156	1404
11	0.04000	1.00	2.76	47.78	3.46	0.0222	6.24	62.40	156	1560
12	0.04000	1.00	2.52	50.94	3.17	0.0203	6.24	68.64	156	1716
13	0.04000	1.00	2.29	53.82	2.88	0.0184	6.24	74.88	156	1872
14	0.04000	1.00	1.83	56.40	2.58	0.0166	6.24	81.12	156	2028
15	0.04000	1.00	1.62	58.70	2.29	0.0147	6.24	87.36	156	2184
16	0.04000	1.00	1.42	60.69	2.00	0.0128	6.24	93.60	156	2340
Roof	0.04000	1.00	1.21	62.40	1.71	0.0109	6.24	99.84	156	2496

Table 2.5.8-5. SP-4 target displacements (FR-16)

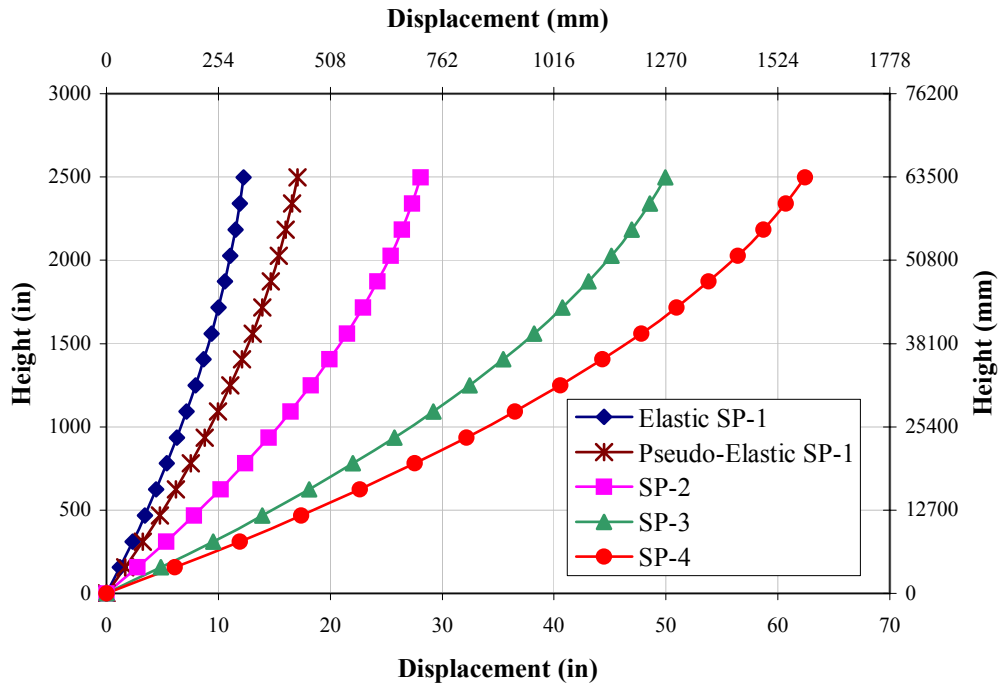


Figure 2.5.8-2. Target displacement profiles (FR-16)

Step 5: Determine effective system displacements.

SDOF System Properties: *Elastic SP-1 (Operational)*

		Gravity: 32.2			
Floor (i)	W_i	M_i	$M_i \Delta_i$	$M_i \Delta_i^2$	$M_i \Delta_i h_i$
Ground	0.00	0	0	0	0
2	182.81	5677	6785	8109	1058480
3	182.81	5677	13245	30898	4132306
4	182.81	5677	19378	66143	9069057
5	182.81	5677	25186	111733	15716311
6	182.81	5677	30669	165670	23921648
7	182.81	5677	35825	226065	33532647
8	182.81	5677	40656	291145	44396885
9	182.81	5677	45162	359247	56361943
10	182.81	5677	49341	428819	69275399
11	182.81	5677	53195	498423	82984833
12	182.81	5677	56724	566733	97337821
13	182.81	5677	59926	632535	112181945
14	182.81	5677	62803	694725	127364782
15	182.81	5677	65354	752314	142733912
16	182.81	5677	67580	804424	158136913
Roof	182.81	5677	69480	850288	173421364
Total:	2925.00	90839	701311	6487269	1151626247

$\Delta_{d,sys}$	9.25	in.	
$M_{eff,sys}$	75816		83% of total
$h_{eff,sys}$	1642		66% of total
$\Delta_{y,sys}$	12.88	in.	
k	0.78		
$\mu_{\Delta,sys}$	0.72		

Table 2.5.8-6. Elastic SP-1 SDOF system properties (FR-16)

SDOF System Properties: SP-2 (Occupiable)

Gravity:		32.2			
Floor (i)	W_i	M_i	$M_i \Delta_i$	$M_i \Delta_i^2$	$M_i \Delta_i h_i$
Ground	0.00	0	0	0	0
2	182.81	5677	15569	42692	2428688
3	182.81	5677	30390	162669	9481599
4	182.81	5677	44464	348226	20809000
5	182.81	5677	57790	588248	36061162
6	182.81	5677	70370	872210	54888353
7	182.81	5677	82202	1190179	76940842
8	182.81	5677	93287	1532809	101868898
9	182.81	5677	103624	1891346	129322789
10	182.81	5677	113214	2257626	158952785
11	182.81	5677	122057	2624076	190409154
12	182.81	5677	130153	2983712	223342166
13	182.81	5677	137501	3330140	257402089
14	182.81	5677	144102	3657556	292239193
15	182.81	5677	149956	3960748	327503745
16	182.81	5677	155062	4235093	362846016
Roof	182.81	5677	159422	4476558	397916273
Total:	2925.00	90839	1609162	34153887	2642412752

$\Delta_{d,sys}$	21.22	in.	
$M_{eff,sys}$	75816		83% of total
$h_{eff,sys}$	1642		66% of total
$\Delta_{y,sys}$	12.88	in.	
k	0.72		
$\mu_{\Delta,sys}$	1.65		

Table 2.5.8-7. SP-2 SDOF system properties (FR-16)

SDOF System Properties: SP-3 (Life Safe)

Gravity:		32.2			
Floor (i)	W_i	M_i	$M_i \Delta_i$	$M_i \Delta_i^2$	$M_i \Delta_i h_i$
Ground	0.00	0	0	0	0
2	182.81	5677	27677	134927	4317668
3	182.81	5677	54026	514113	16856175
4	182.81	5677	79047	1100565	36993779
5	182.81	5677	102738	1859153	64108733
6	182.81	5677	125102	2756615	97579294
7	182.81	5677	146136	3761552	136783719
8	182.81	5677	165843	4844432	181100262
9	182.81	5677	184220	5977587	229907180
10	182.81	5677	201270	7135214	282582728
11	182.81	5677	216990	8293376	338505163
12	182.81	5677	231383	9430003	397052740
13	182.81	5677	244446	10524885	457603714
14	182.81	5677	256182	11559684	519536343
15	182.81	5677	266588	12517921	582228880
16	182.81	5677	275666	13384986	645059584
Roof	182.81	5677	283416	14148134	707406708
Total:	2925.00	90839	2860732	#####	4697622671

$\Delta_{d,sys}$	37.73	in.	
$M_{eff,sys}$	75816		83% of total
$h_{eff,sys}$	1642		66% of total
$\Delta_{y,sys}$	12.88	in.	
k	0.72		
$\mu_{\Delta,sys}$	2.93		

Table 2.5.8-8. SP-3 SDOF system properties (FR-16)

SDOF System Properties: SP-4 (Near Collapse)

Gravity:		32.2						
Floor (i)	W_i	M_i	$M_i \Delta_i$	$M_i \Delta_i^2$	$M_i \Delta_i h_i$	$\Delta_{d,sys}$	47.17	in.
Ground	0.00	0	0	0	0	$M_{eff,sys}$	75816	83% of total
2	182.81	5677	34597	210824	5397085	$h_{eff,sys}$	1642	66% of total
3	182.81	5677	67533	803302	21070219	$\Delta_{y,sys}$	12.88	in.
4	182.81	5677	98808	1719633	46242223	k	0.72	
5	182.81	5677	128423	2904927	80135916	$\mu_{\Delta,sys}$	3.66	
6	182.81	5677	156377	4307211	121974118			
7	182.81	5677	182671	5877425	170979649			
8	182.81	5677	207303	7569425	226375328			
9	182.81	5677	230276	9339979	287383975			
10	182.81	5677	251587	11148772	353228411			
11	182.81	5677	271238	12958401	423131454			
12	182.81	5677	289228	14734379	496315925			
13	182.81	5677	305558	16445133	572004643			
14	182.81	5677	320227	18062006	649420428			
15	182.81	5677	333235	19559251	727786101			
16	182.81	5677	344583	20914041	806324480			
Roof	182.81	5677	354270	22106460	884258385			
Total:	2925.00	90839	3575915	#####	5872028339			

Table 2.5.8-9. SP-4 SDOF system properties (FR-16)

Similar to the discussion in the design of FR-8, the Equivalent Yield Analysis is used.

Step 6: Determine effective system properties and base shear.

Effective System Properties: SP-4 (Near Collapse)

$\zeta_{eff,sys}$	19%		$I_{eff,sys}$	1780406	in ⁴
$T_{eff,sys}$	9.25	sec.	r	0.05	
$K_{eff,sys}$	34981	lbs/in.	$I_{i,sys}$	5753162	in ⁴
$V_{b,sys}$	1650	Kips			

Table 2.5.8-10. SP-4 effective system properties (FR-16)

Effective System Properties: SP-3 (Life Safe)

$\zeta_{eff\ sys}$	15%
$T_{eff\ sys}$	8.41
$K_{eff\ sys}$	42318
$V_{b\ sys}$	1597

sec.

lbs/in.

Kips

$I_{eff\ sys}$	2153826	in ⁴
r	0.05	
$I_{i\ sys}$	5753783	in ⁴

Table 2.5.8-11. SP-3 effective system properties (FR-16)

Effective System Properties: SP-2 (Occupiable)

$\zeta_{eff\ sys}$	8%
$T_{eff\ sys}$	6.5
$K_{eff\ sys}$	70842
$V_{b\ sys}$	1504

sec.

lbs/in.

Kips

$I_{eff\ sys}$	3605587	in ⁴
r	0.05	
$I_{i\ sys}$	5754295	in ⁴

Table 2.5.8-12. SP-2 effective system properties (FR-16)

Effective System Properties: *Elastic* SP-1 (Operational)

$\zeta_{eff\ sys}$	5%
$T_{eff\ sys}$	5.145
$K_{eff\ sys}$	113070
$V_{b\ sys}$	1046
$V_{by\ sys}$	1457

sec. (Yield)

lbs/in (Yield)

Kips

Kips (Yield)

$I_{eff\ sys}$	5754822	in ⁴
----------------	---------	-----------------

Table 2.5.8-13. Elastic SP-1 effective system properties (FR-16)

Step 7: Vertical base shear distribution and analysis.

Equivalent Static Lateral Forces:

Floor (i)	Elastic SP-1		SP-2		SP-3		SP-4	
	F_{yi}	$F_{yi} \Omega_{sys}$	F_i	$F_i \Omega_{sys}$	F_i	$F_i \Omega_{sys}$	F_i	$F_i \Omega_{sys}$
Ground	0	0	0	0	0	0	0	0
2	10	14	15	16	15	17	16	18
3	20	28	28	31	30	33	31	34
4	29	40	42	46	44	49	46	50
5	38	52	54	59	57	63	59	65
6	46	64	66	72	70	77	72	79
7	53	74	77	84	82	90	84	93
8	61	84	87	96	93	102	96	105
9	67	94	97	107	103	113	106	117
10	74	102	106	116	112	124	116	128
11	79	110	114	125	121	133	125	138
12	85	118	122	134	129	142	133	147
13	89	124	128	141	136	150	141	155
14	94	130	135	148	143	157	148	163
15	97	136	140	154	149	164	154	169
16	101	140	145	159	154	169	159	175
Roof	104	144	149	164	158	174	163	180
Total:	1046	1457	1504	1654	1597	1756	1650	1815

Table 2.5.8-14. Equivalent static lateral forces (FR-16)

The system member overstrength factor was determined to be approximately 1.25, with and the plastic hinge sequencing factor was assumed to be 1.2. This leads to a system performance overstrength factor, Ω_{sys} , of approximately 1.5. This factor is then applied to the expected system force-deformation graph determined starting at the *elastic* system as shown in Fig. 2.5.8-3. Thus since a portion of the system overstrength is accounted for in the reduced SP-1 value, the post-yield system overstrength is 1.10 (1.5*0.72). Additionally, the demands per floor where increased to the SP-1 level by dividing the demand by the respective floor rotation ductility (less than unity).

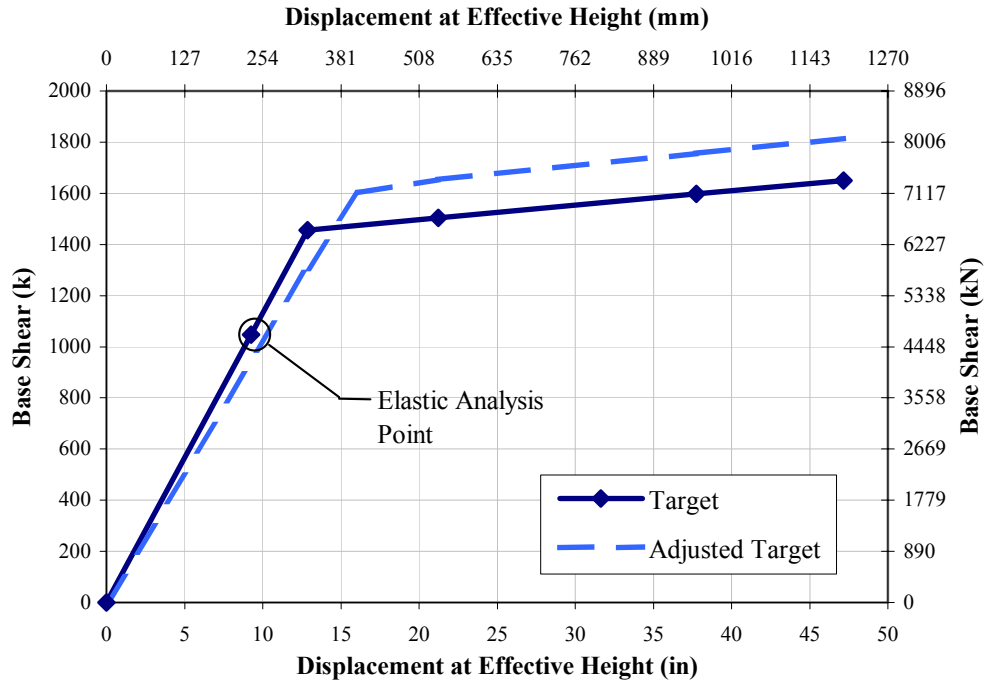


Figure 2.5.8-3. System force-displacement graph (FR-16)

The final frame design is shown in Fig. 2.5.8-4 and the *elastic* SP-1 displacement profile is shown in Fig. 2.5.8-5.

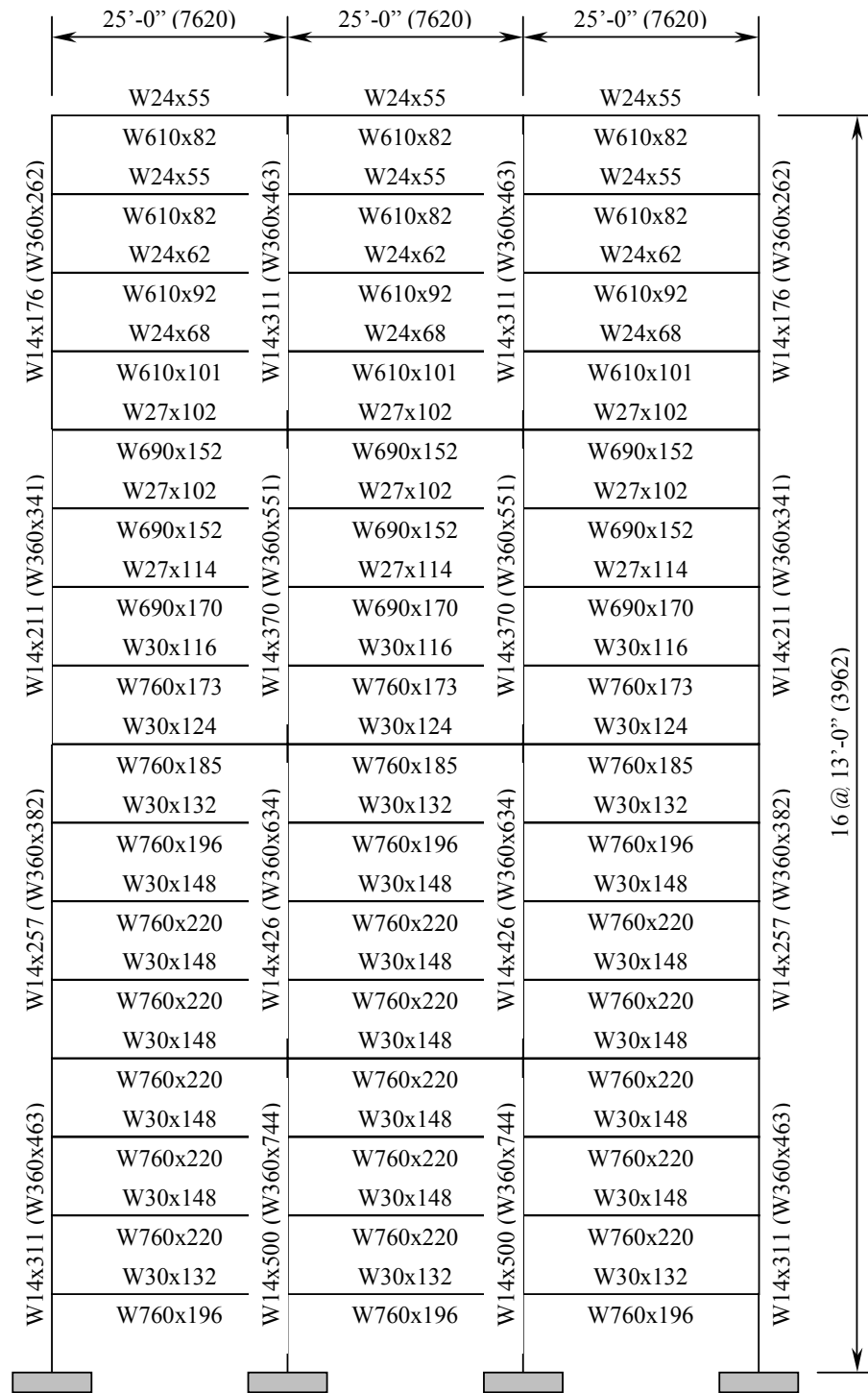


Figure 2.5.8-4. Final frame schematic (FR-16)

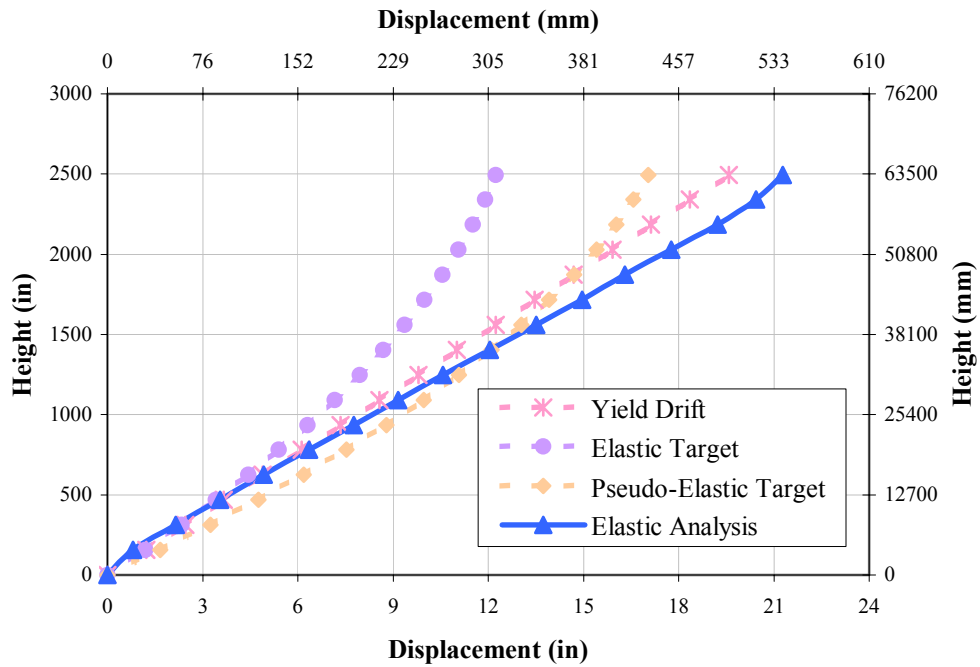


Figure 2.5.8-5. Elastic SP-1 Displacement Profile (FR-16)

Similar to the discussion for FR-8 and FR-8-W27, it is evident that for long period frames the displacement profile diverges from the target profile. Additionally, the assumption of constant shape functions for all performance levels is invalid for long period structures. For this reason, future research is required for these type frames.

PART 3

ADVANCED ANALYSIS

3.0 Introduction

As discussed previously, an elastic 2nd order analysis is used to analyze a frame subjected to the equivalent static lateral seismic forces determined at the SP-1 performance level. Thus the need arises to modify the design base shear (lateral forces) for specific frame configurations (i.e. non-linear displacement profiles) in an attempt to represent a purely elastic system. The demands (moment, shear, and axial forces) from the analysis, including Capacity Design procedures, are then used to design the members in accordance with current steel design theory. It is recommended that steel members be designed in accordance with Load and Resistance Factor Design (LRFD). It is out of the scope of this document to discuss the advantages of using LRFD in lieu of the current design office standard, Allowable Stress Design (ASD), except that a better understanding of failure modes is recognized using a reliability-based design philosophy with performance-based seismic engineering. Additionally, it is recommended that a seismic load factor and resistance factor of unity be used in design.

One draw back of using an elastic analysis is it does not account for member inelastic behavior or the effects of geometric imperfections inherent in LRFD design interaction equations. Additionally, $P-\Delta$ and $P-\delta$ effects (global and local geometric non-linear effects, or 2nd order effects, respectively) shall be included in the analysis. However, few standard elastic analysis software packages account for local $P-\delta$ effects. Alternatively, B_1 and B_2 amplification factors specified in LRFD (1st order elastic analysis) can be used to approximate the global $P-\Delta$ and $P-\delta$ effects for a completely elastic system. However, these factors were derived based on elastic system response and are not suitable for post-yield systems (*Smith, 1996*). Thus an incompatibility exists between the elastic analysis demands and capacities determined from inelastic design interaction equations. That is strength and stability of a system and its members are related, but the interaction is treated separately in the LRFD specifications (*Chen and Kim, 1997*). For the design of elastic systems this discrepancy is of no great importance. However, in seismic engineering, where the members are required to behave and maintain structural integrity in the inelastic region, an elastic analysis will produce conservative demands. This in effect will inherently contribute to the

performance overstrength factor. Furthermore, displacements are used to determine damage levels and since geometric imperfections are accounted for in member design interaction equations and not the analysis, including a push-over analysis, a discrepancy exists in the final ductility prediction.

Currently, the interaction between the system and its members is approximated by the effective length factor, K . Simply, the effective length factor is used to represent the influence of the system on the strength of an individual member (*Chen and Kim, 1997*). However, the alignment chart currently used in steel design does not account for inelastic stiffness reduction of a column and may underestimate the column strength when P_u/P_y is greater than $1/3$ (*Chen and Kim, 1997*). This design methodology allows the design engineer to isolate a member from the system and design the member based on strength curves and interaction equations developed to implicitly account for the effects of yielding and geometric imperfections (stability). This, as previously mentioned, does not satisfy compatibility between the actual inelastic member and the elastic system as assumed in the frame analysis (*Chen and Kim, 1997*). It is outside the scope of this research to define and discuss the calculation of effective length factors or the difficulties associated in accurately predicting system behavior and influence thereof. The reader is therefore referred to other references for detailed discussions (*Chen and Kim, 1997, Chen and Lui, 1991, Chen and Toma, 1994, ASCE, 1994*). Ultimately, the need arises for an analysis/design procedure that combines the behavior of the system and its members thus eliminating any incompatibilities.

Advanced Analysis is any 2nd order inelastic static analysis that captures the limit state strength and stability of a structural system and its individual members (*Chen and Kim, 1997*). Thus predicting the system strength, where as conventional analysis can only define member strengths. Similarly, separate member capacity checks and exhaustive effective length calculations are not required. This can be achieved by incorporating the effects of yielding and geometric imperfections, implicit in design interaction equations and strength curves, into the analysis.

This research aims only to discuss the fundamentals of Advanced Analysis; hence, the reader is referred to work by W.F. Chen and others for detailed discussions on the development of Advanced Analysis procedures, outlined for convenience in Section 3.4,

3.1 Advanced Analysis

The advantages of Advanced Analysis in the design of steel moment frames are outlined in the following (*Chen and Kim, 1997*):

- 1) Advanced Analysis is another tool for structural engineers to use in steel design, and its adoption is not mandatory but will provide a flexibility of options to the designer.
- 2) Advanced Analysis captures the limit state strength and stability of a structural system and its individual members directly, so separate member capacity checks encompassed by the specification equations are not required.
- 3) Compared to the LRFD and ASD, Advanced Analysis provides more information of structural behavior by direct inelastic 2nd order analysis.
- 4) Advanced Analysis overcomes the difficulties due to incompatibility between the elastic global analysis and the limit state member design in the conventional LRFD method.
- 5) Advanced Analysis is user-friendly for a computer-based design, but the LRFD and ASD are not because they require the calculation of K factor on the way from their analysis to separate member capacity checks.
- 6) Advanced Analysis captures the inelastic redistribution of internal forces throughout a structural system, and allows an economic use of material for highly indeterminate steel frames.
- 7) It is now feasible to employ Advanced Analysis techniques that have been considered impractical for design office use in the past because the power of personal computers and engineering work-stations is rapidly increasing.

- 8) Member sizes determined by Advanced Analysis are close to those determined by the LRFD method because the Advanced Analysis method is calibrated against the LRFD column curve and beam-column interaction equations. As a result, advanced analysis provides an alternative to the LRFD.
- 9) Advanced Analysis is time-effective because it completely eliminates tedious and often confused member capacity checks including the calculation of K - factors in the LRFD and ASD.

3.2 Advanced Analysis Methods

Currently there are five (5) types of Advanced Analysis methods:

- 1) Plastic-zone
- 2) Quasi-plastic hinge
- 3) Elastic-plastic hinge
- 4) Notional-load plastic hinge
- 5) Refined-plastic hinge

The refined-plastic hinge (RPH) method is the preferred method for its simplicity and realistic representation of actual behavior (*Chen and Kim, 1997*). In this analysis, stability functions, discussed in Section 2.3, are used to predict 2nd order effects and a two-surface yield model and an effective tangent modulus are used to account for stiffness degradation due to distributed plasticity in framed members (*Chen and Kim, 1997*). Furthermore, the RPH method incorporates three effects that influence the analysis and design of steel members: 1) material, 2) geometric, and 3) connection non-linearities. Connection non-linearity, or semi-rigid connections, will not be discussed in this research since fully rigid beam-to-column connections are assumed. The previous two are discussed subsequently.

3.2.1 Material Non-linearities

Material non-linearities include the effects of yielding associated with flexure and the influence of residual stresses on the capacity of a steel member. To incorporate the flexural yielding effect in the analysis, the element stiffness must degrade parabolically after the member end forces exceed the defined yield function. When the plastic moment capacity is reached, the plastic hinge is modeled as a true hinge with an applied constant plastic moment, M_{pr} , discussed in Section 2.2, otherwise known as a zero length plastic hinge. Modifying the element stiffness matrix in the analysis then modifies the member tangent stiffness to account for the presence of the plastic hinge(s), including the presence of axial forces.

Effect of Plastification at End A Only

$$\begin{Bmatrix} M_A \\ M_B \end{Bmatrix} = \frac{E_t I}{L} \begin{bmatrix} \eta_A S_1 & \eta_A S_2 \\ \eta_A S_2 & \left[S_1 - \frac{S_2^2}{S_1} (1 - \eta_A) \right] \end{bmatrix} \begin{Bmatrix} \theta_A \\ \theta_B \end{Bmatrix} \quad (3.2.1-1)$$

Effect of Plastification at End B Only

$$\begin{Bmatrix} M_A \\ M_B \end{Bmatrix} = \frac{E_t I}{L} \begin{bmatrix} \left[S_1 - \frac{S_2^2}{S_1} (1 - \eta_B) \right] & \eta_B S_2 \\ \eta_B S_2 & \eta_B S_1 \end{bmatrix} \begin{Bmatrix} \theta_A \\ \theta_B \end{Bmatrix} \quad (3.2.1-2)$$

Effect of Plastification at Both Ends

$$\begin{Bmatrix} M_A \\ M_B \end{Bmatrix} = \frac{E_t I}{L} \begin{bmatrix} \eta_A \left[S_1 - \frac{S_2^2}{S_1} (1 - \eta_B) \right] & \eta_A \eta_B S_2 \\ \eta_A \eta_B S_2 & \eta_B \left[S_1 - \frac{S_2^2}{S_1} (1 - \eta_A) \right] \end{bmatrix} \begin{Bmatrix} \theta_A \\ \theta_B \end{Bmatrix} \quad (3.2.1-3)$$

where

E_t = Tangent Modulus defined subsequently

η = Parameter that allows for gradual inelastic stiffness reduction

$$\eta = 1 \text{ for } \alpha \leq 0.5 \quad (3.2.1-4)$$

$$\eta = 4\alpha(1-\alpha) \text{ for } \alpha > 0.5 \quad (3.2.1-5)$$

α = Parameter that measures the magnitude of axial force and bending moment

$$\alpha = \frac{P}{P_y} + \frac{8}{9} \frac{M}{M_p} \text{ for } \frac{P}{P_y} \geq \frac{2}{9} \frac{M}{M_p} \quad (3.2.1-6)$$

$$\alpha = \frac{P}{2P_y} + \frac{M}{M_p} \text{ for } \frac{P}{P_y} < \frac{2}{9} \frac{M}{M_p} \quad (3.2.1-7)$$

S_i = Element stiffness discussed previously in Section 2

This process allows the element stiffness to reduce to account for the effect of plastification at the member end when the force point moves beyond the initial yield surface as shown in Figure 3.2.1-1.

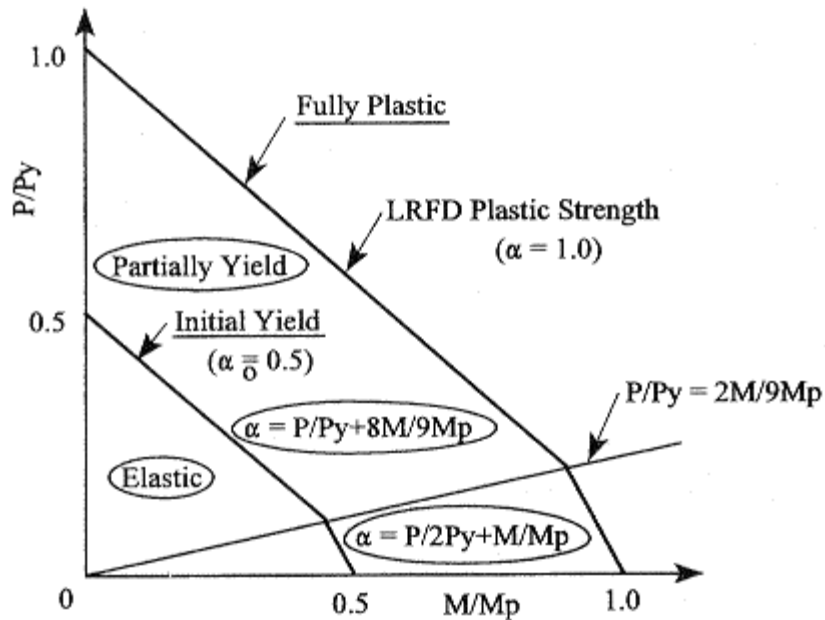


Figure 3.2.1-1. Two-surface stiffness degrading plastic hinge interaction diagram (Chen and Kim, 1997)

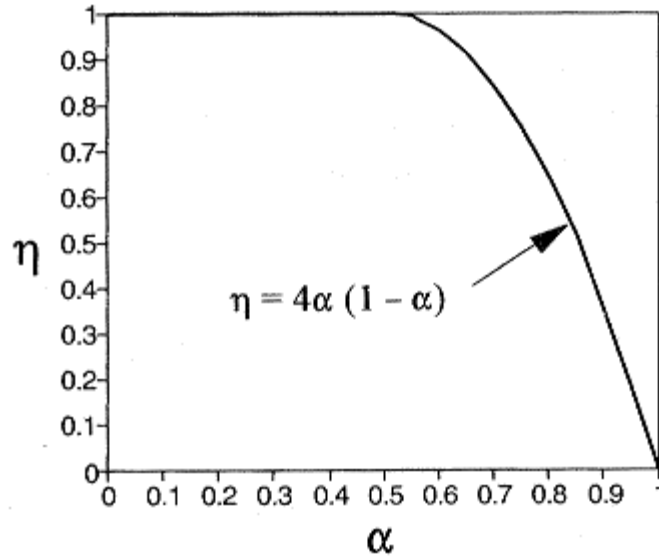


Figure 3.2.1-2. Parabolic plastic hinge stiffness degradation function (Chen and Kim, 1997)

Secondly, the stiffness degradation effect associated with yielding due to residual stress can be accounted for by adjusting the tangent modulus of the material. Although there are several methods for accounting residual stresses, the Column Research Council (CRC) tangent modulus is recommended for its simplicity. In this procedure the Modulus of Elasticity, E , is reduced to account for the reduction of the elastic portion of the cross-section. This is easier to implement than continually determining a modified Moment of Inertia, I_e , for every different section.

$$E_t = 1.0E \text{ for } P \leq 0.5P_y \quad (3.2.1-8)$$

$$E_t = 4 \frac{P}{P_y} E \left(1 - \frac{P}{P_y} \right) \text{ for } P > 0.5P_y \quad (3.2.1-9)$$

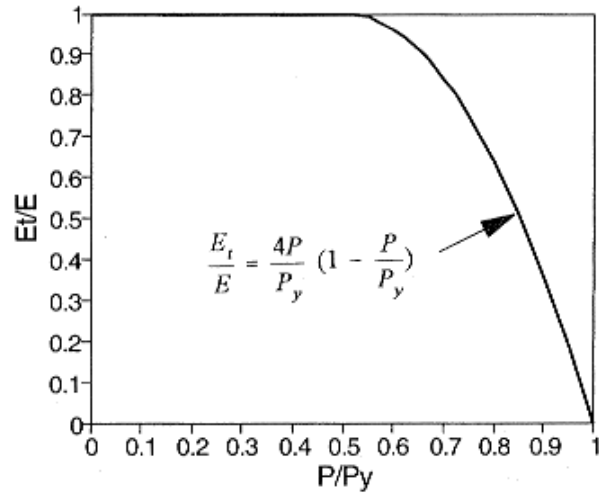


Figure 3.2.1-3. CRC tangent stiffness degradation function (Chen and Kim, 1997)

Similarly, the axial force-deformation curve can be derived.

$$P = \frac{\varepsilon}{\varepsilon_y} P_y \text{ for } P \leq 0.5P_y \quad (3.2.1-10)$$

$$P = \frac{P_y}{1 + \exp\left(2 - \frac{4\varepsilon}{\varepsilon_y}\right)} \text{ for } P > 0.5P_y \quad (3.2.1-11)$$

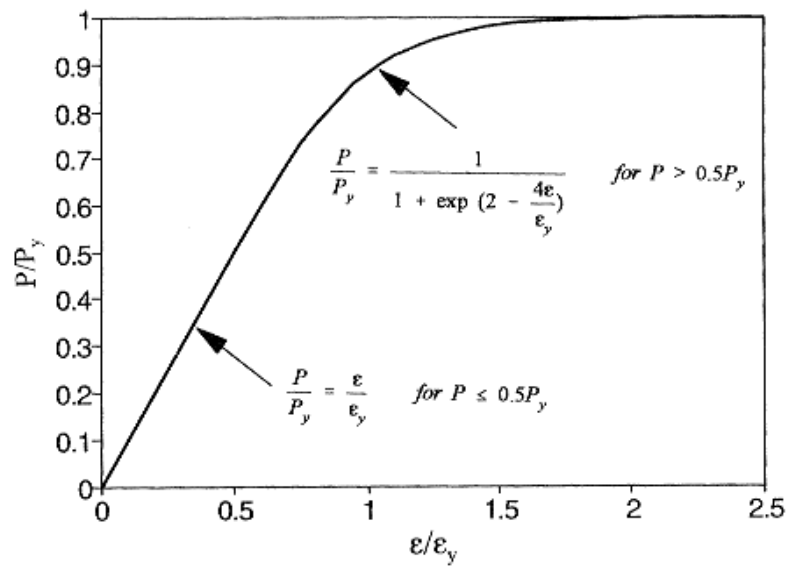


Figure 3.2.1-4. Normalized axial force-strain relationship (Chen and Kim, 1997)

3.2.2 Geometric Non-linearities

Geometric non-linearities include second-order effects ($P-\Delta$ and $P-\delta$) and geometric imperfections (out-of-straightness and out-of-plumbness). Second-order effects are implicitly accounted for in the stability functions discussed in Section 2.3. The presence of geometric imperfections causes additional moments in column members and further degradation of its bending stiffness. There are three methods for incorporating geometric imperfections: 1) explicit imperfection modeling method, 2) equivalent notional load method, and 3) further reduced tangent modulus method. The last is the preferred method for its simplicity because it eliminates the inconvenience of explicit imperfection modeling or the determination of equivalent notional loads. Additionally, this method is not uni-directional. Therefore, Eqs. (3.2.1-8) and (3.2.1-9) can be expanded to include the effect of geometric imperfections.

$$E_t = 1.0E\xi_i \text{ for } P \leq 0.5P_y \quad (3.2.2-1)$$

$$E_t = 4\frac{P}{P_y}E\xi_i\left(1 - \frac{P}{P_y}\right) \text{ for } P > 0.5P_y \quad (3.2.2-2)$$

where

ξ_i = Reduction factor for geometric imperfections

Current steel design codes limit out-of-plumbness to $L/500$ and out-of-straightness to $L/1000$. Research (*Chen and Kim, 1997*) has suggested that this leads to an approximate reduction factor, ξ_i , of 0.85.

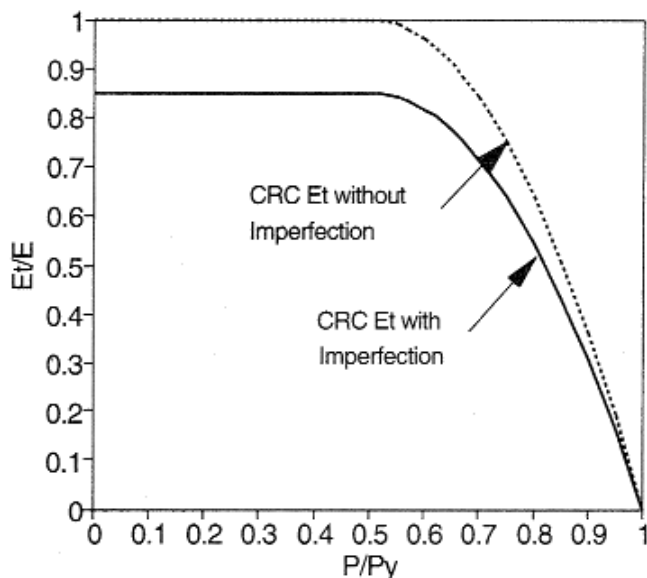


Figure 3.2.2-1. Further reduced CRC tangent stiffness degradation function (Chen and Kim, 1997)

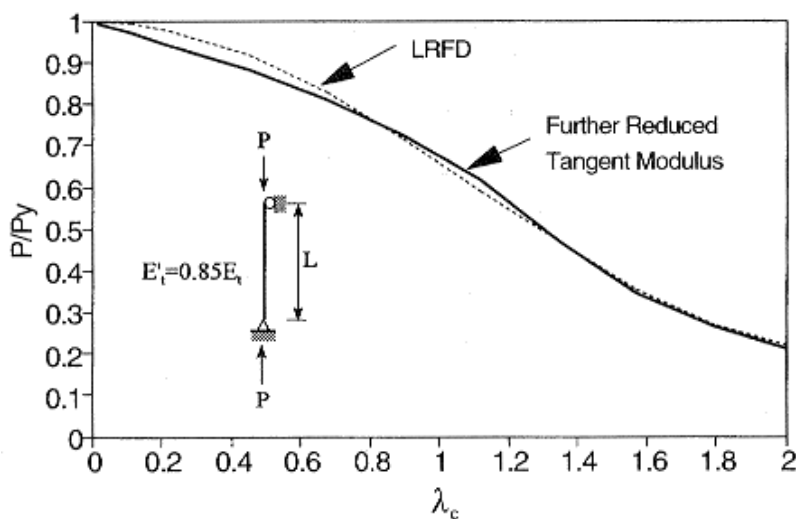


Figure 3.2.2-2. Comparison of strength curves (Chen and Kim, 1997)

3.3 Advanced Analysis and Displacement-Based Design

The benefit of using Advanced Analysis techniques in DBD is that the equivalent static lateral forces corresponding to the MCE or SP-4, in lieu of SP-1, can be used to analyze the system. This further simplifies the design procedure and additionally allows the design engineer to examine the full scope of system inelastic response. However, the goal of this research is not to necessarily incorporate Advanced Analysis techniques into DBD, but to

begin the process of incorporating Advanced Analysis into seismic engineering of steel frames. Although not discussed in this research it seems plausible that the previous stiffness degradation effects should be incorporated into DBD. That is the *equivalent* plastic rotation capacity should be determined incorporating geometric imperfections and the effects of residual stresses. By not incorporating these effects into DBD, the design engineer is given a false sense of ultimate system strength and displacement ductility capacity, for these effects are inherently accounted for in member design equations and not in an elastic analysis. The yielding associated with flexure does not need to be incorporated for this affects the post-yield response of a member.

The previous frames designed in Part 2 were analyzed using PAAP (Practical Advanced Analysis Program written by Seung-Eock Kim) subjected to the equivalent static lateral forces determined at the SP-4 performance level. Since PAAP traces the load-deflection curve of a structure; therefore, being an iterative and incremental analysis program, the lateral forces were reduced by 75 and the load increment scale was set at 150 (twice the reduction value). However, the same load increment scale also iterates the concentrated gravity loads, a reduction factor of 60 was used to insure that the gravity loads were higher than the lateral forces throughout each analysis run. The following sections show the analysis results for the four (4) and eight (8) story frames. Currently, the maximum number of elements permitted in this version of PAAP is 100; therefore, the sixteen (16) story frame could not be analyzed.

One important point that needs to be addressed prior to the subsequent discussion is that PAAP will inherently address member overstrength, including material overstrength if the input variables are modified. For example, F_y can be increased to represent any variation in yield strength. However, PAAP will not completely address plastic hinge sequencing since the SP-4 lateral forces were determined based on an assumed inelastic displacement profile. If the design displacement profile does not account for higher mode response either will the lateral forces. PAAP will incorporate some aspects of hinge sequencing by reducing the load increment of lateral loads on a floor that has formed a yield mechanism while maintaining the same load increment on other elastic floors. However, once a global yield mechanism has formed the analysis diverges unless a strength limit state is reached. Therefore, it seems

plausible to either use a range of target displacement profiles incorporating higher mode effects or variations of lateral forces with a range of plastic hinge sequencing factors.

Furthermore, the concentrated gravity loads cannot be currently applied as constant forces in the analysis. That is they are subject to the same incremental procedure as the lateral loads. There are several reasons for this process, as outlined in many of the references; however, this also indicates that the gravity forces cannot be accurately represented, for limit states are easily reached in columns when the gravity load is continually incremented in excess of required. On the other side, by choosing a relatively low gravity force to offset this effect, the stiffening effect of axial compression is not fully utilized tending towards increased force and displacement demands. This process will have to be revised in order for this program to be used in the analysis of seismic resistant frames.

The subsequent sections show the comparison of displacement profiles at the moment when the frames are subjected to the equivalent lateral forces determined at the SP-1 level. Additionally, the complete force-displacement graphs are shown. Though, there is no formal discussion in the respective sections, a final overall discussion will follow subsequently.

3.3.1 Four (4) Story Frame (FR-4)

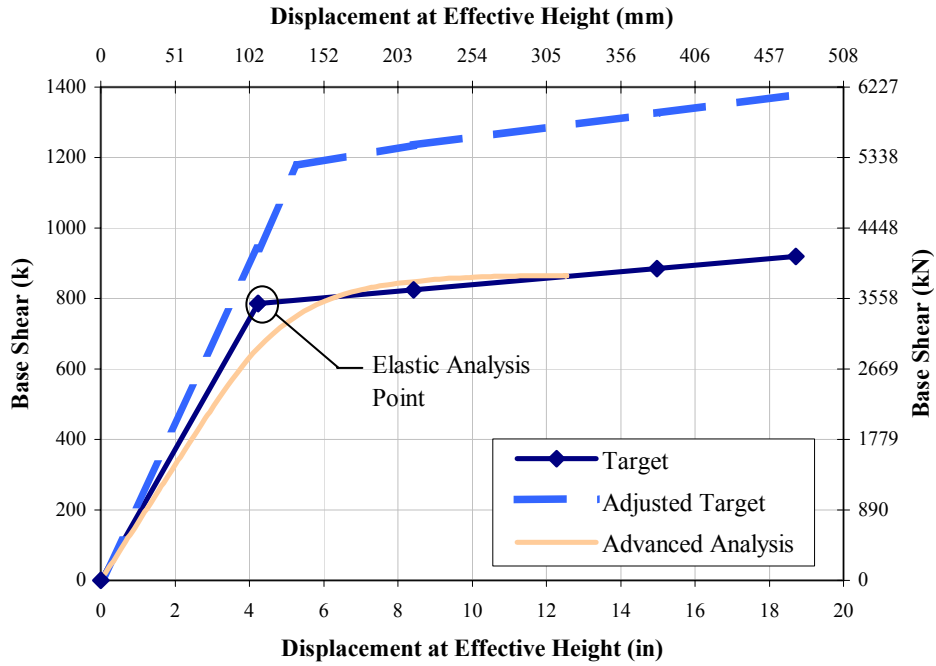


Figure 3.3.1-1. FR-4 System Force-Displacement Graph

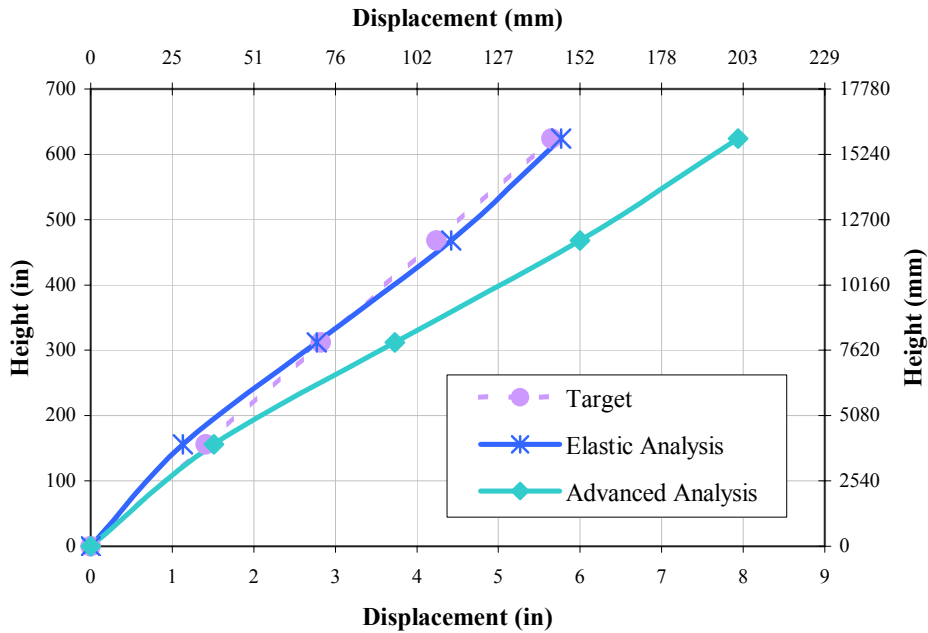


Figure 3.3.1-2. FR-4 SP-1 Displacement Profile

3.3.2 Four (4) Story Frame (FR-4-W21)

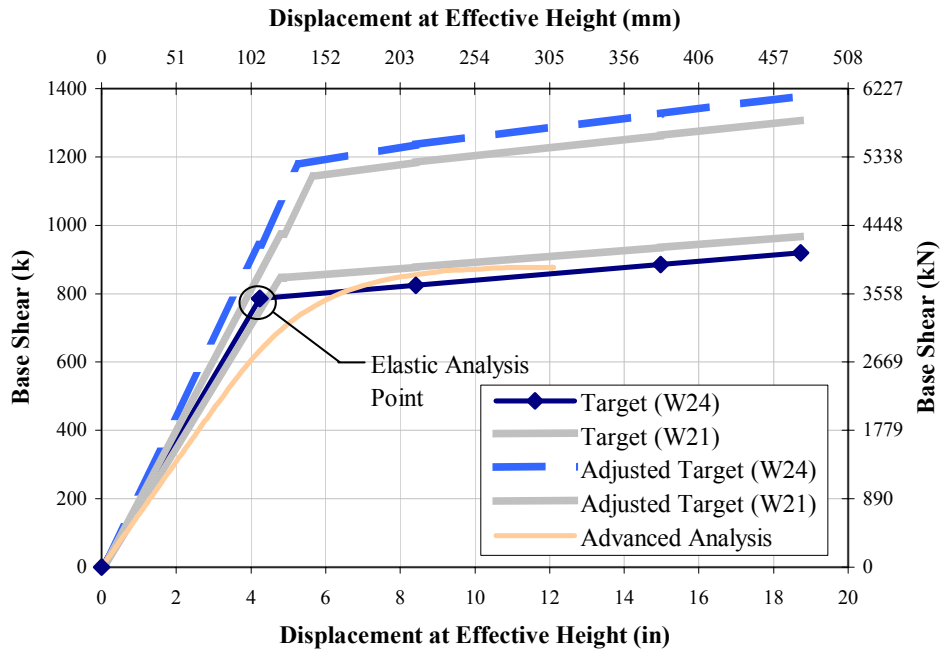


Figure 3.3.2-1. FR-4-W21 System Force-Displacement Graph

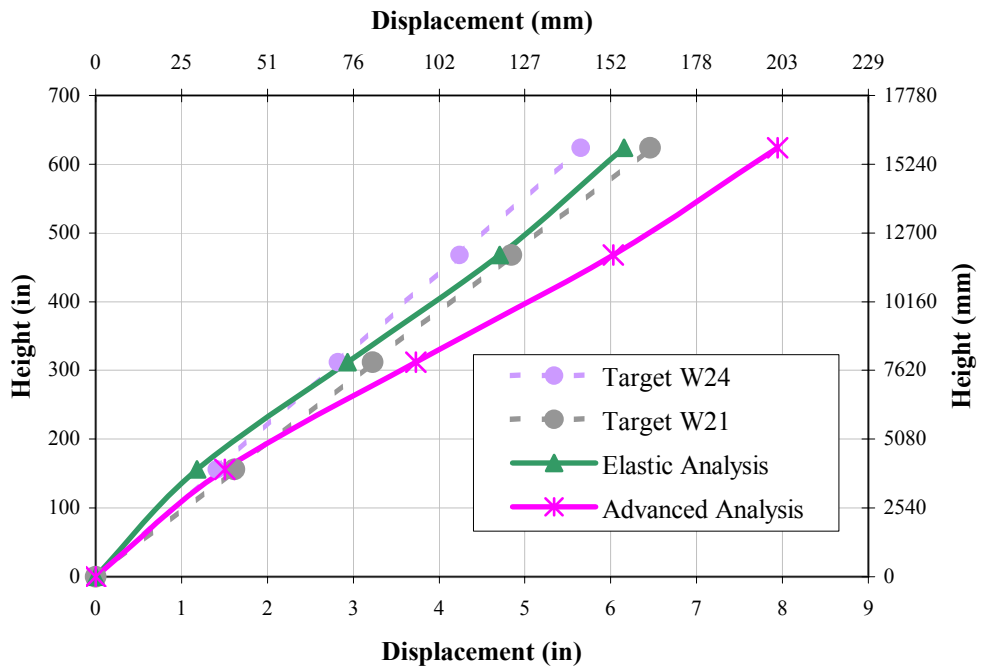


Figure 3.3.2-2. FR-4-W21 SP-1 Displacement Profile

3.3.3 Four (4) Story Frame (FR-4-W24)

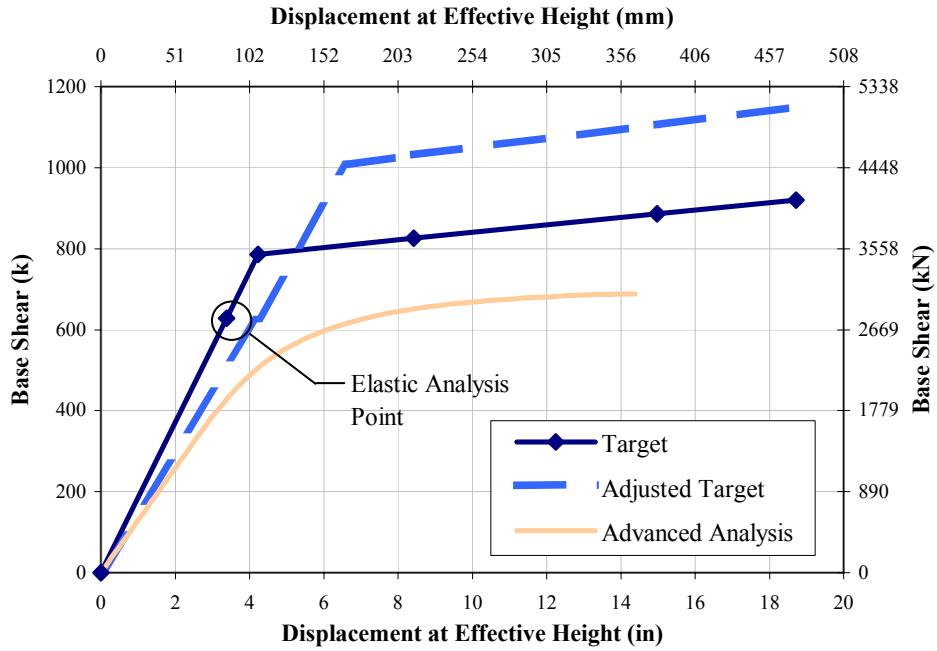


Figure 3.3.3-1. FR-4-W21 System Force-Displacement Graph

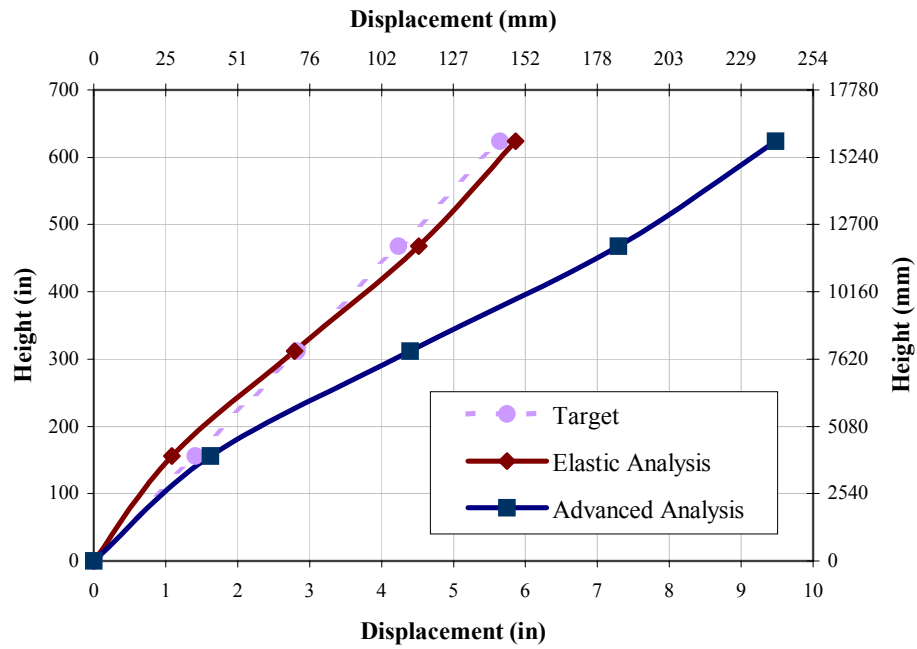


Figure 3.3.3-2. FR-4-W24 SP-1 Displacement Profile

3.3.4 Four (4) Story Frame (FR-4a)

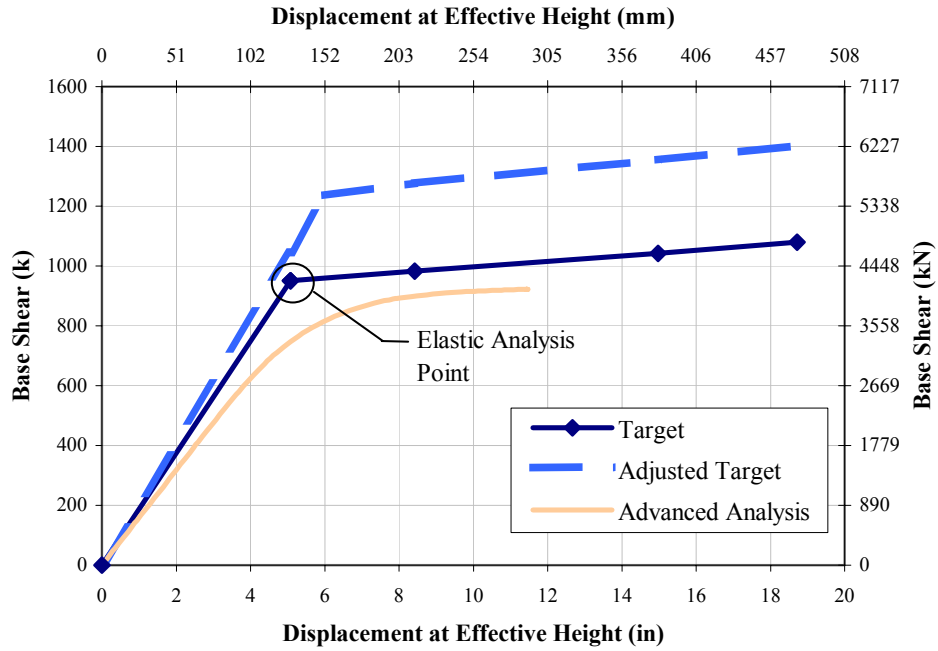


Figure 3.3.4-1. FR-4a System Force-Displacement Graph

There is no displacement profile for this frame since the frame reached a limit state prior to reaching the equivalent SP-1 performance level. As discussed subsequently, this is most likely due to the concentrated gravity loads exceeding the actual value due to load incrementing. Therefore, causing a limit state in one or more of the columns to be reached.

3.3.5 Four (4) Story Frame (FR-4b)

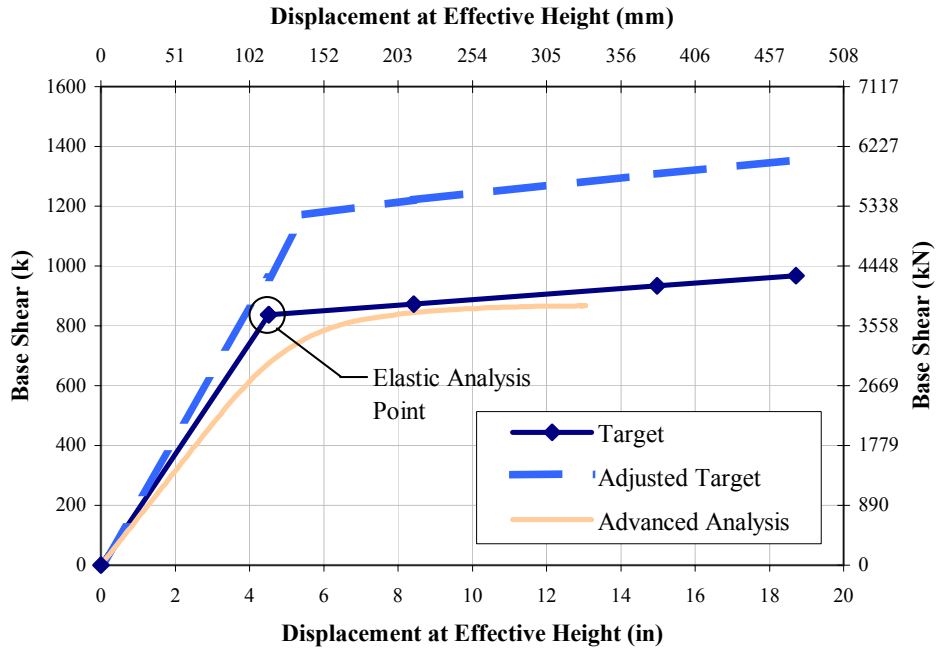


Figure 3.3.5-1. FR-4b System Force-Displacement Graph

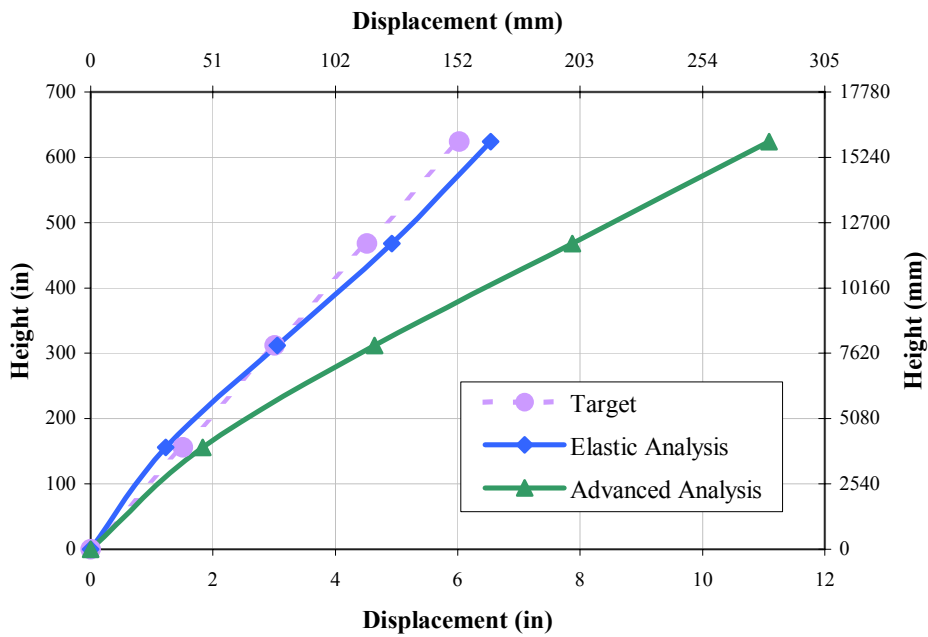


Figure 3.3.5-2. FR-4b SP-1 Displacement profile

3.3.6 Eight (8) Story Frame (FR-8)

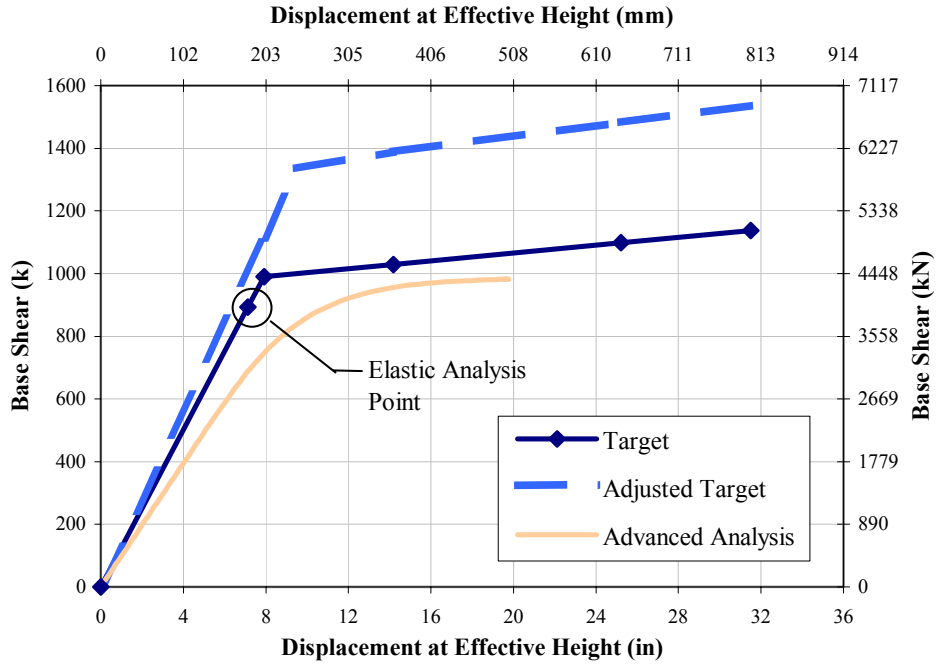


Figure 3.3.6-1. FR-8 System Force-Displacement Graph

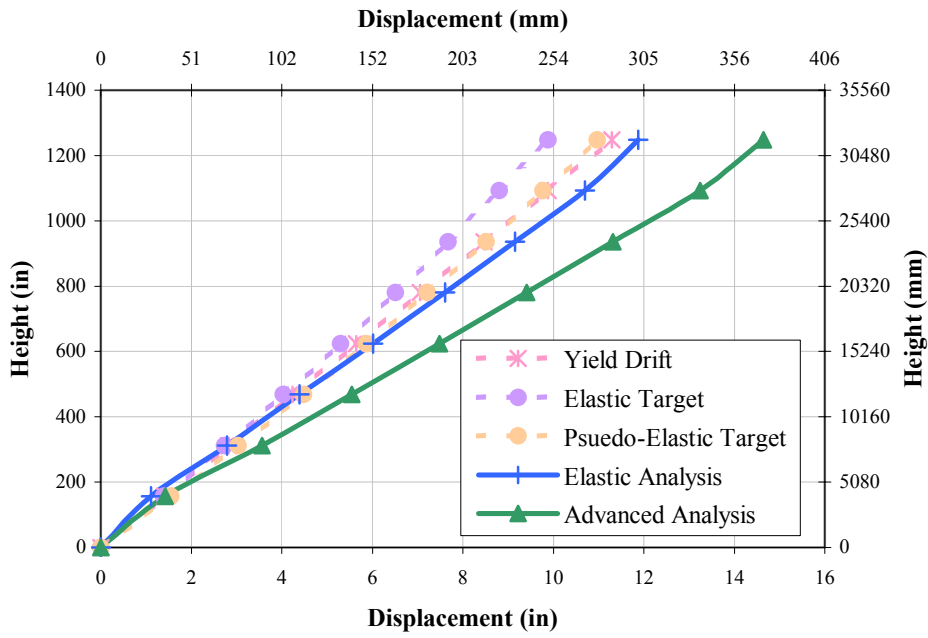


Figure 3.3.6-2. FR-8 SP-1 Displacement Profile

3.3.7 Eight (8) Story Frame (FR-8-W27)

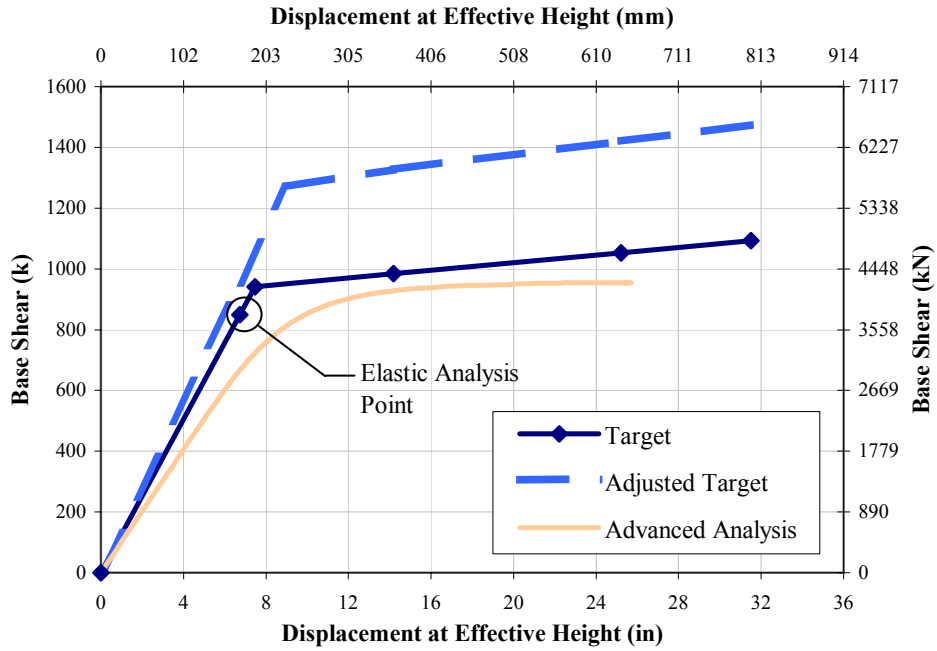


Figure 3.3.7-1. FR-8-W27 System Force-Displacement Graph

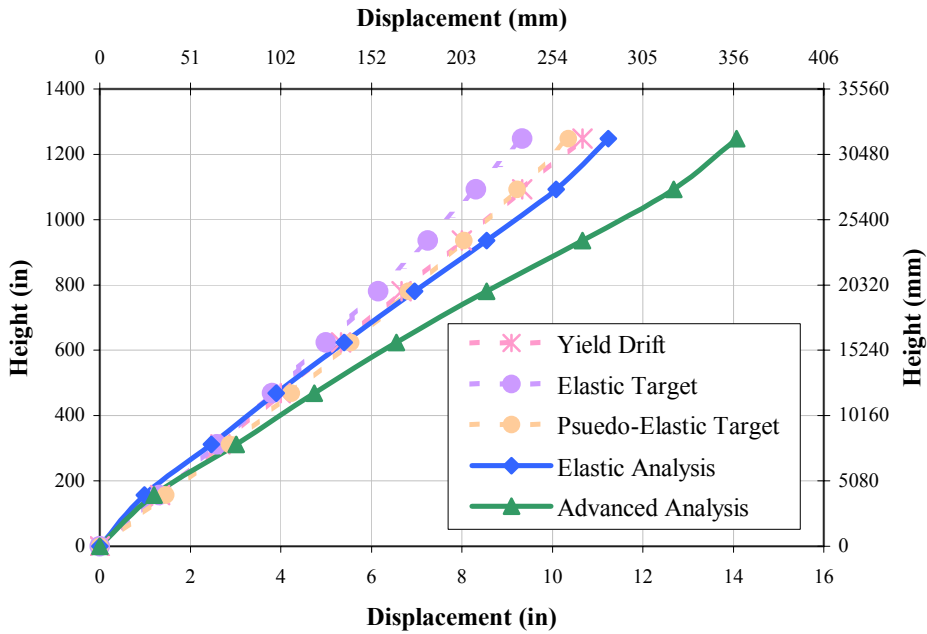


Figure 3.3.7-2. FR-8-W27 SP-1 Displacement profile

As can be seen in the previous displacement profile graphs, the inclusion of geometric imperfections and stiffness degradation functions reduces the bending stiffness of the beams and columns, thus increasing the displacement demands. These effects cannot be seen nor accurately predicted by using an elastic analysis. Furthermore, the force-displacement results are considerably less than that which is predicted by the proposed method. Geometric imperfections automatically produce a 15% reduction in frame stiffness. This, coupled with other non-linear effects, can lead to a decrease in final ductility capacity. It is evident that current force-based designs do not account for the actual stiffness degradation effects included herein in the force reduction factors. Therefore, the maximum ductility of steel frame is grossly over-estimated.

The same displacement response, differing only in magnitude, is recognized at the SP-1 level when compared to the results from the elastic analysis. That is the effects of overstrength are clearly visible. Additionally, the frames still have not formed base hinges and in effect the lower portions behave similar to a braced frame. This clearly signifies that an engineer cannot select a beam based on its respective plastic moment capacity or strong axis Moment of Inertia independently.

As mentioned in Section 3.2, due to the concentrated gravity forces being incremented, and typically resulting in demands in excess of the required value, many columns reach their respective limit state. The analysis program ceases when this occurs and, therefore, the force-displacement graphs stop prior to global stiffness reduction (downward portion of FD response). Ultimately, this affects the validity of using this methodology for examining the full scope of inelastic response. However, since member design is based on pseudo-elastic demands at the SP-1 level, this procedure is recommended in lieu an elastic analysis. This also includes a push-over analysis, erroneously labeled as a non-linear analysis. Furthermore, the procedures outlined within should be incorporated into DBD in order to more accurately predict frame behavior, which cannot be captured by conventional design methodologies.

3.4 References

The following books and articles are recommended for further detailed discussions of Advanced Analysis procedures, verifications, and implementations.

Chen, W.F. and Kim, S.E. (1997) *LRFD Steel Design using Advanced Analysis*, CRC Press, Boca Raton, FL, 441 pp.

Chen, W.F. and Toma, S. (1994) *Advanced Analysis of Steel Frames*, CRC Press, Boca Raton, FL, 383 pp.

Chen, W.F. and Lui, E.M. (1992) *Stability Design of Steel Frames*, CRC Press, Boca Raton, FL, 380 pp.

Chen, W.F. and Sohal, I. (1995) *Plastic Design and Second-order Analysis of Steel Frames*, Springer-Verlag, NY, 509 pp.

Chen, W.F. (2000) *Practical Analysis for Semi-Rigid Frame Design*, World Scientific, NJ, 465 pp.

Kim, S.E. and Chen, W.F. (1996) Practical Advanced Analysis for Braced Steel Frame Design, *J. Struct. Eng.*, ASCE 122(11).

Kim, S.E. and Chen, W.F. (1996) Practical Advanced Analysis for Unbraced Steel Frame Design, *J. Struct. Eng.*, ASCE 122(11).

Liew, J.Y.R., White, D.W., and Chen, W.F. (1993) Second-order refined plastic Hinge Analysis of Frame Design: Part I, *J. Struct. Eng.*, ASCE 119(11).

Liew, J.Y.R., White, D.W., and Chen, W.F. (1993) Second-order refined plastic Hinge Analysis of Frame Design: Part II, *J. Struct. Eng.*, ASCE 119(11).

SSRC (1993) Plastic-Hinge Based Methods for Advanced Analysis and Design of Steel Frames, White, D.W. and Chen, W.F., Eds., SSRC, Lehigh University, Bethlehem, PA, 299 pp.

PART 4

VERIFICATION

4.0 Introduction

The frames designed in Section 2.5 were analyzed in a 2nd order inelastic dynamic analysis to verify the applicability of the proposed design method. *RUAUMOKO* (Carr, 2000) was used for the dynamic analysis using the elasto-perfectly plastic hysteresis discussed in Section 1.2.1. Twelve time-histories were selected to provide a wide analytical range of ground accelerations, intensities (short and long), and duration, shown in Table 4-1. Two of the time-histories were artificially generated by *SIMQKE* (Carr, 1997) to approximate the design MCE. The other ten *actual* time-histories were normalized by the Spectrum Intensity method (Housner, 1952), for the period range of 0.1 to 5 seconds, to approximate the design MCE. Furthermore, the time-histories were modified by the respective MCE PGA Reduction Factors outlined in Section 2.5, including frame dependent EQ I modifiers, in developing the other design earthquake levels (I, II, and III).

Number	TH	Description	+ PGA (% g)	- PGA (% g)	Norm. Factor	Time Step	Duration (sec.)
1	TH-1*	Zone 4, Soil D	0.674	-0.674	1.00	0.02	30.00
2	TH-2*	Zone 4, Soil D	0.674	-0.674	1.00	0.02	30.00
3	TH-3	El Centro (N-S)	0.298	-0.319	2.39	0.02	30.00
4	TH-4	Kobe (N-S)	0.590	-0.834	0.96	0.02	50.00
5	TH-5	Loma Prieta (N-S)	0.570	-0.505	0.81	0.005	25.00
6	TH-6	Cape Mendocino (N-S)	1.497	-0.494	1.08	0.02	30.00
7	TH-7	Tabas (N-S)	0.937	-0.744	0.86	0.02	50.00
8	TH-8	Petrolia (N-S)	0.586	-0.590	1.85	0.02	60.00
9	TH-9	Vina Del Mar (N-S)	0.363	-0.304	2.42	0.005	112.00
10	TH-10	Northridge (N-S)	0.843	-0.590	0.89	0.02	60.00
11	TH-11	Tokachi-Oki (N-S)	0.318	-0.198	2.83	0.02	120.00
12	TH-12	Taft (N-S)	0.156	-0.141	5.18	0.02	50.00

* indicates artificially generated design spectra

Table 4-1. Selected time-histories

The +/- PGA values shown in Table 4-1 are actual values. All time-history design spectrums are included in Appendix B.

4.1 Four (4) Story Frame (FR-4)

4.1.1 Displacement Profiles

Figs. 4.1.1-1 through 4.1.1-4 show the maximum absolute relative displacement envelopes for each time-history analysis representative at each design performance level.

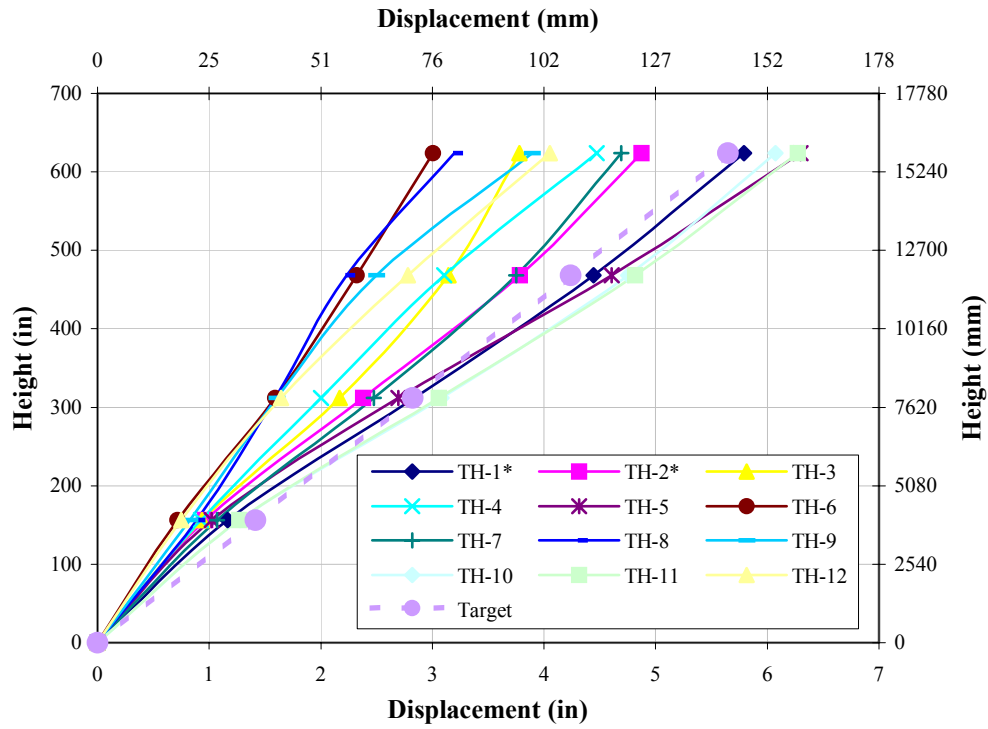


Figure 4.1.1-1. FR-4 Maximum displacement envelopes (SP-1:EQ 1)

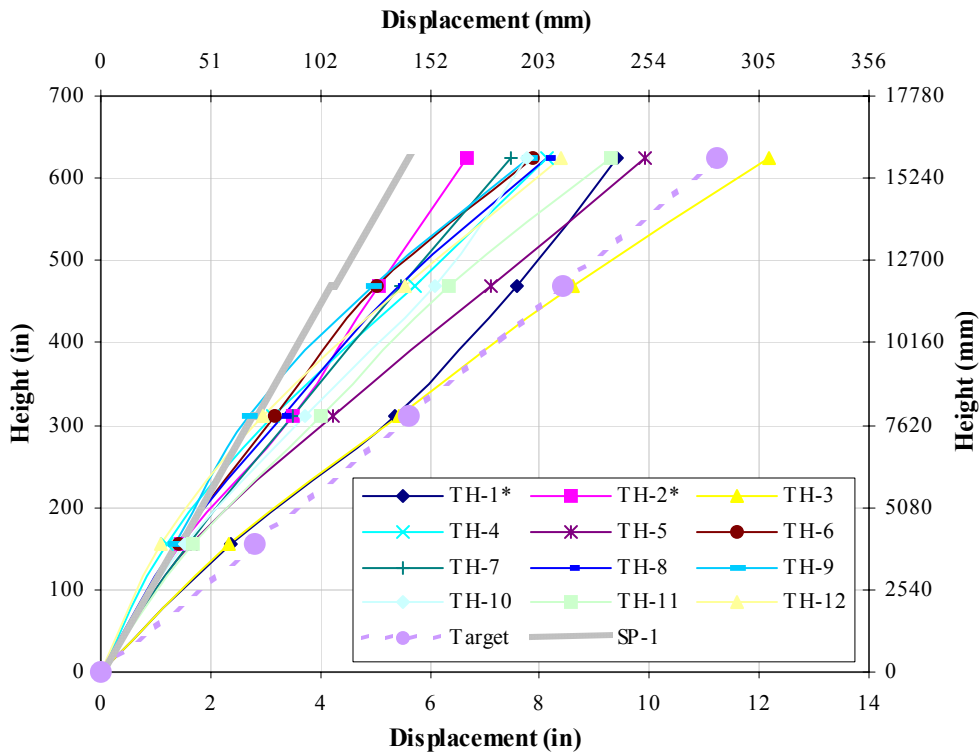


Figure 4.1.1-2. FR-4 Maximum displacement envelopes (SP-2:EQ II)

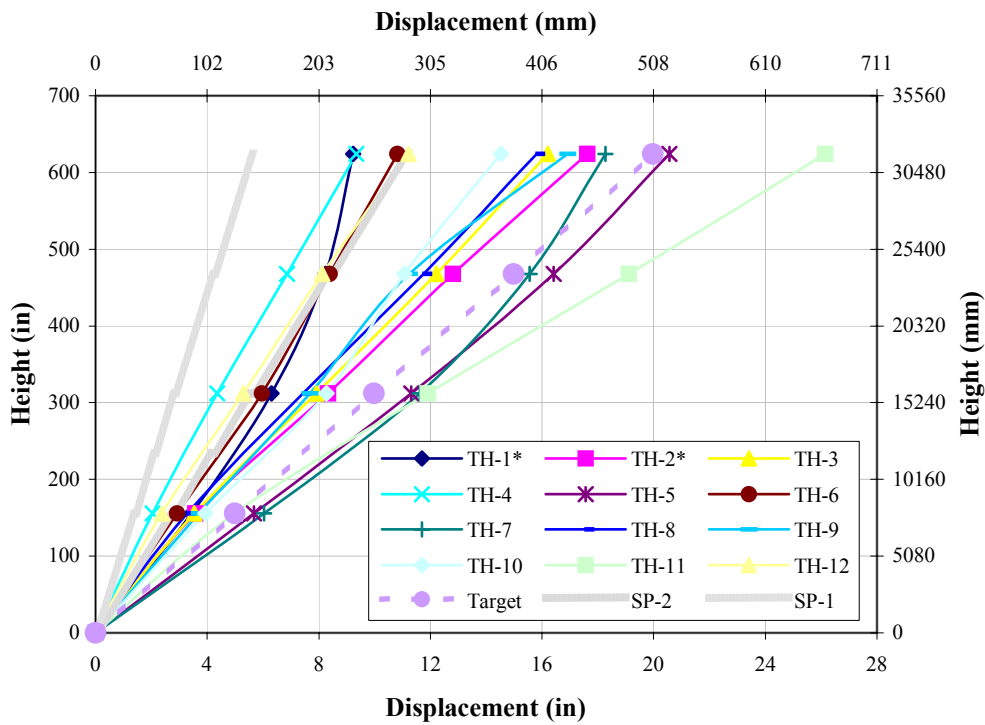


Figure 4.1.1-3. FR-4 Maximum displacement envelopes (SP-3:EQ III)

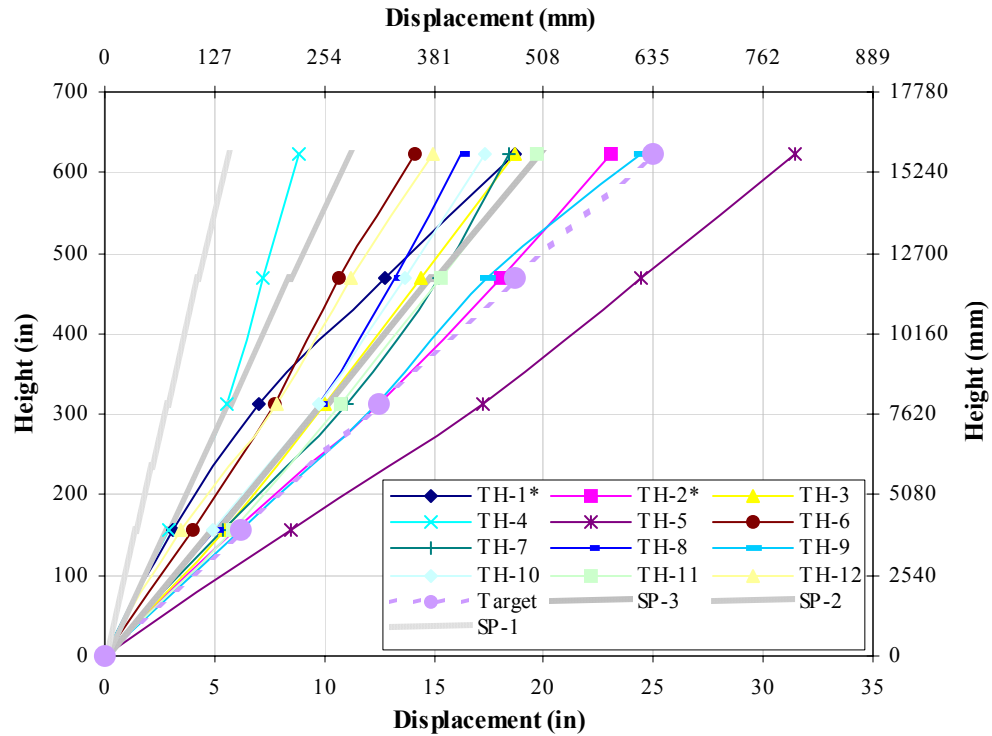


Figure 4.1.1-4. Maximum displacement envelopes (SP-4:EQ IV)

The displacements at the effective height can be extracted from the previous graphs as listed in Table 4.1.1-1.

TH	SP-1 : EQ I (in / mm)		SP-2 : EQ II (in / mm)		SP-3 : EQ III (in / mm)		SP-4 : EQ IV (in / mm)	
	in	mm	in	mm	in	mm	in	mm
TH-1	4.4	113	7.6	193	8.2	209	12.8	324
TH-2	3.8	96	5.1	129	12.8	325	18.1	459
TH-3	3.1	80	8.6	219	12.2	310	14.4	366
TH-4	3.1	79	5.7	146	6.9	174	7.2	183
TH-5	4.6	117	7.1	181	16.4	417	24.4	621
TH-6	2.3	59	5.0	128	8.4	213	10.7	271
TH-7	3.8	95	5.5	139	15.6	395	15.2	386
TH-8	2.2	57	5.4	138	11.8	299	13.2	336
TH-9	2.5	63	5.0	126	11.2	285	17.4	442
TH-10	4.8	121	6.1	154	11.1	281	13.7	347
TH-11	4.8	122	6.3	161	19.1	486	15.3	390
TH-12	2.8	71	5.5	141	8.1	206	11.2	285

Table 4.1.1-1. FR-4 Displacements at effective height

The design, or target, displacement profiles, representative of the desired damage level, are simply a snapshot in time of the maximum allowable nodal displacements for a given performance level. Therefore, when comparing analysis results to limit state values, the maximum nodal displacements should be used. However, not all maximum displacements occur at the same moment in time. As can be seen, good comparison exists at the SP-1 level for the TH-1, 2, 5, 7, 10, and 11. This is due to the respective time-histories having comparable displacements to the design DRS at the effective system period. Also, hinge sequencing effects are not yet prominent since the system is still in the elastic region where member overstrengths dominate the system response. That is the global yield mechanism has not yet formed. Additionally, due to member overstrengths and EQ characteristics, the system is much stronger than required for the other earthquakes (see Section 4.9). Still the linear displacement profile is well represented.

As previously discussed in Section 2.5, it is evident that the base hinges have not formed as expected at the SP-1 level. Similarly, the upper floors dynamically attract higher demands and exhibit greater nodal displacements than expected. This is the first indication of the effect of member overstrengths on system response. That is there is a correlation between plastic hinge sequencing and floor overstrength, and as noted previously, hinge sequencing will affect the actual displacement profiles as seen in several displacement envelopes (since it is assumed that with low-rise frames envelopes are profiles). For example, the top two floors of the four story frame will develop a yield mechanism prior to the stiff lower floors. Likewise, as the upper floors enter the plastic region, the lower floors begin attracting higher demands. As a consequence, the probability of inducing higher mode response independent of earthquake intensity is increased. This process continues until the formation of the global yield mechanism when the response of a frame becomes somewhat sporadic, which is directly related to earthquake intensity. The effect of hinge sequencing can be seen in all post-yield displacement graphs, though it is difficult to evaluate the extent of earthquake induced higher mode response from examining the displacement envelopes. This should not concern the design engineer since increased force demands from hinge sequencing are incorporated in member design. However, there are no procedures for accurately calculating the increased force demands from hinge sequencing other than an iterative analysis procedure

using a complete modal or dynamic analysis. Currently, seismic codes specify an additional top-level concentrated force to represent EQ induced higher mode response; however, this method is crude at best, for it does not consider the stiffness and strength of individual floors.

The previous graphs show the *actual* maximum nodal displacements of the system subjected to the respective earthquakes. However, the maximum nodal displacements do not necessarily occur at the same moment in time. Therefore, in the process of developing a design procedure to represent hinge sequencing, *actual* nodal displacements and interstory drifts as a function of time must be investigated, shown in Figs. 4.1.1-5 through 4.1.1-12. Due to the huge amount of data involved in this kind of analysis, only the artificial time-history (TH-1) will be discussed.

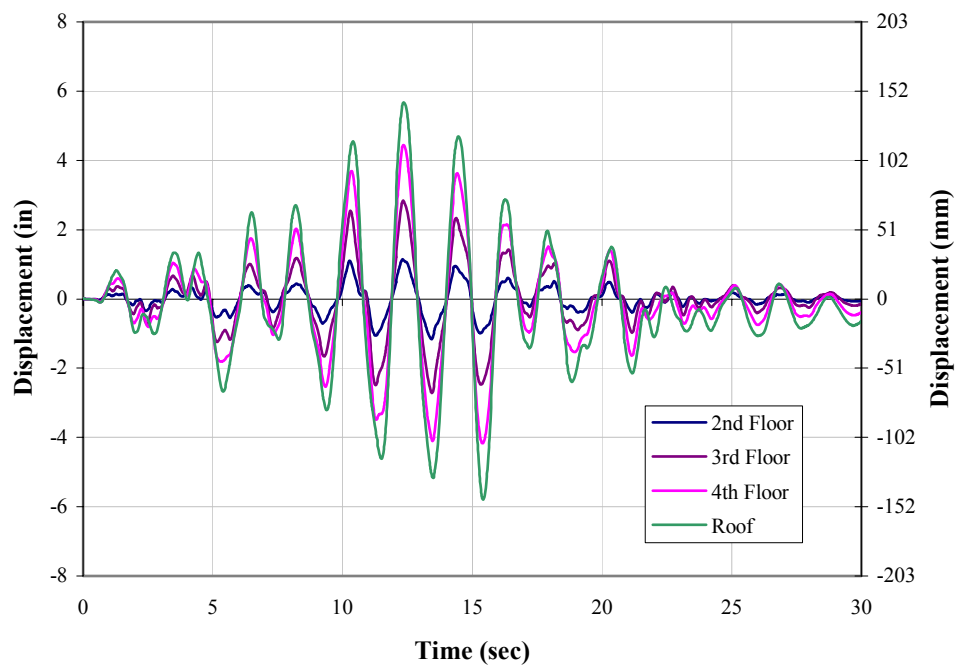


Figure 4.1.1-5. FR-4 Nodal displacements as function of time (TH-1:EQ 1)

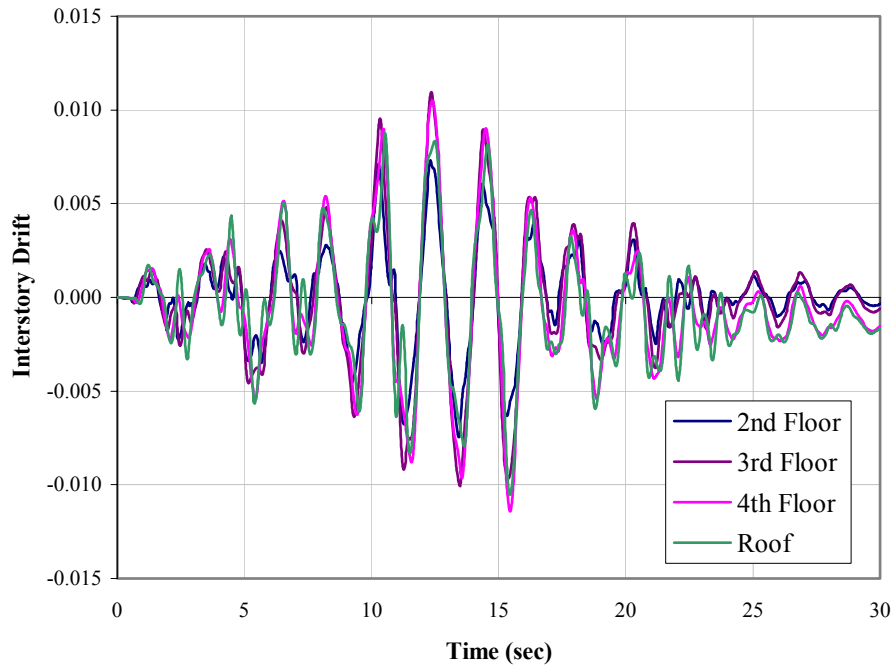


Figure 4.1.1-6. FR-4 Interstory drifts as function of time (TH-1:EQ I)

It is clear that the frame response at the EQ I level is dominated by 1st mode behavior. This should be expected since floors have not in all likelihood developed yield mechanisms leading to hinge sequencing effects. Since the design displacement profile is linear, constant interstory drifts are expected and as can be seen in Fig. 4.1.1-6 discrepancies exist in adjacent interstory drifts at peak displacements regions. This is due to floor overstrengths and the result of no base hinges forming at this earthquake level. It should be mentioned that the 4th floor is the only yield mechanism developed at this earthquake level resulting in the variation in interstory drifts between the 3rd and 4th floors after approximately 20 seconds. This reinforces that member overstrengths dominate system response in low-level earthquakes, prior to period elongation as yield mechanisms begin to form. Likewise, that proportionality exists between floor overstrength and plastic hinge sequencing. However, the contribution of earthquake induced hinge sequencing and its relationship to overstrength induced hinge sequencing is not clear.

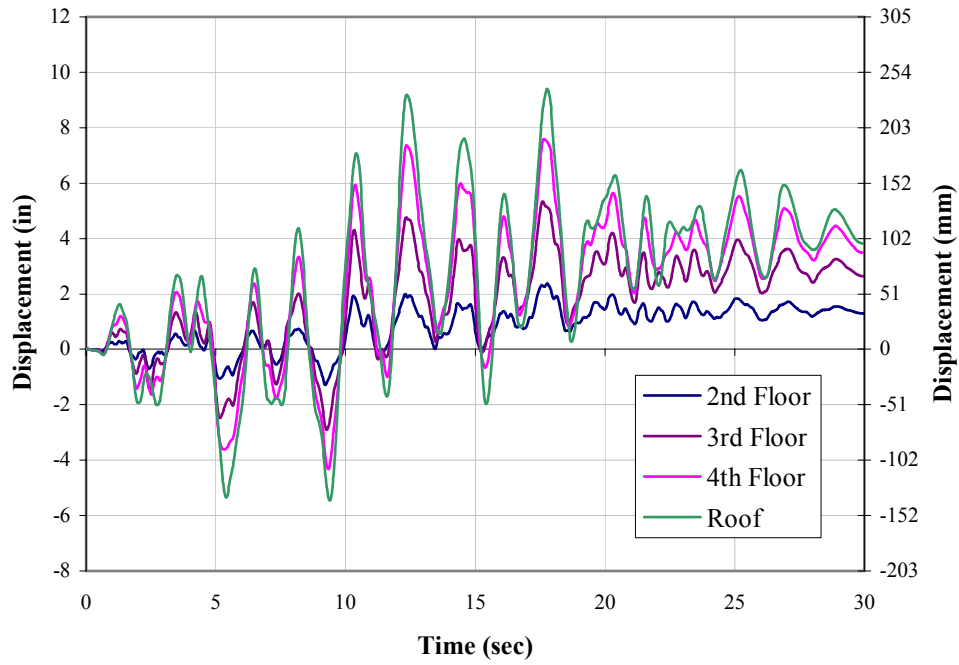


Figure 4.1.1-7. FR-4 Nodal displacements as function of time (TH-1:EQ II)

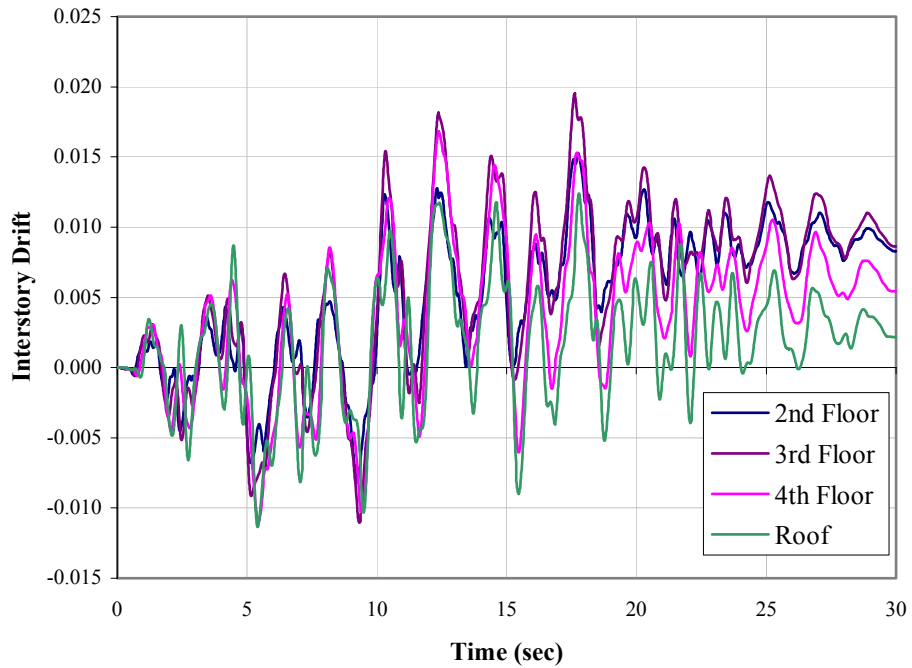


Figure 4.1.1-8. FR-4 Interstory drifts as function of time (TH-1:EQ II)

The same effects discussed at the EQ I level are additionally observed at the EQ II level. The obvious difference is the residual displacements apparent after 20 seconds (same time the 4th floor yield mechanism formed at the EQ I level). Hinge sequencing is also slightly evident prior to 20 seconds indicating the formation of localized yield mechanisms. The global yield mechanism, additionally accompanied with hinge sequencing, forms at approximately 20 seconds and most likely formed at a 1st mode peak displacement region. This is evident due to the variation in interstory drifts between all floors. It should be mentioned that earthquake induced higher mode effects are still not apparent, as the system response still seems to be dominated by the 1st mode, except for a localized response at 22 seconds.

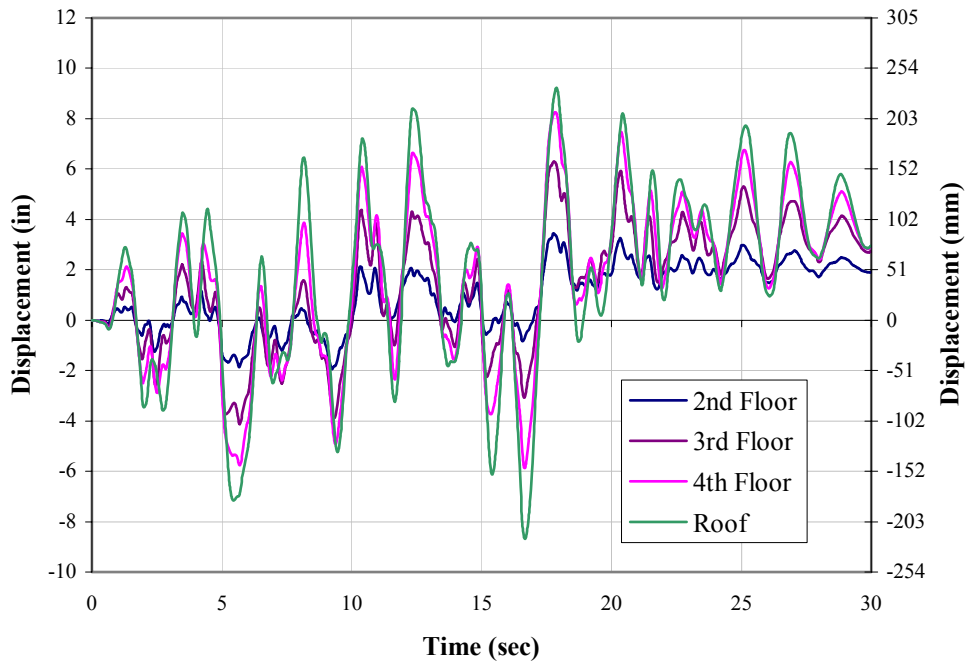


Figure 4.1.1-9. FR-4 Nodal displacements as function of time (TH-1:EQ III)

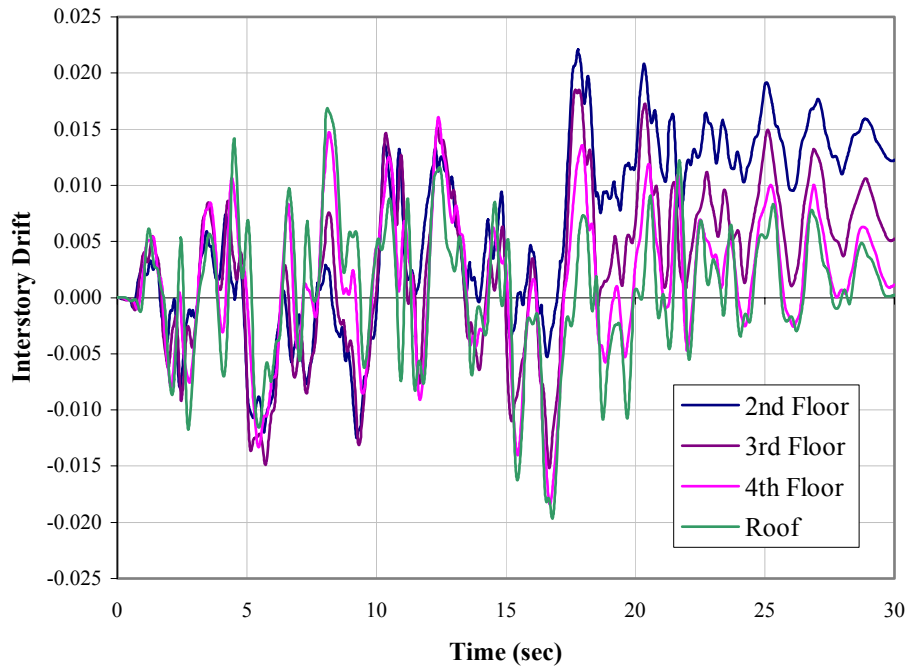


Figure 4.1.1-10. FR-4 Interstory drifts as function of time (TH-1:EQ III)

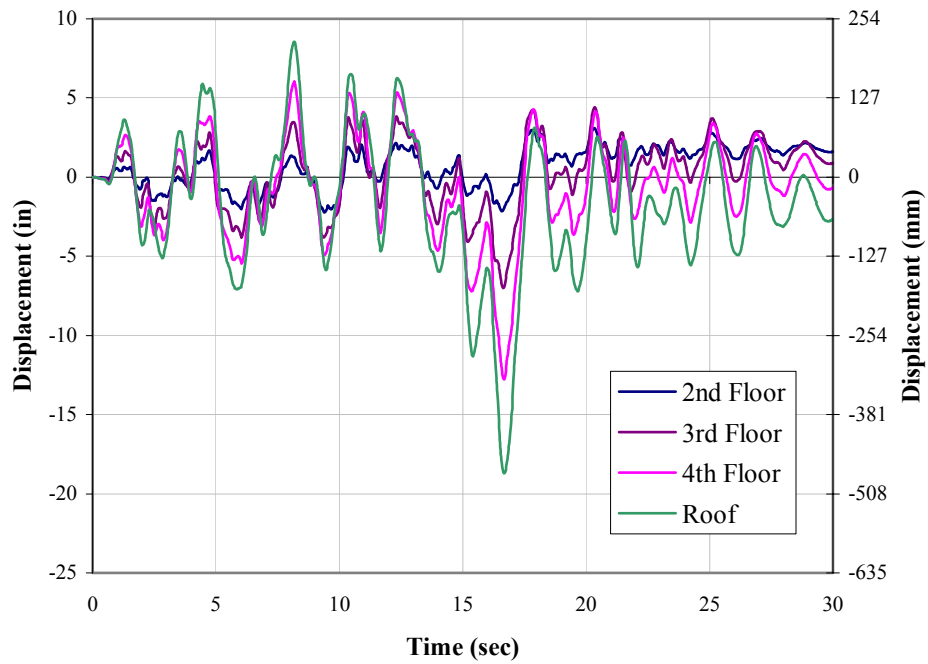


Figure 4.1.1-11. FR-4 Nodal displacements as function of time (TH-1:EQ IV)

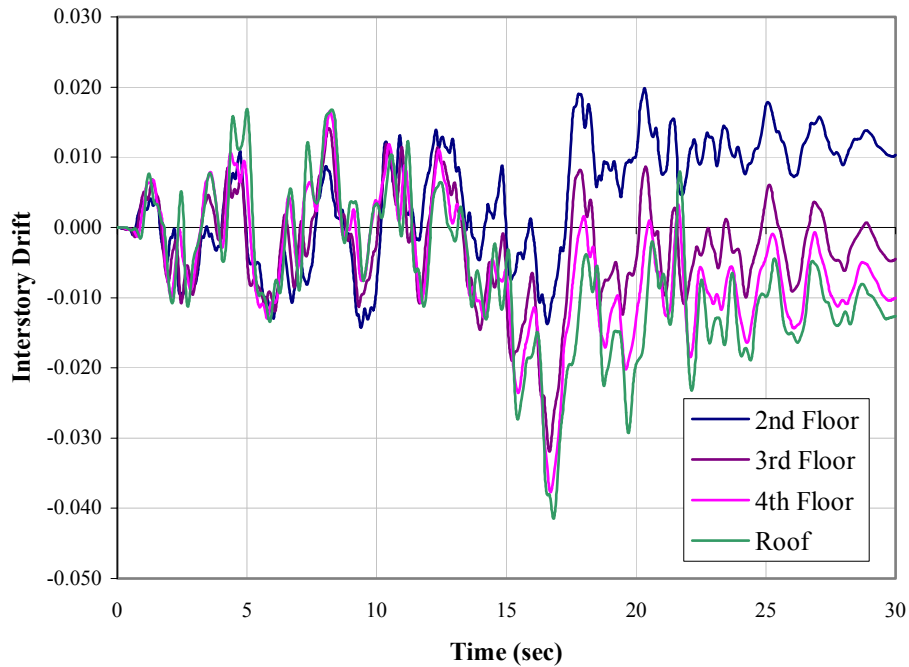


Figure 4.1.1-12. FR-4 Interstory drifts as function of time (TH-1:EQ IV)

Similarly, the same response is seen at the EQ III and EQ IV level except that the global yield mechanism forms earlier. Higher mode response is clearly indicated in the respective graphs. However, this response is mostly likely due to overstrength induced hinge sequencing, which is a system characteristic. A more distinct EQ induced higher mode response can be seen in Fig. 4.1.1-13 (TH-9), due to a significant intensity increase, or spike, at 20 seconds. Thus an extremely high amount of energy is input very quickly into the system and inducing 2nd mode vibration effects. This emphasizes an important difference in system response due to earthquake and system characteristics. As it is seen in the previous graphs, earthquake levels representative of the full design intensity do not necessarily induce higher mode response in low-rise frames; only by specific system characteristics does this effect appear, albeit based on design selections. Hence, the design engineer should be wary of large strength and stiffness deviations in the system. Nonetheless, the importance of incorporating plastic hinge sequencing into the design is apparent.

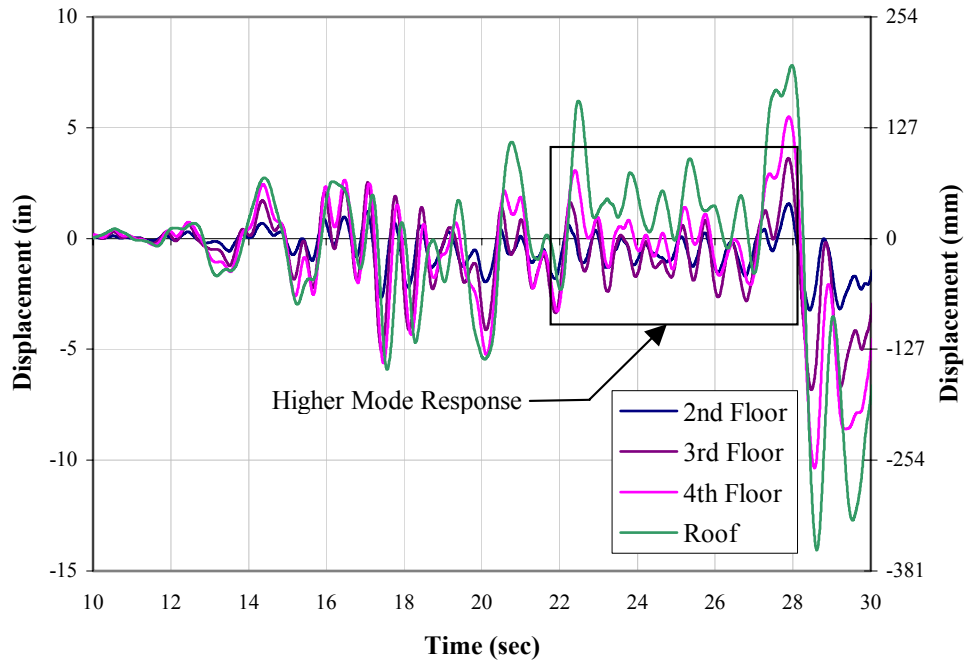


Figure 4.1.1-13. FR-4 Nodal displacements as function of time (TH-9:EQ IV)

Similar to the displacement envelopes, the maximum interstory drifts can be evaluated as seen in Figs. 4.1.1-14 through 4.1.1-17. Again, these do not necessarily occur at the same moment in time nor coincide with the maximum displacements.

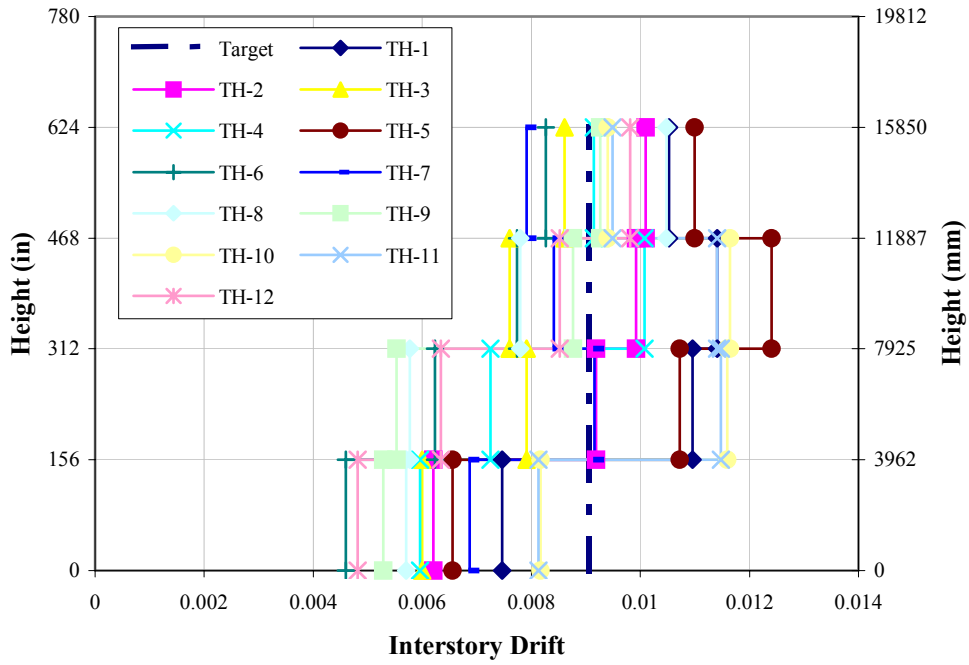


Figure 4.1.1-14. FR-4 Maximum interstory drift envelopes (SP-1:EQ I)

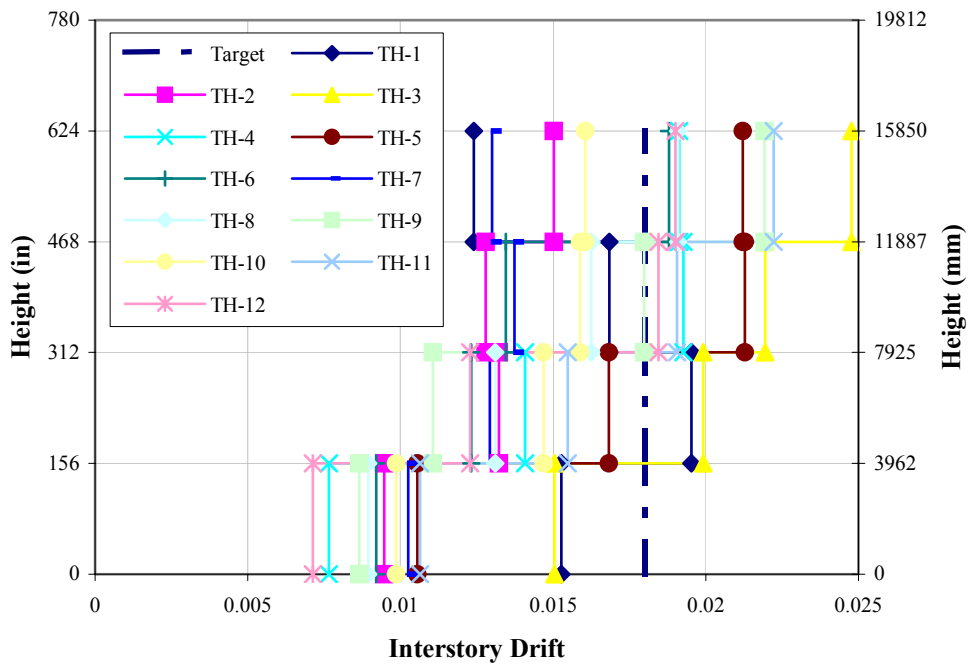


Figure 4.1.1-15. FR-4 Maximum interstory drift envelopes (SP-2:EQ II)

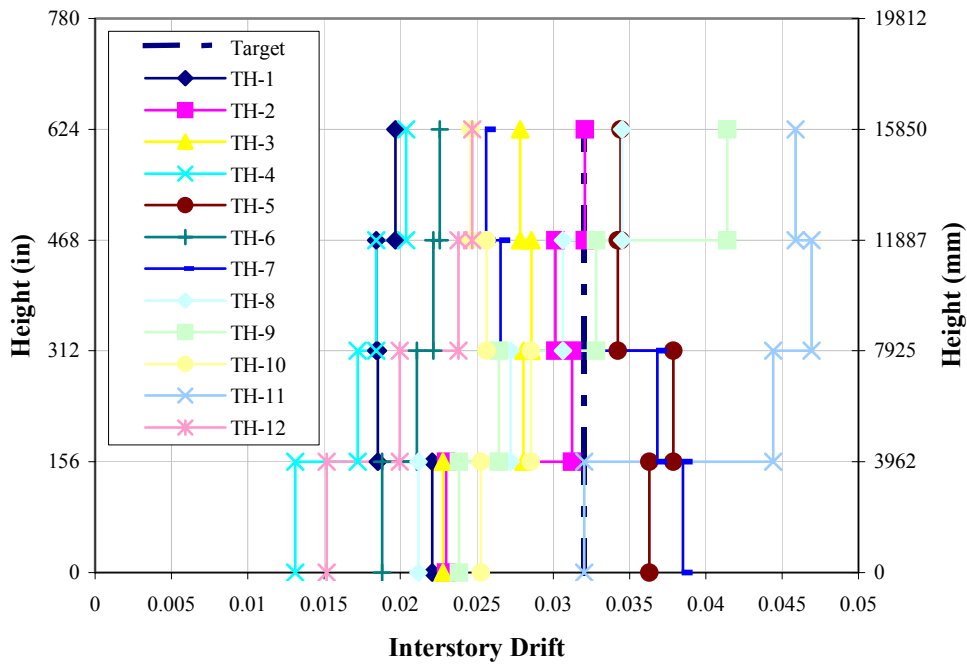


Figure 4.1.1-16. FR-4 Maximum interstory drift envelopes (SP-3:EQ III)

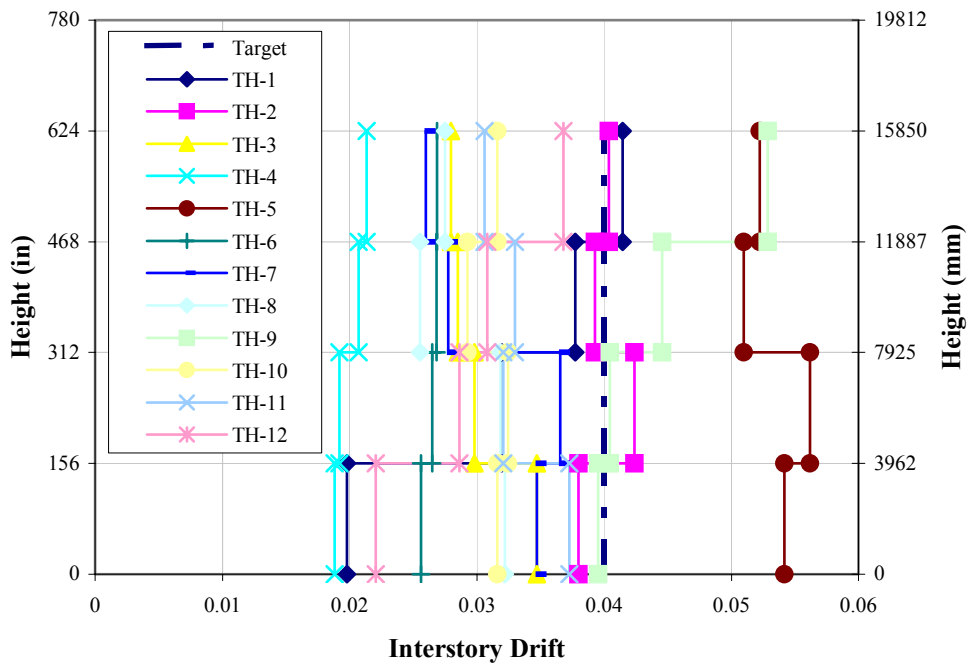


Figure 4.1.1-17. FR-4 Maximum interstory drift envelopes (SP-4:EQ IV)

The previous graphs indicate very different response than the maximum nodal displacements. The effects of hinge sequencing, from EQ characteristics, floor overstrengths, and base hinging, or lack of, are apparent. Additionally, large deviations indicate the possibility of higher mode response. As mentioned previously, higher mode response in low-rise frames is most likely due to the formation of localized yield mechanisms from overstrengths more than EQ intensity.

4.1.2 Base Shear

Table 4.1.2-1 list the maximum absolute base shear envelopes for each time-history analysis representative at each design performance level.

TH	SP-1 : EQ I (k / kN)		SP-2 : EQ II (k / kN)		SP-3 : EQ III (k / kN)		SP-4 : EQ IV (k / kN)	
	TH-1	855	3803	1066	4743	1212	5390	1179
TH-2	702	3121	1026	4564	1344	5978	1203	5352
TH-3	684	3041	1011	4497	1126	5011	1270	5649
TH-4	726	3231	878	3906	1238	5505	1369	6089
TH-5	715	3178	1188	5286	1233	5483	1245	5536
TH-6	556	2475	1093	4860	1130	5028	1194	5309
TH-7	794	3530	1139	5066	1205	5361	1286	5721
TH-8	760	3380	1054	4690	1358	6039	1291	5743
TH-9	670	2982	1105	4917	1252	5569	1356	6033
TH-10	881	3919	1072	4767	1168	5196	1196	5320
TH-11	879	3910	1063	4730	1310	5826	1255	5583
TH-12	588	2615	852	3788	1193	5308	1244	5534

Table 4.1.2-1. FR-4 Maximum base shears

With the base shears and displacement at the effective height determined for each performance level, the system force-displacement graph is constructed and compared to the predicted values. Each mark in Fig. 4.1.2-1 denotes a performance level and consecutively traces the force-displacement response.

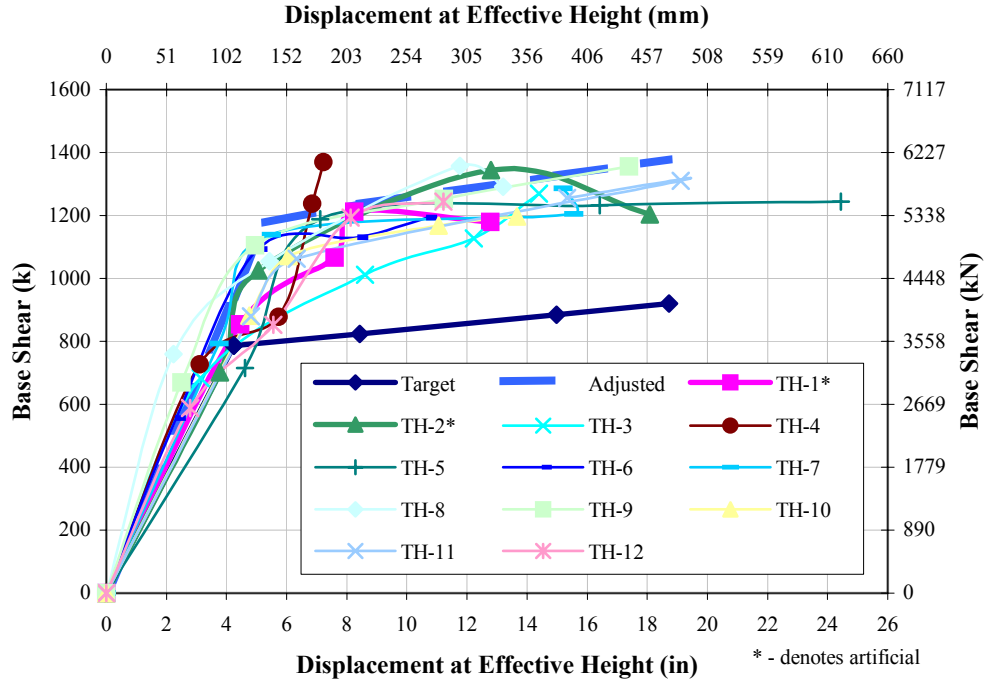


Figure 4.1.2-1. FR-4 System force-displacement graph

There is good comparison between the actual maximum envelopes and “as designed” predicted values. The effects of performance overstrengths on post-yield base shear capacity and nodal displacements are clearly visible, as well as the need to incorporate them into the design of steel frames. For this research the plastic hinge sequencing factor was assumed equal to 1.2 for all cases since the proposed method discussed in Section 2.4.6 is currently purely conceptual. While ultimately this value tends towards an overall good system design, it also causes localized jumps in the graphs (TH-4) due to additional strengthening of beams and columns.

Additionally, a comparison between maximum story shears and design story shears can be performed in an effort to determine the accuracy of the performance overstrength factors. For this frame, the system member overstrength was determined to be 1.25 providing a total system overstrength of approximately 1.5.

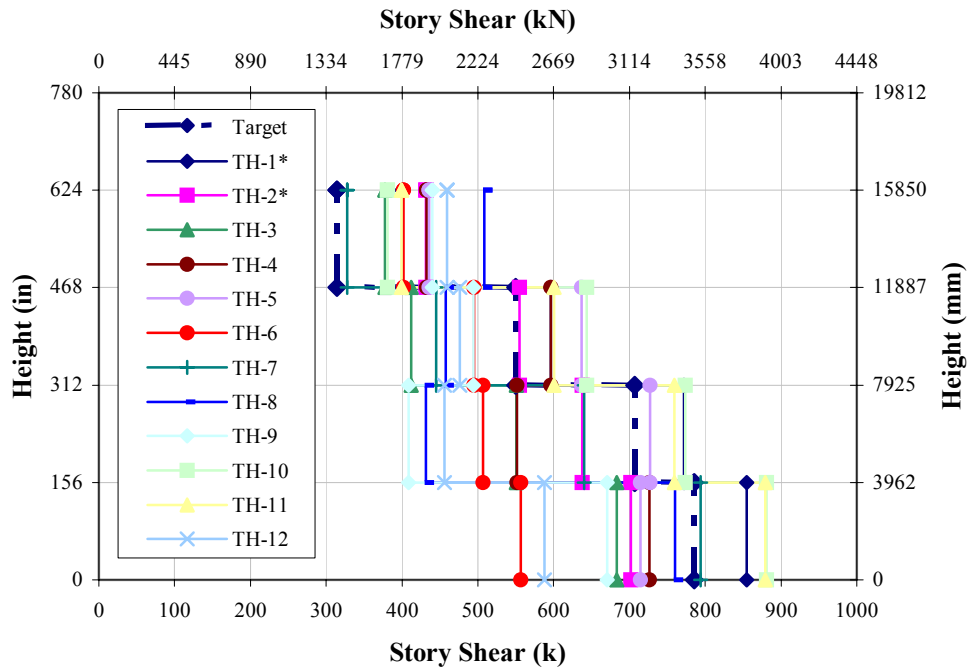


Figure 4.1.2-2. FR-4 Maximum story shear envelopes (SP-1:EQ I)

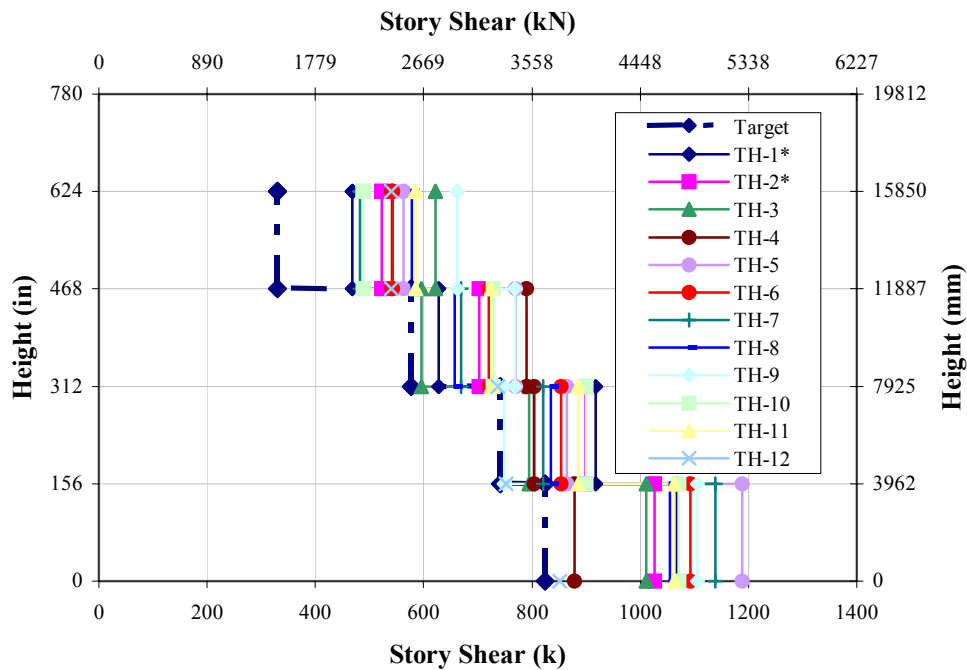


Figure 4.1.2-3. FR-4 Maximum story shear envelopes (SP-2:EQ II)

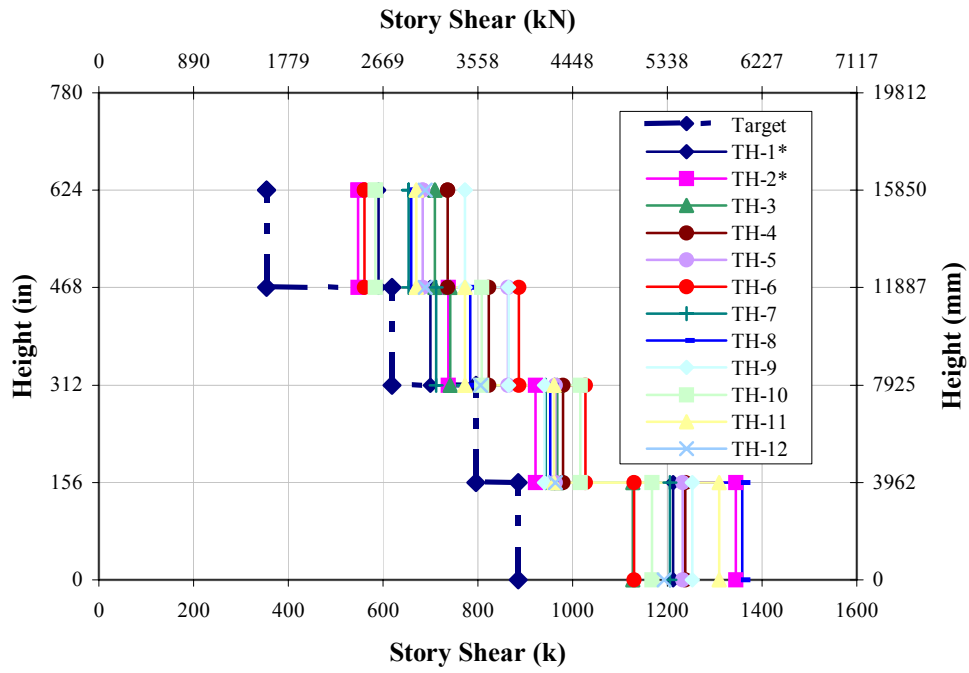


Figure 4.1.2-4. FR-4 Maximum story shear envelopes (SP-3:EQ III)

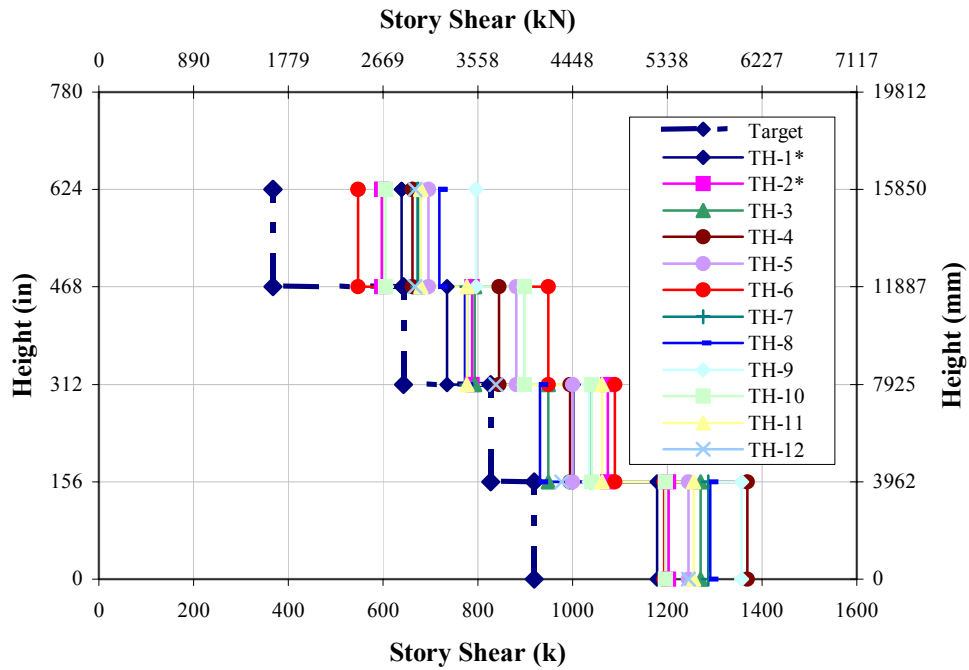


Figure 4.1.2-5. FR-4 Maximum story shear envelopes (SP-1:EQ I)

The effect of individual floor overstrengths on the force demands is evident in the previous graphs. The upper floors, having the higher floor overstrengths, attract higher force demands. Once the system begins to form localized yield mechanisms, the performance overstrength factor is no longer constant due to hinge sequencing. As a side note, once the global yield mechanism forms accompanied by hinge sequencing effects, the base shear decreases due to period elongation as seen in Fig. 4.1.2-3.

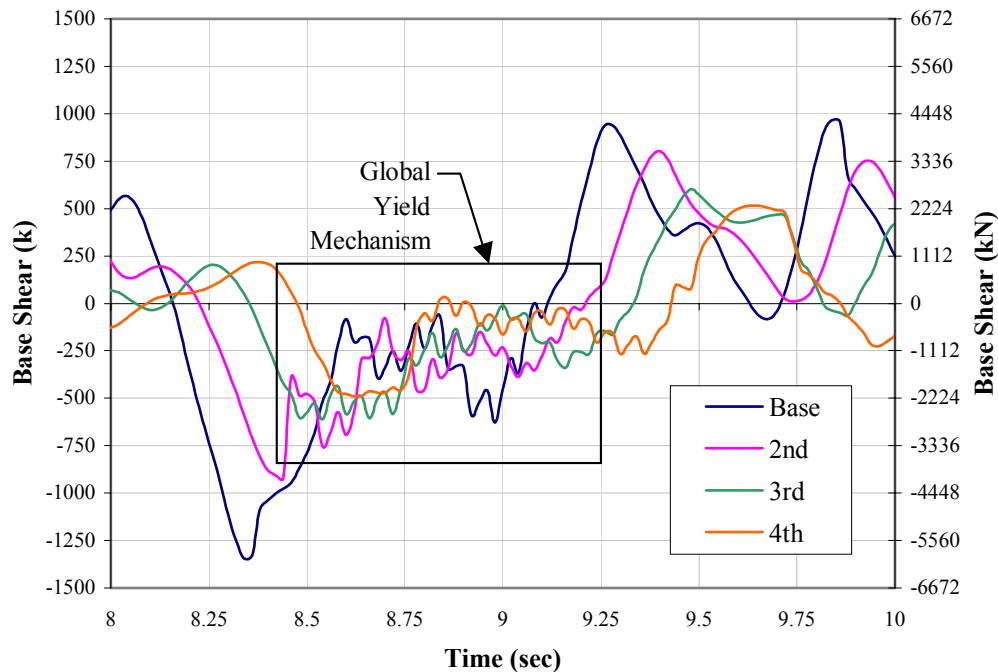


Figure 4.1.2-6. FR-4 story shears as function of time (TH-1:EQ III)

This graph also highlights that plastic hinges in a frame form in a vertical traveling wave. If the floors were designed in accordance with recommended procedures, then floor yield mechanisms will form similarly. Another indication of the effects of hinge sequencing in frames, shown in Fig. 4.1.2-3, is at 8.5 seconds when the story shears in the 3rd and 4th floor exceed the base shear and 2nd floor story shear.

Ultimately, this process results in a good design. It should be mentioned that Capacity Design procedures representing the complexities of frame response during strong ground motion and the uncertainties of earthquake characteristics is the key to a structurally safe structure.

4.2 Four (4) Story Frame (FR-4-W21)

4.2.1 Displacement Profiles

This alternate frame is provided as an example or “what if” situation and will not be discussed formally. Additionally, only the two artificial earthquakes will be used in the analysis.

Figs. 4.2.1-1 through 4.2.1-4 show the maximum absolute relative displacement envelopes for each time-history analysis (TH-1 and 2) representative at each design performance level.

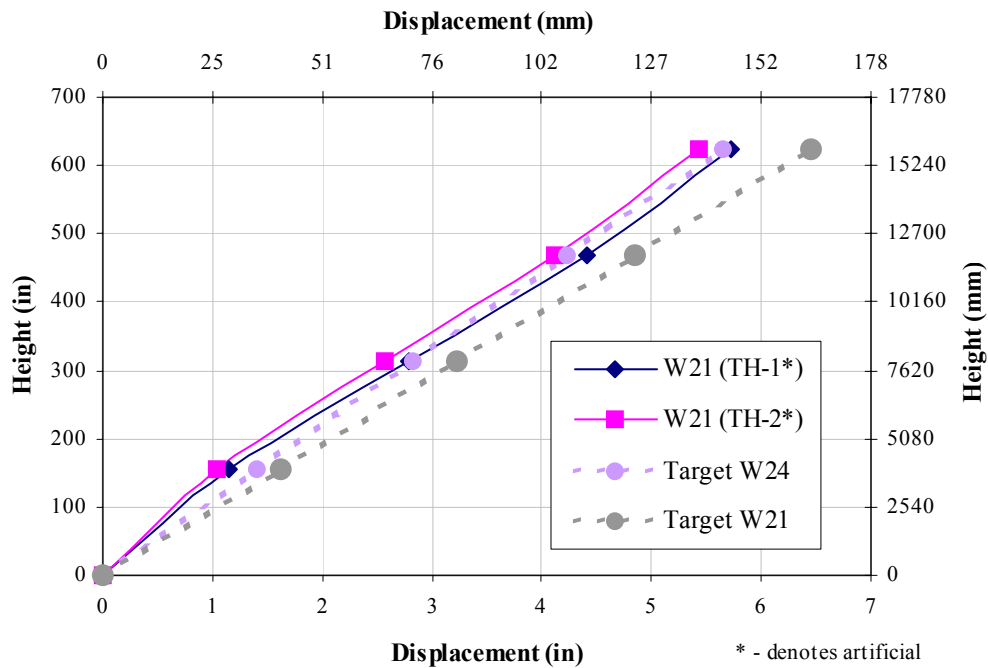


Figure 4.2.1-1. FR-4-W21 Maximum displacement envelopes (SP-1:EQ I)

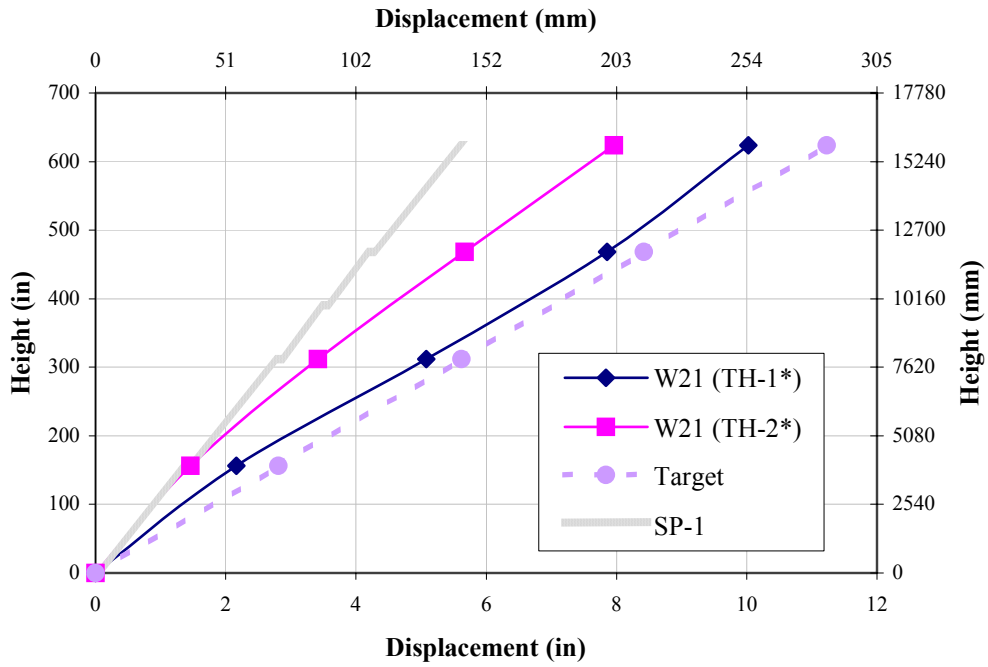


Figure 4.2.1-2. FR-4-W21 Maximum displacement envelopes (SP-2:EQ II)

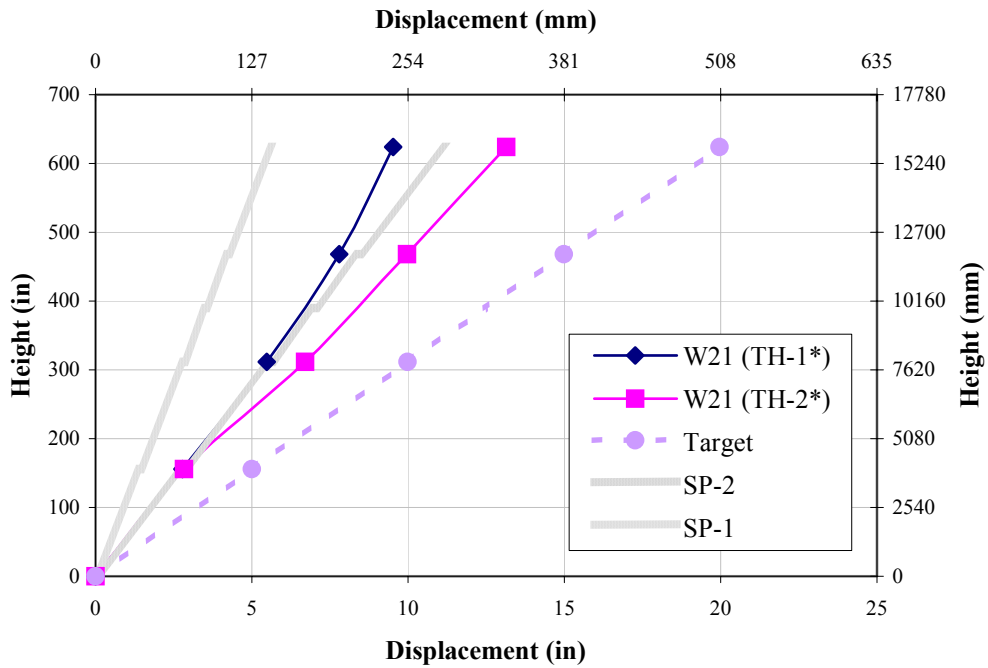


Figure 4.2.1-3. FR-4-W21 Maximum displacement envelopes (SP-3:EQ III)

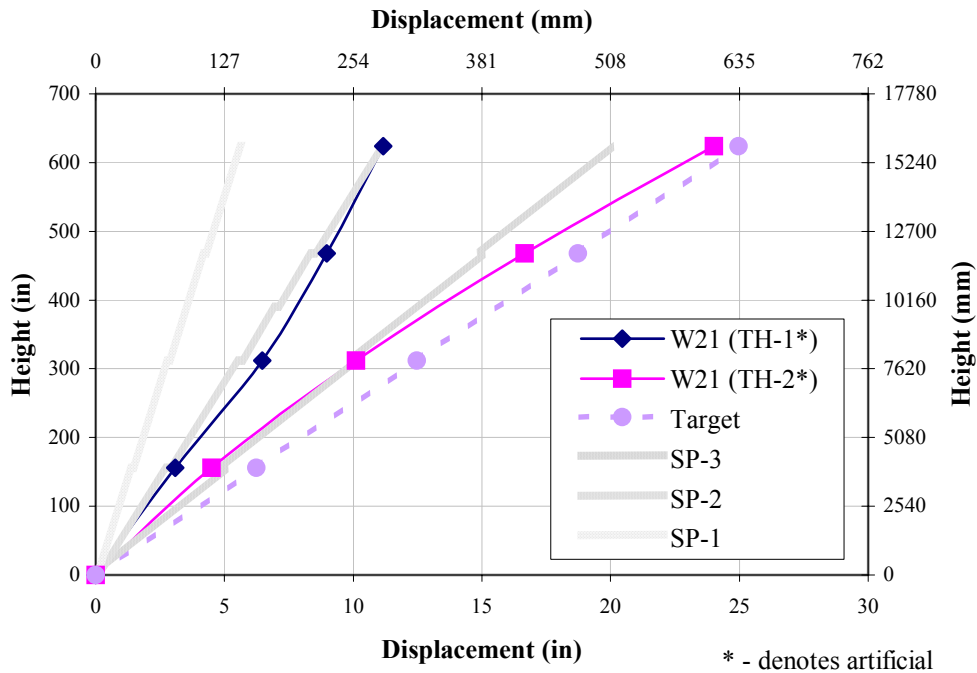


Figure 4.2.1-4. FR-4-W21 Maximum displacement envelopes (SP-4:EQ IV)

TH	SP-1 : EQ I (in / mm)		SP-2 : EQ II (in / mm)		SP-3 : EQ III (in / mm)		SP-4 : EQ IV (in / mm)	
	TH-1	4.4	112	7.9	199	7.8	198	9.0
TH-2	4.1	105	5.7	144	10.0	253	16.7	423

Table 4.2.1-1. FR-4-W21 Displacement at effective height

As can be seen, good comparison exists at the SP-1 level for TH-1 and 2 and it is evident that the base hinges have not formed as expected. Post-yield results are somewhat sporadic due to the *actual* DRS (see Section 4.9).

By investigating nodal displacements as a function of time, the maximum interstory drifts can be evaluated as seen in Figs. 4.1.1-5 through 4.1.1-8. Again, these do not necessarily occur at the same moment in time as the maximum displacements.

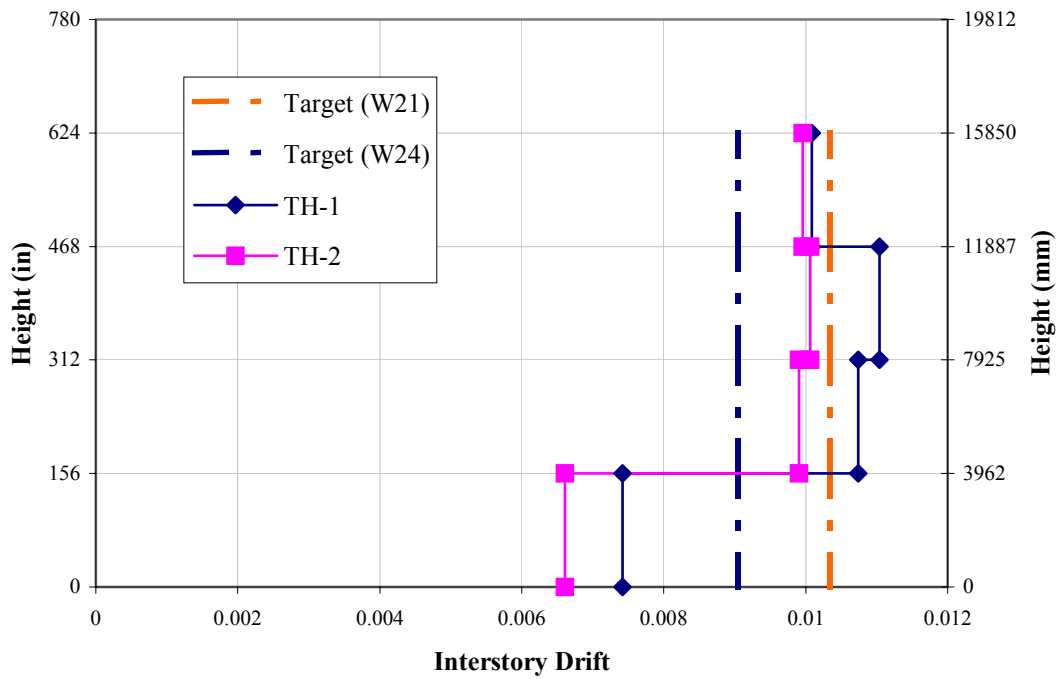


Figure 4.2.1-5. FR-4-W21 Maximum interstory drift envelope (SP-1:EQ I)

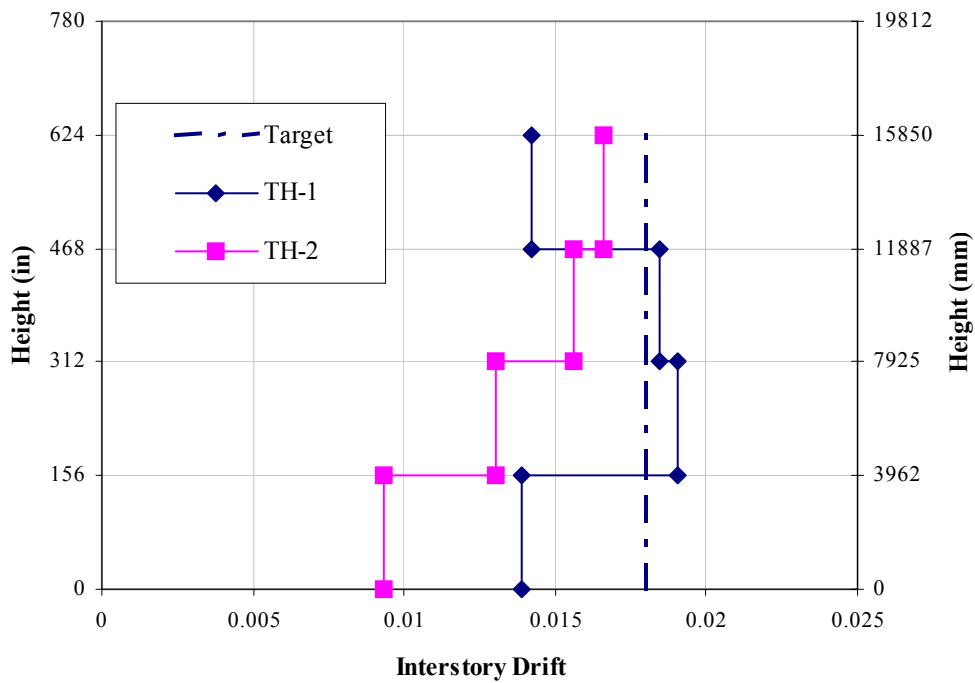


Figure 4.2.1-6. FR-4-W21 Maximum interstory drift envelope (SP-2:EQ II)

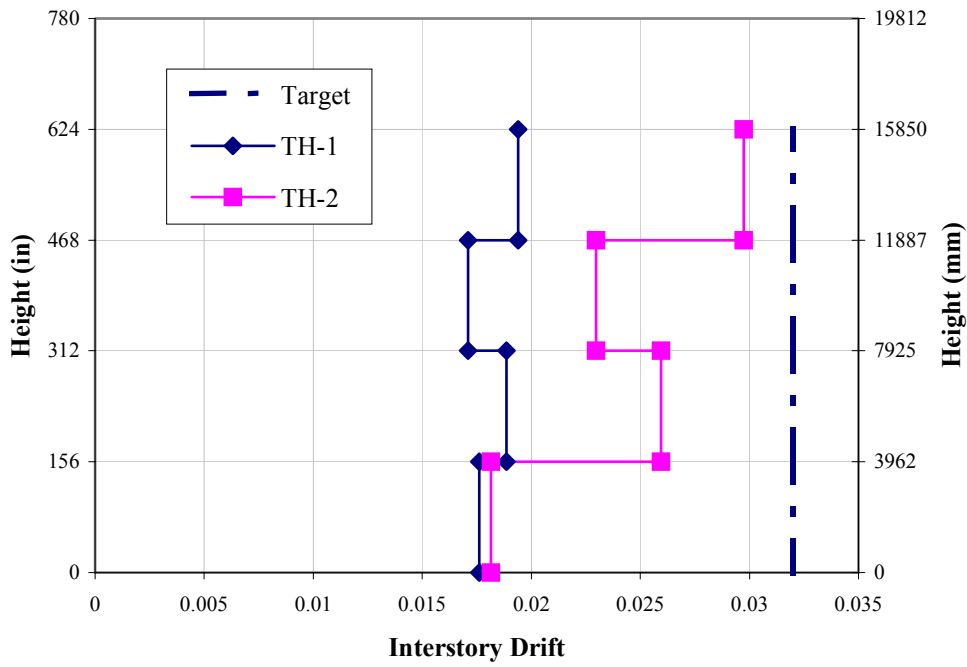


Figure 4.2.1-7. FR-4-W21 Maximum interstory drift envelope (SP-3:EQ III)

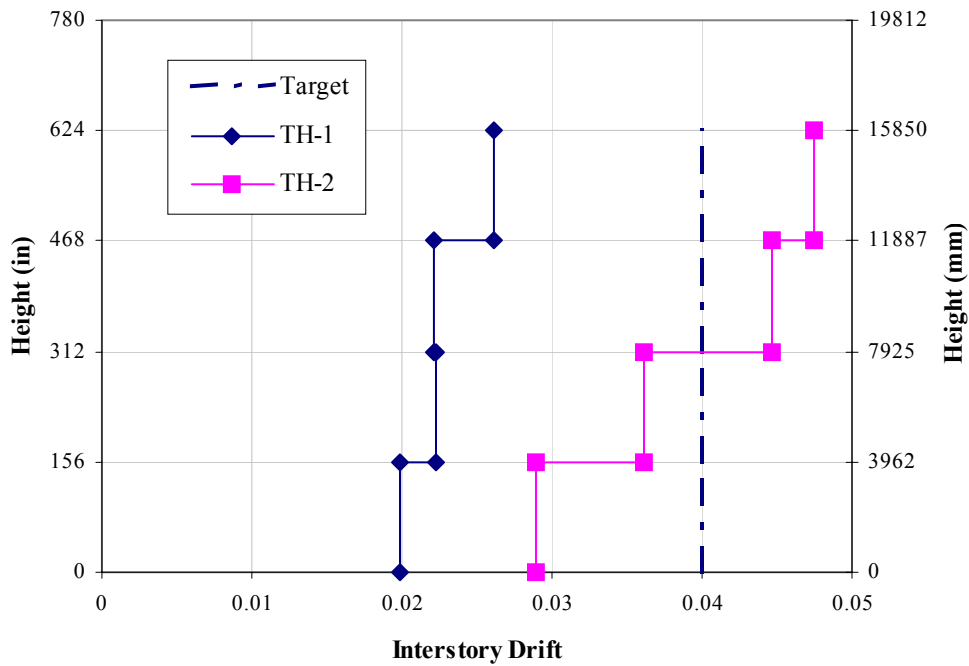


Figure 4.2.1-8. FR-4-W21 Maximum interstory drift envelope (SP-4:EQ IV)

4.2.2 Base Shear

TH	SP-1 : EQ I (k / kN)		SP-2 : EQ II (k / kN)		SP-3 : EQ III (k / kN)		SP-4 : EQ IV (k / kN)	
TH-1	813	3617	1084	4819	1160	5159	1183	5261
TH-2	697	3099	985	4381	1164	5179	1180	5249

Table 4.2.2-1. FR-4-W21 Base shears

With the base shears and displacement at the effective height determined for each performance level, the system force-displacement graph is constructed and compared to the predicted values shown in Fig. 4.2.2-1.

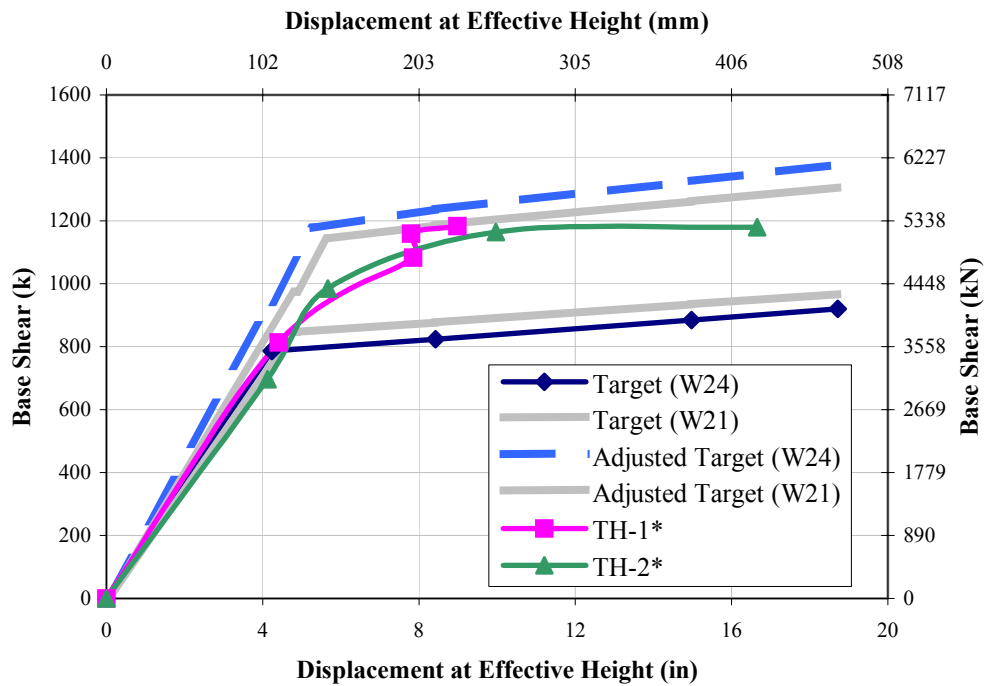


Figure 4.2.2-1. FR-4-W21 System force-displacement graph

There is good comparison between the actual maximum envelopes and predicted values. Additionally, the system tends towards the predicted W21 values. This emphasizes the importance of accurate target calculations while consistently maintaining the initial assumptions on the final frame behavior.

4.3 Four (4) Story Frame (FR-4-W24)

4.3.1 Displacement Profiles

This alternate frame is provided as an example or “what if” situation and will not be discussed formally. Additionally, only the two artificial earthquakes will be used in the analysis.

Figs. 4.3.1-1 through 4.3.1-4 show the maximum absolute relative displacement envelopes for each time-history analysis representative at each design performance level.

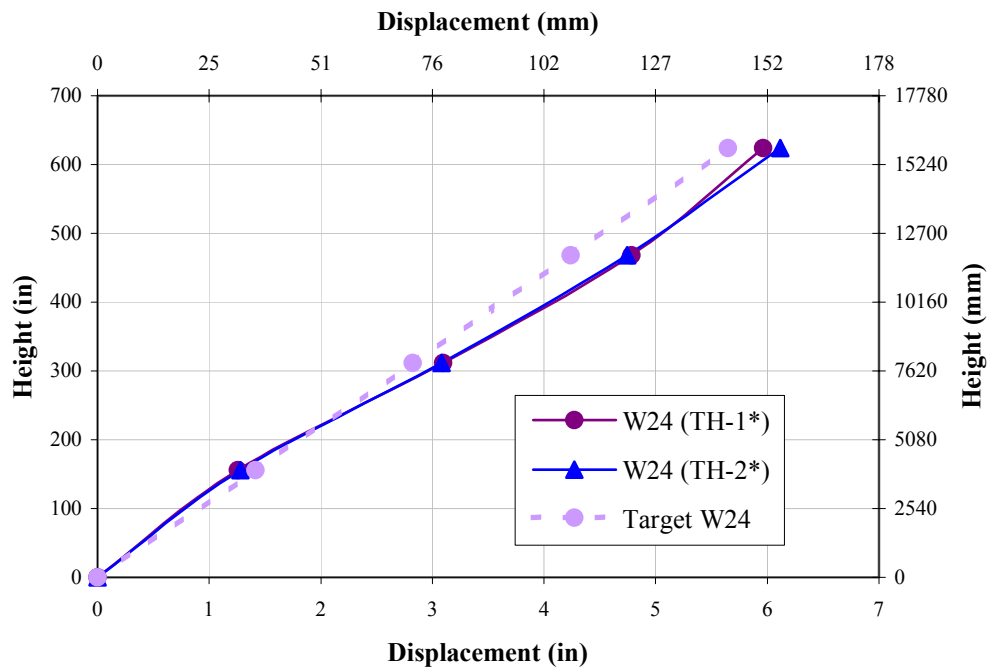


Figure 4.3.1-1. FR-4-W24 Maximum displacement envelopes (SP-1:EQ 1)

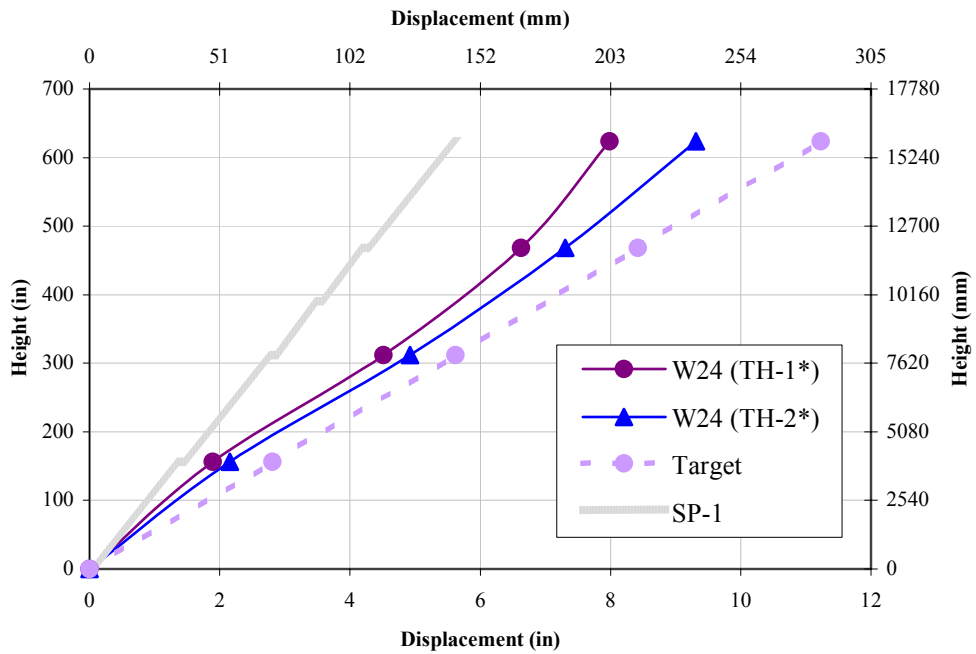


Figure 4.3.1-2. FR-4-W24 Maximum displacement envelopes (SP-2:EQ II)

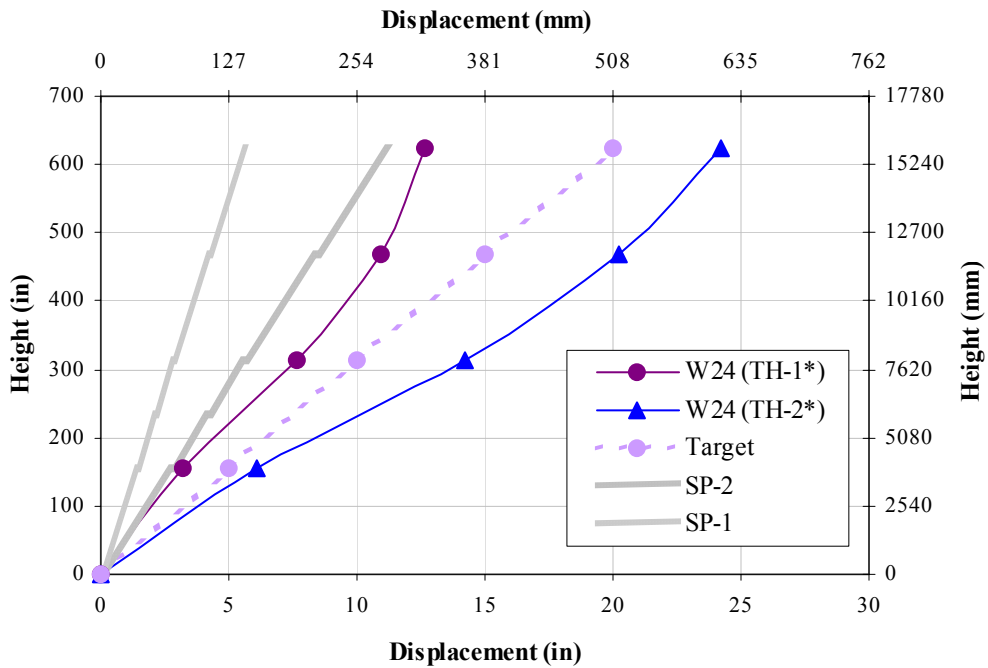


Figure 4.3.1-3. FR-4-W24 Maximum displacement envelopes (SP-3:EQ III)

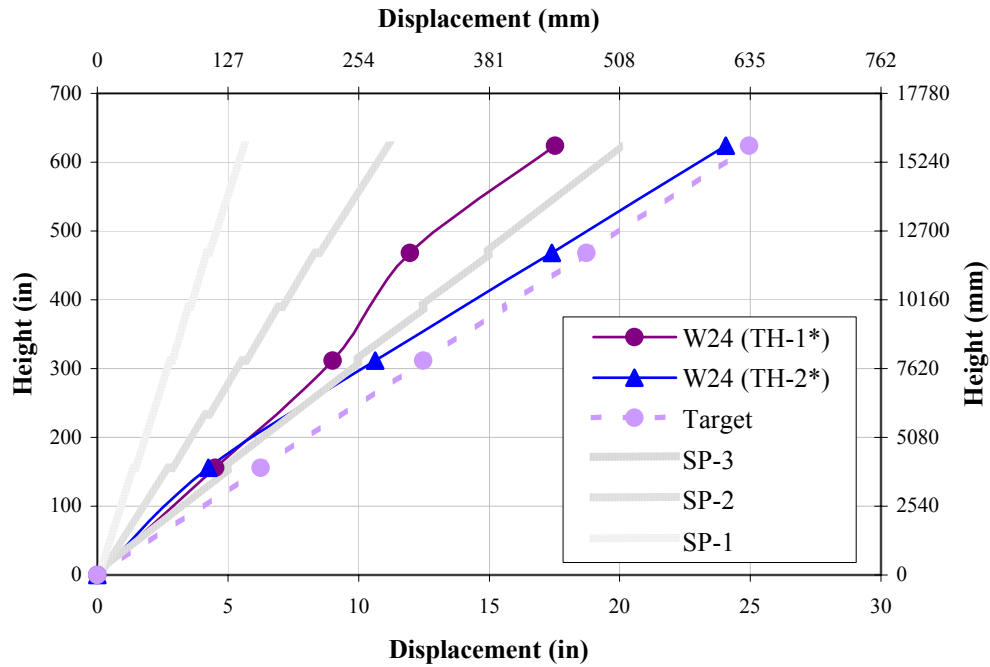


Figure 4.3.1-4. FR-4-W24 Maximum displacement envelopes (SP-4:EQ IV)

TH	SP-1 : EQ I (in / mm)		SP-2 : EQ II (in / mm)		SP-3 : EQ III (in / mm)		SP-4 : EQ IV (in / mm)	
	TH-1	4.8	121	6.6	168	10.9	278	12.0
TH-2	4.7	121	7.3	185	20.2	513	17.4	442

Table 4.3.1-1. FR-4-W24 Displacement at effective height

Similar to FR-4-W21, reasonable comparison exists at the SP-1 level for TH-1 and 2, whereas post-yield results deviate due to differences in the *actual* DRS and hinge sequencing.

By investigating nodal displacements as a function of time, the maximum interstory drifts can be evaluated as seen in Figs. 4.3.1-5 through 4.3.1-8.

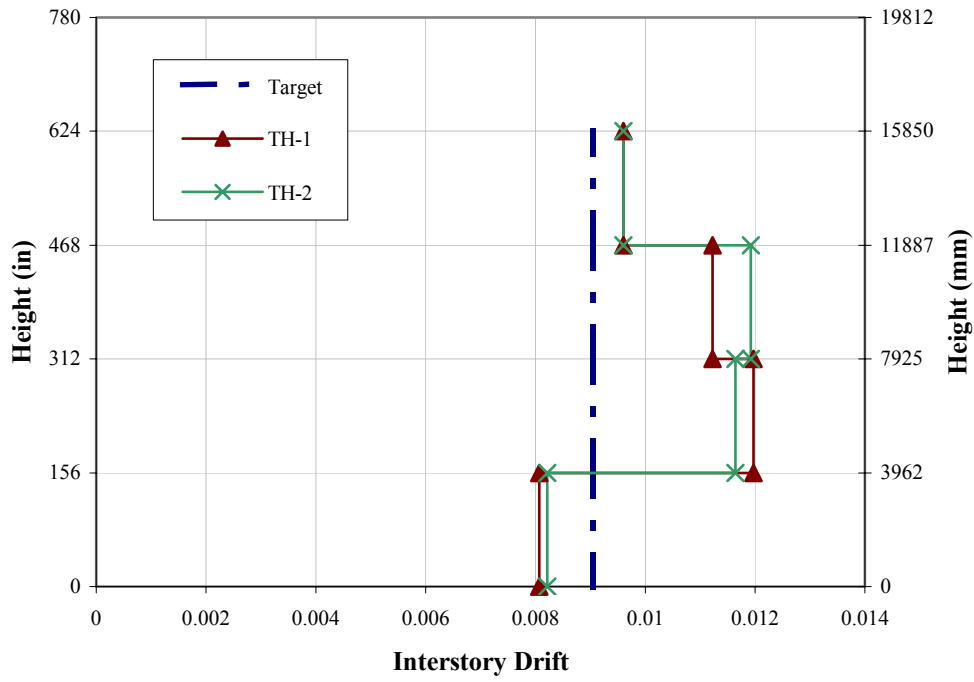


Figure 4.3.1-5. FR-4-W24 Maximum interstory drift envelope (SP-1:EQ I)

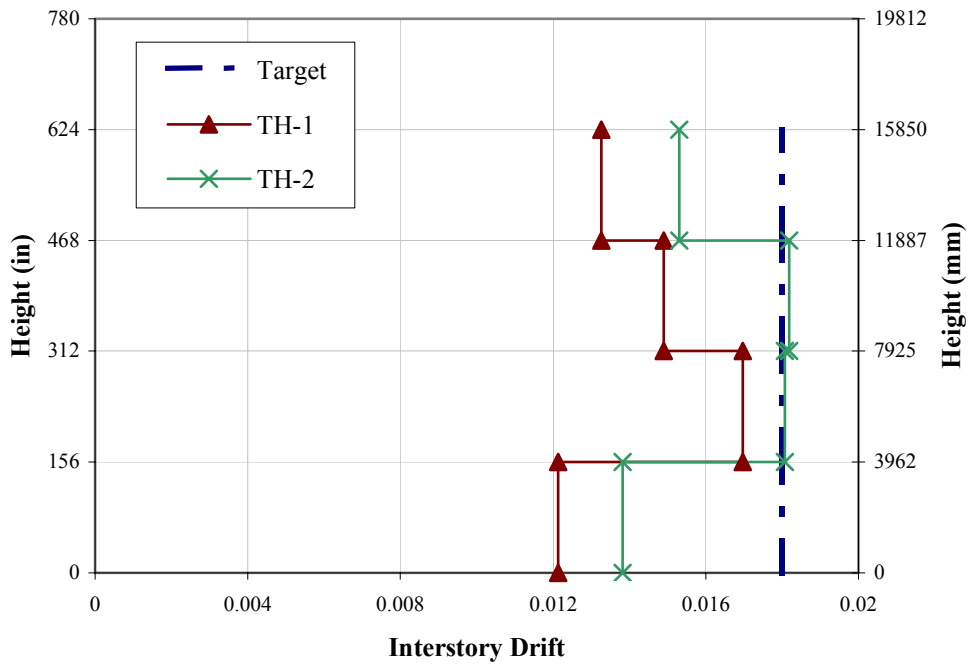


Figure 4.3.1-6. FR-4-W24 Maximum interstory drift envelope (SP-2:EQ II)

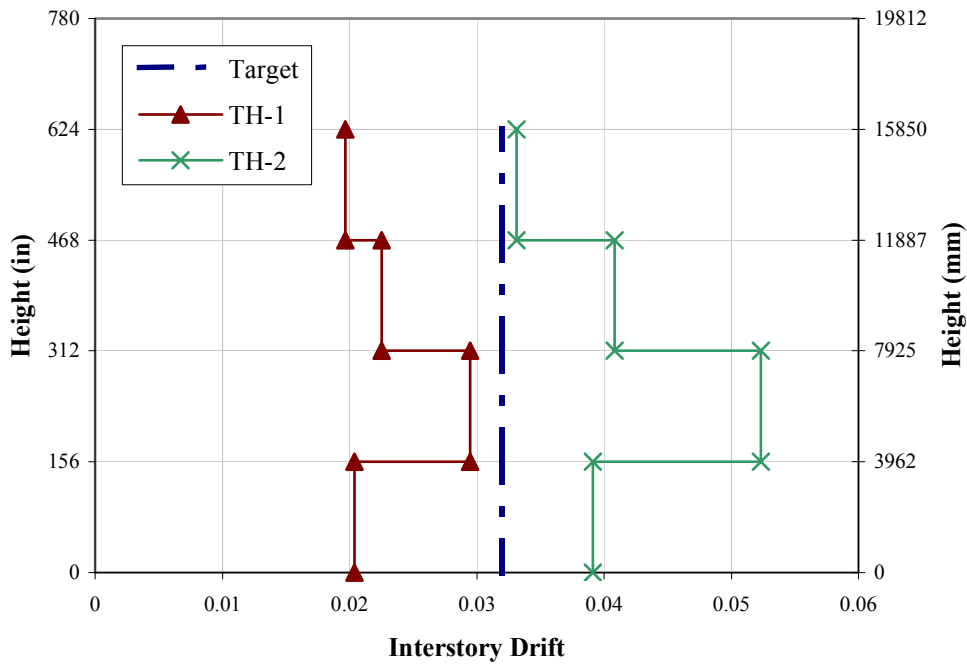


Figure 4.3.1-7. FR-4-W24 Maximum interstory drift envelope (SP-3:EQ III)

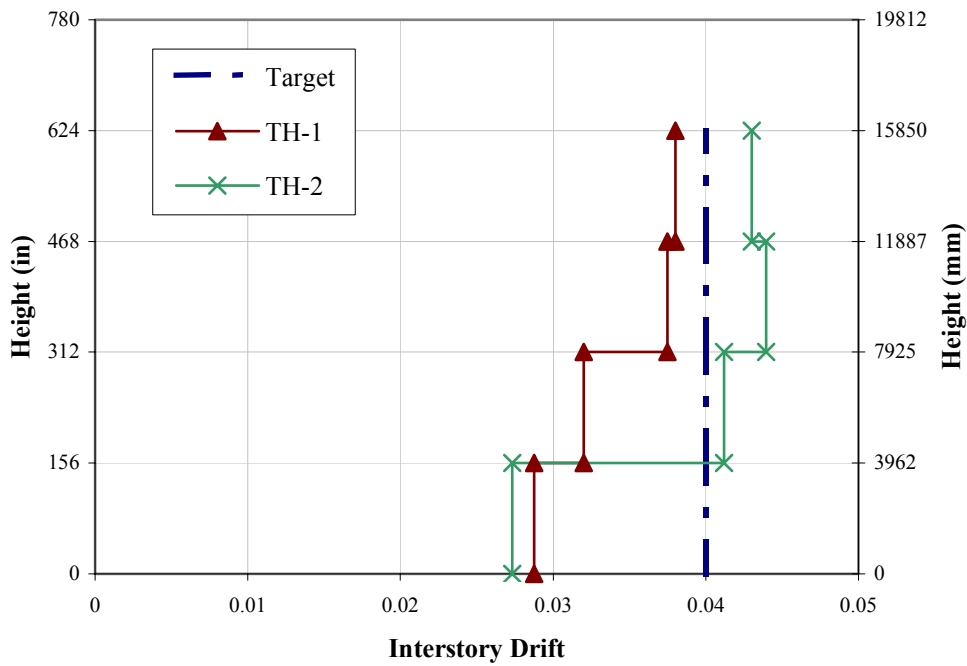


Figure 4.3.1-8. FR-4-W24 Maximum interstory drift envelope (SP-4:EQ IV)

4.3.2 Base Shear

TH	SP-1 : EQ I (k / kN)		SP-2 : EQ II (k / kN)		SP-3 : EQ III (k / kN)		SP-4 : EQ IV (k / kN)	
TH-1	655	2912	850	3781	978	4350	1036	4607
TH-2	678	3016	763	3392	1010	4493	1011	4495

Table 4.3.2-1. Base shears (FR-4-W24)

With the base shears and displacement at the effective height determined for each performance level, the system force-displacement graph is constructed and compared to the predicted values shown in Fig. 4.3.2-1.

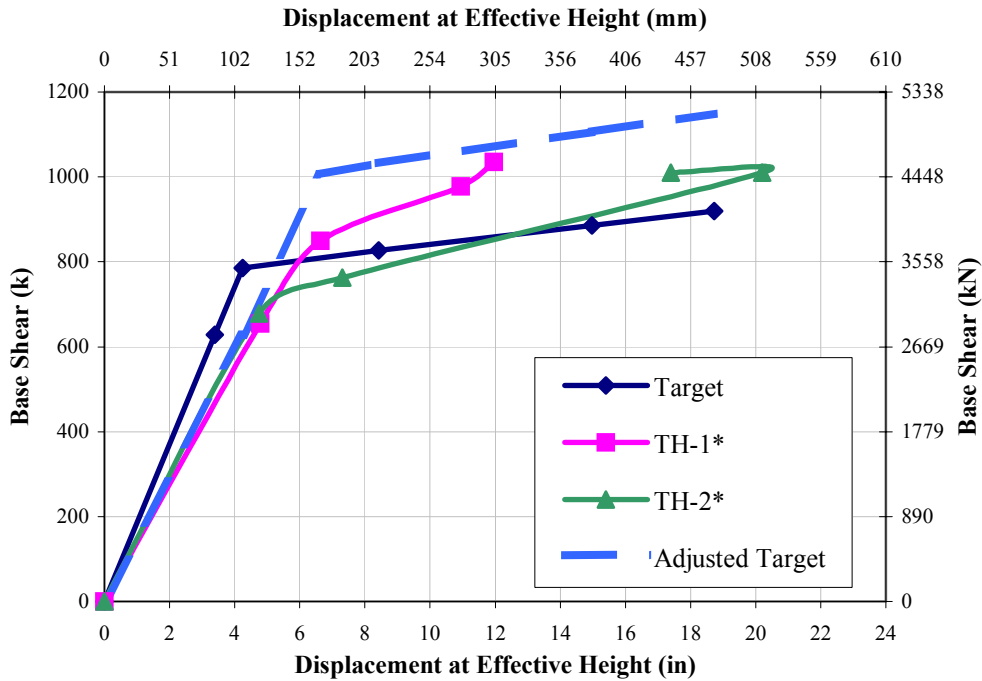


Figure 4.3.2-1. FR-4-W24 System force-displacement graph

As can be seen in Fig. 4.3.2-1, this process under-predicts damage levels. Therefore, it is not recommended and, additionally, all overstrength factors should be applied to post-analysis results.

4.4 Four (4) Story Frame (FR-4a)

4.4.1 Displacement Profiles

This alternate frame is provided as an example configuration and will not be discussed formally. Additionally, only the two artificial earthquakes will be used in the analysis.

Figs. 4.4.1-1 through 4.4.1-4 show the maximum absolute relative displacement envelopes for each time-history analysis representative at each design performance level.

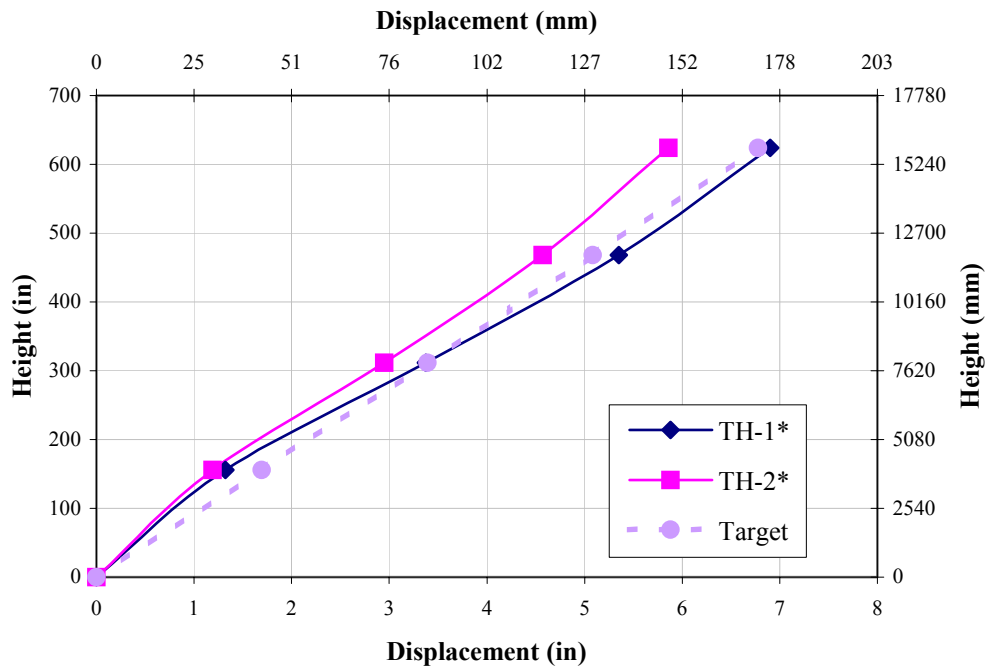


Figure 4.4.1-1. FR-4a Maximum displacement envelopes (SP-1:EQ I)

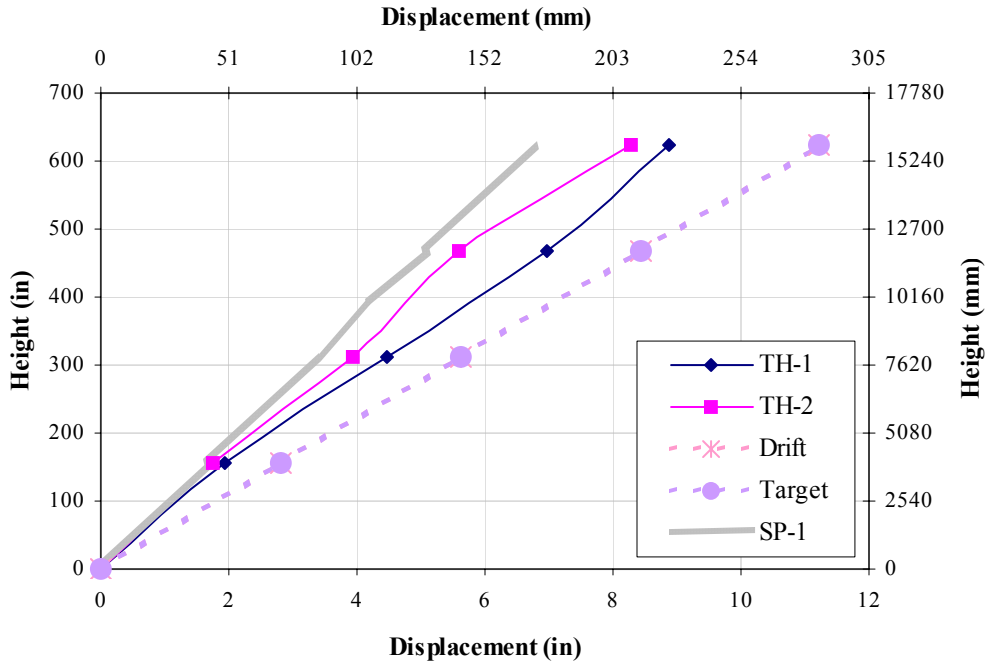


Figure 4.4.1-2. FR-4a Maximum displacement envelopes (SP-2:EQ II)

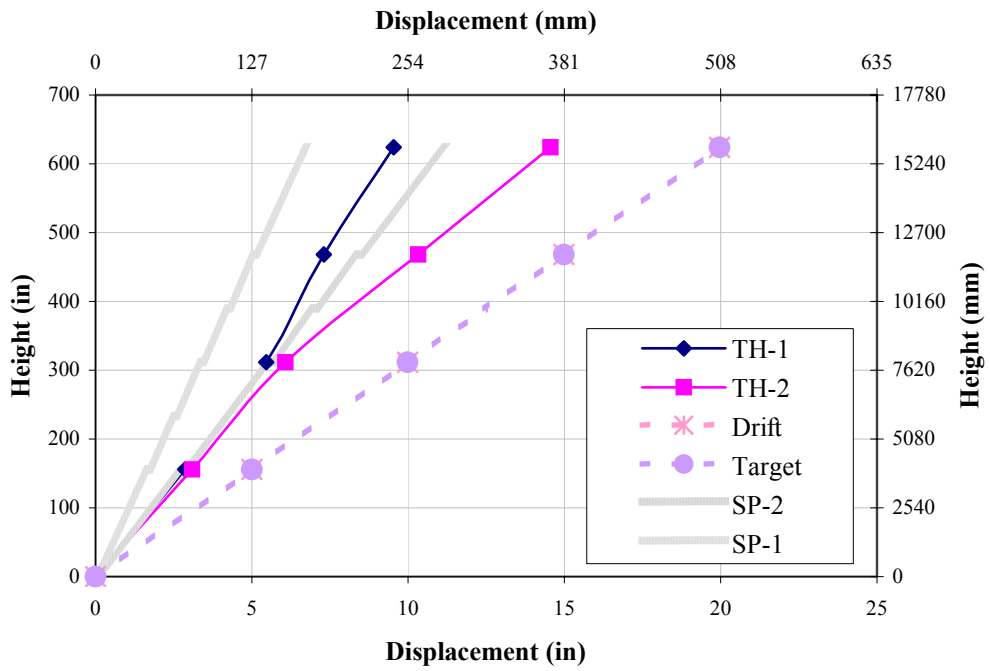


Figure 4.4.1-3. Fr-4a Maximum displacement envelopes (SP-3:EQ III)

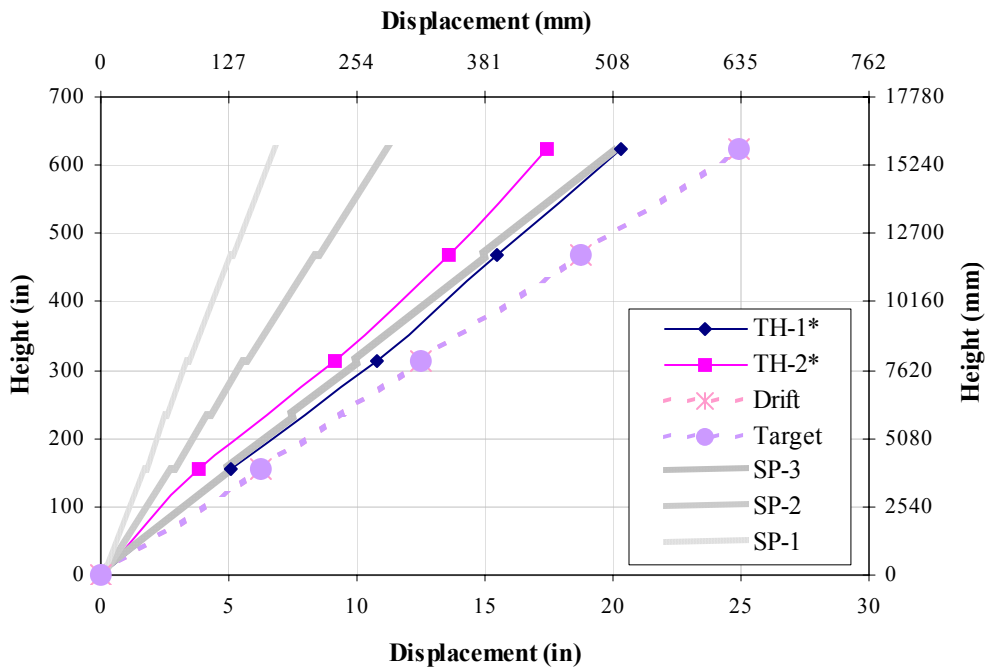


Figure 4.4.1-4. FR-4a Maximum displacement envelopes (SP-4:EQ IV)

TH	SP-1 : EQ I (in / mm)		SP-2 : EQ II (in / mm)		SP-3 : EQ III (in / mm)		SP-4 : EQ IV (in / mm)	
	TH-1	5.4	136	7.0	177	7.3	186	15.4
TH-2	4.6	116	5.6	142	10.3	262	13.6	345

Table 4.4.1-1. FR-4a Displacement at effective height

Similar to the previous discussions, good comparison exists at the SP-1 level for TH-1 and 2, whereas post-yield results deviate due to differences in the *actual* DRS and hinge sequencing.

By investigating nodal displacements as a function of time, the maximum interstory drifts can be evaluated as seen in Figs. 4.3.1-5 through 4.3.1-8.

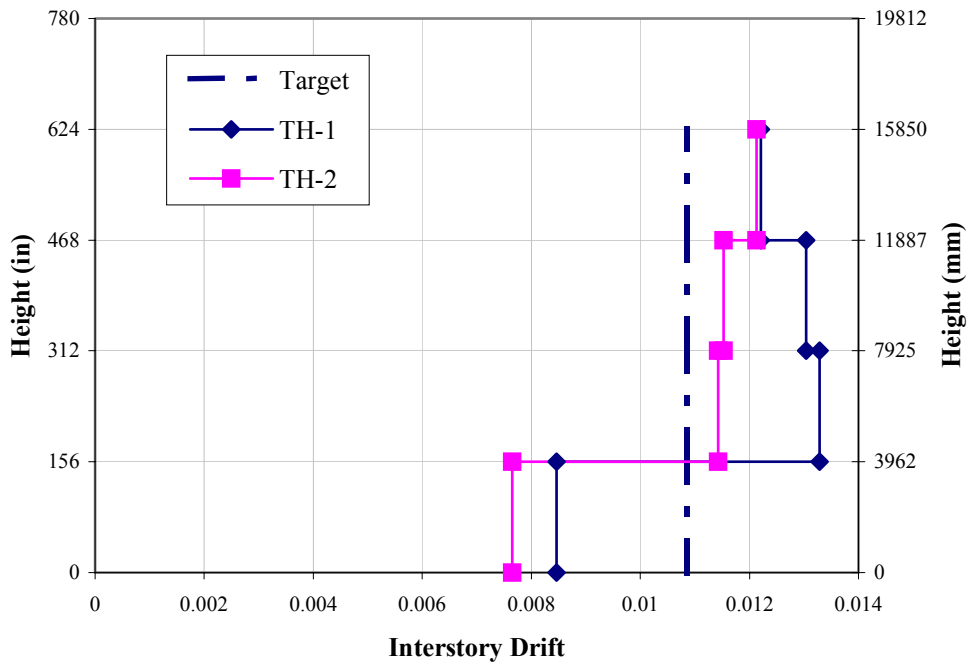


Figure 4.4.1-5. FR-4a Maximum interstory drift envelope (SP-1:EQ I)

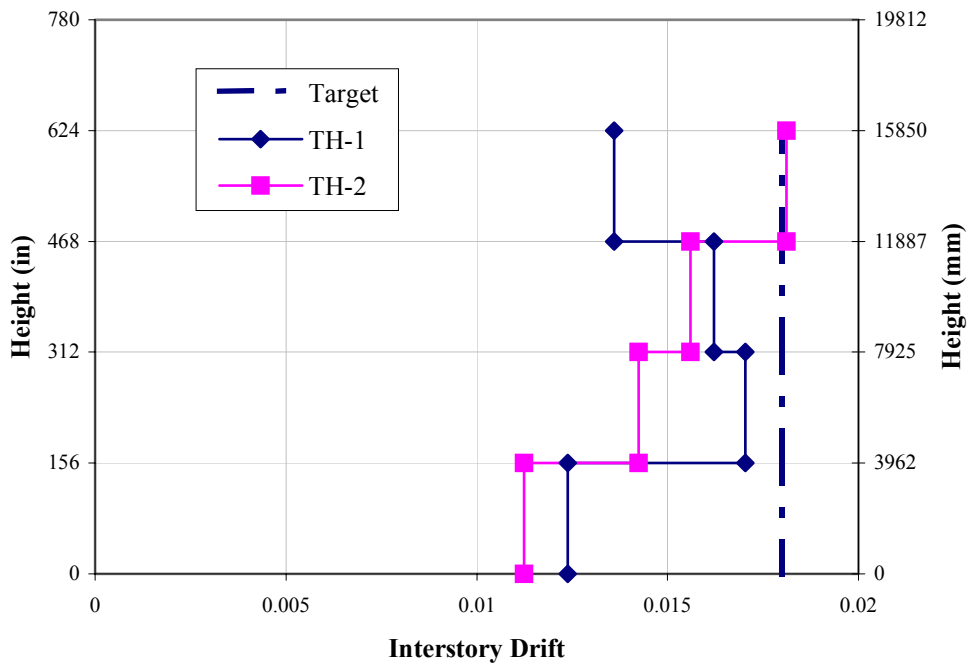


Figure 4.4.1-6. FR-4a Maximum interstory drift envelope (SP-2:EQ II)

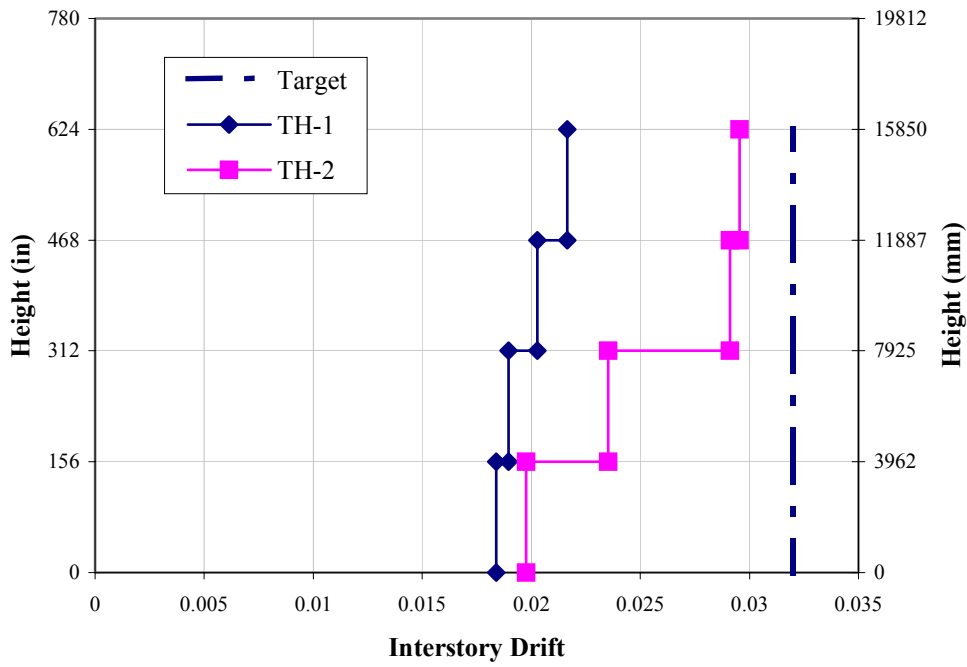


Figure 4.4.1-7. FR-4a Maximum interstory drift envelope (SP-3:EQ III)

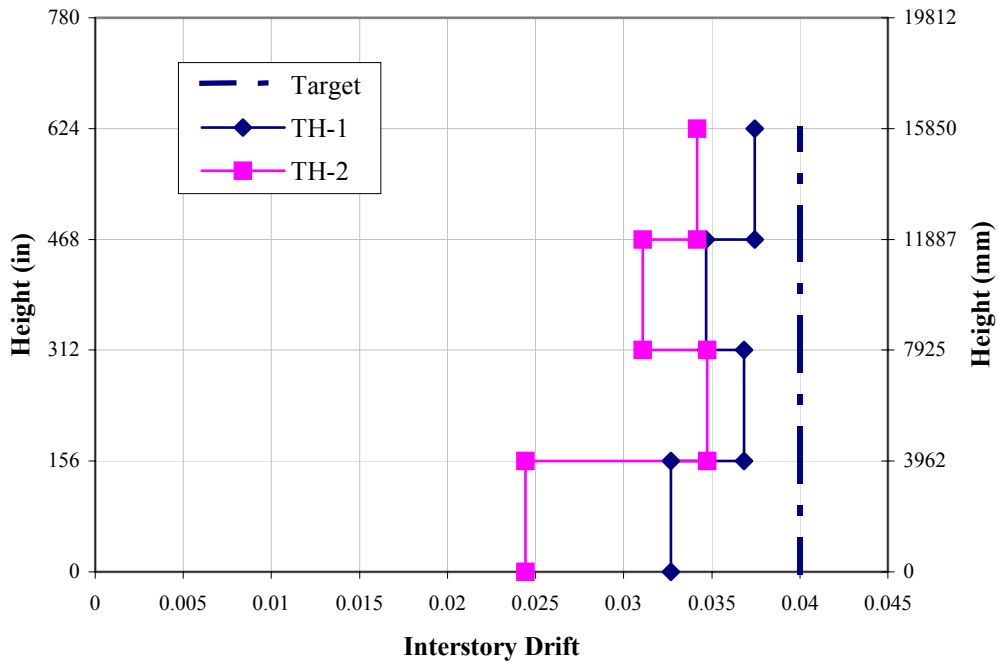


Figure 4.4.1-8. FR-4a Maximum interstory drift envelope (SP-4:EQ IV)

4.4.2 Base Shear

TH	SP-1 : EQ I (k / kN)		SP-2 : EQ II (k / kN)		SP-3 : EQ III (k / kN)		SP-4 : EQ IV (k / kN)	
TH-1	965	4292	1084	4823	1208	5371	1198	5330
TH-2	848	3770	1073	4771	1177	5235	1213	5394

Table 4.4.2-1. FR-4a Base shears

With the base shears and displacement at the effective height determined for each performance level, the system force-displacement graph is constructed and compared to the predicted values shown in Fig. 4.3.2-1.

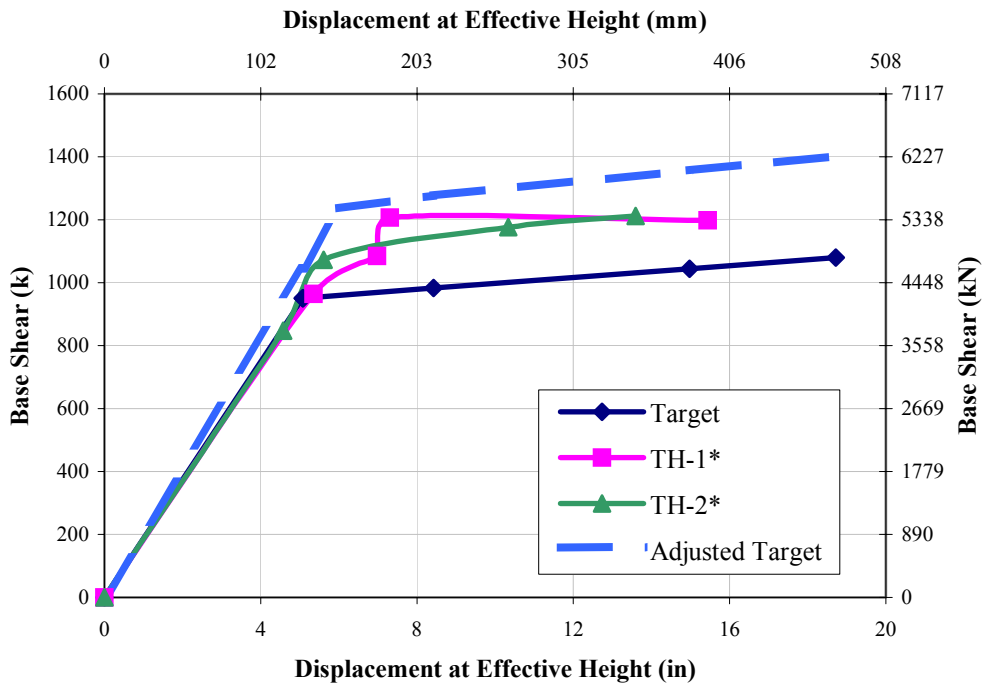


Figure 4.4.2-1. FR-4a System force-displacement graph

There is good comparison between the actual maximum envelopes and predicted values. The effects of performance overstrengths on post-yield base shear capacity and nodal displacements are clearly visible, as well as the need to incorporate them into the design of steel frames.

Additionally, a comparison between maximum story shears and design story shears can be performed in an effort to determine the accuracy of the performance overstrength factor.

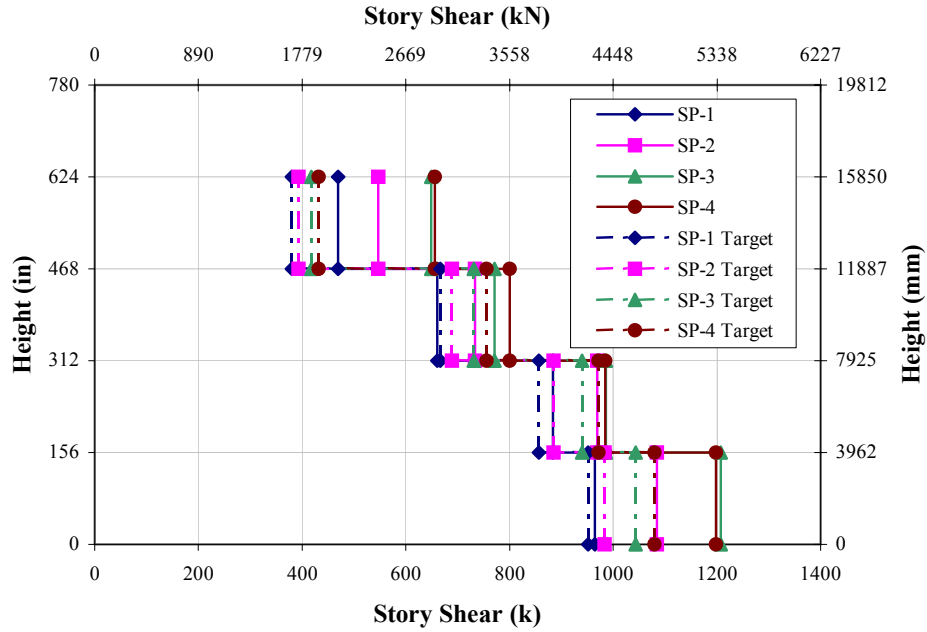


Figure 4.5.2-2. FR-4a Maximum story shears (TH-1)

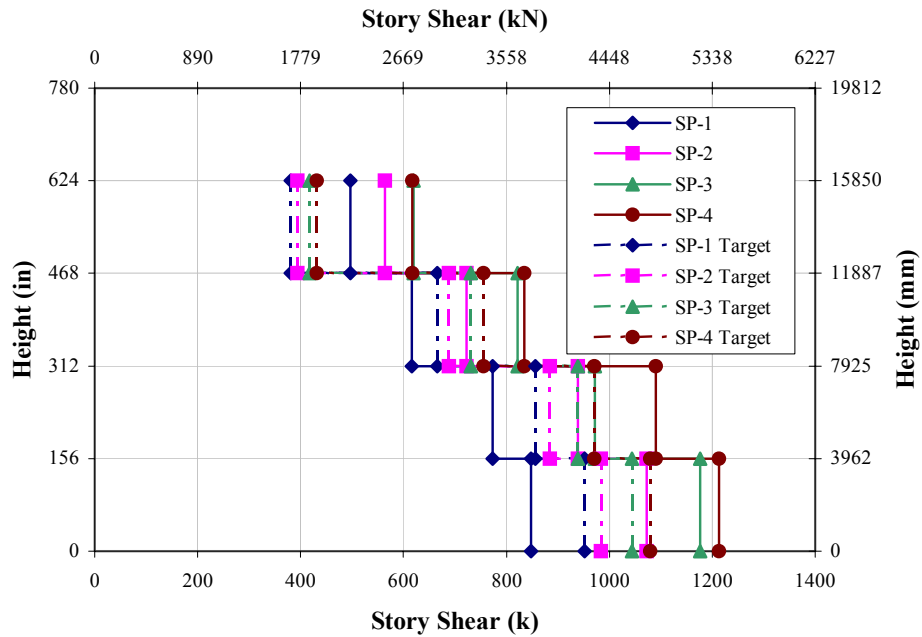


Figure 4.5.2-3. FR-4a Maximum story shears (TH-2)

4.5 Four (4) Story Frame (FR-4b)

4.5.1 Displacement Profiles

This alternate frame is provided as an example configuration and will not be discussed formally. Additionally, only the two artificial earthquakes will be used in the analysis.

Figs. 4.5.1-1 through 4.5.1-4 show the maximum absolute relative displacement envelopes for each time-history analysis representative at each design performance level.

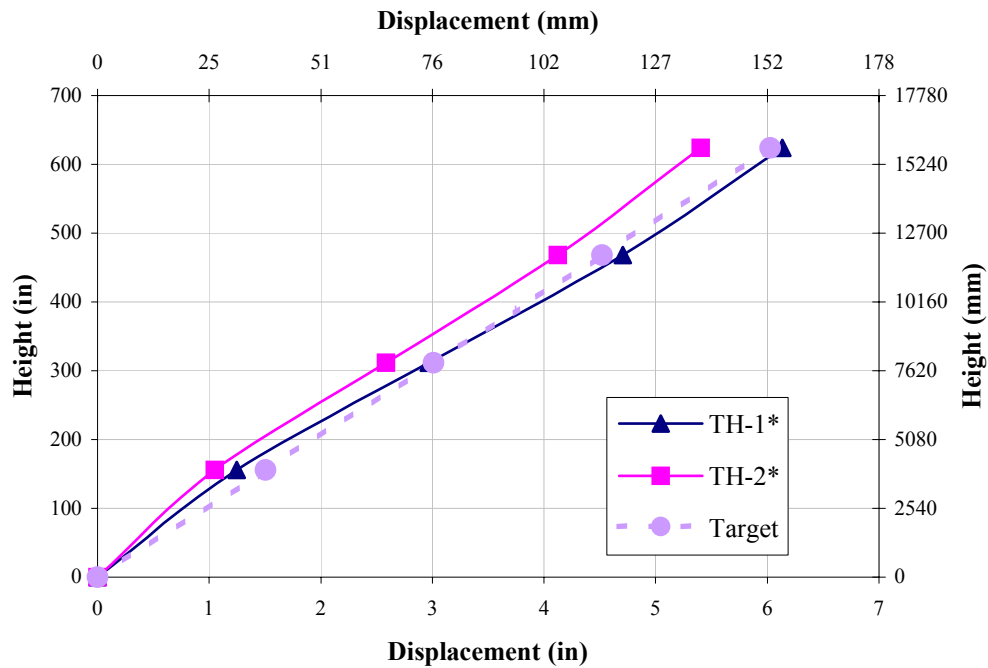


Figure 4.5.1-1. FR-4b Maximum displacement envelopes (SP-1:EQ I)

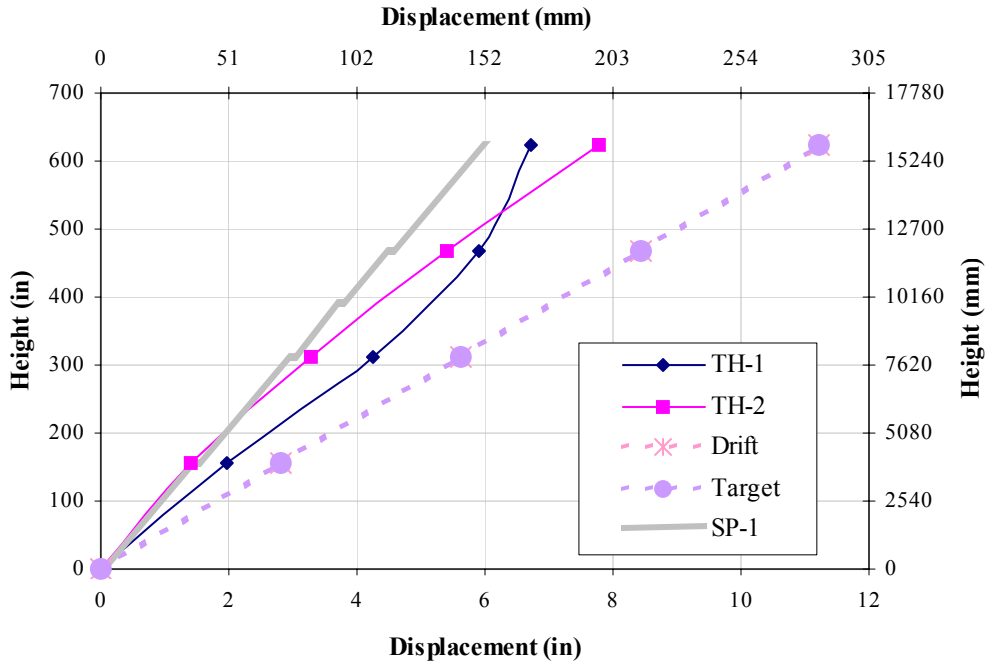


Figure 4.5.1-2. FR-4b Maximum displacement envelopes (SP-2:EQ II)

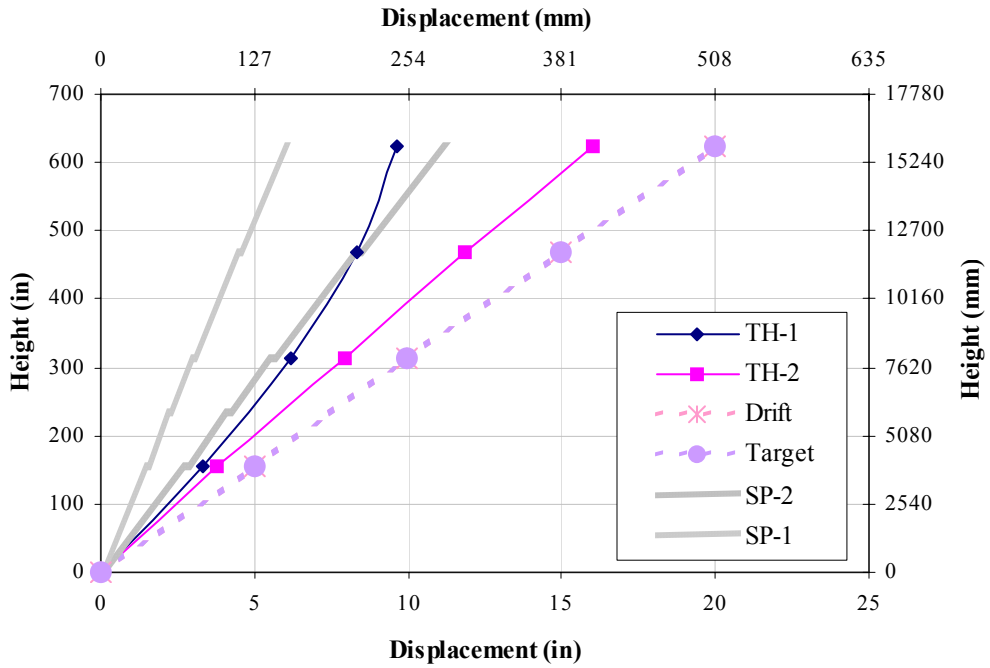


Figure 4.5.1-3. Fr-4b Maximum displacement envelopes (SP-3:EQ III)

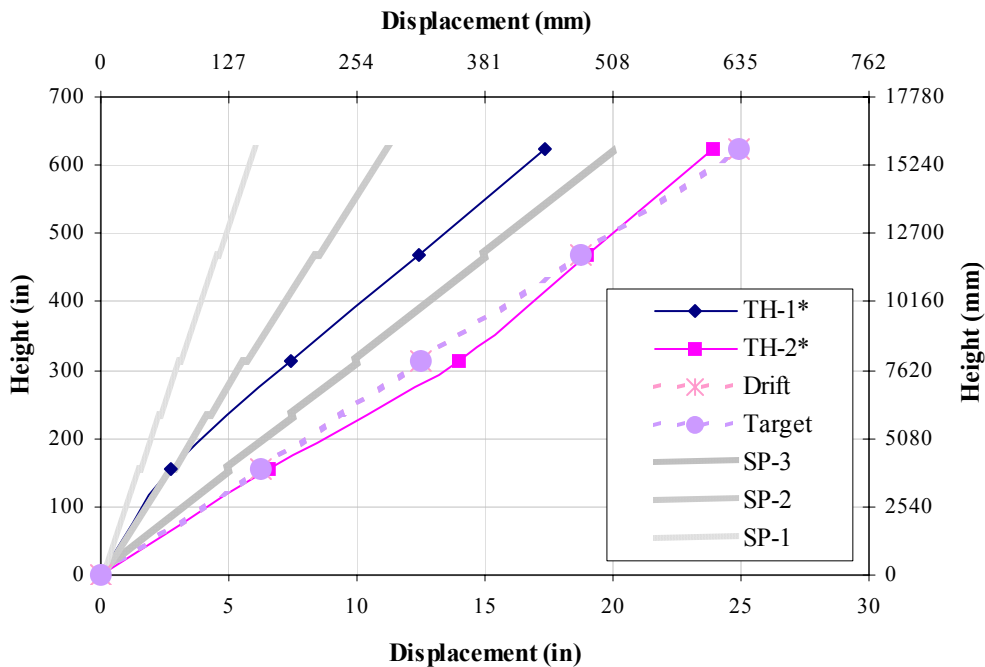


Figure 4.5.1-4. FR-4b Maximum displacement envelopes (SP-4:EQ IV)

TH	SP-1 : EQ I (in / mm)		SP-2 : EQ II (in / mm)		SP-3 : EQ III (in / mm)		SP-4 : EQ IV (in / mm)	
	TH-1	4.7	120	5.9	150	8.3	211	12.4
TH-2	4.1	105	5.4	137	11.9	301	19.0	483

Table 4.5.1-1. FR-4b Displacement at effective height

Similar to the previous discussions, good comparison exists at the SP-1 level for TH-1, whereas post-yield results deviate due to differences in the *actual* DRS and hinge sequencing.

By investigating nodal displacements as a function of time, the maximum interstory drifts can be evaluated as seen in Figs. 4.3.1-5 through 4.3.1-8. Again, these do not necessarily occur at the same moment in time as the maximum displacements.

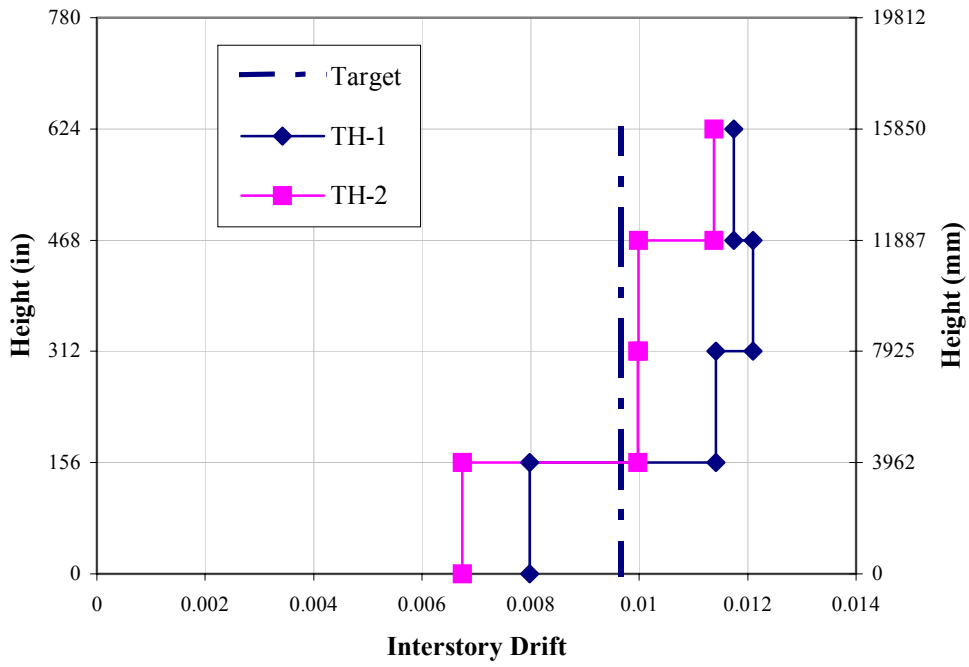


Figure 4.5.1-5. FR-4b Maximum interstory drift envelope (SP-1:EQ I)

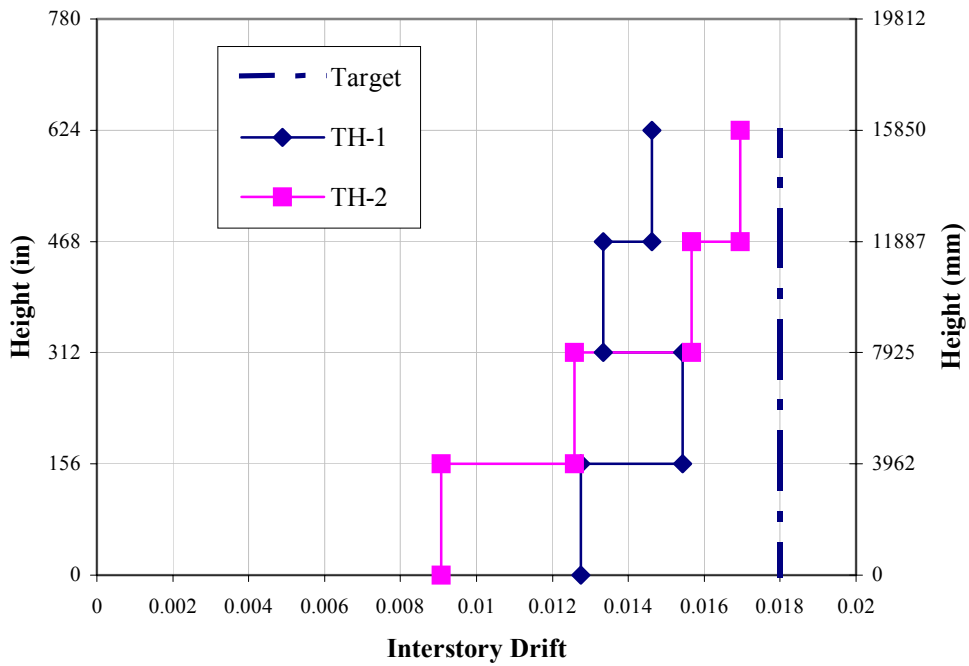


Figure 4.5.1-6. FR-4b Maximum interstory drift envelope (SP-2:EQ II)

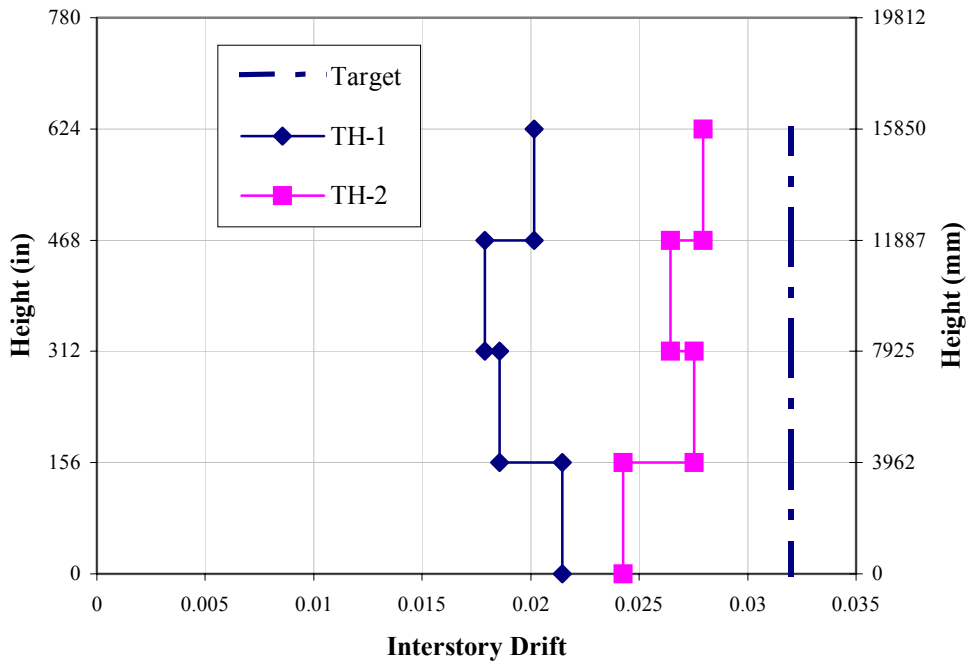


Figure 4.5.1-7. FR-4b Maximum interstory drift envelope (SP-3:EQ III)

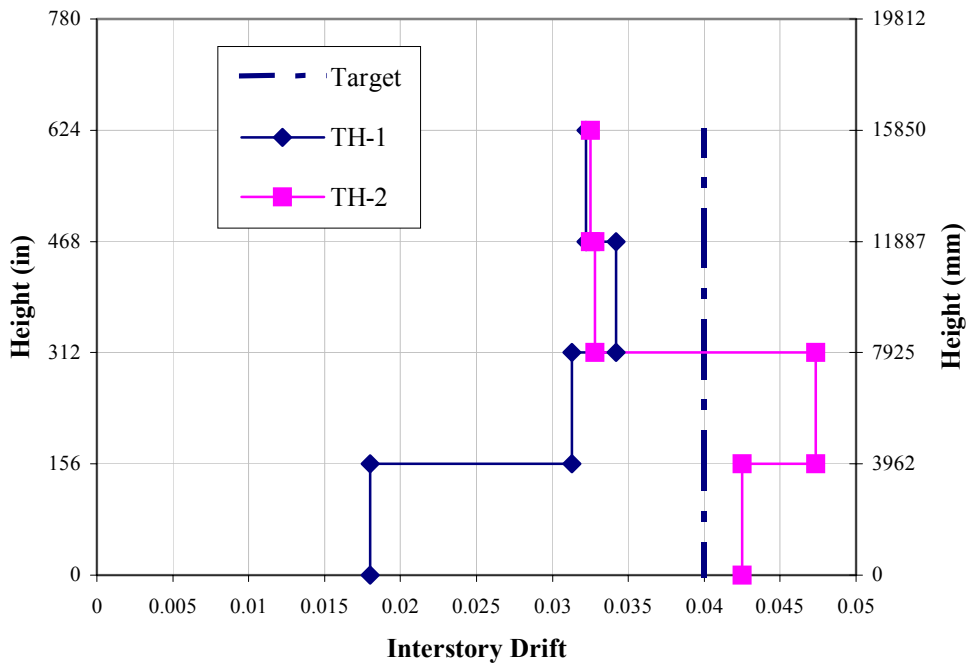


Figure 4.5.1-8. FR-4b Maximum interstory drift envelope (SP-4:EQ IV)

4.5.2 Base Shear

TH	SP-1 : EQ I (k / kN)		SP-2 : EQ II (k / kN)		SP-3 : EQ III (k / kN)		SP-4 : EQ IV (k / kN)	
TH-1	890	3957	1083	4819	1206	5362	1181	5255
TH-2	738	3284	1060	4714	1258	5594	1312	5837

Table 4.5.2-1. FR-4b Base shears

With the base shears and displacement at the effective height determined for each performance level, the system force-displacement graph is constructed and compared to the predicted values shown in Fig. 4.3.2-1.

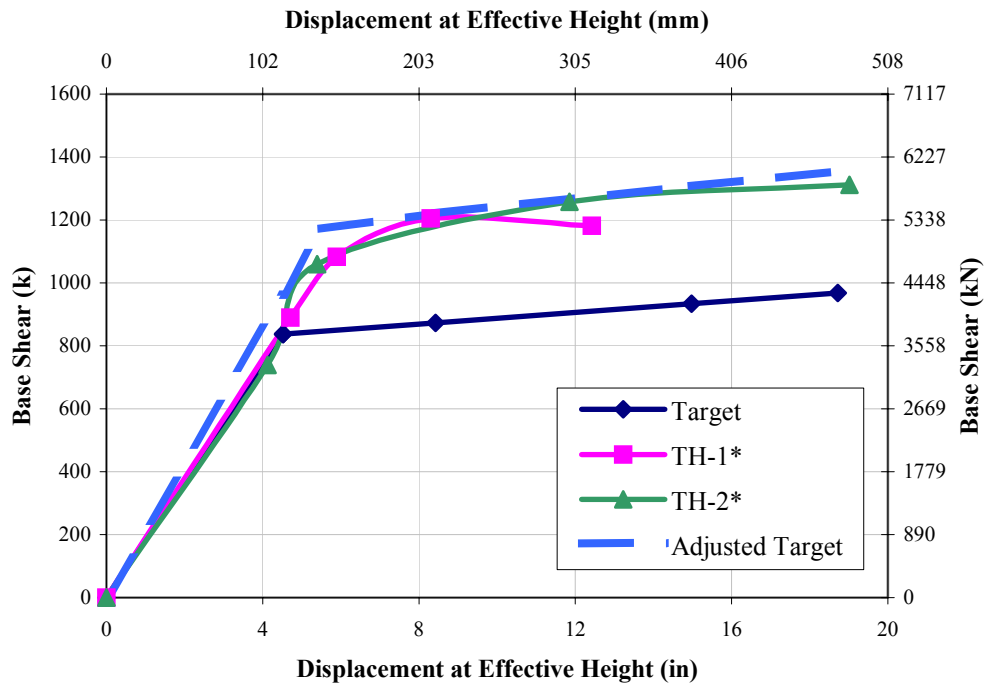


Figure 4.5.2-1. FR-4b System force-displacement graph

There is good comparison between the actual maximum envelopes and predicted values. The effects of performance overstrengths on post-yield base shear capacity and nodal displacements are clearly visible, as well as the need to incorporate them into the design of steel frames.

Additionally, a comparison between maximum story shears and design story shears can be performed in an effort to determine the accuracy of the performance overstrength factor.

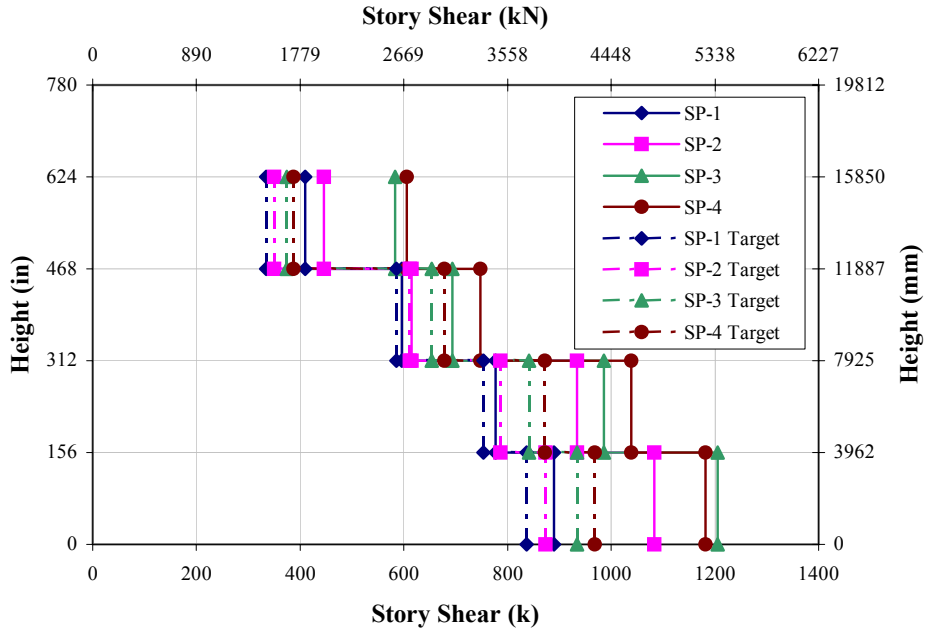


Figure 4.5.2-2. FR-4b Maximum story shears (TH-1)

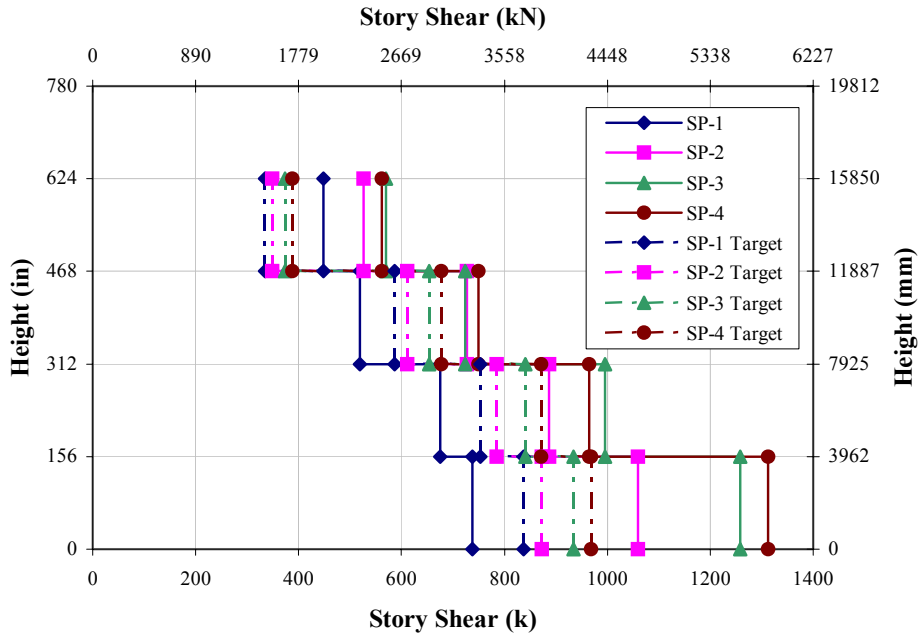


Figure 4.5.2-3. FR-4b Maximum story shears (TH-2)

4.6 Eight (8) Story Frame (FR-8)

4.6.1 Displacement Profiles

Figs. 4.6.1-1 through 4.6.1-4 show the maximum absolute relative displacement envelopes for each time-history analysis representative at each design performance level.

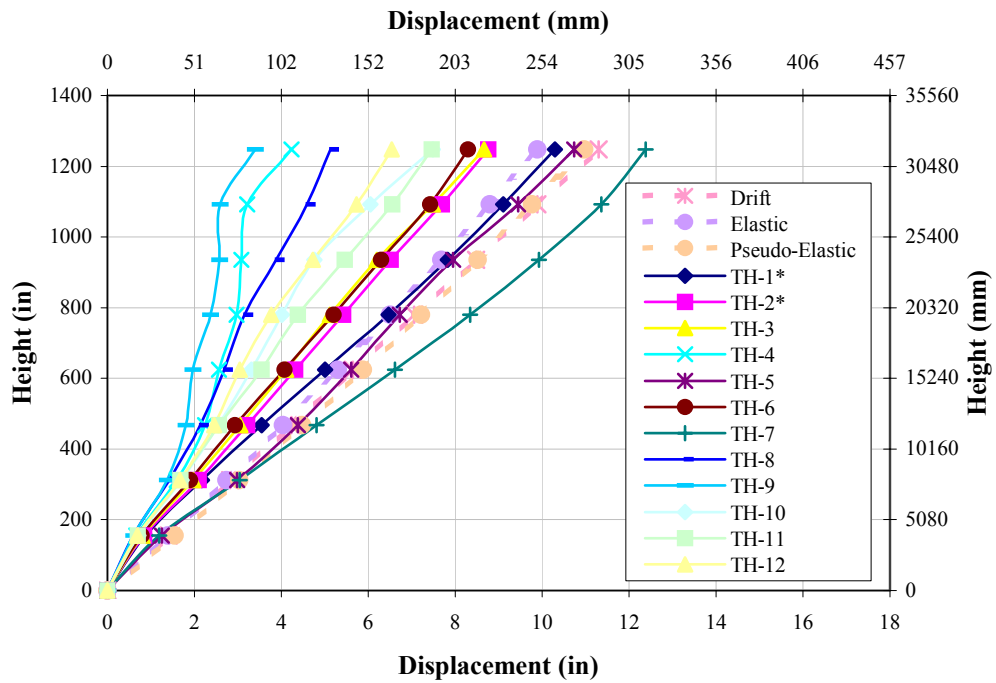


Figure 4.6.1-1. FR-8 Maximum displacement envelopes (SP-1:EQ 1)

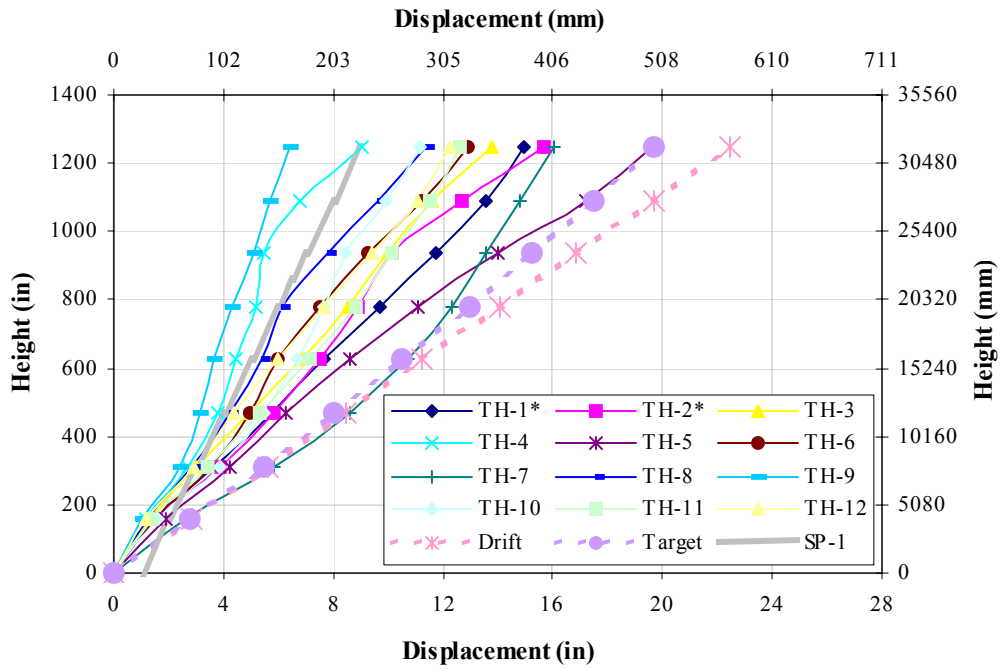


Figure 4.6.1-2. FR-8 Maximum displacement envelopes (SP-2:EQ II)

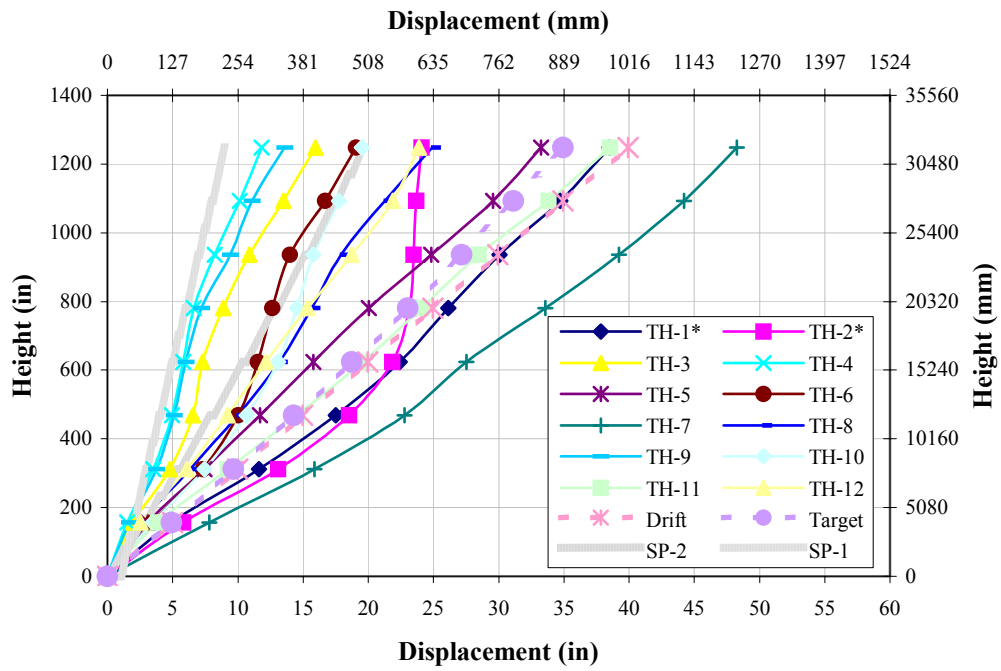


Figure 4.6.1-3. FR-8 Maximum displacement envelopes (SP-3:EQ III)

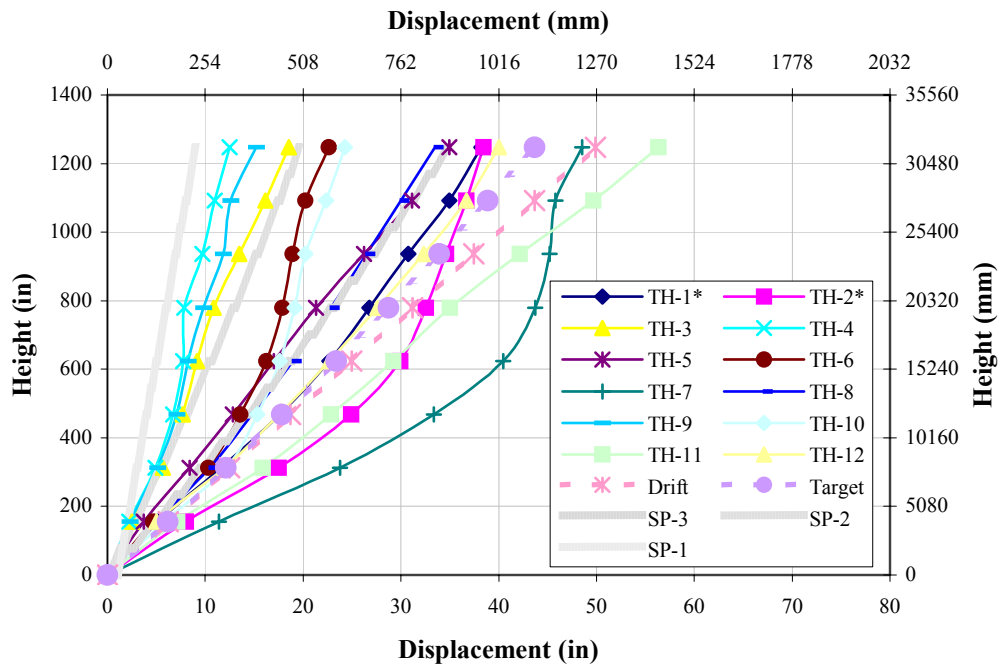


Figure 4.6.1-4. FR-8 Maximum displacement envelopes (SP-4:EQ IV)

TH	SP-1 : EQ I (in / mm)		SP-2 : EQ II (in / mm)		SP-3 : EQ III (in / mm)		SP-4 : EQ IV (in / mm)	
TH-1	7.3	185	10.9	277	28.5	723	29.2	741
TH-2	6.1	155	9.6	245	23.3	593	33.8	859
TH-3	5.8	146	9.4	239	10.1	256	12.4	315
TH-4	3.0	77	5.3	136	7.6	193	9.0	228
TH-5	7.5	190	12.8	326	22.9	582	24.3	617
TH-6	5.9	149	8.5	217	13.4	341	18.5	470
TH-7	9.3	236	13.1	332	37.0	939	44.6	1134
TH-8	3.6	91	7.1	182	17.0	432	25.0	636
TH-9	2.5	63	4.8	122	8.5	217	11.0	280
TH-10	4.5	113	8.1	207	15.3	388	19.8	502
TH-11	5.0	128	9.6	245	26.7	679	39.3	999
TH-12	4.3	110	8.7	221	17.4	441	30.4	773

Table 4.6.1-1. FR-8 Displacement at effective height

As can be seen, good comparison exists at the SP-1 level for the TH-1, 2, 5, 6, and 7. Additionally, deviations in displacement envelopes indicate the possibility of earthquake induced higher mode response for long period frames.

The previous graphs show the *actual* maximum nodal displacements of the system subjected to the respective earthquakes. However, the maximum nodal displacements do not necessarily occur at the same moment in time. Therefore, in the process of developing a design procedure to represent hinge sequencing, *actual* nodal displacements and interstory drifts as a function of time must be investigated, shown in Figs. 4.1.1-5 through 4.1.1-12. Due to the huge amount of data involved in this kind of analysis, only the artificial time-history (TH-1) will be discussed.

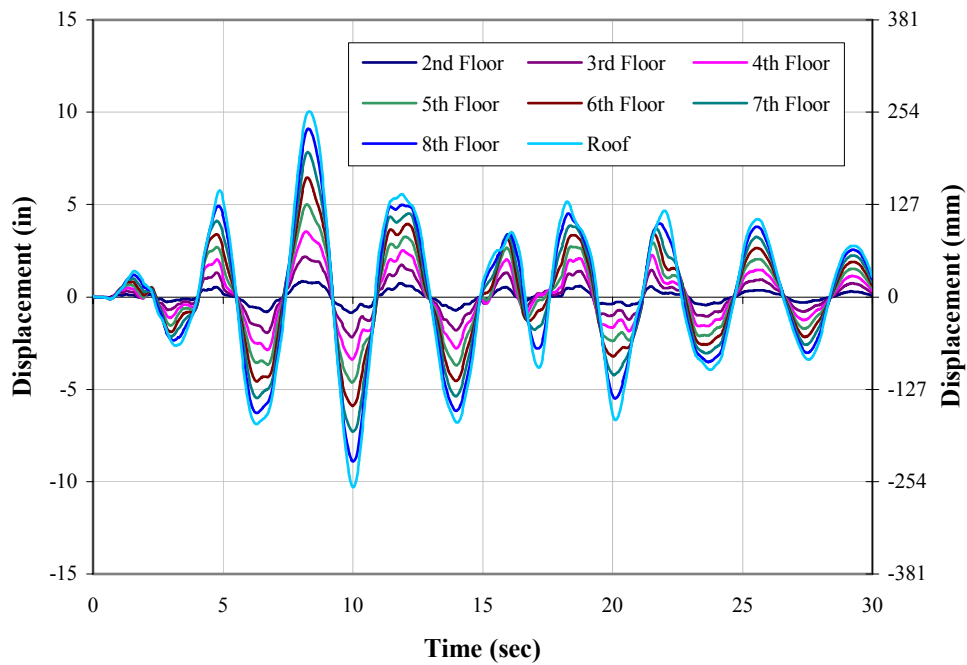


Figure 4.6.1-5. FR-8 Nodal displacements as function of time (TH-1:EQ 1)

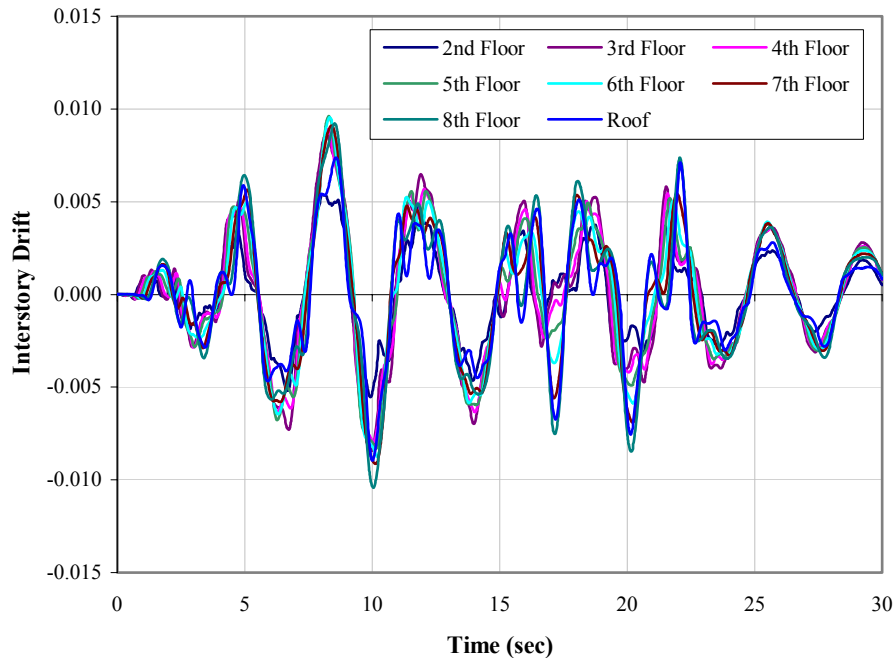


Figure 4.6.1-6. FR-8 Interstory drifts as function of time (TH-1:EQ I)

It clear that the frame response at the EQ I level is dominated by 1st mode behavior. This should be expected since floors have not in all likelihood developed yield mechanisms leading to hinge sequencing effects. Since the design displacement profile is non-linear, slight deviations in interstory drifts are expected. As can be seen in Fig. 4.6.1-6, discrepancies exist in adjacent interstory drifts at peak displacements regions. This is due to floor overstrengths and the result of no base hinges forming at this earthquake level, indicating possible hinge sequencing effects. It should be mentioned that no yield mechanism developed at this earthquake level. Also, the difficulty in examining EQ induced higher mode response in long period frames at low-level earthquakes is that confusions can arise from lagging. This occurs when a frame sways but upon reversal the upper floors, due to momentum, continue in the opposite direction of the lower floors.

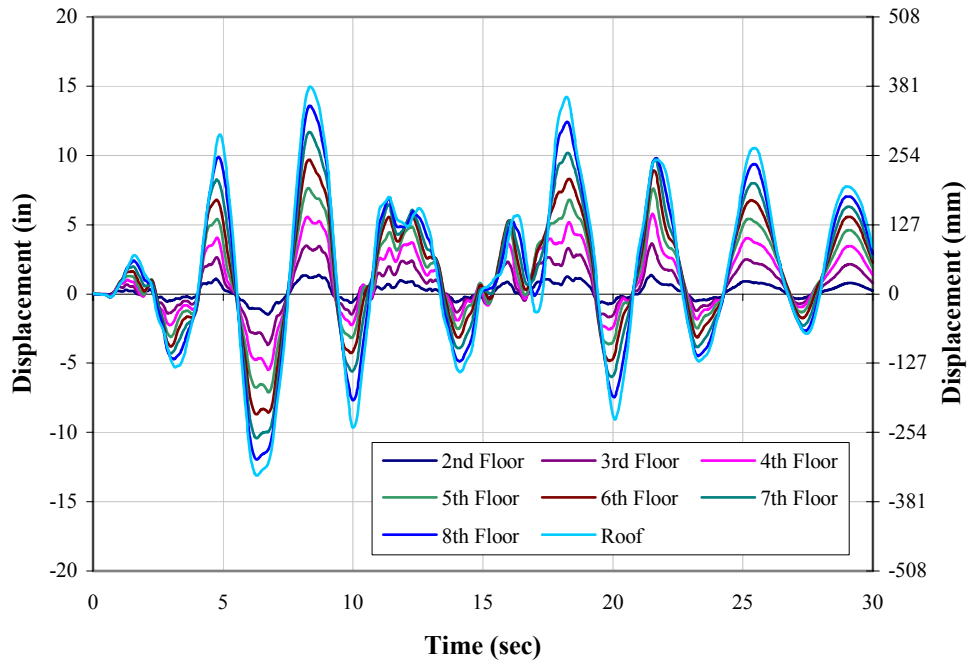


Figure 4.6.1-7. FR-8 Nodal displacements as function of time (TH-1:EQ II)

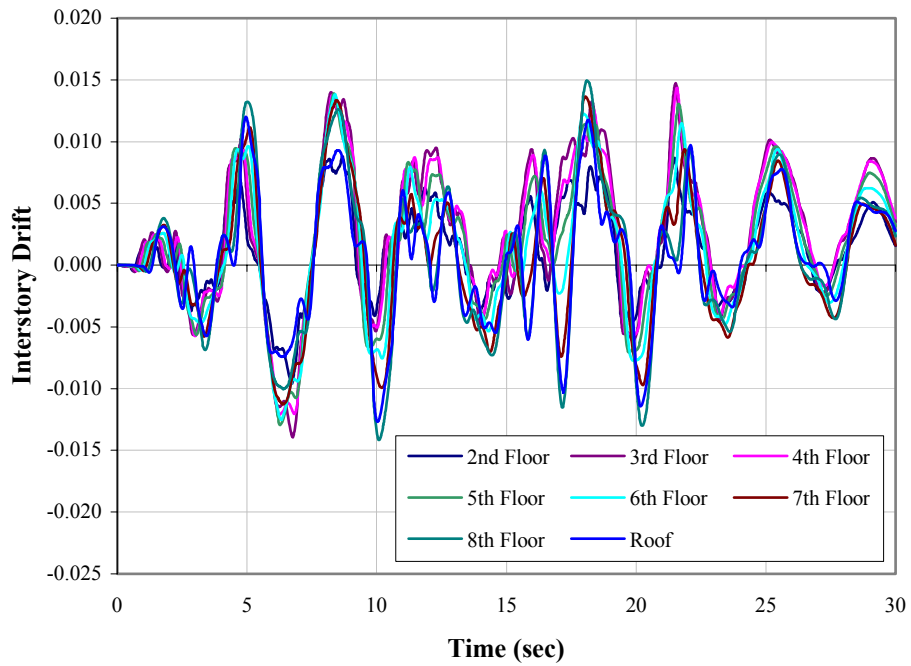


Figure 4.6.1-8. FR-8 Interstory drifts as function of time (TH-1:EQ II)

The same effects discussed at the EQ I level are additionally observed at the EQ II level. The drift discrepancies at 7 seconds are due to yield mechanisms forming in the 7th and 8th floor. Additionally, the global yield mechanism, additionally accompanied by hinge sequencing, forms at approximately 9 seconds. This is evident due to the variation in interstory drifts. It should be mentioned that higher mode effects are still not apparent, as the system response still seems to be dominated by the 1st mode, except for localized lagging responses.

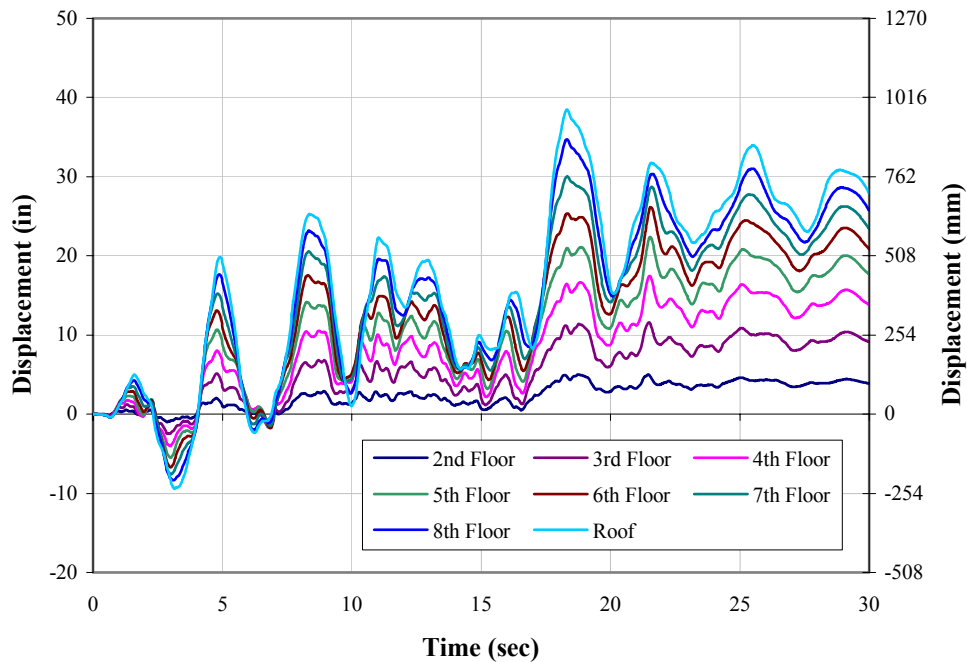


Figure 4.6.1-9. FR-8 Nodal displacements as function of time (TH-1:EQ III)

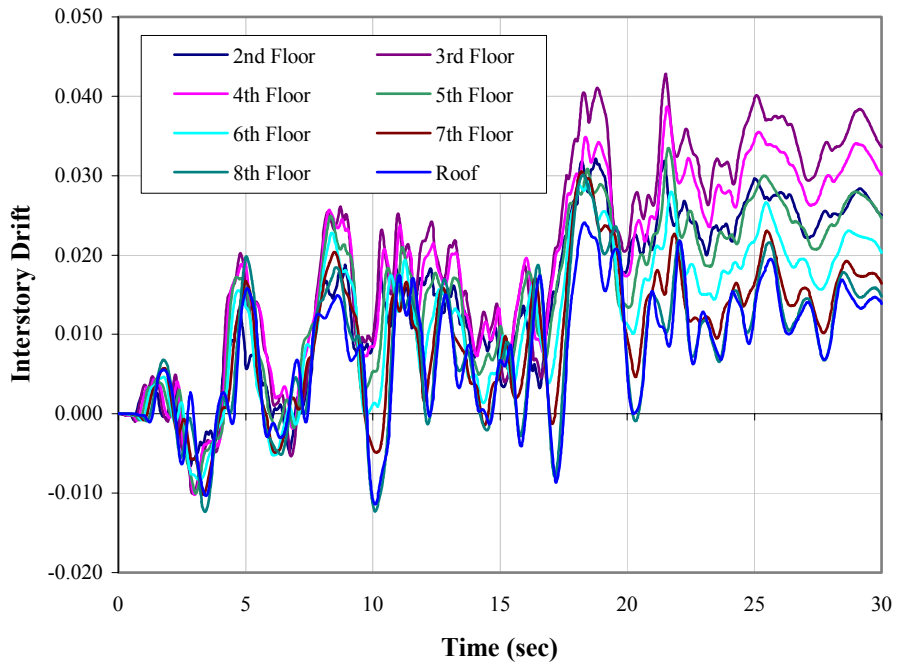


Figure 4.6.1-10. FR-8 Interstory drifts as function of time (TH-1:EQ III)

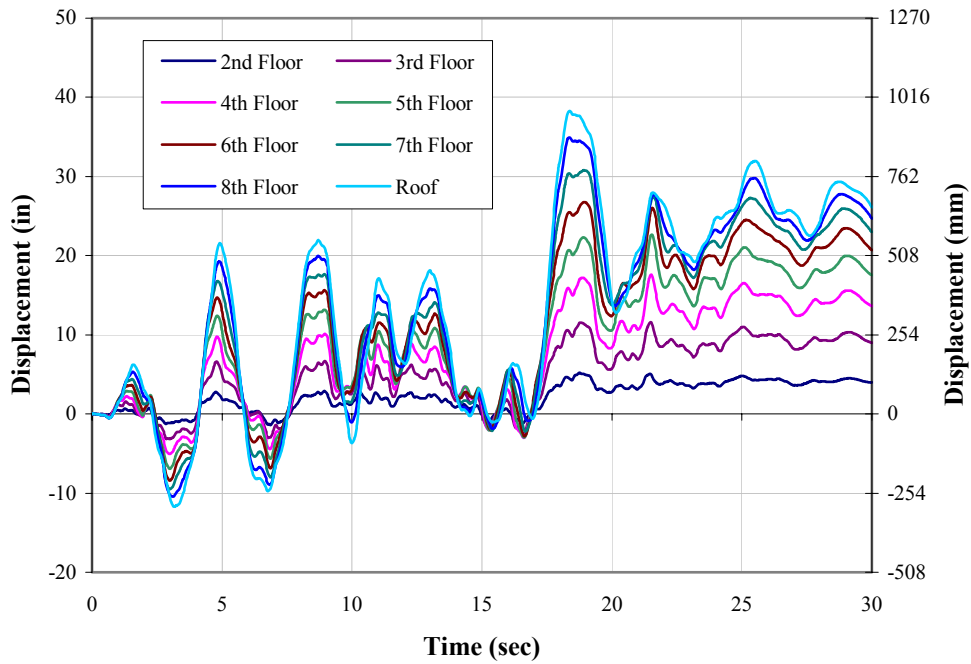


Figure 4.6.1-11. FR-8 Nodal displacements as function of time (TH-1:EQ IV)

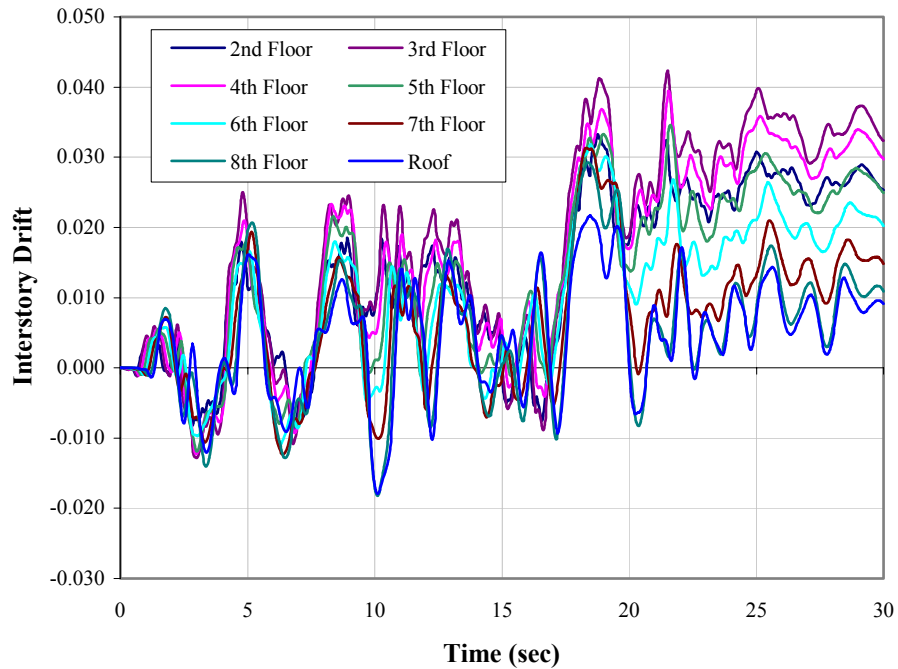


Figure 4.6.1-12. FR-8 Interstory drifts as function of time (TH-1:EQ IV)

Similarly, the same response is seen at the EQ III and EQ IV level except that the global yield mechanism forms earlier and leads to residual displacements. Hinge sequencing accompanied with slight higher mode response is clearly indicated in the respective graphs. However, this effect is mostly due to hinge sequencing from system characteristics more than earthquake intensity.

By investigating nodal displacements as a function of time, the maximum interstory drifts can be evaluated as seen in Figs. 4.6.1-13 through 4.6.1-16. Again, these do not necessarily occur at the same moment in time as the maximum displacements.

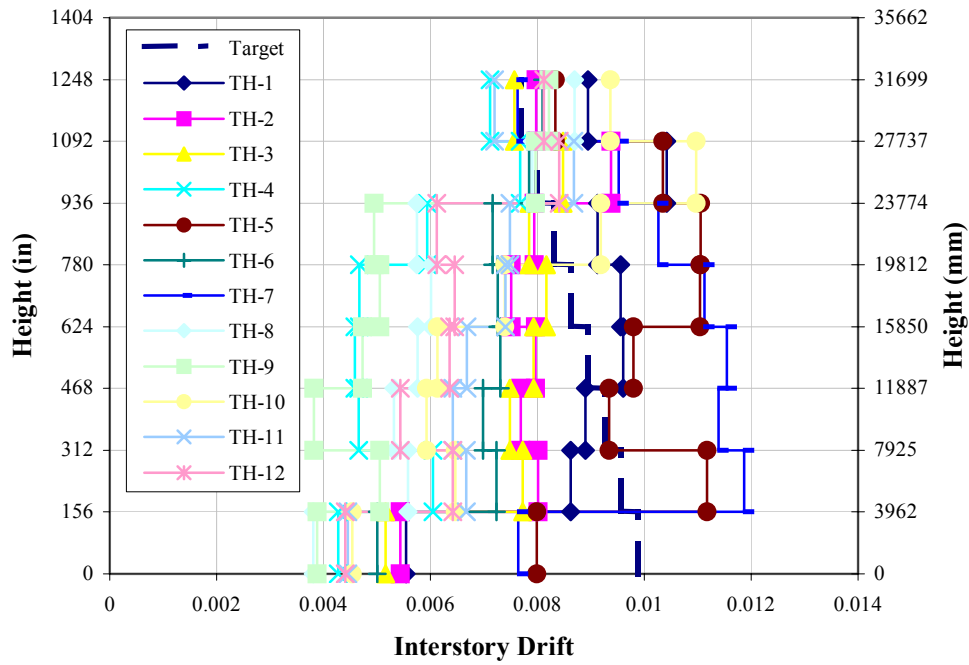


Figure 4.6.1-13. FR-8 Maximum interstory drift envelope (SP-1:EQ I)

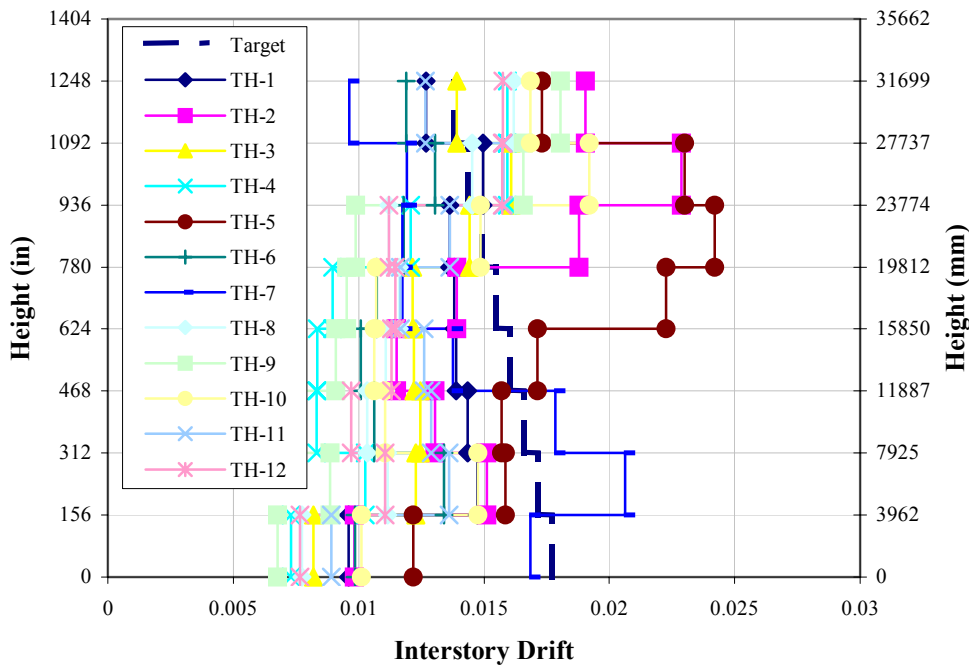


Figure 4.6.1-14. FR-8 Maximum interstory drift envelope (SP-2:EQ II)

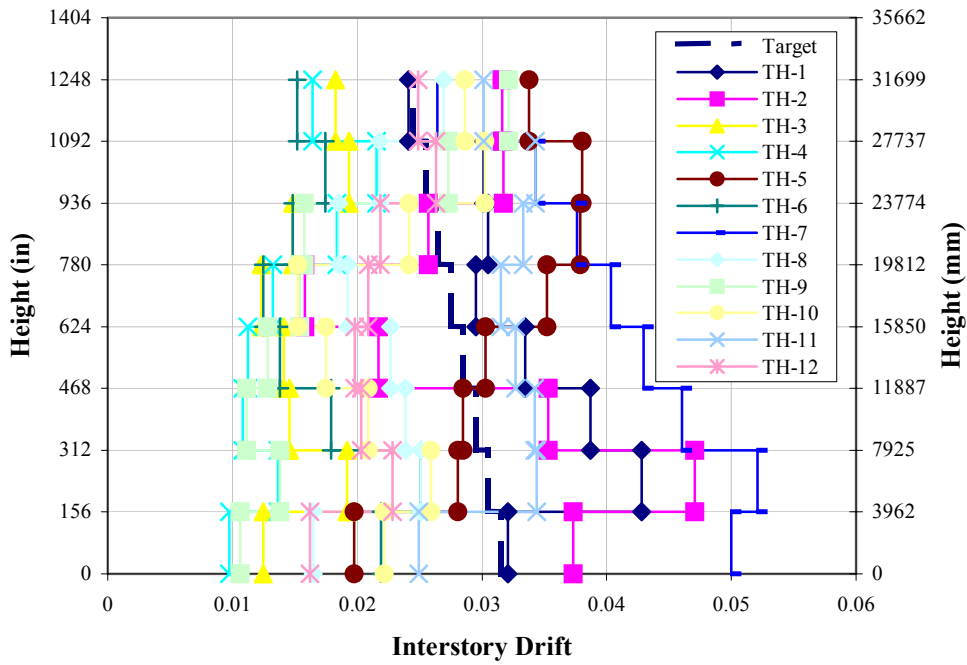


Figure 4.6.1-15. FR-8 Maximum interstory drift envelope (SP-3:EQ III)

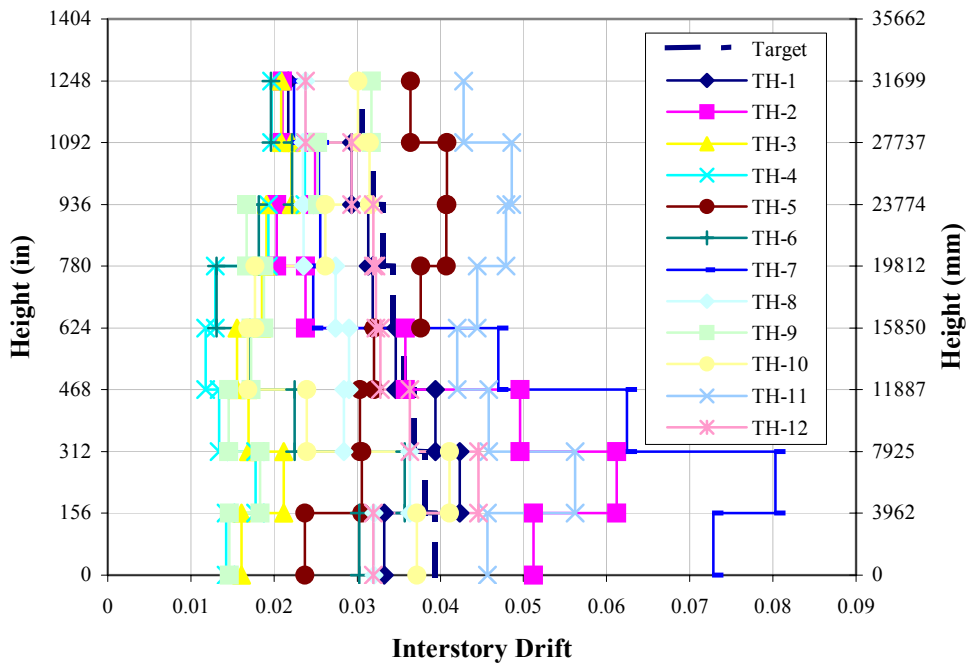


Figure 4.6.1-16. FR-8 Maximum interstory drift envelope (SP-4:EQ IV)

4.6.2 Base Shear

TH	SP-1 : EQ I (k / kN)		SP-2 : EQ II (k / kN)		SP-3 : EQ III (k / kN)		SP-4 : EQ IV (k / kN)	
TH-1	711	3165	1128	5017	1264	5623	1376	6121
TH-2	712	3166	1173	5217	1449	6443	1401	6230
TH-3	699	3110	1182	5256	1265	5626	1322	5882
TH-4	585	2604	1025	4559	1385	6159	1444	6422
TH-5	1047	4657	1248	5550	1365	6071	1333	5930
TH-6	692	3077	1289	5736	1302	5789	1350	6003
TH-7	989	4400	1228	5463	1306	5807	1608	7152
TH-8	527	2342	1053	4685	1383	6152	1456	6476
TH-9	545	2424	955	4248	1382	6145	1514	6734
TH-10	610	2715	1200	5336	1361	6052	1377	6126
TH-11	604	2687	1178	5240	1311	5830	1368	6087
TH-12	587	2609	1034	4597	1303	5795	1373	6107

Table 4.6.2-1. FR-8 Base shears

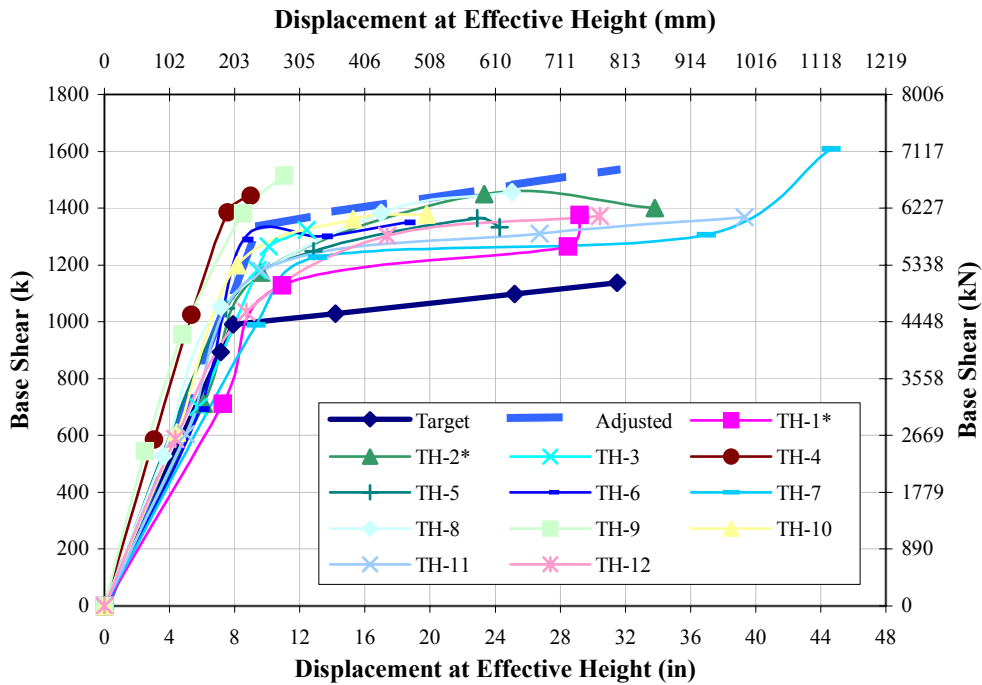


Figure 4.6.2-1. FR-8 System force-displacement graph

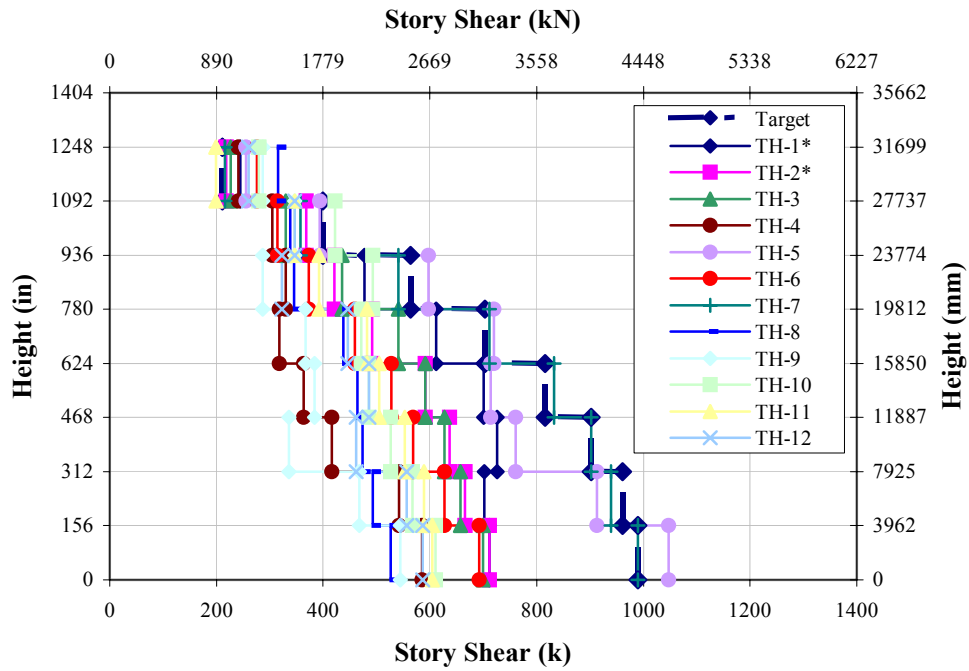


Figure 4.6.2-2. FR-8 Maximum story shear envelopes (SP-1:EQ I)

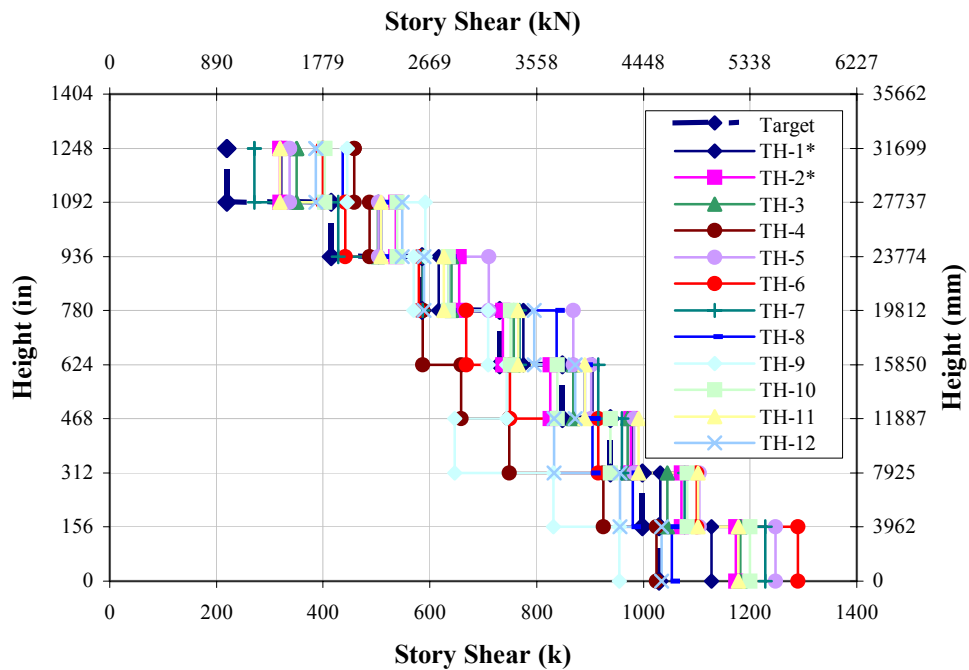


Figure 4.6.2-3. FR-8 Maximum story shear envelopes (SP-2:EQ II)

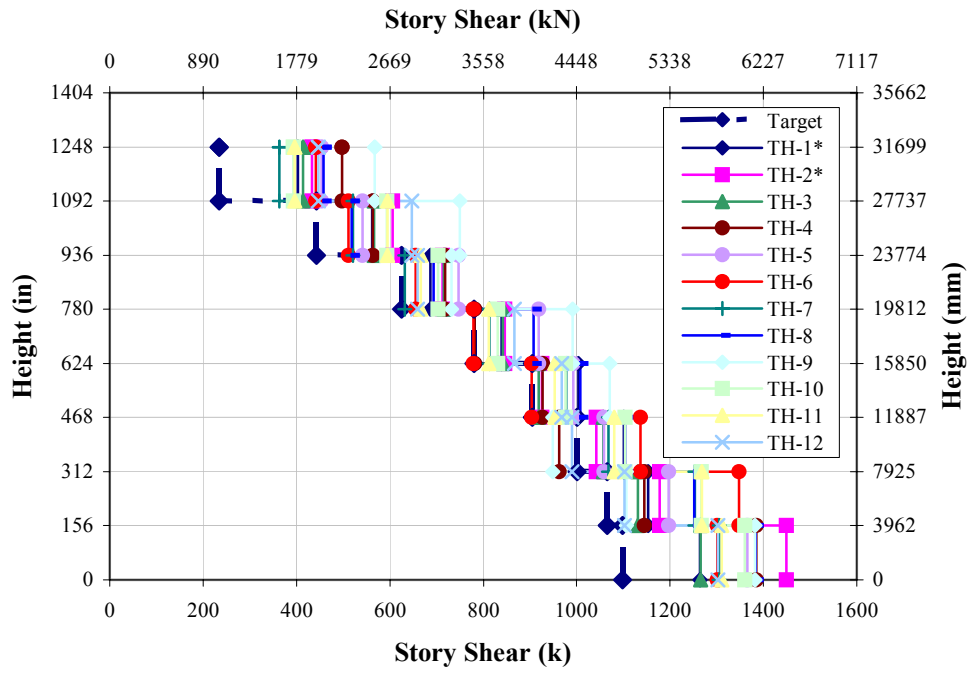


Figure 4.6.2-4. FR-8 Maximum story shear envelopes (SP-3:EQ III)

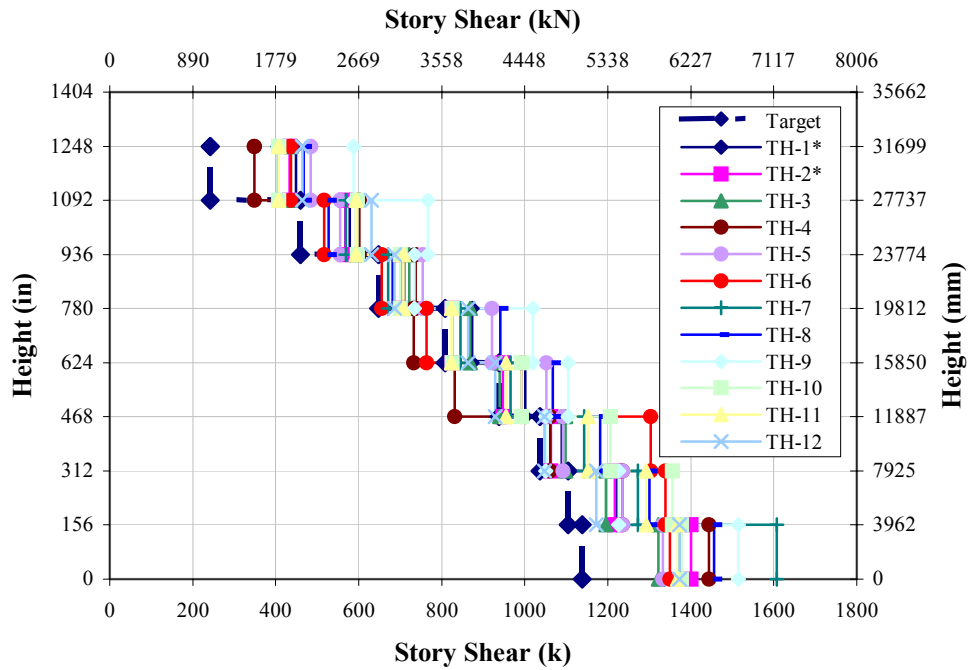


Figure 4.6.2-5. FR-8 Maximum story shear envelopes (SP-4:EQ IV)

4.7 Eight (8) Story Frame (FR-8-W27)

4.7.1 Displacement Profiles

Figs. 4.7.1-1 through 4.7.1-4 show the maximum absolute relative displacement envelopes for each time-history analysis representative at each design performance level.

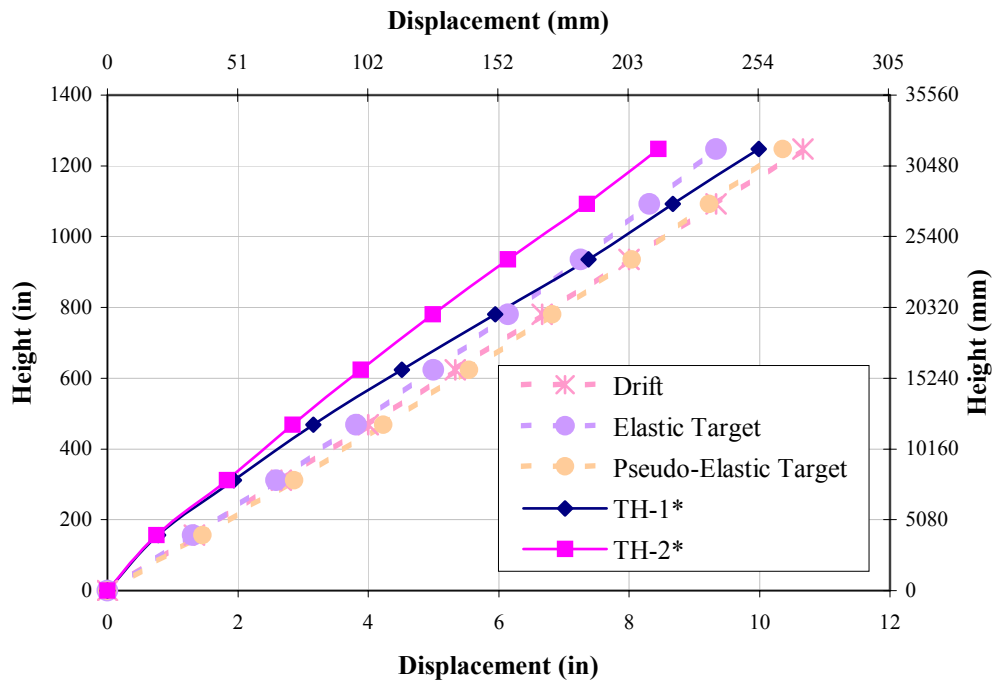


Figure 4.7.1-1. FR-8-W27 Maximum displacement envelopes (SP-1:EQ I)

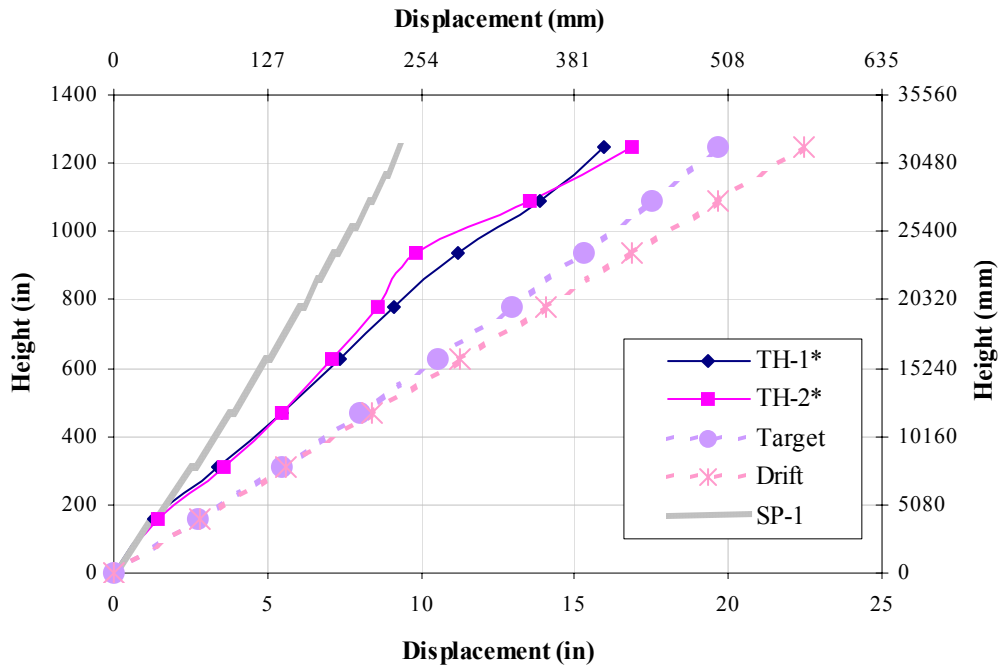


Figure 4.7.1-2. FR-8-W27 Maximum displacement envelopes (SP-2:EQ II)

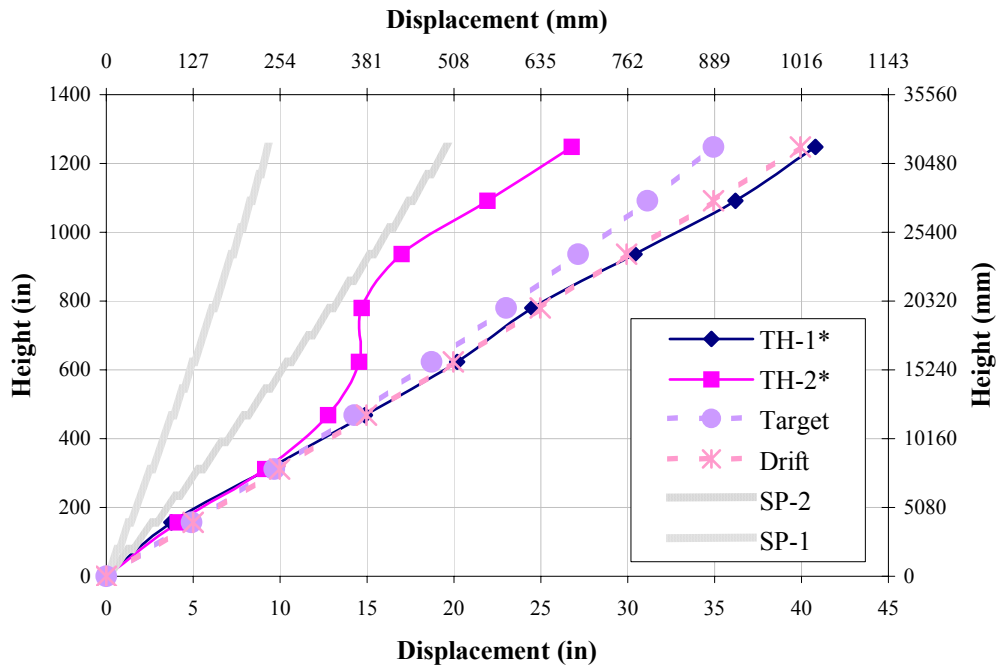


Figure 4.7.1-3. FR-8-W27 Maximum displacement envelopes (SP-3:EQ III)

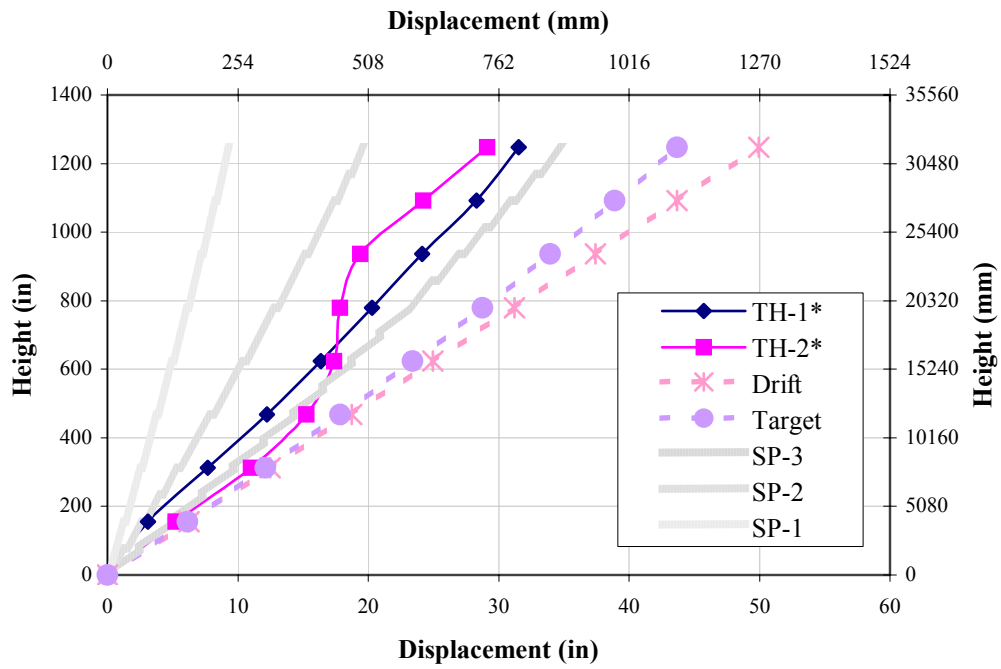


Figure 4.7.1-4. FR-8-W27 Maximum displacement envelopes (SP-4:EQ IV)

TH	SP-1 : EQ I (in / mm)		SP-2 : EQ II (in / mm)		SP-3 : EQ III (in / mm)		SP-4 : EQ IV (in / mm)	
	TH-1	6.8	173	10.4	264	28.0	712	22.6
TH-2	5.7	144	9.3	237	16.1	408	18.8	477

Table 4.7.1-1. FR-8-W27 Displacement at effective height

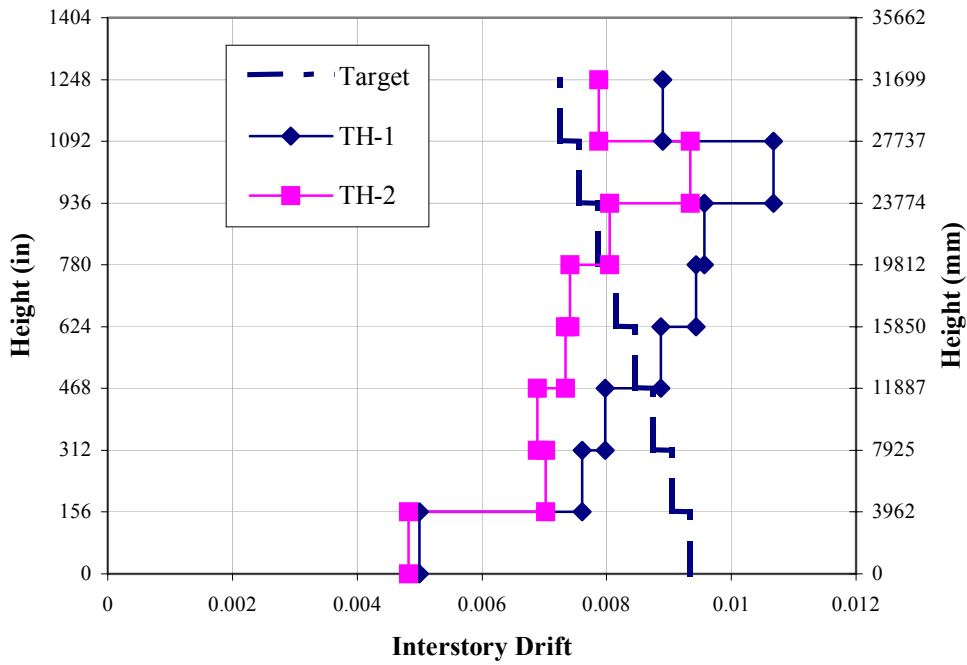


Figure 4.7.1-5. FR-8-W27 Maximum interstory drift envelope (SP-1:EQ I)

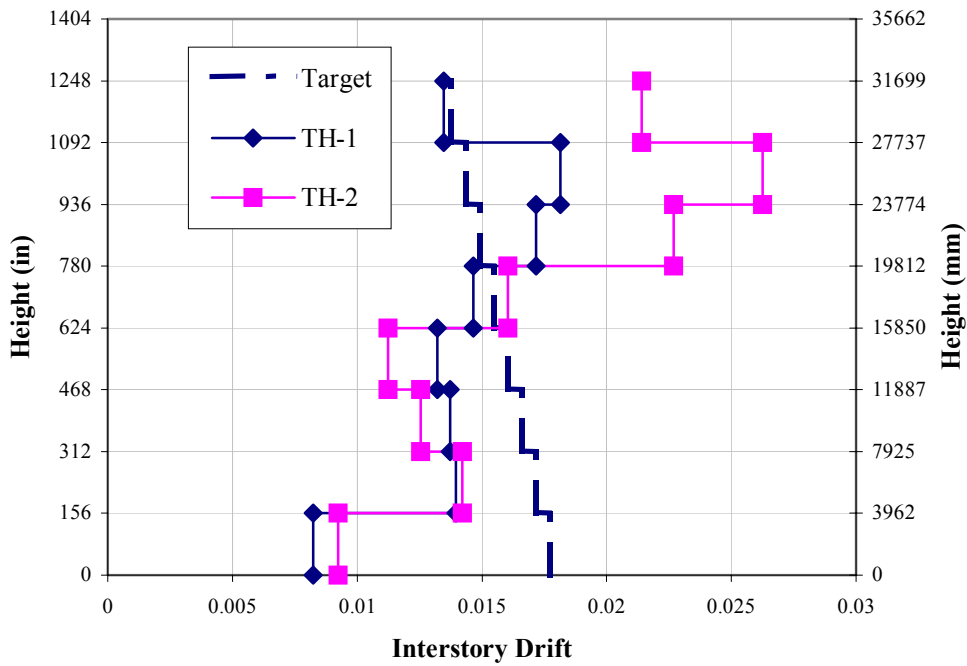


Figure 4.7.1-6. FR-8-W27 Maximum interstory drift envelope (SP-2:EQ II)

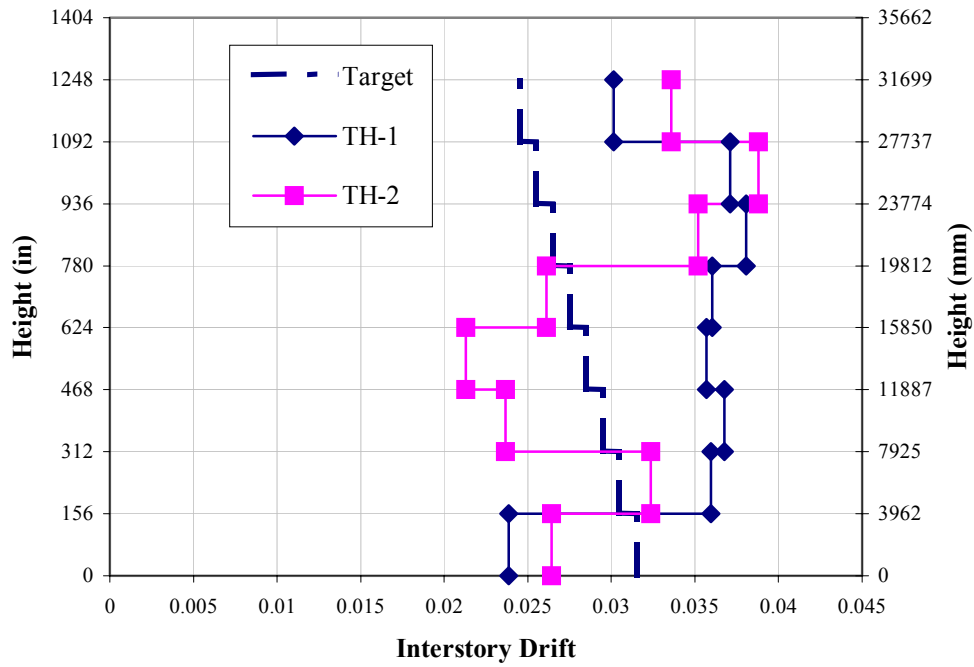


Figure 4.7.1-7. FR-8-W27 Maximum interstory drift envelope (SP-3:EQ III)

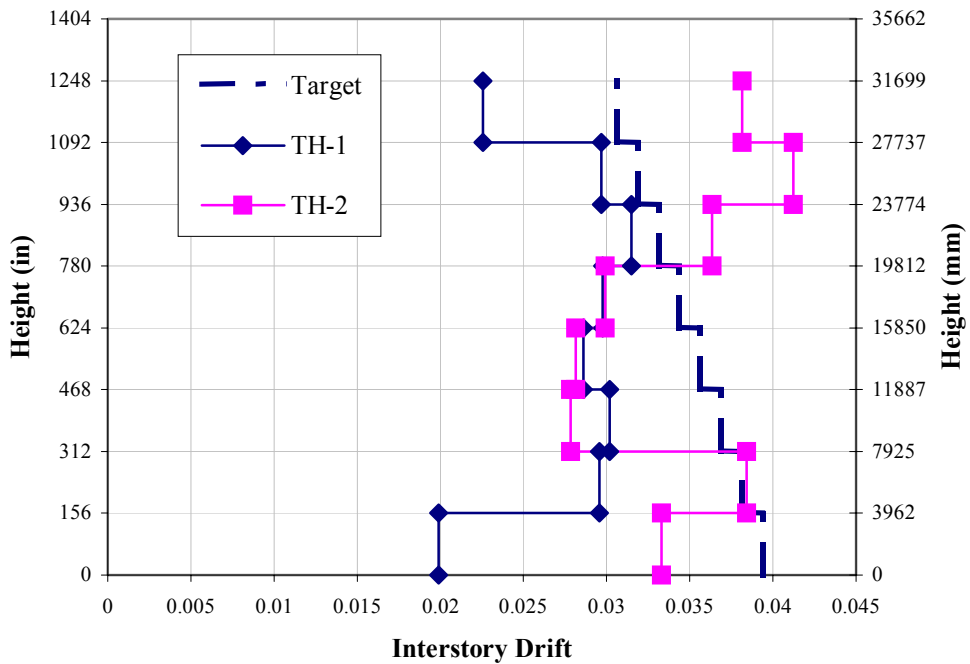


Figure 4.7.1-8. FR-8-W27 Maximum interstory drift envelope (SP-4:EQ IV)

4.7.2 Base Shear

TH	SP-1 : EQ I (k / kN)		SP-2 : EQ II (k / kN)		SP-3 : EQ III (k / kN)		SP-4 : EQ IV (k / kN)	
TH-1	686	3053	1122	4989	1333	5929	1438	6395
TH-2	679	3022	1187	5278	1351	6009	1502	6680

Table 4.7.2-1. FR-8-W27 Base shears

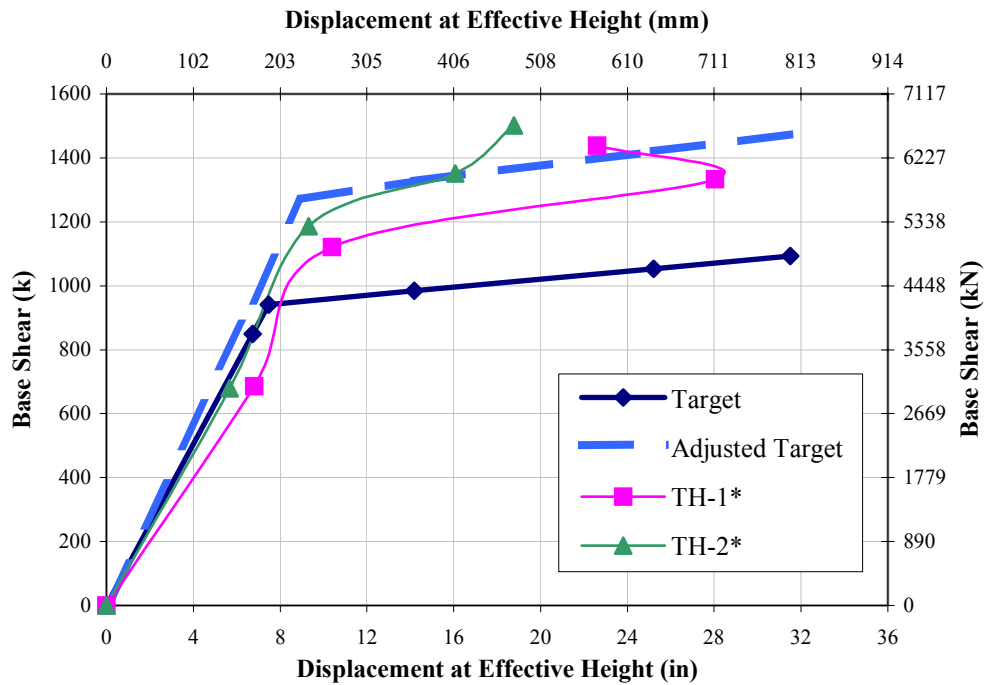


Figure 4.7.2-1. FR-8-W27 System force-displacement graph

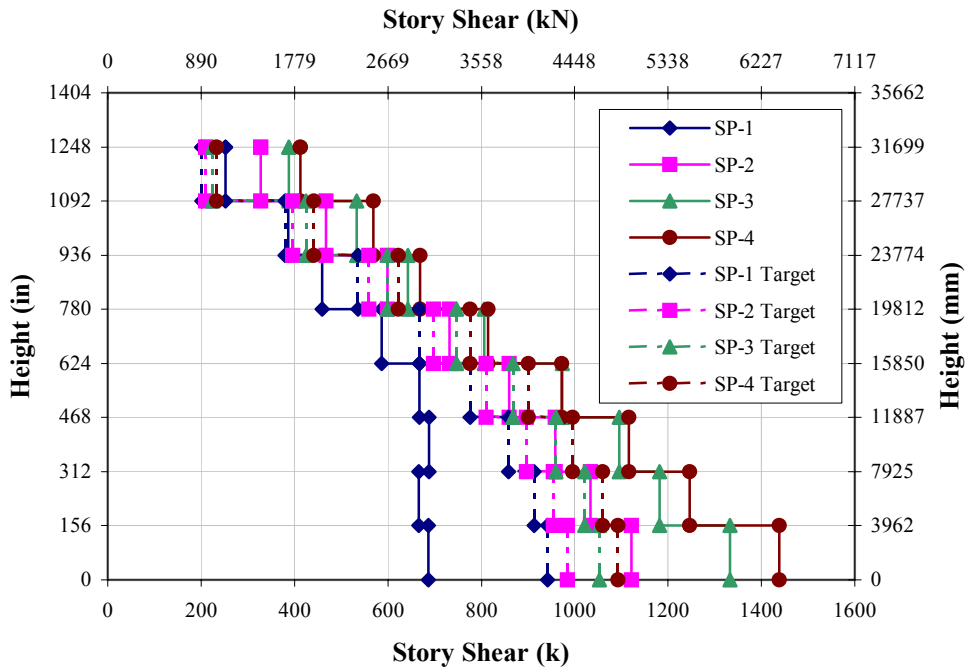


Figure 4.7.2-2. FR-8-W27 Maximum story shears (TH-1)

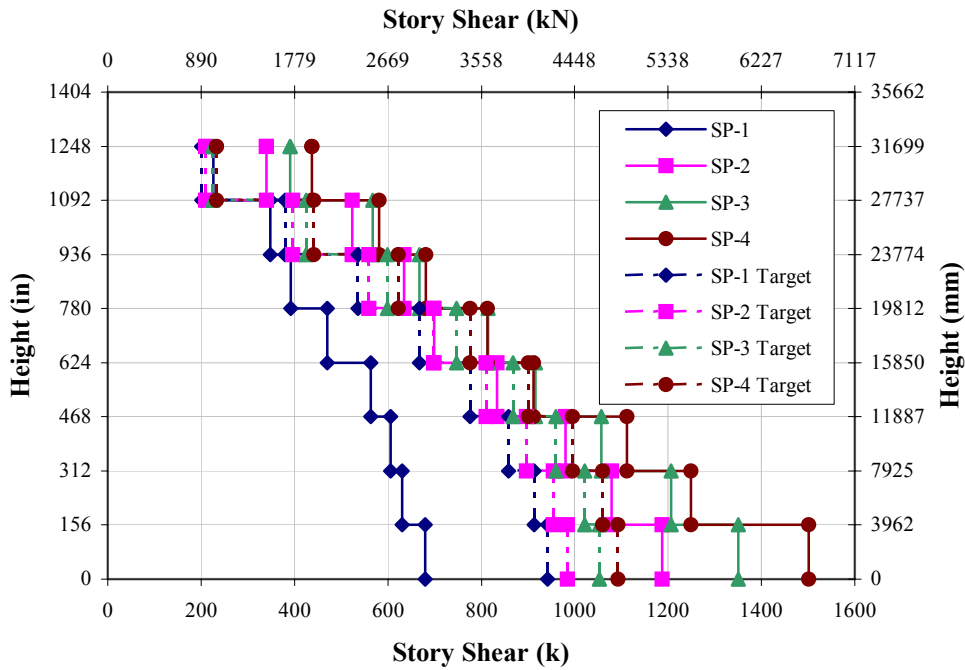


Figure 4.7.2-3. FR-8-W27 Maximum story shears (TH-2)

4.8 Sixteen (16) Story Frame (FR-16)

4.8.1 Displacement Profiles

Figs. 4.8.1-1 through 4.8.1-4 show the maximum absolute relative displacement envelopes for each time-history analysis representative at each design performance level.

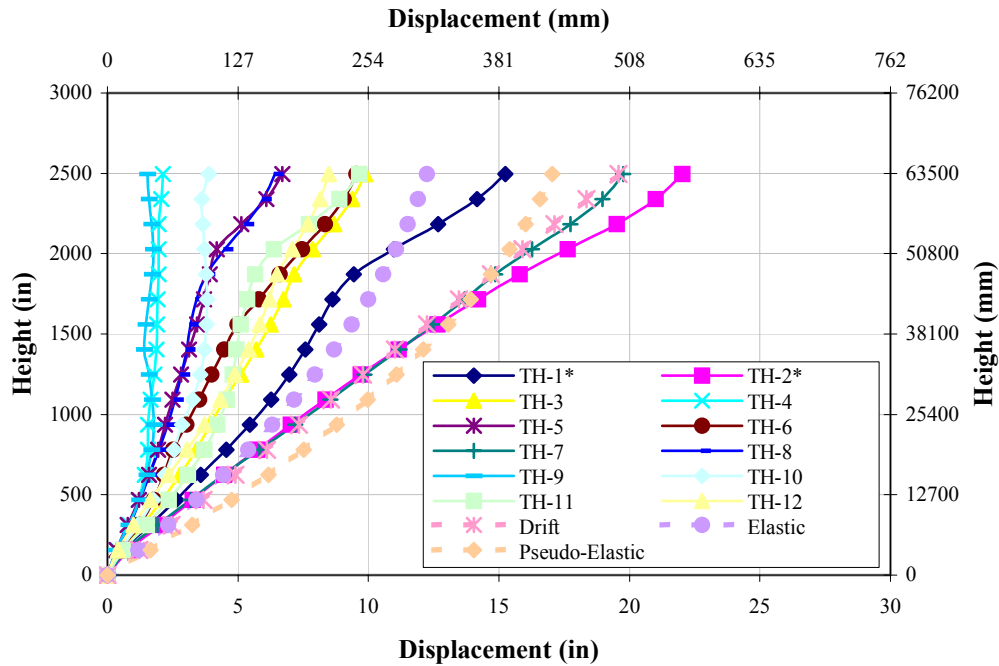


Figure 4.8.1-1. FR-16 Maximum displacement envelopes (SP-1:EQ I)

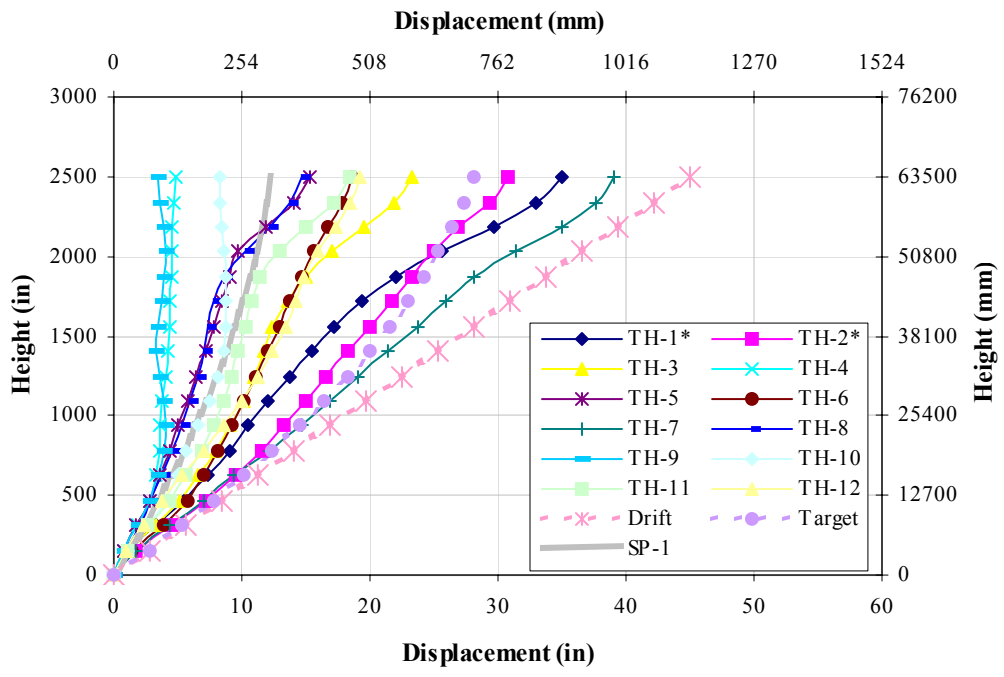


Figure 4.8.1-2. FR-16 Maximum displacement envelopes (SP-2:EQ II)

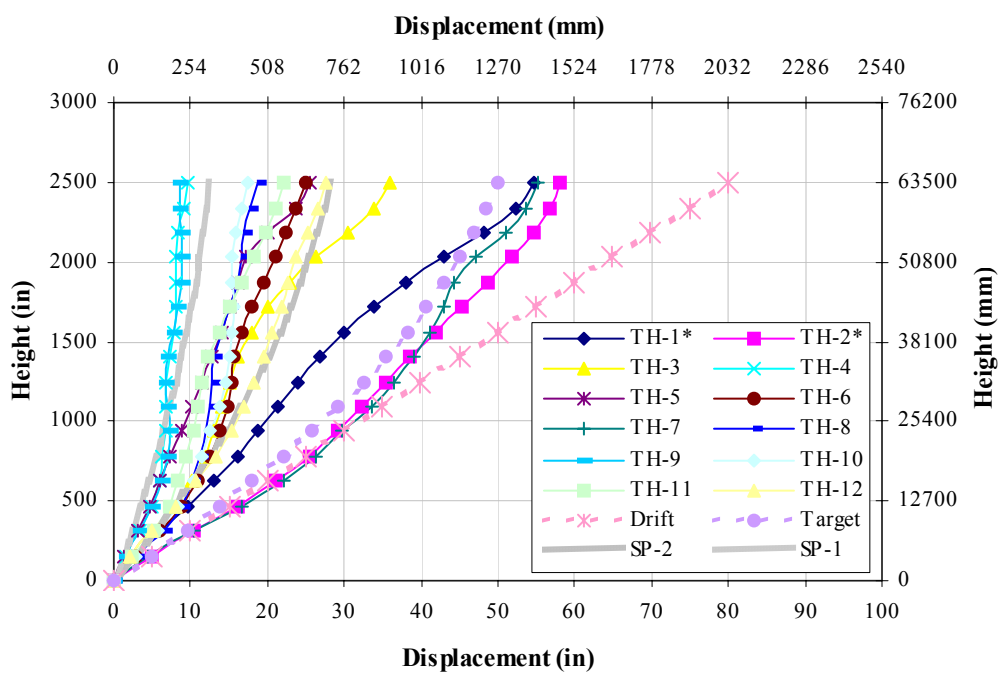


Figure 4.8.1-3. FR-16 Maximum displacement envelopes (SP-3:EQ III)

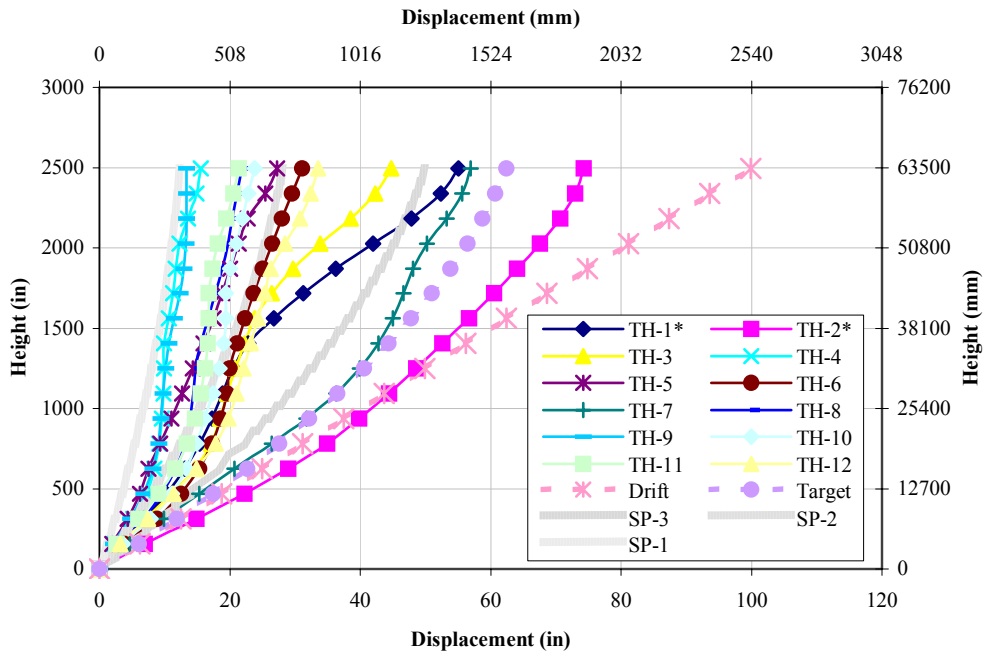


Figure 4.8.1-4. FR-16 Maximum displacement envelopes (SP-4:EQ IV)

TH	SP-1 : EQ I (in / mm)		SP-2 : EQ II (in / mm)		SP-3 : EQ III (in / mm)		SP-4 : EQ IV (in / mm)	
	in	mm	in	mm	in	mm	in	mm
TH-1	8.4	213	18.3	466	32.0	813	29.1	739
TH-2	13.5	342	20.9	531	43.7	1111	58.7	1491
TH-3	6.5	165	13.1	332	19.1	484	25.2	640
TH-4	1.9	49	4.4	111	7.9	200	11.0	279
TH-5	3.6	91	8.2	208	14.5	370	18.2	462
TH-6	5.4	138	13.4	340	17.4	441	23.0	585
TH-7	13.1	333	24.8	631	42.1	1069	45.9	1165
TH-8	3.3	84	7.5	192	14.6	371	17.2	438
TH-9	1.5	39	3.5	90	8.0	204	11.9	303
TH-10	3.8	97	8.7	222	15.5	394	19.4	492
TH-11	5.2	133	10.6	268	14.5	369	16.8	426
TH-12	6.0	153	13.8	351	21.3	540	24.9	632

Table 4.8.1-1. FR-16 Displacement at effective height

As can be seen, reasonable comparison exists at the SP-1 level for the TH-1, 2, and 7. It is clear that EQ induced higher mode response, accompanied with hinge sequencing, dominate displacements for long period frames at all performance levels.

Similarly, the *actual* interstory drifts as a function of time can also be determined. Figs. 4.8.1-5 through 4.8.1-12 show *actual* displacements and interstory drifts as a function of time. Due to the huge amounts of data involved in this kind of analysis, only the artificial time-histories (TH-1) will be discussed in detail.

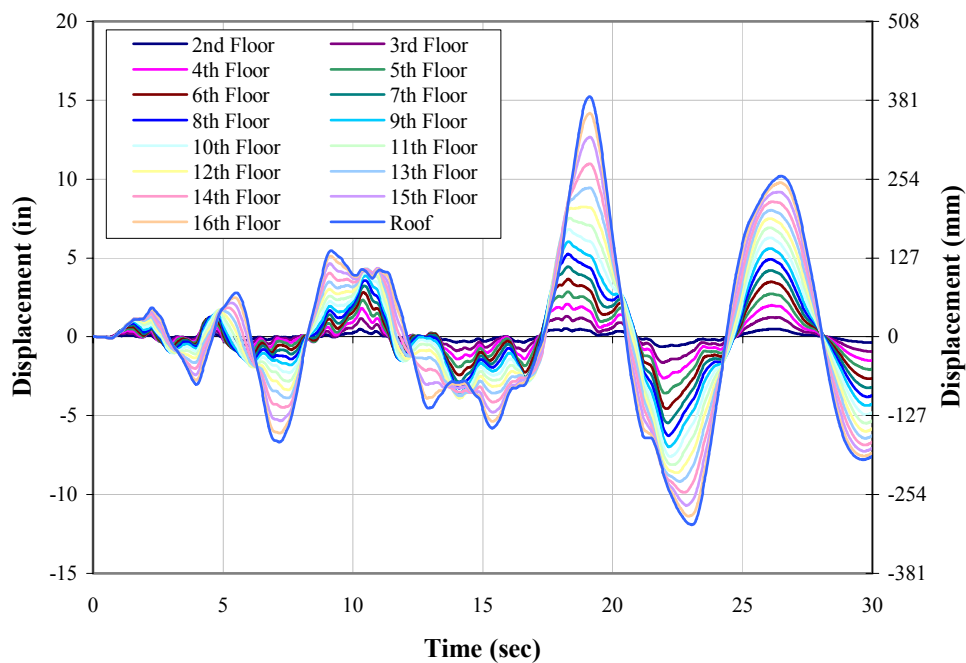


Figure 4.8.1-5. FR-16 Nodal displacements as function of time (TH-1:EQ 1)

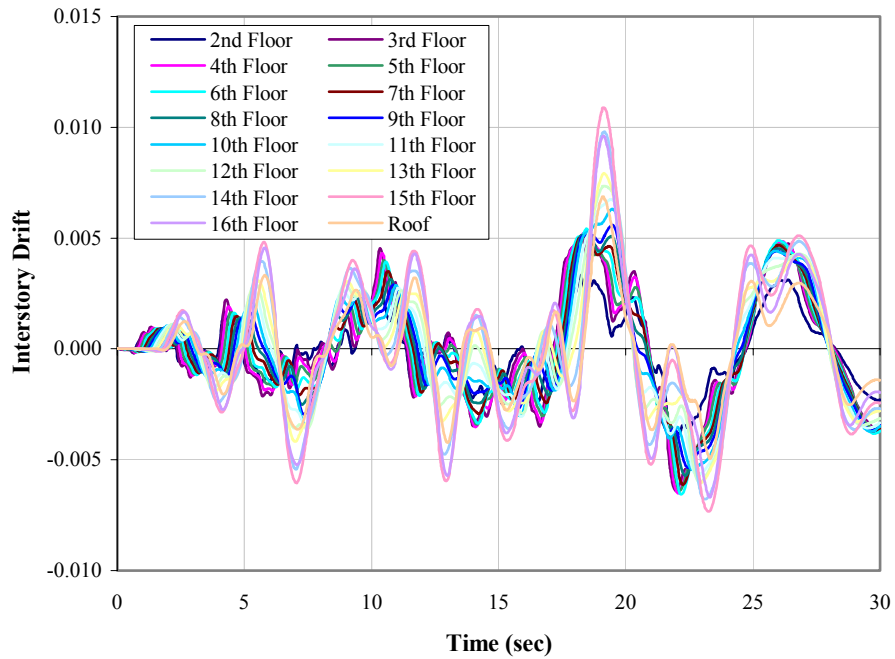


Figure 4.8.1-6. FR-16 Interstory drifts as function of time (TH-1:EQ I)

It clear that the frame response at the EQ I level is dominated by 1st mode behavior with lagging effects prominently exhibited. As can be seen in Fig. 4.8.1-6, discrepancies exist in adjacent interstory drifts at peak displacements regions in the upper floors due to floor overstrengths. It should be mentioned that no floor yield mechanism developed at this earthquake level.

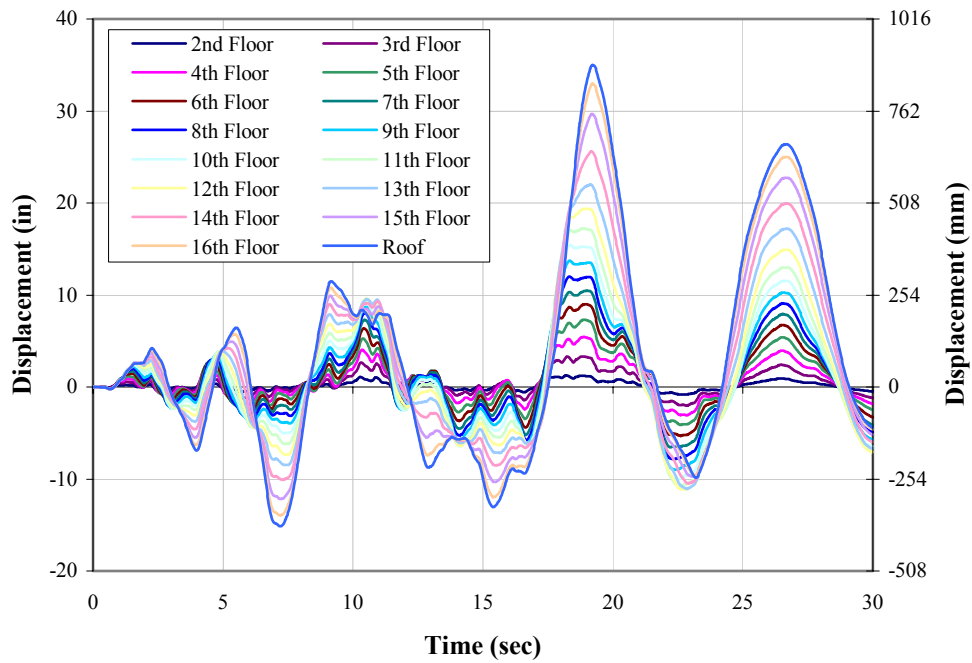


Figure 4.8.1-7. FR-16 Nodal displacements as function of time (TH-1:EQ II)

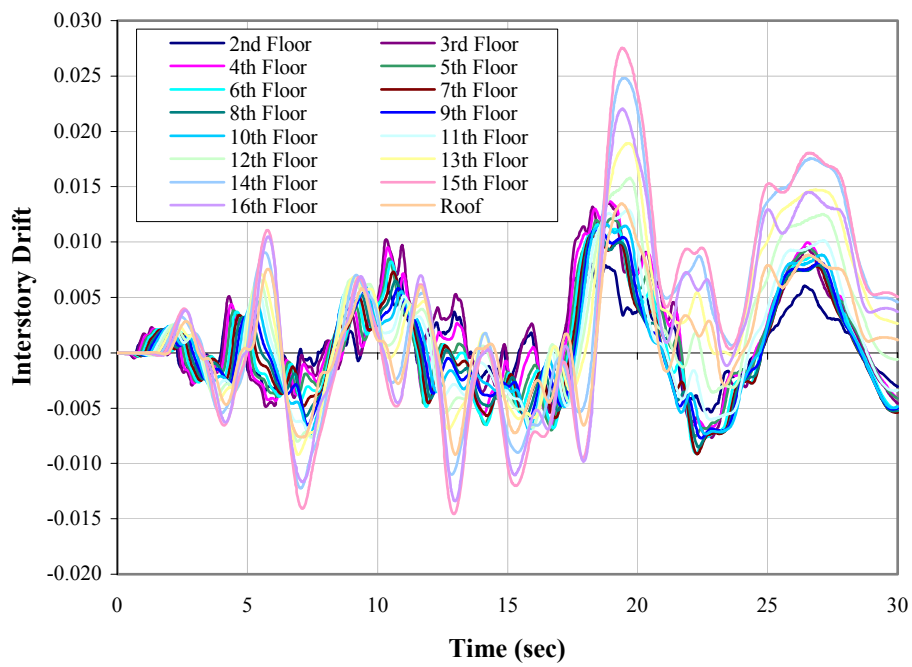


Figure 4.8.1-8. FR-16 Interstory drifts as function of time (TH-1:EQ II)

The same effects discussed at the EQ I level are additionally observed at the EQ II level. The obvious difference being the magnitude of interstory drifts due to the formation of floor yield mechanisms in the 14th and 15th floors, prominent lagging effects prior to 7 seconds, and higher mode response between 10 and 17 seconds. Additionally, as expected with long period structures, the global yield mechanism does not form simultaneously but in vertical traveling waves. This effect can be seen by the change in interstory drifts after 17 seconds.

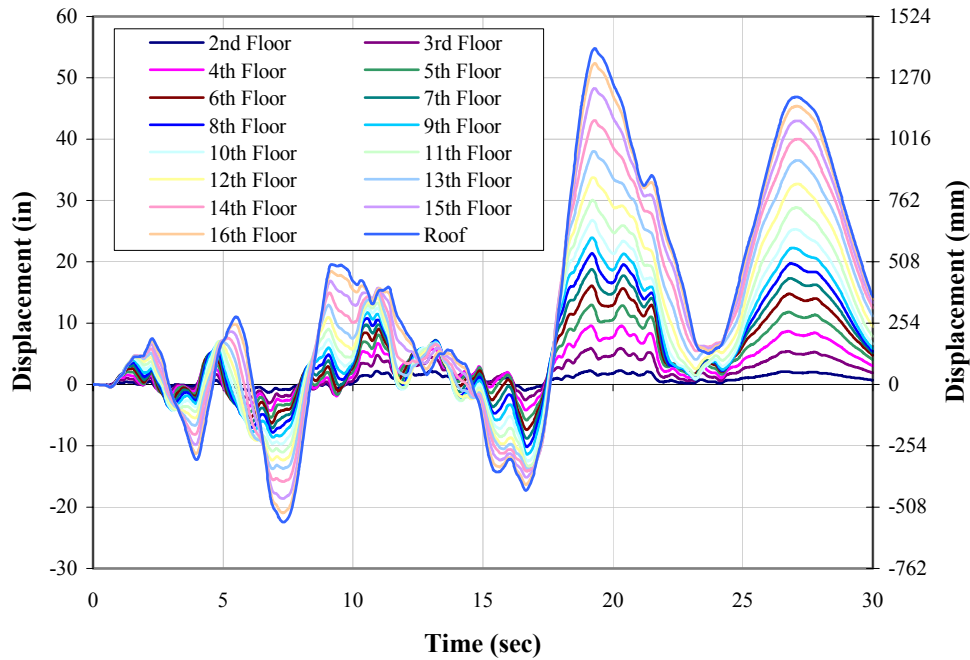


Figure 4.8.1-9. FR-16 Nodal displacements as function of time (TH-1:EQ III)

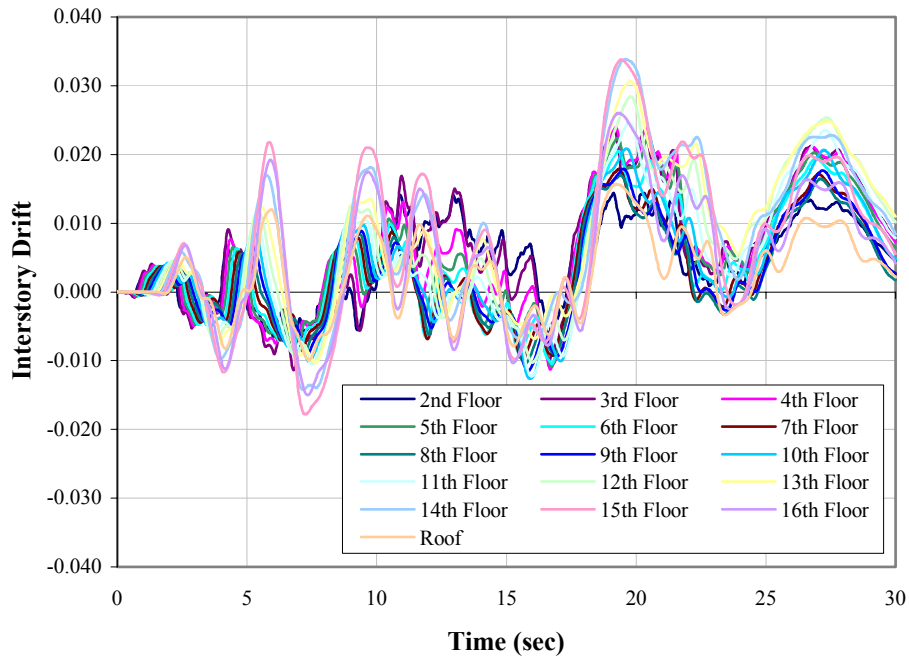


Figure 4.8.1-10. FR-16 Interstory drifts as function of time (TH-1:EQ III)

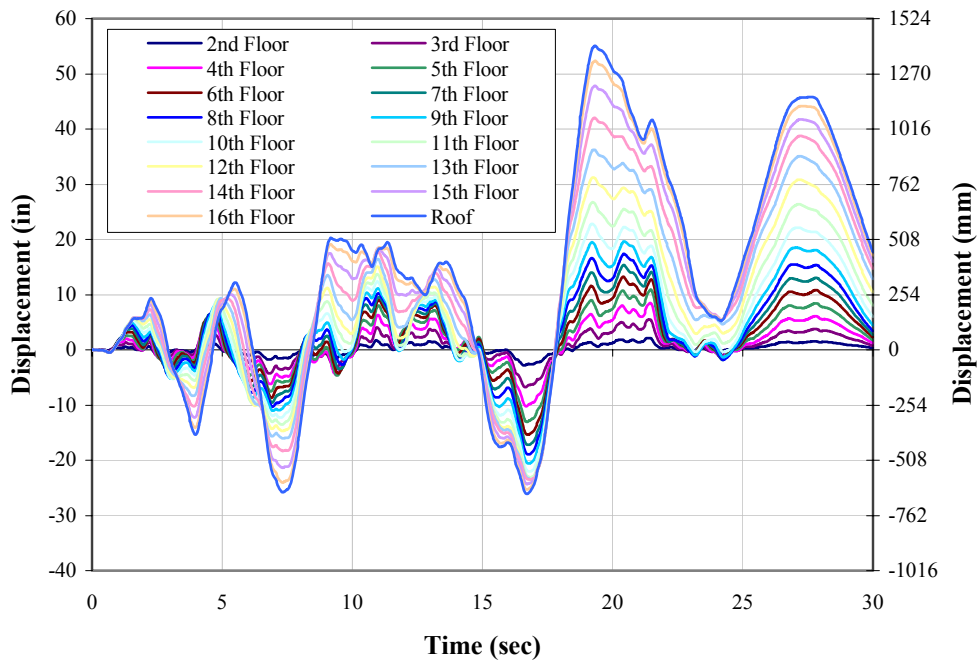


Figure 4.8.1-11. FR-16 Nodal displacements as function of time (TH-1:EQ IV)

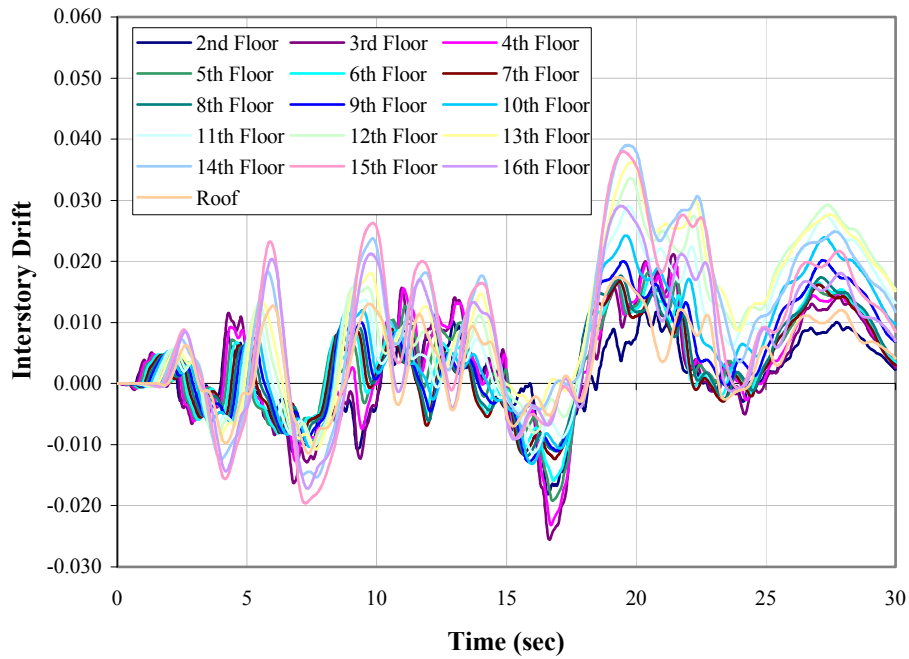


Figure 4.8.1-12. FR-16 Interstory drifts as function of time (TH-1:EQ IV)

Similarly, the same response is seen at the EQ III and EQ IV level except that the global yield mechanism forms about 19 seconds. Hinge sequencing accompanied with higher mode response is clearly indicated in the respective graphs.

By investigating nodal displacements as a function of time, the maximum interstory drifts can be evaluated as seen in Figs. 4.8.1-13 through 4.8.1-16. Again, these do not necessarily occur at the same moment in time as the maximum displacements.

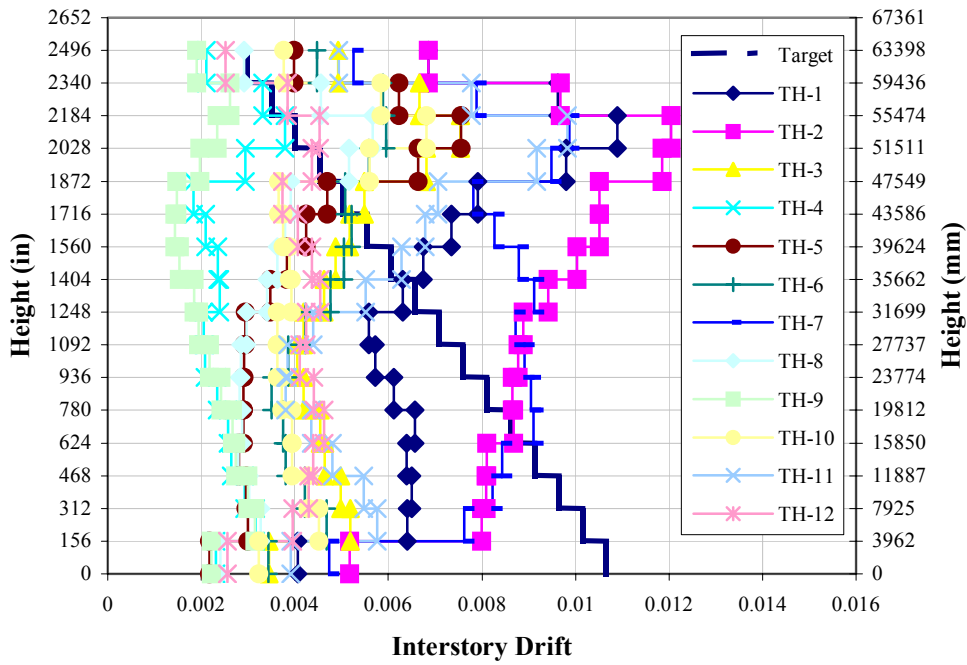


Figure 4.8.1-13. FR-16 Maximum interstory drift envelope (SP-1:EQ I)

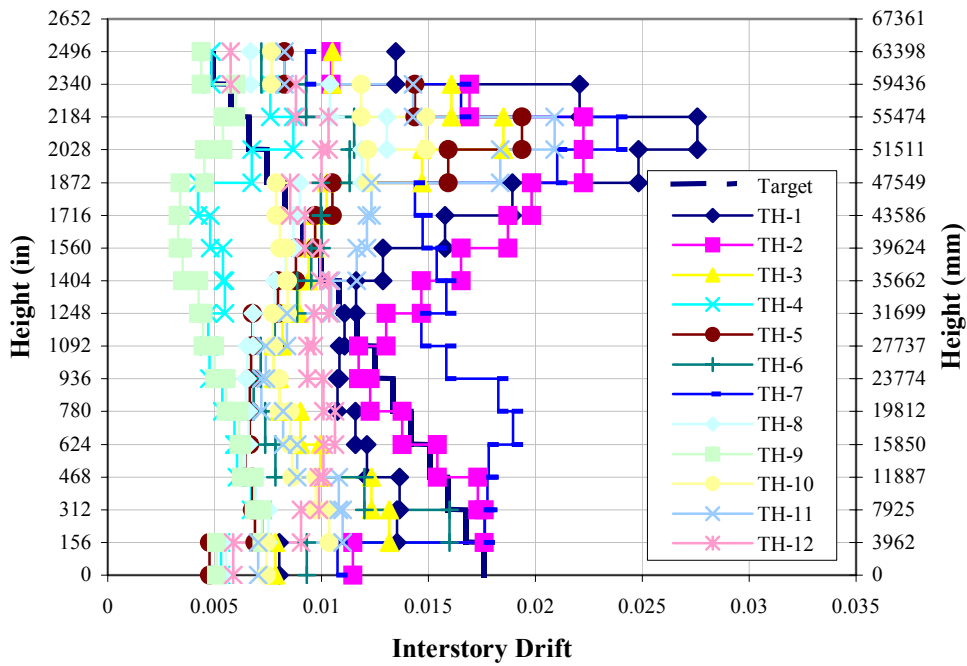


Figure 4.8.1-14. FR-16 Maximum interstory drift envelope (SP-2:EQ II)

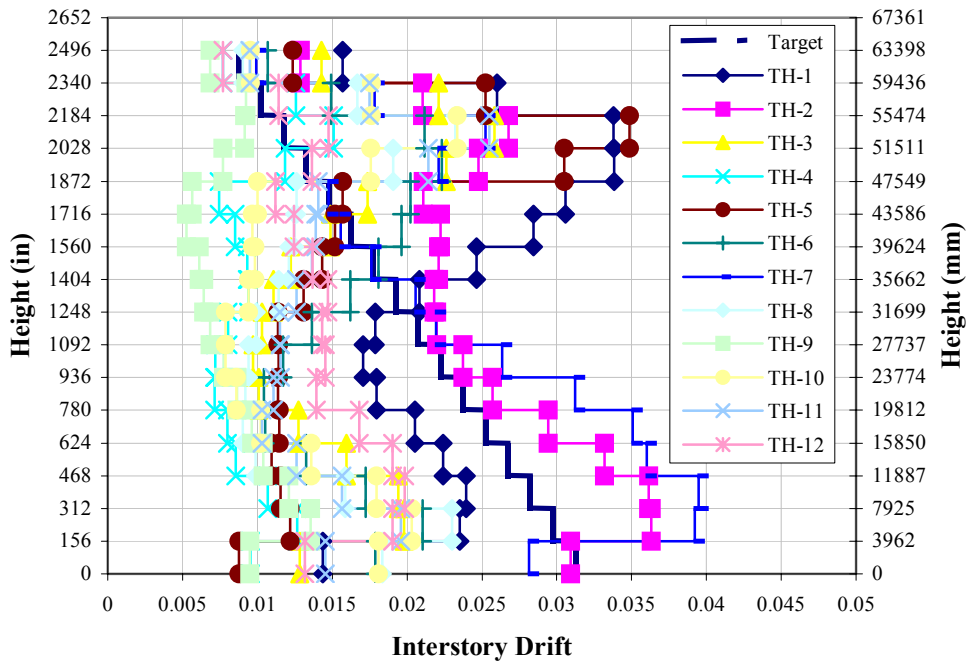


Figure 4.8.1-15. FR-16 Maximum interstory drift envelope (SP-3:EQ III)

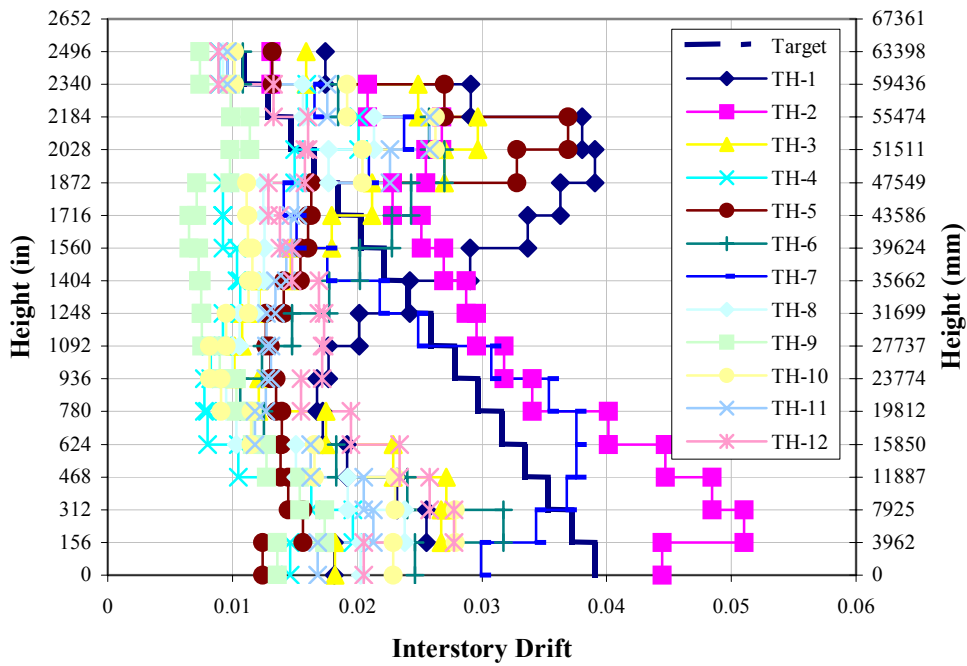


Figure 4.8.1-16. FR-16 Maximum interstory drift envelope (SP-4:EQ IV)

4.8.2 Base Shear

TH	SP-1 : EQ I (k / kN)		SP-2 : EQ II (k / kN)		SP-3 : EQ III (k / kN)		SP-4 : EQ IV (k / kN)	
TH-1	681	3028	1260	5603	1567	6972	1555	6916
TH-2	867	3855	1370	6092	1448	6440	1570	6982
TH-3	591	2628	1206	5366	1509	6712	1549	6891
TH-4	372	1656	853	3796	1419	6310	1653	7354
TH-5	346	1539	753	3350	1277	5679	1308	5816
TH-6	628	2794	1415	6296	1610	7161	1624	7225
TH-7	676	3006	1094	4866	1213	5394	1228	5462
TH-8	391	1738	896	3985	1410	6271	1450	6452
TH-9	346	1539	793	3529	1343	5973	1524	6781
TH-10	508	2261	1166	5185	1421	6322	1472	6549
TH-11	583	2594	1074	4778	1382	6148	1374	6113
TH-12	390	1734	894	3975	1285	5714	1376	6119

Table 4.8.2-1. FR-16 Base shears

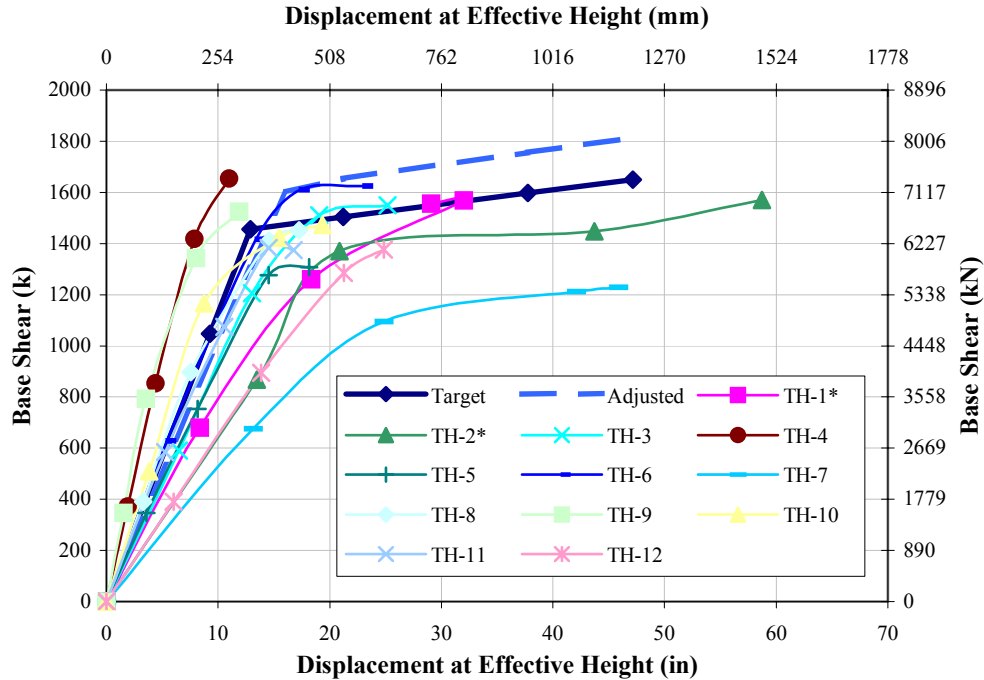


Figure 4.8.2-1. FR-16 System force-displacement graph

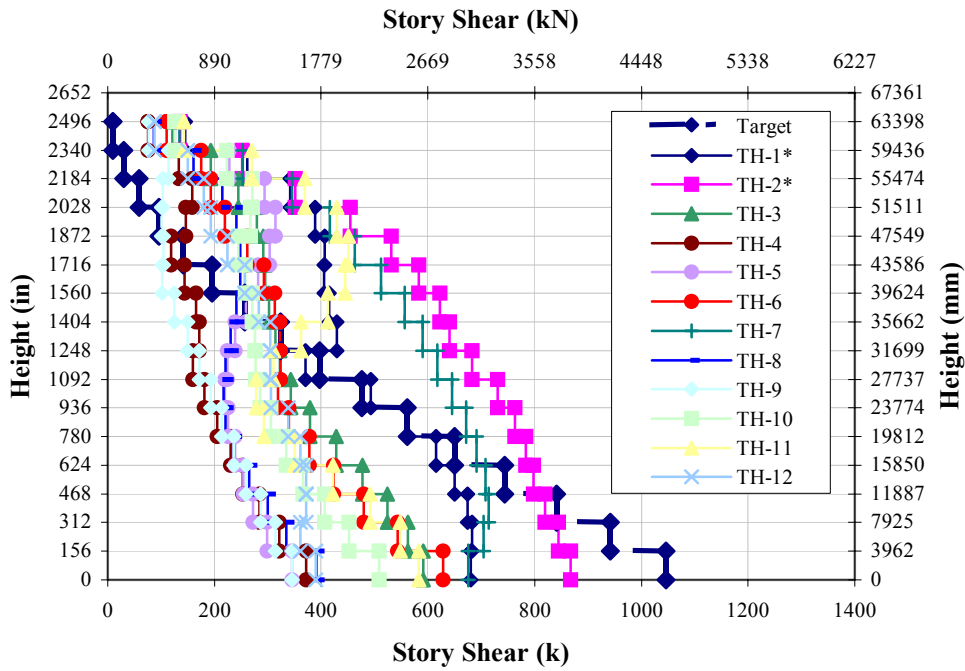


Figure 4.8.2-2. FR-16 Maximum story shear envelopes (SP-1:EQ I)

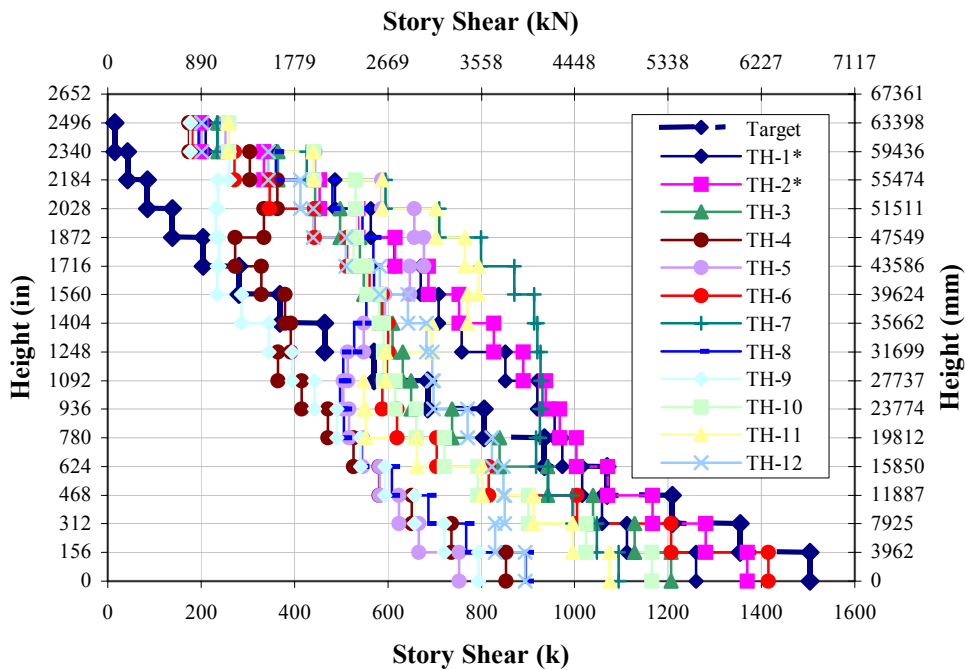


Figure 4.8.2-3. FR-16 Maximum story shear envelopes (SP-2:EQ II)

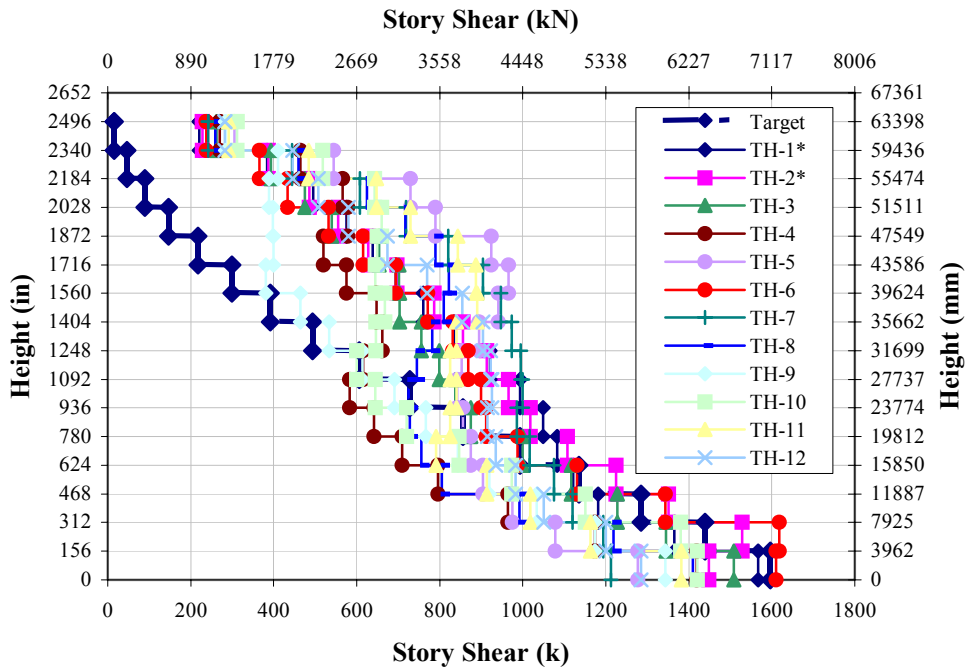


Figure 4.8.2-4. FR-16 Maximum story shear envelopes (SP-3:EQ III)

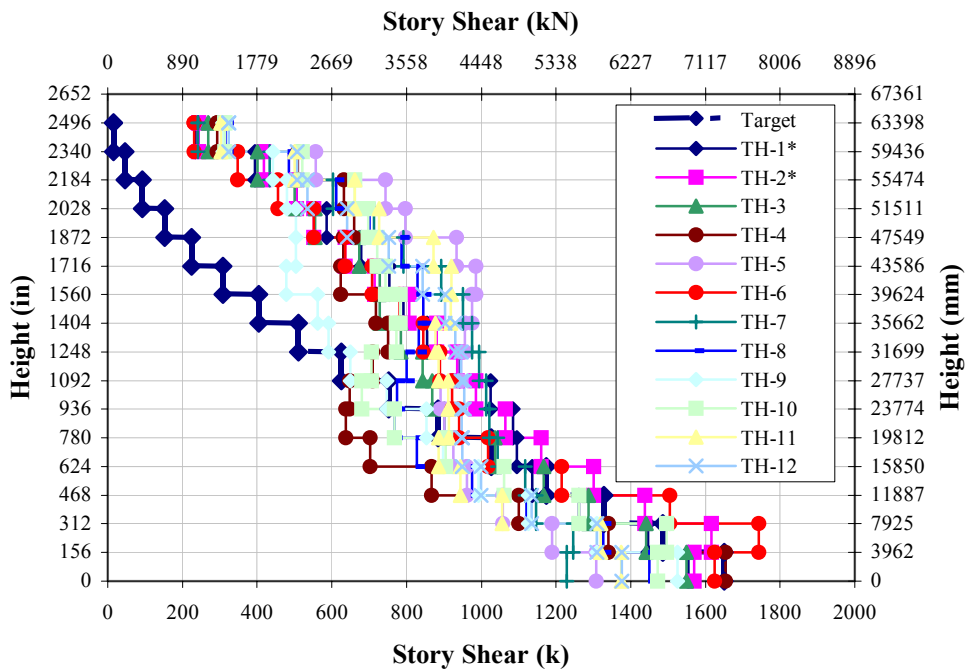


Figure 4.8.2-5. FR-16 Maximum story shear envelopes (SP-4:EQ IV)

4.9 Sources of Variation

Variations in the analytical results are evident in all the previous displacement graphs. This is mainly due to some of the normalized earthquake records not representing the design MCE, notably in the long period region, partly due to the normalization process (i.e. selected period range for intensity comparison). Additionally, variations occur in trying to represent an actual earthquake with the simplified codified spectrum and, similarly, some records are not representative of an *actual* earthquake at the selected location. Ultimately, the DRS for these earthquakes will not correspond to the design MCE DRS and will discrepancies are evident in the final analytical results. Figs. 4.9-1 through 4.9-5 illustrate this fact for 5%, 10%, 15%, 20%, and 25% damping levels.

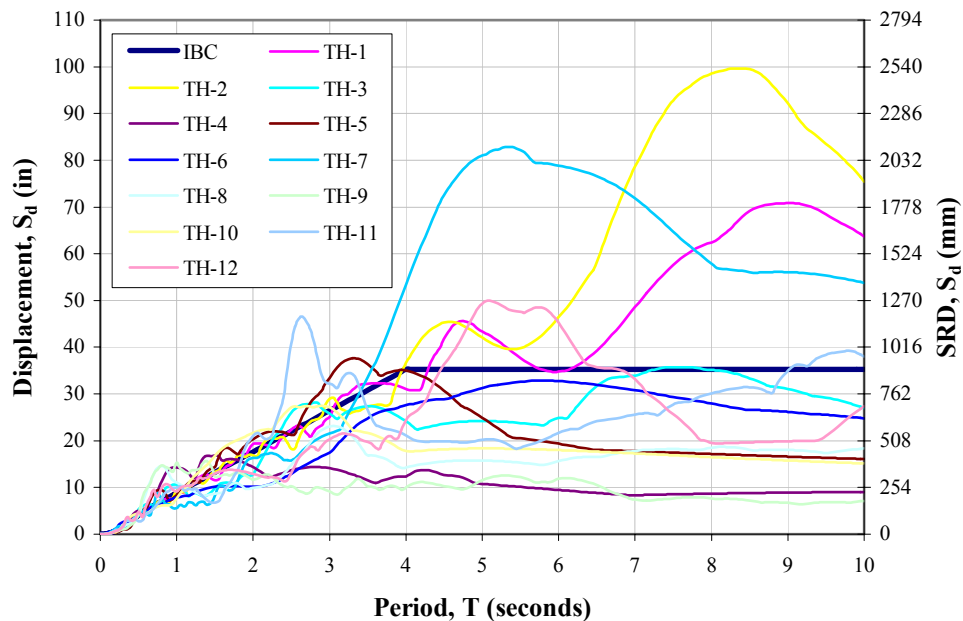


Figure 4.9-1. MCE (EQ IV) Design displacement response spectrums (5% damping)

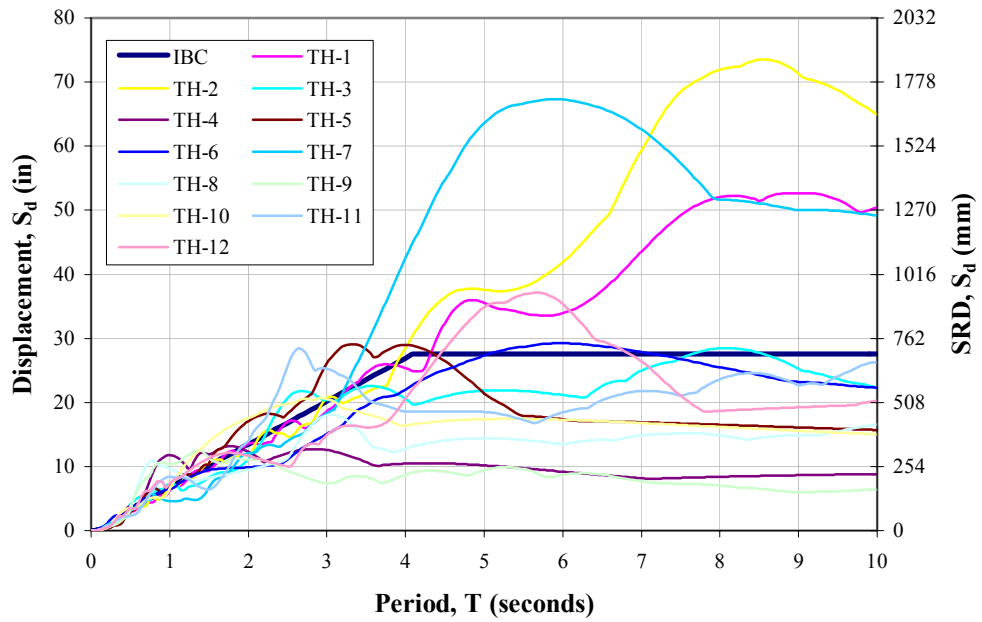


Figure 4.9-2. MCE (EQ IV) Design displacement response spectrums (10% damping)

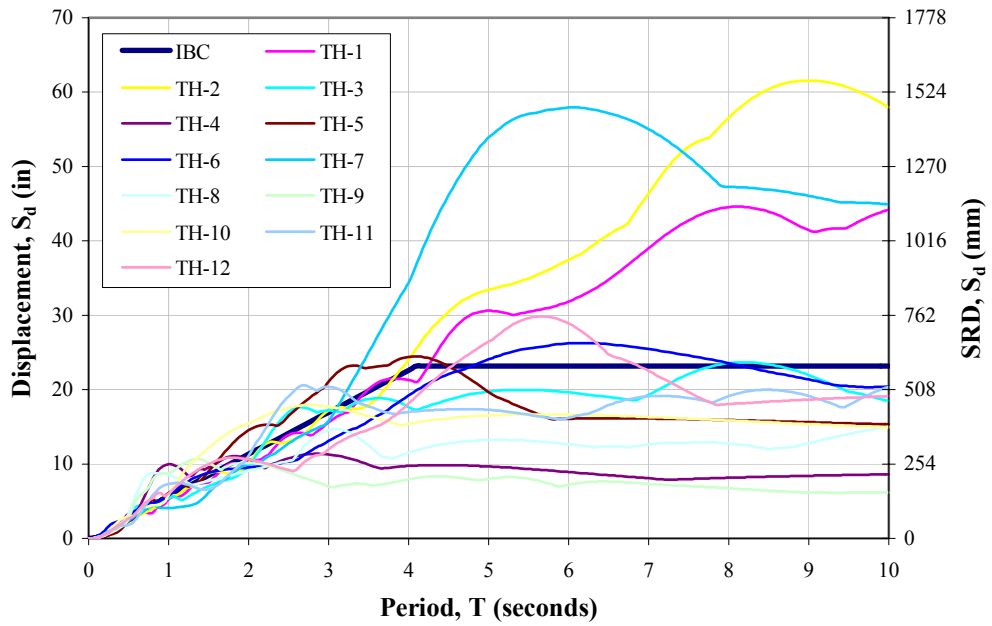


Figure 4.9-3. MCE (EQ IV) Design displacement response spectrums (15% damping)

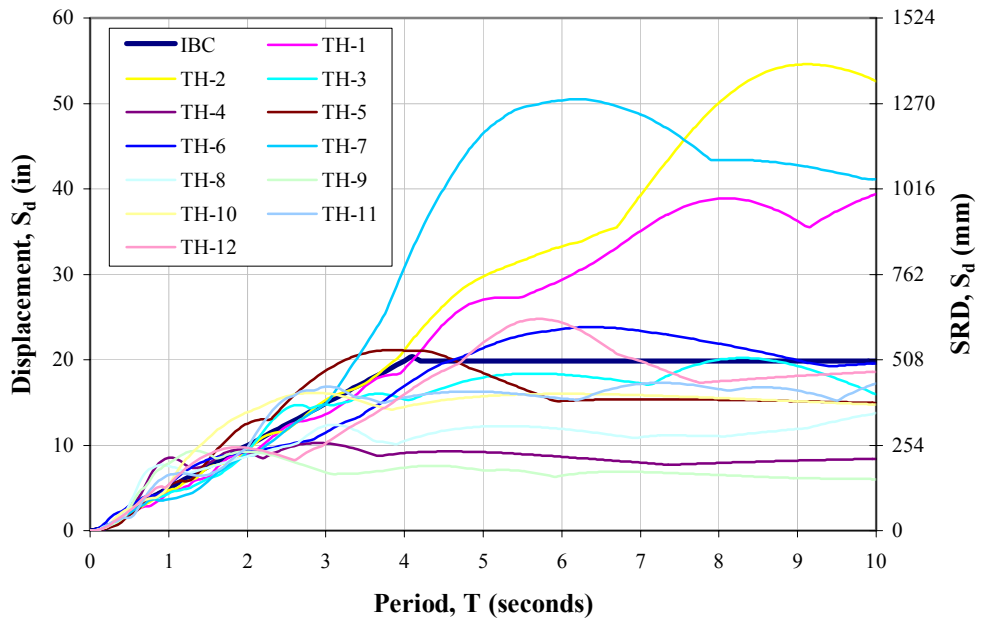


Figure 4.9-4. MCE (EQ IV) Design displacement response spectrums (20% damping)

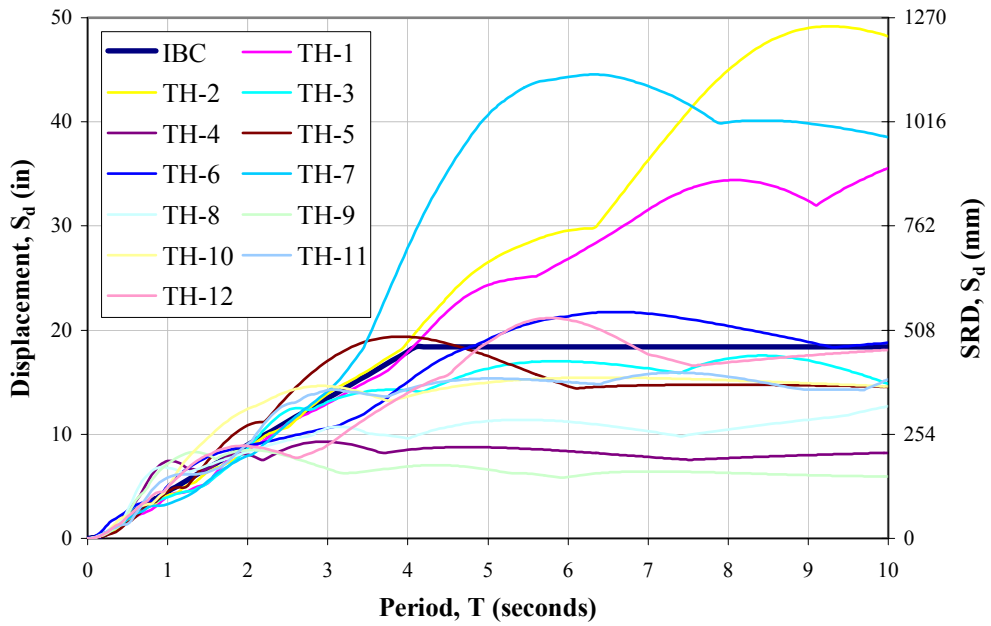


Figure 4.9-5. MCE (EQ IV) Design displacement response spectrums (25% damping)

As seen in the previous graphs, several normalized earthquake records in fact due not serve the intended purpose of approximating the design MCE at various levels of system damping. Hence, a better comparison procedure to demonstrate the validity of the proposed method is to evaluate the displacement results against the expected displacement from the *actual* DRS at the respective effective periods. Figs. 4.9-6 through 4.9-8 show the variation for the ratio of displacements at the effective height using the effective periods from Section 2.5 for FR-4, 8, and 16.

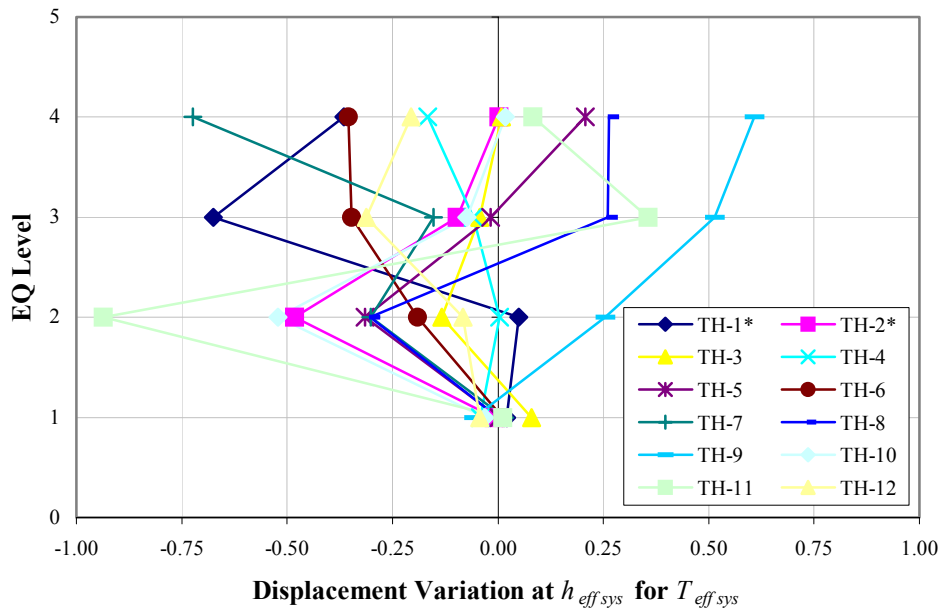


Figure 4.9-6. Displacement variations at effective system height (FR-4)

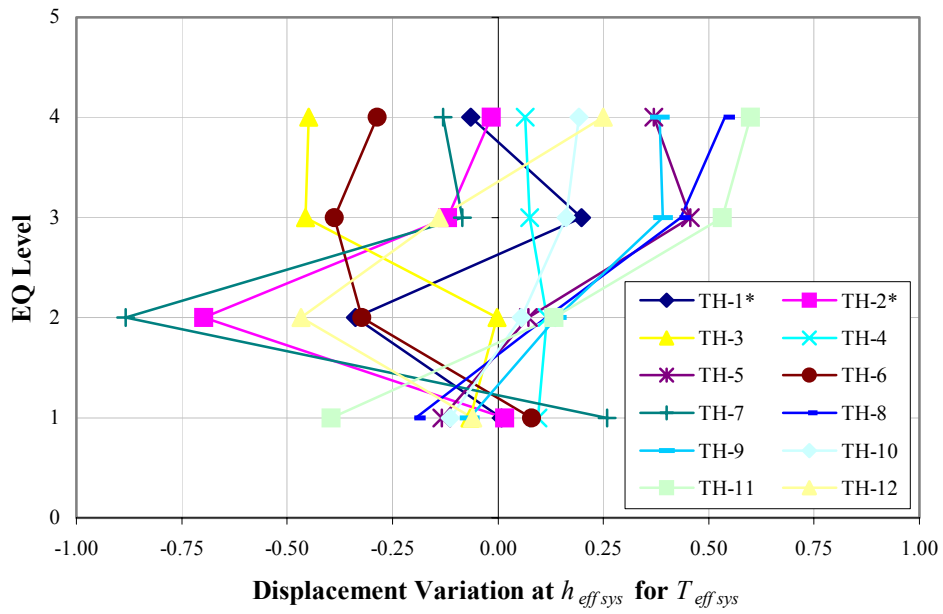


Figure 4.9-7. Displacement variations at effective system height (FR-8)

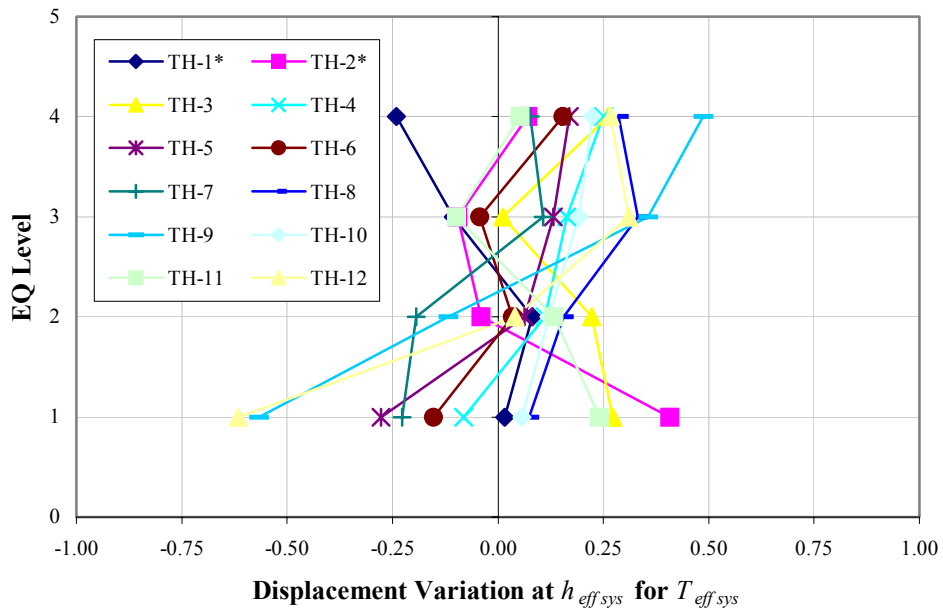


Figure 4.9-8. Displacement variations at effective system height (FR-16)

However, the use of the constant design effective period to determine the expected displacement is misleading since each DRS would in fact provide a different design effective period. As seen in Figs. 4.9-9 through 4.9-11, there is a range of effective periods for each target displacement representing the complete spectrum of selected earthquake records.

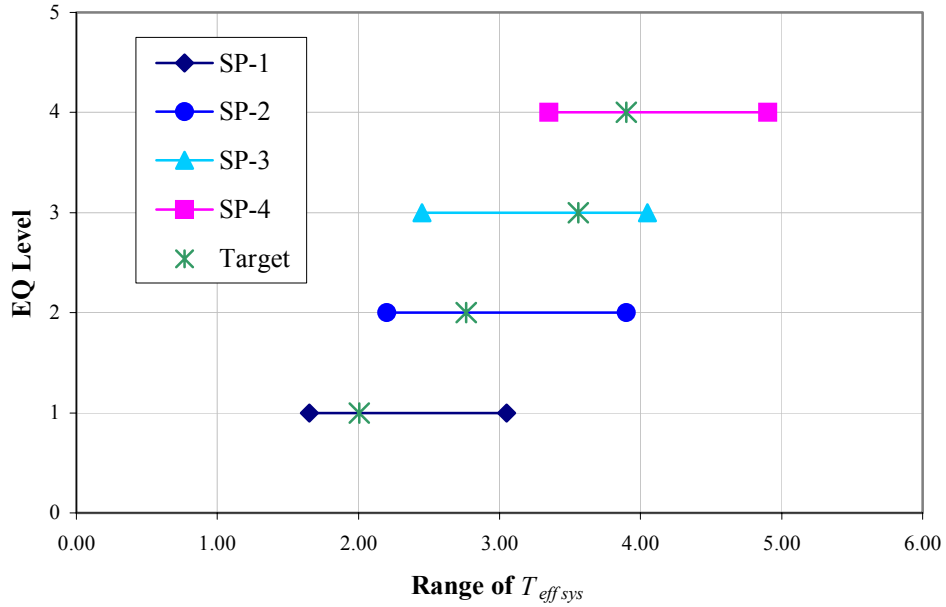


Figure 4.9-9. Range of effective system periods (FR-4)

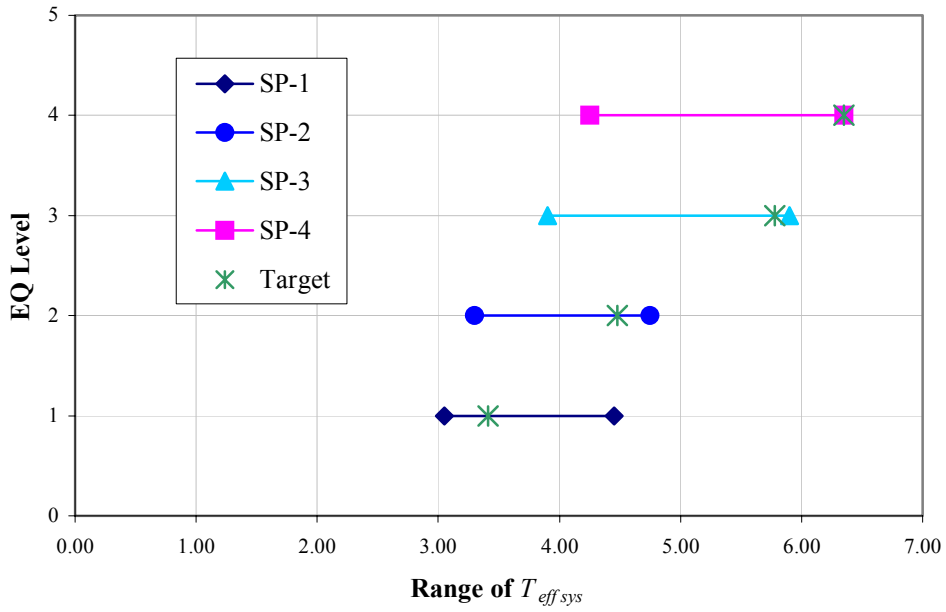


Figure 4.9-10. Range of effective system periods (FR-8)

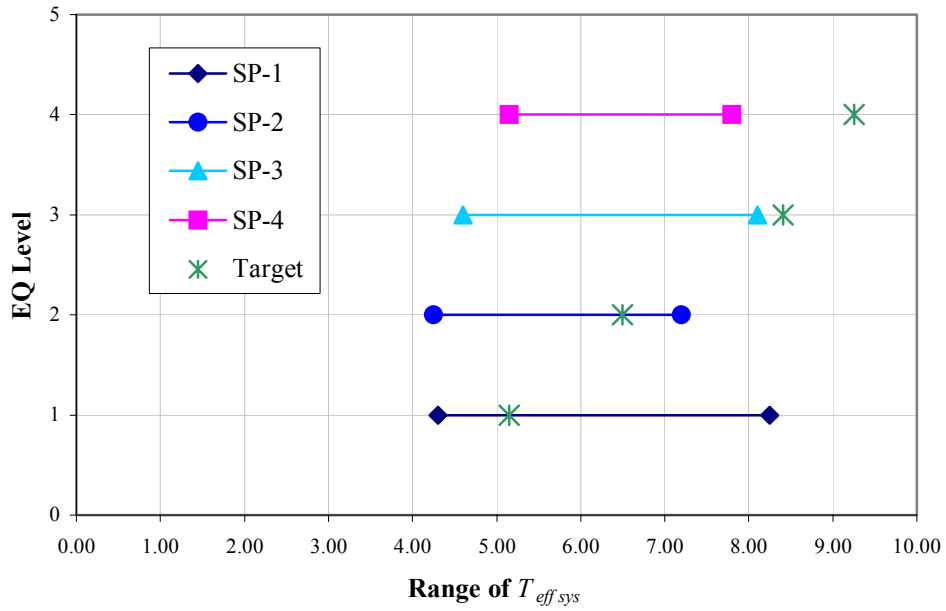


Figure 4.9-11. Range of effective system periods (FR-16)

Likewise, this will lead to variations in base shear, system nodal displacements, and design force demands. This emphasizes the differences in response based on earthquake characteristics and the importance of including all possible variations in the final design of a structure.

Additionally, variations also originate from the use of conceptual procedures. For example, the use of constant design displacement shape functions for all performance levels. While for linear profiles this provides good comparison, long period frames tend to provide higher variations in analytical results. Furthermore, it has been shown that stiffness is proportional to strength; therefore, any variation in overstrength factors could in fact alter the system response.

In conclusion, it is evident for short period structures, typical of low-rise frames, that there is good comparison between the predicted results from the proposed method and *actual* response from the dynamic analysis. Furthermore, earthquake induced higher mode effects are not prominent, whereas overstrength effects control the response along the entire force-displacement range. As system periods increase, thus escalating the complexity of predicting the various response levels, higher mode effects from earthquake characteristics and overstrength are prominent, especially in the inelastic region.

PART 5

CONCLUSION AND FUTURE RESEARCH

5.0 Conclusion

This research has proposed an alternate viable seismic design philosophy that inherently eliminates the current restrictions and erroneous assumptions observed in current FBD. Although a direct comparison between the two philosophies was not included, a steel frame designed in accordance with DBD is more efficient by means of ductility capacity and behavior. Additionally, the design engineer has a better sense of the various degrees of damage.

While the procedures outlined herein, including the Equivalent Yield Analysis, give good comparisons at low-level earthquakes (EQ I and II), post-yield behavior is sporadic at best due to the effects of performance overstrengths and earthquake characteristics. Additionally, the difficulty of predicting the post-yield response of long period frames is noted. Hence, the requirement to incorporate Capacity Design into the design of steel frames is recommended.

Due to the direct relationship between hinge sequencing and member/floor overstrengths, difficulties arise in the direct assessment of the plastic hinge sequencing factor prior to member design. A dynamic amplification factor applied to the design displacement profiles to represent a possible range of design targets should only represent the possibility of higher mode effects associated with earthquake characteristics. Thus the hinge sequencing factor would then only represent the effects of floor overstrengths and associated higher mode response due to system characteristics. In fact, by including a dynamic amplification prior to member design in an effort to represent the entire range of hinge sequencing (higher modes and floor overstrengths) the design engineer would be placed in a loop tending towards current force-based methods. Whereas the design would ultimately become an iterative process and would possibly result in a stronger and stiffer frame than typically required. Therefore, it is recommended that the plastic hinge sequencing factor for both earthquake and overstrength induced higher mode response be determined and applied during the member design stage.

Furthermore, an interesting conclusion from DBD is that the design base shear is proportional to the square of seismic intensity, whereas force-based methods assume a linear relationship between design base shear and seismic intensity (*Priestley and Kowalksy, 2000*)

The following is a recap of the DBD methodology for the design of seismic resistant steel moment frames.

- 1) Determine target drifts and drift ratios based on assumed controlling maximum drift for specified structural performance levels defined in accordance with performance objectives set forth by SEAOC, Appendix B.
- 2) Determine design earthquake levels from target drift ratios and develop design response spectrums for each respective earthquake for 5%, 10%, 20%, 30% 40% and 50% damping levels. Additionally, determine damping vs. ductility relationship based on selected hysteresis.
- 3) Initial beam depth(s) can be approximated by selecting a beam depth with a plastic moment capacity range that can easily satisfy at least twice the plastic moment demand of a simply supported beam subjected to the design gravity loads, normally $0.9(\text{Dead} + 0.3 \text{ Live})$. The loads may be applied either uniformly or by several concentrated loads. It should be noted that the uniform approximation is conservative compared to concentrated applied loads.
- 4) Determine beam plastic rotation capacities using beam depths from Step 3.

$$\theta_p = 0.42\phi_m^o \varepsilon_y \frac{L_b}{d} \quad (\text{based on } S_F = 1.14 \text{ and } \lambda = 1.10)$$

Use rotation charts to determine required beam depths for unsymmetric beam lengths.

- 5) Develop design displacement profiles (nodal displacements) based on post-yield drifts from Step 1. The *elastic* and pseudo-elastic profile can be determined from the system plastic rotation capacity determined in Step 4.
- 6) Determine effective system mass.
- 7) Determine effective height from design displacement profile and effective mass.
- 8) Determine system displacement at effective height

- 9) Determine yield displacement at effective height using yield drift.
- 10) Determine system displacement ductility demand.
- 11) Determine effective damping using system ductility demand.
- 12) Determine effective period by entering respective DRS with system displacement and effective damping.
- 13) Determine effective system stiffness and base shear and verify controlling performance level. Repeat process if necessary
- 14) Construct system force-displacement graph.
- 15) Distribute yield base shear from Step 13 in accordance with mass distribution and yield displacement profile, including reductions from Equivalent Yield Analysis. Analyze system in an elastic analysis (static inelastic analysis is preferred).
- 16) Determine member and system performance overstrength factors and apply Capacity Design procedures in the member design.
- 17) Iterate analysis and member selection, including overstrengths, until convergence on the moment demand and displacement profile.
- 18) Increase base shear obtained from Step 13 by the system overstrength factor from 16 and 17 and adjust the target force-displacement graph.
- 19) Verify system using push-over analysis or non-linear static analysis using full lateral loads determined from maximum base shear, or non-linear dynamic analysis with respective time-histories.

Additionally, Advanced Analysis procedures were investigated to outline their use in the design and analysis of seismic resistant frames. It was shown that by incorporating uncertainties inherent in member design codes the engineer could design a more efficient

frame and, at the same time, gain a better understanding of maximum ductility capacities. It is recommended that the principles outlined in Part 3 be incorporated into DBD.

As illustrated within this document, the proposed method is relatively simple, with the only complexities stemming from the determination of the numerical performance overstrength factor. Additionally, current seismic design does not offer an analysis solution incorporating Capacity Design, which has been proven to be unmistakably valuable, nor the advantages of investigating post-yield frame response. Ultimately, the proposed method has much greater potential for producing effective structures since it directly deals with the proportionality between strength and stiffness (*Priestly and Kowalsky, 2000*). However, certain simplifications and procedures need to be further researched in an effort to better represent uncertainties and accuracy of the proposed procedures. Finally, it is the inclusion of Capacity Design procedures that guarantees the structural safety of seismic resistant steel moment frames.

5.1 Future Research

The following is a list of future research needs for the continual development of the proposed method.

- 1) Stiffness degradation should be accounted for in the inelastic dynamic analysis and the design displacement profiles.
- 2) The column-to-beam stiffness factor, λ , should be researched for validity and accuracy.
- 3) The effect of transverse loads on the *equivalent* plastic rotation capacity should be investigated.
- 4) DBD methods for semi-rigid and braced frames should be investigated.
- 5) Advanced Analysis procedures should be incorporated into DBD methods.
- 6) More accurate and appropriate time-histories should be used, or a better normalization process utilized.

- 7) Performance overstrengths factors should be further researched for accuracy, including the correlation between floor overstrength and plastic hinge sequencing. Additionally, overstrengths for strain rate and strain hardening should be investigated.
- 8) Capacity Design procedures for the design of beams and columns should be researched for validity and accuracy.
- 9) The use of RBS and RCS should be investigated and incorporated in the proposed DBD methods.
- 10) The effect of composite action should be researched and incorporated in the proposed DBD methods.
- 11) Demand Factor and Resistance Design methods should be incorporated in the proposed DBD methods.
- 12) Effective damping vs. ductility relationship should be further researched.
- 13) Second order effects should be incorporated into the design acceleration and displacement response spectrums.
- 14) Displacement profiles at the Pseudo elastic and inelastic levels, including target drift values should be researched for validity and accuracy. Special attention should also be given to predicting behavior of long period structures.

PART 6

APPENDIX AND REFERENCES

APPENDIX A: Design Response Spectrums

The following design response spectrums were constructed in accordance with IBC/NEHRP 2000 seismic provisions as stipulated in IBC 2000/FEMA 368 using the peak ground accelerations (PGA) from Table A-1 developed in Section 2.5.

Performance Level ²	PGA Reduction Factor	PGA
SP-1 – Operational	0.125 ¹	0.084 ¹
SP-2 – Occupiable	0.45	0.30
SP-3 – Life Safe	0.80	0.54
SP-4 – Near Collapse ³	1.00	0.67

Notes:

1. Based on a target drift of 0.005 – requires modification as previously discussed
2. Base Structural Objective (BSO) is chosen with no limits placed for restricting non-structural damage.
3. With BSO, SP-4 corresponds to the MCE (EQ IV).

Table A-1. Design Peak Ground Accelerations

A.1 Acceleration Response Spectrums

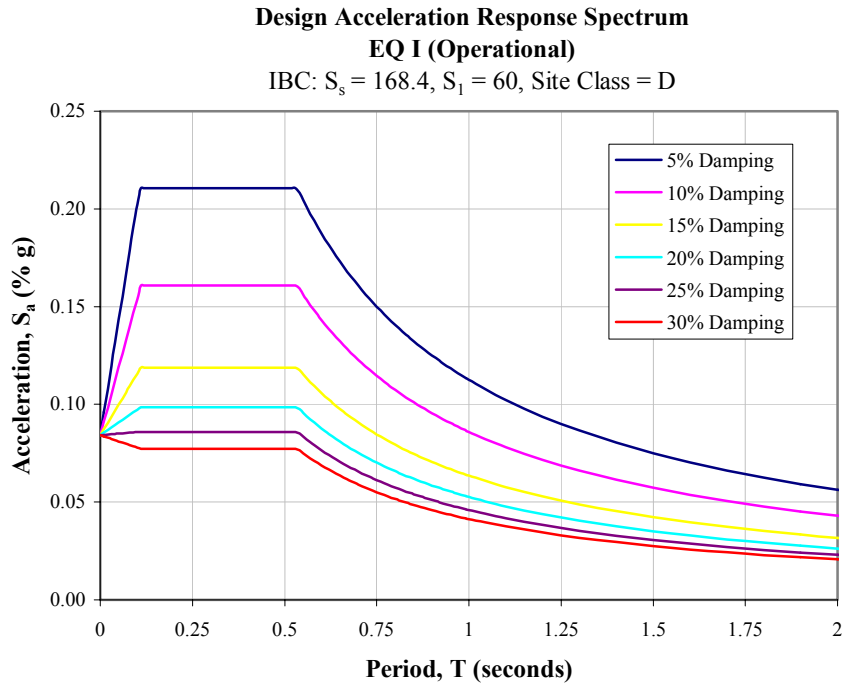


Figure A.1-1. EQ I Acceleration Response Spectrum

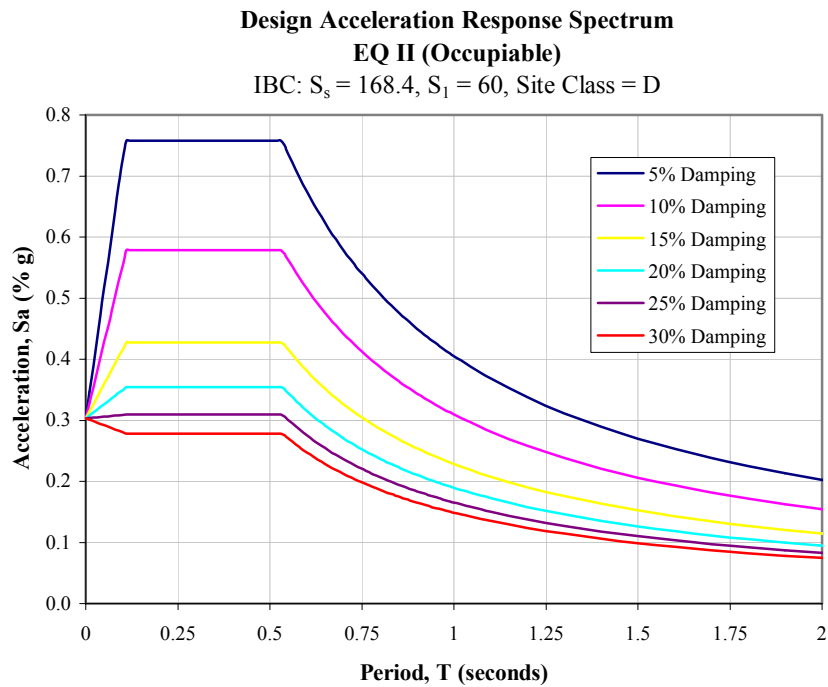


Figure A.1-2. EQ II Acceleration Response Spectrum

**Design Acceleration Response Spectrum
EQ III (Life Safe)**

IBC: $S_s = 168.4$, $S_1 = 60$, Site Class = D

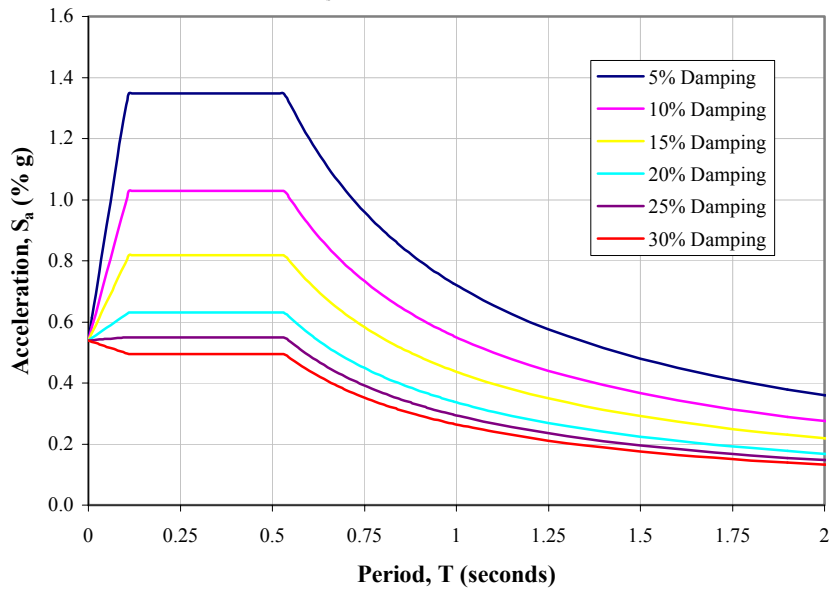


Figure A.1-3. EQ III Acceleration Response Spectrum

**Design Acceleration Response Spectrum
EQ IV (MCE - Collapse)**

IBC: $S_s = 168.4$, $S_1 = 60$, Site Class = D

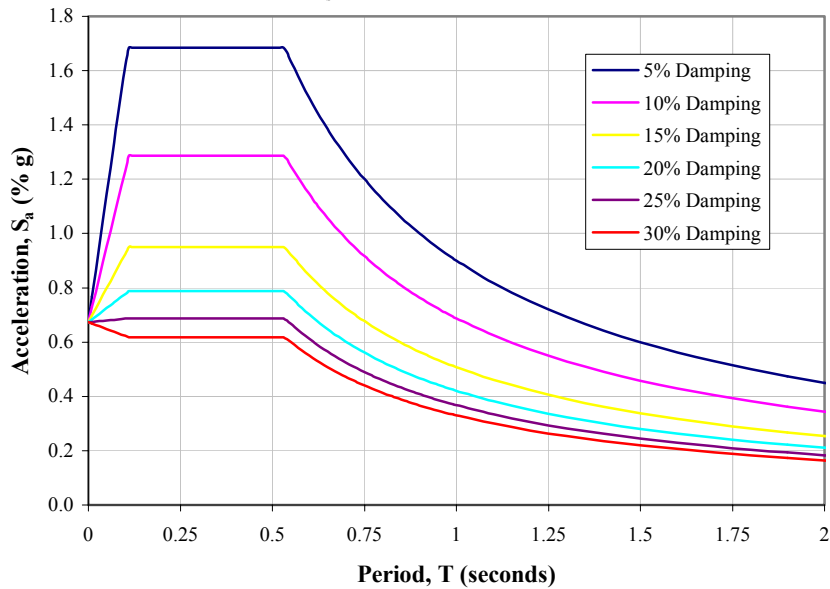


Figure A.1-4. EQ IV Acceleration Response Spectrum

A.2 Displacement Response Spectrums

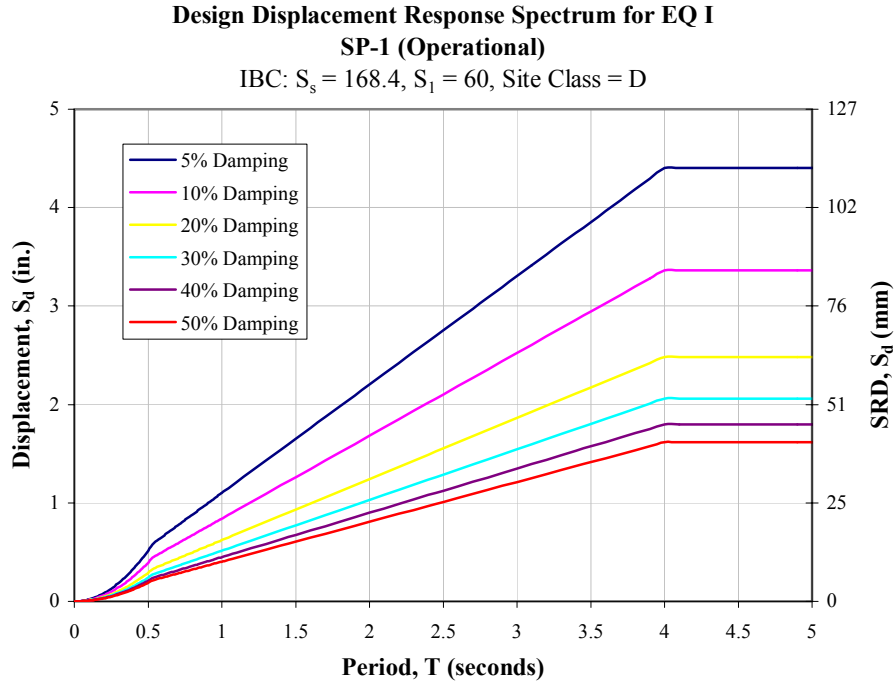


Figure A.2-1. EQ I Displacement Response Spectra

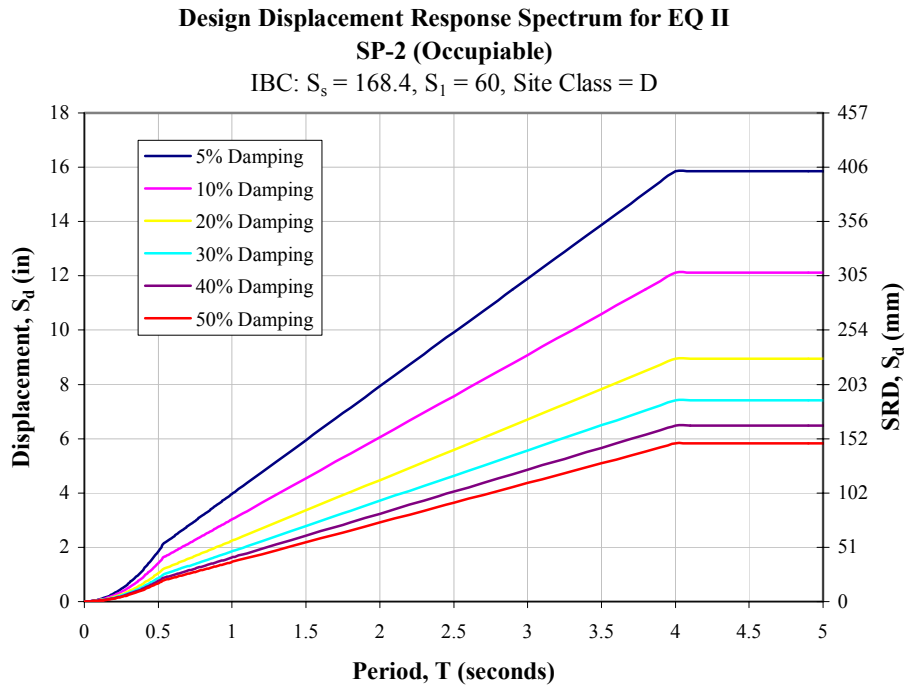


Figure A.2-2. EQ II Displacement Response Spectra

**Design Displacement Response Spectrum for EQ III
SP-3 (Life Safe)**

IBC: $S_s = 168.4$, $S_1 = 60$, Site Class = D

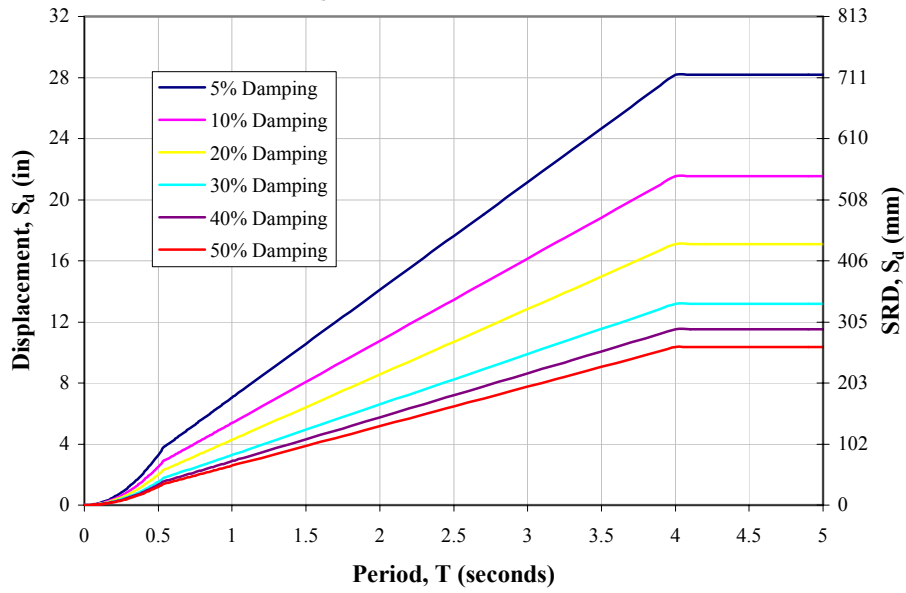


Figure A.2-3. EQ III Displacement Response Spectra

**Design Displacement Response Spectrum for EQ IV
SP-4 (MCE - Collapse)**

IBC: $S_s = 168.4$, $S_1 = 60$, Site Class = D

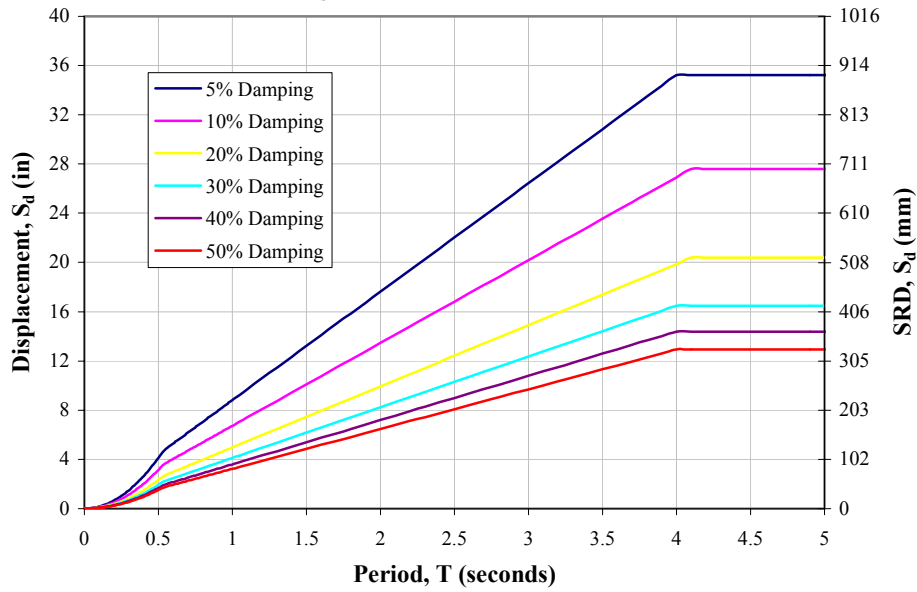


Figure A.2-4. EQ IV Displacement Response Spectra

A.3 Velocity Response Spectrums

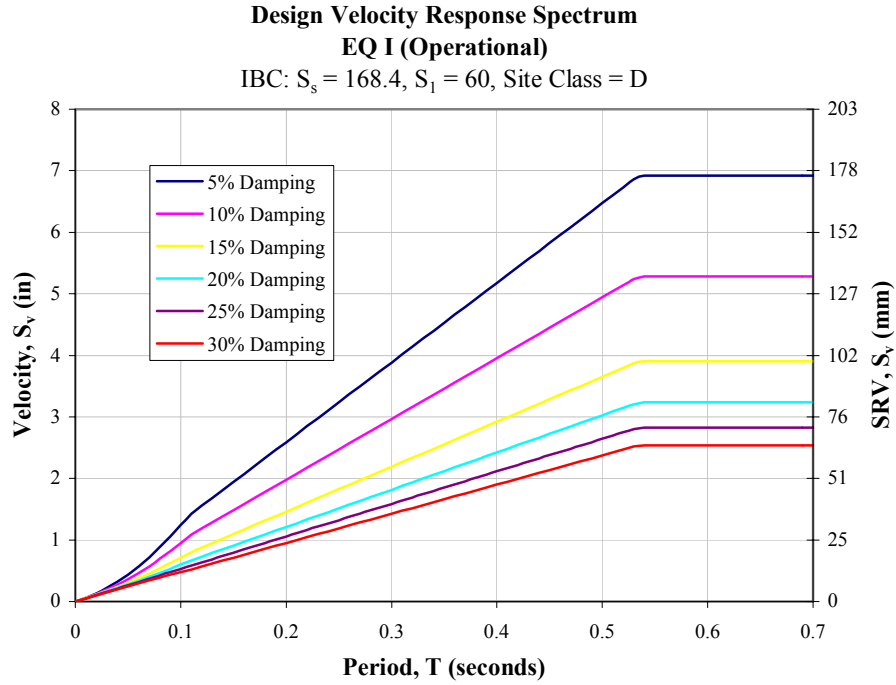


Figure A.3-1. EQ I Velocity Response Spectra

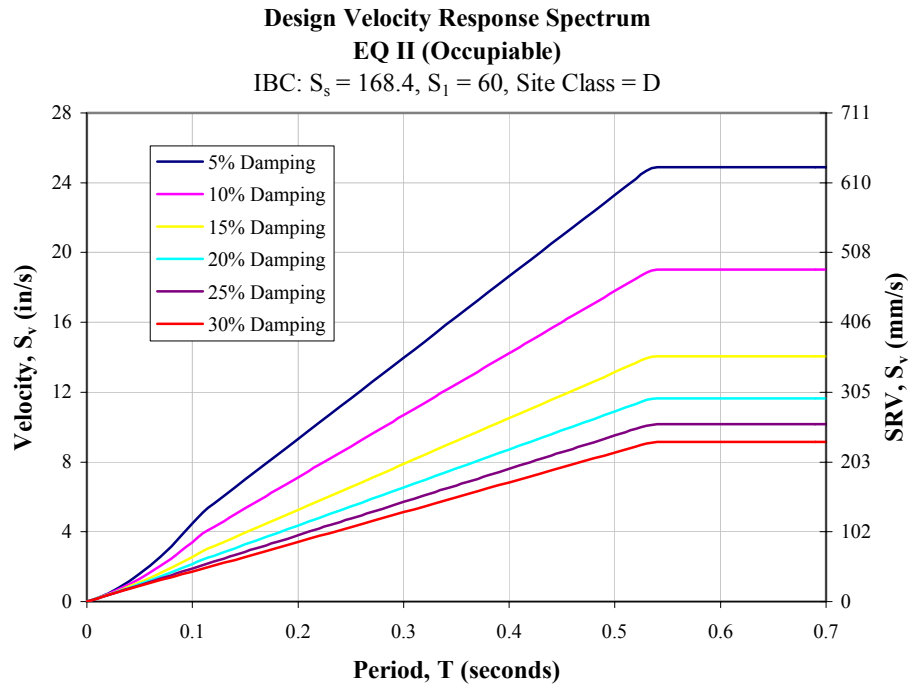


Figure A.3-2. EQ II Velocity Response Spectra

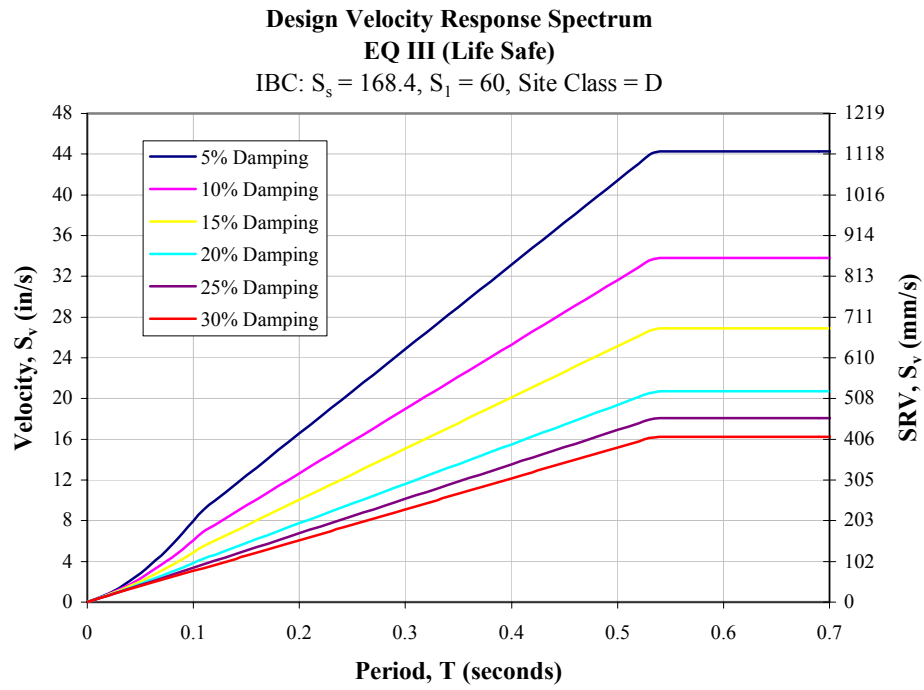


Figure A.3-3. EQ III Velocity Response Spectra

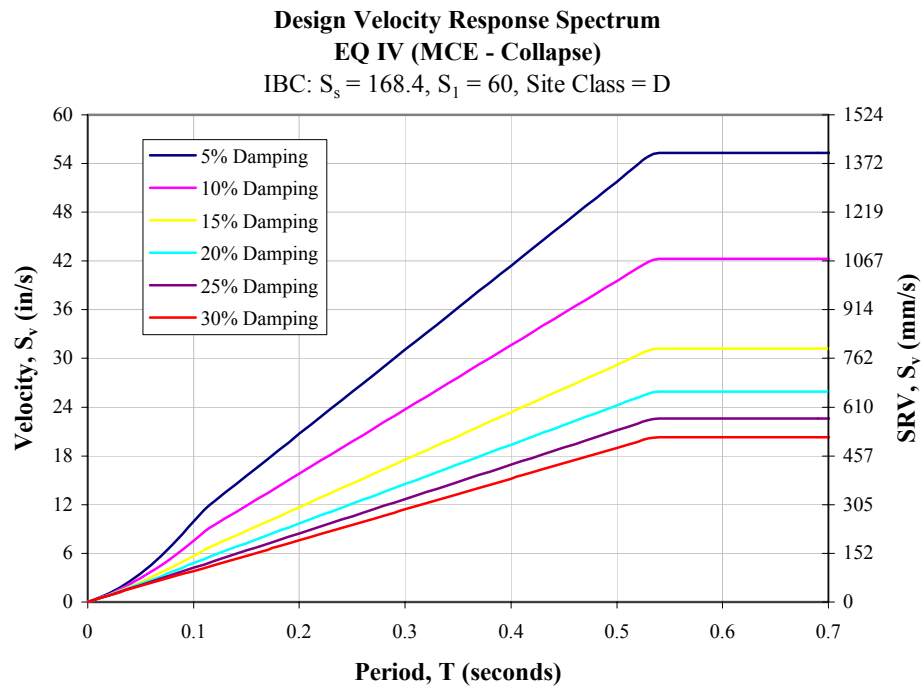


Figure A.3-4. EQ IV Velocity Response Spectra

B.1 TH-1 Design Response Spectrums (Artificial)

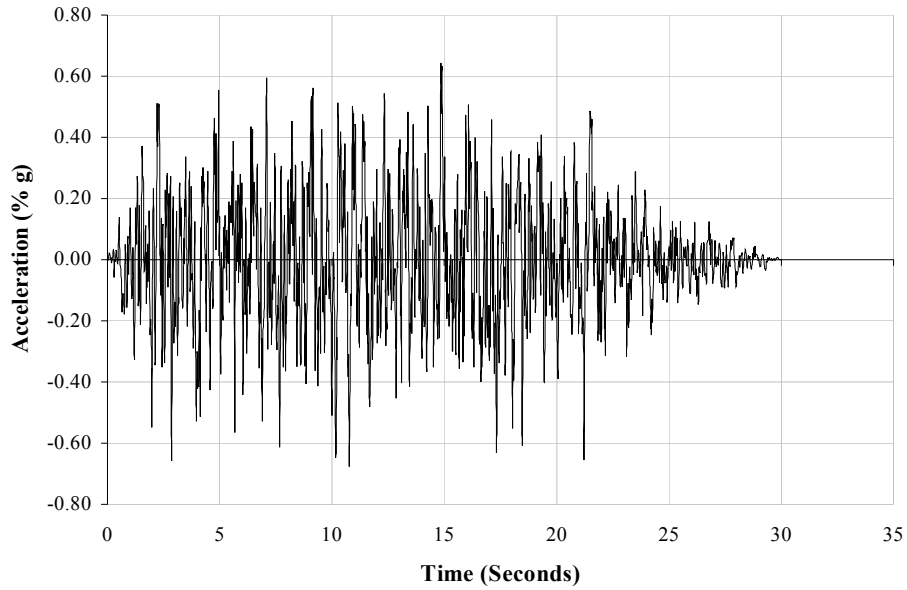


Figure B.1-1. Time-History (TH-1)

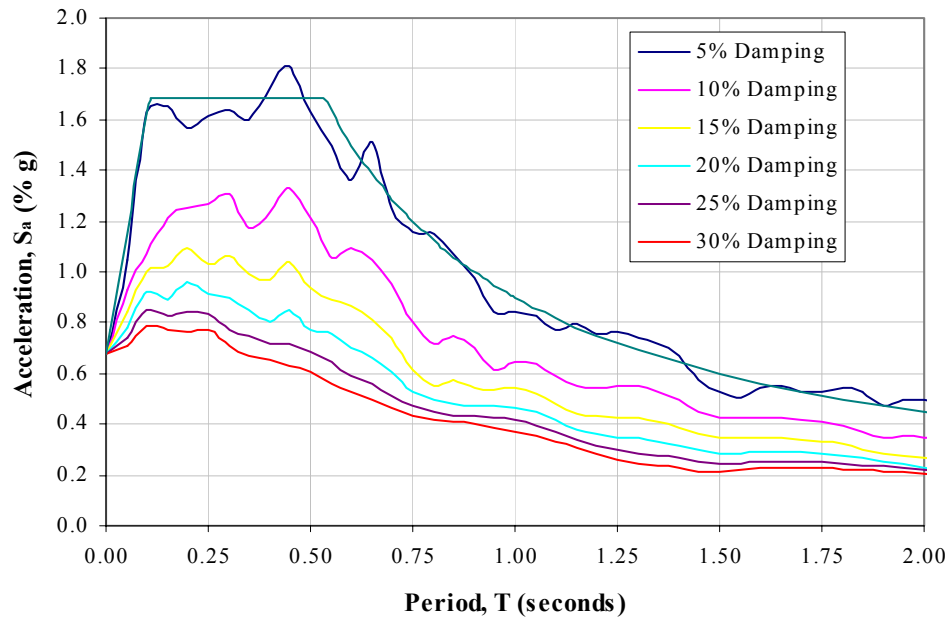


Figure B.1-2. Acceleration Response Spectra (TH-1)

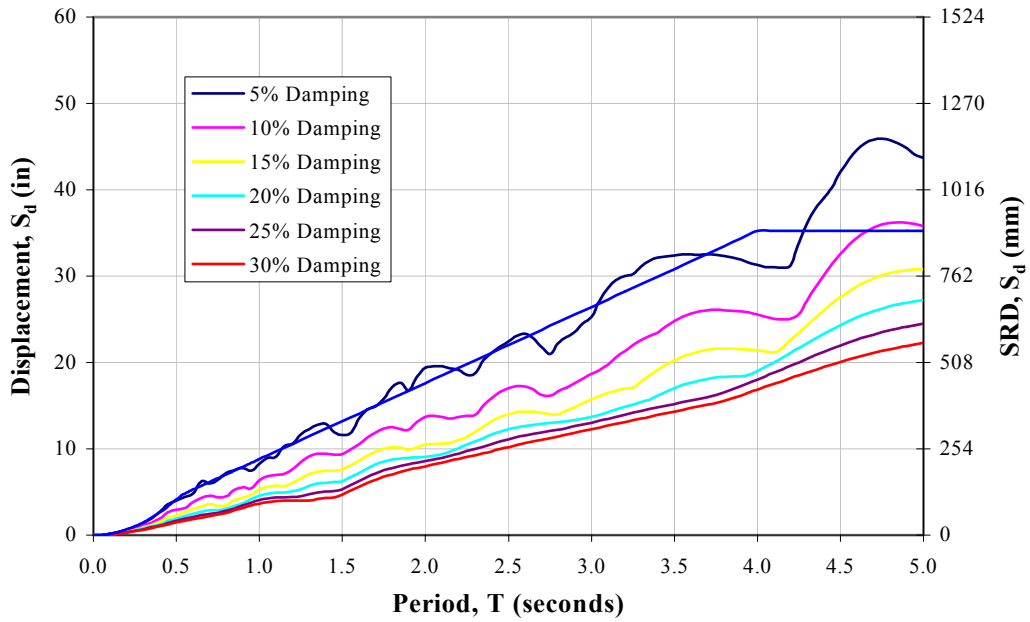


Figure B.1-3. Displacement Response Spectra (TH-1)

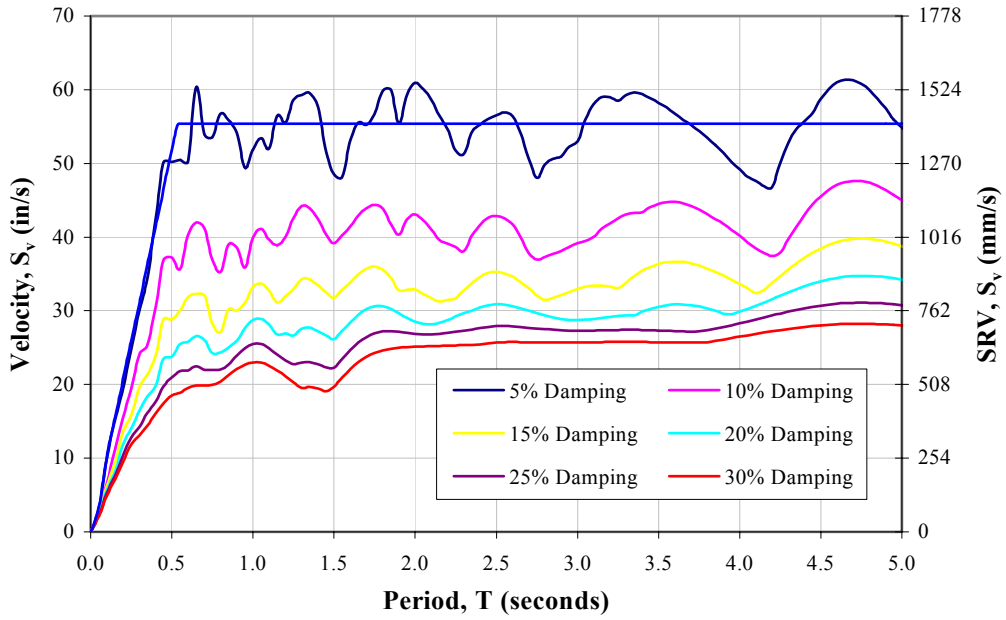


Figure B.1-4. Velocity Response Spectra (TH-1)

B.2 TH-2 Design Response Spectrums (Artificial)

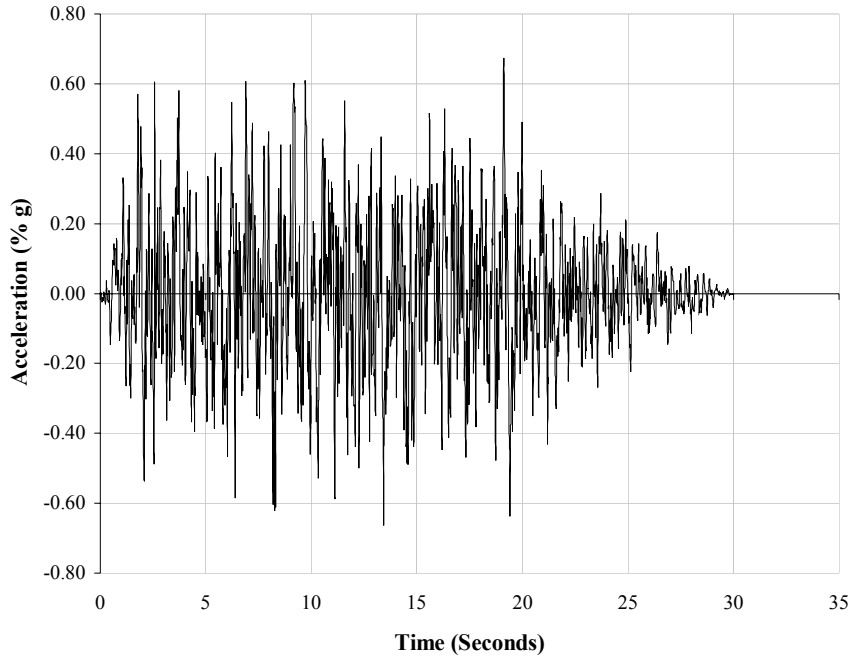


Figure B.2-1. Time-History (TH-2)

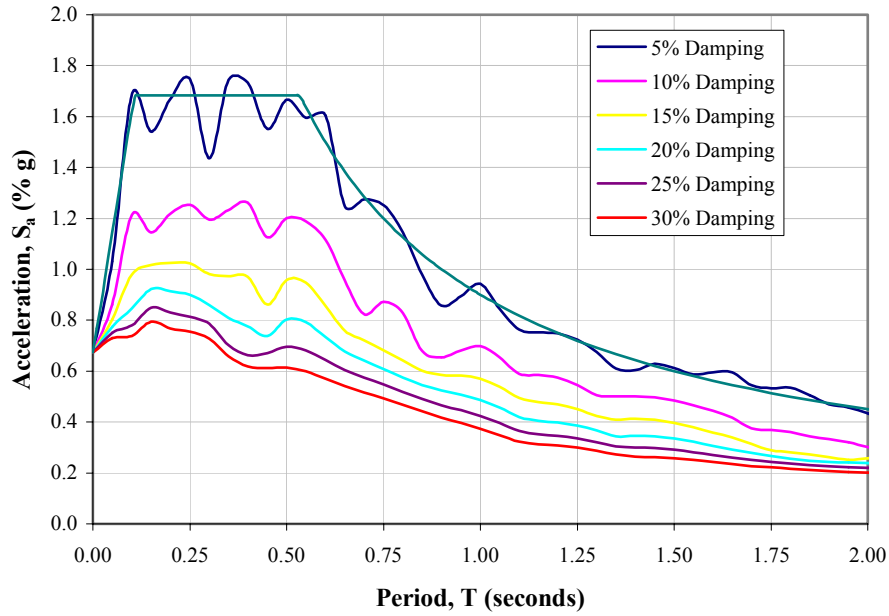


Figure B.2-2. Acceleration Response Spectra (TH-2)

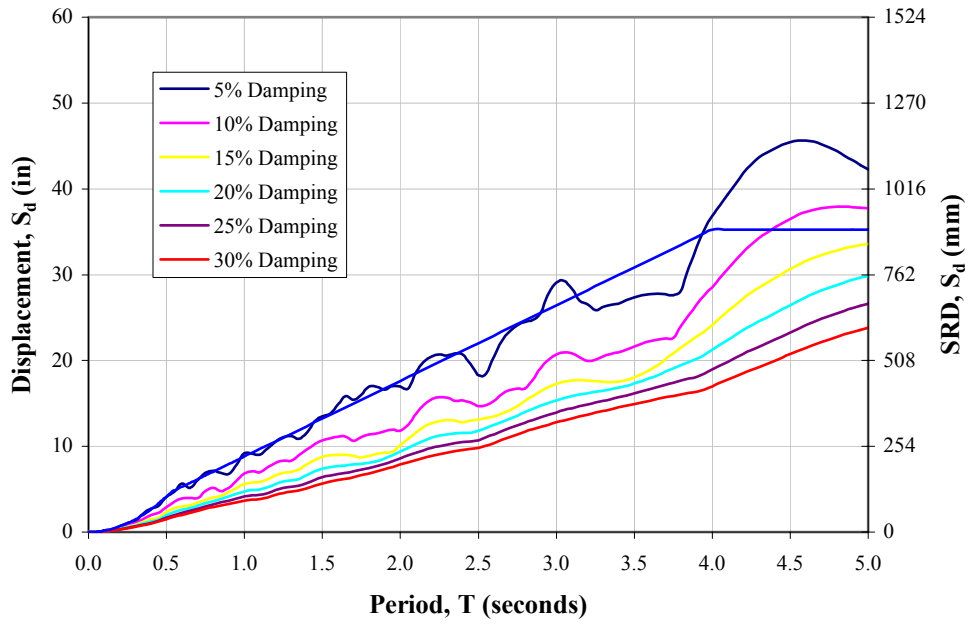


Figure B.2-3. Displacement Response Spectra (TH-2)

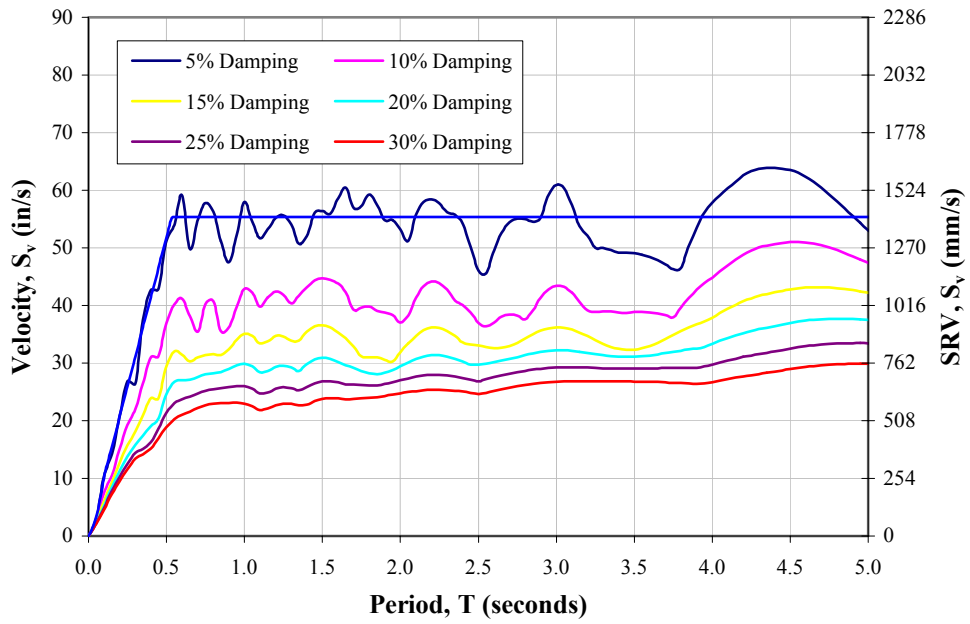


Figure B.2-4. Velocity Response Spectra (TH-2)

B.3 TH-3 Design Response Spectrums (El Centro)

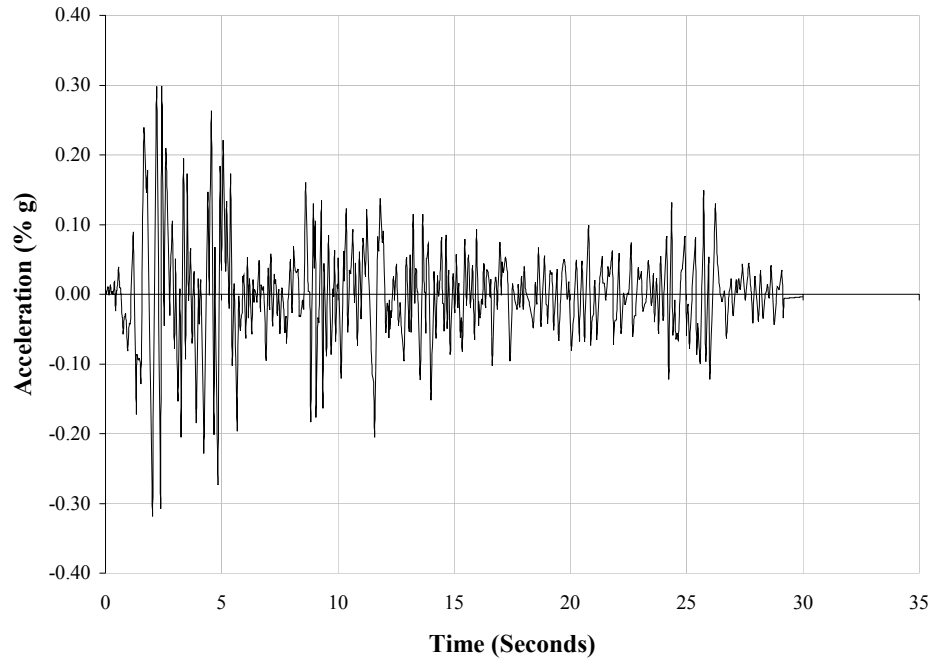


Figure B.3-1. Time-History (TH-3)

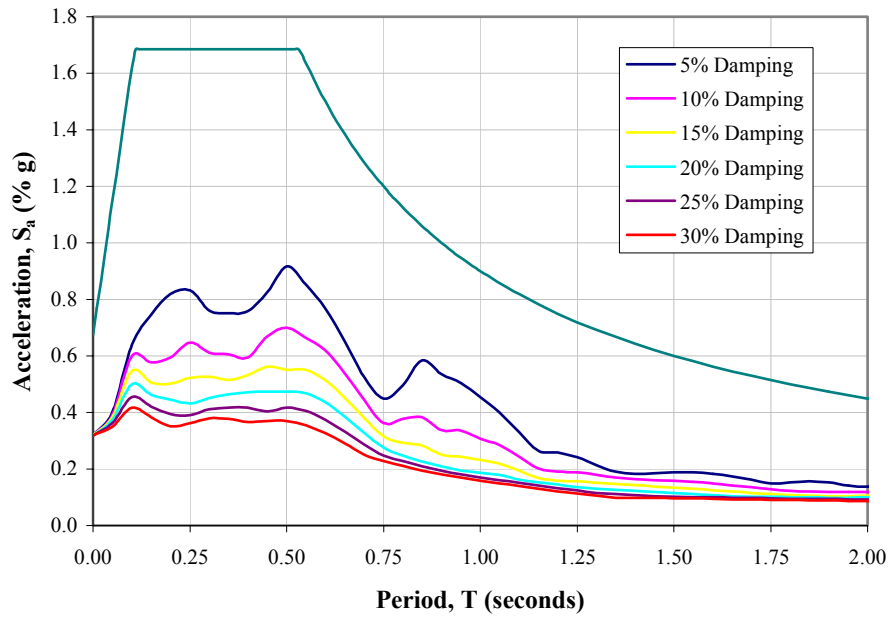


Figure B.3-2. Acceleration Response Spectra (TH-3)

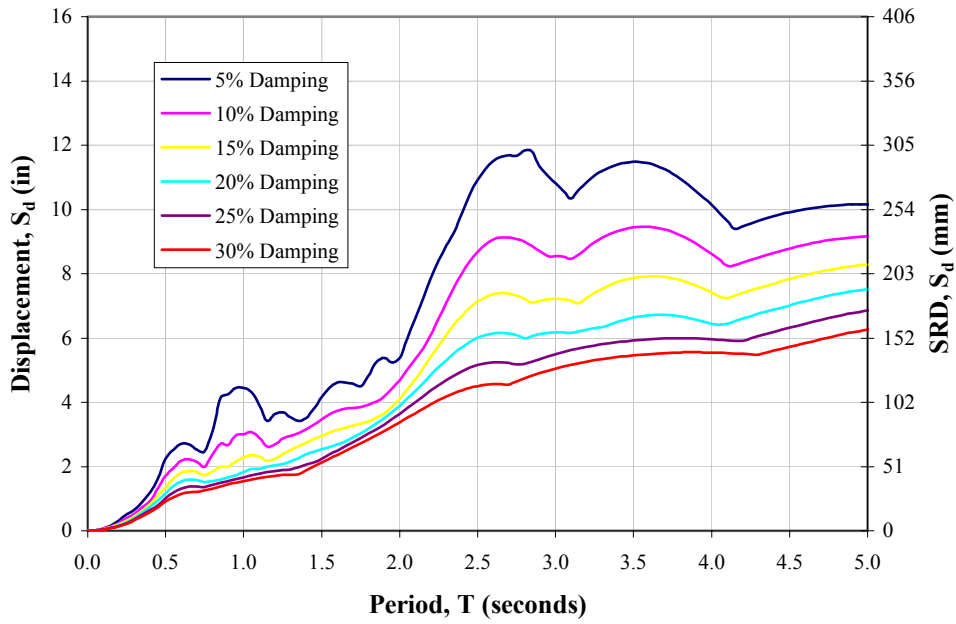


Figure B.3-3. Displacement Response Spectra (TH-3)

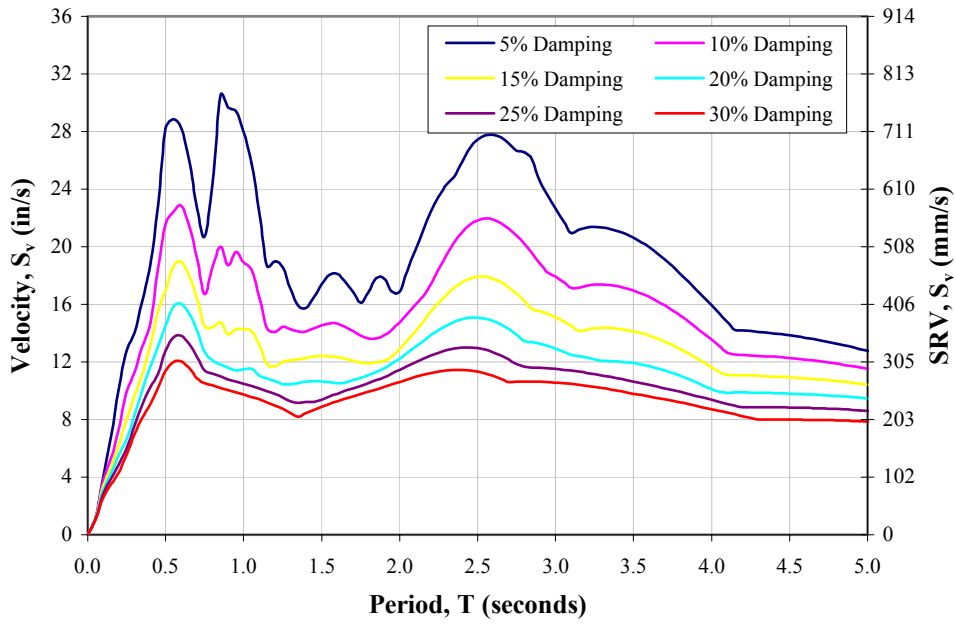


Figure B.3-4. Velocity Response Spectra (TH-3)

B.4 TH-4 Design Response Spectrums (Kobe)

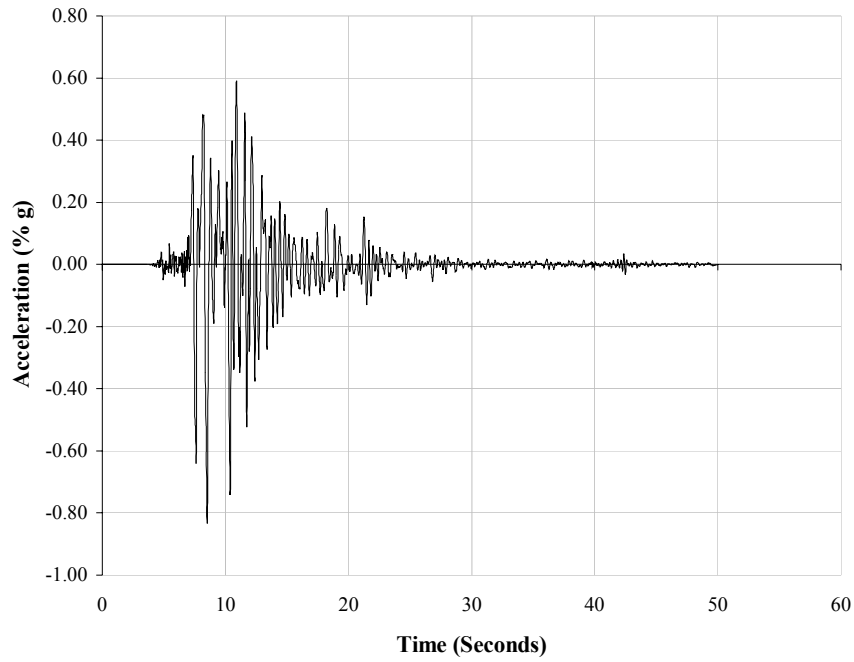


Figure B.4-1. Time-History (TH-4)

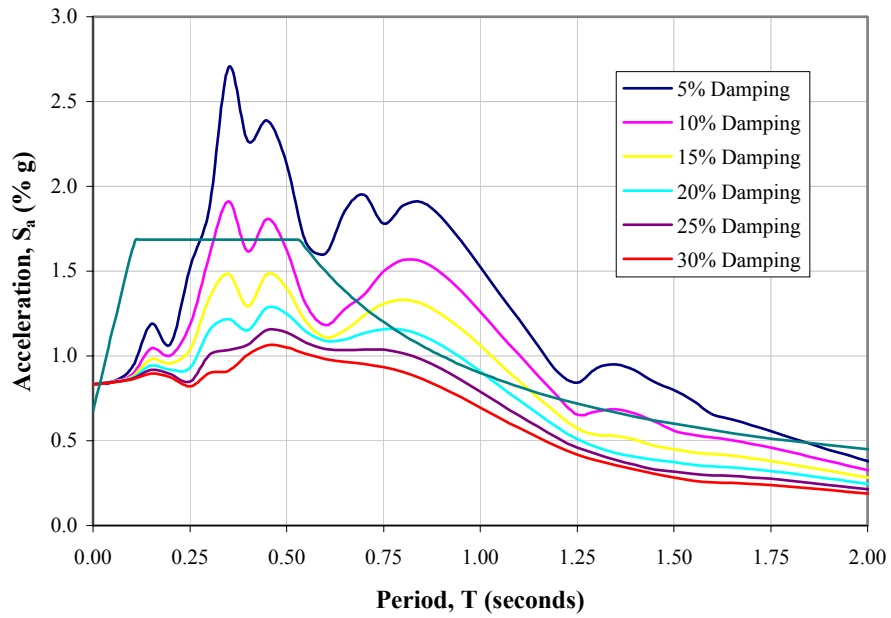


Figure B.4-2. Acceleration Response Spectra (TH-4)

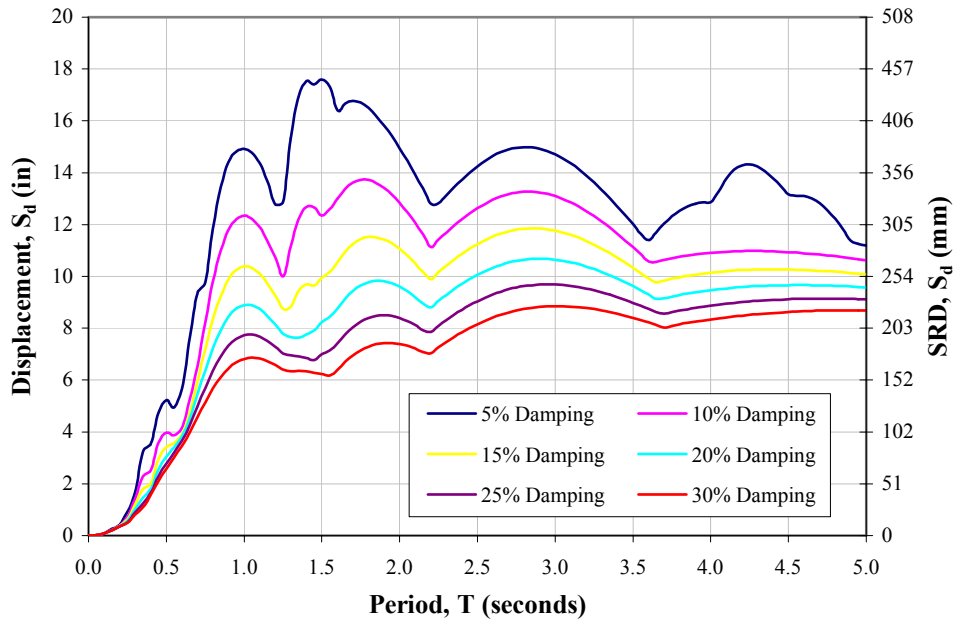


Figure B.4-3. Displacement Response Spectra (TH-4)

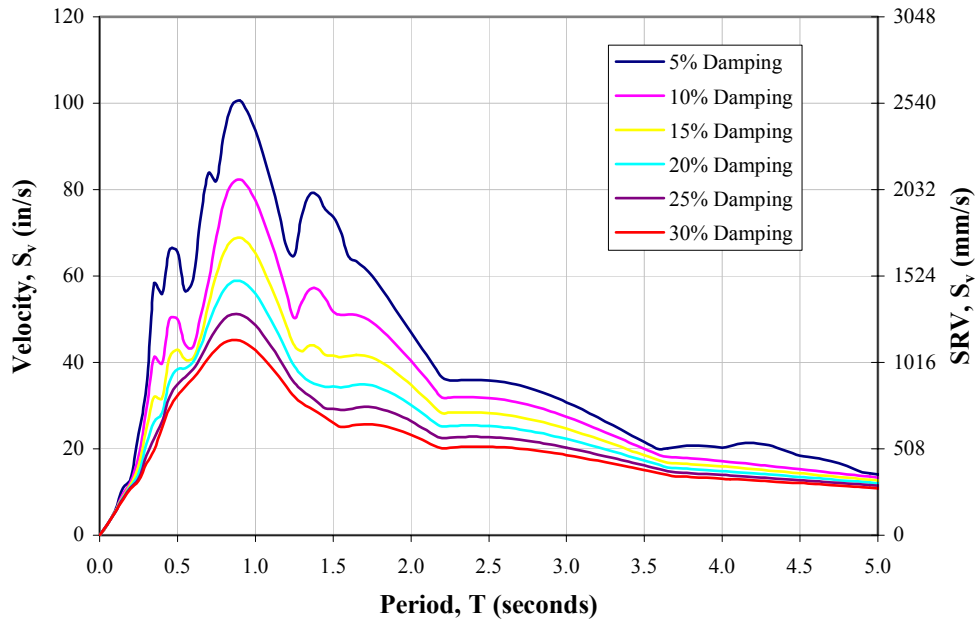


Figure B.4-4. Velocity Response Spectra (TH-4)

B.5 TH-5 Design Response Spectrums (Loma Prieta)

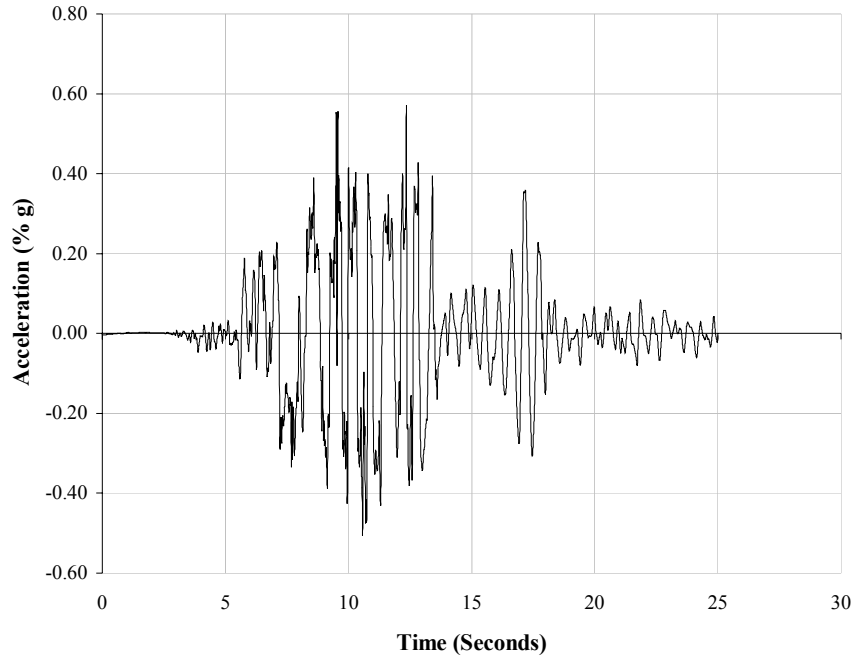


Figure B.5-1. Time-History (TH-5)

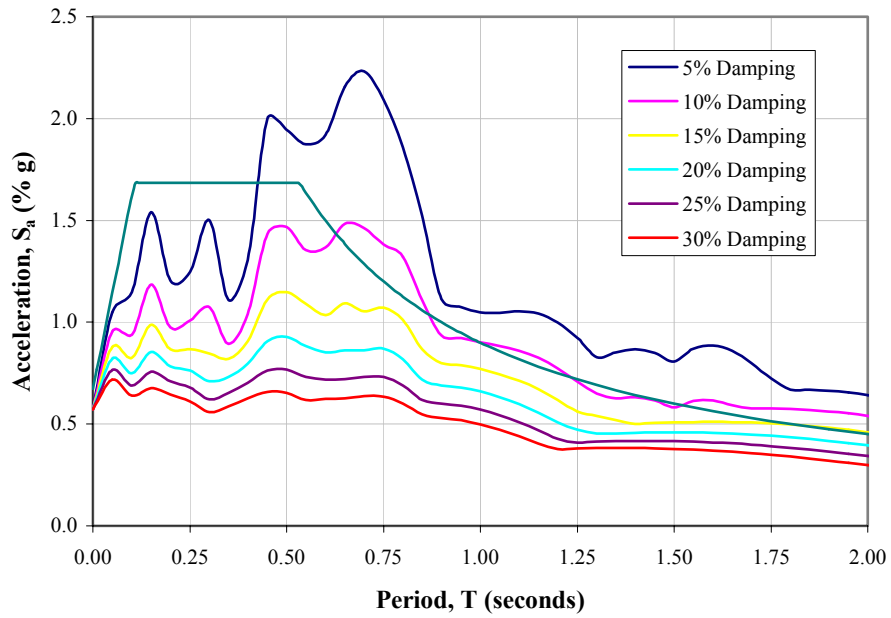


Figure B.5-2. Acceleration Response Spectra (TH-5)

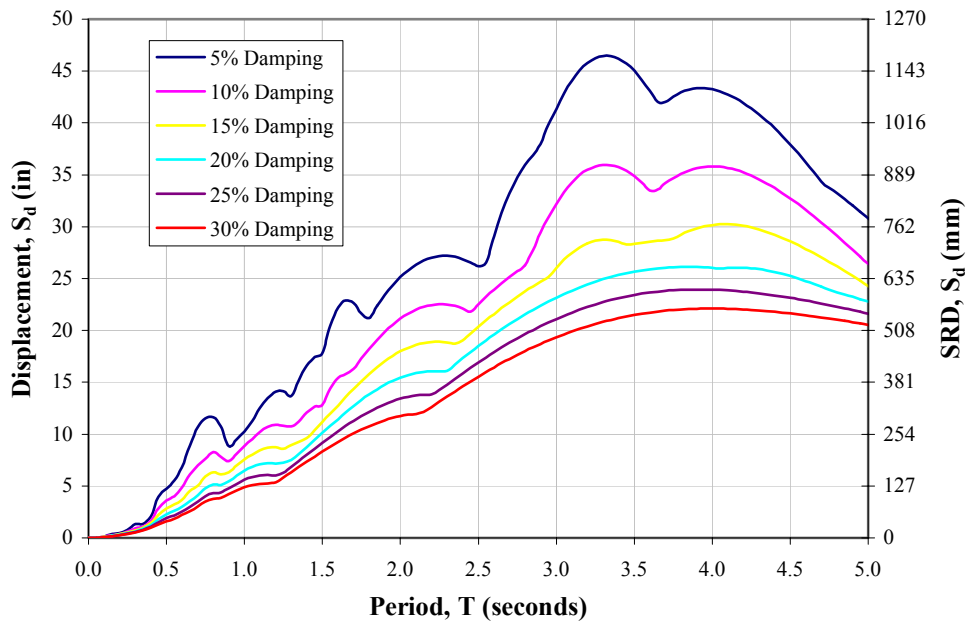


Figure B.5-3. Displacement Response Spectra (TH-5)

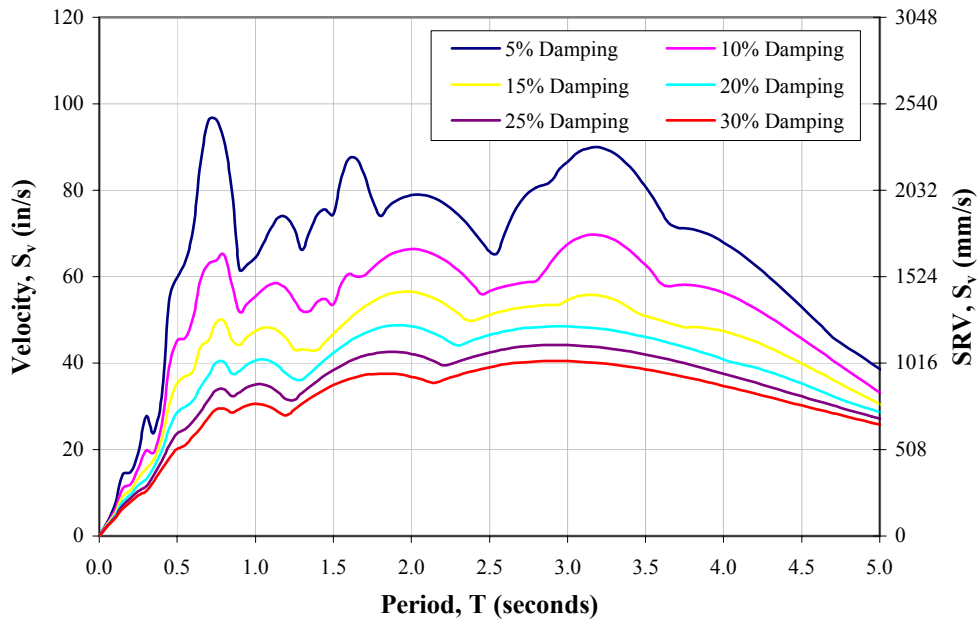


Figure B.5-4. Velocity Response Spectra (TH-5)

B.6 TH-6 Design Response Spectrums (Cape Mendocino)

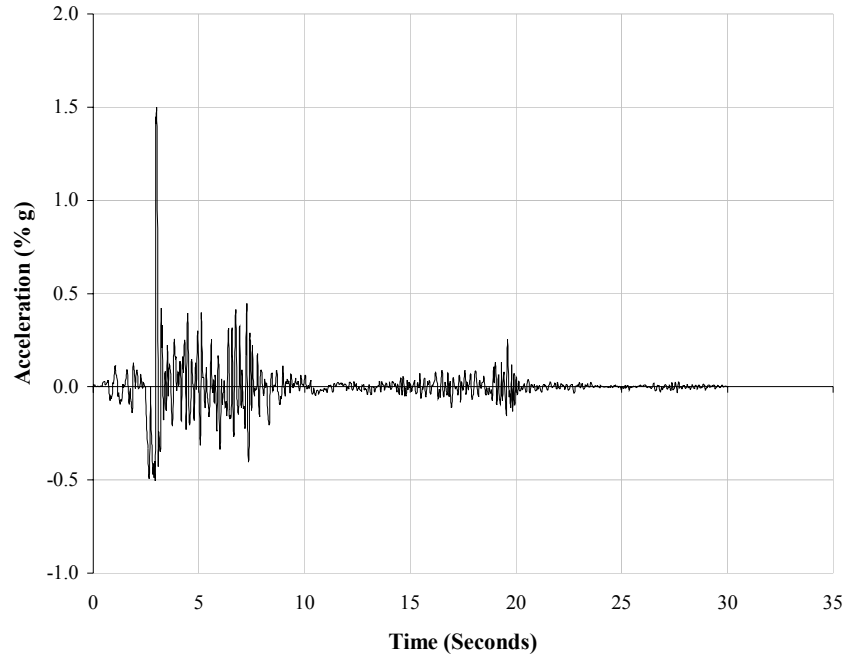


Figure B.6-1. Time-History (TH-6)

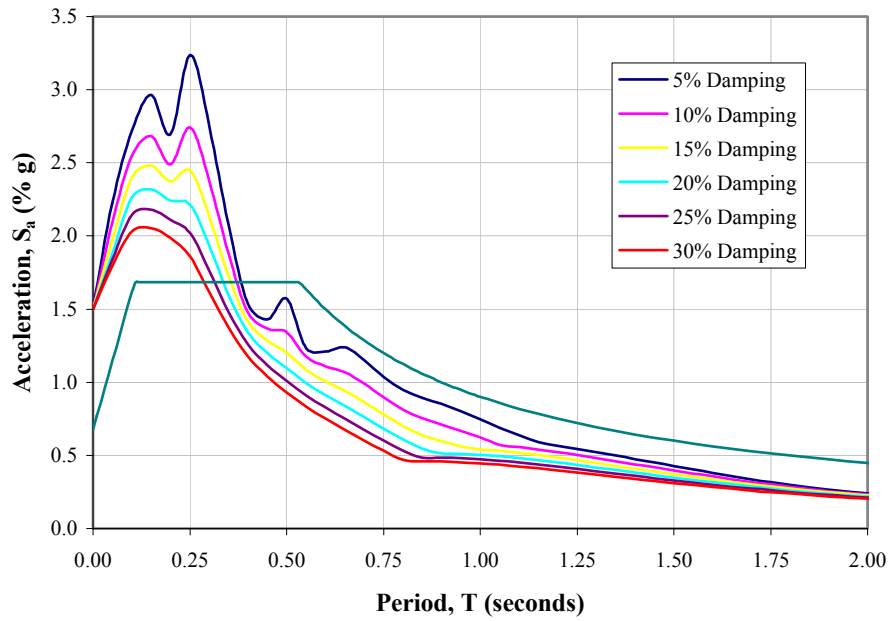


Figure B.6-2. Acceleration Response Spectra (TH-6)

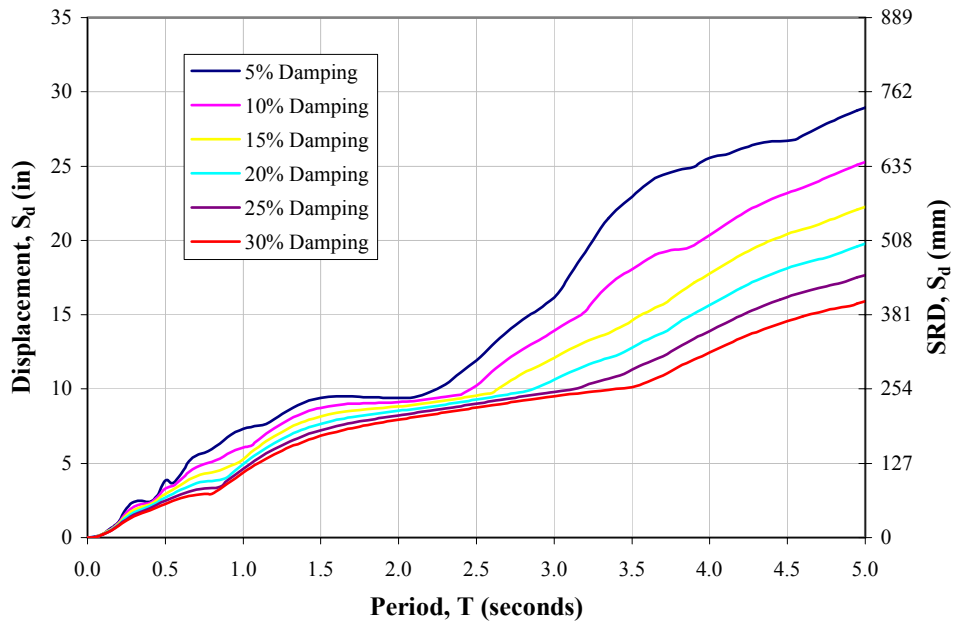


Figure B.6-3. Displacement Response Spectra (TH-6)

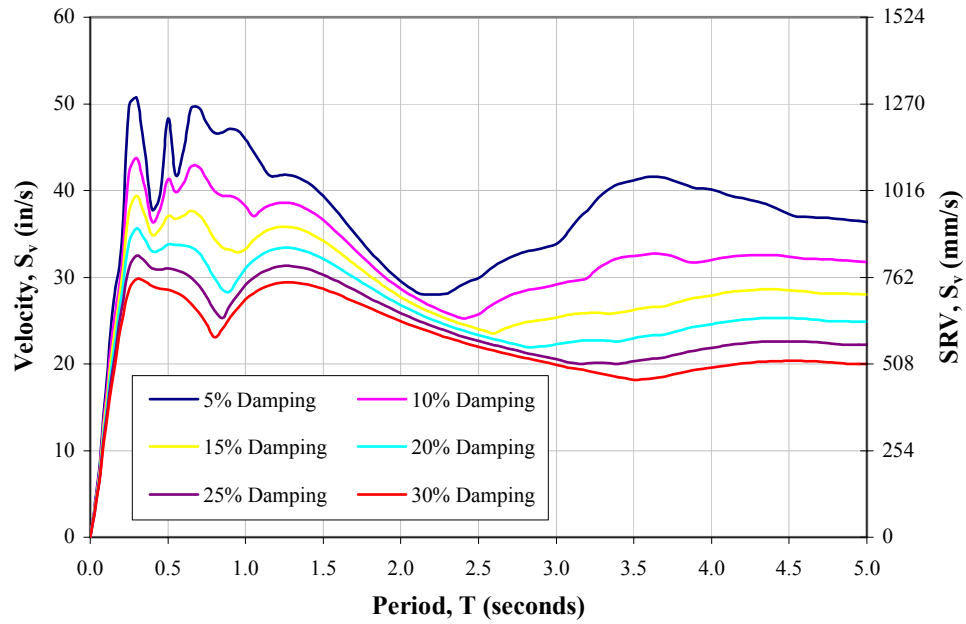


Figure B.6-4. Velocity Response Spectra (TH-6)

B.7 TH-7 Design Response Spectrums (Tabas)

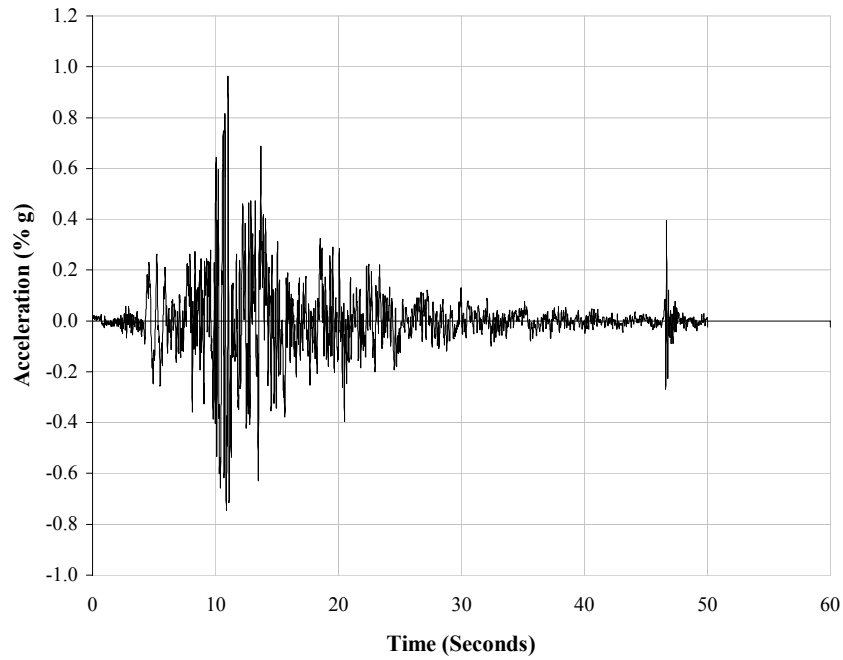


Figure B.7-1. Time-History (TH-7)

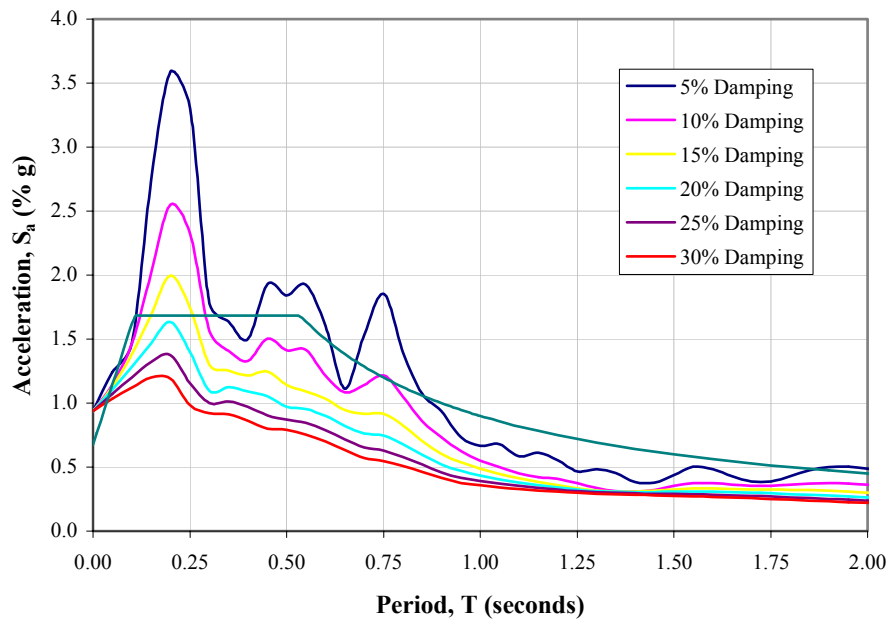


Figure B.7-2. Acceleration Response Spectra (TH-7)

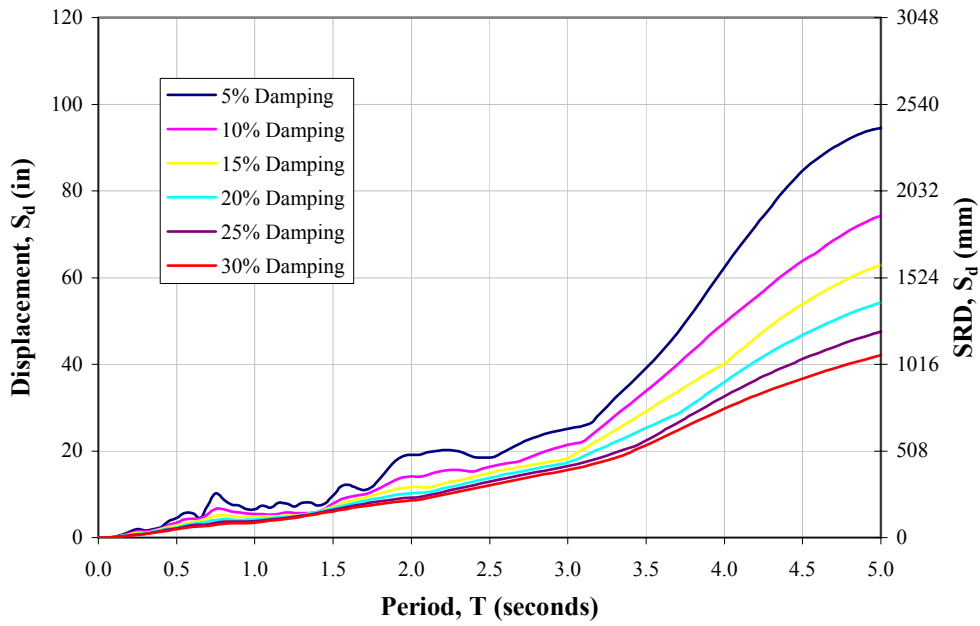


Figure B.7-3. Displacement Response Spectra (TH-7)

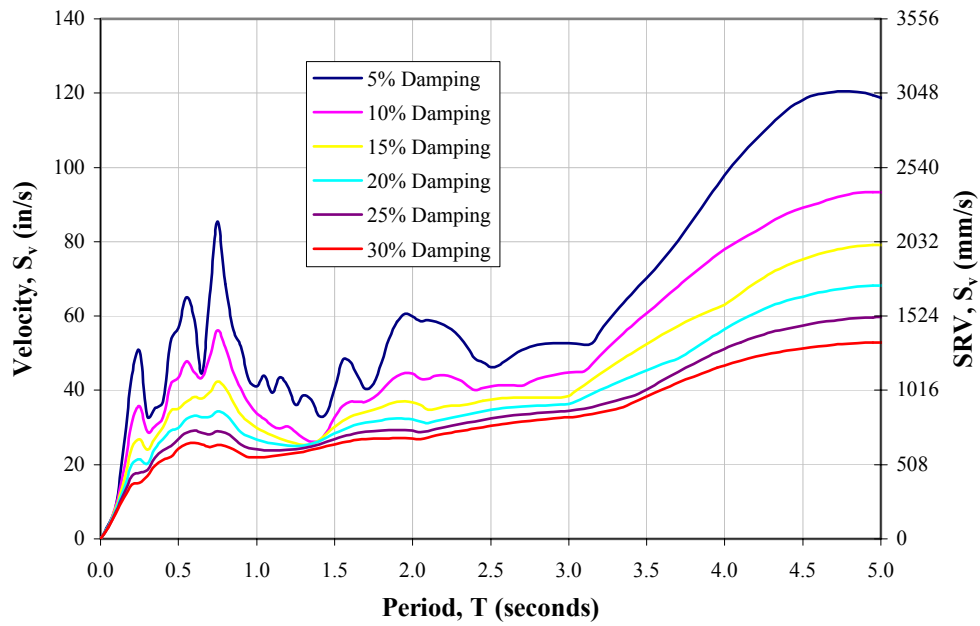


Figure B.7-4. Velocity Response Spectra (TH-7)

B.8 TH-8 Design Response Spectrums (Petrolia)

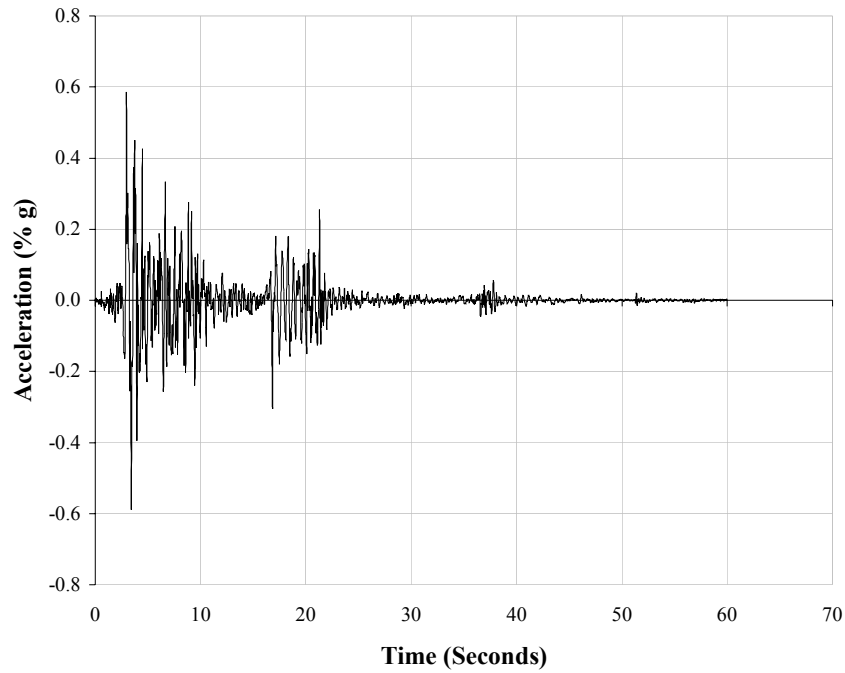


Figure B.8-1. Time-History (TH-8)

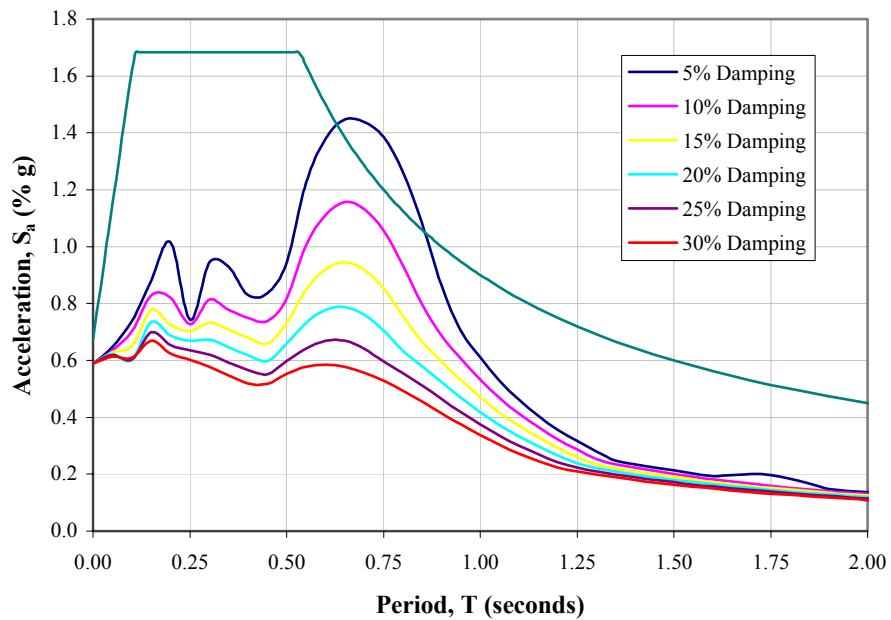


Figure B.8-2. Acceleration Response Spectra (TH-8)

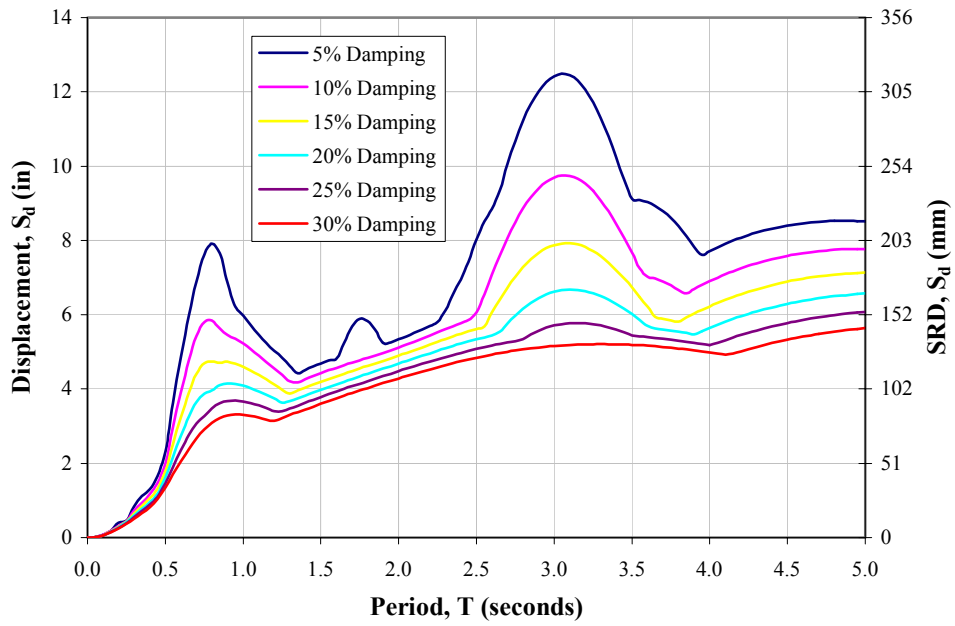


Figure B.8-3. Displacement Response Spectra (TH-8)

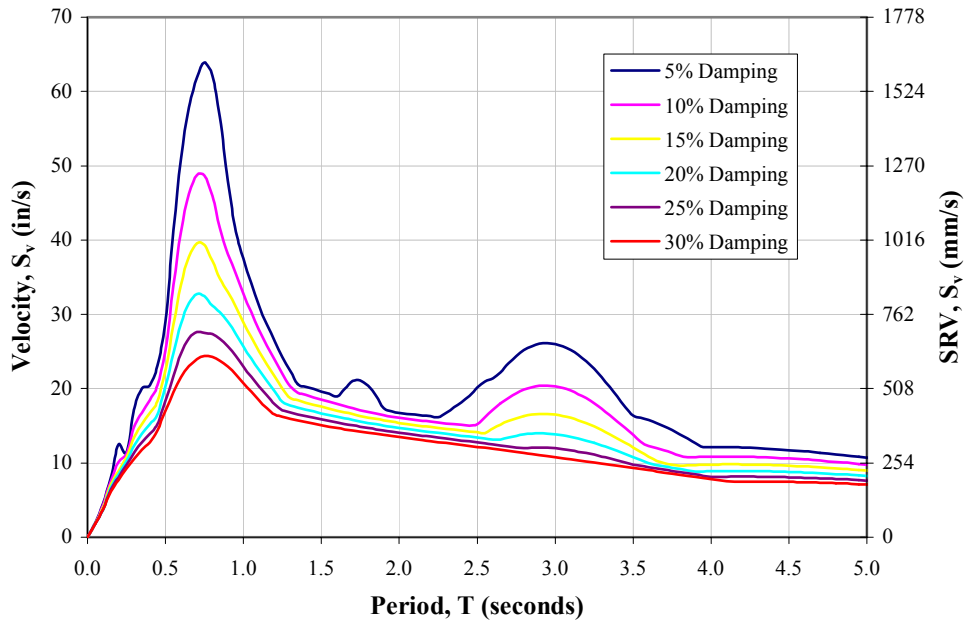


Figure B.8-4. Velocity Response Spectra (TH-8)

B.9 TH-9 Design Response Spectrums (Vina Del Mar)

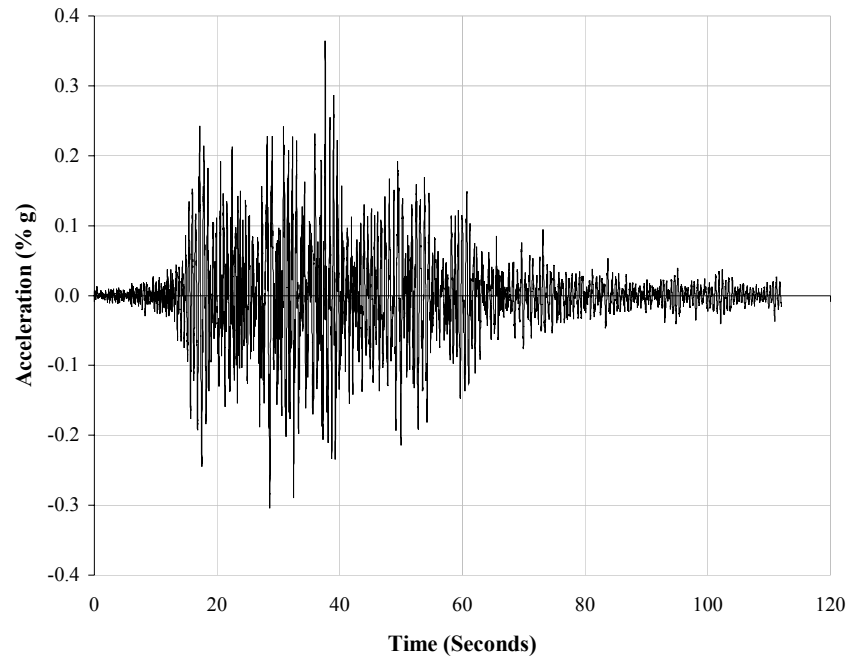


Figure B.9-1. Time-History (TH-9)

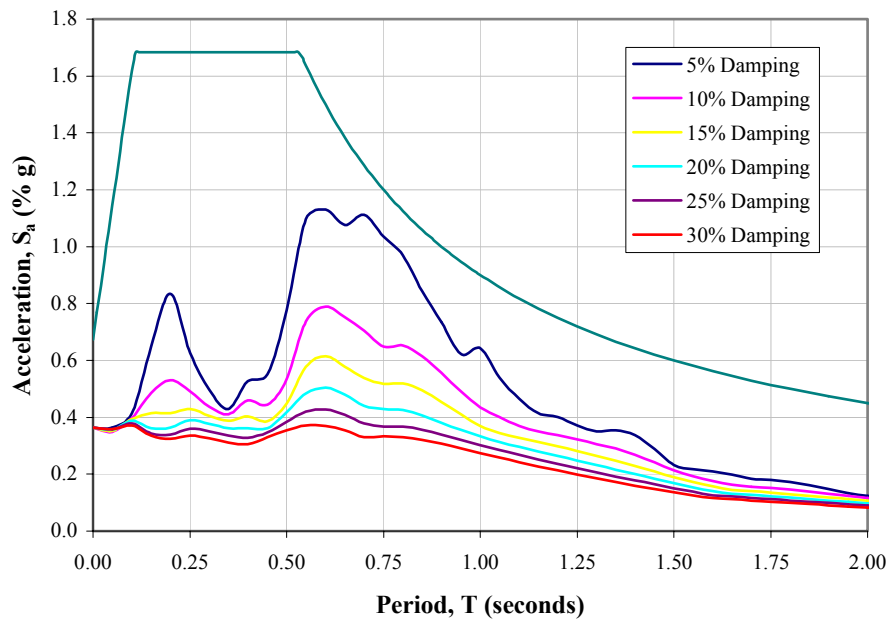


Figure B.9-2. Acceleration Response Spectra (TH-9)

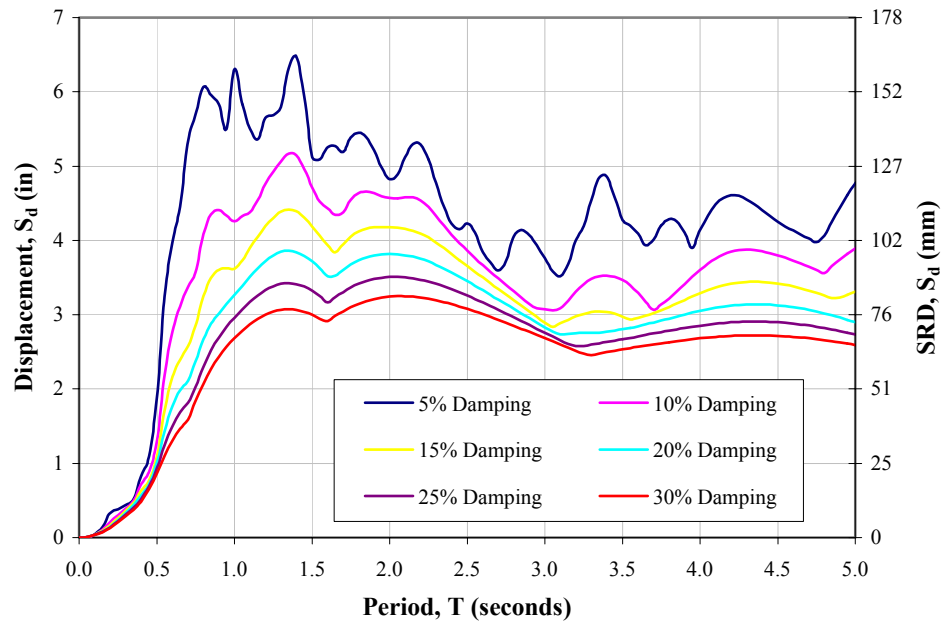


Figure B.9-3. Displacement Response Spectra (TH-9)

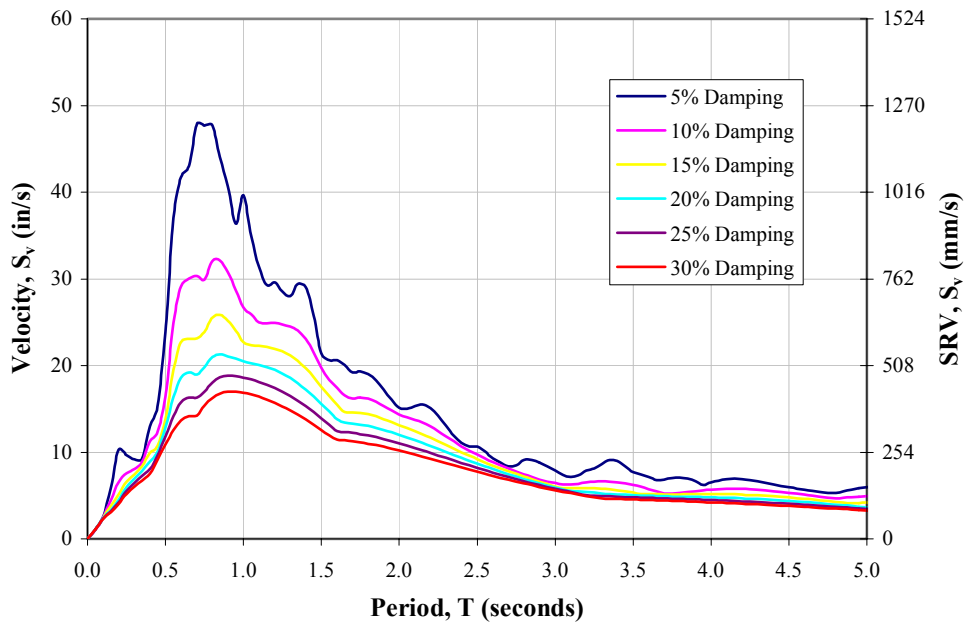


Figure B.9-4. Velocity Response Spectra (TH-9)

B.10 TH-10 Design Response Spectrums (Northridge)

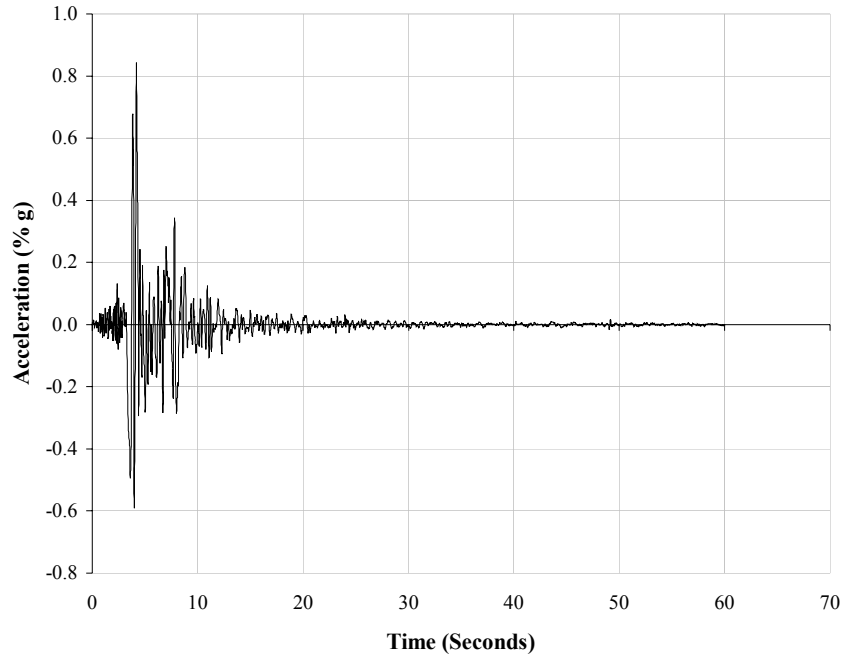


Figure B.10-1. Time-History (TH-10)

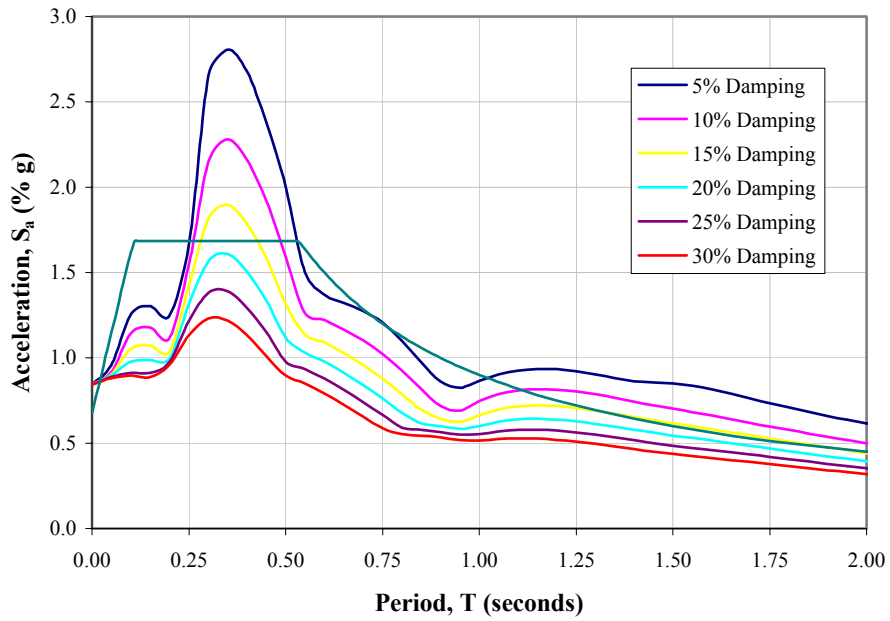


Figure B.10-2. Acceleration Response Spectra (TH-10)

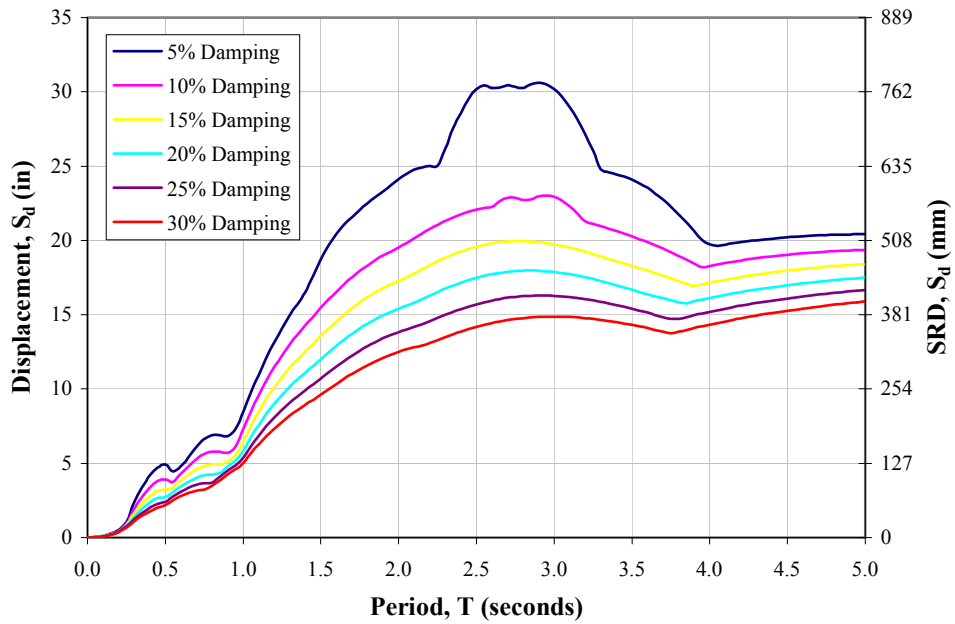


Figure B.10-3. Displacement Response Spectra (TH-10)

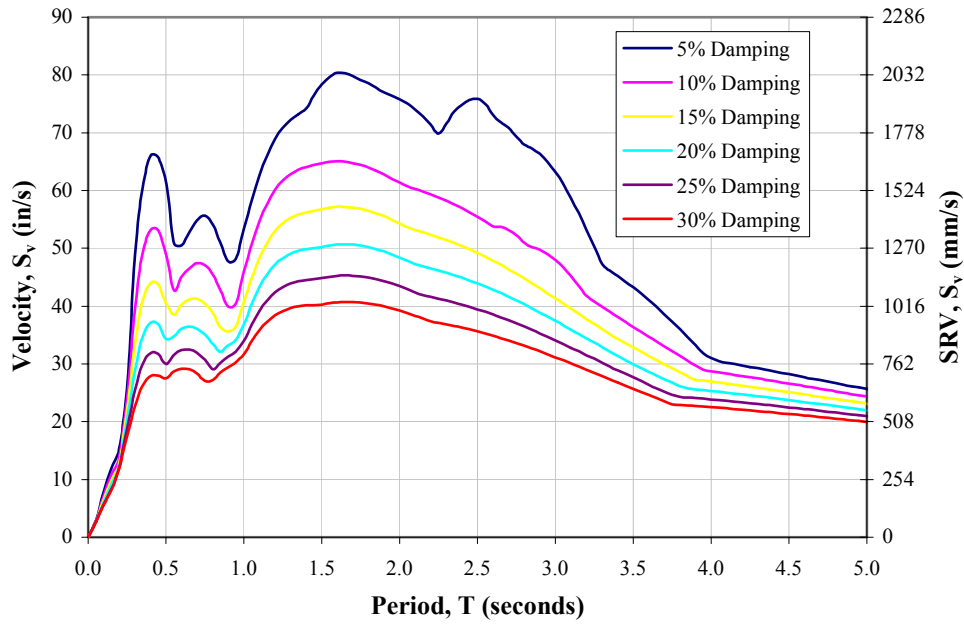


Figure B.10-4. Velocity Response Spectra (TH-10)

B.11 TH-11 Design Response Spectrums (Tokachi-Oki)

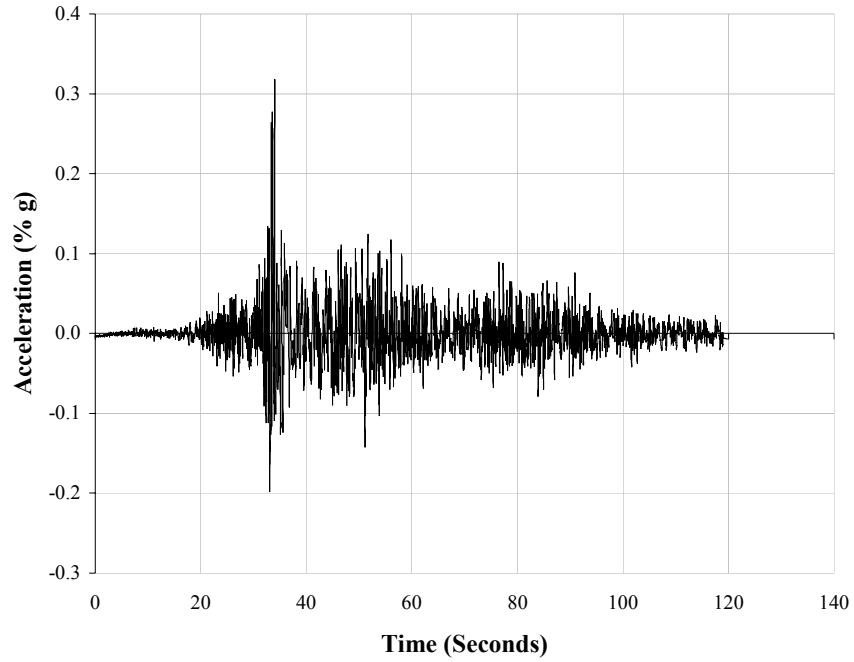


Figure B.11-1. Time-History (TH-11)

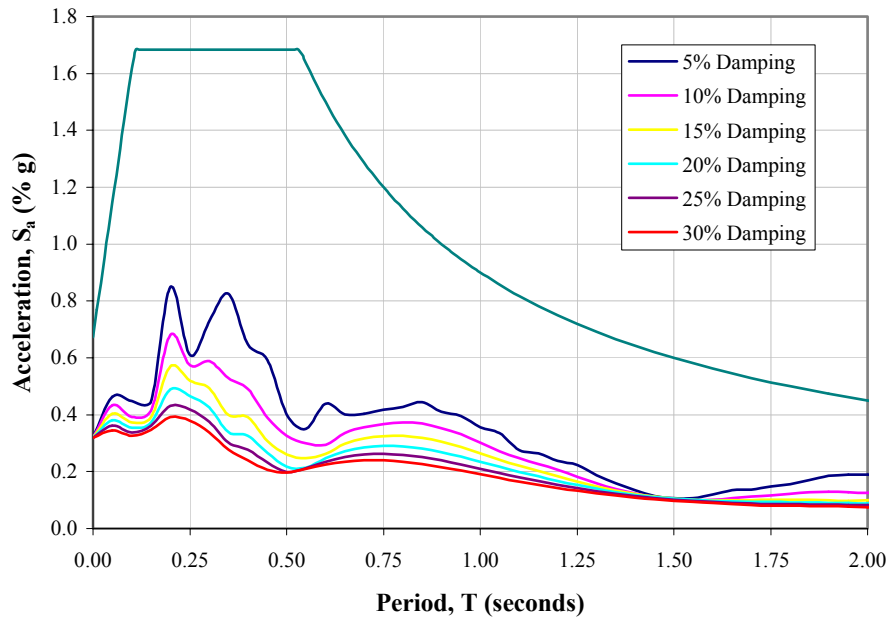


Figure B.11-2. Acceleration Response Spectra (TH-11)

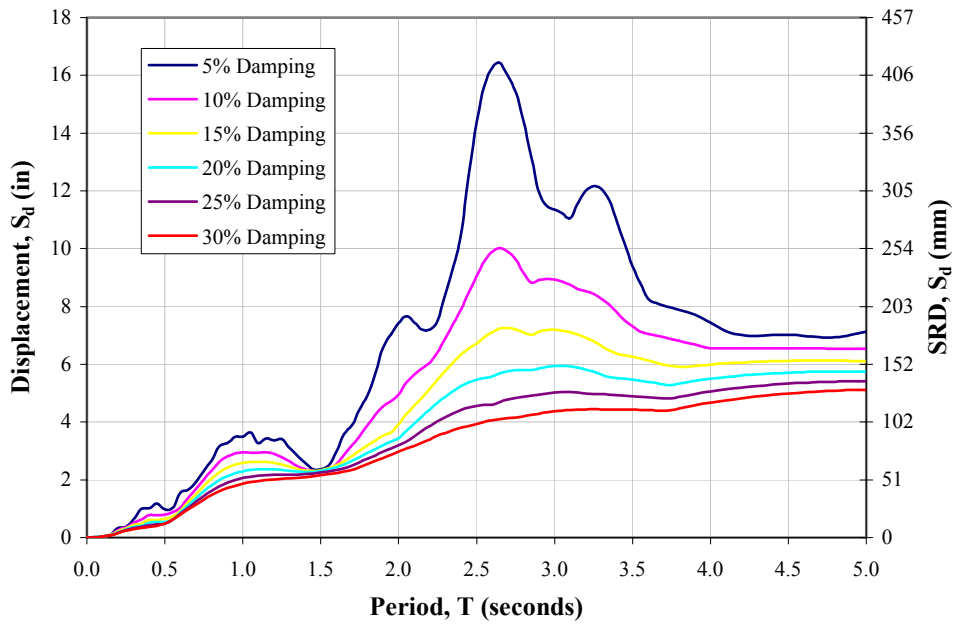


Figure B.11-3. Displacement Response Spectra (TH-11)

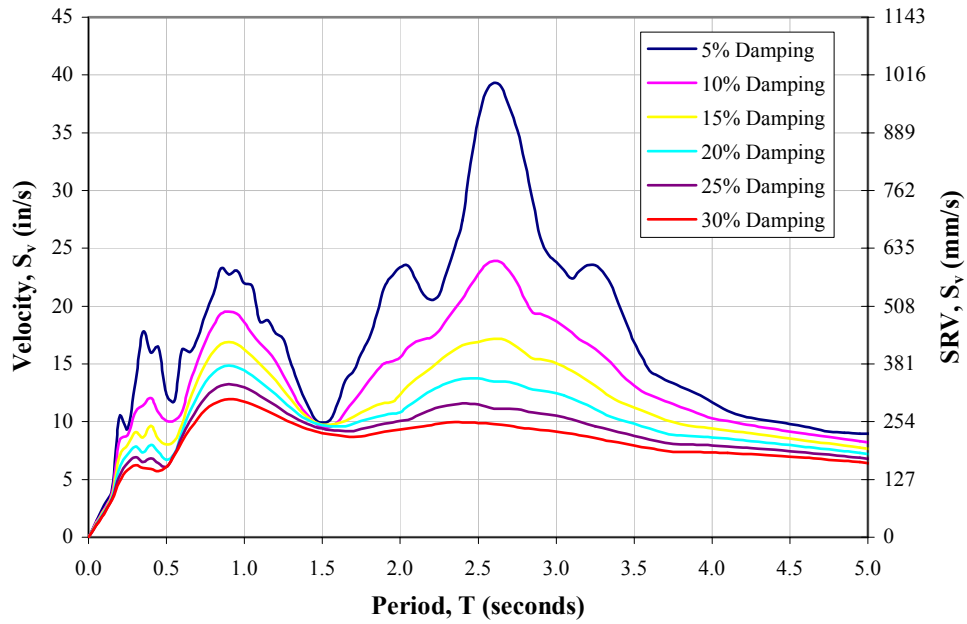


Figure B.11-4. Velocity Response Spectra (TH-11)

B.12 TH-12 Design Response Spectrums (Taft)

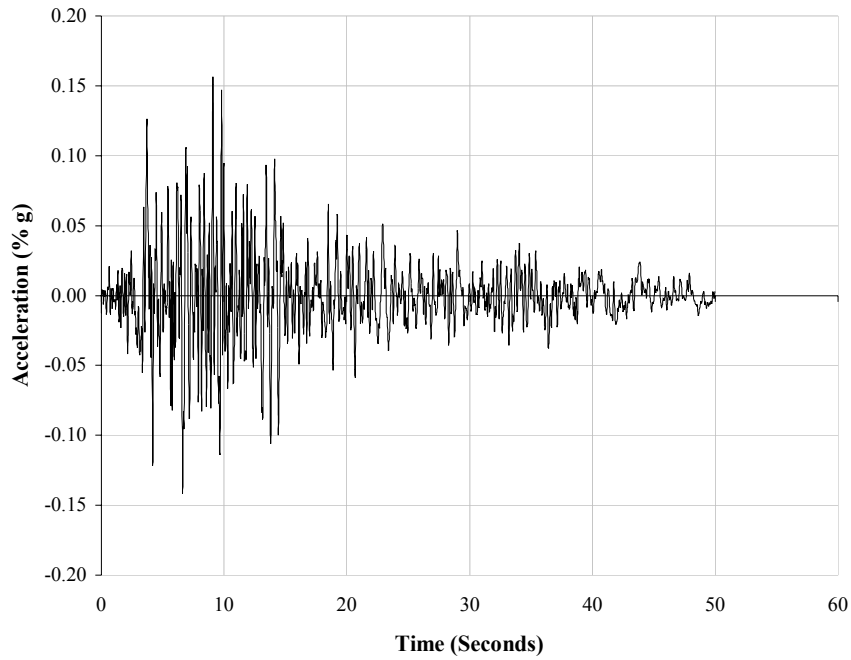


Figure B.12-1. Time-History (TH-12)

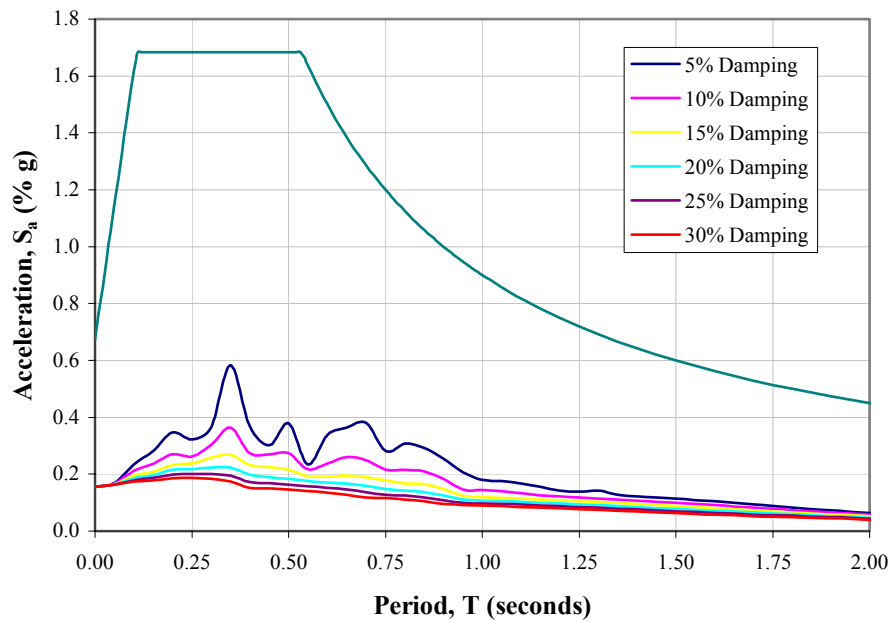


Figure B.12-2. Acceleration Response Spectra (TH-12)

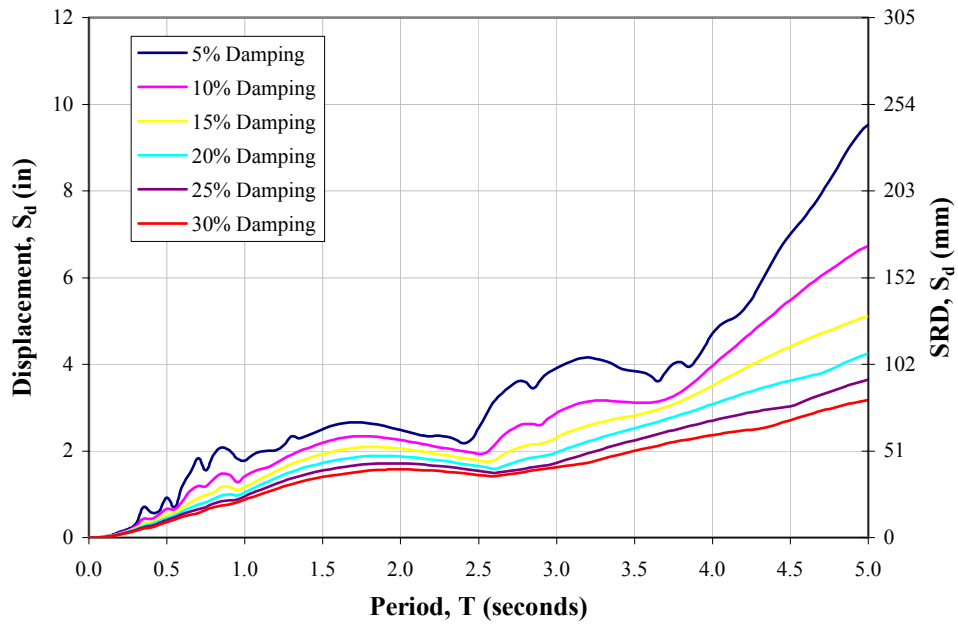


Figure B.12-3. Displacement Response Spectra (TH-12)

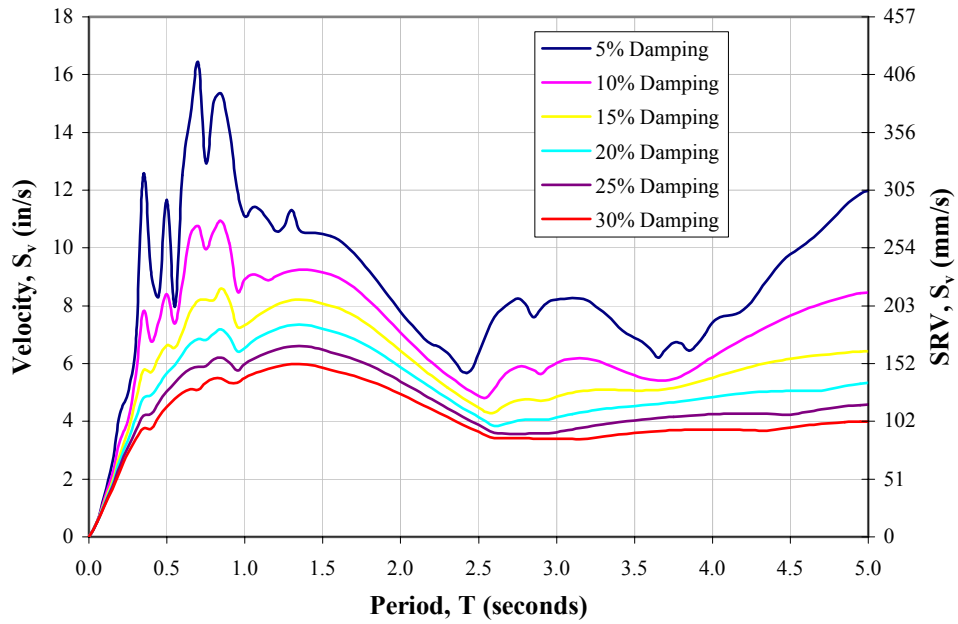


Figure B.12-4. Velocity Response Spectra (TH-12)

APPENDIX C: References

The following documents were used in the preparation of this document. References on the topic of Advanced Analysis and steel frame analysis are included in Section 3.4, and will not be re-stated here.

AISC. 2000. *Load and Resistance Factor Design Specification for Structural Steel Buildings*. Chicago: American Institute of Steel Construction

AISC. 2001. *Seismic Provisions for Structural Steel Buildings*. Chicago: American Institute of Steel Construction

Bruneau, M., Uang, C.M., and Whittaker, A., *Ductile Design of Steel Structures*, McGraw Hill, NY, 1998, 485 pp.

Carr, A.J., "Ruaumoko – Program for Inelastic Dynamic Analysis", Dept. of Civil Engineering, University of Canterbury, 1996.

Carr, A.J., "SIMQKE – Program for Artificial Earthquake Generation", Dept. of Civil Engineering, University of Canterbury, 1997.

Chopra, A.K., *Dynamics of Structures – Theory and Applications to Earthquake Engineering*, Prentice Hall, NJ, 2001, 844 pp.

EC8. Eurocode 9: Design Provisions for Earthquake Resistant Structures, 1994.

FEMA-350. 2000. *Recommended Seismic Design Criteria for New Moment-Frame Buildings*. Federal Emergency Management Agency, Washington, D.C..

FEMA-368. 2001. *NEHRP Recommended Provisions for Seismic Regulations for New Buildings and Other Structures*. Federal Emergency Management Agency, Washington, D.C..

Housner, G.W. "Spectrum intensities of strong-motion earthquakes", *Proc. Symp. On Earthquake and Blast Effects Structures*, C.M. Duke and M. Feigen, eds., Los Angeles: University of California, 1952, p. 21-36.

ICBO. 2000. *International Building Code*. International Conference of Building Officials. Whittier, CA.

Mazzolani, F.M., *Moment Resistant Connections of Steel Frames in Seismic Areas*, E&FN Spon, London, 2000, 644 pp.

Mazzolani, F.M. and Piluso, V., *Theory and Design of Seismic Resistant Steel Frames*, E&FN Spon, London, 1996, 497 pp.

Mazzolani, F.M., Montuori, R., and Piluso, V., "Performance-based design of Seismic Resistant MR Frames", *Behavior of Steel Structures in Seismic Area – STESSA 2000*, F.M. Mazzolani, Ed., Montreal, Canada, 2000, p. 611-618.

Mesa, A. and Priestley, M.J.N., "Dynamic Amplification of Seismic Moment and Shear Forces in Cantilever Walls", Master's Thesis, Rose School, Pavia, Italy, 2002, 95 pp.

Paulay, T. and Priestley, M.J.N., *Seismic Design of Reinforced Concrete and Masonry Buildings*, Wiley, NY, 1992, 744 pp.

Priestley, M.J.N., "Brief Comments on Elastic Flexibility of Reinforced Concrete Frames and Significance to Seismic Design", *Unpublished*, 2000.

Priestley, M.J.N., "Myths and Fallacies in Earthquake Engineering – Conflicts between Design and Reality", Tom Paulay-Symposium "Lateral Force Transfer in Buildings", San Diego, CA, 1993.

Priestley, M.J.N. and Kowalsky, M.J., "Direct Displacement-Based Seismic Design of Concrete Buildings", *Bulletin of the New Zealand Society for Earthquake Engineering*, Vol. 33 (4) 2000.

Priestley, M.J.N., Seible, F., and Calvi, G.M., *Seismic Design and Retrofit of Bridges*, Wiley, NY, 1996, 686 pp.

Salmon, C.G. and Johnson, J.E., *Steel Structures – Design and Behavior*, Harper Collins, NY, 1996, 1024 pp.

SEAOC. 1999. *Recommended Lateral Force Requirements and Commentary*. Structural Engineers Association of California. Sacramento, CA.

Shibata, A. and Sozen, M., “Substitute Structure Method for Seismic Design in Reinforced Concrete.” *Journal of the Structural Division*, ASCE Vol. 102 (6) 1976.

Smith, J.C., *Structural Steel Design – LRFD Approach*, Wiley, NY, 1996, 540 pp.

Takeda, T. Sozen, M., and Nielson, N., “Reinforced Concrete Response to Simulated Earthquakes”, *Journal of the Structural Division*, ASCE, Vol. 96(12) 1970.

Uang, C.M. and Fan, C.C., "Cyclic Instability of Steel Moment Connections with Reduced Beam Sections", *Behavior of Steel Structures in Seismic Area – STESSA 2000*, F.M. Mazzolani, Ed., Montreal, Canada, 2000, p. 747-753.

Uang, C.M. and Yu, Q.S., "Effects of Lateral Bracing and System Restraint on the Behavior of RBS Moment Connections", *Behavior of Steel Structures in Seismic Area – STESSA 2000*, F.M. Mazzolani, Ed., Montreal, Canada, 2000, p. 755-762.

Uang, C.M. and Bertero, V.V., “UBC Seismic Serviceability Regulations: Critical Review”, *Journal of Structural Engineering*, ASCE, Vol. 117(7) 1991.

Uang, C.M. and Maarouf, A., “Deflection Amplification Factor for Seismic Design Provisions”, *Journal of Structural Engineering*, ASCE, Vol. 120(8) 1994.